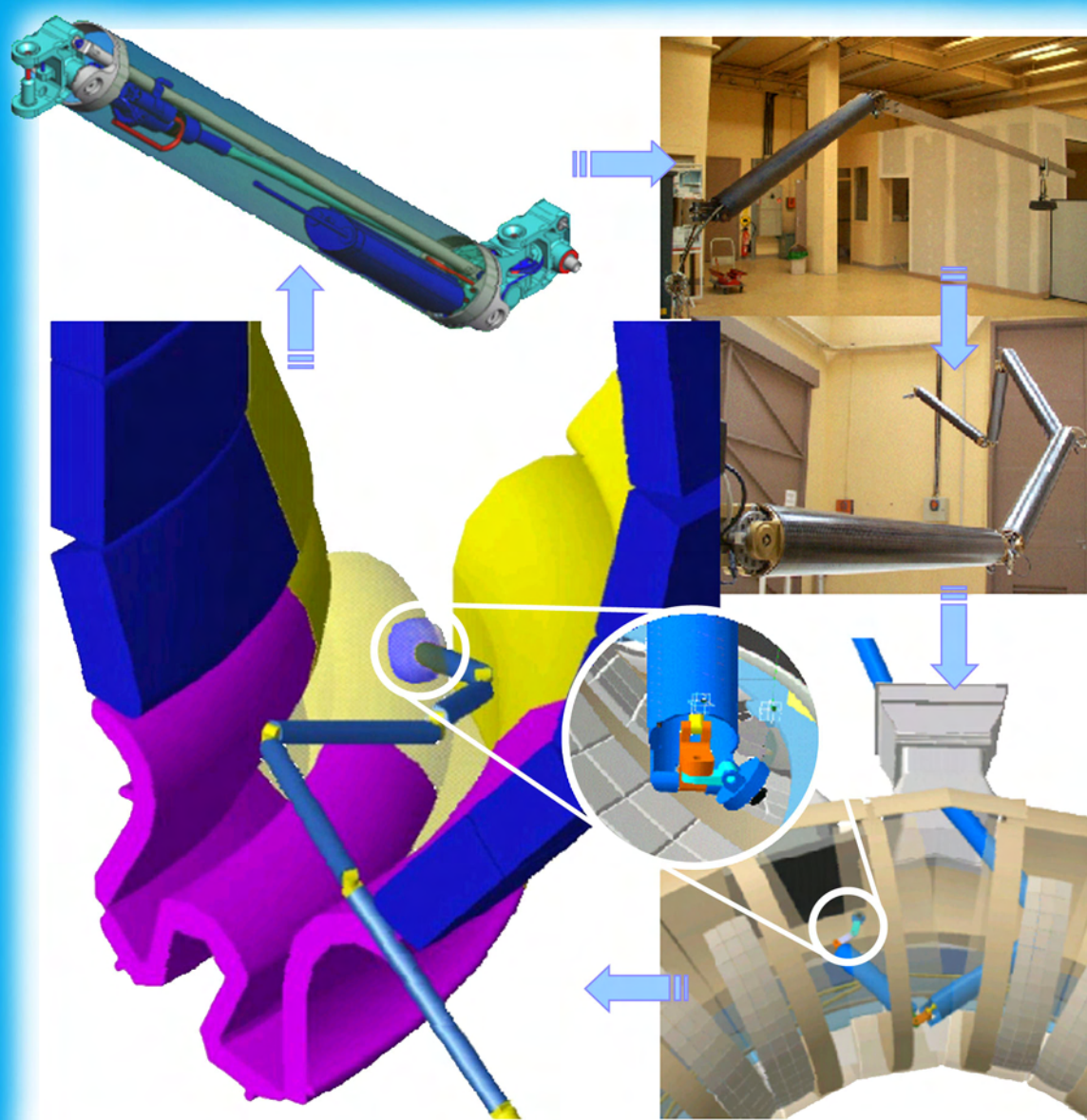


# FUSION TECHNOLOGY

## Annual Report of the Association EURATOM-CEA 2004 (full report)

Compiled by : Ph. MAGAUD and F. Le VAGUERES



ASSOCIATION EURATOM-CEA  
DSM/DRFC  
CEA/CADARACHE  
13108 Saint-Paul-lez-Durance (France)



# FUSION TECHNOLOGY

## Annual Report of the Association EURATOM-CEA

### 2004

(full report)

Compiled by : Ph. MAGAUD and F. LE VAGUERES

ASSOCIATION EURATOM-CEA  
DSM/DRFC  
CEA CADARACHE  
13108 Saint-Paul-Lez-Durance (France)

Tél. : 33 - 4 42 25 46 59  
Fax : 33 - 4 42 25 64 21  
e-mail : [dirdrfc@drfc.cad.cea.fr](mailto:dirdrfc@drfc.cad.cea.fr)  
Web : <http://www-fusion-magnetique.cea.fr>

This report is also available on-line at : <http://www-fusion-magnetique.cea.fr>

*Cover : The Articulated Inspection Arm (AIA), an articulated multipurpose tool to demonstrate the feasibility of close inspection of the ITER Divertor cassettes and Vacuum Vessel first wall. The AIA is able to operate under temperature (120°C) and vacuum ( $10^{-6}$  Pa).*



# CONTENTS

|                           |   |
|---------------------------|---|
| <b>INTRODUCTION</b> ..... | 1 |
|---------------------------|---|

|  |   |
|--|---|
| <b>EFDA TECHNOLOGY PROGRAMME</b> ..... | 3 |
|--|---|

## **Physics Integration**

### **Plasma Edge**

|                |   |   |
|----------------|---|---|
| TW3-TPP-ERDIAG | Evaluation of Laser Ablation Optical Emission Spectroscopy (LA-OES) method for graphite co-deposited layer characterization ..... | 5 |
|----------------|---|---|

### **Heating and Current Drive**

|              |  |    |
|--------------|--|----|
| CEFDA01-645  | TW2-TPHN-NBDES1: Support to neutral beam physics and testing 1 ..... | 9  |
| CEFDA03-1129 | TW3-TPHI-ICRDES1: ITER ICRF Antenna and matching system design ..... | 13 |

### **Diagnostics**

|                              |   |    |
|------------------------------|---|----|
| CEFDA02-1003<br>CEFDA03-1111 | TW2-TPDS-DIASUP4 and TW3-TPDS-DIASUP1:<br>Support to the ITER diagnostic design ..... | 17 |
| TW2-TPDS-DIADEV-D02          | Development of diagnostic components - First mirror study .....                       | 19 |

## **Vessel-In Vessel**

### **Vessel-Blanket and Materials**

|                 |   |    |
|-----------------|---|----|
| CEFDA03-1067    | TW3-TVM-MDB: Rules for design, fabrication and inspection<br>Establishment and Operation of a Material Database .....   | 23 |
| CEFDA03-1091    | TW4-TVM-LIP: Rules for design, fabrication and inspection<br>Modification of ITER materials documents and assessment<br>of material data for licensing TBM's design rules ..... | 25 |
| TW0-T508/05     | Development of Be/CuCrZr brazing techniques .....   | 27 |
| TW1-TVV-HIP     | Improvement of HIP Fabrication techniques .....   | 31 |
| TW2-TVV-ROBOT   | Dynamic test rig for Intersector Welding Robot (IWR)<br>for VV sector field joining .....   | 33 |
| TW3-TVM-JOINT   | Characterization of the CuCrZr/SS junction strength<br>for different blanket manufacturing conditions .....   | 35 |
| TW3-TVV-DISFREE | Further development of the hybrid MIG/Laser welding technique<br>for VV sector field joining .....  | 39 |

|                |   |    |
|----------------|---|----|
| TW3-TVV-ROBASS | Long detection range seam tracker .....   | 43 |
| TW4-TVV-OSWELD | Qualification of multiple phased array UT for one sided welds during VV manufacture ..... | 45 |

## **Plasma Facing Components**

|              |   |    |
|--------------|---|----|
| CEFDA01-585  | TW1-TVP-TESTAN: Monitoring and analysis of thermal fatigue testing of divertor prototypes - 200 kW electron beam gun test ..... | 49 |
| CEFDA02-583  | TW1-TVV-DES: Destructive examination of primary first wall panels and mock-ups .....  | 55 |
| CEFDA03-1029 | TW3-TVB-JOINOP: Optimization of Be/Cu alloy joints for primary first wall panels .....  | 59 |
| CEFDA03-1051 | TW4-TVD-ACCEPT: Study on acceptance criteria for the ITER divertor vertical target .....  | 63 |
| CEFDA03-1077 | TW3-TVB-INMOCK: Fabrication of primary first wall mock-ups for in-pile experiments .....  | 67 |
| TW0-T438-01  | Development and testing of time resolved erosion detecting techniques .....   | 71 |

## **Remote Handling**

|                |  |    |
|----------------|--|----|
| TW4-TVR-AIA    | Articulated Inspection Arm (AIA) .....   | 73 |
| TW4-TVR-Radtol | Radiation tolerance assessment of standard electronic components for remote handling ..... | 77 |
| TW4-TVR-WHMAN  | Development of a water hydraulic manipulator .....   | 83 |

## **Magnet Structure**

|                |   |     |
|----------------|---|-----|
| CEFDA03-1015   | TW2-TMSM-COOLINL: Mock-ups for the TF and CS Terminal regions and Cooling Inlets .....  | 87  |
| CEFDA03-1120   | TW3-TMSC-ASTEST: Tests of advanced Nb <sub>3</sub> Sn strands<br>Extensive characterization of industrial advanced Nb <sub>3</sub> Sn strands developed for ITER TF coils system .....  | 91  |
| CEFDA04-1127   | TW4-TMSC-SAMAN1: Manufacture of sub-size samples .....  | 93  |
| CEFDA04-1134   | TW4-TMSC-BARBEN: Bending strain effects of single strands<br>Study of bending strain effect on critical properties of Nb <sub>3</sub> Sn strands jacketed with stainless steel for various bending amplitudes and temperatures .... | 95  |
| TW1-TMC-CODES  | Design and Interpretation Codes<br>Determination of thermohydraulic properties of cable-in-conduit conductors with a central channel .....  | 99  |
| TW1-TMS-PFCITE | Poloidal Field Conductor Insert (PFCI) .....  | 103 |
| TW2-TMST-TOSKA | TFMC testing with the LCT coil .....  | 105 |
| TW3-TMSC-ELRES | Experimental assessment of the effect of electrical resistances on the V-I characteristics of superconductive cables .....  | 109 |

## **Tritium Breeding and Materials**

### **Breeding Blanket**

#### **Helium Cooled Pebble Bed (HCPB) blanket**

|                   |  |     |
|-------------------|--|-----|
| TW2-TTBB-002b-D01 | Blanket manufacturing techniques - First wall HIPping with open channels .....   | 113 |
| TW4-TTBB-005-D01  | HCPB breeder and neutrons multiplier materials<br>Procurement and quality control of $\text{Li}_2\text{TiO}_3$ pebbles ..... | 115 |

#### **Helium Cooled Lithium Lead (HCLL) blanket**

|                  |   |     |
|------------------|---|-----|
| TW2-TTBC-001-D01 | Helium Cooled Lithium Lead - TBM design, integration and analysis<br>Blanket system design and analysis - Integration and testing in ITER ..... | 117 |
| TW2-TTBC-002-D01 | Blanket manufacturing techniques<br>Fabrication processes for HCLL and HCPB TBMs .....  | 123 |
| TW2-TTBC-002-D03 | Testing of small-scale mocks-ups to qualify manufacturing technologies .....  | 127 |
| TW2-TTBC-005-D01 | Helium Cooled Lithium Lead - Safety and Licensing<br>Test Blanket Module (TBM) accidental safety study .....                                    | 129 |
| TW4-TTBC-001-D01 | TBM design, integration and analysis - Testing programme<br>and engineering design of the first HCLL TBM for ITER H-H phase .....               | 133 |

### **Structural materials development**

#### **Reduced Activation Ferritic Martensitic (RAFM) steels**

|                   |   |     |
|-------------------|---|-----|
| TW2-TTMS-001b-D02 | Irradiation performance - Neutron irradiation to 70 dpa at 325°C and PIE .....  | 135 |
| TW2-TTMS-004a-D04 | Eurofer : Fusion welds development - Evaluation of a welding process<br>adapted to the Test Blanket Module's geometry : Assembly of the horizontal<br>cooling plates with the continuous wave YAG laser welding process ..... | 139 |
| TW2-TTMS-004b-D01 | Tubing process qualification - Advanced process development and testing<br>for the production of TBM's cooling channels .....   | 143 |
| TW2-TTMS-004b-D02 | Qualification of fabrication processes - Processing of high quality welds<br>according to TBM design .....  | 145 |
| TW2-TTMS-005b-D03 | Rules for design, fabrication and inspection<br>Fracture Mechanics Assessments of TBM's .....   | 151 |
| TW4-TTMS-005-D01  | Rules for design, fabrication and inspection<br>Update Data Base and Appendix A of DEMO-SDC .....   | 155 |
| TW4-TTMS-007-D02  | Modelisation of irradiation effects<br>Ab-initio defect energy calculations in the Fe-He system .....   | 157 |

#### **Advanced materials**

|                                      |  |     |
|--------------------------------------|--|-----|
| TW3-TTMA-001-D04<br>TW3-TTMA-002-D04 | SiC/SiC ceramic composites - Divertor and Plasma Facing Materials .....                    | 161 |
| TW4-TTMA-001-D04                     | Modelling of the mechanical behaviour of advanced 3D SiC <sub>f</sub> /SiC composite ..... | 163 |

### **Neutron source**

|                  |  |     |
|------------------|--|-----|
| TW4-TTMI-001-D01 | IFMIF accelerator facilities - Accelerator system design ..... | 167 |
|------------------|--|-----|

## **Safety and Environment**

|                        |   |     |
|------------------------|---|-----|
| SEA5-1                 | Validation of computer codes and models .....   | 171 |
| TW1-TSW-002            | Waste and decommissioning strategy .....  | 175 |
| TW3-TSS-SEA5.3         | Ice formation on cryogenic surfaces .....   | 181 |
| TW3-TSW-002            | Assessment of radioactive waste in ITER hot cell facility .....   | 183 |
| TW4-TSS-SEA5.5-D02&D05 | Validation of the PAXITR and PACTITER code<br>against fusion-specific experiments .....                       | 187 |
| TW4-TSS-SEA5.5-D11     | Validation of the PACTITER code against fusion-specific experiments<br>Development of the PACTITER code ..... | 191 |

## **System Studies**

### **Power Plant Conceptual Studies (PPCS)**

|                    |   |     |
|--------------------|---|-----|
| TW2-TRP-PPCS15-D03 | Waste management strategy on mode A and B .....   | 193 |
| TW4-TRP-002-D02b   | Conceptual design of a HCLL reactor - Tritium control &<br>management analysis, thermo-hydraulic and thermo-mechanical analyses ..... | 197 |
| TW4-TRP-002-D04    | Conceptual design of a HCLL reactor - Design Integration .....  | 201 |

## **ITER Site Preparation**

### **European ITER Site Studies (EISS)**

|                |   |     |
|----------------|---|-----|
| CEFDA03-1069   | European ITER Site Studies (EISS)   |     |
| CEFDA03-1082   | TW3-TES-EISSg1: EISS 3 generic tasks CEA  |     |
| CEFDA04-1161   | TW3-TES-EISS2c: EISS 3 stage 2  |     |
| TW4-TES-COLABA | TW3-TES-EISS4F: European ITER site study 4 – Cadarache<br>TW4-TES-COLABA: Cadarache site for ITER -<br>Collaboration with Local Authorities ..... | 207 |

### **Site and Plant Layout**

|              |   |     |
|--------------|---|-----|
| CEFDA03-1083 | TW3-TEP-CRYO2: Design of ITER cryoplant/cryo-distribution system<br>(auxilliary coldboxes, cryoline...) ..... | 211 |
|--------------|---|-----|

## **Design Support and Procurement**

### **Design Support**

|              |   |     |
|--------------|---|-----|
| CEFDA03-1098 | TW3-TDS-MAGCEA: Detailed engineering and manufacturing studies of the ITER<br>magnet system: Poloidal Field (PF) coil windings and cold test assessment ..... | 215 |
|--------------|---|-----|

## **JET Technology**

### **Physics Integration**

#### **Heating Systems**

|              |   |     |
|--------------|---|-----|
| CEFDA03-1031 | JW3-EP-ICRH and JW4-EP-ICRH: Contribution to ICRH |     |
| CEFDA04-1146 | components antenna limiter .....                  | 219 |

#### **Diagnostics**

|              |   |     |
|--------------|---|-----|
| CEFDA03-1044 | JW3-EP-IRV: Diagnostics enhancement - Wide angle IR endoscope ..... | 221 |
|--------------|---|-----|

### **Vessel-In Vessel**

#### **Plasma Facing Components**

|            |   |     |
|------------|---|-----|
| JW0-FT-3.1 | Internal PFC components behaviour and modelling ..... | 223 |
|------------|---|-----|

#### **Safety and Environment**

|                 |  |     |
|-----------------|--|-----|
| JW3-FT-2.15-D01 | Detritiation of soft housekeeping materials (mainly plastics) .....  | 227 |
| JW3-FT-2.15-D02 | Detritiation of vacuum oil and organic liquids .....   | 231 |
| JW4-FT-3.19     | Laser decontamination/Tritium removal - Studies on Tokamak wall surfaces<br>decontamination by pulsed repetition rate lasers ..... | 235 |

## **Heating Systems Technology Project**

|                 |  |     |
|-----------------|--|-----|
| CEFDA03-1047    | TW3-THHN-IITF1: The first ITER NB injector and<br>the ITER NB test facility: design .....  | 239 |
| CEFDA04-1140    | TW4-THHN-ADSD2: Neutral beam development for EFDA extension .....  | 243 |
| TW3-THHE-CCGDS1 | Coaxial cavity gyrotron and test facility - Design, support to the industrial<br>development and preparation of the technical specifications .....                                 | 247 |
| TW3-THHI-GTFDS1 | Fusion diacrode, IC RF generator, IC power supply and IC test facility -<br>Design, support to the industrial development<br>and preparation of the technical specifications ..... | 249 |

|   |            |
|---|------------|
| <b><i>UNDERLYING TECHNOLOGY PROGRAMME</i></b> ..... | <b>251</b> |
|---|------------|

## **Vessel-In Vessel**

### **Plasma Facing Components**

|                   |   |     |
|-------------------|---|-----|
| UT-VIV/PFC-Damage | Study of damage mechanisms in plasma facing components .....  | 253 |
| UT-VIV/PFC-HIP    | Improvement of reliability, performance and industrial relevancy<br>of HIP processes for PFC components ..... | 255 |

|                    |   |     |
|--------------------|---|-----|
| UT-VIV/PFC-NanoSiC | Nanocrystalline silicon carbide (SiC)<br>Optimization of the preparation of NanoSiC .....                     | 259 |
| UT-VIV/PFC-Pyro    | Application of a tricolour pyroreflectometer to plasma facing components<br>in-situ infrared monitoring ..... | 263 |

## **Remote Handling**

|                  |  |     |
|------------------|--|-----|
| UT-VIV/AM-ECIr   | Remote handling techniques - Radiation effects on electronic components .....                              | 267 |
| UT-VIV/AM-Hydro  | Technologies and control for remote handling systems .....   | 273 |
| UT-VIV/AM-Vacuum | Technologies for vacuum and temperature and magnetic field conditions<br>for remote handling systems ..... | 275 |

## **Tritium Breeding and Materials**

### **Breeding Blanket**

|              |  |     |
|--------------|--|-----|
| UT-TBM/BB-He | Helium components technology - Problems and outline of solutions ..... | 279 |
|--------------|--|-----|

### **Materials Development**

#### **Structural Materials**

|                     |   |     |
|---------------------|---|-----|
| UT-TBM/MAT-LAM/Opti | Development of new RAFM steels with regard to creep properties .....  | 283 |
| UT-TBM/MAT-Modpulse | Pulsed irradiation of the martensitic alloy Eurofer<br>Irradiations by krypton ions at 350 and 550°C at high flux during short time ..... | 287 |

## **Safety and Environment**

|                  |   |     |
|------------------|---|-----|
| UT-S&E-LASER/DEC | Laser decontamination/Tritium removal – Modelling of lasers surface heating ....  | 291 |
| UT-S&E-LiPbwater | Recalculation of the LIFUS experiment (interaction between lithium-lead<br>and water) with the 3D version of SIMMER ..... | 295 |

|  |     |
|--|-----|
| <b><i>APPENDIX 1 : Directions contribution to the fusion programme</i></b> ..... | 299 |
|--|-----|

|   |     |
|---|-----|
| <b><i>APPENDIX 2 : Allocations of tasks</i></b> ..... | 303 |
|---|-----|

|   |     |
|---|-----|
| <b><i>APPENDIX 3 : Reports and publications</i></b> ..... | 309 |
|---|-----|

|  |     |
|--|-----|
| <b><i>APPENDIX 4 : CEA tasks in alphabetical order</i></b> ..... | 317 |
|--|-----|

|  |     |
|--|-----|
| <b><i>APPENDIX 5 : CEA sites</i></b> ..... | 321 |
|--|-----|

# INTRODUCTION

European research on controlled thermonuclear fusion is carried out in an integrated programme with the objective to develop a safe, clean and economically viable energy source. Part of this programme is under the responsibility of the *European Fusion Development Agreement* (EFDA) which provides a framework covering the activities in the field of technology (both Next Step and Reactor) and the collective use of the Joint European Torus (JET).

This annual report summarizes activities performed by the Euratom-CEA Association in 2004 within the frame of the European Technology Programme (both “EFDA” activities and “Underlying Technology” programme). It does not include keep-in touch activities in the frame of Inertial Confinement Energy, reported in a specific issue performed by the European Commission.

This full report is also available on line at “<http://www-fusion-magnetique.cea.fr>”. In each section, the tasks are sorted out according to the EFDA main fields : Physics (TP) , Vessel/In-Vessel (VIV), Magnets (TM), Tritium breeding and Materials (TT), Safety and Environment (TS), System Studies (TS), JET technology activities (TJ),... The Euratom-CEA Association is involved in all these topics (figure 1).

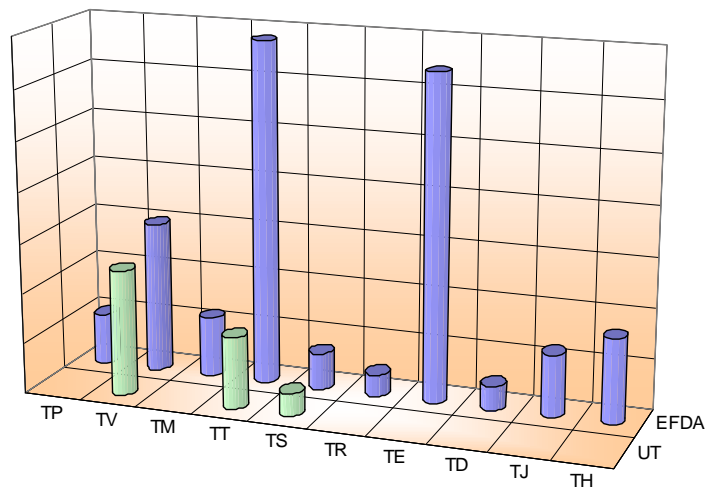
- Euratom-CEA activities carried out in the field “**Physics Integration**” are mainly linked to neutral beam developments and to the development of diagnostic components. In particular, in-situ diagnostics of the plasma facing surface have been studied.
- Plasma Facing Component (PFC) developments, Vacuum Vessel/Blanket activities and Remote handling studies are carried out inside the field “**Vessel/In-Vessel**”. The manufacturing of the ITER Primary First Wall (PFW) panel by HIP forming has been investigated. A dummy mock-up was produced to validate the manufacturing feasibility. In collaboration with BAE Systems, the Euratom-CEA Association has investigated a new welding process, able to improve welding productivity by several times compared to the ITER welding reference process. It is based on a hybrid laser/TIG process called Hybrid Laser Conduction Welding (HLCW). A ITER first wall mock-up (a combination of copper alloy as heat sink material, stainless steel as structural material and beryllium tiles as an armour material) have been successfully manufactured using induction brazing. This process limits the over-temperature exposure of the CuCrZr copper alloy. The Euratom-CEA Association performs a R&D program to demonstrate the feasibility of close inspection of the ITER Divertor cassettes and Vacuum Vessel first wall. The work performed includes design, manufacture and testing of an articulated multipurpose tool demonstrator called Articulated Inspection Arm (AIA), able to operate under temperature (120°C) and vacuum ( $10^{-6}$  Pa). In 2004, a single module prototype was manufactured and successfully tested in a specific device at Cadarache.
- In the field “**Magnets**”, Euratom-CEA Association was involved to provide input information for establishing the final dimension details of the ITER cryoplat. The Euratom-CEA Association is also involved with the design of different parts of the ITER magnet system: thermohydraulic properties of cable-in-conduit conductors with a central channel, design and fabrication of mock-ups for some critical parts of the ITER coils (He inlet), tests of ‘high performance’ Nb<sub>3</sub>Sn superconducting strands, joints development.
- The Field “**Tritium Breeding and Materials**” includes for a large part reactor relevant activities. Within the frame of test breeding module (TBM), activities mainly concerned the improvement and completion of the TBM engineering design. After a first design step in which the main structure, its functional features, its mounting sequence and manufacturing characteristics were defined, the second step, relied on the optimization of the design and manufacturing of the module as well as its integration to the supporting frame. A planning and list of test requirements for the qualification of the HCLL TBM was defined. A preliminary testing programme for the HCLL TBMs in ITER has been proposed on the basis of the foreseen ITER scenario and of the TBM testing strategy and mock-ups test objectives. Manufacturing of relevant mock-ups are under progress. Within the frame of the Helium Cooled Pebble Bed (HCPB) concept programmes, studies about the development of Li<sub>2</sub>TiO<sub>3</sub> pebbles are on going. A new batch of 1 kilogram of pebbles with the size distribution in the range 0.6 to 0.8 mm was produced in 2004. The characteristics of pebbles are in agreement with the specifications for the Li<sub>2</sub>TiO<sub>3</sub> pebbles. Two kilograms of pebbles were delivered for the HE-FUS 3 mock-up tests at ENEA and one sample of optimized <sup>6</sup>Li enriched Li<sub>2</sub>TiO<sub>3</sub> pebbles was delivered for the irradiation experiment at NRG. Euratom-CEA has a significant involvement in the development of structural materials for a fusion reactor, mainly focused in Europe on the EUROFER, a reduced activation martensitic steel. The irradiation behaviour of this alloy at high doses and for irradiation temperatures lower than 400°C is performed in irradiation experiments conducted in the BOR60 reactor of the Russian Research Institute of Atomic Reactors. As expected, all materials harden during irradiation, but RAFM steels and in particular EUROFER 97, present the lower level of hardening and the higher ductility compared to

conventional 9Cr1Mo steels. ODS-Fe-14%Cr-Y<sub>2</sub>O<sub>3</sub> ferritic alloy, having a fine grain structure, display also an interesting behaviour as RAFM steels. Euratom-CEA Association is also involved in the modelling irradiation effects programme by providing a database of Ab-initio defect energy calculations in the Fe-He system.

- **“Safety and Environment”** studies realized by Euratom-CEA cover different parts of this topic such as code validation experiment. The PACTITER code, an adaptation of the PACTOLE code developed for Pressurized Water Reactor, has been used for predicting the Activated Corrosion Products activities in the various Primary Heat Transfer Systems or Tokamak Water Cooling Systems (TWCS). A new tests campaign has been performed in 2004 in the new CORELE-2 loop to determine release rates of 316L under ITER TCWS operating conditions.
- Activities performed in the field **“System studies”** are dedicated to the Power Plant Conceptual Studies (PPCS). In 2004, activities were focused on the reactor model AB, based on a Helium-Cooled Lithium-Lead (HCLL) blanket. The model AB reactor is a suitable near term fusion power reactor able to supply 1.5 GWe to the grid with a gross efficiency of near 44%. Because of the high pumping power required by He-cooled systems, the net efficiency is reduced to about 35%. The HCLL blanket allows to achieve a TBR of 1.13.
- Activities carried out in the Field **“JET technology”** are devoted to the study of different processes which can be used for tritium removal from carbon materials, “Housekeeping” materials, vacuum oil and organic liquids. 2004 activities have also been devoted to the plasma facing components thermo-mechanical modelling, and to the JET diagnostics and divertor enhancement.

Three specific operational divisions of the CEA, located on four sites (see appendix 5), are involved in the Euratom-CEA fusion activities:

- the Nuclear Energy Division (DEN) , for In-vessel component design (first wall, divertor, blanket, ...), neutronics, structural materials and safety activities,
- the Technology Research Division (DRT), for activities dedicated to materials (elaboration, breeding materials) and robotics,
- the Physical Sciences Division (DSM), which includes the Controlled Fusion Research Department (DRFC) operating Tore Supra and responsible for plasma physics, cryoplant and magnet and plasma facing component activities.



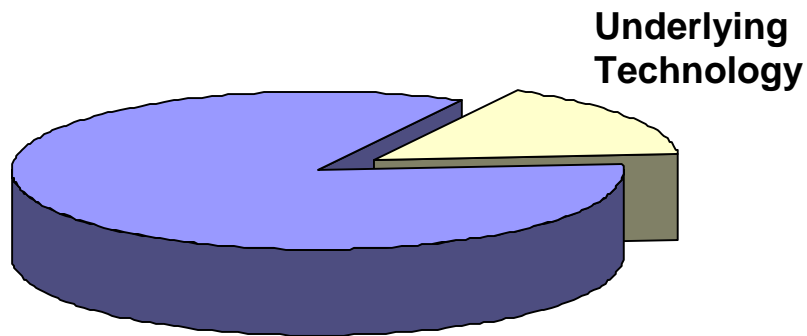
- |  |   |
|--|---|
| TP : Physics                                 | TR : System studies                     |
| TV : Vessel/In-Vessel                        | TE : ITER Site Preparation              |
| TM : Magnets                                 | TD : Design Support and Procurement     |
| TT : Tritium breeding and Materials          | TJ : JET Technology                     |
| TS : Safety and Environment                  | TH : Heating Systems Technology Project |
| EFDA : European Fusion Development Agreement |   |
| UT : Underlying Technology                   |   |

Figure 1 : breakdown of the work carried out by Field

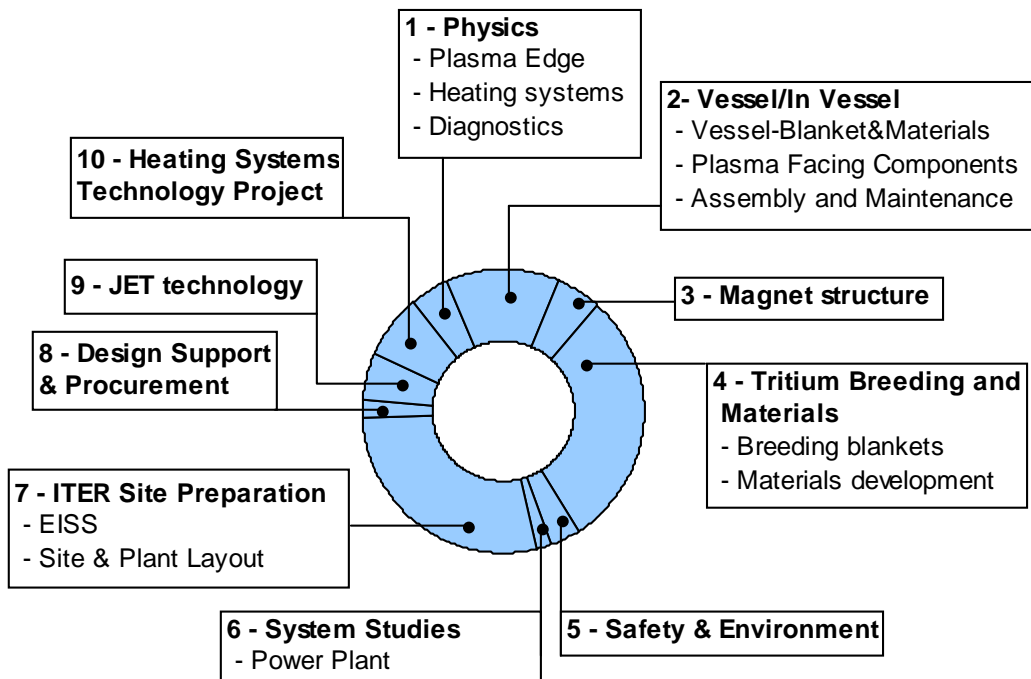
The Euratom-CEA programme in Technology is also completed by specific R&D collaborations with industry in the fields of safety (Technicatome) and with the French National Centre for Scientific Research in the Plasma Facing Component activities.

Progress in fusion technology is constant over the years and this report once again highlights a number of important steps that have been accomplished in this domain. Euratom-CEA, together with other European Institutions is on the foreground of technological advances which are of prime importance for the success of the ITER construction. On the longer term, progress in technology will improve the vision of an electricity producing reactor and will increase the credibility of fusion energy as a genuine energy for the future. The authors and the editors should be commended for their dedicated contribution in making this report available.

# EUROPEAN FUSION DEVELOPMENT AGREEMENT TECHNOLOGY PROGRAMME



## EFDA technology programme





## TW3-TPP-ERDIAG

### Task Title: EVALUATION OF LASER ABLATION OPTICAL EMISSION SPECTROSCOPY (LA-OES) METHOD FOR GRAPHITE CO-DEPOSITED LAYER CHARACTERIZATION

#### INTRODUCTION

In-situ diagnostics of the plasma facing surface is regarded crucial for fusion investigations. A further development of the diagnostics is seen essential in dealing with erosion and deposition in nuclear fusion experiments. The application of new materials such as beryllium (instead of graphite) and carbon fibre composite (CFC) requires also further improvement and development of the diagnostics. It should be stressed that the available diagnostics can not completely explain the matter transport from plasma to the component surface in modern TOKAMAK reactors. Within the frames of our investigations on laser detritiation [1-2], some ablation and thermal measurements were made and analysed. The rigid nuclear safety rules in working with tritium and beryllium limited the investigations. Thus, the laboratory measurements were made only with a few available samples of TexTor and TORE SUPRA graphite.

Laser Ablation Optical Emission Spectroscopy (LA-OES) diagnostics (in some publications referred as LIBS - Laser Induced Breakdown Spectroscopy) was under study. The possibility to make in-situ completely optical measurements inside the vacuum chamber is regarded as an advantage of this method. LA-OES is applied for a surface quantitative or qualitative elemental analysis. The analysis allows to detect the atomic lines emitted by plasma induced after the nanosecond laser pulse interaction with the surface. Generally, LA-OES is applied with the nearly Gaussian laser beam [3-4]. The craters are conical. Each laser pulse results in a sample ablation from different depths. This paper demonstrates that it is possible to use a "homogeneous" laser beam to form cylindrical craters when each laser pulse ablates the sample from a definite depth. The possible LA-OES application to determine both the composition and the thickness of a co-deposited layer was under investigation. In our experiments, thin (up to 10  $\mu\text{m}$ ) and thick (50  $\mu\text{m}$ ) layers were studied. Our previous experiments [5] demonstrated that LA-OES allows to detect certain impurities of a co-deposited layer. The development of the diagnostics to analyse the hydrogen and the impurities contents in a co-deposited layer was the aim of our recent investigations. Hydrogen contents measurements are of the fundamental importance for future TOKAMAK (ITER). The hydrogen Balmer series line ( $n=3 \rightarrow n=2$ ) in the visible spectral range at 656 nm was observed and detected. The isotopic shift between hydrogen and deuterium line is 0.2 nm. As H-line width was  $\approx 2$  nm (a full width at half maximum), it was not possible to distinguish hydrogen isotopes. The energy of the upper transition level is  $\approx 12$  eV. Thus, it was necessary to create hot plasma on the sample by high laser fluence.

#### 2004 ACTIVITIES

LA-OES method in application to graphite tile with a co-deposited layer was studied on the DPC/SCP/LRSI installation (figure 1) that was modified and adjusted for graphite co-deposited layer investigations. The second harmonic (532 nm, 6 ns) of Nd-YAG laser (Brilliant, Quantel) was focused onto the surface by the lens (100 mm or 250 mm focal length). The laser pulse energy was  $\approx 60$  mJ (without the diaphragm 2) and  $\approx 20$  mJ (with the diaphragm 2). The diaphragms were applied to homogenise the laser beam intensity distribution that was hyper-Gaussian with 2.5 rad beam divergence. The diameters of the diaphragm 1 and diaphragm 2 were 6 mm and 3 mm, respectively. A graphite sample was placed in a specially developed sealed sell to protect (especially, against the oxygen molecules) the treated surface and laser plasma by argon. The cell was filled with argon, 1 bar pressure. Two optical fibers were used to collect the plasma light and to transport it to the spectrometer entrance slits.

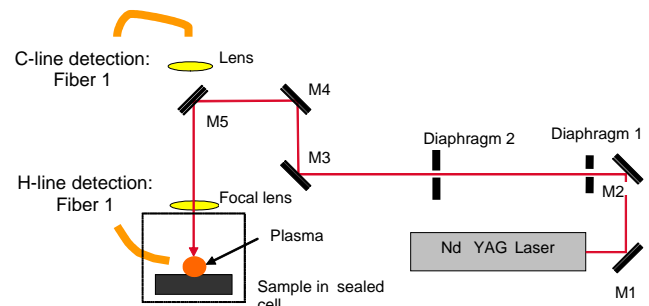


Figure 1 : LA-OES installation

The spectral analysis of the laser plasma plume was made with two 1-meter focal length Czerny Turner spectrometers (Acton Research and THR 1000, Jobin Yvon) supplied with ICCD cameras (ICCD I Max, Roper Scientific) to detect the time resolved spectral line intensity. One spectrometer was adjusted to detect carbon CI-line ( $\lambda = 247.856$  nm,  $E_k = 7.685$  eV,  $g_i = 1$ ,  $g_k = 3$ ,  $A_{ki} = 0.34 \times 10^8 \text{ s}^{-1}$ ), while the other – for hydrogen line detection ( $\lambda \approx 656.281$  nm, 656,274 nm and 656,286 nm,  $E_k \approx 12.088$  eV,  $g_i = 6$ ,  $g_k = 16$ ,  $A_{ki} = (0.696 + 0.435 + 0.0014) \times 10^8 \text{ s}^{-1}$ ).

The experiments with non-homogeneous laser beam and high (40-100 J/cm<sup>2</sup>) laser fluence were performed with 60 mJ laser beam (without the diaphragm 2). The beam was focused onto the TexTor graphite surface by the lens (100 mm focal length) in 0.25-0.4 mm diameter spot to provide 40-100 J/cm<sup>2</sup> laser fluence on the sample. 1200 laser shots were applied for one crater ablation in air at 1 bar pressure.

The laser spot diameter on the target was estimated as  $D_L \approx \Theta_L \times F \approx 0.0025 \text{ rad} \times 100\text{mm} = 0.25 \text{ mm}$ , where  $\Theta_L$  is the laser beam angular divergence. After the graphite surface ablation with 1200 pulses, the crater diameter on the sample surface was determined as 0.4 mm. The “conical” crater depth was 0.35 mm or higher. The spectral line intensities of hydrogen (656.2852 nm), carbon (247.856 nm), and also of some impurities (B, Si, and Fe) were detected for each laser pulse. The ICCD cameras with 1  $\mu\text{s}$  delay and 10  $\mu\text{s}$  gate time were chosen for application. The spectral line intensities (as a function of the number of the applied pulses) decreased and vanished after 150 pulses application for impurities (B, Si and Fe) and after 300-400 pulses for H and C.

The experiments with non-homogeneous laser beam and medium (20-26 J/cm<sup>2</sup>) laser fluence were performed with two diaphragms (figure 1). Diaphragm 2 was placed at the distance  $s_1 = 1250 \text{ mm}$  from the focusing lens with the focal length  $F = 250 \text{ mm}$ . The sample was placed in the lens  $F$  focal position. Six craters were formed after 1200 pulses. Laser ablation rate was of 0.5  $\mu\text{m}$  per pulse. The face surface with a co-deposited layer and the backside surface of TexTor tile were under study. 1200 analytical spectra were detected for each crater. For the typical crater diameters of 300-400  $\mu\text{m}$  that were determined with the mechanical profilometer and the optical microscope, the laser spot surface was  $\approx 0.001 \text{ cm}^2$ . The optical microscope observations confirmed the “conical” crater shape. Spectral line measurements were performed with ICCD camera 10  $\mu\text{s}$  gate time, 0.1  $\mu\text{s}$  delay for H and 0.8  $\mu\text{s}$  delay for C. The typical laser plasma spectra with hydrogen, carbon, and impurity lines are presented (figure 2 and figure 3).

The hydrogen and carbon lines were observed over  $\approx 600$  pulses. The ratio of H/C line intensities for face and backside TexTor tile surfaces are presented on figure 4 and figure 5. The H/C line intensity ratio is high (3÷6) for the face surface with a co-deposited layer during 30 pulses.

Then, the H/C ratio decreases to a constant value 1.5 and 1 for the face and backside surface, respectively. The B, Fe, Si, and Cu impurity traces were detected during  $\approx 3$  pulses for the backside surface and during  $\approx 300$  pulses for the face surface.

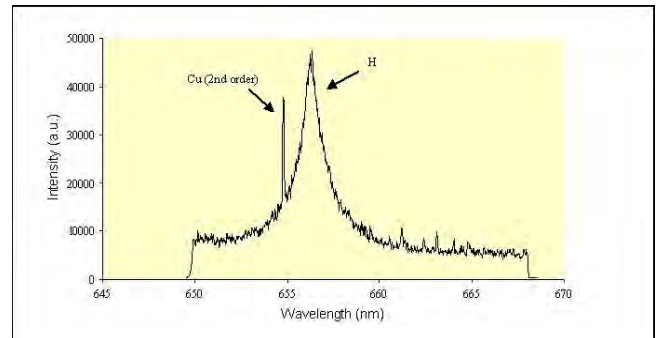


Figure 2 : Typical spectrum in the red range. Gain of ICCD - 255, delay - 0.1  $\mu\text{s}$ , gate time - 10  $\mu\text{s}$ , one crater, 1200 spectra were accumulated

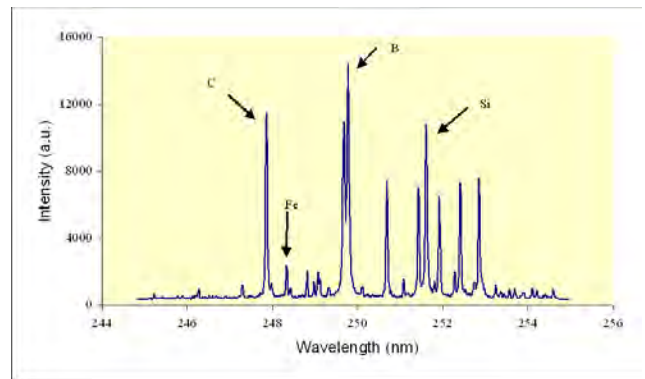


Figure 3 : Typical spectrum in the VU range. Gain of ICCD - 160 ; Delay - 0.8  $\mu\text{s}$  ; Gate time - 10  $\mu\text{s}$  ; one crater; 1200 spectra were accumulated.

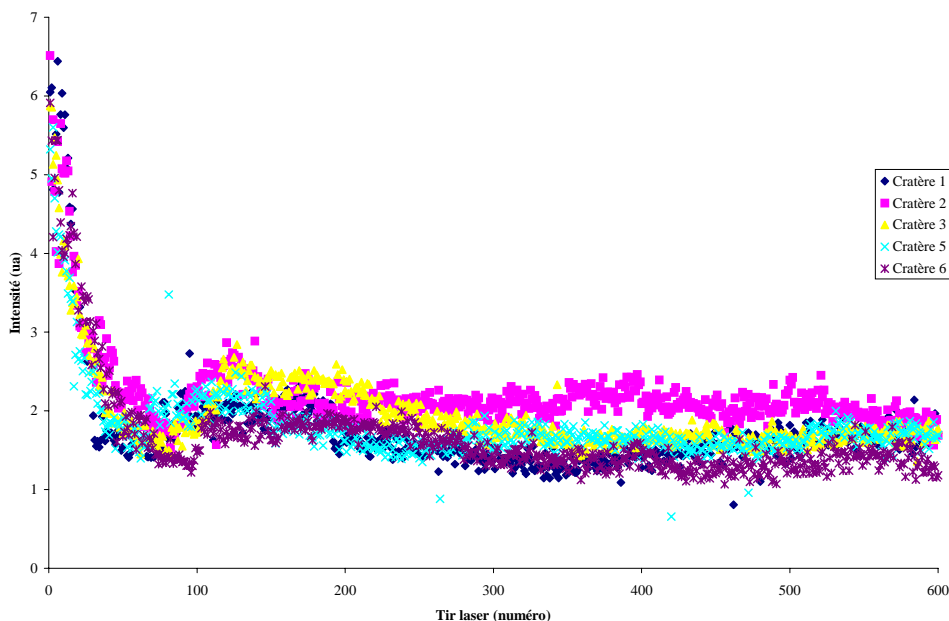


Figure 4 : The ratio of H/C line intensities for six craters on the face surface (with a co-deposited layer) as a function of the pulse number

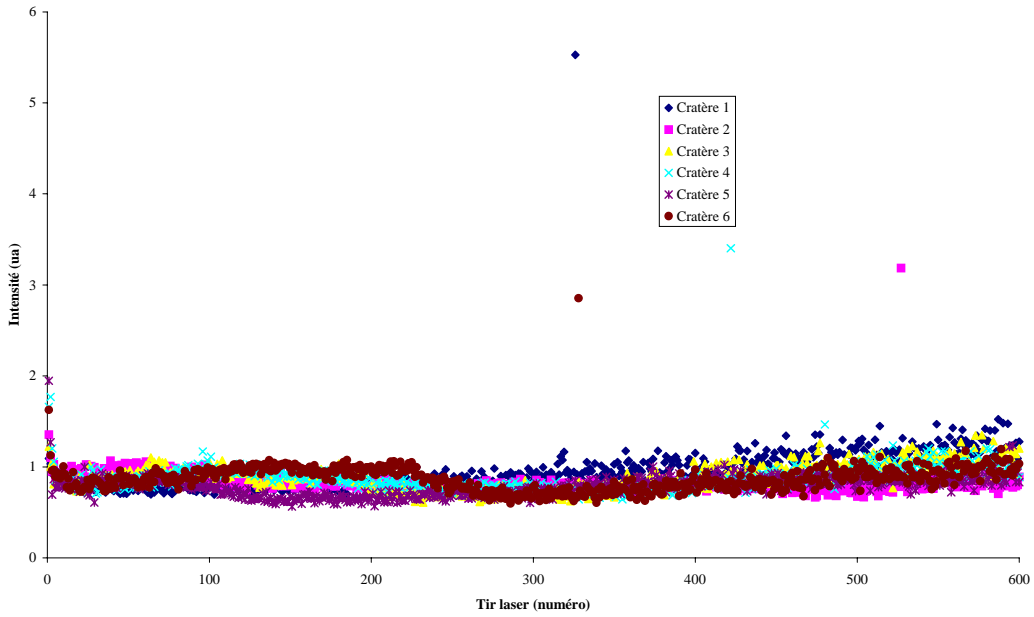


Figure 5 : The ratio of H/C line intensities for six craters on the backside surface (without a co-deposited layer) as a function of the pulse number

The experiments with “homogeneous” laser beam and low ( $4.5 \text{ J/cm}^2$ ) laser fluence were performed with the diaphragm 2 aperture ( $D_2=3\text{mm}$  diameter) being imaged on the sample (TexTor graphite with and without a co-deposited layer). The graphite sample was placed at the distance  $b=s/[(s/F)-1]$  from the lens F. For  $F = 250 \text{ mm}$  and  $s = 1250 \text{ mm}$ , the distance  $b = 312.5 \text{ mm}$ . In this case, the laser spot diameter on the graphite sample is

$D_s = D_2/[(s/F)-1] = 750\mu\text{m}$  that corresponds to the laser spot surface  $0.25 \pi D_s^2 \cong 4.4 \times 10^{-3} \text{ cm}^2$ . For the laser energy  $E \cong 20 \text{ mJ}$ , the laser fluence was  $4.5 \text{ J/cm}^2$ . In this case, the spectral line intensities were very weak or undetectable.

To avoid the effect of the atmospheric water hydrogen (vapour water molecules can dissociate in laser plasma and result in the atomic hydrogen), a sealed cell with argon was developed. It was used to study LA-OES spectral lines in neutral atmosphere. The experiments with “homogeneous” laser beam and medium ( $20 \text{ J/cm}^2$ ) laser fluence were performed with the sealed cell with argon under 1 bar pressure. 13 mJ laser pulse energy was applied. The 3 mm diameter diaphragm 2 was placed at 2250 mm from the focusing lens  $F = 250 \text{ mm}$ .

The sample surface was at 235 mm from the focusing lens. The graphite ablation rate was  $\approx 0.25 \mu\text{m}$  per pulse. Figure 6 presents a crater form obtained with “homogeneous” laser beam for Al-target with a relatively low surface roughness.

The experimental parameters were as follows: the ICCD camera gate time -  $10 \mu\text{s}$ , the delay -  $0.4 \mu\text{s}$  for carbon spectral line detection, and  $0.1 \mu\text{s}$  for hydrogen spectral line. 600 spectra were detected for each crater. The argon gas application resulted mainly in the spectral line intensities increase. Both in air and in argon, the H/C ratio and line intensity changes with the pulse number were almost the same.

Thus, the application of argon environment should not be considered critical for the co-deposited layer analysis. The argon application manifested itself as a black re-deposition around the craters. The black circular zone was not detected with ablation in air, but was observed in Ar. It is considered to be resulting from the graphite powder re-deposition. The graphite powder appeared in the laser plasma plume after its cooling and condensation into micro particles. Ar was keeping hydrogen atoms from oxidation. In air, oxygen gave rise to  $\text{CO}_2$  and, thus, suppressed the black circle formation around the crater.

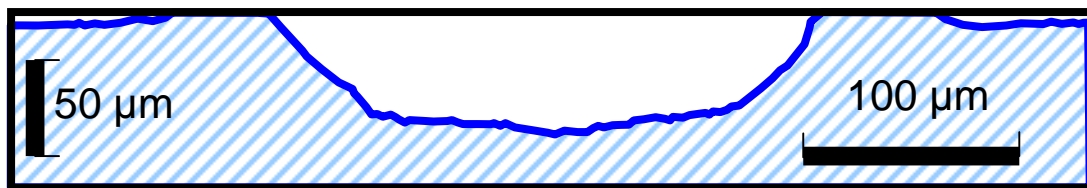


Figure 6 : Crater form obtained with “homogeneous” laser beam on Al-target

## CONCLUSIONS

---

To study LA-OES specific applications to graphite co-deposited layer, a special laser installation was developed and implemented. The installation was used to make time resolved spectral measurements on laser plasma in the controlled environment (argon or air). The experiments with high and medium laser fluence demonstrated the necessity "to homogenise" the laser beam.

The analytical transition wavelengths for hydrogen, carbon, and other impurities (B, Fe, Si, Cu) were determined. For LA-OES measurements, a sufficiently high laser fluence (10-20 J/cm<sup>2</sup>) was required. This requirement resulted from a high energy of the analytical transition of the upper levels for hydrogen (12 eV) and carbon (7.7 eV).

Hydrogen was detected on two sides of the TexTor tile samples (with and without co-deposited layer). In our experiments, hydrogen was detected even in the bulk graphite (for 100- 1000 pulse range). The H/C spectral line intensity ratios were different for face and backside surfaces. The hydrogen spectral line intensity was higher on the surface with a co-deposited layer. On a thick co-deposited layer, the H/C ratio was observed up to 30 pulses. The significant H/C ratio was observed only for the initial 5 pulses on a backside surface on a thin co-deposited layer.

A sealed cell with argon was developed and implemented to study LA-OES spectral lines in neutral atmosphere. The argon gas application resulted in the spectral line intensities increase. The H/C ratio and line intensity changes with the pulse number were practically the same both in air and argon. The argon effect manifested itself as a black re-deposition around the craters. The black circular zone was observed in Ar, but was not detected with ablation in air.

The results of our investigations should be regarded rather optimistic for in-situ LA-OES applications in fusion reactors. On the basis of the obtained results, certain ways to improve the LA-OES analytical performances are envisaged. Thus, the study on LA-OES future improvement and optimization (LA with homogeneous beam of 20 J/cm<sup>2</sup> laser fluence, LA-OES with ultra short laser pulses [6], two pulse plasma reheating [7], etc.) should be considered important.

## REFERENCES

---

- [1] A. Semerok et al. - Studies on graphite surfaces detritiation by pulsed repetition rate nanosecond lasers - CEA report NT DPC/SCP/04-076-A, 2004, pp. 39.
- [2] A. Semerok et al. - Studies on TOKAMAK wall surfaces decontamination by pulsed repetition rate lasers - CEA report NT DPC/SCP/05-111-A, 2005, pp.50.
- [3] C. Geertsen et al, Spectrochemica Acta, B 51, (1996) 1403-1416
- [4] B. Sallé et al, Spectrochemica Acta, B-59 (2004) 1413-1422.
- [5] F. Le Guern et al., J. Nucl. Material, 335 (2004) 410-416.
- [6] A. Semerok et al, Laser and Particle Beams. 20, (2002), 67-72.
- [7] A. Semerok, Ch. Dutouquet, Thin Solid Films, 435-434 (2004) 501-505.

## TASK LEADER

---

Alexandre SEMEROK

DEN/DPC/SCP/LILM  
CEA-Saclay  
F-91191 Gif-sur-Yvette Cedex

Tél. : 33 1 69 08 65 57  
Fax : 33 1 69 08 78 84

E-mail : asemerok@cea.fr

**Task Title: TW2-TPHN-NBDES1: SUPPORT TO NEUTRAL BEAM PHYSICS AND TESTING 1**

**INTRODUCTION**

The European concept for a 1 MeV, 40 A negative ion based accelerator for the neutral beam system on ITER, the SINGle APerture, SINGle Aperture (SINGAP), is an attractive alternative to the ITER reference design, the so-called Multi-Aperture, Multi-Grid (MAMuG) accelerator. A prototype SINGAP accelerator has been used for several years and produced D<sup>-</sup> beams with an energy of 910 keV, 60 A/m<sup>2</sup> simultaneously [1]. The measured beam profiles on the target agree well with the ones predicted by beam optics calculations [2]. However with this prototype accelerator it was not possible to produce beams with optics acceptable to ITER. Therefore a new accelerator, the “ITER-like” accelerator, has been built in order to demonstrate that the beam optics required for ITER can be achieved [3]. A new ion source has also been built which is fully water cooled to allow repetitive pulsing at the required power levels.

**2004 ACTIVITIES**

**THE NEW ITER-LIKE ACCELERATOR AND THE NEW ION SOURCE**

The new ion source is a revised version of the earlier prototype “Drift Source” [4]. The source is mounted inside the vacuum. The side plates are made by Cu deposition and contain water cooling channels and the CoSm magnets which provide the fast electron confinement.

The top, bottom and back plates are made of water cooled OFHC copper. They contain no magnets and the cooling water channels were created by deep drilling.

The pre-accelerator consists of a plasma grid, an extraction grid and a pre-acceleration grid. Each grid is mounted on a circular stainless steel (SS) grid support plate. Each support plate is supported on alumina post insulators from a common SS base plate. The extraction grid and the pre-acceleration grid have aperture patterns of 5 x 5 with a horizontal and vertical pitch of 20 mm. A 20 mm high “kerb” made of stainless steel is fitted at the exit of the pre-accelerator.

This kerb modifies the electric field such that the outer beamlets are “pushed” towards the beam centre in order create adequately parallel beamlets at the exit of the post-accelerator.

Four different plasma grids have been made, with the number of apertures varying from 3 to 25. The Cadarache 1 MV power supply has a current limit of 100 mA. This limits the numbers of apertures on the plasma grid to three when 200 A/m<sup>2</sup>, 1 MeV beams are to be produced.

However, for comparison of experiment and modelling it is more suitable to use rows of 5 apertures and reduce the beam energy. The plasma grid with 25 apertures will be used when the SINGAP accelerator will be tested at the megavolt test stand at JAERI, Naka in Japan in the near future, where a 1 MV – 1 A power supply is available.

A cross section of the “ITER-like” accelerator with the ion source can be seen in figure 1.

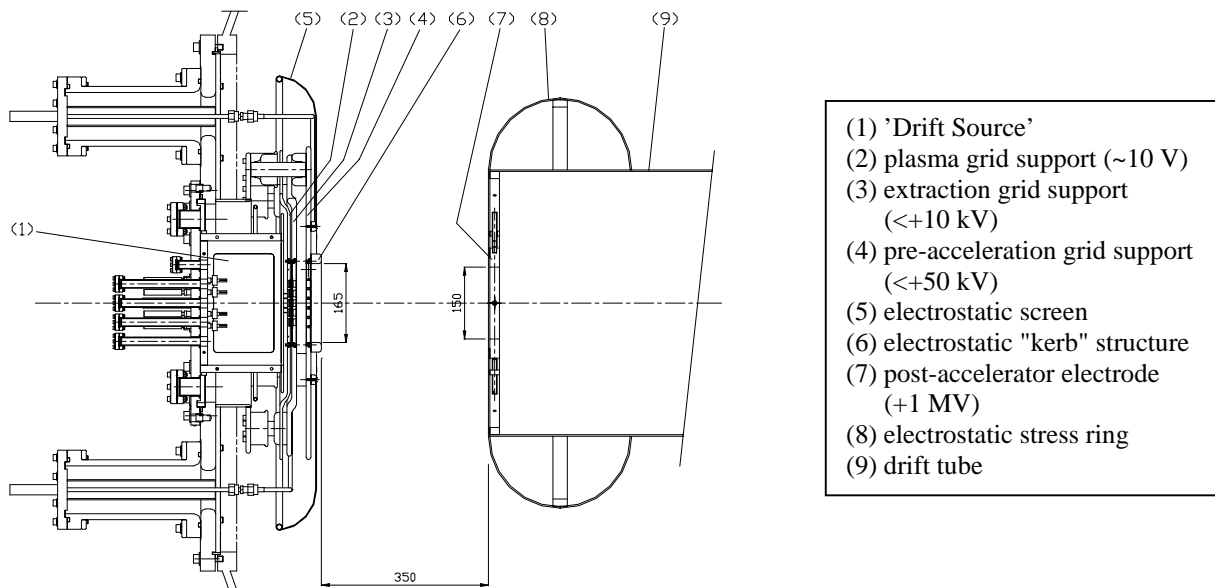


Figure 1 : Vertical section of the “ITER-like” SINGAP Beam Source

The 4 plasma grids have each two heater elements embedded in the source side of the grids to enable heating of the plasma grid to  $\approx 300\text{ }^\circ\text{C}$  for efficient negative ion production with Cs seeding of the source [5].

The extraction grid and the pre-acceleration grid are both water cooled through horizontal channels between the aperture rows and incorporate CoSm magnets for electron suppression and/or ion trajectory correction. Since the grids are rather complex they were manufactured using electrolytic Cu deposition.

The beamlets formed in the pre-accelerator are accelerated to an energy of 1 MeV in one step across the main acceleration gap of 350 mm. The post-accelerator electrode has only one large square opening and is made of OFHC Cu. It can be displaced vertically and horizontally, thus providing aperture offset beam steering to simulate the vertical steering ( $\pm 0.55^\circ$ ) required on ITER or for correcting for beam misalignment.

Both the pre-accelerator and the post-accelerator have been provided with electro-polished SS screens to reduce the electrostatic stresses and they are arranged to ensure that the beam optics is not influenced by fringe fields.

**VOLTAGE HOLDING**

Breakdown free HV pulses up to 940 kV were achieved after only 160 minutes of accumulated voltage on-time. Helium gas with a pressure of about 0.05 Pa was added into the vacuum tank in order to suppress dark currents [6]. Higher voltages have not been attempted in order to minimise the risk of damaging the 1 MV power supply.

**BEAM OPTICS SIMULATIONS**

The first comparisons between simulations and experiments have been done for SINGAP in the ITER-like configuration. Shot 7545 was chosen for the simulation because the the three beamlets are well resolved, which facilitates the detailed comparison with the simulations.

Shot 7545 had 1.8 s of  $28\text{ A/m}^2$   $D^-$  beams, 13 mA in total, as determined from the energy deposited onto the 19 mm thick Mitsubishi MFC 1A graphite target.

Taking stripping losses into account, the extracted current density from the source was  $36\text{ A/m}^2$ .

The extraction voltage was 2.5 kV, the pre-acceleration voltage 18 kV and the post-acceleration voltage 625 kV.

The source pressure was 0.4 Pa, the plasma grid was at  $225\text{ }^\circ\text{C}$  and caesium was introduced. The result of the simulation can be seen on the right in figure 2.

The simulation procedure is described in detail in [2]. An addition to the previously described procedure is that the calculated temperature profiles are now corrected for the time and temperature dependent 3D heat diffusion occurring during the transit from the exposed front towards the rear face of the carbon target where the temperature distribution is measured experimentally.

**EXPERIMENTAL DATA**

The measured infra red data is shown on the left in figure 2 and on the right, the calculated power density as seen from the back of the target.

We see from the data in figure 2:

- The two beamlets on the right are vertically 30 mm apart (the calculation gives 23 mm).
- The lower two beamlets are horizontally 11 mm apart (the calculation gives 12 mm).
- The power density profile is wider than calculated, but the central part not by very much.

The reason why the beamlets are vertically further apart than calculated is not yet clear.

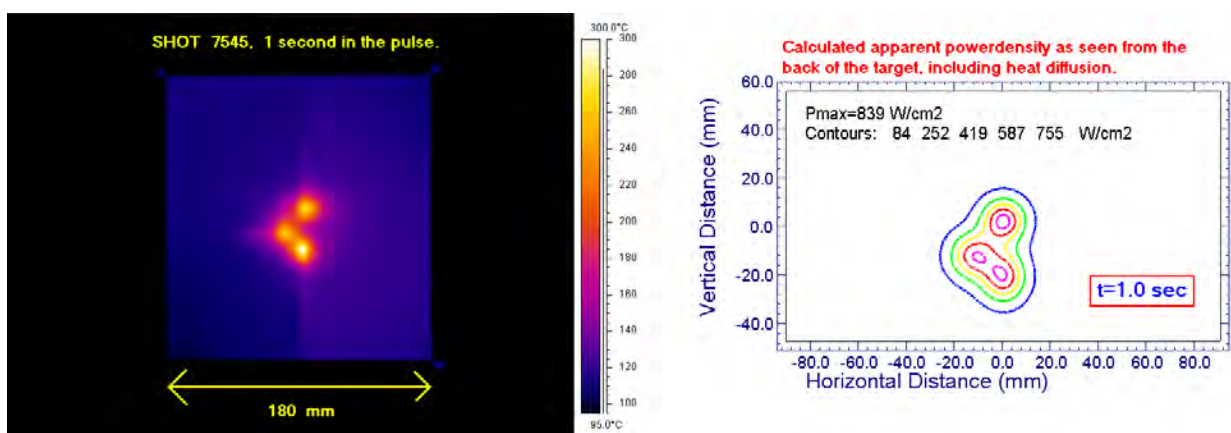


Figure 2 : Infra red data taken from the back of the carbon target for shot 7545 ( $28\text{ A/m}^2 D^-$ ) is shown on the left The calculated power density is shown on the right

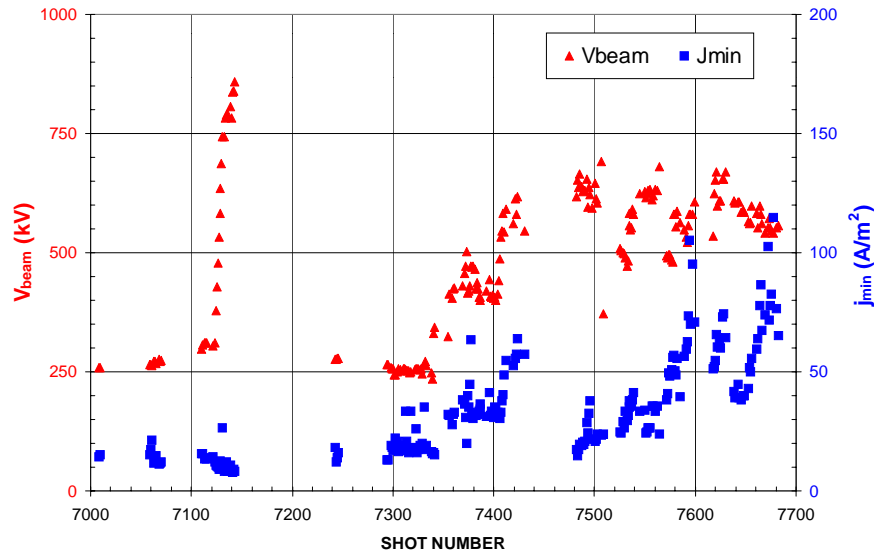


Figure 3 : D beam energies and current densities for the shots done so far with the “ITER-like” accelerator  
The current densities in this graph are slightly over evaluated due to slightly different software being used

With the experimental profile information available, we have tried to determine the actual beam optics. If we assume that the starting positions of the beamlets are correct and adjust the steering angles to match the measured positions on the target, the beamlet positions at the target will be correct, but the current density will still be too high. The measured power density indicates that the beamlet optics are worse than those calculated; either the beamlet divergence is higher than calculated, or the beamlet profile not the assumed simple Gaussian. Simply degrading the beamlet divergence to match the peak power density results in calculated profiles that are too narrow at the edge and too wide in the centre (smearing out the individual beamlets). A reasonable match can be found if it is assumed that the beamlet profile is bi-Gaussian with 60 % with a divergence of  $\approx 3$  mrad and 40 % with a 7 mrad divergence.

### HIGHER BEAM ENERGIES AND CURRENTS

There has been a limited number of shots done so far with the new “ITER-like” accelerator. They are all displayed in figure 3. All shots were done with deuterium. Caesium was gradually introduced to the source from shot number 7280 onward. At the end of the shots shown here we had introduced 1.9 g of Cs. Beam energy of 850 keV was obtained in shot 7143 with a current density of 15 A/m<sup>2</sup>.

This shot was done without caesium. Breakdown free shots with Caesium gave beams with an energy of 580 keV and a current density of 85 A/m<sup>2</sup>.

### CONCLUSIONS

HV conditioning pulses have demonstrated that the ITER-like accelerator can hold 930 kV without breakdowns. D<sup>-</sup> beams have been produced at 850 keV with a current density of 15 A/m<sup>2</sup>.

A current density of 85 A/m<sup>2</sup> has been achieved at 580 keV. The power is measured calorimetrically on the graphite target.

The first experiments have so far confirmed some aspects of the design of the new ITER-like accelerator, but not all. In particular the experiment data suggest that the beamlets have a bi-Gaussian power density distribution (60% with a divergence of  $\approx 3$  mrad and 40% with a 7 mrad) as opposed to the single Gaussian with 2.5 mrad divergence of the simulation.

The positions of the beamlets relative to each other are correct (within 1 mrad), except the central beamlet, which is almost 3 mrad too high. The reasons for these differences are not yet understood. Further experiments and simulations will be carried out in an attempt to understand the differences between the calculated and experimental beam profiles and the accelerated current density.

### REFERENCES

---

[1] L. Svensson, D. Boilson, H.P.L. de Esch, R.S. Hemsworth, A. Krylov and P. Massmann - 22<sup>nd</sup> SOFT, Helsinki, 2002.

[2] H.P.L. de Esch, R.S. Hemsworth and P. Massmann - Updated physics design ITER-SINGAP accelerator, submitted to Fusion Engineering and Design.

[3] P. Massmann, L. Svensson, H.P.L. de Esch and R.S. Hemsworth - Design and fabrication of the “ITER-like” D<sup>-</sup> acceleration system, to be presented at 23<sup>rd</sup> SOFT Venice, 2004.

[4] A. Simonin, G. Delogu, C. Desgranges, M. Fumelli, RSI 70 (1999) 4542.

- [5] Y. Okumura - Advanced Negative Ion Beam Technology to Improve the System Efficiency of Neutral Beam Injectors, 18<sup>th</sup> International Conference on Fusion Energy, Sorrento, Italy, 4-10 October 2000.
- [6] P. Massmann, D. Boilson, H.P.L. de Esch, R.S. Hemsworth and L. Svensson - 20<sup>th</sup> ISDEIV - Tours, 2002.
- [7] A. Krylov, R.S. Hemsworth - Gas losses and related beam losses in the ITER NBI, submitted to Fusion Engineering and Design.

## **TASK LEADER**

---

Lennart SVENSSON

DRFC/SCCP/GIDEA  
CEA-Cadarache  
F-13108 Saint-Paul-Lez-Durance Cedex

Tél. : 33 4 42 25 61 69  
Fax : 33 4 42 25 62 33

E-mail : [lennart.svensson@cea.fr](mailto:lennart.svensson@cea.fr)

## **REPORTS AND PUBLICATIONS**

---

Experimental results with the new ITER-like 1 MV SINGAP accelerator - L. Svensson, D. Boilson, H.P.L. de Esch, R.S. Hemsworth and P. Massmann - 10<sup>th</sup> International Symposium on the Production and Neutralization of Negative Ions and Beams, Kiev, 13-17 September 2004.

Design and Fabrication of the "ITER-like" SINGAP D<sup>-</sup> Acceleration System – P. Massmann, L. Svensson, H.P.L. de Esch and R.S. Hemsworth - 23<sup>rd</sup> symposium of fusion technology 20-24 September 2004.

**Task Title: TW3-TPHI-ICRDES1: ITER ICRF ANTENNA AND MATCHING SYSTEM DESIGN**

**INTRODUCTION**

The elements of the ITER Ion Cyclotron array described in the ITER Reference Design are a modification of the Tore Supra antenna concept (figure 1a), aimed to obtaining resilience to fast resistive load variations, such as those due to ELMs [1]. In figure 1b) it is shown that the in the modified structure, hereafter referred to as ITER-like structure (ILS), unlike in the original one, the input Voltage Standing Wave Ratio (VSWR) can be limited below a specific value, independent of resistive load variations, which depends on the circuit input resistance  $R_0$ .

The basic element of the array consists of 2 short-circuited current straps, connected to a tuning network, in series with two variable capacitive reactances, connected in parallel to the input of a RF power source, via a step-up impedance transformer.

The circuit resilience to load variations arises, in part, from the fact that the input admittances of the two sections are complex conjugate, and their imaginary parts cancel out when paralleled.

In a dense array, such as the ITER Ion Cyclotron array, (figure 2) a certain level of non conductive (i.e. inductive, and to less extent, capacitive) direct coupling between array elements is present at the plasma end, and most of all, an apparent inter element reactive and resistive coupling is reflected by the plasma load, back to the exciting array elements. It has been suggested [2] that inter-strap coupling in the ITER array would impair the overall load resilience of the proposed array.

**2004 ACTIVITIES**

**EFFECTS OF COUPLING AND LOAD ASYMMETRIES ON LOAD RESILIENCE**

In this paper it is shown that full load resilience and perfect impedance match can be preserved by the closed-loop control of the ILS currents.

It is also shown that, in any case, for a predictable behaviour of the ITER array, all array current *must* be controlled, and this should be performed around symmetry conditions that *must* be automatically preserved against unpredictable load variations (due to plasma and random breakdown conditions) to optimize the radiation spectrum, and to avoid control instabilities. If control is lost, the power level of the array must be very rapidly stopped, to prevent equipment damage.

Finally it shown that the ITER array operation is possible, with the hardware described in the ITER Reference Design, and with a suitable array control and protection system, for reasonable assumption on the range of parameter in ITER operation.:

More in detail it is also shown that:

1. An arbitrarily loaded ITER like structure, described by an arbitrary impedance matrix :

$$Z_L = \begin{pmatrix} R_{s1} + 1i X_{s1} & R_{m2} + 1i X_{m2} \\ R_{m1} + 1i X_{m1} & R_{s2} + 1i X_{s2} \end{pmatrix}$$

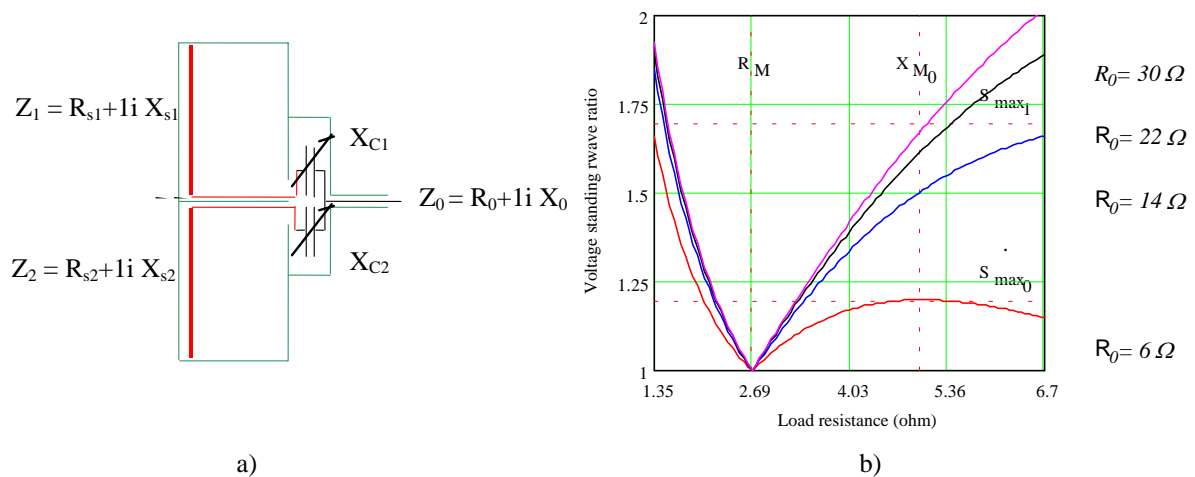


Figure 1 : a) layout of the ITER like structure with tuning element in series, b) Input VSWR as function of load resistance

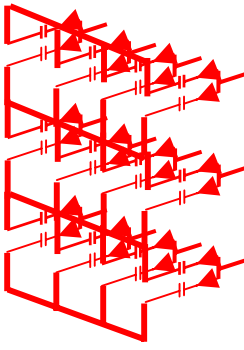


Figure 2 : Sketch of the IC array according to a recent CEA proposal

2. Can be matched to any resistive input impedance  $R_0$ , within the limits acceptable to high power sources ( $VSWR < 1.5$ ), while preserving full load resilience. The number of circuit elements necessary for tuning depends on the level of coupling between the two ILS half sections and on the amount of asymmetry in the diagonal terms of the matrix, while asymmetry in the non diagonal terms is generally negligible.
3. For reasonable values of the coupling coefficient ( $k_p \sim -20$  dB), and for the ITER antenna parameter range, two elements are sufficient to match the ILS.
4. Load asymmetries, in particular if associated with coupling, further complicates the analysis, but the overall picture does not change if the asymmetry in diagonal terms of the matrix is within 10% of the input resistance  $R_0$ .
5. For large values of inter element coupling, four tuning elements are needed to preserve both load resilience and impedance match. This is in general achieved with load dependent RF voltage unbalances in the tuning circuit, which play no role in the plasma coupling process, but may set a limit to the operation of the array, if its dielectric properties are limited.
6. For a large array of coupled elements, such as the ITER IC array, a tight vectorial control of *all* array currents is mandatory, for a stable and efficient operation, independent of the type of array elements and load resilience. Unpredictable, load dependent and severe control instabilities, leading to suppression of the power flow by the RF protection system(s) may occur if the control is lost.
7. On the other hand, the electrical behaviour of an ILS, in which the currents are controlled in closed loop by the internal tuning system, is predictable, and not different from the one of a single strap, since the vectorial relation between input and strap currents is preserved by feedback.

It can be shown that the input impedance of an individual RL circuit (such as a loaded short-circuited current strap) can be perfectly matched to an arbitrary resistive impedance (such as the one of a RF power

source) by two purely reactive elements, one in series and the other in parallel. Linking two straps in a ITER-like structure has always practical advantages compared with individually matched elements, because, in addition to load resilience, even if four matching elements are to be used, they can be physically separated in two sections, one within the resonant part of the circuit and the other in the transmission line. As the first pair already significantly reduces the load VSWR, the second can be located at the generator end, since transmission losses are greatly reduced.

## CONTROL AND MATCHING

On control issues, we discuss:

1. A general array control strategy of the array  $k_p$  spectrum control, including power phase, impedance matching control, also addressing the problem of monitoring, control and system protections
2. A procedure for automatic impedance match acquisition and upholding in vacuum and on plasma.

The automatic impedance matching system of a complex array such as the one of ITER is deeply integrated within the overall control and protection system and its operation and stability depends on most, if not all, system parameters.

At the current level of technology, impedance tuning at the power level relevant to fusion devices still requires the mechanical control of the geometry of actively cooled components using vacuum pressurized gas as dielectrics. At an operating frequency of 60 MHz, typical for ITER, the radiation wavelength is  $\lambda = 6$  m. Tuning elements based of transmission line sections are therefore bulky and inconvenient for control purposes.

Dimensions of the tuning components can be reduced, if a combination of line sections and lumped circuit elements are used. This allows the construction of tuning equipment having a faster response, and adequate power performances can be obtained in reduced volumes by increasing the dielectric rigidity of the dielectric medium.

For the design of these components, however, a simple analytic approach is insufficient and an adequate electrical and thermal characterization by FEM analysis should be provided.

In the case of ITER, the geometry of the in-vessel equipment is heavily constrained by environmental conditions due to the need of:

- Minimizing electric field and maximizing the dielectric strength in any point of the system.
- Providing adequate nuclear shielding against neutron fields.

- Implementing in the design an adequate structural hardness to support large electro-magnetic and gravitational loads, due to plasma disruptions and a sufficient flexibility to accept important differential thermal loads.
- Providing a safe vacuum/tritium confinement.
- Allowing intensive water cooling of all components and support structures.
- Permitting remote handling operation on the system.
- Facilitating Hot Cell maintenance, repairs and dismantling.
- Minimizing waste inventory.

In view of these constraints, a simple electrical description of the array control system is insufficient. A description of geometry and electrical properties of the control components and a detailed explanation of how these integrate in the system is needed.

### **PROPOSALS FOR UPGRADES FOR THE REFERENCE DESIGN**

In the paper the discussion of the matching system is part of a wider context, including recent proposals [3] for an upgrade of the ITER IC Reference Design.

The proposed changes have the purpose of:

- Upgrading the array performance.
- Improving the dielectric strength in most part of the array.
- Greatly simplifying the array layout.
- Facilitating maintenance in Hot Cell and, possibly, in situ.
- Implementing an effective vectorial control of the array currents.
- Providing means for breakdown detection and protection.

The new design includes modifications to:

- Strap layout
- VTL layout
- Tuning components and vacuum feed trough

The geometry of the array is significantly changed compared to previous proposals and this has required a substantial revision of the array electrical analysis.

## **REPORTS AND PUBLICATIONS**

---

- [1] G. Bosia - Fusion Science & Technology - 43 pp. 153-159, (2003).
- [2] A. Messiaen - Proc of the 15th Topical Conference on RF Power in Plasmas - AIP CP 694, 142, (2003).
- [3] G. Bosia - Proposals for upgrades to the ITER Reference design - CEA CNN/NTT (2004).

## **TASK LEADER**

---

Giuseppe BOSIA in collaboration with S. BREMOND  
L. NICOLAS  
K. VULLIEZ

DSM/DRFC/SCCP  
CEA-Cadarache  
F-13108 Saint-Paul-Lez-Durance Cedex

Tél. : 33 4 42 25 49 22  
Fax : 33 4 42 25 62 33

E-mail : giuseppe.bosia@cea.fr



**CEFDA02-1003**  
**CEFDA03-1111**

## **Task Title: TW2-TPDS-DIASUP4 and TW3-TPDS-DIASUP1: SUPPORT TO THE ITER DIAGNOSTIC DESIGN**

### **INTRODUCTION**

ITER requires an extensive set of diagnostic systems to provide several key functions in support of the design goals that include: protection of the device, input to plasma control systems, evaluation and analysis of plasma performance. The process of adapting the design of the diagnostic systems from the original ITER design in 1998 was begun during the EDA Extension Phase. However, considerable detailed design work remains to optimize the measurement capability of the individual systems and to prepare procurement packages for individual diagnostics.

The overall objective of these tasks is to advance the design of several ITER diagnostic systems for which the EU has developed conceptual designs, to re-evaluate their performance for the most recent analysis of plasma conditions, to provide support for the ITER IT in the preparation of the relevant ITER documentation and in evaluating the cost.

These studies have been carried out under two contracts: CEFDA02-1003 signed in August 2003 and CEFDA03-1111 signed in April 2004. However, the technical scope and completion dates of the second contract were modified in a supplementary agreement, signed in Brussels on 31 December 2004, to reflect the revised emphasis of the expected European contribution to ITER diagnostics. The main changes were to cancel a further study that had been planned for polarimetry, to change the focus of the reflectometer study onto the plasma position system and to extend the scope of the other studies. Studies covered by the first contract were completed during 2004 but studies under the second contract, because of the revisions to its technical content and the extension of the completion dates, will extend into 2005. The work involves studies of the following diagnostic systems.

### **BOLOMETRY**

The first phase of this study agreed, in collaboration with the ITER IT, a generic design for the bolometer camera and carried out analysis of the thermal response, defined the cooling requirements and assessed the sensitivity of the bolometer. The second phase (carried out in collaboration with the HAS and IPP fusion Associations) is advancing a number of design and integration issues concerning ITER bolometers. CEA's main contribution is to perform a detailed design analysis of the bolometer camera housing and the internal camera structure for several different camera locations in the ITER vessel.

The study also involves optimization of the camera collimator designs and preliminary assessments of various technical issues including connectors and cables.

### **THERMOGRAPHY**

The study has developed a conceptual design for thermographic measurements in the ITER divertor region based on a novel method using optical fibres (figure 1).

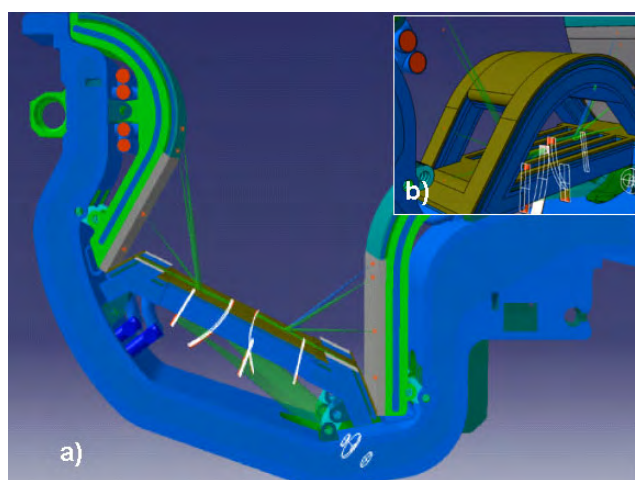


*Figure 1 : Thermography diagnostic system for ITER divertor - a) Side view in 3D of optical design implanted in the divertor cassette - b) Passage of inner target viewing lines through dome window*

### **POLARIMETRY**

CEA has contributed to a collaborative study led by the FOM Fusion Association. CEA's specific role has been to characterize the change of optical performance in the infrared region of the spectrum of a corner cube reflector when exposed to plasma. This work is linked to the ITER first mirror studies that are described elsewhere in this report.

### **MOTIONAL STARK EFFECT**

This collaborative study was led by CEA and involved also the FOM, UKAEA and VR fusion Associations. CEA's contribution was to perform an initial feasibility study of the possibility of diagnosing the current density profile in ITER by means of the Motional Stark Effect (MSE) using the ITER heating beams. One area of particular importance was to determine the feasibility of MSE at high Lorenz electric field and the CEA study concluded that this is possible. The overall conclusion is that most of the difficulties foreseen with MSE on ITER can be resolved.

## WIDE-ANGLE VIEWING

This is a new collaborative study, led by CEA and involving the ENEA and FOM Associations, to perform a design analysis of the optical layouts of the ITER wide-angle viewing systems, with particular emphasis on the systems to be installed on the main horizontal ports. The wide-angle plasma viewing system is an extensive and complex diagnostic with as many as 18 cameras. The original specification, based on a study from the original ITER design in 1998, needs to be brought up to date to take account of recent changes in the ITER design and significant advances in the techniques and expertise for this diagnostic method. An important issue is to assess the extent to which this diagnostic system can complement or even replace other systems.

## CALORIMETRY

CEA has carried out an initial study of the feasibility of a diagnostic system for fusion power based on calorimetric measurements of the ITER machine cooling systems.

## Q-PROFILE DETERMINATION

This is a 2-part study with the DCU Association (University College Cork) responsible for the first stage and CEA for the second stage. The CEA study has provided expert advice on the determination of MSE measurements in ITER with particular emphasis on the optimization and number of MSE viewing lines and channels.

## REFLECTOMETRY

CEA is participating in a collaborative design study (led by the IST Fusion Association) of the plasma position reflectometer systems for ITER. CEA is assessing an existing design for the antenna and estimating antenna loss over the relevant frequency range. CEA is contributing also to the performance analysis of waveguides.

## CONCLUSION

---

Studies covered by the EFDA02-1003 contact are completed: generic design for the bolometer camera [1], conceptual design for thermographic measurements [2], optical performance of the polarimeter system [3], feasibility study of the possibility of diagnosing the current density profile in ITER by means of the Motional Stark Effect [4].

Tasks under the EFDA03-1111 are running according to the revised planning agreed in December 2004.

## REPORTS AND PUBLICATIONS

---

- [1] Thermal analysis of the ITER reference bolometers, Final report - DIAG/NTT-2004.027, 10/2004.
- [2] Preliminary final report for the EFDA task TWP2002 TW2-TPDS-DIASUP-231 concerning task 2.3 Thermography - part II : CEA, 12/2004.
- [3] Support of the ITER Diagnostic design : Polarimetry - Final report - DIAG/NTT 2005-003, 01/2005.
- [4] Design analysis of motional stark effect diagnostic for ITER - DIAG/NTT-2004.029, 11/2004.

## TASK LEADER

---

Peter STOTT

DSM/DRFC/SCCP/GCBD  
CEA-Cadarache  
F-13108 Saint-Paul-Lez-Durance Cedex

Tél. : 33 4 42 25 66 94  
Fax : 33 4 42 25 62 33

E-mail : peter.stott@cea.fr

## TW2-TPDS-DIADEV-D02

### Task Title: DEVELOPMENT OF DIAGNOSTIC COMPONENTS FIRST MIRROR STUDY

#### INTRODUCTION

First mirrors will be the plasma facing components of optical diagnostic systems in ITER. Attention is concentrated on two processes, which can lead to degradation of mirror optical properties, namely:

- sputtering by charge exchange (CX) neutrals and ions during plasma operation and conditioning procedures such as discharge cleaning, which leads to erosion;
- deposition of material eroded from the divertor (e.g., limiters in TS) and first wall, which leads to surface contamination [1]. In the frame of an EFDA contract, metallic mirror samples (22 mm in diameter, 4 mm thick) of three different materials- mono-crystalline molybdenum (mc-Mo), polycrystalline stainless steel (SS) and copper (Cu) - were installed in TS for long-term plasma exposure during the experimental campaign 2003-2004 [2]. The task included also post exposure mirror analysis. The final report has been delivered according the due date (end 2004).

#### 2004 ACTIVITIES

##### OPERATION CONDITION

Mirror materials and the experimental layout of mirror exposure have been described in Technofusion 2003.

During the roughly one year exposure period, about 1400 plasma pulses (mainly D<sub>2</sub>) of more than  $I_p = 200$  kA ( $n_{e0} \sim 2-4 \cdot 10^{19} \text{ m}^{-3}$ ) have been performed with a cumulative pulse length of  $\sim 26000$  s (7 h 10). The accumulation of injected energy in TS between March 2003 and April 2004 was roughly 37 Gigajoules (GJ) composed of  $\sim 13$  GJ ohmic,  $\sim 22$  GJ lower hybrid and  $\sim 2$  GJ ICRH. In addition wall conditioning procedures of glow discharges in He ( $t = 362$  h,  $I = 7 \mu\text{A}/\text{cm}^2$ ;  $U_a = 300$  V,  $p = 0.3$  Pa), in D<sub>2</sub> ( $t = 606$  h,  $I = 7 \mu\text{A}/\text{cm}^2$ ,  $U_a = 400$  V,  $p = 0.3$  Pa) and 13 h of boronisation, alternating with plasma operation, have been performed during this exposure time. A major water leak of an actively cooled in-vessel component in September 2003 led to local mirror "splashing" (the mirrors have not been cleaned after that, before further exposure).

##### POST EXPOSURE MIRROR ANALYSES

Surface roughness and 3D surface profiles have been measured by confocal microscopy (CM). Surface topography and chemical analyses were performed by SEM imaging, EDX, XPS and SIMS.

Reflectivity measurements were carried out using a spectrophotometer equipped with an integrating sphere operating in the spectral range of 250-2500 nm. Optical constants  $n$  (refraction index) and  $k$  (extinction coefficient) were measured by ellipsometry in the range between 300-850 nm. All measurements were compared with results obtained on virgin reference samples.

##### Mc-molybdenum (A-D, B-D)

The surface roughness of the mc-molybdenum samples showed nearly no deterioration ( $R_a \sim 0.7$  nm) and, within the accuracy of the CM measurement method, a net-erosion depth of roughly  $0.12 \mu\text{m}$ . SEM imaging revealed an almost unchanged surface aspect. Some not regular shaped microparticle structures on the surface can be seen; their density is similar than on SS but lower than on Cu surfaces. The elongated form of the particles may indicate shaping by water drops due to an in-situ water leak ("splashing"), which occurred during sample exposition. The composition of these particles measured by EDX is dominated by C and O. XPS measurements on the mirror surface show C1s, Mo 3d, Fe 2p and O 1s lines. The molybdenum line shows a triplet revealing the presence of the bulk material coated with a thin molybdenum trioxide layer (the mirror samples were air exposed after removal from TS). SIMS surface analyses show carbon deposits enriched with hydrogen, deuterium, boron and oxygen (figure 1).

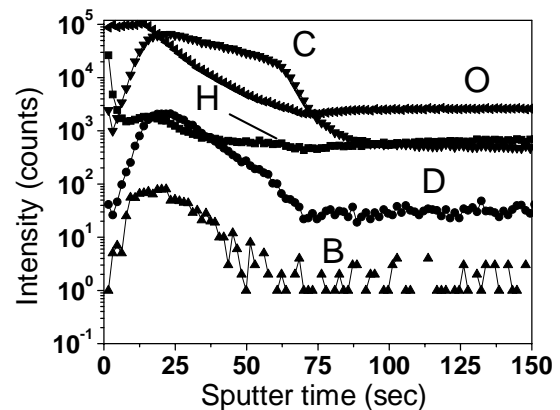


Figure 1 : SIMS spectrum of mc-molybdenum (A-D) mirror sample exposed in TS

In order to estimate the deposited film thickness on the exposed mc-Mo mirror sample, the SIMS facility was calibrated using a Dektak-6M mechanical profiler. A carbon deposit thickness of 12 nm was estimated. This thickness is also in some way confirmed by colorimetry: 10-15 nm thick deposits are still transparent, but 20-25 nm thick ones can be already seen by the unaided eye [3].

The total and the specular reflectivity show a slight decrease compared to the virgin sample. Specular values are compared to SS and Cu in figure 2. This decrease is more pronounced in the UV region. The diffuse reflectivity remains very low (< 2 %). Since the diffusive component of the reflectivity is linked to the roughness of the material, we can deduce that the roughness has not evolved sensibly during exposure (plasma and conditioning procedures), which has been confirmed by surface roughness measurements. We can assume that the decrease of the specular reflectivity is due to light absorption in the thin layer of carbon deposited.

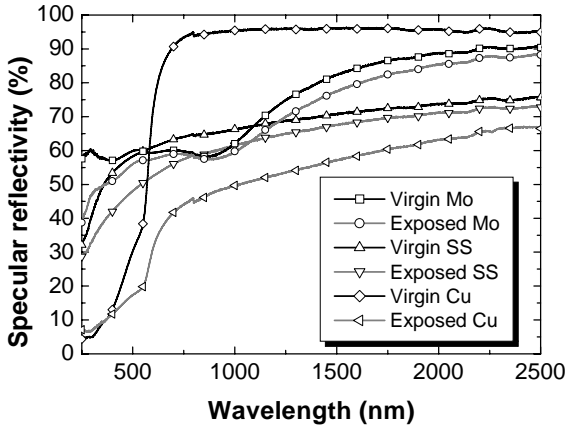


Figure 2 : Specular reflectivity versus wavelength of exposed (mc-Mo, SS, Cu) and virgin reference samples

**Stainless steel (A-B, B-B)**

The exposed stainless steel sample showed a Ra of 5.7 nm (however, virgin reference samples varied between 1.6 to 8 nm) and a net-erosion depth of roughly 0.22 μm.

A low scale grain-to-grain relief and in-grain topography is visible in SEM. The density of microparticles for the SS surface is similar to that for the Mo sample and, therefore, lower as for Cu. Again the composition of these particles is dominated by C and O. Traces of other impurities such as Mo and Si are observed. SIMS analyses of the mirrors show surface contaminations with oxygen and boron impurities. Also hydrogen and deuterium is observed.

A decrease of both, the total and specular reflectivity (figure 4), is observed after exposure. Diffuse reflectivity is higher especially in the UV region (< 6 %). While SIMS analyses do not allow us to make solid conclusions of the existence of a deposited layer, results from former simulation experiments [1] showed, that such a small erosion depth (~0.22 μm) cannot lead to a significant reflectance drop as observed.

**Copper (A-G, B-G)**

The most dramatic surface aspect change, which is clearly visible by the unaided eye, were observed on the copper mirrors with Ra of 47 and 69 nm, respectively (virgin reference sample varied between 7 to 8 nm) and an important net-erosion depth of roughly 2.6 and 2.33 μm, respectively (figure 3).

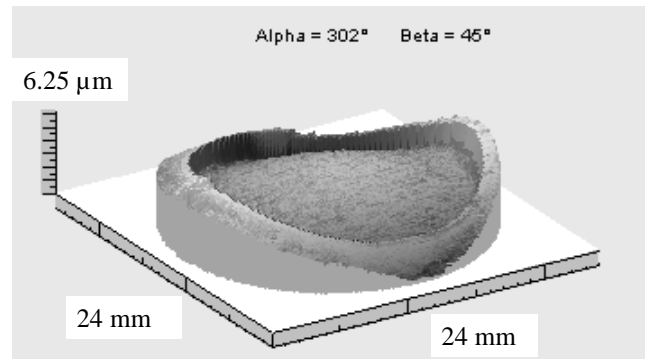


Figure 3 : Confocal microscopy synthesised 3D image of exposed copper (A-G) mirror sample of 22 mm in diameter

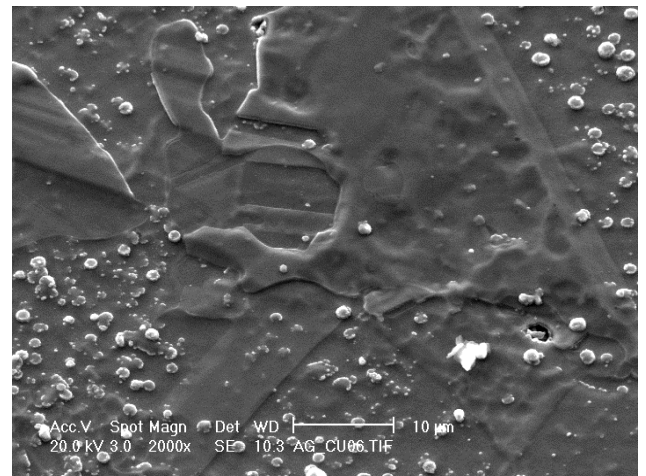


Figure 4 : SEM image of exposed copper (A-G) mirror sample

A strong grain-to-grain relief and in-grain topography is visible in SEM. The grain-to-grain steps seems to be weakened by a deposited layer, which shows an additional erosion topography. The original topography has drastically changed (figure 4). The microparticle density is much higher than for Mo and SS specimens, very different in form and size and depends on grain orientation. The composition of some of these particles with size up to 1 μm is dominated by C and O. XPS spectra show impurities like carbon, boron, silicon and oxygen. Moreover a fitting procedure applied to the copper line reveals the presence of a layer of copper oxide.

Copper is present in two states, as an oxide layer and as a bulk non-oxidized material (the mirror samples were also air exposed after removal from TS). SIMS analyses at the mirror center show contaminations with oxygen and boron impurities. Also hydrogen and a small amount of deuterium can be distinguished. However, these analyses cannot provide us with firm conclusions on the existence of a deposited layer.

The diffuse reflectivity reaches extreme values of about 50 % and, consequently, the specular component ~ 40 % at 800 nm. Therefore, we can assume that the drop of specular reflectivity is mainly due to erosion processes. As for the other mirror materials, relative reflectivity measurements in the FIR (119 μm) showed no significant modifications after exposure.

## GLOW DISCHARGE EXPERIMENTS

Mirrors have endured during the one year exposure in TS, conditioning procedures by means of alternating (between plasma operation) glow discharges. In order to verify the influence of erosion due to physical sputtering by ions, virgin reference mirror samples of the same fabrication batch have been exposed ex-vessel to He ( $t = 402$  h,  $I = 9 \mu\text{A}/\text{cm}^2$ ,  $U_a = 300$  V,  $p = 1.5$  Pa) and  $\text{D}_2$  ions ( $t = 214$  h,  $I = 9 \mu\text{A}/\text{cm}^2$ ,  $U_a = 400$  V,  $p = 1.5$  Pa) in a special laboratory equipment. After each (He and additional  $\text{D}_2$ ) exposure period, surface roughness and profile measurements were performed by CM. From the synthesized 3D images it can be seen that the eroded surface of (TS and ex-vessel) exposed mirrors is not homogeneous and has no rotational symmetry, which complicates, in general, the interpretation of erosion depth. Note, that the mentioned erosion depths are obtained between the exposed mirror border and its shadowed area and, therefore, may not represent correctly an average value. A variety of effects may have led to erosion pattern inhomogeneities, such as: original surface imprecisions, field potential inhomogeneities, particle incidence ("configuration factor"), surface roughness, etc. The laboratory (ex-vessel) results normalized for TS conditioning procedures (exposure time, current density) are in good agreement with TS global net-erosion for Cu, while SS and Mo values diverge up to a factor of 2-3 (table 1). Nevertheless these results show, that erosion due to conditioning procedures is important.

## NUMERICAL SIMULATIONS

Numerical simulations were undertaken to characterize the plasma near the mirror samples exposed in Tore Supra, in terms of particle fluxes and energies. The effort was divided into two tasks, assuming that erosion will primarily be caused by CXS neutrals, which are dominant over ion fluxes from the plasma by two orders of magnitude, and deposits formed by carbon eroded and re-deposited from the TPL (toroidal pump limiter):

- Simulations with the 3-D Monte Carlo code EIRENE have been carried out to calculate the CXS fluxes near the samples.
- A model describing carbon erosion and re-deposition processes in the Tore Supra CIEL geometry using the BBQ 3-D Monte Carlo scrape-off layer impurity transport code coupled to a core radial impurity transport code (ITC / SANCO / MIST) has been developed, allowing to estimate the expected carbon deposition on the mirror samples.

It was found during the simulation of the plasma conditions, that at the mirror location the CXS and carbon fluxes are minimized due to the geometry of the TS CIEL configuration, thus also minimizing the effect of erosion and deposition during plasma operation. Glow discharges, used for wall conditioning, on the contrary are more or less homogeneous, and their effect is more important at the sample location than the plasma (also due to the long duration of conditioning compared to plasma operation).

The current status of the BBQ simulations allows to give an indication of the order of magnitude for the carbon deposition ( $0.086 \mu\text{m}$ ). But the interplay of erosion/deposition and the complex sequence of events (plasma operation, glows, leak) makes it extremely difficult to simulate the exact progression of the erosion. However the tendency of calculation results confirm the experimental measurements in the sense, that erosion due to physical sputtering by ions during conditioning procedures dominates over erosion from CX neutrals during plasma operation (table 1).

*Table 1 : Comparison between measured (CM) laboratory (ex-vessel) erosion results normalized for TS conditioning procedures (current density, exposure time), TS net-erosion and erosion values from numerical simulations*

| Exposed mirror sample material | Normalized He (362 h) glow-erosion ( $\mu\text{m}$ ) | Normalized He (362 h) + $\text{D}_2$ (606 h) glow-erosion ( $\mu\text{m}$ ) | Net-erosion in TS ( $\mu\text{m}$ ) | Erosion (num. simul.) plasma + glows ( $\mu\text{m}$ ) |
|--------------------------------|--|---|-------------------------------------|--|
| Mc-Molybdenum                  | $\sim 0.061$   | $0.061 + 0.25 = 0.31$   | $\sim 0.12$                         | 0.107  |
| Stainless Steel                | $\sim 0.3$   | $0.3 + 0.17 = 0.47$   | $\sim 0.22$                         | 0.5185   |
| Copper OFHC                    | $\sim 0.31$  | $0.31 + 2.53 = 2.84$  | $\sim 2.68$                         | 1.008  |

## CONCLUSIONS

The long-term plasma exposure experiment of mirror samples in Tore Supra clearly demonstrate, that the mirror optical properties were degraded due to two opposite processes: (i) deposition of contaminating films (on Mo samples), which are, however, difficult to detect on SS and Cu, (ii) sputtering by CX neutrals during plasma operation and especially ions during alternating long lasting conditioning procedures. The simultaneous demonstration of opposite processes, such as erosion/contamination-deposition observed during mirror exposure in TS suggest, that periods of time when sputtering predominates over deposition (during long lasting glow discharge procedures) and, on the contrary, deposition predominates over sputtering (during plasma operation), having been alternated. Erosion due to physical sputtering by ions during glow discharge procedures in TS was important.

## REFERENCES

- V. Voitsenya, A. Costley, V. Bandourko, et al., Diagnostic first mirrors for burning plasma experiments, Rev. Sci. Instr. 72 (2001) 475.
- P. Wienhold et al., Nucl. Instr. and Meth. in Phys. Res. B 94, (1994), 503-510.

## REPORTS AND PUBLICATIONS

---

- [2] M. Lipa, B. Schunke, Ch. Gil et al. - First mirror study in Tore Supra - EFDA ref. TW2-TPDS-DIADEV-D02, Final report, January 2005.

## TASK LEADER

---

Manfred LIPA  
Beatrix SCHUNKE  
Christophe GIL

DSM/DRFC/SIPP  
CEA-Cadarache  
F-13108 Saint-Paul-Lez-Durance Cedex

Tél. : 33 4 42 25 4658  
Fax : 33 4 42 25 49 90

E-mail : lipa@drfc.cad.cea.fr

---

**Task Title: TW3-TVM-MDB: RULES FOR DESIGN, FABRICATION AND INSPECTION**  
**Establishment and Operation of a Material Database**

---

**INTRODUCTION**

---

Material research represents a significant part of the European and Worldwide efforts on Fusion research. The properties of new and existing materials need to be known in detail by Designers, by Licensing Authorities and not the least by Material Scientists. The present requirement for a materials Database comes firstly from a need by ITER to establish the status of Fusion materials data for licensing purposes and secondly to consolidate the data so that it is easily available to material researchers in the future, to identify holes in our existing knowledge base and to help establish directions for future material research.

The data that are subject of this proposal are those that have been measured and collected as part of the European Fusion program in support of NET and ITER over the past two decades.

The database constructed shall in the first instance, concentrate on the mechanical properties and thermal properties of both structural and plasma facing materials collected as part of the Next Step activities.

For this purpose UKAEA has been granted a contract as leading Association, with CEA and HAS (Hungarian Academy of Sciences) as supporting associations.

The final task report is expected to describe the following aspects of the work done:

- A description of the database and its structure.
- A list of procedures generated during the database activity.
- A list of users of the database.
- A list of contributors to the database and their contribution.
- A list of reports referred to by the database.

As one of the supporting associations, CEA will advise the leading Association, UKAEA, throughout the project on the following issues:

- The definition of the detailed database structure and format of the information.
- The collection of data.
- Checking of data.
- Maintenance of database.
- Installation, running of database and development of criteria to access and use the database.

**2003-2004 ACTIVITIES**

---

Two meetings were held in 2003 and one in 2004, where the progress of work was examined. During the first meeting CEA was asked to help UKAEA with examples of the database format files.

These were sent to EFDA and UKAEA and included format files for data collection (product, chemical compositions, tension, impact, impact plots, fracture, creep, fatigue), all with definitions of fields in the databases.

Also CEA supplied UKAEA with an example of the Internet server used at CEA for consulting materials properties databases. It was emphasized that in this Intranet system all actions are performed on the server side and the user only needs a simple browser for consulting the databases, extracting data and plotting the figures. Furthermore, the databases can be on local and remote stations. The server in response to a user's request will instantly fetch data from local or remote servers and presents them on the screen. Since then, UKAEA has presented the latest status of their database, data entry and searching, data templates and administrative tools. They have now extended these by proposals for data qualification and implementation, as well as, future work (short term and long term).

CEA has provided extended comments to all parties and two short assessment reports analyzing the work done at UKAEA. It is noted that the progress of the work so far has been satisfactory and promising. The fact that the database uses free and open access software is in particular appreciated. Also the fact that the database can be consulted and maintained via a browser satisfies another main objective of this task.

However, there are still some concerns, particularly when new and lesser-known materials are added to database. Most of these will be resolved as the work proceeds and more experience is gained. For this reason the flexibility of the database is important. To ensure perennially of the database it has been proposed and accepted by UKAEA, that the actual data should be independent of the database structure and should permit downloading with all links in a way to be picked up by another database system.

Also, a working server configuration should be installed on another server outside the actual UKAEA or JET servers, e.g. at EFDA. With regards to the proposed future work, these are welcomed but should not be at the expense of data collection and verification.

## **CONCLUSIONS**

---

The establishment and operation of a materials database for ITER is proceeding satisfactorily. The database has incorporated most of the initial recommendations and in its final form is expected to cover the rest.

## **REPORTS AND PUBLICATIONS**

---

F. Tavassoli, CEA / France, Report on the TW3-TVM-MDB Meeting, September 9, 2003, Place: UKAEA Fusion, Culham Science Centre, Abingdon, England,

EU Materials properties Database / Data analysis meeting, EFDA Garching, 24-25 June 2004.

A. T. Peacock, V. Barabash, F. Gillemot, P. Karditsas, G. Lloyd, J-W Rensman, A-A. F. Tavassoli and M. Walters, EU contributions to the ITER Materials Properties Data Assessment, SOFT, Venice, 20-24 September 2004.

## **TASK LEADER**

---

Farhad TAVASSOLI

DEN/DMN  
CEA-Saclay  
F-91191 Gif-sur-Yvette Cedex

Tél. : 33 1 69 08 60 21  
Fax : 33 1 69 08 80 70

E-mail : [tavassoli@cea.fr](mailto:tavassoli@cea.fr)

**Task Title: TW4-TVM-LIP: RULES FOR DESIGN, FABRICATION AND INSPECTION**  
**Modification of ITER materials documents and assessment of material data for licensing TBM's design rules**

**INTRODUCTION**

The properties of materials used in fusion components need to be known in detail by designers, by licensing authorities and the materials specialists.

ITER Materials Properties Handbook is a document that provides such information in an internationally accepted format.

The main objective of this task is to update and expand the existing ITER MPH files and as a first step this is done for materials used in the vacuum vessel.

CEA's contribution in this task consists of:

- Assist ITER International Team (ITER-IT) and EFDA CSU in revising the ITER materials properties Handbook files.
- Participate in ITER materials working groups for defining the materials to be assessed.
- Participate in ITER materials database groups for defining the materials data to be put in a European database.

**2004 ACTIVITIES**

**DESCRIPTION OF THE WORK PERFORMED IN 2003 AND 2004**

- a) The first work performed was updating of the existing ITER materials documentation. This documentation, notably the Materials Properties Handbook (MPH), needed to be updated to include the results of recent R&D activities, references to the correct codes and standards and the inclusion of material properties, which are not well covered at the present time, for example fracture toughness.

CEA's contribution mainly covered results on the stainless steel type 316LN-IG. At the request of the ITER-IT also the existing fusion weld metal references were also described. An example of CEA contribution to a ITER Question and updating of MPH files on 316LN-IG steel for vacuum vessel is done hereafter.

ITER Question: Data and equation given for  $R_m$  in RCC-MR edition 2002 for 316LN under subsection Z, A3.1S.31 do not match.

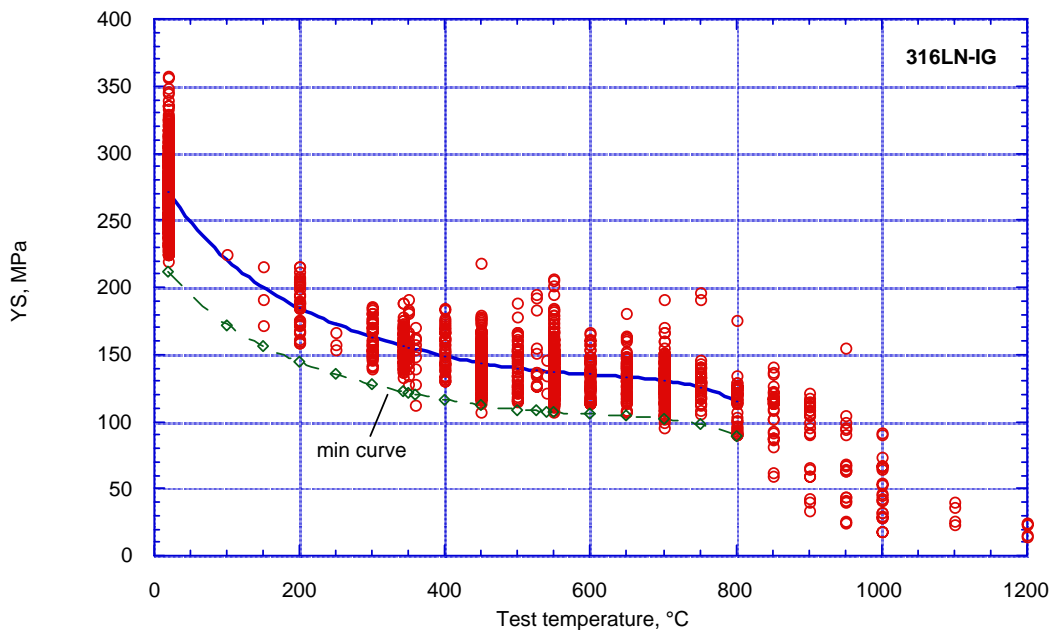


Figure 1 : Plot of  $R_p$  versus temperature for steel Type 316LN

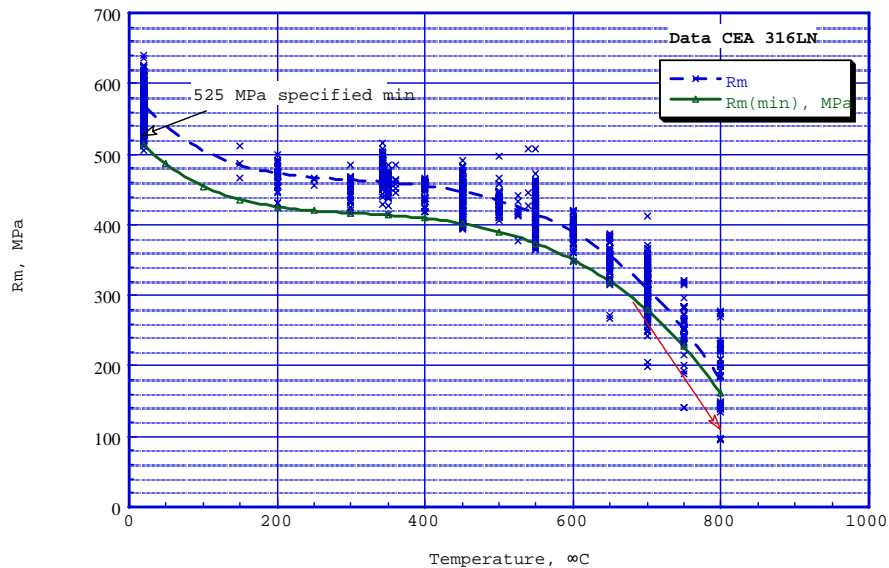


Figure 2 : Plot of  $R_m$  versus temperature for steel Type 316LN

CEA Contribution was :

- To show that the CEA database is compatible with those used in RCC-MR edition 2002. Figure 1 below shows the source data used to obtain average and minimum  $R_p$  recommended curves. The results obtained are the same as those used in RCC-MR.
  - Next, to extend the analysis to  $R_m$ , for which data are not presented in the same manner, see figure 2. Here the values deducted from the min curve also correspond to the RCC-MR, except at room temperature and at temperatures above 650°C. The reason for this is that the room temperature  $R_m$  value is a code specified value for this type of steel (must take preference over data in the plot). At temperatures above 650°C, the fitted equation does not cover the data scatter, hence use of lower values as shown by red arrow.
- b) The second work performed involved the preparation of new component specific documents. Specifically these documents would summarize all the material property recommendations needed for the design of specific components. CEA's main contribution was towards a document prepared by ITER-IT on the vacuum vessel.
- c) The third work performed was to support both the above-mentioned activities by reviewing the data available within the database to ensure that it has been produced with the correct standards and the necessary data trace-ability.
- It is possible in the future that this task will provide the model for which In-vessel materials will be reviewed. This, however, will depend on the experience gained (see also TW3-TVM-MDB ).
- d) Future work proposed is on Type 316LN-IG joints. Such information need to be combined with those available at ITER and presented as MPH files.

## CONCLUSIONS

ITER Materials Properties Handbook for vacuum vessel materials in general and type 316LN-IG in particular has been updated. Extension of the work to type 316 steel joint as well as substantiation of the documents on other materials are in progress or envisaged for the next phase of the activities.

## REPORTS AND PUBLICATIONS

F. Tavassoli, CEA / France, Report on the TW3-TVM-MDB Meeting, September 9, 2003, Place: UKAEA Fusion, Culham Science Centre, Abingdon, England.

EU Materials properties Database / Data analysis meeting, EFDA Garching, 24-25 June 2004.

A. T. Peacock, V. Barabash, F. Gillemot, P. Karditsas, G. Lloyd, J-W Rensman, A-A. F. Tavassoli and M. Walters, EU contributions to the ITER Materials Properties Data Assessment, SOFT, Venice, 20-24 September 2004.

## TASK LEADER

Farhad TAVASSOLI

DEN/DMN  
CEA-Saclay  
F-91191 Gif-sur-Yvette Cedex

Tél. : 33 1 69 08 60 21

Fax : 33 1 69 08 80 70

E-mail : tavassoli@cea.fr

Not available on line

## TW4-TVV-OSWELD

### Task Title: QUALIFICATION OF MULTIPLE PHASED ARRAY UT FOR ONE SIDED WELDS DURING VV MANUFACTURE

#### INTRODUCTION

The objective of the 2004 activity deals with qualification studies of non destructive testing methods for the one sided welds during VV manufacture. This work is connected with previous tasks performed between 2001 and 2003.

Initial studies were performed to investigate ultrasonic techniques relevant for defect detection in different kind of welds (EB weld or TIG weld).

New techniques were needed to improve the whole inspection coverage of the weld thickness. Two mock-ups were manufactured: an EB Weld mock-up and a TIG weld mock-up (weld roots were machined to obtain a smooth state of surface around the weld). These specimens contain surface breaking and embedded notches, as well as side-drilled holes for calibration purposes.

Main objectives of task achieved in 2002 were to design phased arrays probes using simulation and to carry out experiments, for most relevant configurations studied in 2001. Techniques evaluated in these works showed a potential interest but needed some optimizations, particularly for TIG weld inspection.

That is why new phased array probes were designed and manufactured in 2003. These transducers were carried out using dynamical inspection techniques based on angular scanning associated with beam focusing.

#### 2004 ACTIVITIES

##### GEOMETRICAL CONSTRAINTS

All studied methods take into account the geometrical constraints. These constraints are the following:

- Just one side access is available to the probes and instrumentation device (which means that X-ray inspection, for instance, would not be possible for this assembly).
- The presence of the poloidal ribs on the upper surface of the shell limits the distance for probes scanning over the welds. Therefore, even if two inspections may be performed from both sides (left and right) of the weld, the scanning displacement may be limited to 80 mm from the weld axis.

Apart from their improved flexibility and adaptability to perform different UT techniques, phased arrays here again provide a way to overcome such limited access thanks to beam-steering. It also has to be recalled that the weld type, as well as the final geometry of the component and limits quotations are not known yet, so that the suggested techniques presented in this report should still be modified in case of new requirement from the weld or assembly design.

##### DESCRIPTION OF NON DESTRUCTIVE TESTING METHODS

Further experimental trials have been carried out on both mock-ups to ensure the respect of the maximal available area of 80 mm from the weld centre axis.

##### Electron-Beam Weld inspection

###### *Description of the inspection technique*

The inspection technique consists in an angular scan associated with a focusing along the weld axis. A 5 MHz linear phased array is used in pulse echo mode to generate ultrasonic beams from 40° to 80° respectively focused at 60 and 5 mm depth.

This technique offers the possibility to cover a large depth of inspection with only one transducer and without any mechanical displacement. For that case, the geometrical requirement related to the maximal available area is respected, that is to say 80 mm from the weld center axis.

Following sketch illustrates the configuration of inspection.

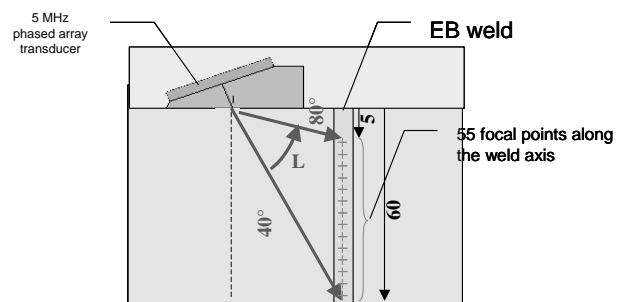


Figure 1 : Illustration of the EB weld inspection

##### *Experimental results*

Acquisitions were carried out on a mock-up including an EB weld. This mock-up contains inner surface breaking and embedded notches.

All inner surface-breaking notches (from 1 to 10 mm high) were detected and located. Depth sizing was possible with a good accuracy on the higher notches (10 and 4 mm). Both 10 and 4 mm high notches embedded into the weld were correctly detected, located and sized.

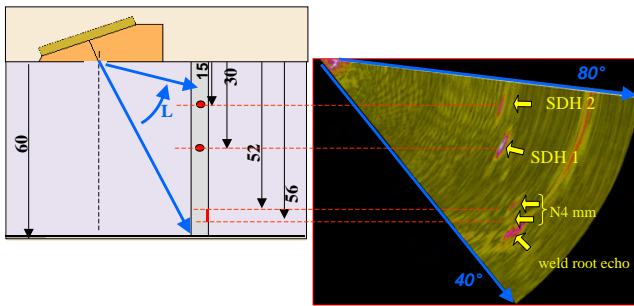


Figure 2 : Example of angular scan carried out on the EB weld mock-up

**TIG Weld inspection**

*Description of the inspection technique*

The most difficult area to inspect concerns the inner part of the weld. For this reason, the inspection technique studied in the framework of this work concerns the thickness of the weld from 20 mm in depth to 60 mm. The first 20 mm in depth will be subsequently studied.

The inspection technique consists in an angular scan associated with a focusing along a constant radius of curvature. Two linear phased arrays are configured as a dual-element transducer. Delay laws are calculated to generate longitudinal waves from 25° to 60° focused along a 75 mm radius of curvature.

Low signal to noise ratio obtained with previous transducers (2 and 5 MHz in pulse echo mode) [2] lead to define a specific transducer for the TIG weld inspection. This probe is composed of two linear arrays of 32 elements (1.2x20 mm<sup>2</sup> for each element) with a 2 MHz frequency. Dual element configuration is efficient to reduce back-scattering noise in coarse-grained material as in TIG weld. The probe wedge allows to naturally generate 45° longitudinal waves focused at 60 mm depth.

For all acquisitions carried out in the framework of this study, the probe has been fixed at the limit of the maximal available area, that is to say 80 mm. Acquisitions have been performed from both sides (left and right) of the weld. As for the previous study on EB weld mock-up, the angular scan offers the possibility to cover a large depth of inspection without any mechanical displacement.

Following sketches (figure 3) illustrates the configuration implemented on the TIG weld mock-up.

*Experimental results*

The TIG weld mock-up contains inner surface breaking and embedded notches. Experimental results showed that embedded and surface breaking notch greater than 2 mm are detected and sized before the weld.

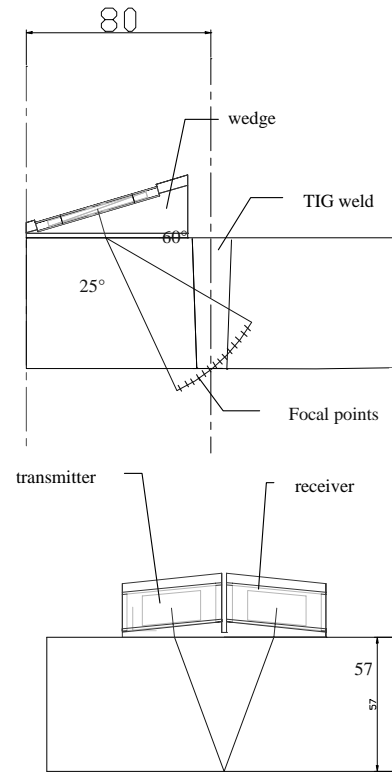
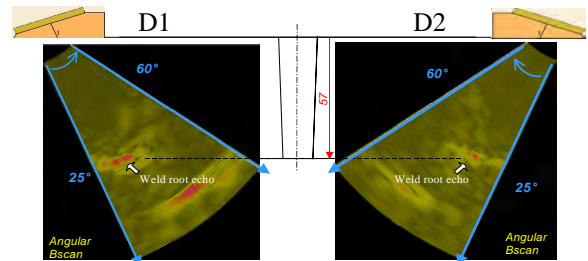


Figure 3 : Illustration of the TIG weld inspection

Through the weld, inspection performances are altered. Inner surface breaking and embedded notches equal to or greater than 4 mm were detected. 4 and 10 mm high embedded notches can be sized but with lesser accuracy. No inner surface breaking notch is sized. Following figure displays acquisitions carried out on the TIG weld for an area free of defect. We note false calls due to the weld root in both directions. As a consequence the noise level is greater for inner surface breaking defects than for embedded defects.



Following picture illustrates a result obtained on a 4 mm high embedded notch.

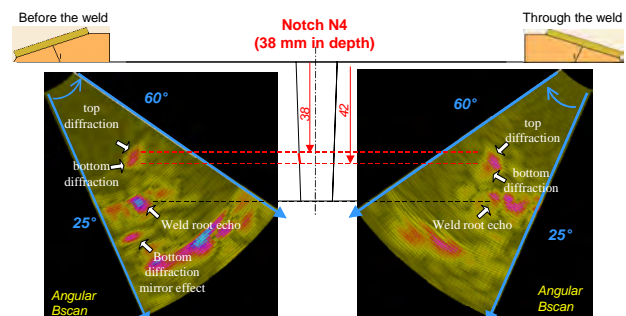


Figure 4 : Example of angular scan carried out on the TIG weld mock-up

### QUALIFICATION OF METHOD

Among the kind of studied welds, EFDA indicated that the TIG weld seems to provide the best interest. Thus, this part aims to evaluate the validity range of the method previously defined for the TIG weld inspection. This is achieved using simulation software tools of CIVA software.

CIVA is an expertise software for NDT developed by the CEA. This software gathers simulation, processing and imaging tools in order to directly compare experimental and computed data.

Ultrasonic tools allow to predict the beam propagation from the transmitter to the area being inspected and also to calculate the interaction with acoustic discontinuities within the area (defects or boundaries).

#### Parametric study

This study aims to consider a large range of defects that may be expected in such a kind of weld. These defects can vary in terms of size, orientation, position. The effects of these three parameters on the method of inspection performances have been evaluated thanks to the simulation.

##### Defect size influence

The first studied parameter concerns the influence of the defect size. Simulations were carried out with flaw sizes equal to 1, 2, 4 and 10 mm high.

We note that the corner echo amplitude decreases of 8 dB when the defect size come from 10 to 1 mm. Simulations confirm that only inner surface breaking notches greater than 2 mm can be sized.

Following figure corresponds to simulations of inspection on a 1 and a 10 mm high inner surface breaking notches. Corner echoes are detected in both cases, but diffraction echoes are not detected on the 1 mm high notch.

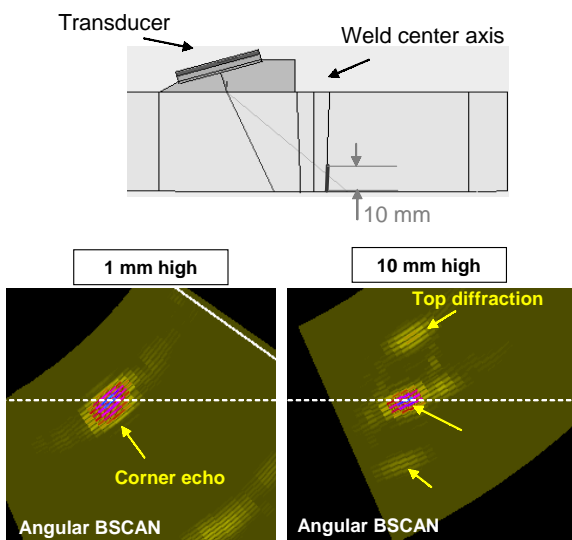


Figure 5 : Simulation of inspection on a 10 mm high inner surface breaking notch

##### Defect orientation influence

This part deals with the influence of the defect orientation. Two different angles are considered: tilt angle, from 0° to 90° around the fusion line, and skew angle from 0° to 10°.

If we consider a 10 mm high inner surface breaking notch, when the tilt angle comes from 2° (along the fusion line) to 10°, the corner echo amplitude decreases of 5 dB.

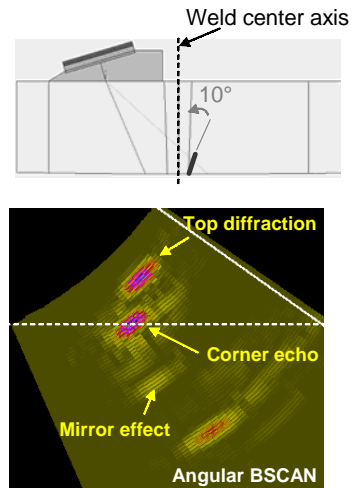


Figure 6 : Simulation of inspection on a 10 mm high inner surface breaking notch with a 10° tilt angle

Effects of skew angles from 0° (along the fusion line) to 10° have been evaluated. Simulation results allow to evaluate the ability of detection considering experimental results obtained in terms of signal to noise ratio.

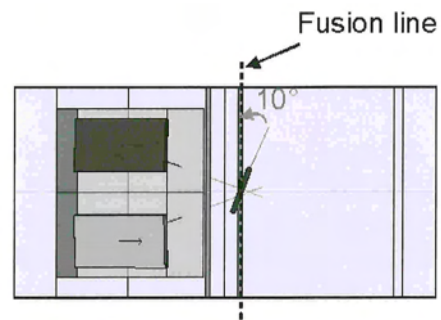


Figure 7 : Example of a 10 mm high inner surface breaking notch with a 10° skew angle (Top view)

##### Defect location influence

Other simulations have been carried out to appreciate the influence of the defect location on the detection.

Defects embedded in the TIG weld mock-up have been taken into account in the simulation. We note that the angular scan from 25° to 60° is not enough.

Thus, if the maximal angle is extended to 70°, we observe that the method of inspection is efficient to inspect the weld from 20 mm in depth to the backwall.

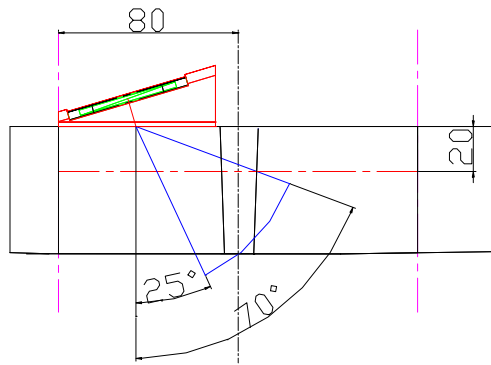


Figure 8 : Inspection from 20 mm in depth to the backwall

### Geometrical influence

All experimental studies have been carried out on planar mock-ups. The geometry of the final component is not determined yet. Several geometries have been submitted by EFDA. Following image is an example of the possible geometries. In that case, main difficulties of inspection come from permanent geometrical echoes that could hide the presence of a defect along the fusion line.

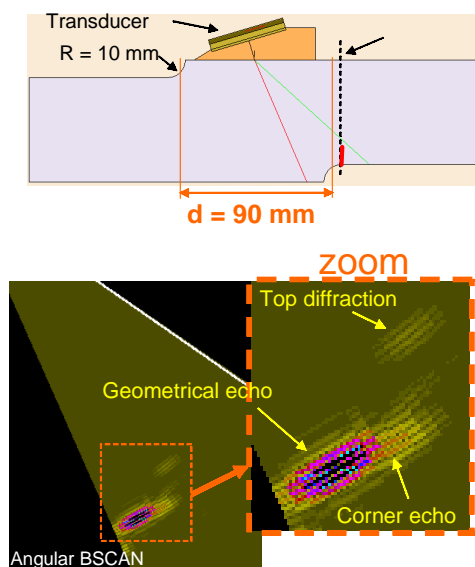


Figure 9 : Simulation of inspection on a 10 mm high inner surface breaking with a possible geometry

In that example, simulation shows that the defect is too close from the radius of curvature to be correctly detected. The difference between the amplitudes of the corner echo on the defect and the geometrical echo is of 17 dB.

## CONCLUSIONS

Further experimental trials have been carried out on both mock-ups to ensure the respect of the maximal available area of 80 mm from the weld centre axis. These acquisitions have shown the validity of the methods defined in 2003 on flaws contained into both mock-ups.

Since EFDA indicates that the TIG weld seems to provide the best interest, the validity range of the method of inspection defined for this weld has been particularly studied using simulation tools of CIVA.

This study aimed to consider a large range of defects that may be expected in such a kind of weld. These defects can vary in terms of size, orientation, position. The effects of these three parameters on the method of inspection performances have then been evaluated. The geometry of the final component is not yet defined. Several geometries have been submitted by EFDA and studied by means of simulation.

## REPORTS AND PUBLICATIONS

- [1] 'Development of phased array techniques for the inspection of one sided welds in ITER vacuum vessel', SYSSC/04-RT0143/Rev. 0 September 2004.
- [2] 'Development of ultrasonic non destructive testing method for the vessel inter-sector weld of ITER: development of dynamic phased array techniques', SISC/03-RT0096/Rev. 0, September 2003.
- [3] 'Development of ultrasonic non destructive testing method for the vessel inter-sector weld of ITER: simulation of welding process', DECS/SISC/LMUS/02-RT0052, July 2002.

## TASK LEADER

Philippe BREDIF

DRT/DeTECS/SYSSC/LMUS  
CEA-Saclay  
F-91191 Gif-sur-Yvette Cedex

Tél. : 33 1 69 08 34 68  
Fax : 33 1 69 08 75 97

E-mail : philippe.bredif@cea.fr

**Task Title: TW1-TVP-TESTAN: MONITORING AND ANALYSIS OF THERMAL FATIGUE TESTING OF DIVERTOR PROTOTYPES 200 kW electron beam gun test**

**INTRODUCTION**

This contract concerns the monitoring and the analysis of thermal fatigue testing of PFCs at FE200 facility. Four mock-ups were tested from April 2003 to December 2004:

- Hypervapotron armoured with CFC flat tiles (mock-up HVCFC-8)
- CuCrZr/SS first wall mock-ups (mock-up FW7)
- CFC monoblocks (mock-up Baffle)
- CFC and W monoblocks (mock-up VTFS)

The contract is now completed, a final report [1] including analysis of the 4 testing campaign (18 intermediate reports) was available in April 2005.

**2004 ACTIVITIES**

**HYPERVAPOTRON ARMOURED WITH FLAT TILES (MOCK-UP HVCFC-8)**

The hypervapotron concept adapted to a CuCrZr heat sink armoured with Carbon Fibre Composite (CFC) or Tungsten was envisaged for the vertical targets of the ITER divertor since the beginning of ITER EDA, but finally abandoned for two main reasons : it was suspected that the joint

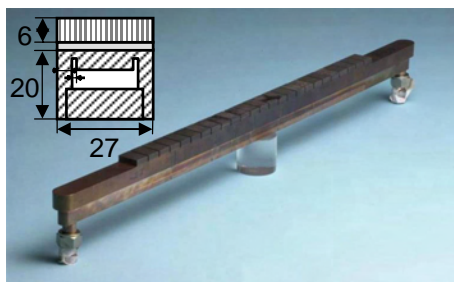
temperature between CFC or W and CuCrZr may be too high as well as a possible occurrences of a “cascade tile failure” effect.

Last experimental results accompanied with progress in modelling have shown excellent behaviour of flat tiles armoured hypervapotron with regards to the two mentioned supposed disadvantageous arguments : temperature of the armour/heat sink joint - strongly dependent on the flow velocity – can be driven below a tolerated limit even under ITER slow-transient heat flux of 20 MW/m<sup>2</sup> and cascade tile failure occurrence under ITER nominal heat flux of 10 MW/m<sup>2</sup> was not experimentally observed.

In order to validate the hypervapotron concept as a design solution for the ITER divertor, thermal fatigue testing has been successfully performed on a medium scale mock-up (figure 1b).

**Mock-ups description**

The mock-up was manufactured by Plansee AG : it consisted of a CuCrZr heat sink (741 mm length x 27 mm width) armoured with 25 flat tiles (18.5 mm length x 6 mm thick) of the 3D carbon fibre composite (CFC) material SEPCarb NS31 assembled with pure Copper by Active Metal Casting (AMC) (figure 1a). The manufacturing route respected the main technological features of a TORE SUPRA toroidal limiter finger element: in first AMC tiles were electron beam welded on the CuCrZr bar, then fins and slots inspired from neutral beam JET design were machined into the bar, afterwards, the bar was closed with a thick CuCrZr rear plug including hydraulics connections then electron beam welded onto the sidewalls. The mock-up was equipped with 6 K-type thermocouple positioned at the Copper/CuCrZr joint.



a)

| ITER spec.           | FE200                  | TSEFEY-M               |
|----------------------|------------------------|------------------------|
| 3000 cycles          | 3000 cycles            | 3000 cycles            |
| 10 MW/m <sup>2</sup> | 15 MW/m <sup>2</sup>   | 15 MW/m <sup>2</sup>   |
| 300 cycles           | 800 cycles             | 1000 cycles            |
| 20 MW/m <sup>2</sup> | 5 MW/m <sup>2</sup>    | 25 MW/m <sup>2</sup>   |
| Critical             | a few cycles           | a few cycles           |
| Heat Flux            | > 30 MW/m <sup>2</sup> | > 30 MW/m <sup>2</sup> |

b)

Figure 1 : a) view of the mock-up and b) main results of the HHF testing

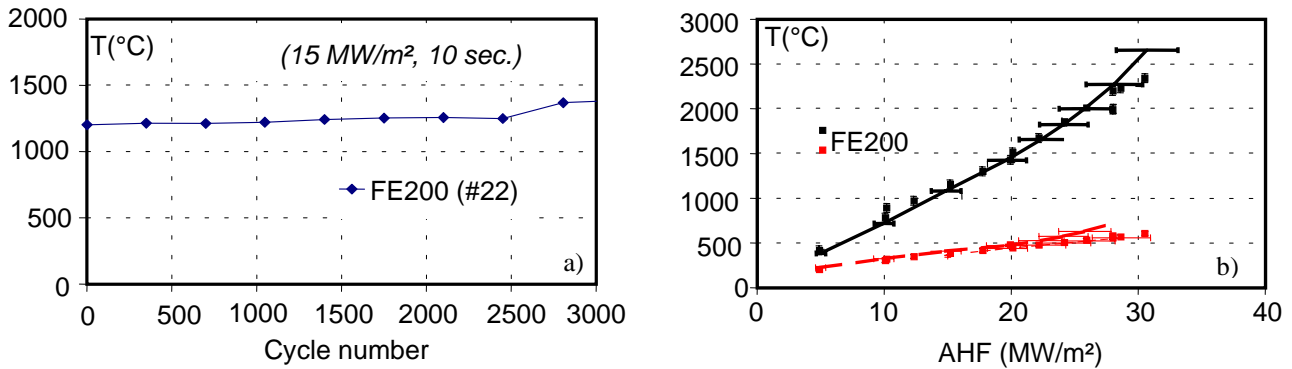


Figure 2 : a) Steady-state surface temperature evolution during fatigue at 15 MW/m<sup>2</sup>  
 b) Comparison between modeling (black lines = pyrometers, dashed lines = thermocouples)  
 and measurements [9 m/s, 120°C, 35 bar]C

### Fatigue testing at 15 MW/m<sup>2</sup>

3000 pulses of 10 seconds duration were performed during a first step of fatigue on the two mock-ups at 15 MW/m<sup>2</sup>. Surface temperature was found almost constant at 1200°C up to 1500 cycles (figure 2a), then increased smoothly up to 1350°C at the 3000<sup>th</sup> cycle.

CFC/Copper/CuCrZr joint was examined afterwards and did not show any degradation.

### Fatigue testing at 25 MW/m<sup>2</sup>

This step of fatigue was interrupted after 800 cycles of 10 sec. due to the continuous occurrence of local strong sublimation, much severe in the lowest thermal conductivity direction.

A metallographic examination of the joint was performed above the sublimed area and demonstrated the presence of CFC cones empty of Copper.

This phenomena of Copper “re-melting” (so called because the Copper was already melted during AMC process)– not observed in the past with fluxes in the range of 10 MW/m<sup>2</sup> - may be attributed to the high value of deposited heat flux leading to a local high convective (and marginally radiative) heat flux at the joint CFC/Copper near a local initial detachment of the tile.

### Critical Heat Flux

A few increasing of power by steps of minimum 30 sec. was performed at the two facilities up to a stable value of 30 MW/m<sup>2</sup> absorbed heat flux. Shots were stopped due to high surface temperature (> 2300°C), critical heat flux was not observed.

### Modelling

A 3D modelling of the hypervapotron mock-up featuring orthotropy of CFC NS31, dependence on temperature of the materials thermal properties and heat transfer coefficient was built with the finite element code CAST3M of CEA (figure 2b).

### Conclusion

A CuCrZr heat sink hypervapotron armoured with flat tiles of Carbon Fibre Composite Sepcarb NS31 was manufactured by Plansee AG with respect to the main technological features of a TORE SUPRA toroidal limiter finger element, then fatigue tested at FE200 in Le Creusot : full ITER design specifications were achieved with margins, this result shows that the hypervapotron cooling concept is a mature industrial solution for ITER divertor plasma facing components.

### CuCrZr FIRST WALL SAMPLE MANUFACTURED BY HIPPING (MOCK-UP FW7 = PH/S-7F AND PH/S-7FB)

A manufacturing route for the production of Primary First Wall Panels (PFW) involves a high temperature HIPing at 1040°C for joining the CuCrZr alloy heat sink materials to the 316L Stainless Steel (SS) back plate. Beryllium (Be) armour is then joined by HIPping at a temperature range of 560-580°C. In order to allow the retention of sufficient mechanical strength with the CuCrZr, two alternative routes are being considered : high temperature HIP quenching, i.e. HIP cycle with fast cooling within the HIP furnace, followed by an ageing heat treatment or a high temperature HIP cycle with a subsequent solution annealing heat treatment with fast cooling also followed by an ageing heat treatment. In comparison with the prime aged heat treatment, all the above heat treatment cycle slightly degrade the tensile strength of the CuCrZr alloy. Mock-ups were manufactured following the above alternative routes (PH/S-7F and PH/S-7Fb) and tested in FE200 to compare their fatigue behaviour.

### MOCK-UP DESCRIPTION

The mock-up FW7 consists in 2 elements respectively named PH/S-7F and PH/S-7Fb mounted on a cooled structure. These two elements are made of a 20 mm thick CuCrZr heat sink HIPped onto a 30mm thick Stainless Steel back plate; 4 Stainless Steel cooling tubes of outer diameter 12 mm, thickness 1 mm, are inserted in between the two CuCrZr half-shells.

Each element is equipped with 2 type K thermocouples located at two deepness (Tref 1 and 3 at 30 mm, 2 and 4 at 40 mm).

The cooling tubes are welded to inlet and outlet manifolds for connection to water supply system, allowing the parallel flowing of the 2 elements. Dimensions of each element are 250mm x 88mm x 50mm (figure 3).

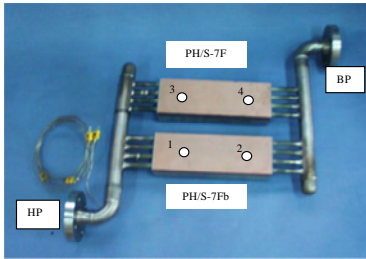


Figure 3 : View of the mock-up FW7 (reference view from the gun :

HP an BP in correspondence with FE200 connections)

**Fatigue testing at 5 MW/m<sup>2</sup>**

The cooling water conditions for these tests were selected at inlet temperature 100 °C, flow rate 3kg/s (i.e. 4.8 m/s), inlet pressure 3.3 MPa (ITER first wall relevant conditions).

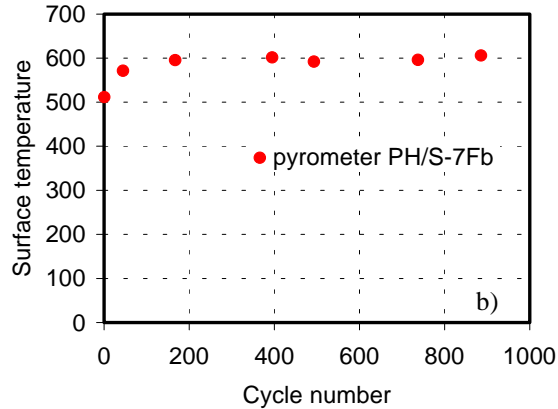
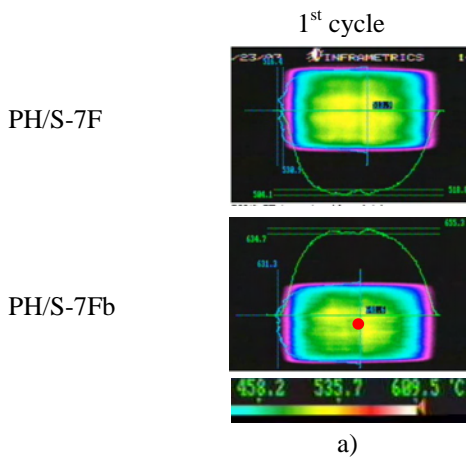


Figure 4 : a ) FW7 under 5 MW/m<sup>2</sup> absorbed into the water, b) Surface temperature constant during fatigue

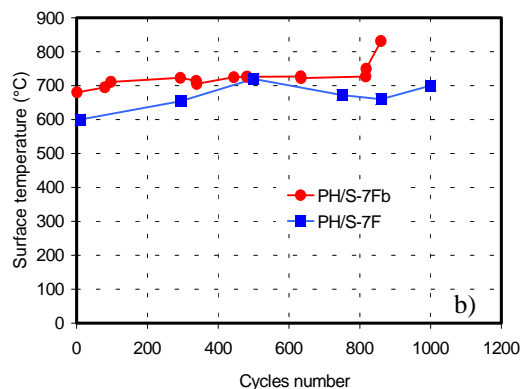
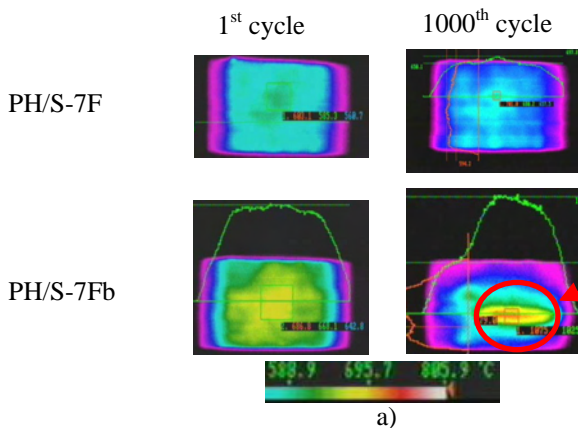


Figure 5 : a ) FW7 under 7 MW/m<sup>2</sup> absorbed into the water, b) Surface temperature during fatigue

Both of the elements resisted successfully the step of fatigue 1000 cycles at 5 MW/m<sup>2</sup> 15 sec. ON / 15 sec. OFF: no obvious observation of surface temperature was observed during this step except during the first cycles, this slight increasing of 50°C being attributed to the previous sandblasting of the mock-ups.

**Fatigue testing at 7 MW/m<sup>2</sup>**

During the step of fatigue at 7 MW/m<sup>2</sup> 15 sec. ON / 15 sec. OFF, a steep increase of temperature was detected onto the element PH/S-7Fb (from 720°C to 820°C, see figure 4b). The fatigue step was interrupted on this mock-up and continued on PH/S-7F up to 1000 cycles without indication of defect propagation.

A non destructive examination was performed in SATIR test bed before FE200 testing and did not show presence of defects, hot spots in red are mainly due to emissivity artefacts but not to flaws between the half-shells of copper and/or the SS tubes (see the intermediate report on SATIR examination for more details) (figure 6).

A numerical treatment on SATIR test bed using camera CEDIP device was developed during the period : it allows the effects of emissivity to be corrected. A flaw detection on the 3<sup>rd</sup> tube is well correlated with FE200 picture

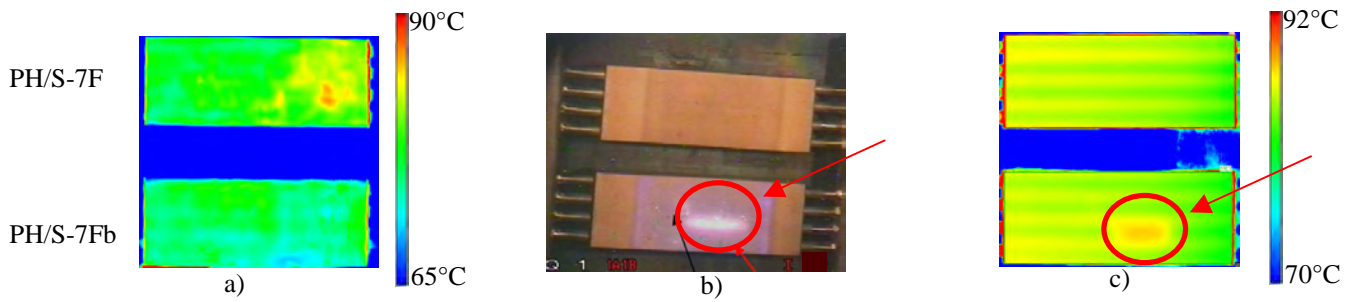


Figure 6 : SATIR most contrasted transient view a) before FE200 testing with analogic device (emissivity effects disturbs the picture) ; b) during cooling down phase at the end of FE200 HHF testing campaign ; c) after FE200 testing with normalized film of temperature

**Conclusion**

Two samples of Primary First Wall Panels (PFW) sustained up to 5 MW/m<sup>2</sup>, 1000 cycles without damage. The element PH/S-7F could sustain 1000 cycles 7 MW/m<sup>2</sup> without damage but the element PH/S-7Fb failed after 860 cycles at 7 MW/m<sup>2</sup>. Post-testing metallographic analysis (performed by the manufacturer in a separate contract) will allow the manufacturing route to be optimized.

**CFC AND W MONOBLOCKS (MOCK-UP VTFS)**

HHF tests on this components were performed and reported in fusion technology 2003, the analysis was presented at SOFT22 conference [3].

**CFC MONOBLOCKS (MOCK-UP BAFFLE)**

**Mock-up description**

The Baffle mock-up is made of two CFC monoblocks elements (panel B and panel C) manufactured by Plansee with the processes Active Metal Casting (AMC<sup>®</sup>) to attach CFC-NB31 to Copper and low temperature HIPing (550°C) to bond Copper to CuCrZr internal tube. Each element is composed with two rails, the *straight part* of each rail has a length of 680 mm (overall length = 780 mm), consisting in 170 CFC monoblocks bonded to a tubular heat sink. Panel B rails are attached onto the SS backplate by means of steel pads, which are electron beam welded onto the support structure whereas Panel C has the CFC monoblocks mechanically attached by means of dove-tail rails (see figure 7).

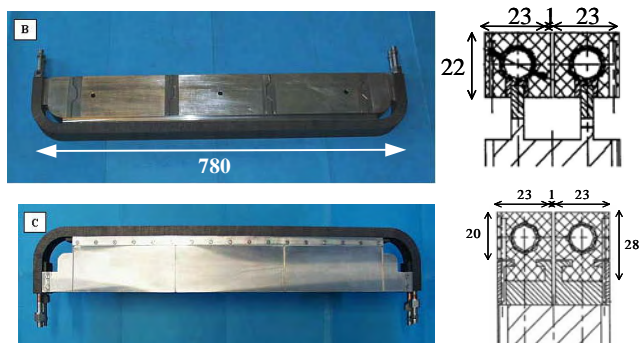


Figure 7 : Mock-up baffle : panels B and C

**SATIR examination and FE200 screening at 5 MW/m<sup>2</sup>**

A synthesis of non destructive testing performed on the mock-up was reported in [4]. Main conclusions are the following:

- Defects at the CuCrZr/Cu joint can be reliably detected by ultrasounds.
- By comparing images from ultrasounds with those from SATIR and FE200 infrared imaging, one can extract defects at the Cu/CFC joint. Those ones have higher contribution to the thermal response of the components. The analysis of experimental data, compared with Finite Element calculations, allows the determination of possible defect location and extension, for each inspection method.
- For baffle C (ITER reference design), manufacturing defects at the Cu/CFC joint preferably appeared at an angle of 45° or 90° along the tube (with 0° corresponding to the top of the monoblock, i.e. the plasma facing surface) with an extension ranging from 45° to 135°. Under SATIR testing, these defects led to a DTref not exceeding 7.5°C.
- Propagation of such defects will be assessed during the HHF testing.

**Fatigue testing at 10 MW/m<sup>2</sup>**

Two zones of the mock-up endured a cycling step of 3000 cycles at 10 MW/m<sup>2</sup> (10 sec. ON / 10 sec. OFF).

Each zone of 140 mm length is composed with 68 monoblocks (two rows of 34 monoblocks, 4 mm each)

This first step of fatigue operated at 10 MW/m<sup>2</sup> did not pointed out propagation of defect, a second step of 20 MW/m<sup>2</sup> is foreseen in 2005 in a separate contract. Studies on damage propagation will be performed in parallel.

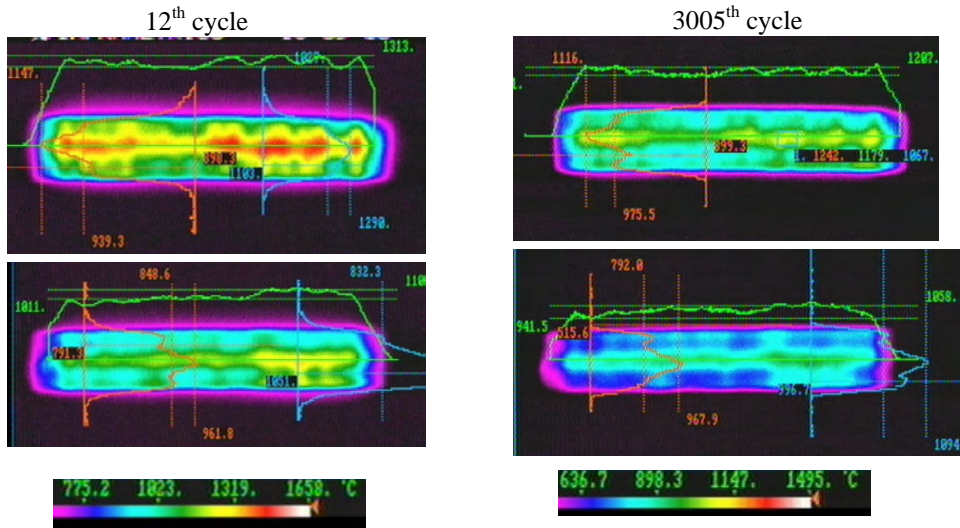


Figure 8 : 12<sup>th</sup> and 3005<sup>th</sup> cycle under 10 MW/m<sup>2</sup> absorbed into the water

## REPORTS AND PUBLICATIONS

- [1] Contract EFDA 01/585 - Final report - CFP/NTT-2005.008 - March 2005, F. Escourbiac.
- [2] A mature industrial solution for ITER divertor plasma facing components: hypervapotron cooling concept adapted to Tore Supra flat tile technology - F. Escourbiac, I. Bobin-Vastra, V. Kuznetsov, M. Missirlian, B. Schedler, J. Schlosser, Proc. 23<sup>rd</sup> SOFT-23, 20-24 Sept., Venice, Italy.
- [3] Results and analysis of high heat flux tests on a full scale vertical target prototype of ITER divertor - Proc. 23<sup>rd</sup> SOFT-23 - 20-24 Sept., Venice, Italy - M. Missirlian, F. Escourbiac, M. Merola, I. Bobin-Vastra, J. Schlosser, A. Durocher.
- [4] Synthesis of non-destructive testing of the baffles prototypes designed for the ITER divertor (panels B and C) - CFP/NTT-2004.015 - S. Fouquet.

## TASK LEADER

Frédéric ESCOURBIAC

DSM/DRFC/SIPP

CEA-Cadarache

F-13108 Saint-Paul-Lez-Durance Cedex

Tél. : 33 4 42 25 44 00

Fax. : 33 4 42 25 49 90

E-mail : frederic.escourbiac@cea.fr



Not available on line

**Task Title: TW4-TVD-ACCEPT: STUDY ON ACCEPTANCE CRITERIA FOR THE ITER DIVERTOR VERTICAL TARGET**

**INTRODUCTION**

This study on acceptance criteria for the ITER divertor vertical target components was performed under European contract 03-1051 with EFDA organization [a] [1].

The divertor system is aimed at exhausting the alpha particles and helium produced by the fusion reaction as well as other impurities resulting from plasma-wall interaction. It is made of 54 modules or “cassettes”, located at the bottom of the vacuum vessel. Each cassette supports a set of three actively cooled carbon fibre composite (CFC) or tungsten (W) armoured plasma facing components (PFCs): an inner and an outer vertical target that must tolerate high heat loads (10 - 20 MW m<sup>-2</sup>), and a dome (figure 1). The reference design is “monoblock” (or “tube in tile”) geometry for the CFC part and “flat tile” geometry for the W armour. A high-quality bonding between the armour and the heat sink is essential to ensure the lifetime of the components.

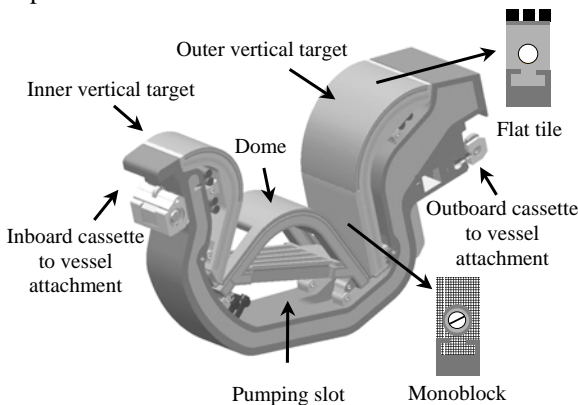


Figure 1 : Schematic view of the ITER divertor

With Tore Supra toroidal pump limiter (TPL), CEA has developed a large experience of acceptance criteria for actively-cooled high heat flux elements armoured with CFC flat tiles using infrared thermography (“SATIR” infrared test bench at CEA). The testing protocol consists in inducing a thermal transient within the heat sink structure by an alternative hot/cold water flow. The surface temperature of the tiles is monitored by an infrared camera. The transients are compared with those of a reference element, afterwards the maximum difference of temperature – called  $\Delta T_{ref\_max}$  – is evaluated for each tile. For Tore Supra TPL tiles, the applied acceptance criterion was  $\Delta T_{ref\_max} = 3^{\circ}C$ , i.e. the maximum acceptable difference of temperature between the controlled tile and the reference element during a cooling down transient. The transient infrared thermography method is well established for flat tiles. The work is now focused on control and acceptance of CFC monoblocks for the ITER divertor.

**2004 ACTIVITIES**

**ANALYSIS OF THE EXPERIMENTAL DATABASE: EXPERIENCE GAINED WITH THE ITER VERTICAL TARGET MOCK-UPS**

In the frame of the ITER divertor design, various mock-ups or prototypes have been manufactured and controlled using ultrasounds or transient infrared thermography [2]. They were also extensively tested under high heat flux loading (FE200 facility at Framatome, Le Creusot). The identified mock-ups are PRODIV (a 500 mm long CFC monoblock component), VTMS (Vertical Target Medium Scale), VTMSdef (Vertical Target Medium Scale with calibrated defects), which are prototypes for the divertor, Baffle samples, Critical Heat Flux CFC monoblocks, Round Robin Tests samples, VTFS (Vertical Target Full Scale), Baffle prototypes [3].

The identification of the manufacturing defects within CFC monoblocks and the evaluation of their possible propagation is essential, in order to be able to take the decision of the acceptance. Considering the monoblock geometry, a methodology based on the experience of the existing mock-ups has been developed to determine reliably the location (CuCrZr/Cu or Cu/CFC joint), position ( $\theta$ ) and extension ( $\Delta\theta$ ) of the defects (figure 2).

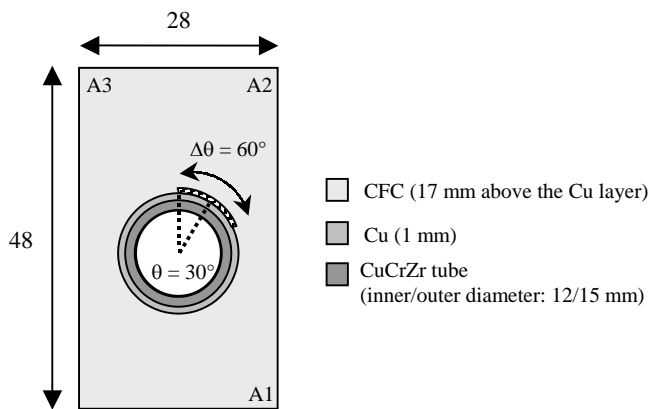


Figure 2 : CFC monoblock geometry;  $\theta$  is the position and  $\Delta\theta$  the extension of the defect

To start with, ultrasonic inspection of the components gives precise information (position and extension) about the defects located at the CuCrZr/Cu joint. Defects above 2 mm can be distinguished. The second step consists in transient infrared thermography (SATIR) examination of the top surface and the lateral surfaces of the monoblocks. While the inspection of the top surface provides poor information in case of large CFC thickness (17 mm), a better detection is gained from the lateral surfaces (CFC thickness of 5.5 mm).

For a chosen defect, the experimental  $\Delta T_{ref\_max}$  profile is compared to a set of theoretical profiles obtained from Finite Element calculations (figure 3). On this basis, it is possible to deduce the value of  $\theta$  (position of the defect) from the  $\Delta T_{ref\_max}$  profile, and the one of  $\Delta\theta$  (extension of the defect), considering the  $\Delta T_{ref\_max}$  amplitude.

It worth being noticed that with a 1 mm thick Cu compliant layer, a defect located at the CuCrZr/Cu joint has almost as much influence on the thermal response of the component as a defect positioned at the Cu/CFC joint (figure 4). After high heat flux tests (for example 1000 cycles at 10 MW/m<sup>2</sup>) the defect propagation can be deduced by comparing the experimental  $\Delta T_{ref\_max}$  profiles taken before and after the high heat flux loading.

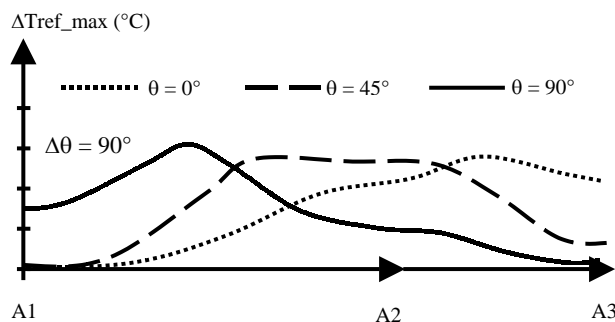


Figure 3 : Calculated  $\Delta T_{ref\_max}$  profiles for various defect positions and fixed extension (SATIR water velocity 3.2 m.s<sup>-1</sup>)

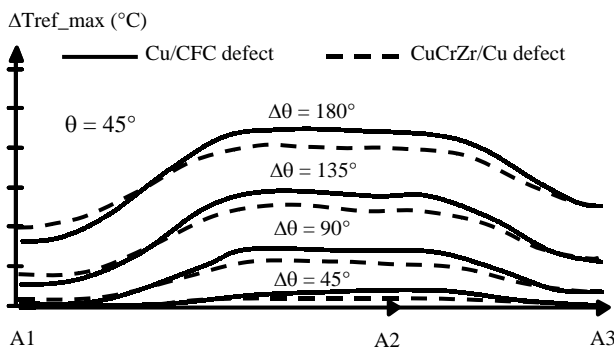


Figure 4 : Calculated  $\Delta T_{ref\_max}$  profiles for various defect extensions and fixed position, either at the CuCrZr/Cu joint or at the Cu/CFC joint (SATIR water velocity 3.2 m.s<sup>-1</sup>)

## DEFINITION OF ACCEPTANCE CRITERIA FOR THE ITER DIVERTOR

The design conditions for high heat flux testing of the vertical target CFC monoblocks are the following: i) the wall heat flux must stay below 26 MW/m<sup>2</sup> (considering a wall critical heat flux of 36 MW/m<sup>2</sup> with a safety factor of 1.4) during normal operation (10 MW/m<sup>2</sup>) and transient operation (20 MW/m<sup>2</sup>) ii) reasonably the surface temperature of the CFC part should stay below 2000°C (to limit the erosion) [b] iii) the temperature of the Cu part must stay below 550°C during normal operation (to avoid crack formation). Considering this, the maximum acceptable defect is shown on figure 2 (Cu/CFC joint,  $\theta = 30^\circ$ ,  $\Delta\theta = 60^\circ$ ).

According to finite element (FE) calculations (using the existing SATIR water parameters: P = 1.2 MPa, V = 4.9 m.s<sup>-1</sup>, T ranging from 95°C to 5°C), the corresponding  $\Delta T_{ref\_max}$  value is 3°C.

## TESTING PROCEDURE OF THE COMPONENTS

The whole testing procedure for the CFC monoblocks for the ITER divertor shall be performed using two complementary techniques. First, the quality of the CuCrZr/Cu joint could be checked by ultrasounds. Next, the components shall be controlled on the "SATIR" infrared test bench to measure the  $\Delta T_{ref\_max}$  values for each monoblock. Finally, the following criteria, based on  $\Delta T_{ref\_max}$ , shall be applied. If the element is doubtful, a closer examination of the defects based on the methodology presented in §1 shall be performed. When the element is rejected it can be either repaired or remanufactured. In addition to the cut-off value, the statistical distribution of  $\Delta T_{ref\_max}$  shall be within a specified scatter band to account for 1) possible variation of the material properties, 2) geometrical tolerances, 3) accuracy and repeatability of the SATIR test measurements [b] [c].

## VALIDATION OF THE INFRARED THERMOGRAPHY TESTING PROCEDURE

In order to validate the proposed methods and criteria, mock-ups with artificial defects will be manufactured and controlled on SATIR test bed, high heat flux tested (10 MW/m<sup>2</sup> and 20 MW/m<sup>2</sup>) and then again SATIR tested. These samples were designed in 2003 [4], then updated in 2004 [5].

Two companies will supply the required mock-ups in 2006, under a separated contract. The following components (see figure 5) will be fabricated by each company:

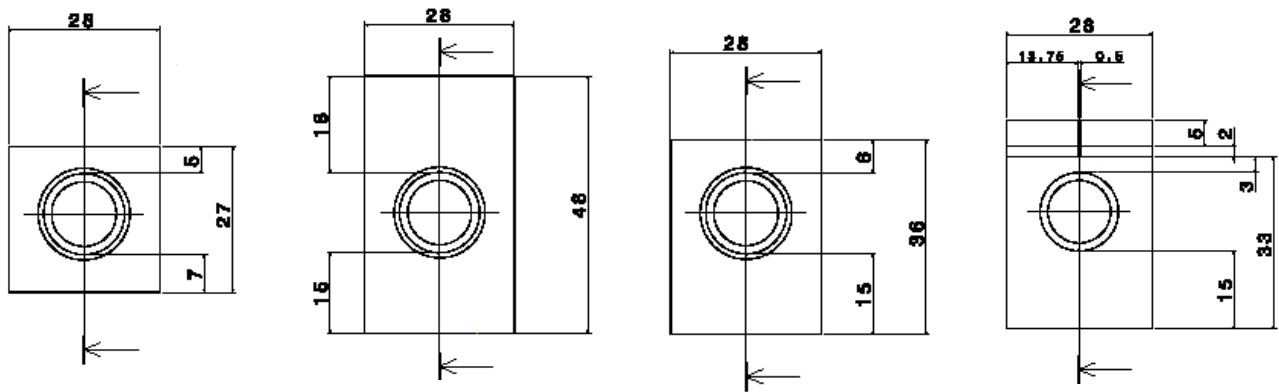
- 26 CFC monoblocks "short" (16 with Cu/CFC defects, 8 with CuCrZr/Cu defects, 2 without defects), with an armour thickness of 4 mm to enable the high heat flux testing while keeping the maximum surface temperature within acceptable levels).
- 2 CFC monoblocks "high" (delivered without defects), with an armour thickness of 17 mm to be fully consistent with the ITER design. These mock-ups will be used to assess the defect detection capability of the infrared examination. They are not intended to be high heat flux tested.
- 14 W monoblocks (6 with Cu/W joint defects, 6 with CuCrZr/Cu defects, 2 without defects).
- 14 W flat tiles (6 with Cu/W defects, 6 with CuCrZr/Cu defects, 2 without defects).

This is a total of  $56 \times 2 = 112$  mock-ups, of which 112 - 4 = 108 mock-ups to be heat flux tested.

The dimensions of the samples are presented in table 1.

Table 1 : Dimensions of the samples

| Dimensions (mm)                     | CFC monoblocks "short" | CFC monoblocks "high" | W monoblocks | W Flat tiles |
|-------------------------------------|------------------------|-----------------------|--------------|--------------|
| Quantity                            | 26                     | 2                     | 14           | 14           |
| Height                              | 27                     | 48                    | 36           | 40           |
| Width                               | 28                     | 28                    | 28           | 28           |
| Axial length                        | 20                     | 20                    | 12           | 25           |
| Armour thickness above the Cu layer | 4                      | 17                    | 5            | 5            |
| Pure Cu interlayer thickness        | 1                      | 1                     | 1            | 1            |
| CuCrZr tube inner/outer diameter    | 12/15                  | 12/15                 | 12/15        | 12/15        |



(a) CFC monoblock "short" (b) CFC monoblock "high" (c) W monoblock (d) W flat tile

Figure 5 : Design of the mock-ups for the validation of the infrared thermography testing procedure

Table 2 : Specifications for the artificial defects to be introduced in the mock-ups (2 mock-ups per each defect)

|                          | CFC monoblocks "short"   | W monoblocks  | W flat tiles             |
|--------------------------|--|---|--------------------------|
| <b>Cu / armour joint</b> | $\Delta\theta = 20, 35, 50, 65^\circ$ at $\theta = 0^\circ$ and $\theta = 45^\circ$                          | $\Delta\theta = 15, 30, 45^\circ$ at $\theta = 0^\circ$ | 2, 4, 6 mm (at the edge) |
| <b>CuCrZr / Cu joint</b> | $\Delta\theta = 40^\circ$ at $\theta = 0^\circ$ and $\Delta\theta = 20, 40, 60^\circ$ at $\theta = 45^\circ$ | $\Delta\theta = 15, 30, 45^\circ$ at $\theta = 0^\circ$ | 2, 4, 6 mm (at the edge) |

For each geometry, preliminary Finite Element calculations were performed so as to determine the possible calibrated defects that would be acceptable under high heat flux and detectable with SATIR [6]. The hypothesis of traversing strips defects was retained for the analyses. This decision is in line with the experimental evidence and artificial defects of this type can be easily machined. Table 2 indicates the specifications for the calibrated defects to be introduced in the mock-ups (2 mock-ups per each defect).

## CONCLUSIONS

A study on the detection of bonding defects and acceptance criteria for plasma facing components for the ITER divertor vertical target was performed in the frame of this contract. The main non-destructive technique for the inspection of CFC monoblocks is the infrared thermography ("SATIR", CEA Cadarache). The parameter  $\Delta T_{ref\_max}$  is used to establish if the tested element contains unacceptable defects.

The cut-off value is dictated by the risk of the occurrence of the critical heat flux and of plasma poisoning by the eroded carbon.

All that will be validated and the defect propagation will be assessed by manufacturing and high heat flux testing mock-ups with calibrated defects, which were designed during the study. The same methodology shall be applied for W armoured components however the low emissivity of such material may lead to poor detection.

This task is now completed and the final report has been published [7].

## REFERENCES

[a] EFDA Technology Workprogramme 2004 - Study on acceptance criteria for the ITER divertor - 10<sup>th</sup> April 2003.

- [b] E. D'Agata, R. Tivey - Toward the development of the workable acceptance criteria for the divertor CFC monoblock armour - Proc. 23<sup>rd</sup> Symp. on Fusion Technology (SOFT) - Venice, Sept. 20-24 (2004), to be published.
- [c] M. Merola, W. Dänner, M. Pick and the EU ITER Participating Team - EU R&D on divertor components - Proc. 23<sup>rd</sup> Symp. on Fusion Technology (SOFT) - Venice, Sept. 20-24 (2004), to be published.

## REPORTS AND PUBLICATIONS

---

- [1] S. Fouquet, J. Schlosser, M. Merola, A. Durocher, F. Escourbiac, A. Grosman, M. Missirlan, C. Portafaix - Acceptance criteria for the ITER divertor vertical target - 7<sup>th</sup> International Symposium on Fusion Nuclear Technology (ISFNT) - Tokyo, May 22-27 (2005), to be published.
- [2] S. Fouquet - Study on acceptance criteria for the ITER divertor - Intermediate report 2: experimental database, CFP/NTT-2004.014.
- [3] S. Fouquet - Synthesis of non-destructive testing of the baffles prototypes designed for the ITER divertor (panels B and C) - CFP/NTT-2004.015.
- [4] S. Fouquet - Study on acceptance criteria for the ITER divertor - Intermediate report 1: design of the samples with artificial defects - CFP/NTT-2004.003.
- [5] M. Merola, S. Fouquet - Study of acceptance criteria for the ITER divertor: summary report of the progress meeting on the 7<sup>th</sup> December 2004 - Cadarache, CFP/CRR-2004.014.
- [6] C. Portafaix, S. Fouquet - Study on acceptance criteria for the ITER divertor - Intermediate report 3: Thermal calculations for CFC and W monoblocks - CFP/NTT-2004.030.
- [7] S. Fouquet, J. Schlosser - Study on acceptance criteria for the ITER divertor - Final report - CFP/NTT-2004.035.

## TASK LEADER

---

Jacques SCHLOSSER

DSM/DRFC/SIPP/GCFP  
CEA-Cadarache  
F-13108 Saint-Paul-Lez-Durance Cedex

Tél. : 33 4 42 25 25 44  
Tél. : 33 4 42 25 49 90

E-mail : jacques.schlosser@cea.fr

Not available on line

Not available on line

Not available on line

Not available on line

# Task Title: DEVELOPMENT AND TESTING OF TIME RESOLVED EROSION DETECTING TECHNIQUES

## INTRODUCTION

Carbon based material is widely used as plasma facing component in present fusion device due to its good thermo-physical properties. It is the material retained in the ITER divertor, nevertheless, physical and chemical sputtering yield of carbon are important and this leads to high erosion rate. As a consequence, the large carbon source reacts with the plasma and creates a very complex Plasma Wall Interaction physic. In particular, redeposition may occur when carbon atoms or ion return to the wall; because of the reactivity of carbon with hydrogen, carbon layers are built up with a large hydrogen isotope content. In the case of ITER, the tritium retention in these carbon redeposited layers may limit the operation for safety reason. So far, only basic erosion and redeposition measurements have been undertaken in present tokamak and none of them can provide in situ a time resolved erosion/redeposition measurement. From bibliography analysis [1], Speckle interferometry has been retained as the most promising technique. Preliminary experiments [2] showed the feasibility of such technique on a carbon fibre material and provided qualitative and quantitative information on surface displacement. It was also shown [3] that 2 wavelengths are required for a tokamak application. By using a second laser, the relative displacement and the shape of the object have been successfully measured [4].

## 2004 ACTIVITIES

The two lasers, a Dye pumped by a Yag doubled in frequency, have been installed and commissioned in a clean room in 2003. During the year 2004, experiments on several samples have been performed on this new optical bench. Measurements on a set of 2 coins, using 3 wavelengths at 562, 562.05 and 562.8 nm, demonstrated that it is possible to measure large amplitude depth (2 mm) with a good resolution (1 μm).

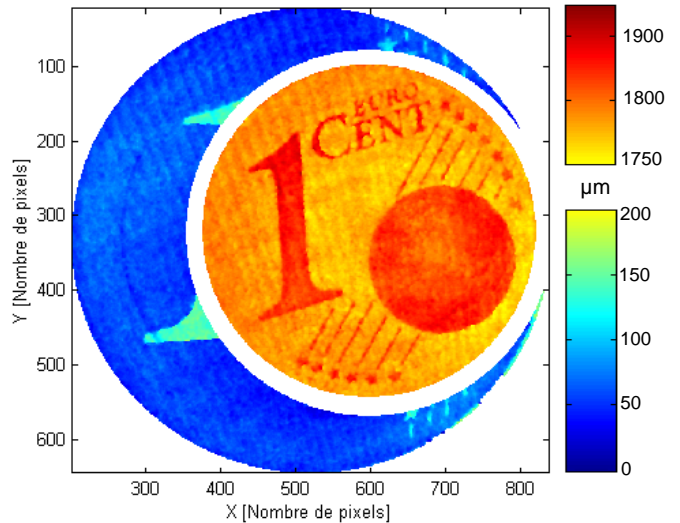


Figure 1 : 3D Reconstruction of 2 superposed coins (1 € and 1 cent)

Two-wavelength Speckle interferometry experiments on CFC tiles ablated with a ruby laser have been performed using 562 and 562.3 nm ; thickness and volume on the ablated area have been measured.

Comparison of these results with those obtained by microscopy are in very good agreement and confirmed the possibility to measure erosion on CFC by means of speckle interferometry.

In order to improve the analysis of the 3D image obtained with Speckle interferometry, a dedicated Image Analysis software, written in Matlab, has been developed.

This software allows to apply filters on the phase image prior to the unwrap process, to perform rotation, subtraction of images, removal of shape, measure of volume etc.

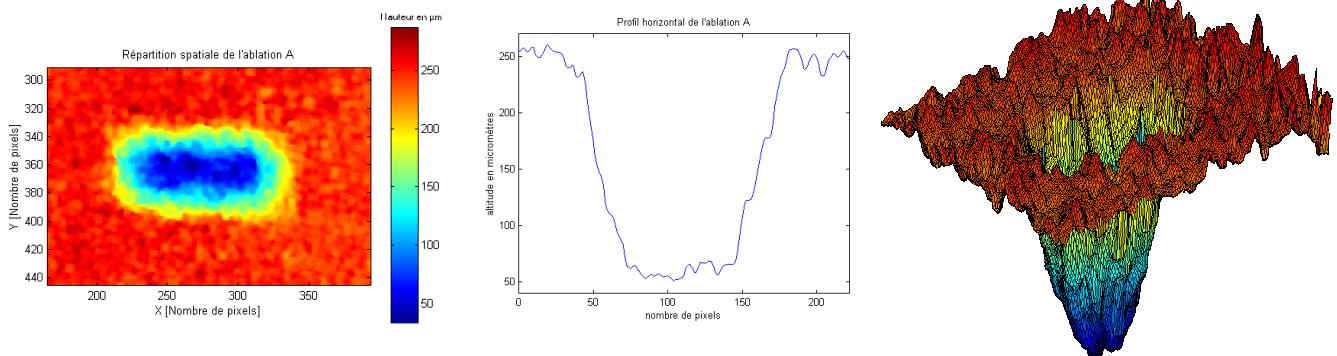


Figure 2 : 3D Image of the ablated zone, horizontal depth profile and 3D view of the crater

Finally, experiments at long distance has been investigated. Both the reference and the analysis beam, in order to save the coherence of the two beams, have been extended from 55 to 145 cm. Except the lateral resolution which decreases due to the larger field of view, there is no visible effect, in particular the depth resolution is unchanged. From this result, we can conclude that measurement at long distance will not be an issue in a tokamak.

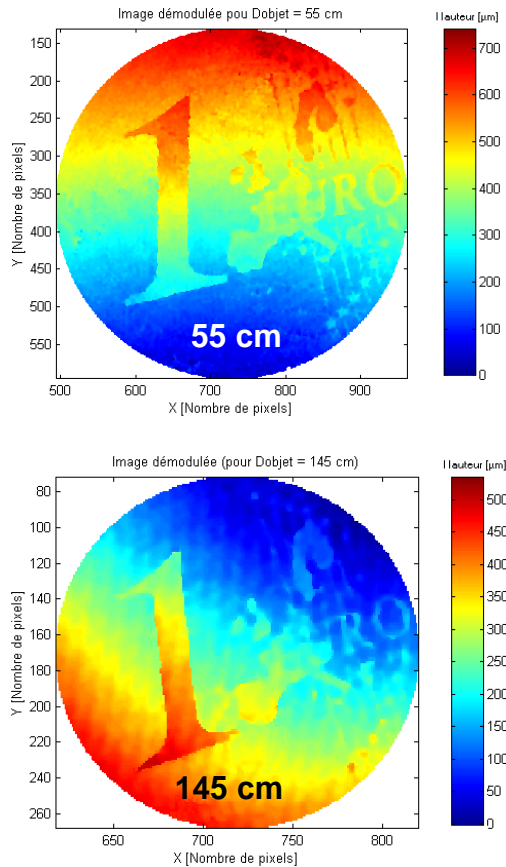


Figure 3 : 2D Images of I€ coin taken at a distance of 55 cm and 145 cm

The Final report on this task T438-01 has been sent to and accepted by EFDA in November. This task is now finished.

## CONCLUSIONS

Speckle interferometry optical bench is now fully operational in laboratory in CEA Cadarache. Additional development needs to be done in laboratory, prior to the installation of a Speckle interferometry diagnostic on a tokamak. In particular, the effects of the vibrations need to be investigated in detail.

The task T438-01 is finished and further developments are needed that could be done under a new task agreement, if any.

## REFERENCES

- [1] G. Roupillard - CFP/NTT.2000.031 - CEA Cadarache, 2000.
- [2] CEA rapport DSM/DRFC T438-01 2000.
- [3] A. W. Koch, M. Ruprecht, and R. Wilhelm - Laser Speckle Techniques for in situ-Monitoring of Erosion and Redeposition at Inner Walls in Large Experimental Fusion Devices - Max-Planck-Institut Für Plasmaphysik Garching bei München (1995).
- [4] CEA rapport DSM/DRFC T438-01 2002.

## REPORTS AND PUBLICATIONS

Mesures tridimensionnelles par microscopie confocale - DIAG/CRM-2004.001 (2004) - P. Dore, E. Gauthier.

Procédure d'entretien du laser en salle blanche du bâtiment 507 - DIAG/NTT-2004.015 (2004) - P. Dore.

Mesure de Vibration sur le Limiteur Pompé Toroïdal - DIAG/NTT-2004.016 (2004) - P. Dore.

Mesure de Vibration sur le Limiteur Pompé Toroïdal (en choc et hors choc) - DIAG/NTT-2004.031 (2004) - P. Dore.

Final report TW0-T438-01 - CFP/NTT-2004.033 (2004) - E. Gauthier, P. Dore.

Etude de l'érosion des composants face au plasma par interférométrie de speckle - 5<sup>ème</sup> Colloque Int. Francophone : Méthodes et Techniques Optiques pour l'Industrie, (2004) - P. Dore, E. Gauthier.

## TASK LEADER

Eric GAUTHIER

DSM/DRFC/SIPP  
CEA-Cadarache  
F-13108 Saint-Paul-Lez-Durance Cedex

Tél. : 33 4 42 25 42 04  
Fax : 33 4 42 25 49 90

E-mail : eric.gauthier@cea.fr

---

**Task Title: ARTICULATED INSPECTION ARM (AIA)**

---

**INTRODUCTION**

This project takes place in the Remote Handling (RH) activities for the next step of the fusion reactor ITER. The aim of the R&D program is to demonstrate the feasibility of close inspection of the divertor cassettes and the Vacuum Vessel first wall of ITER. We assumed that a long reach and limited payload carrier penetrates the first wall using the 6 penetrations evenly distributed around the machine and foreseen for the In-Vessel Viewing System (IVVS). The need to access closer than the IVVS to the vacuum vessel first wall and the divertor cassettes had been identified. This is required when considering inspection with other processes as camera or leak detection. The work performed under the EFDA-CSU Workprogramme includes the design, manufacture and testing of an articulated device demonstrator called Articulated Inspection Arm (AIA). The first phase of the project concerned the analysis to define a realistic conceptual design of the equipment that fit the requirements of inspection operation inside the vacuum vessel.

A scale one mock-up (previously called In Vessel Penetration (IVP)) was manufactured, focusing on the electro mechanical test in air and at room temperature of a single module. The test campaign of a 2 degrees of freedom module was finally successfully performed and gave confidence of structural resistance of the system which was the first essential design driver to verify. In parallel, a feasibility study of operation under vacuum and temperature was performed to select the possible applicable technologies. At this step it has been identified the need for developments of specific new technologies in particular for bearings, actuators and electronics. This development required proof of principle test phase. Therefore a scale one full module with 2 degrees of freedom was manufactured and tested under vacuum and temperature conditions at Tore Supra facilities.

**2004 ACTIVITIES**

**MANUFACTURE OF A VACUUM AND TEMPERATURE MODULE DEMONSTRATOR**

To satisfy ITER operational condition (T° & vacuum), IVP original design had been upgraded with all selected suitable technologies. This Prototype is now called AIA (Articulated Inspection Arm).

The main design options that were chosen are:

- Use of metallic alloys for the structure materials such as titanium.
- Some other non organic materials could also be used like Vespel.
- Use of welding processes for assembly of the structure parts.
- Use of needle bearings with dry lubricant.
- HCMOS military electronics components with a dedicated robot network. Electronics and lubricated roller screw and gear box will be embedded in tight boxes with tight feed through.

To be tested under realistic operating conditions of vacuum and temperature, the AIA demonstrator will be manufactured with respect of CEA Tore Supra (TS) constraints.

In particular, design will be compatible with TS dimensions, then the elevation axis will have + - 45 ° range and the complete robot total length will be 7.4 meter.



*Figure 1 : AIA sub assemblies and parts*

### DEMONSTRATOR MODULE TEST CAMPAIGN

The objectives of the tests are proof of principle of design options of the AIA. Especially to evaluate performances under in service and baking conditions in terms of functioning, lifetime and outgassing.

Main parameters involved are loading capabilities, speed, accuracy and ability to sustain ITER VV conditions.

The module was set-up in a specific vacuum vessel (ME60) at CEA Tore Supra facility that can be baked up to 230°C under high vacuum conditions. Representative loading was applied.

First test performed on the module was the leak detection which has proved the tightness of the boxes in which the electronics, the actuators and the sensors are embedded.

Functioning of the system under vacuum and at working temperature of 120°C was verified. The efficiency of the actuators was the same than in air at room temperature, the speed was slightly lower. The survey of temperature of the motor and the power electronics component showed an increasing of 40°C during 3 full range pitch movements. This good result shows that despite vacuum conditions, thermal exchange is working properly through the AIA structure and this gives confidence on the in service capabilities of the system.

During all the test campaign, monitoring of vacuum and the outgassing rate of the module were recorded. The baking was performed during one week at 200°C. The final spectrum was compared to the initial one and shows a good conditioning of the module. At the end of the baking, the pressure of the vessel reached a good level and was  $9.7 \cdot 10^{-6}$  Pa at 120°C. Most of the greases were outgassed.

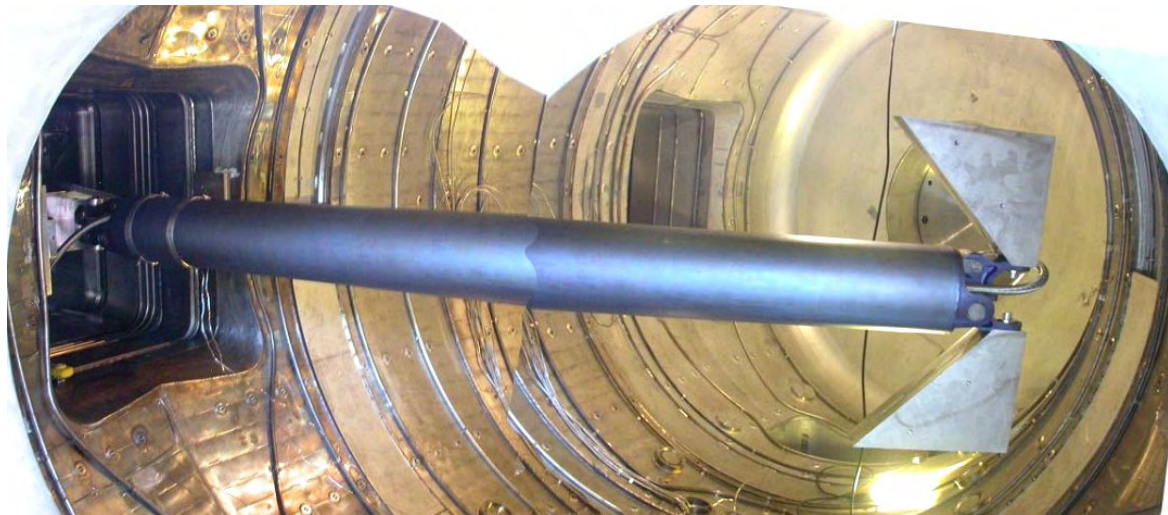


Figure 2 : AIA Prototype module in the ME60 vacuum vessel

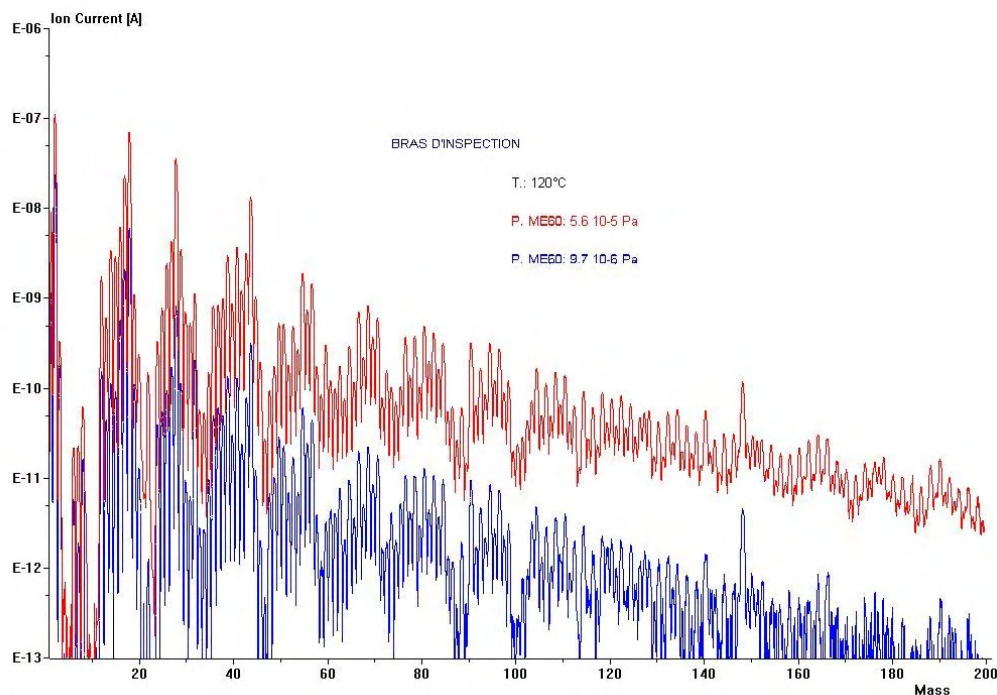


Figure 3 : Initial and final spectra of the module

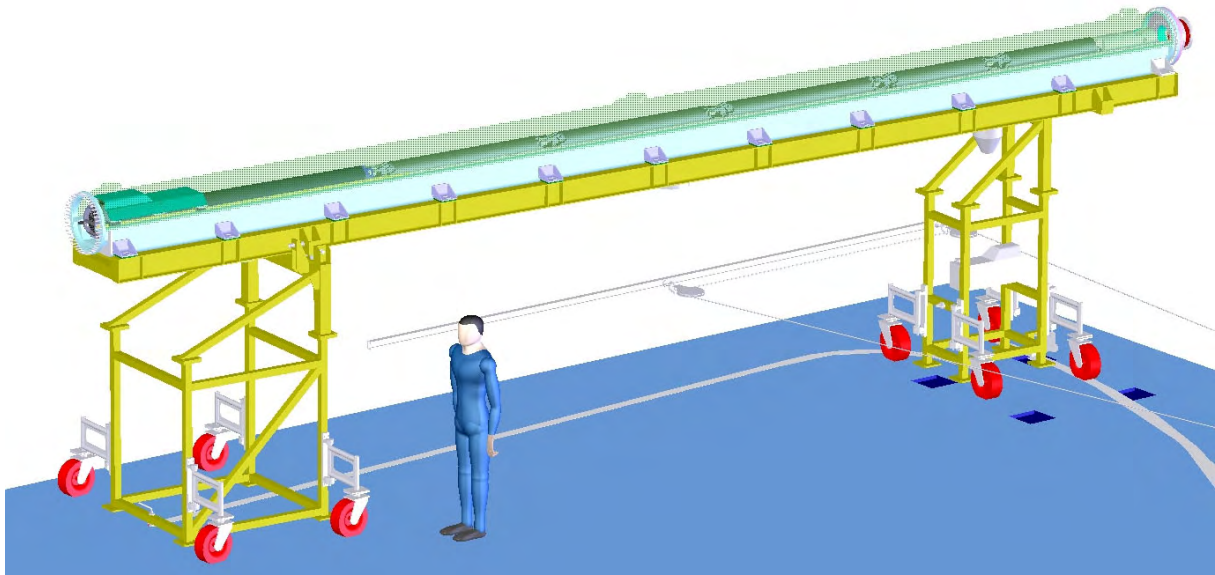


Figure 4 : AIA storage cask design

## DESIGN OF THE AIA DEPLOYMENT SYSTEM AND STORAGE CASK

The storage cask is a longitudinal box which contains the robot and its deployment system. It is equipped of 2 rails to guide the robot inside the torus and should afford the mechanical solicitations due to the overhang mounting of the robot.

The deployer has 3 main functions: to sustain the robot, to make a translation inside the storage cask, and to provide power supply.

The translation move will be provided by an electrical actuator mounted inside a sealed box. The torque of the motor is transmitted through a magnetic coupling.

The storage cask is shown in the next figure with the deployment system in carrying the AIA 5 modules.

## CONCLUSIONS

The IVP feasibility study performed in 2001 - 2003 was continued with the design and manufacture of a vacuum and temperature prototype module. A test campaign under ITER relevant conditions was performed during this year. In parallel, the design of storage cask and the deployment system was performed to carry the AIA system to be tested on Tore Supra.

Following promising first results obtained on the prototype segment, the complete AIA robot will be manufactured. Demonstration of the AIA behaviour and reliability in real temperature and vacuum tokamak environment is planned on Tore Supra for the next years. Several processes are foreseen to be developed and demonstrated on the AIA robot carrier that could be considered very useful for ITER maintenance.

## REFERENCES

- [1] European Fusion Technology Programme - Task TW0-DTP/01.2, Task TW0-DTP/01.4, Task TW1-TVA/IVP, Task TW2-TVA/IVP, Task TW3-TVR/IVV.
- [2] European Fusion Technology Programme - Task TW4-TVR/AIA December 1<sup>st</sup>, 2003.

## REPORTS AND PUBLICATIONS

CEA/DTSI/SRSI/LPR/03RT.104/Issue 0 - Articulated Inspection Arm, Manufacture report.

CEA/DTSI/SRSI/LPR/04RT.103/Issue 0 - Articulated Inspection Arm, AIA prototype module test campaign report.

CEA/DTSI/SRSI/LPR/04RT.104/Issue 0 - Articulated Inspection Arm, Deployer design report.

SOFT 2004 Paper 393: ITER Articulated Inspection Arm (AIA): R&d progress on Vacuum and Temperature technology for remote handling.

SOFT 2004 Paper 389: ITER Articulated Inspection Arm (AIA) : Geometric calibration issues of a long-reach flexible robot.

## **TASK LEADER**

---

Jean-Pierre FRICONNEAU

DRT/LIST/DTSI/SRSI  
CEA-Fontenay aux Roses  
Boîte Postale 6  
F-92265 Fontenay aux Roses Cedex

Tél. : 33 1 46 54 89 66  
Fax : 33 1 46 54 75 80

E-mail : [jean.pierre.friconneau@cea.fr](mailto:jean.pierre.friconneau@cea.fr)

# TW4-TVR-RADTOL

## Task Title: RADIATION TOLERANCE ASSESSMENT OF STANDARD ELECTRONIC COMPONENTS FOR REMOTE HANDLING

### INTRODUCTION

The proof of feasibility under severe environment done on the last term of year 2003 [1], allowed validating two main embedded converting functions used for sensors such as resolvers and Linear Variable Displacement Transducers (LVDT).

The phase difference between analog input and output signals coming from a BRT resolver was sampled with enough precision to be counted with, at, least an 8 bits counter.

The pseudo-tracking loop ADC conversion for LVDT output signals was effective with an 8 bits DAC converter.

This document presents the complementary functions and modifications highlighted by the results of the irradiation campaigns, but also some requests of EFDA team and ITER end-users.

Two printed cards, one for the resolver and framing functions, the other one for floating ground and ADC conversion, were achieved using polyimid material (which is hardened and supports very high temperature). An irradiation campaign was achieved at IRSN facility, IRMA, at room temperature. High temperature tests were made in our laboratory climatic oven. Results are presented.

Low Voltage Differential Signal (LVDS) components, previously evaluated in [2], were implemented to drive output signals on bifilar links.

A sine analog generator was defined and implemented to generate input for both resolvers and LVDT sensors.

The counter function was extended to 12 bits, which leads to the use of a clock frequency of 20 MHz to cover the maximum  $2\pi$  angle between the resolver's input and output signals. Also, a clear function was added to this counter in order to deliver an absolute 12 bits value for each phase measurement.

A preliminary test of the prototype was done at Mol. Results are contrasted but useful.

A full data link test-bed was defined and evaluated under radiation on IRMA, IRSN facility at Saclay. Despite some difficulties to assume a correct progress of the experiment, results are useful and need to be confirmed.

### 2004 ACTIVITIES

The functional block summarizes the added or redesigned developments all along 2004 (see figure 1).

The resolver coding the phase angle as  $Asin(\phi)$  and  $Acos(\phi)$  was left because of analog multiplier function (AD634 component) unable to support radiation.

Added or redesigned functions are presented below.

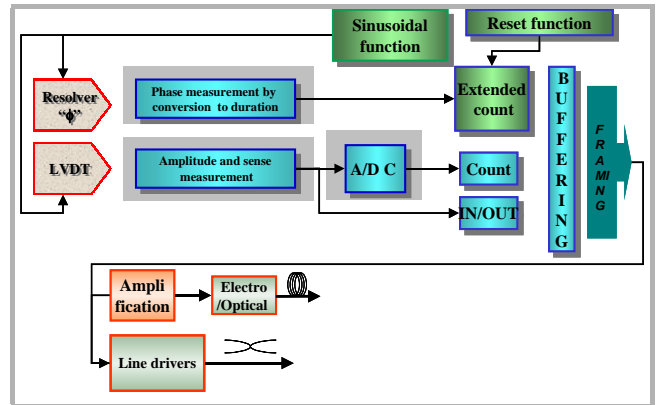


Figure 1 : Synoptic diagram of the electronic functions available on 2004

### RESOLVER BRT OR RESOLVER “φ”:

The only resolver retained for the future multiplexor needs  $Asin(\omega t)$  and  $Acos(\omega t)$  as inputs and delivers a  $Asin(\omega t + l - \phi)$  as output.

The design of electronic functions and the global positive results of radiation campaigns of the mock-ups were detailed on [1][2][3].

To increase embedded autonomy and improve wire reduction and thus beneficiate of enhanced AUC components, some functions were redefined or added before making the printed board prototype.

The serialiser necessary to deliver the frame of the digital coded value coming from the position angle conversion uses three recent AU16374 synchronized latches. A particular design reconstitutes a shift register commonly used to serialize digital.

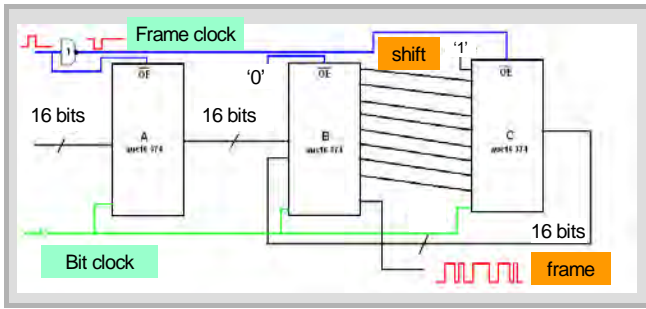


Figure 2 : Principle of serialiser using AUC16374 D-latches

Figure 2 summarizes the association between these three elements. More details are provided in [5].

Figure 3 represents some of the chronograms of main signals coming from the function. The frame clock is closely dependant of the signal frequency delivered to the resolver inputs. In the implementation retained for the prototype, frame emission and counter values latching are alternatively on the rise front of the clock.

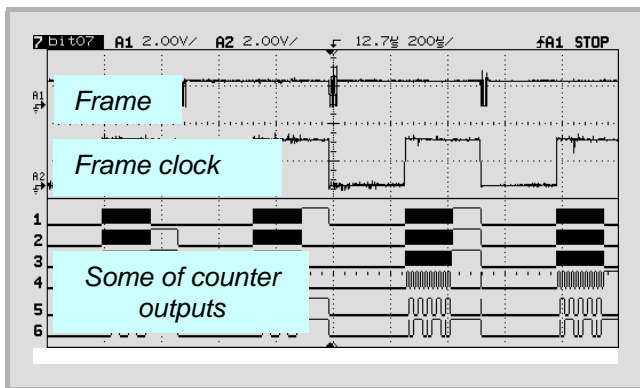


Figure 3 : Chronograms of serialiser mechanism

The printed board prototype was realized with a later addition of LVDS lines drivers piggy-back modules used to transmit data to the control desk. As reported on figure 4, it was possible to identify the different functions previously studied and the two recently added ones.

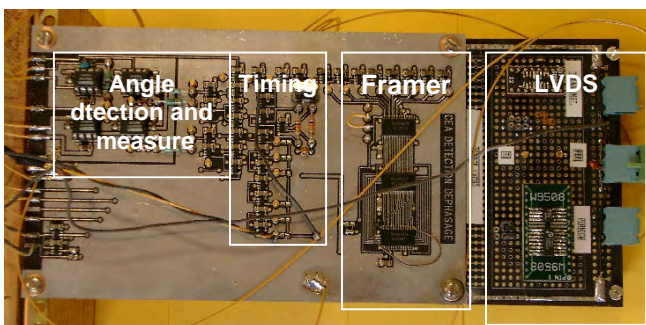


Figure 4 : Printed board of the prototype

The prototype was submitted to an intermediate irradiation to evaluate the prototyping transfer. The experiment done at IRMA facility, up to 5 MGy, provided very interesting results.

The chronograms of figure 5, taken 15 meters away from the prototype on the control test-bed desk, show coherent frame and clock frame signals while validating a good behaviour of all internal functions. Post-irradiation measures confirmed the assertion, especially counters and LVDS drivers (not shown).

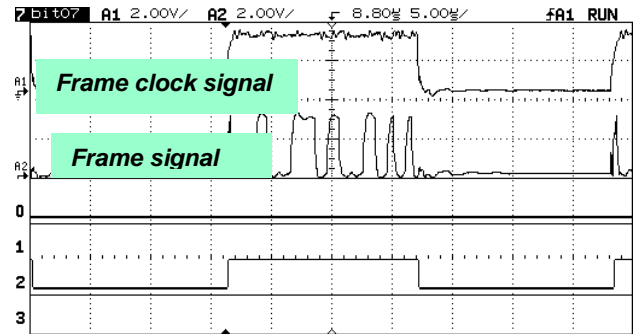


Figure 5 : Frame delivered at the level of the control desk after 2.7 MGy

After the irradiation campaign (IRSN facility did not include thermostatic bottles), high temperature tests were done and the results are presented on figure 6.

After some stresses at different temperature up to 150°C, no erroneous states were observed both on analog and digital signals.

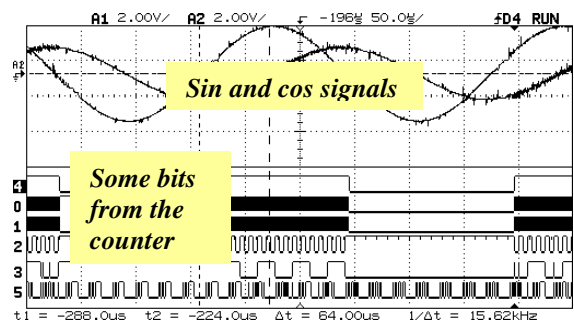


Figure 6 : Temperature tests (laboratory oven)

New upgrades were later done on the prototype.

The sinusoidal resolver reference input was designed, realized in order to suppress extra wires and increase the autonomy of the multiplexor.

The resonator was a Wien Bridge structure calculated to deliver a frequency signal of  $f_{res} \approx 3.7 \text{ kHz}$  corresponding to the resolver's requirements with  $R = 4.3 \text{ k}\Omega$  and  $C = 10 \text{ nF}$ .

An automatic gain control inserted in the feedback loop and assumed by a FET transistor stabilized the amplitude and the quality of the sinusoidal output to a correct level (see figure 7).

The corresponding frame clock signal is very close to that delivered until now by a function generator. The counter period is about of 270  $\mu\text{s}$  for a  $2\pi$  full phasing between input and output resolver signals.

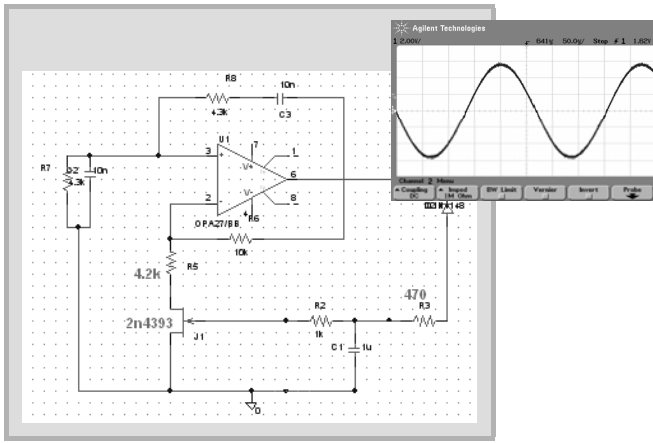


Figure 7 : Sinusoidal function delivered to the resolver input

The 12 bit counter was also defined and realized with some recent AUC74 flip-flops (BGA packaging) with “clear” in place of AUC79. These flip-flops allow an absolute coding of the angle with high precision. To obtain an efficient sampling of 270/4096  $\mu$ s, 66 ns, a timer using 20 MHz quartz was added giving a 50 ns sampling period.

All these new functions were implemented on a printed board prototype and mounted above the mother board previously studied. The resulting laboratory test is summarized in figure 3 which shows the counting operation of the time period corresponding to the absolute position of the angle. Also visible on figure 3, the reset effect on all the flip-flops outputs after frame was latched and sent.

The two cards were irradiated at MOL facility to quicker reach high dose level.

The results obtained were very contrasted after about 10 MGy. A gap appearing between 5 and 10 MGy might not be clearly seen and positively managed, mainly for two reasons: one was the multiple functions simultaneously tested and their interaction during radiation, the other the great difficulty to easily change any parameter.

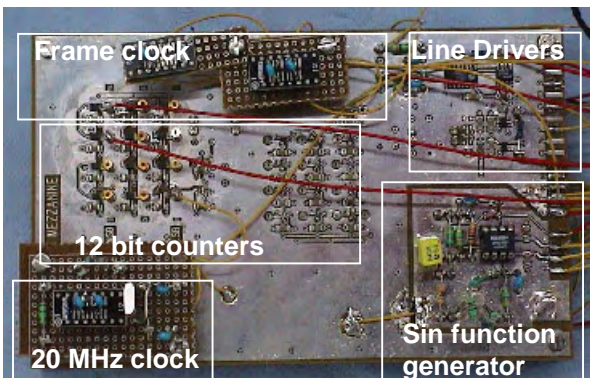


Figure 8: Piggy-back prototype with new functions

The drift observed on logic supply, about 3.3-3.5 V at the end of irradiation was above the 2.8 V expected threshold . All the timer functions were still efficient after increasing voltage supply.

Post-irradiation controls showed an extra degradation of the OPAs which could be corrected by increasing the supply up to +/- 15 V (experiments were done with a +/-7.5 V as for 2003 campaigns).

AUC74 BGA packaging was responsible of the full failure of the counter mechanism and the destruction of most flip-flops. The functionality of the others was kept at 2.8 V. LVDS remained functional for PERICOM components.

**VIRTUAL GROUND SUPPLY/ADC AND LVDT FUNCTIONS**

The post-degradation control of 2003 experiment enabled modifying the virtual ground supply [1] [3] [4] by increasing positive and negative levels to +/-7.5V to enable a correct behaviour of all the OPAs used for the multiple functions included in the multiplexer concept. A power stage was also added to drive the ground current coming from both logic and analog components. The electronic scheme is presented on figure 9.

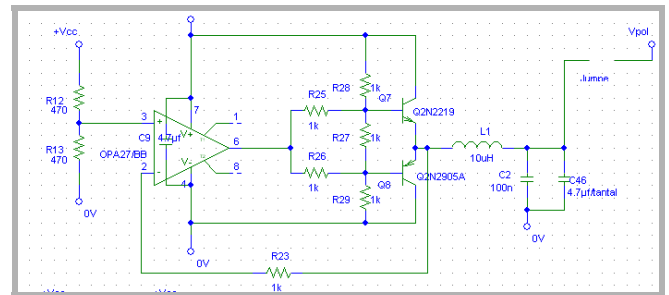


Figure 9 : Design of a new virtual ground supply

Concerning logic supply and reference voltage, only minor adaptations to those new conditions were identified, as for ADC and LVDT functions. A printed circuit was designed and realized, including all these functions. Some very short wires were added to assume signal exchanges between the two cards.

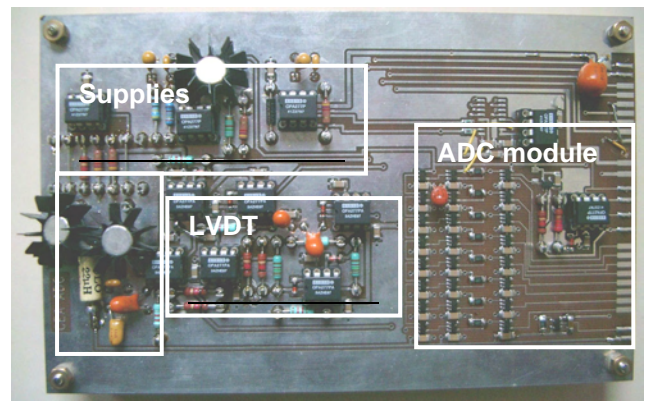


Figure 10 : Printed board of ADC/LVDT/virtual ground supply

To fulfill the validation of the multiplex prototype, the board was irradiated with the resolver board at IRMA, IRSN (Saclay), up to 5 MGy as represented on figure 11.

To enhance the experiment, the resolver board was fully supplied by the virtual ground supply. Some intermediate clocks are given by the resolver board. Most sensible data were read through a control desk 15 meters away from the irradiated board.

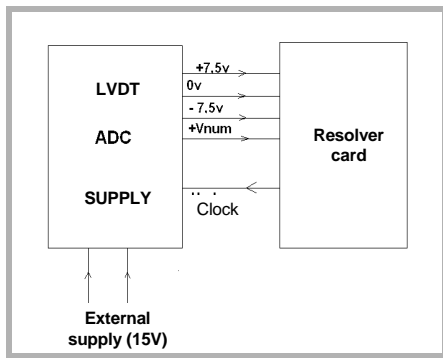


Figure 11 : Synoptic of irradiation test principles

As for resolver board, most of the results were very satisfactory. The LVDT measurements reported on figure 12 showed the regular and homogeneous evolution of analog and digital data recorded all along the campaign. It should be clear that for any positions of the LVDT, drifts were visible on the analog value while ADC conversion seems to be correct up to 350-400 hours with unavailability of the conversion.

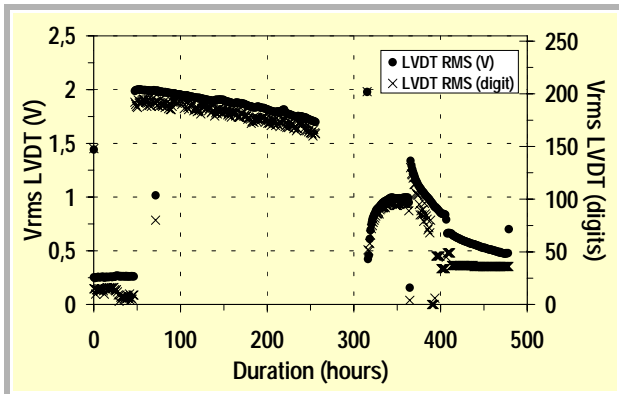


Figure 12 : Analog and digital values of LVDT position

No failures were observed on virtual ground supplies while current was decreasing as shown on figure 13.

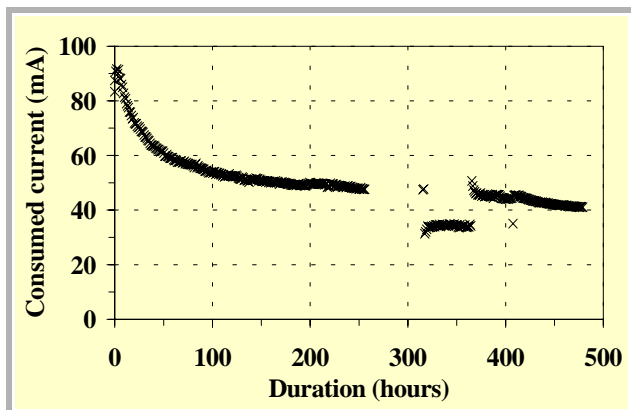


Figure 13 : Current evolution during irradiation

The post irradiation controls showed that the drifts or the failures only proceed of the OPAs load current drifts . Some simple arrangements of hazardous bias reestablished a full functionality of both ADC and LVDT conversions.

New up-grades were later done to perform the prototype.

A sinusoidal LVDT reference input was designed and realized on the model of the resolver. To respect the characteristics of the LVDT, the calculated parameters were  $f_{res} \approx 5 \text{ kHz}$  with  $R = 6.8 \text{ k}\Omega$  and  $C = 4.7 \text{ nF}$ .

The LVDT positive or negative position detection function was rebuilt in a way very close to phase detection function of the resolver board and added as a piggy-back to the mother board.

The common irradiation of the resolver and LVDT cards (figure 14) at MOL up to 10 MGy provided very contrasted results also for this card.

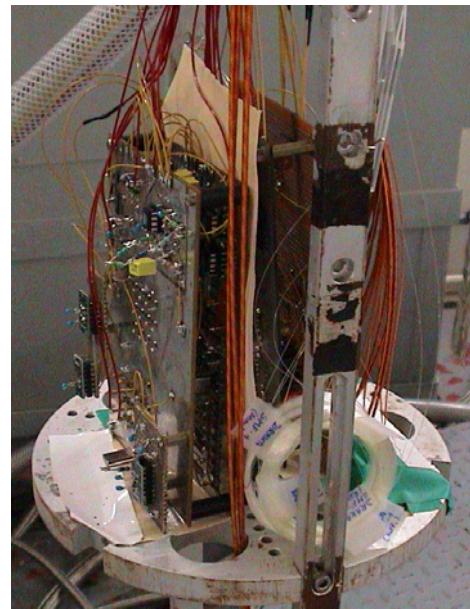


Figure 14 : Boards' placement on the bottle before irradiation

The exploitation of recorded data provided enough information to understand the behaviour of the experiment during the radiation.

After a few tens of hours, the current consumed by the prototypes, probably by logic flip-flops, exceeded the limit given to external supply (180 mA) and obliged it to fall at about 6 V.

Virtual ground and logic supplies became unable to drive any components and LVDT homogeneous values became very inconsistent.

A compromise between the increasing external and the virtual ground supply gave sometimes enough voltage to restart the logic functions and deliver a correct ADC binary converted value (see figure 17 during the first hundreds of hours).

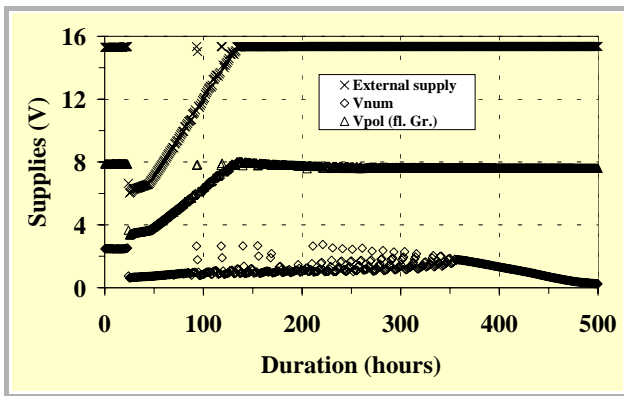


Figure 15 : Virtual ground supplies during radiation

Nevertheless, after a full recovery of supplies (see figure 15 and figure 16) after about 150 h, the only logic supply seemed too low to maintain a permanent correct behaviour of all the logic functions.

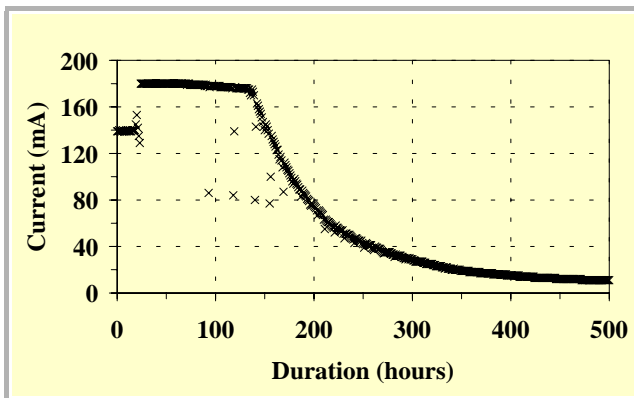


Figure 16 : External current during irradiation

It is possible that the OPA became unable to deliver enough current to drive the full logic functions implying a global diminution of global consumed current, the other reasons could also be the continuous destruction of AUC74 (BGA packaging) components.

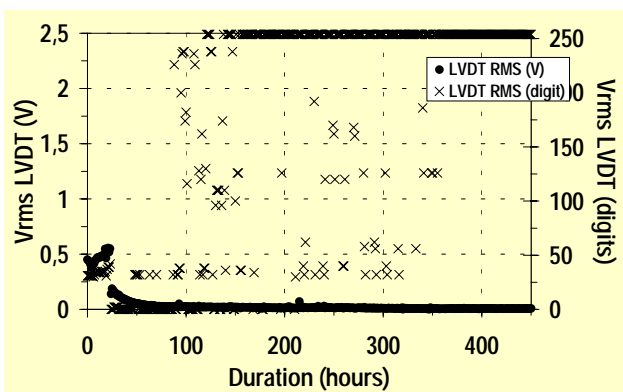


Figure 17 : LVDT measurement during radiation

The post-irradiation control confirmed the important drift observed for the supply of OPAs and DAC (at least +/- 15V) but in any case the lost of the components.

For the last experiment of the year, some functions were upgraded or redefined.

Mainly, the 20 MHz counter was redefined and hand-wired to deliver a 12 bits value with AUC74 in an identical packaging. All OPA were exchanged but, unfortunately, no logic and DAC components.

An embedded mechanical test bed developed by tasks partners allowed regular movements of the resolver in order to deliver dynamic frame of the angle position. Some digital inputs were also positioned by switches activated by lifters.

### FULL MULTIPLEXER EXPERIMENT

An irradiation campaign was realized at IRMA, IRSN facility at Saclay, commonly with SCK team, to validate the full multiplexer with either bifilar and optical transmission (figure 18).

The mean received dose by this important test-bed was close to 4.5 MGy.

The very short time dedicated to the adaptation of our modules to the test-bed did not enable easy pre-irradiation and later on-line controls of our boards.

Some failures occurred during the campaign mainly for this reason but were compensated by direct investigations, voltage adjustments and easy recovery (opening could be requested easily).

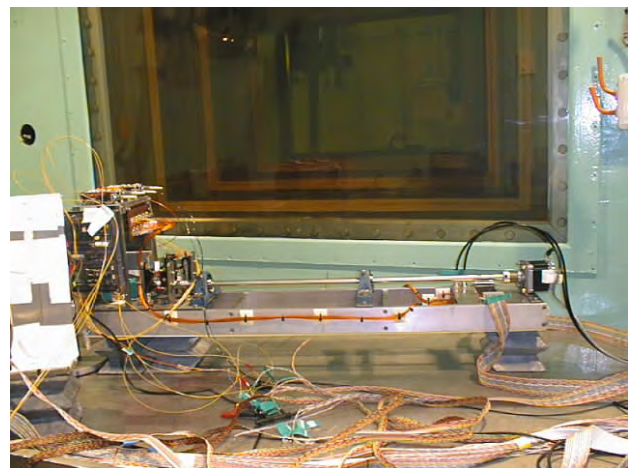


Figure 18 : Mechanical test-bed used for full validation of the multiplexer

During this irradiation the influence of the non equivalent radiation state of all these boards clearly appeared.

Some were recent with new components, other partially upgraded and some remained in correct state even after one or two irradiation campaigns.

The encountered failures were always solved by an adjustment of logic supply also used for LVDS lines drivers.

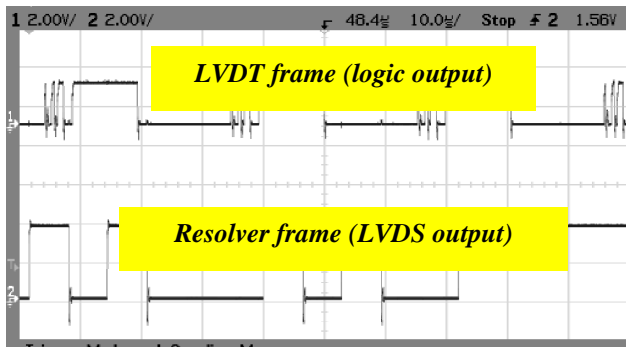


Figure 19 : Frame signals coming from LVDT and resolver boards

The recorded frames signals of figure 19 taken at the control desk and those of figure 20 taken during a break inside the cell on test points were obtained after at least 3 MGy. They gave good signals.

More details of the final experiment are given in [6].

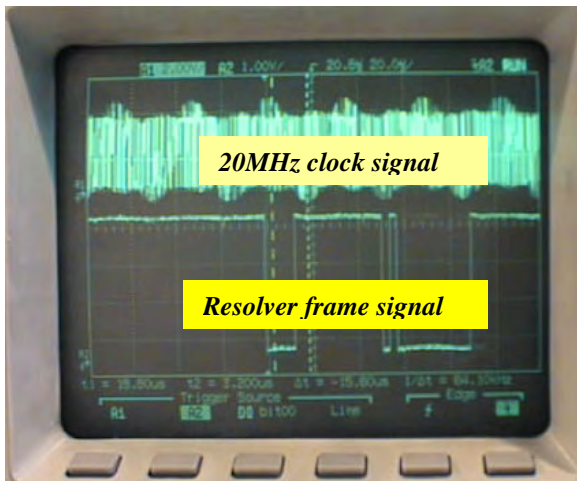


Figure 20 : Inside cell measurements

## CONCLUSION

During this year, many new very useful functions were added and a 20MHz counter was finally validated with AUC74 reset flip-flops enabling 12 bit scale for the angle position.

The final experiment showed the necessity to avoid any mixing of different radiation degraded boards.

The expected validation of the full multiplexer module must be confirmed by another experiment with fully upgraded cards.

Most of the results already acquired led to correctly validate this concept.

## REPORTS AND PUBLICATIONS

- [1] Fusion Technology : Annual Report of the Association EURATOM/CEA 2003 Task TW3-TVR-RADTOL.
- [2] Fusion Technology : Annual Report of the Association EURATOM/CEA 2002 pp 91-95.
- [3] TW3-TVR-RADTOL June report DRT/LIST/DTSI/SARC/03-813/AG.
- [4] TW3-TVR-RADTOL December report DRT/LIST/DTSI/SARC/04-042/AG.
- [5] TW4-TVR-RADTOL June report DRT/LIST/DTSI/SARC/04-335/AG.
- [6] TW4-TVR-RADTOL December report to be published .

## TASK LEADER

Alain GIRAUD

DRT/LIST/DTSI/SARC/LCSD  
CEA-Saclay  
F-91191 Gif-sur-Yvette Cedex

Tél. : 33 1 69 08 64 30  
Fax : 33 1 69 08 20 82

E-mail : alain.giraud@cea.fr

**TW4-TVR-WHMAN****Task Title: DEVELOPMENT OF A WATER HYDRAULIC MANIPULATOR****INTRODUCTION**

Due to the high level of radiations, the nominal maintenance in ITER will be carried out with help of robotic means. In reduced volumes, hydraulic applications can provide powerful actuators. Therefore, they become an interesting technology to design a heavy duty manipulator for operations in space constrained areas. Operating in a fusion reactor requires a cleanliness level that oil hydraulic cannot ensure. Pure water hydraulics therefore proposes a good alternative and developments are today focusing on that direction.

Although basic hydraulic elements like pumps, valves, filters running with pure water are already available on the market, actuators are not so many. Linear actuators are already available on shelf but compact rotary actuators are still missing. Although some R&D developments are providing powerful actuators in compact design, the size of the existing industrial products would make a big and heavy component. The design of the actuator was sometimes quickly adapted to water without real endurance tests and their reliability steel needs to be tested.

A reflection was carried out to propose an actuator design compatible with ITER's specific requirements.

**2004 ACTIVITIES****USING WATER AS A FLUID MEDIUM**

Compared to oil, water has the following drawbacks:

- Has a low viscosity.
- Has a higher density.
- Creates erosion.
- Corrodes the internal surfaces.
- Has a high vapour pressure.
- Has poor lubricant properties.
- Is a living environment.
- Reduced operating temperature range.

Although water hydraulics is not new, the number of industrial and therefore of industrial products available on the market can still be considered as confidential compared to oil hydraulics and lots of work is still done in research laboratories.

According to all the publications, material selection and build quality are essential parameters to consider when designing water hydraulics systems.

Water has a viscosity that is generally one thirtieth that of hydraulic oil. The effects are a higher acceleration rate, faster flow velocities and greater energy creating altogether a bigger potential of destruction.

Low viscosity also gives the ability to go through smaller cracks.

High vapour pressure creates systems highly susceptible to cavitation which leads to erosion of internal surfaces.

Effects of water's low viscosity on the design are most of the time solved by machining with tighter part tolerances.

For pure water hydraulics products, clearances are now typically found between 2  $\mu\text{m}$  and 10  $\mu\text{m}$ . General rules are talking about clearance order of a third or less compared to oil hydraulics.

Typical films thicknesses for hydrodynamic lubrication are of 0.1  $\mu\text{m}$  for water compared to 10  $\mu\text{m}$  for oil. Ten times less is needed for both cases in elasto-hydrodynamic regime. In fact the film thickness becomes unacceptable with water because the build quality can't provide such accuracy.

Therefore, roller bearings and all classical rolling elements can not be used with the classical specifications related to lifetime or load capacity in water applications, even if they are made of corrosion resistant materials.

Bearings with plastic bushing are seen in many applications where the loads are low but the most common solution is a combination of PEEK and stainless steel. They are generally limited to systems operating at pressures lower than 160 bars.

Material choice is probably one of the most difficult aspects in the design of water hydraulics components. Stainless steel is widely used to fight against corrosion. Pistons, cylinder blocks, valve plates are typical part now made with that material while housings are using more and more cast bronze.

Due to poor lubrication, it is assumed that there will be a relatively high coefficient of friction and that surface wear will take place. Because of corrosion stainless steel should be used for all the power transmission parts, but friction of stainless steel with other materials is usually high. Metal-metal contact seems out of question and all publications agreed on the fact that one of the rubbing surfaces must be non-metallic.

Leakage and erosion problems are sometimes solved by manufacturers through the use of new ceramic materials. Among them: aluminum oxides and Zirconias.

Association of ceramic materials also needs to be made carefully. Two materials with a high toughness operating against each other are often worn heavily after standard test durations.

### AVAILABLE PRODUCTS

Power-packs units are widely developed products. Compact sized units are available in manufacturers catalogues providing the fact that pressure and flow rates are staying at relatively low values.

It seems like operating at 200 bars which is the typical value used with hydraulic manipulators should already being considered upper than the standard values.

Low viscosity of water has a direct impact on the internal leakage of the components and therefore on size and performances provided by the power pack to achieve sufficient operating speed. Actuation means like motors or cylinders are already available in industrial catalogues.

Motors are usually based on axial pistons operating on a swashplate for high speed applications and on the vane type motors for applications requiring high torque at low speeds. But all these motors can not deliver high torques during stops of the actuator. Because these situations are the most common configurations during operations with manipulators, designing a manipulator can not be made without additional devices such as clutches. This therefore goes against the backdrivability of the system required for force feedback applications and against the compactness of the design.

Using cylinders to drive rotation often leads to limitation of strokes and reduces the operating area of the manipulator. For that reason they should not be used as standard actuators in the design of a manipulator.

For these reasons previous work concentrated on the adaptation of rotary vane actuators from oil to water. A prototype, AQUA, was successfully tested at the Institute of Hydraulics and Automation in Tampere (Finland). Sealing proved to be efficient but according to the designers improvements still need to be done on the bearings and long term tests were not carried on.

### DESIGN OF A WATER HYDRAULICS ROTARY ACTUATOR TEST BENCH

Work made at IHA (university of Tampere) proved the principle of operating a rotary actuator with water. Fine position and force control schemes were achieved and showed good performances. Improvements were made in order to find an appropriate design and material for the seals. Control, sealing and main design are already considered as having found an answer.

These new test series will therefore work in two directions:

- Find a solution to the uncertainty on the bearings.
- Perform an endurance test.

Using stainless steel bearing is necessary if we use water as a fluid medium. Stainless steel tapered roller bearings are not yet available on the market, even if some manufacturers are listing them in catalogues. Angular contact ball bearings are available but can't stand the same load within the same dimensions. Adaptation of the standard design of rotary actuators will be necessary to take this constraint into account.

Design of the actuator for the test bench is an adaptation of one joint of the Samm modular hydraulic arm from Cybernetix. An adaptation of the flanges was made to provide the necessary space for angular contact ball bearing or bearing configuration made of ball thrust bearings and ball bearings.

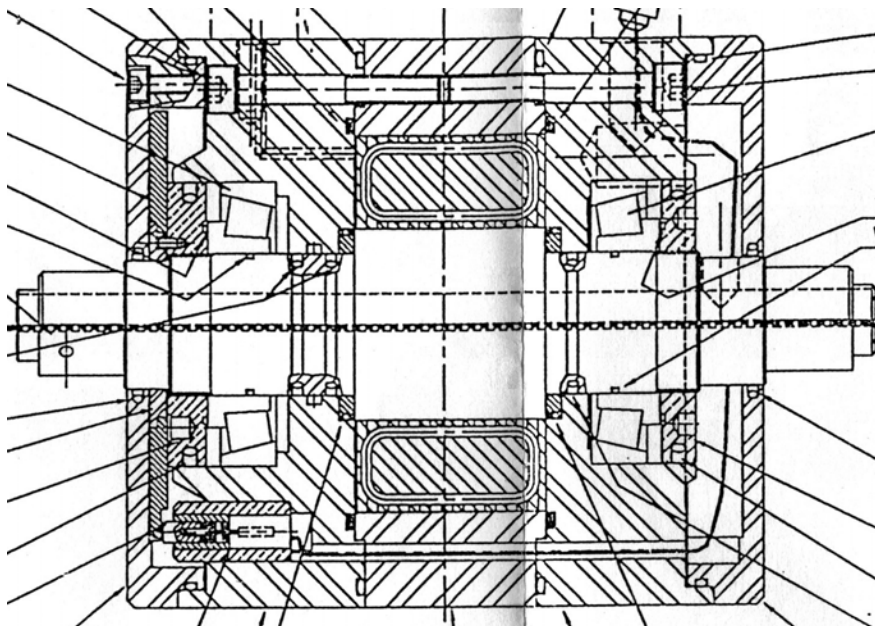


Figure 1 : SAMM rotary vane actuator

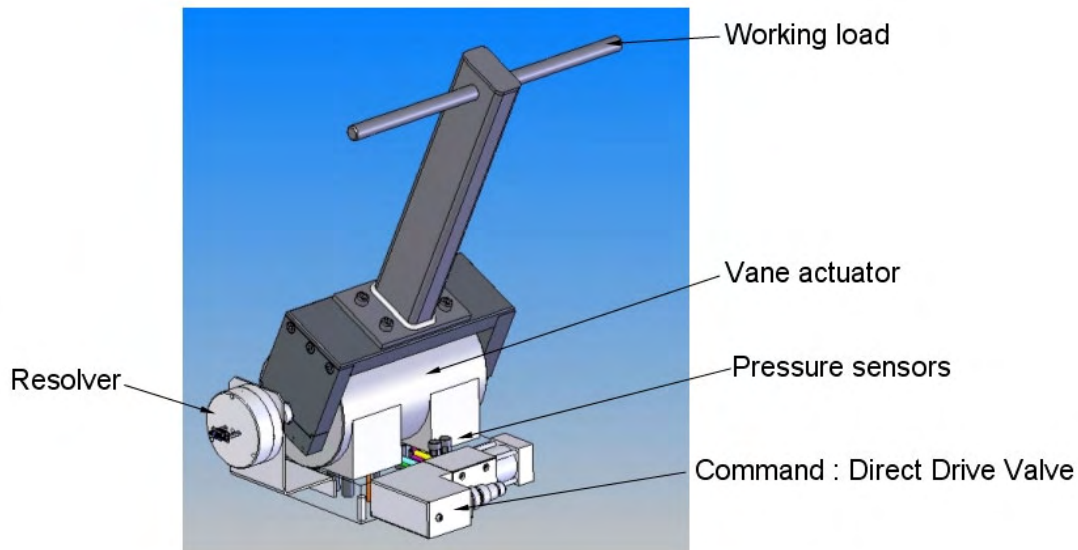


Figure 2 : Test bench

The most interesting bearing technology suitable for water is probably hybrid ball bearings.

In those bearings, balls are usually made of Silicon Nitride and rings of martensitic stainless steel. Friction between ceramic and stainless steel is lower than stainless steel against itself thus limiting heating of the bearing. Hardness is also very different between balls and raceways and that gives a significant advantage to this design.

The bearing manufacturer ISO proposes both stainless steel and hybrid bearings angular contact ball bearings suitable for our applications.

Test series will be performed with both components to find the best product.

The test bench is composed of the elements of the figure 2.

Position measurements will be made with help of a resolver.

Water will be provided to the actuator through a Moog D633 Direct Drive Valve. This product is not directly designed for water but is used in glycol water applications. Its performances should be enough for long term tests. Two pressure sensors will measure the pressure in the two chambers of the actuator.

Load adjustment will be made at the end of the arm.

## CONCLUSIONS

---

After an analysis of the consequences of using water as a fluid medium a brief overview of technological solutions found by industrial companies or research labs to address the problem were listed. The industrial products offer is today centered on components like: pumps, filters, on-off valves.

In fact, components that one can consider being provided with relatively simple technological functions. In terms of advanced components like motors and proportional valves or servo-valves, designs or performances limitations are precluding their use in for robotic manipulators.

Starting from the design of one oil hydraulic actuator this task designed a mock-up to study both the influence of different kind of bearings and long term issues during endurance tests. Commissioning of the components of the mock –up is now finished and the test phase will start soon.

## REPORTS AND PUBLICATIONS

---

DTSI/SCRI/LPR/05RT006 TW4-TVR-WHMAN - Water hydraulic manipulator - Definition of a single axis water hydraulic mock-up.

## TASK LEADER

---

Jean-Pierre FRICONNEAU

DTSI/SCRI/LPR  
CEA-Fontenay aux Roses  
Boîte Postale 6  
F-92265 Fontenay aux Roses Cedex

Tél. : 33 1 46 54 89 66

Fax : 33 1 46 54 75 80

E-mail : jean-pierre.friconneau@cea.fr



**CEFDA03-1015**

---

**Task Title: TW2-TMSM-COOLINL: MOCK-UPS FOR THE TF AND CS  
TERMINAL REGIONS AND COOLING INLETS**

---

**INTRODUCTION**

---

The Euratom-CEA Association is requested through the contract EFDA 03-1015 to assist the EFDA Close Support Unit Garching and the Superconducting Coils and Structures Division of the ITER International Team (ITER-IT) in the detailed design and manufacture of relevant mock-ups for some critical areas of the Toroidal Field (TF), Central Solenoid (CS) and Poloidal Field (PF) coil windings.

Mechanical testing at cryogenic temperatures of the mock-ups under relevant loads and number of cycles will be carried out at FZK Karlsruhe (TW3-TMSM-CRYTEST) and ENEA Brasimone (TW1-TMS-SHKEYS). Euratom-CEA is requested to design the mock-ups in close collaboration with these two Groups and EFDA/ITER, coordinate the testing activity and report on the final test results. Euratom-CEA is responsible for the definition of the testing conditions (loads, number of cycles, temperature, etc.) under review and approval of EFDA/ITER.

The work include three main activities:

- Design, manufacture and assistance to testing of mock-ups and samples of the Toroidal Field (TF) coil helium inlet.
- Design, manufacture and assistance to testing of mock-ups and samples of the Central Solenoid (CS) helium inlet.
- Design, manufacture and assistance to testing of mock-ups and samples of the bonded tails at the extremity of the windings of the Poloidal Field (PF) coils.

**2004 ACTIVITIES**

---

**DEVELOPMENT OF THE TF COIL HELIUM INLET****Design**

The TF coil conductor consists of a circular Nb<sub>3</sub>Sn cable-in-conduit with a central cooling channel cooled by supercritical helium. The material used for the conductor jacket is stainless steel. The jacket inner diameter is 40.2 mm and the jacket wall thickness is 1.6 mm. The winding uses a one-in-hand conductor (about 800 m long) in a double pancake configuration inserted into a radial plate.

The cooling inlets are located at the two innermost turns of each double pancake into the joggle region where the conductor from the first pancake come out of his radial plate groove to go into the groove of the second pancake. The total length of the inlet region is 700 mm.

The design of the ITER TF helium inlet is developed on the basis of ITER drawings which defines the space allowed for the inlet region.

The helium pipe connected to the inlet has to fit into the double pancake thickness without interference with the coil case.

Taken into account these space limitations, the proposed design for the inlet is as follows: The conductor jacket is locally cut on a length of 98 mm. The cable wrapping is removed at this location.

The sub-cable wrappings is cut only at the outer surface of the cable. A grid in two halves with a thickness equivalent to the jacket plus the wrappings is placed on the bare cable.

The two halves of the grid are spot welded one against the other but the grid is not welded to the jacket ends to allows cable deformation independent to the grid during TF coil operation. The grid uses two inner longitudinal grooves to distribute helium all along the length of the inlet.

The helium is then distributed on all the cable outer area by a set of grooves on the inner circumference of the grid. The grooves have a depth of 0.5 mm. The width of the grooves at the inner circumference of the grid is limited at 2 mm with a pitch of 8 mm.

This layout limits the unsupported length of the strands to 2 mm and then avoid the risk of strands deformation due to Lorentz forces when the coil operates.

The mechanical stiffness of the inlet is insured by two half shells which are then placed to recover the grid and are longitudinally welded one against the other. These longitudinal welds have to be performed without welding of the grid with the shells to allows independent deformation of the shells under the hoop force during TF operation with respect to the grid.

The shells are then welded on the conductor jacket at their two ends. All the shells welds have to be helium tight.

A special helium pipe has been previously welded on to the corresponding half shell using an elliptic shape to reduce the stress concentration around the hole. Figure 1 shows this design.

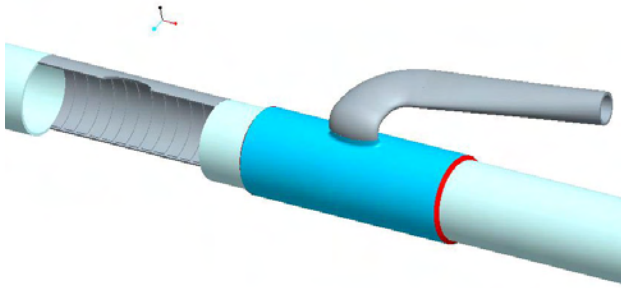


Figure 1 : TF inlet design proposal  
(The mechanical shells are shifted to show one half grid)

The strain experienced by the TF coils at helium inlets during operation is  $\varepsilon \sim (6 \pm 5) \times 10^{-4}$ , where  $6 \cdot 10^{-4}$  is the essentially static strain due to the toroidal field alone and  $\pm 5 \cdot 10^{-4}$  is the cyclic out-of-plane strain (translated into stress, this gives a stress of  $\sigma \sim 120 \pm 100$  MPa).

Normally, the number of cycles should be 1 200 000 (factor 20 on the ITER number of cycles) but to reduce the number of cycles to 30 000, it was suggested to double the strain (this strain corresponding to an average tensile stress  $\sigma \sim 440$  MPa).

### Analysis

A 3D straight FEM model was built for global analysis and a 2D local model was built for analysis of the weld between the shells and the jacket. After optimization of the geometry, the maximum stress around the elliptic helium hole remains to be lower than 700 MPa when a peak value at the shells weld location of 858 MPa appears on the jacket. These values have been considered to be acceptable by EFDA.

### Manufacture

The components for the manufacture of five mechanical and hydraulic mock-ups have been fabricated and delivered to CEA (figure 2).

Four mock-ups will be completed in 2005 for welding procedure determination and mechanical qualification in the FzK facility while one hydraulic mock-up will be tested in the OTHELLO test facility for pressure drop measurement and flow distribution characterization among petals.



Figure 2 : The components of a TF inlet

## DEVELOPMENT OF THE CS COIL HELIUM INLET

### Design

The CS conductor consists of a Nb<sub>3</sub>Sn cable-in-conduit with a central cooling channel, cooled by supercritical helium. The material used for the conductor jacket is stainless steel. The jacket inner diameter is 33.2 mm and the jacket outer square section is 49.9 mm × 49.9 mm.

The CS modules are wound as hexa-pancakes (6 pancakes with a single conductor length) and quad-pancakes (4 pancakes with a single conductor length). Helium inlets are at the crossover regions on the inner bore between each double pancake and outlets are at the crossover regions and joints on the outside. The high field region is therefore cooled by the coldest helium. There are three helium inlets for each hexa-pancake and two for each quad-pancake.

The main issue associated with the CS helium inlet is its structural behaviour. This is because the inlets are located at the CS inner diameter, where cyclic tensile stresses are highest. In the CS jacket, the maximum stress occurs at initial magnetization and reaches 470 MPa in the vertical sidewalls of the jacket. This stress is due to the combined effect of the toroidal hoop stress and the vertical magnetic load acting on the CS stack. The helium inlet region requires, therefore, a local reinforcement to allow the opening in the conductor jacket without excessive stress intensification. The inlet must also provide a good distribution of helium in the six sub-cables of the conductor. A design of this inlet was suggested by ITER-IT to achieve these requirements. The inlet is manufactured by machining an elongated narrow slot for the helium inlet. This slot must be long enough to allow direct access for the helium to the sub-cables. A cover with a structural reinforcement around the helium inlet opening is then welded above the slot.

### Analysis

A FEM model relevant to this proposed design was previously built and has led to an optimization of the design to reach a maximum stress concentration factor of 1.30.

To qualify this design on a mechanical mock-up, with an average stress in the inlet region of 405 MPa, a tensile force of 664 kN would be necessary which is not compatible with the FzK test facility capability of 500 kN. In addition, EFDA asked to reduce the number of cycles from 1 200 000 to 30 000 by doubling the loading.

The mock-up design was adapted to the facility capability by a reduction of the mock-up cross section by cutting longitudinally the conductor in order to test only the cover side part. A comparison of the stresses distribution between a complete and reduced mock-up was performed [1]. This reduction of the mock-up leading to a modification of the mock-up bending, a shift of the pulling point was needed to get representative stress concentration factor on this reduced mock-up. A FEM analysis was performed to adjust the mock-up cross section as well as the shift value to be representative (figure 3).

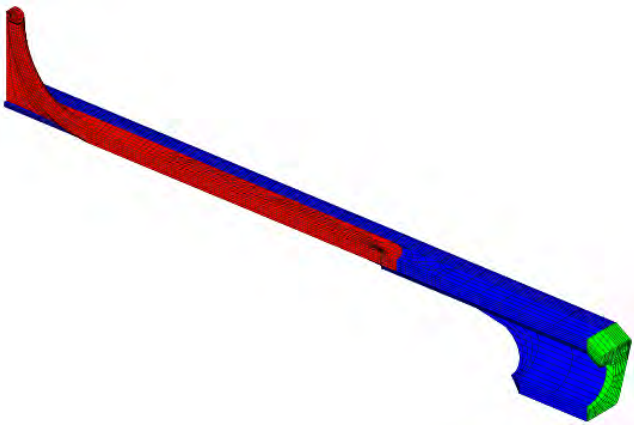


Figure 3 : F.E. Model of the reduced CS mock-up

The complete design drawings of the corresponding mechanical qualification mock-up were issued. In parallel, a manufacture test was performed on a similar PF conductor sample with square jacket and has qualify the feasibility and machining process for the narrow groove manufacture (figure 4).



Figure 4 : Manufacture test of the narrow groove

A more fabricable value of the radius of the ends of the groove of 2 mm instead of 1 mm has been chosen. In agreement with EFDA. This increases very locally the stress concentration factor from 1.30 to 1.57.

No samples of CS conductor being available during year 2004, the manufacture and tests of this mock-up have been delayed

### DEVELOPMENT OF THE BONDED TAILS OF THE PF COIL WINDINGS

#### Design

The ITER PF coils design of the winding packs consists of a stack of double pancakes made of NbTi cable-in-conduit conductor, with a square section jacket in stainless steel 316LN.

Electrical joints are necessary for the connections between double-pancakes and the terminals; at each joint, a structural element is required to transfer the operating hoop load on the conductor. In the present design, this is provided by a conductor tail welded to the conductor jacket and bonded to the adjacent turns of the pancake. The load is therefore transmitted to adjacent turns and to the bulk of the coil, through shear stresses in the insulation.

The highest hoop load occurs in PF5 Coil, and it results in a tensile load in the conductor jacket of 250 kN and a tensile stress of 150 MPa. This is also the load to be carried and transmitted by the bonded tail. In the framework of the CEA/EFDA Contract 00-541 a design was developed using a hollow profiled tail.

The scope of the present task is to develop the manufacturing and assembly of the coil tails to the level of an industrial process and, ultimately, to build a mock up, representing the main features of the coil tail, and to subject it to fatigue tests, at LN temperature, at the ENEA (Brasimone, Italy).

#### Manufacture

At first the work has concentrated on qualifying the process for manufacturing the prototype tails, within the strict tolerances required, and four tails have been produced (figure 5).

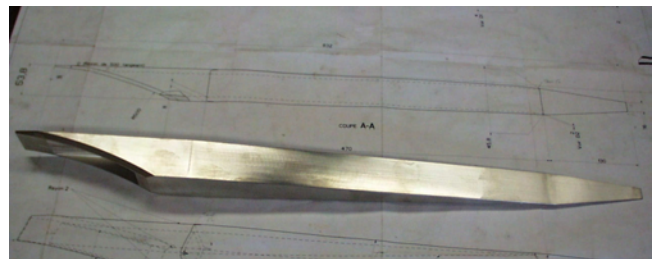


Figure 5 : Manufacture of a prototype PF Coil

This has been followed by the process qualification of welding the tails to the PF conductor jacket, bent at 500 mm radius, as foreseen for the PF pancake conductor exits (figure 6). All parts have been manufactured with the nominal dimension as PF5 coil and have been made in steel 316LN especially forged.



Figure 6 : Coil Tail welded to a mock-up PF conductor exit

At present the overall mock-up, inclusive of parts representative of the adjacent conductor is in the process of being assembled and impregnated. The mock-up includes two of the coil tails previously manufactured and steel plates simulating the inertia of the adjacent conductors (figure 7). Further stress analysis performed on the mock-up F.E. model has highlighted tensile stresses in the G10 epoxy-glass fillers caused by the cool-down to LN temperature.

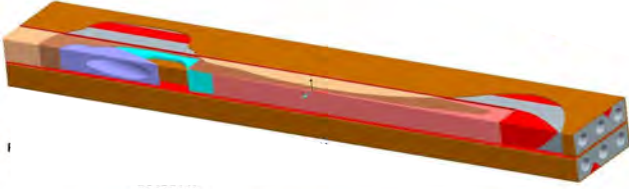


Figure 7 : PF Coil Tail mock-up for fatigue testing

To reduce the filler thermal contraction and overcome this problem, the mock-up filler parts will be made with special G10 at high (80 %) glass content. In parallel a structure has been designed and it is being fabricated, to interface the mock-up to the test machine, such to convert the compressive force of the machine in tensile force applied to the mock-up. The limited space to bolt the mock-up to the structure and the application of the pre-load on the bolts has required the manufacture of special Inconel 767 tensioners. The applied test load will be twice the nominal for 60 000 cycles.

## CONCLUSION

---

The task COOLINL is devoted to design and fabrication of mock-ups for three different items: the TF helium inlet, the CS helium inlets and the PF bonded tails. During the year 2004, the following actions were performed:

The TF inlet design was defined. Local and global FEM analysis were performed for optimization and have led to acceptable stress level with a double loading to reduce the number of cycles. The components for the fatigue life as well as for the hydraulic mock-ups were manufactured. The fatigue life as well as hydraulic qualification is planned in 2005.

A CS inlet, design of a reduced mock-up compatible with the test facility capability and the doubling of the loading imposed by EFDA was defined. A corresponding FEM analysis was performed to get representative stress concentration level with respect to the real complete inlet. The mock-ups manufacture was delayed due to the unavailability of CS conductor samples.

The components for the PF tail mock-up were manufactured. A FEM of the PF tail mock-up was built and has led to define the final design and the materials for the structure of the fatigue life mock-up. All the components are under fabrication. The mock-up assembly and tests are planned in 2005.

## REPORTS AND PUBLICATIONS

---

- [1] P. Decool - EFDA contract 03-1015 : CS cooling inlets comparison between A full and a half mockup - Note AIM/NTT/2004.004.

## TASK LEADER

---

Patrick DECOOL

DSM/DRFC/STEP  
CEA-Cadarache  
F-13108 Saint-Paul-Lez-Durance Cedex

Tél. : 33 4 42 25 43 50  
Fax : 33 4 42 25 26 61

E-mail : [decool@drfc.cad.cea.fr](mailto:decool@drfc.cad.cea.fr)

---

**Task Title: TW3-TMSC-ASTEST: TESTS OF ADVANCED Nb<sub>3</sub>Sn STRANDS EXTENSIVE CHARACTERIZATION OF INDUSTRIAL ADVANCED Nb<sub>3</sub>Sn STRANDS DEVELOPED FOR ITER TF COILS SYSTEM**

---

**INTRODUCTION**

This action is part of a global R&D program extension devoted to the Nb<sub>3</sub>Sn material. Nb<sub>3</sub>Sn is the superconducting material used in the ITER TF and CS Coils.

However the models built in the framework of the ITER EDA phase (CSMC, CSIC, TFMC, TFCI) has shown reduced performances compared to those expected and consequently a specific EU R&D program was launched.

An action was started with industrial companies to stimulate them in developing a new generation of superconducting strands with specifications adapted to the ITER TF Coils system:

- $I_C(4.2\text{ K}, 12\text{ T}) > 200\text{ A}$  with a target value of 280 A.
- $Q_{\text{hyst}} < 500\text{ mJ}\cdot\text{cm}^{-3}$ .

Six companies were concerned : Alstom (F), Outokumpu Italy (I), Outokumpu Finland (FIN), EAS (D), SMI (NL), Oxford Instruments (GB).

The strand qualification is planned in two steps :

- a global assessment of all EU stations involved in this task, for which a benchmarking strand from SMI is tested in all laboratories. Results are then compared and must remain within a defined scattering to be accepted,
- two strands are tested by each EU laboratories with possibility of cross-checking between laboratories.

The tests involve :

1. geometrical measurements with diameter, filament twist pitch and Cu/nonCu ratio,
2. electrical measurements with  $J_C(4.2\text{K}, 10-14\text{ T})$ ,
3. magnetic measurements with  $Q_{\text{hyst}}(+/- 3\text{ T})$ .

Actions #1 and #3 are planned to be performed at CEA Cadarache while action #2 is to be performed at CEA Saclay.

**2004 ACTIVITIES**

**QUALIFICATION OF THE EU LABORATORIES FACILITIES**

The test facility used for the electrical measurements is the CEATACES test facility, located at CEA Saclay in the DAPNIA laboratory. The test facility used for the AC losses magnetic measurements is the SUSI facility located at CEA Cadarache.

All required tests were performed with the SMI strand. It is to be noted that less characterizations were planned for this qualification step (no filament twist pitch or strand diameter). Test mandrels were provided by CEA, handling and heat treatments were performed by CEA.

**Geometrical tests**

The cross section micrograph is shown in figure 1.

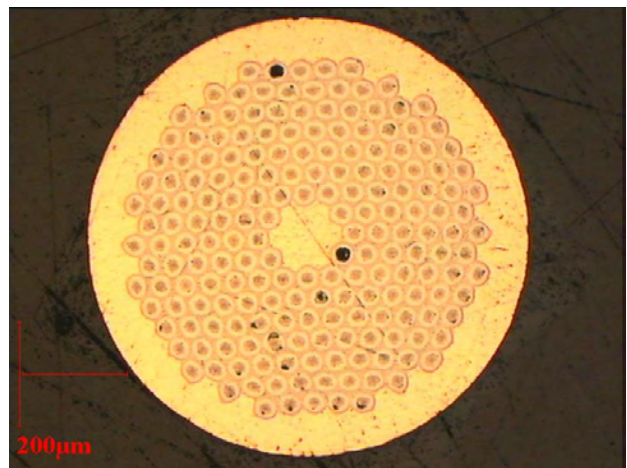


*Figure 1 : Micrographic view of the SMI strand cross-section.*

Cu/nonCu ratio has been evaluated to 0.827.

**Electrical tests**

For those tests, stability measurements were encountered and were solved by the addition of strand extra lengths in the Cu/Ti transition part of the mandrel. Results are shown in figure 2.

## CONCLUSION

During the year 2004 the ASTEST actions progressed as follows:

- The benchmarking step was completed with the SMI strand. All tests were assessed by EFDA in comparison with all other EU laboratories involved. The CEA tests facilities were thus accepted for ITER advanced strands qualification.
- The critical current tests were achieved on the first industrial strand (Oxford Instruments) and the remaining are planned for early 2005.

## REFERENCES

- [1] L. Zani, H. Cloez, C. Meuris, P. Chesny, J-M. Gheller, L. Kulbicki, L. Vieillard - Task TW3-TMSC-ASTEST Deliverable 1 : Intermediate report on test of advanced Nb<sub>3</sub>Sn strands - Note AIM/NTT-2004.014 (2004).

## TASK LEADER

Louis ZANI

DSM/DRFC/STEP  
CEA-Cadarache  
F-13108 Saint-Paul-Lez-Durance Cedex

Tél. : 33 4 42 25 29 67  
Fax : 33 4 42 25 26 61

E-mail : louis.zani@cea.fr

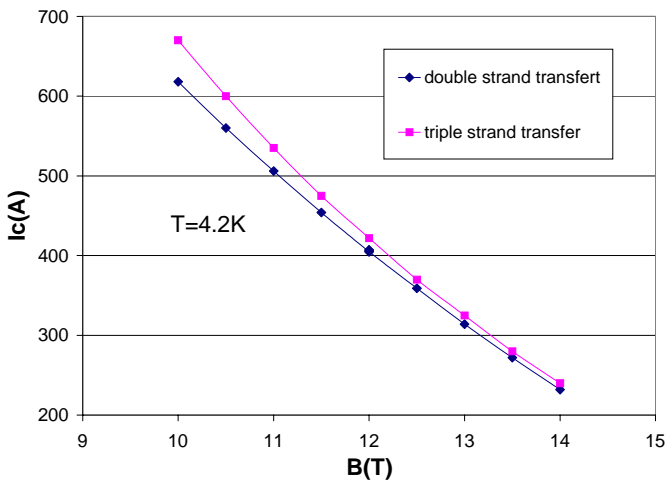


Figure 2 : Critical current results for two SMI samples. The difference between samples lays in the strand extra length added for stabilization

### Magnetic tests

$Q_{hyst}(+/- 3T)$  have been evaluated to  $1370 \text{ mJ.cm}^{-3}$

This step was completed and the corresponding deliverable report was sent to EFDA [1]. All results were compared between EU laboratories and found acceptable by EFDA. CEA was thus allowed to enter the second step of the strands qualification process.

### INDUSTRIAL STRANDS CHARACTERIZATION

The first strand from Oxford Instruments was provided to CEA by EFDA and all billets available were prepared for characterizations (Hysteresis losses, critical current, Cu/nonCu...).

Critical current tests were performed in early December 2004 at CEA Saclay and results can be seen in figure 3.

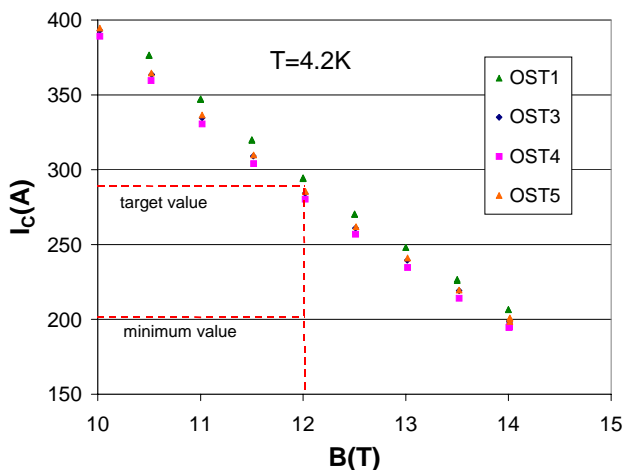


Figure 3 : Critical current results for four OST samples (four different billets)

The remaining tests on OST strands are planned for the first semester of 2005. All tests for the second strand will start as soon as it is received from EFDA in CEA Cadarache.

CEFDA04-1127

---

**Task Title: TW4-TMSC-SAMAN1: MANUFACTURE OF SUB-SIZE SAMPLES**


---

**INTRODUCTION**


---

The tests of the TF model coil in 2001 – 2002 have shown that the performance of the conductor was lower than expected [1]. This initiated in Europe an advanced strand procurement to take advantage of the progresses in Nb<sub>3</sub>Sn during these last ten years. New high performance strands have been ordered by EFDA to industry.

In the framework of the SAMAN task, CEA has to explore the sensitivity of these high performance Nb<sub>3</sub>Sn strands to stainless steel jacketing on subsize samples, as concern the critical properties. This will be done by ordering and manufacturing these samples in the industry and then by participating to the tests at FZK (Germany) in the FBI test facility. 2004 has been devoted to the writing of the specifications of these samples and to ordering their fabrication in the industry.

**2004 ACTIVITIES**


---

**SCOPE OF SUPPLY**

Strands of ‘high performance’ Nb<sub>3</sub>Sn superconductor, meeting ITER specifications, have been produced by the industry. The contract to be placed in industry, within this task, concerns the manufacturing of sub-size conductor samples, made of these strands. The samples are required for a test program with two objectives :

1. Characterization of the cable performances, depending on cabling parameters. For this purpose, for each type of sample to be manufactured, one or more parameters are varied with respect to the reference parameter value.
2. Performance comparisons of conductors made with strands provided by different manufacturers. In this case, various samples, all of the same type, are to be manufactured with strands provided by five different strand suppliers.

The supply contract is divided in two lots according to these two objectives.

**DESCRIPTION OF THE SAMPLES**

This type of samples has been already manufactured in the framework of a previous contract [2]. A section of the sample can be seen in figure 1, in the particular case of 36 strands. The strands are taken in a jacket. Copper tubes are inserted at both extremities for the electrical contact to the current leads of the power supply.

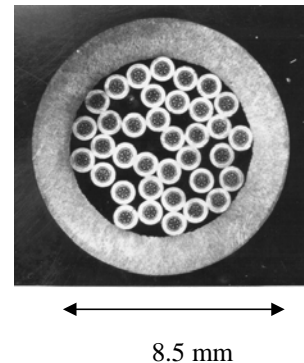


*Figure 1 : Section of a sample manufactured in the framework of a previous task [2]*

The sub-size cable samples to be manufactured as part of this contract are summarised in tables 1 and 2.

The samples for the sample characterization tests constitute the first lot. They are presented in table 1 This lot corresponds to a total of 24 samples plus 3 prototypes.

The samples for the superconducting strand manufacturer comparison tests, constitute the second lot. They are presented in table 2. This lot corresponds to a total of 20 samples.

EFDA will provide to CEA the strands to be used by the manufacturer :

- (a) The Nb<sub>3</sub>Sn superconductor strand, size Ø 0.81 mm.
- (b) The copper strand size Ø 0.81 mm, (type : OFHC copper, chromium plated with 2µm plating thickness, unless otherwise specified for few samples with no chromium plating).

The manufacturer will be responsible for the supply of all other materials required, in particular :

- (c) Type 316L stainless steel tube.
- (d) Copper tube made of ‘high purity’ copper with RRR higher than 80 (RRR is the electrical resistance ratio between ambient temperature and 20 K →  $R_{293K}/R_{20K}$ ).

The manufacturer will be responsible for the cabling of the copper and Nb<sub>3</sub>Sn strands and for the ‘jacketing’ of the cable with the stainless steel and copper tubes to its final dimensions. The cabling is to be performed ‘without torsion’, according to the standard practice in the cabling industry. For the jacketing with the steel and copper tube the preferred manufacturing method is by ‘hammering’

Table 1 : Samples for characterization program (first lot)

| 1st Triplet made of :       | Samples 3X3<br>Twist pitch 45/ 85mm<br>Void fraction 32% |                  | Samples 3X3X5<br>Cr coating |                          |                            |                          | Samples 3X3X3X5<br>Twist pitch<br>45/85/125/160 mm<br>Cr coating<br>Void fraction 32 % |
|-----------------------------|--|------------------|-----------------------------|--------------------------|----------------------------|--------------------------|--|
|                             |  |                  | Twist pitch<br>45/85/125mm  |                          | Twist pitch<br>35/65/110mm |                          |  |
|                             | Cr coating   | No<br>Cr coating | Void fraction<br>32 %       | Void<br>fraction<br>25 % | Void fraction<br>45 %      | Void<br>fraction<br>32 % |  |
| 0 Cu strand<br>3 SC strands | 2  |                  | 2                           |                          |                            |                          |  |
| 1 Cu strand<br>2 SC strands | 1 prototype<br>+<br>2                                    | 2                | 1 prototype<br>+<br>2       | 2                        | 2                          | 2                        | 1 prototype<br>+<br>2  |
| 2 Cu strands<br>1 SC strand | 2  |                  | 2                           |                          |                            |                          | 2  |
| Total                       | 8 + 1 prototype  |                  | 10 + 1 prototype            |                          |                            | 2                        | 4 + 1 prototype  |

Table 2 : Samples for supplier comparison assessment program (second lot)

| 1st Triplet made of :       | Samples 3X3X5 | Twist pitch 45/85/125 mm<br>Cu-Cr coating<br>Void fraction 32 % |   |   |   |   | Samples 3X3X3X5 | Twist pitch 45/85/125/160 mm<br>Cu- Cr coating<br>Void fraction 32 % |   |   |   |   |
|-----------------------------|---------------|---|---|---|---|---|-----------------|--|---|---|---|---|
|                             |               | SC Strand Supplier  |   |   |   |   |                 | SC Strand Supplier   |   |   |   |   |
|                             |               | A   | B | C | D | E |                 | A  | B | C | D | E |
| 1 Cu strand<br>2 SC strands |               | 2   | 2 | 2 | 2 | 2 |                 |  |   |   |   |   |
| 2 Cu strands<br>1 SC strand |               |   |   |   |   |   | 2               | 2  | 2 | 2 | 2 | 2 |

**STATUS OF THE TASK**

A call for tender has been sent in October 2004 according to the specifications presented above. The Nexans company (France) has been selected to manufacture the samples. The first prototypes are expected to be ready in June 2005.

**CONCLUSION**

2004 has been devoted to the writing of the specifications of the samples to be manufactured. A call for tender has been launched in industry based on these specifications; Nexans has been chosen and the first prototypes are expected to be delivered in June 2005.

**REFERENCES**

[1] J.L. Duchateau et al - Exploring the limits of a very large Nb<sub>3</sub>Sn conductor: the 80 kA conductor of the ITER Toroidal Field Model Coil - 2004 Supercon. Sci. Techno. 17, p.241-249.

[2] W. Specking, J.L. Duchateau - First results of strain effects on critical current of incoloy jacketed Nb<sub>3</sub>Sn CICC's - 1997 - 15<sup>th</sup> Conference on Magnet Technology Beijing (China).

**TASK LEADER**

J.L. DUCHATEAU

DSM/DRFC/STEP  
CEA-Cadarache  
F-13108 Saint-Paul-Lez-Durance Cedex

Tél. : 33 4 42 25 49 67  
Fax : 33 4 42 25 26 61

E-mail : duchat@drfc.cad.cea.fr

CEFDA04-1134

---

**Task Title: TW4-TMSC-BARBEN: BENDING STRAIN EFFECTS OF SINGLE STRANDS**  
**Study of bending strain effect on critical properties of Nb<sub>3</sub>Sn strands jacketed with stainless steel for various bending amplitudes and temperatures**

---

## INTRODUCTION

---

This action is part of a global R&D program extension devoted to the Nb<sub>3</sub>Sn material. This task aims at investigating a possible influence of bending strain on strand performances. In order to perform tests on strands in relevant conditions to that occurring in a cable-in-conduit conductor, the tested samples will use jacketed single strands. For this 316L stainless steel tubes will be used for the jacket.

The bending efforts will be imposed by changing curvature radius of the jacketed strand (practically changing support mandrels radius).

Three main parameters will be explored:

1. the bending strain applied, typically for a maximum bending strain of 0.25 % and 0.5 % on the filamentary zone,
2. the strand structural parameters (manufacturer i.e. process, filaments twist pitch), in order to evaluate the reliability of previously developed models [1],
3. the temperature (no bending applied in these conditions).

Practically this work will be done in collaboration with ENEA Frascati (Italy). Critical properties of jacketed strands at T = 4.2 K and B = 12 T will be measured in an ENEA dedicated facility. The actions are globally shared as follows:

In a first step CEA should define on a typical jacketed strand a method for imposing a controlled bending strain. All needed tools and all method options should be performed at CEA except for the jacketed strand provided by ENEA. The qualification of the method will derive from comparative tests in the ENEA facility.

In second step CEA transfer the know-how to ENEA, which is in charge of the defined supports manufacturing and all samples handling (with various manufacturers and twist pitches). All critical current measurements will be performed in the ENEA facility.

In a third step CEA will characterize a defined jacketed strand at variable temperature with no bending applied. The final analysis of all experimental results will be achieved commonly between CEA and ENEA.

## 2004 ACTIVITIES

---

### BENDING TOOLS AND PROCEDURE

#### Design

As mentioned earlier the bending will be applied by modifying sample curvature radius on its support mandrel. Two options are possible for bending: expansion (radius increase) or reduction (radius decrease). Besides, the strand ends for current injection may be unjacketed before or after heat treatment.

CEA decided to test each of those methods and the choice will be made after comparison of J<sub>c</sub>(4.2 K, 12 T).

At CEA the heat treatment and testing mandrels have been designed for expansion and reduction options, trying to avoid any extra or uncontrolled strain (mainly torsion).

For reduction method the heat treatment is performed on a high diameter mandrel and transferred to the testing mandrel at low diameter (figure 1 left part) by help of an adapted set-up.

For expansion method, the transfer is to be held by an intermediate cone with specifically designed grooves to avoid torsion and follow as well as possible the natural spring expanding.

#### Manufacture

Manufacturing have been completed in early December. Jacketed strands were also provided at that date, allowing early handling tests.

Some pictures of the support pieces can be seen in figure 1.

The next action program is the completion of the additional tools required for the transfer method.

Then reduction method will be tested first on dummy samples after an ITER-like heat treatment. Basically three points will be investigated : jacket removal phase without damaging strand, soldering onto Cu pieces, the transfer and the maintain of strand onto the mandrel. This is expected to be completed about march 2005.



Figure 1 : Support systems for jacketed strands  
Left picture is for the reduction method and right picture is for the expansion method.

**EXPERIMENT FOR VARIABLE TEMPERATURE TESTS**

The Variable Temperature Cryostat (VTC) already used for single strands characterization [2, 3] is required for the study of jacketed strands critical properties at various temperatures. A picture of a superconducting strand wounded onto the VTC test mandrel is shown in figure 2.

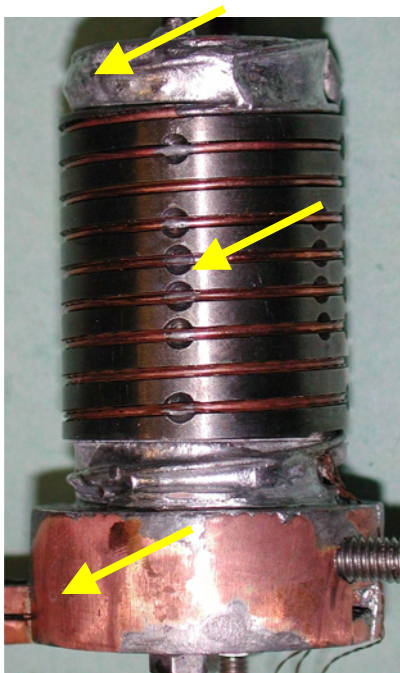


Figure 2 : Equipped mandrel for the VTC qualification at high temperature - The location of the three temperature probes (not visible on the picture) are shown by arrows

The system was recently upgraded as the regulation system was coupled with the acquisition system by adding a regulation module to the DAS Labview program (National Instruments). The qualification of this new configuration was quasi achieved with a testing campaign [4] in GHMFL laboratory (CNRS, Grenoble) performed in December 2004.

An example of temperature ramp obtained is given in figure 3 showing a satisfactory temperature homogeneity (< 30 mK).

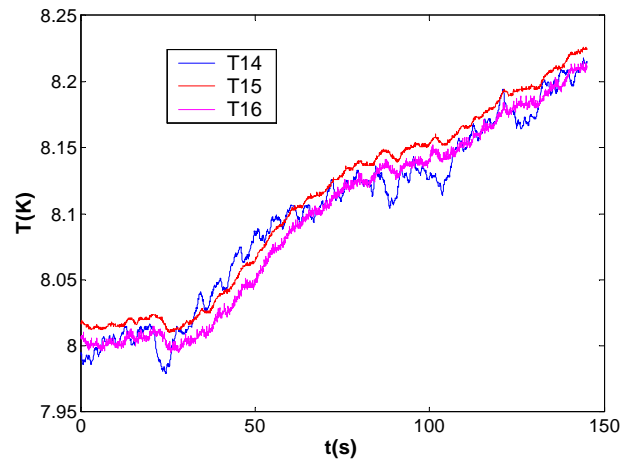


Figure 3 : Example of controlled temperature ramp performed with the Labview regulation system installed on the VTC set-up. The T14, T15 and T16 temperature probes are located at top, center and bottom of the mandrel

However an extra campaign would be required for statistics and for use with the stainless steel pieces required in the task, planned in CEA Cadarache between march and april 2005. The final measurements at GHMFL should occur before summer 2005.

**CONCLUSION**

During the year 2004 the BARBEN actions progressed as follows:

- The jacketed strands transfer method was defined with 4 options to be compared.
- The adapted mandrels for heat treatment and for measurements were designed and manufactured.
- The first OST superconducting strand was jacketed.
- The upgraded VTC facility was qualification was nearly achieved with a campaign in GHMFL (CNRS, Grenoble).

All remaining actions on this task are planned to be completed during the year 2005.

## REFERENCES

---

- [1] J.W. Ekin - Current transfer in multifilamentary superconductors. I. Theory, J. Appl. Phys. Vol. 49 n°6, pp.3406-3409 (1978).
- [2] L. Zani, JP. Serries, H. Cloez, Z. Bej and E. Mossang - Characterization of transport properties variations with magnetic field and temperature of ITER-candidate NbTi strands, Physica C 372-376 pp. 1311-1314 (2002).
- [3] L. Zani, E. Mossang, M. Tena, J-P. Serries and H. Cloez -  $J_c(B,T)$  characterization of NbTi strands used in ITER PF-relevant Insert and Full-scale sample, presented at ASC2004 (2004).

## REPORTS AND PUBLICATIONS

---

- [4] L. Zani, M. Tena, H. Cloez, J-P. Serries, S. Girard - Tâche BARBEN : qualification du système de régulation du Cryostat à température Variable en configuration Nb<sub>3</sub>Sn, Note AIM/NTT-2005.003, (2005).

## TASK LEADER

---

Louis ZANI

DSM/DRFC/STEP

CEA-Cadarache

F-13108 Saint-Paul-Lez-Durance Cedex

Tél. : 33 4 42 25 29 67

Fax : 33 4 42 25 26 61

E-mail : louis.zani@cea.fr



## TW1-TMC-CODES

---

### Task Title: **DESIGN AND INTERPRETATION CODES** **Determination of thermohydraulic properties of cable-in-conduit conductors with a central channel**

---

#### INTRODUCTION

---

The thermohydraulics of cable-in-conduit conductors has to be well described, to allow proper design of the cryogenic system of ITER. The pressure drop of central channels representative of ITER has to be characterized. The recooling time of forced flow coils and the quench behaviour are driven by the heat transfer coefficient between the annular area and the central channel. This coefficient can hardly be theoretically evaluated; only experiments, possible at room temperature, can bring information about this coefficient.

These experimental activities are led at CEA Cadarache on dedicated facilities in collaboration with Politecnico di Torino.

#### 2004 ACTIVITIES

---

##### MEASUREMENT OF CENTRAL SPIRAL PRESSURE DROP

The pressure drop measurements were carried out on central spiral samples tested in the OTHELLO test facility at Cadarache. The experimental work was completed in 2003. Following the previous qualification of the TFMC spirals (specially Showa and Cortaillod with inner and outer diameters equals to 10 and 12 mm respectively), with the determination of the friction factor as a function of the Reynolds Number, it seemed pertinent to characterize other spirals with different geometrical (hydraulic) parameter and to estimate the influence of these parameter on the friction factor.

New spirals were supplied by the Mécaessorts company, with inner and outer diameter respectively of 6 and 8 mm on one hand and 8 and 10 mm on the other hand. These spirals have been characterized and the friction factors determined experimentally in the OTHELLO test facility with pressurized nitrogen. Some friction factor fits indicating the tendency with the Reynolds Number could be given. The important results of these experimental measurements is that the S8, C8 and I8 spirals show a much higher friction factor –nearly 0.4- than the TFMC central spiral which was only between 0.1 and 0.2.

$$\text{Spiral I8} \quad f_{EU,I8} = 0.54 \cdot RE^{-0.03}$$

$$\text{Spiral I10} \quad f_{EU,I10} = 0.36 \cdot RE^{-0.038}$$

Nevertheless, the influence of the geometrical parameters considered is difficult to evaluate without a parametric study. The present design of the ITER Toroidal Field Cable In Conduit Conductor includes a central spiral with inner and outer diameters of 7 and 9 mm respectively (with a gap to twist pitch length ratio equal to 0.5). A first approximation of the friction factor of this type of spiral could be given, by linear interpolation of the previously tested central spirals results.

$$\text{Spiral I9} \quad f_{EU,I9} = 0.45 \cdot RE^{-0.034} \quad (\text{interpolated})$$

Nevertheless, experimental tests (in the OTHELLO test facility) of such spirals samples would be very useful for a more precise determination of the friction factor and could be used for further parametric study and the assessment of refined theoretical models of the central spiral hydraulics.

##### EXPERIMENTAL EVALUATION OF THE HEAT TRANSFER COEFFICIENT BETWEEN ANNULAR AND CENTRAL CHANNELS OF ITER CONDUCTORS

An important parameter of the ITER magnets cryogenic cooling system is the recooling time. The cable-in-conduit conductor (CICC) being cooled by a high speed flow (1m/s) in the central channel in parallel with a slow speed flow (0.1m/s) in the annular area, the recooling time is depending on:

- The heat transfer coefficient between the two parallel channels.
- The fluid velocity in each channel.

A numerical and analytical model was developed to predict the temperature evolution along a CICC after a temperature step at the inlet. This model relies on the heat transfer coefficient between the two parallel channels, but also the heat transfer coefficient between the jacket and the water.

To evaluate this heat transfer coefficient, a new facility named HECOL and operating in relevant Reynolds number up to 70°C in pressurised water was built in 2003. A sample of TFMC conductor with Cortaillod spiral specially instrumented was used for the tests (figure 1).

After the first test campaigns, performed in collaboration with POLITO, experimental heat transfer coefficients have been determined. An upgrading of the facility was performed and a new test campaign showed poor accuracy of the temperature measurements.

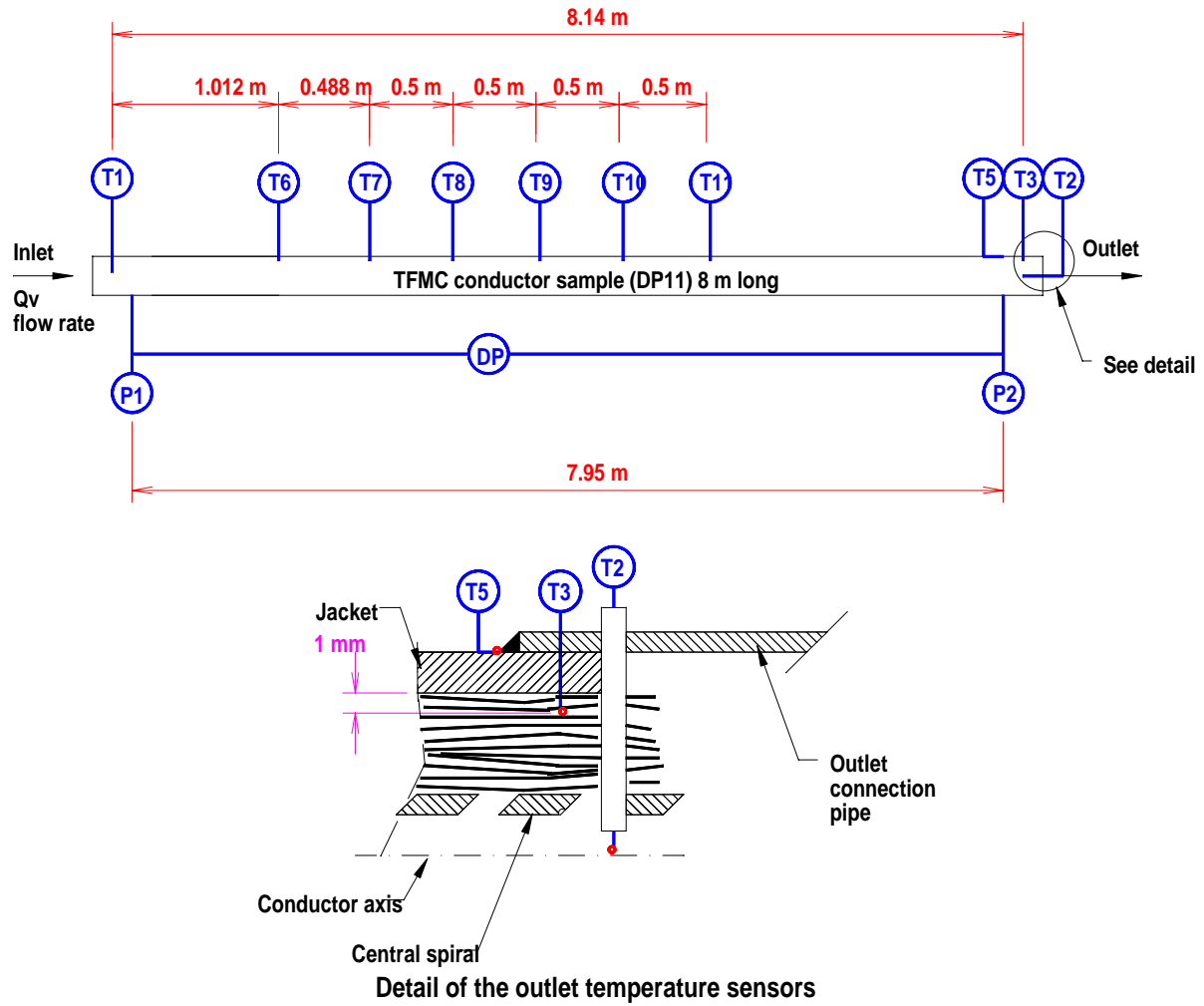


Figure 1 : Sample instrumentation for heat transfer measurement

At the beginning of 2004, an upgraded version of the data acquisition system providing more accuracy was installed, the conductor sample was insulated and a calibration of all the temperature sensors was performed. A final test campaign was engaged with transient tests by imposing a temperature step at the inlet. The corrected temperature evolution was measured at different location along the conductor (figure 2).

For the evaluation of the global heat exchange coefficient in CICC, the convective heat exchange was first determined with the Reynolds-Colburn analogy. A steady state model, with a characteristic space constant  $\Lambda$  was then developed and presented. This parameter governs the mixing temperature between the two channels of the CICC and permits to express the annular channel temperature as well as the central hole channel temperature in a heated zone and non-heated zone.

From the measurement of the characteristic space constant on our sample and applying this model within the HECOL test conditions, the global heat exchange coefficient of ITER CICC type conductor was determined between 15000 and 30000 W/m<sup>2</sup>.K as an increasing function of the fluid volumetric mass flow rate (0.2 up to 1.8 l/s) and with the temperature (or Prandtl number) as parameter.

The convective heat exchange coefficient in each channel ( $h_{convb}$  and  $h_{convh}$ ) as well as the bundle mass flow ratio  $\alpha$  and the characteristic space constant  $\Lambda$  could also be determined.

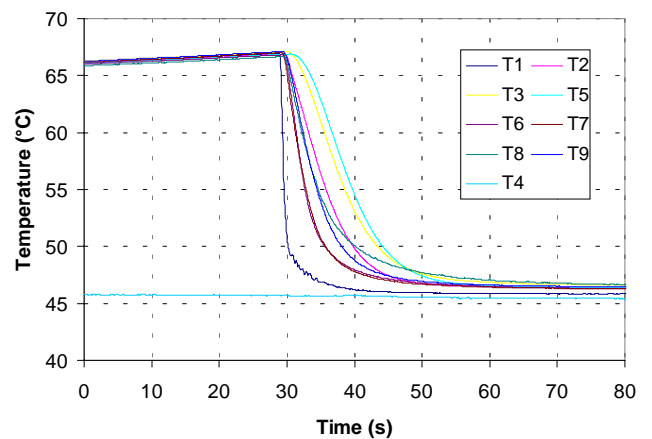


Figure 2 : Corrected temperatures for a typical shot from 65 down to 45 °C at 1.5 l/s

The results obtained with a corresponding thermohydraulic transient numerical tool (code M&M) confirm the global heat transfer coefficient range presented with the steady state model application.

Furthermore, the steady state characteristic space constant model, with the corresponding heat transfer correlation were applied to cold tests, specially the PF-FSJS. A good agreement of the calculated analytical value of the space constant on one hand and the experiments on the other hand was observed.. Typically, the global heat transfer coefficient  $h_{\text{perfor}}$  for the PF-FSJS is between 300 and 450 W/m<sup>2</sup>.K. For the TFMC tests, in the TOSKA test facility, the global heat transfer coefficient  $h_{\text{perfor}}$  is comprised between 400 and 600 W/m<sup>2</sup>.K.

As for the PF-FSJS experiment, it would be interesting to perform some steady state tests in the HECOL test facility in order to verify the characteristic space constant predicted by the model with experimental results by measurements of the temperature profile along the conductor. These steady state tests would be worthwhile by varying the mass flow rate (Reynolds number), the water temperature (Prandtl number) and the sensor locations (radial direction); with heating on a determined length, they also are representative of what happens on the CICC during nuclear heating of the TF Coils.

## CONCLUSION

---

During the year 2004, an analysis of the tests of seven central spirals relevant to ITER type conductors tested in GN2 at room temperature in the OTHELLO test facility during the year 2003 was carried out. This analysis led to conclude that the smaller diameter spirals (8 mm) presents friction factor about twice higher than the old larger ITER spirals (12 mm). An interpolation led to predict the friction factor of the new ITER spirals design. However, a set of spirals much closer to the new ITER spiral design would be very useful for a more precise determination of the friction factor and could be used for further parametric study and the assessment of refined theoretical models of the central spiral hydraulics.

For the evaluation of the heat transfer coefficient between annular area and central channel of ITER cable-in-conduit conductors, the dedicated experimental facility HECOL which operates in pressurized water at 70°C was upgraded and the accuracy of the last results was satisfactory. A steady state model, with a characteristic space constant  $\Lambda$  was then developed and has confirm the results obtained with a corresponding thermohydraulic transient numerical tool (code M&M) on the global heat transfer coefficient range.

The steady state characteristic space constant model, with the corresponding heat transfer correlation were applied to cold tests. A good agreement of the calculated analytical value of the space constant on one hand and the experiments on the other hand was observed.

It was suggested to perform some steady state tests in HECOL to verify the characteristic space constant predicted by the model. A final report on all these task activities was issued [1].

## REPORTS AND PUBLICATIONS

---

- [1] Task CODES: Deliverable 4, Experimental investigation to determine the heat transfer coefficient between annular area and the central channel of ITER-FEAT conductors as an input to codes development, S. Nicollet, H. Cloez, P. Decool, J.L. Duchateau, A. Martinez, M. Tena, B. Renard, J.P. Serries.

## TASK LEADER

---

Patrick DECOOL

DSM/DRFC/STEP

CEA-Cadarache

F-13108 Saint-Paul-Lez-Durance Cedex

Tél. : 33 4 42 25 43 50

Fax : 33 4 42 25 26 61

E-mail : [decool@drfc.cad.cea.fr](mailto:decool@drfc.cad.cea.fr)



**TW1-TMS-PFCITE**

**Task Title: POLOIDAL FIELD CONDUCTOR INSERT (PFCI)**

**INTRODUCTION**

Within the framework of the ITER project, the EU PT has been asked to manufacture a model coil, called Poloidal Field Conductor Insert (PFCI), to be tested in the JAERI test facility in Naka, Japan. The development, manufacture and testing of the PFCI coil shall support the design of the ITER PF conductors and coils.

The main objective of the model coil tests is to get a complete knowledge and understanding of the behaviour of high current NbTi cable-in-conduit conductors and related joints under operating conditions as foreseen for the ITER Poloidal Field (PF1 & PF6) coils. A conductor representative of the ITER PF1 & PF6 coils shall be wound in a single layer coil and equipped with a numerous instrumentation composed of inductive heaters, voltage taps, temperature and pressure sensors, strain gauges, etc. The coil shall be inserted inside the bore of the ITER CS Model Coil (CSMC) at the JAERI test facility in Naka (Japan) and tested in 2005.

The coil winding features a square conductor with a NbTi superconducting cable inserted in a thick wall, stainless steel jacket. Superconducting joints are required to connect the coil to the current leads. Another joint is located at an intermediate location in the winding to test an ITER-relevant joint under magnetic field operating conditions similar to the ones foreseen in the ITER PF coils. The upper and lower terminations shall connect the winding to the existing CSMC Insert busbar system of the Naka facility, as well as to the cryogen supplies.

The work of CEA within task PFCITE covers the following items:

- Participation to definition and review of the test procedure.
- Participation to operational campaigns of the PFCI and reporting of the results.
- Analysis of the results, including thermo-hydraulic, electro-magnetic, and structural simulations of the real operating conditions of the coil.
- Analysis of impact of results on ITER PF coils design.

The NbTi cable for the PFCI was delivered to Ansaldo in August 2002 from the Russian Federation, the jacketing was completed at Ansaldo in June 2003. Fabrication of the coil is running at Tesla (UK) under monitoring by EFDA/CSU Garching, however problems in the joint design and fabrication were discovered during the tests of the PFCI-FSJS in SULTAN.

A new R&D was then launched at Tesla to get an acceptable joint resistance (i.e.  $\leq 5 \text{ n}\Omega$ ) and new tests by CRPP on small pieces of improved joint look satisfactory. The coil (including impregnation) should be completed by mid March 2005. The fabrication of the mechanical structure is carried out in parallel (expected to be ready in Feb. 2005). Final acceptance and shipment to the CSMC test facility are foreseen end of March 2005, and assembly in the Naka facility during summer 2005. Testing programme at JAERI should start end of 2005.

**2004 ACTIVITIES**

For 2004, our activities were reduced because of the delay taken in the fabrication of the PFCI at Tesla (UK). The model developed by CEA to predict joint performance under transient (code JUST) was applied to the study of the behaviour of the PFCI intermediate joint in the reference pulse field scenario. The JUST code is now considered as one of the tools to be used for the analysis of the PFCI test results [1].

The reference pulse field scenario consists of a discharge of the CSMC from 21.2 kA to zero, with a decay time constant of 20 s, without current in the PFCI. Figure 1 shows the power dissipated in the intermediate joint during the discharge, with a separation of the contributions due to the radial field variation and to the axial field variation. It can be seen in this figure that the two contributions are almost equivalent in term of peak power which is quite different in the ITER PF6 joints due to a relative higher radial field variation.

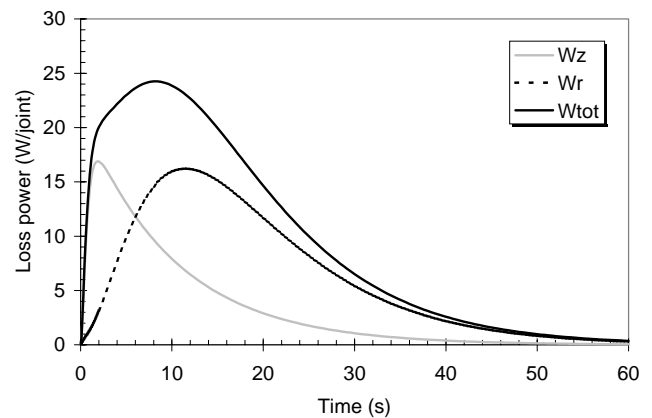


*Figure 1 : Computed loss power in the ITER PFCI intermediate joint during a CSMC discharge from 21.2 kA within 20 s: contribution of radial field variation (Wr), contribution of axial field variation (Wz), total loss power (Wtot)*

The helium outlet temperature at the joint is shown in figure 2, where it can be seen that the temperature increases of about 1 K at the maximum. Figure 3 gives the minimum temperature margin in the joint during this scenario. In figure 3, DTcs\_o corresponds to the margin with the average current (here equal to 0) in the strands, while DTcs+ includes the loop current flowing through the strands.

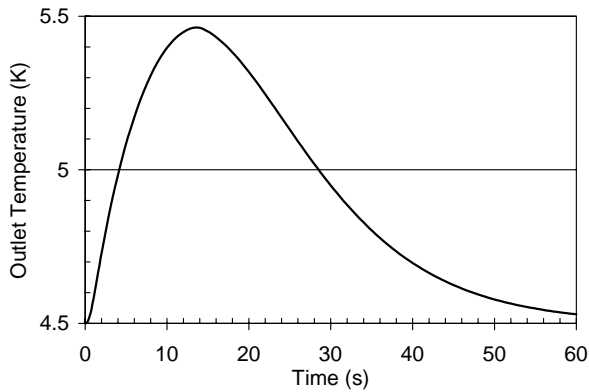


Figure 2 : Computed evolution of helium outlet temperature in PFCI intermediate joint during a CSMC discharge from 21.2 kA within 20 s

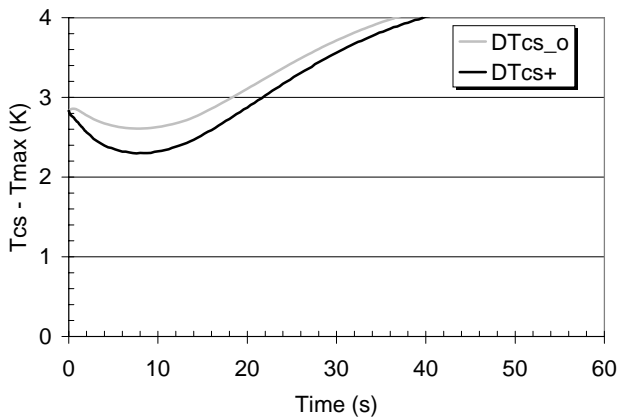


Figure 3 : Computed evolution of temperature margin in PFCI intermediate joint during a CSMC discharge from 21.2 kA within 20 s (DTcs\_o with transport current only, DTcs+ with adding loop current)

## CONCLUSIONS

The Poloidal Field Conductor Insert is under fabrication in industry and should be tested in the CSMC facility (Naka, Japan) end of 2005. CEA is participating in the definitions of both the PFCI instrumentation and the testing programme. The model developed by CEA (code JUST) for the analysis of the ITER PF joint behaviours was applied to the PFCI intermediate joint during the reference pulse field scenario.

This analysis has shown that radial and axial field variation will give equivalent contributions at variance with the ITER PF6 joints in which the former is predominant, and that the helium temperature rise will be quite measurable ( $\approx 1$  K). This model is a part of the useful tools to be used for the assessment of the testing programme as well as for the PFCI test analysis.

## REFERENCES

- [1] R. Zanino et al - Preparation of the ITER Poloidal Field Conductor Insert (PFCI) Test - presented at the 2004 Applied Superconductivity Conference, October 3-8 Jacksonville FL (USA).

## TASK LEADER

Daniel CIAZYNSKI

DSM/DRFC  
CEA-Cadarache  
F-13108 Saint-Paul-Lez-Durance Cedex

Tél. : 33 4 42 25 42 18  
Fax : 33 4 42 25 26 61

E-mail : daniel.ciazynski@cea.fr

## TW2-TMST-TOSKA

### Task Title: TFMC TESTING WITH THE LCT COIL

#### INTRODUCTION

In the framework of the TOSKA Task, CEA was asked by EFDA to participate to the testing of the ITER Poloidal Field Conductor Insert Full Size Joint sample (PFIS) in the SULTAN facility at CRPP in Villigen. The PFIS was tested in 2004.

This sample aimed to test electrically both the conductor and the joints used in the Poloidal Field Coil Insert (PFCI) to be tested in the CSMC facility (JAERI, Naka, Japan). The PFIS as well as the PFCI were designed by EFDA which also followed up the fabrication in industry at TESLA (UK).

The two conductor legs are identical except that one leg (W) has the regular ITER geometry with steel wraps around the last but one cabling stage (petal), while the other leg (NW) has no such wraps and thus requires a slightly higher compaction to keep the final void fractions equivalent (see Figures 1a and 1b). The conductor with wraps is identical to the one used in the fabrication of the PFCI.

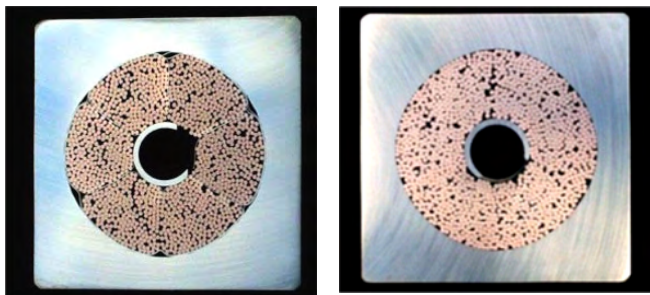


Figure 1a : Cross-section of PFIS left leg conductor (with wraps)

Figure 1b : Cross-section of PFIS right leg conductor (w/o wraps)

Both legs make use of the same NbTi strand, fabricated by Bochvar VNIINM (Moscow, Russia). This strand is 0.73 mm in diameter (see table 1).

#### 2004 ACTIVITIES

##### MEASUREMENT OF RRR ON PFIS JOINT SLEEVES

During the first PFIS Test Group meeting, CEA pointed out that the electrical resistivity of the joint copper sleeves was not known. A high resistivity of the CuCrZr could be expected with a significant impact on the joint resistance. CEA and CRPP received each a piece of joint sleeve from Tesla for measurement.

The results are summed up in table 2.

Table 2 : Results of resistance measurements on a piece of PFIS copper sleeve

| T (K) | Current (A) | Voltage drop (μV) | Resistance (μΩ) | Resistivity (10 <sup>-8</sup> Ω.m) |
|-------|-------------|-------------------|-----------------|------------------------------------|
| 300   | 7.46        | 1059 ± 12         | 142.0 ± 1.6     | 2.40 ± 0.03                        |
| 4.2   | 74.5        | 3920 ± 65         | 52.6 ± 0.9      | 0.891 ± 0.015                      |

The residual resistivity RRR ratio is therefore:  $RRR = 2.69 \pm 0.02$ , i.e.  $RRR \sim 2-3$ . The CEA measurements are also consistent with the CRPP measurements giving a resistivity of about  $9.5 \times 10^{-8} \Omega.m$  at 4.2 K and a RRR of about 2.6.

The contribution to the joint resistance can be estimated to  $3.7 \cdot 10^{-9} \Omega$ , therefore not negligible when dealing with joint resistance within the nΩ range.

Table 1 : PFIS and ITER PF coil conductor characteristics

|  | PFIS <sub>W</sub>   | PFIS <sub>NW</sub>  | ITER PF1&6        |
|--|---------------------|---------------------|-------------------|
| NbTi strand diameter (Ni coated), mm   | 0.73                | 0.73                | 0.73              |
| Ratio of copper to non copper sections | 1.41                | 1.41                | 1.6               |
| Cabling pattern                        | (3x4x4x5x6)         | (3x4x4x5x6)         | (3x4x4x5x6)       |
| Number of strands                      | 1440                | 1440                | 1440              |
| Cu cross section, mm <sup>2</sup>      | 353                 | 353                 | 371               |
| Non-Cu cross section, mm <sup>2</sup>  | 250                 | 250                 | 232               |
| Cable space diameter, mm               | 37.53               | 36.89               | 38.2              |
| Cabling twist pitches, mm              | 42/86/122/158/≈ 500 | 42/86/122/158/≈ 530 | 45/85/125/165/425 |
| Steel spiral for central channel, mm   | 10 x 12             | 10 x 12             | 10 x 12           |
| Estimated void fraction, %             | 33.5                | 34.3                | 34.5              |
| Outer conductor size, mm×mm            | 50.35 x 50.45       | 49.82 x 49.78       | 53.8x53.8         |

## JOINT RESISTANCE

The bottom joint resistance was found to be unexpectedly high during the conductor test, this was also the case for the two upper termination resistances, with one of them (the left one) being particularly high. The measured values are reported below:

- Hairpin (bottom) joint resistance  $\approx 10 \text{ n}\Omega$
- PFIS<sub>W</sub> (left leg) termination resistance  $\approx 18 \text{ n}\Omega$
- PFIS<sub>NW</sub> (right leg) termination resistance  $\approx 6 \text{ n}\Omega$

These high values cannot be explained only by the use of high resistivity copper sleeves and likely a high (and not reproducible) resistance between strands and copper sleeve has to be considered. Such a high interface resistance is related to the manufacturing process of the joint.

The high bottom joint resistance played a negative effect in the test of the conductor legs by preventing to operate the conductors at low temperature and high current, and by perturbing significantly the current sharing experiment (non linear increase of current  $\rightarrow$  non constant inductive voltage, and increase of operating temperature as current increases).

Finally, the tests of the bottom joint in SULTAN (usually performed by lifting up the sample) were cancelled due to the poor behaviour of this joint.

## ELECTRICAL TESTS

The PFIS conductor performances have been found to be lower than expected by any models for both legs. Better predictions are obtained using the CEA strand data compared to the VNIINM data (i.e. using lower strand performances) [1]. CEA performed a comparison of the results provided by different models issued by different institutions and laboratories [2].

Dramatic current limitation (quench) can be explained by highly uneven current distribution among petals as well as among strands inside petals.

Uniformity can be improved by current redistribution among petals and strands which can explain the better stability of the unwrapped conductor leg and the better performances measured on both legs at low current. However, no model is presently capable to explain the full behaviour of the PFIS conductors.

The interpolation of the PFIS DC experimental results, rescaled with the NbTi area with respect to the ITER PF coils (at  $B_{\max} = 6 \text{ T}$ ,  $T_{\text{op}} = 5.0 \text{ K}$ ) are compared to the PF-FSJS conductor test results and to the ITER operating specifications in table 3.

It can be seen in this table, that the PF-FSJS conductors had better performances than the PFIS (the worst PF-FSJS leg being better than the best PFIS leg), although the PF-FSJS itself did not reach the ITER operating specifications. It should be also noted that the PF-FSJS conductors have their original ITER wraps.

The explanations for these poor performances lie in the lower strand properties (as compared to ITER operating specifications) and to highly uneven current distribution in the PFIS, likely due to an uneven contact resistance distribution between cable and copper sleeves, also related to a high joint resistance.

*Table 3 : Comparisons between sample performances and ITER PF coil specifications*

| Conductor                              | PFIS wrapped | PFIS unwrapped | PF-FSJS EM leg | PF-FSJS Alstom leg | ITER PF1&6  |
|--|--------------|----------------|----------------|--------------------|-------------|
| $T_q \text{ (K)}$                      | 5.80         | 6.05           | 6.25           | 6.40               | 6.50        |
| $\Delta T_{\text{margin}} \text{ (K)}$ | <b>0.80</b>  | <b>1.05</b>    | <b>1.25</b>    | <b>1.40</b>        | <b>1.50</b> |

## THERMOHYDRAULICAL TESTS

The central channel of Cable in Conduit conductors is self-justified to reduce the cryogenic power associated with helium circulation and hence the operating costs. But the inhomogeneity in the He flow within the cable, brings complexity and a discrepancy in temperature between the central and annular channels under heat load. The thermohydraulics of cable samples can be explored at low temperatures in the Sultan facility at CRPP/Villigen, using the same sample (PFIS) as for the superconductivity critical properties investigations.

Due to the thermometer layout of the PFIS, this study was carried out using only the AC loss deposition provided by a dipole on a conductor section. The two legs of the PFIS are asymmetric because the superconducting strand petals are directly inserted in the jacket in the right leg, whereas they are wrapped in stainless steel tape in the left leg (see figures 1a and 1 b). The eddy currents created by the AC field and generating heat have a reduced intensity on the left leg relevant to the ITER conductor design.

Results and theoretical expectations according to the steady state model developed by CEA [3] for heat transfer coefficients are summarized in table 4 for each leg at 10 g/s with AC heating.

Though this kind of heating is instructive given its representativeness of AC losses in the final coil use, these experiments do not provide accurate thermal results concerning the space constant  $\Lambda$ , and associated heat transfer coefficient  $h$  between the two conductor channels. The reason is mainly that the exact length of the heat deposition and its homogeneity is uncertain.

On the PFIS experiments, AC losses heat up the right leg without wrappings more than the left, as expected. The minimum power used in these 10 g/s experiments is 25 W/m assuming a deposition length of 0.4 m. The left leg temperatures heat up especially less than expected. The PFIS AC loss upstream temperature is slightly rising even at very low power, which is disturbing and may be also a sign of wide heating length.

Table 4 : PFIS AC power, characteristic length  $\Lambda$  and resulting heat transfers at 10g/s

| Expected values                              | $\Lambda=0.48$ m                         |  |   |   |
|--|--|--|---|---|
|  | h=418 W/m <sup>2</sup> K<br>hp=13.1 W/mK |  |   |   |
| AC frequency                                 | 4 Hz                                     | 3 Hz                                     | 2 Hz                                    | 1 Hz                                    |
| Left leg W=<br>(wraps) $\Lambda$ =<br>h=     | 37 W<br>0.7 m<br>285 W/m <sup>2</sup> K  | 25 W<br>0.75 m<br>265 W/m <sup>2</sup> K | 15 W<br>0.8 m<br>250 W/m <sup>2</sup> K | 10 W<br>1 m<br>200 W/m <sup>2</sup> K   |
| Right leg W=<br>(no wraps) $\Lambda$ =<br>h= | 54 W<br>0.35 m<br>570 W/m <sup>2</sup> K | 36 W<br>0.35 m<br>570 W/m <sup>2</sup> K | 21 W<br>0.4 m<br>500 W/m <sup>2</sup> K | 14 W<br>0.4 m<br>500 W/m <sup>2</sup> K |

It is not possible to experimentally evaluate the respective channel mass flow rates. We can evaluate channel mass flow balance, but there remains some uncertainty in the empirical law used. Similarly, it is not possible to evaluate mass exchange between annular and central channels. Of course the respective mass flows strongly influence physical phenomena and experimental evaluation of heat transfer rates.

The next conductor tests in Sultan will be instrumented with an annular heater on the conductor and thermometers in an appropriate way similar to the PF-FSJS configuration in order to have enough close downstream data and derive thermal parameters in a more accurate way.

## CONCLUSION

In the framework of the TW2-TMST-TOSKA task, CEA has participated to the tests and the analysis of the PF Insert Sample (PFIS). Final report has been delivered to EFDA [4].

Two campaigns have been devoted to these tests: one for electrical tests and the other for thermohydraulic tests.

The first conclusion of these tests is that the measured joint electrical resistance exhibits a very high value (10 n $\Omega$ ), which is far above that measured for the PF-FSJS (1.6 n $\Omega$ ), previous NbTi joint sample developed in Europe in the framework of Task M50. Consequently, the ITER specification (< 2 n $\Omega$ ) is not met and the PFIS joint design is not qualified. The poor electrical performances in comparison with expectation were found partly due to the lower strand properties and partly due to highly uneven current distribution induced at the level of the joint.

As for the thermohydraulic tests, a simple method for estimation of the heat exchange between central channel and annular region has been defined by CEA. This method is based on the observation of the temperature distribution downstream during steady state heating of a piece of conductor. This study delivered heat exchange coefficients which are acceptable for ITER conductors but with insufficient accuracy. This has to be improved by testing further samples with extended instrumentation.

## REFERENCES

- [1] L. Zani et al. - Jc(B,T) characterization of NbTi strands used in ITER PF-relevant insert and full-scale sample - to be published in IEEE Trans. Appl. Supercond., June 2005.
- [2] D. Ciazynski et al. - DC Performances of ITER NbTi Conductors: Models vs. Measurements - to be published in IEEE Trans. Appl. Supercond., June 2005.
- [3] S. Nicollet et al. - Evaluation of the ITER cable-in-conduit conductor heat transfer - presented at 20th Int. Cryo. Eng. Conf. Beijing, 2004.
- [4] J.L. Duchateau et al. - Task TW2-TMST-TOSKA : Deliverable 4 Final report on the testing of a full size joint sample - February 2005 Internal CEA Note AIM/NTT- 2005.002.

## TASK LEADER

J.L. DUCHATEAU

DSM/DRFC/STEP  
CEA-Cadarache  
F-13108 Saint-Paul-Lez-Durance Cedex

Tél. : 33 4 42 25 49 67  
Fax : 33 4 42 25 26 61

E-mail : duchat@drfc.cad.cea.fr



## TW3-TMSC-ELRES

---

### Task Title: **EXPERIMENTAL ASSESSMENT OF THE EFFECT OF ELECTRICAL RESISTANCES ON THE V-I CHARACTERISTICS OF SUPERCONDUCTIVE CABLES**

---

#### INTRODUCTION

---

Task ELRES aims at investigating experimentally the effect of the joint-to-strands resistance values and of different percentages of joint-to-strand connections on the possible variation of the "global" V-I characteristic of a NbTi ITER-type cable, limited at the last but one stage. The samples will have different joint resistances and different fraction of directly connected strands. This activity also investigates the effect of the strand-to-strand transverse resistances, which have been shown to change considerably with cycling and to affect the values of critical current and "n" parameter of s/c cables.

Five joint samples have to be fabricated and tested, each sample contains two different legs which leads to test in fact 10 different legs. The first three joint samples are fabricated using already existing conductor lengths remaining from task M50. Extra conductor lengths (with a different cable void fraction) are fabricated in industry using already existing NbTi strands. The last two joint samples are fabricated using this new conductor. The samples are tested (V-I or V-T characteristics) in the JOSEFA facility at Cadarache. Complementary tests are carried out to measure conductor interstrand resistances.

The task activities can then be summarized as follows:

- Definition of samples and of testing procedure.
- Fabrication of 3 samples using existing (from task M50) conductors.
- Fabrication of new conductor lengths using existing (from task M50) NbTi strands.
- Fabrication of 2 samples using new conductor lengths.
- Test of 5 samples in the JOSEFA test facility (CEA Cadarache).
- Additional characterization of samples (interstrand resistances).

#### 2004 ACTIVITIES

---

The definition of the samples and of the testing procedure was performed in 2003. Also during this year the qualification of detailed manufacturing processes (Nickel removal, insulation of contacts) was carried out. Therefore our activities in 2004 were concentrated on the fabrication and the tests of the samples.

#### FABRICATION OF NEW CONDUCTORS

Using remaining NbTi (Alstom and Europa Metalli) strands from task M50, new conductor lengths (about 2 x 10 m) had to be fabricated to complete task ELRES (these lengths are referred as the ELRES conductors). This fabrication included the multi-stage cabling of 108 strands as well as the compaction of the cable inside a 316L steel jacket. The final void fraction of the cable was fixed to 32 % (slightly lower than the 36 % of the M50 conductors) in agreement with EFDA, so as to introduce a variation in the interstrand resistances.

The manufacture of these two lengths was started at NEXANS in December 2003. Unfortunately, the first samples were rejected since their twist pitches did not fulfil the technical specification for cabling. Some trials with additional lengths of strand provided by CEA were performed at the beginning of year 2004. An acceptable cable geometry was finally reached with regard to the specification and the two additional lengths were produced and delivered to CEA at the end of May 2004.

#### FABRICATION OF FIVE SAMPLES

During the manufacture of the first batch of three samples (using the M50 conductors) some cracks were detected at the TIG weld locations between termination box and cover, and between jacket and termination. These cracks were located on all of the legs being in manufacture, a non-conformity in the materials used was suspected. A first try to re-melt the weld being not successful, investigations and welding tests have shown that this was not due to the jacket or terminations material. A further detailed control of the welding filler rods has finally shown that some rods of high Nickel content filler had been mixed with the regular filler foreseen for the welds.

All the welds were then milled and welded again with the good filler material. Note that in the case of the cover/termination weld, the milling and new welding were performed in parallel in a way not to release the compaction pressure inside the terminal. The visual inspection was then satisfactory. After a dye penetrant test which did not show any crack, a final helium tightness test was performed with vacuum inside the legs and helium atmosphere outside. A leak rate lower than  $10^{-6}$  Pa.m<sup>3</sup>.s<sup>-1</sup> was then measured.

The five samples with their names and characteristics are given in table 1. A picture of the five samples completed is presented in figure 1.

Table 1 : Definition and characteristics of the ELRES samples

| Sample name                    | ELRES-0              | ELRES-1              | ELRES-2              | ELRES-3                | ELRES-4                |
|--------------------------------|----------------------|----------------------|----------------------|------------------------|------------------------|
| Left leg conductor             | Int CuNi strand M50  | Int CuNi strand M50  | Int CuNi strand M50  | Int CuNi strand ELRES  | Int CuNi strand ELRES  |
| Right leg conductor            | Ni plated strand M50 | Ni plated strand M50 | Ni plated strand M50 | Ni plated strand ELRES | Ni plated strand ELRES |
| Joint insulated area (default) | 0 %                  | 25 %                 | 50 %                 | 25 %                   | 50 %                   |

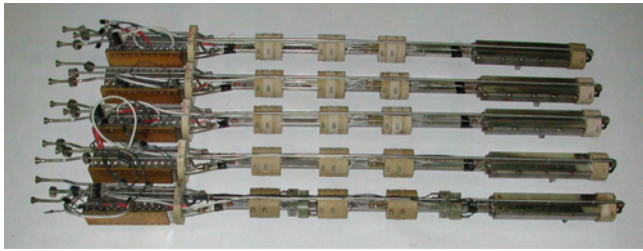


Figure 1 : The five ELRES samples completed and ready for testing

All the left legs make use of the Alstom (AL) NbTi strand with internal CuNi barrier, and all the right legs make use of the Europa Metalli (EM) NbTi strand with Ni plating. The first sample (ELRES-0) is the reference sample, without default in the bottom joint. The other samples have an unconnected length (25% or 50% of total overlapping length) in their bottom joints.

The samples are fully instrumented with 5 temperature sensors (T in figure 2), 14 voltage taps on the conductor legs (RV and LV in figure 2), 2 voltage taps on the bottom joint (RV8 and LV8 in figure 2), 2 pick-up coils for magnetization measurement (RPU1 and LPU1 in figure 2), 4 sets of 4-quadrant Hall probes (2 sets H1-H4 and H5-H8 per leg, see figure 2) for current distribution measurement.

The reference sample ELRES-0 was delivered in September 2004 for testing. The last sample (ELRES-4) was delivered end of November 2004 for testing.

A report on the manufacture of the samples was issued and delivered to EFDA by the end of 2004 [1].

**IMPROVEMENT OF THE JOSEFA FACILITY**

The cryogenic part of the JOSEFA facility was modified (simplification of the hydraulic paths) and repaired. In addition, a new data acquisition system, based on a 16-bit National Instruments system controlled under Labview™, was installed.

This system allows measurements with the required accuracy for plotting V-T or V-I characteristics of samples (the critical field of 10 μV/m corresponds to a voltage drop of 1.7 μV over 170 mm in these experiments). The facility was ready in September 2004 for testing the first sample.

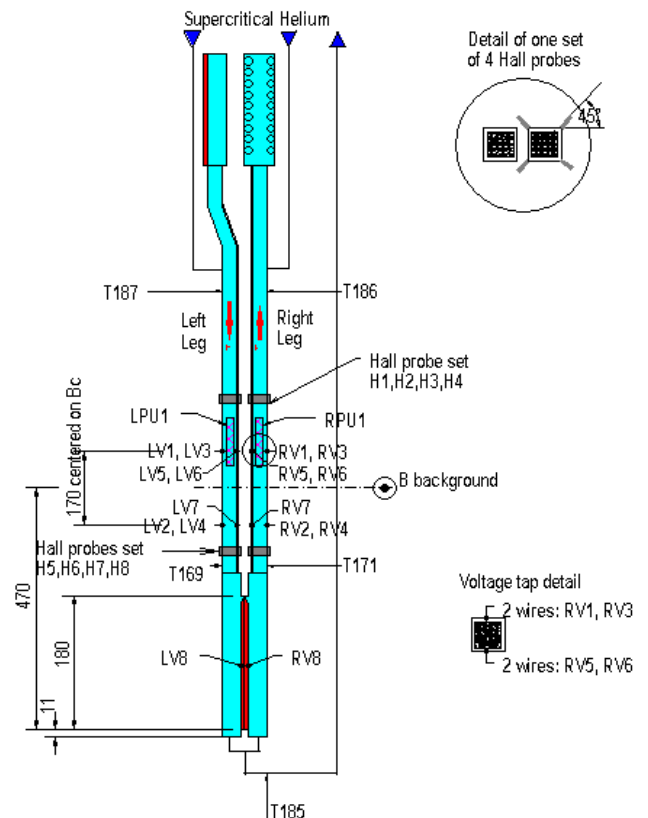


Figure 2 : Scheme of instrumentation of an ELRES sample

**TESTS OF THE SAMPLES**

Only the first reference sample ELRES-0 could be tested in 2004. this test was also the full test of the upgraded JOSEFA facility. The V-T characteristic was preferred to the V-I characteristics because its interpretation is direct, as a matter of fact, the variations of the self field and of the Joule heating in the joints (and in the current leads) tend to pollute the V-I characteristics (i.e. increase of field and temperature with current).

However, it became rapidly obvious that the plot of a correct V-T characteristics required a very low temperature gradient along the tested leg (< 0.05 K between T187 and T169, or between T186 and T171, see figure 2). Indeed, the situation is much more difficult (and much more accurate) in the ELRES samples than in the SULTAN samples, because the electric potential on the jacket is very close to the strand potential due to the lack of wrappings in the conductor.

In the SULTAN samples, the voltage taps located on the steel jacket pick an average (among the strands) cable voltage because of the high electric resistance between the strands and the jacket, then the V-T characteristics almost always looks nice, in fact blurred (there is no significant cross electric gradient). In the ELRES samples, each voltage tap picks a voltage close to a strand voltage, and there may be a high voltage cross gradient on the jacket if the electric field is not uniform along the strands (in case of thermal gradient for example). This phenomenon is particularly clear when comparing the two voltage drops (V1-V2) and (V5-V7) corresponding to taps located on opposite conductor sides.

In the perfect situation (uniform current distribution among strands and uniform temperature profile along the measured length), each strand develops the same voltage drop along the measured length and as a consequence (V1-V2) is equal to (V5-V7). This is the situation generally observed at low transport current (see figure 3). As soon as there is a significant temperature gradient along the measured length, the strands are no more equipotential and (V1-V2) is not equal to (V5-V7), this is the case shown in figure 4, which is generally (but not systematically) observed at higher transport current. A way to smooth the curves is then to consider the average value between these two voltage drops, one then recovers more or less a SULTAN-like experiment (see figure 4 for the effect of averaging on scattered curves). Note that the voltage threshold of 1.7  $\mu\text{V}$  corresponds to the critical electric field criterion of 10  $\mu\text{V}/\text{m}$ .

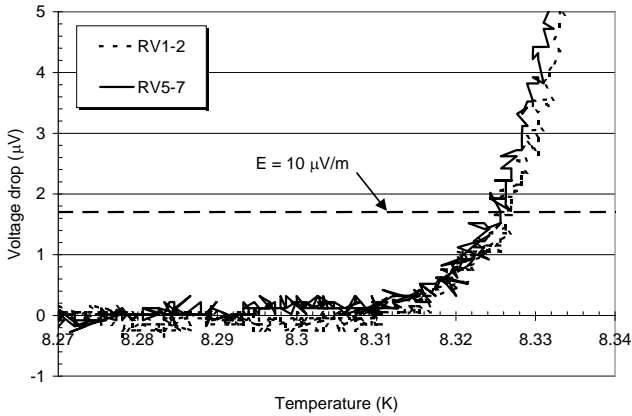


Figure 3 : Measured voltage drops on ELRES-0 at 2 T and 1 kA

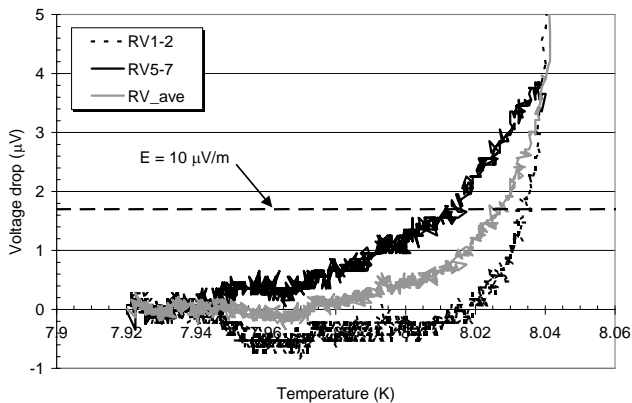


Figure 4 : Measured voltage drops on ELRES-0 at 2 T and 5 kA (RV\_ave is average between RV1-2 and RV5-7)

The ELRES-0 conductor critical current @ 10  $\mu\text{V}/\text{m}$  under a 3.4 T field are plotted in figure 5. Also plotted is the expected performance using the strand characteristics under the same magnetic field (extrapolation from strand experimental range using fitting curves). The surprisingly better performances of the conductors can be explained by some inaccuracy in the extrapolation of the strand performances. Note that the two legs behave similarly which is logical with regard to the similar strand performances. Note also that generally the conductors were stable up to 6 kA at the critical electric field (although limit at 6 kA) and that no degradation of transport properties were observed at variance with the full size NbTi conductors tested in SULTAN (PF-FSJS and PFCI-FSJS).

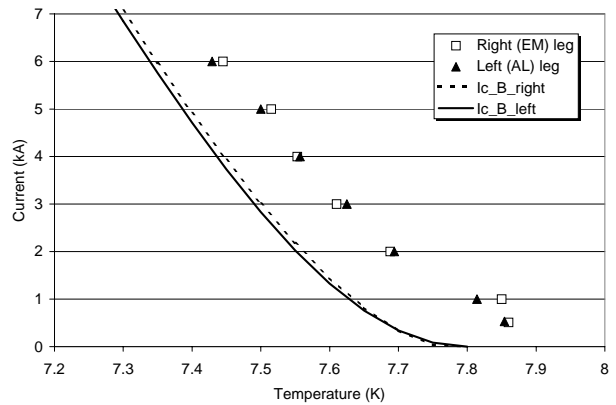


Figure 5 : Critical current on ELRES-0 sample compared to extrapolations from strands ( $I_{c\_B}$ ) at 3.4 T

The half-joint resistance is about 2.9 n $\Omega$  on the left leg while it is about 1.0 n $\Omega$  on the right leg. These values are rather low (extrapolated to below 0.9 and 0.3 n $\Omega$  respectively for a full size joint resistance) which shows that the contacts between strands and copper soles are good. The higher value on the left leg is explained by the internal CuNi barrier which cannot be removed from the strands at variance with the Ni plating.

## CONCLUSIONS

The fabrication of the five ELRES samples (including the two samples with the new conductor delivered by NEXANS) was completed at the end of 2004. the fabrication report was delivered to EFDA in December 2004.

The first reference sample ELRES-0 was tested successfully at the end of 2004, this test was also the test of the full upgraded JOSEFA facility.

The second sample ELRES-1 was tested successfully in January 2005. Due to the maintenance programme on the cryogenic system during the shut down of Tore Supra, helium supply will not be available before mid March 2005. The 3 remaining samples should be tested in the JOSEFA facility between mid March and May 2005. The final report should be delivered by the end of May 2005.

## REPORTS AND PUBLICATIONS

---

- [1] P. DECOOL and H. CLOEZ - Task TW3-TMSC-ELRES : Milestone #2 Manufacturing of Samples (Cable and Joints) - CEA Note DRFC (STEP/GCRY), AIM/NTT-2004.029, December 15, 2004.

## TASK LEADER

---

Daniel CIAZYNSKI

DSM/DRFC  
CEA-Cadarache  
F-13108 Saint-Paul-Lez-Durance Cedex

Tél. : 33 4 42 25 42 18

Fax : 33 4 42 25 26 61

E-mail : [daniel.ciazynski@cea.fr](mailto:daniel.ciazynski@cea.fr)

Not available on line

Not available on line

Not available on line

Not available on line

**TW2-TTBC-001-D01**


---

**Task Title: HELIUM COOLED LITHIUM LEAD -  
TBM DESIGN, INTEGRATION AND ANALYSIS  
Blanket system design and analysis - Integration and testing in ITER**


---

**INTRODUCTION**

In 2002, EU has endorsed the decision to concentrate the work on blanket modules for testing in ITER on a single coolant, helium.

Up to that time, two different coolants were envisaged for the EU Breeding Blankets: i) pressurized water for the Water Cooled Lithium Lead (WCLL) concept and ii) pressurized He for the HCPB concept (Helium-Cooled pebble-Bed).

In this frame, the general objective of the EU Task TW2-TTBC-001-D01 is to develop and optimize (with regard to tritium breeding, heat removal and shielding capability) a Helium Cooled Lithium Lead (HCLL) breeding blanket concept for DEMO and its corresponding Test Blanket Module (TBM) to be tested in ITER.

**2004 ACTIVITIES**

2004 activities mainly concerned the improvement and completion of the TBM engineering design.

After a first design step in which the main structure, its functional features, its mounting sequence and manufacturing characteristics were defined, the second step, relied on the optimization of the design and manufacturing of the module as well as its integration to the supporting frame.

A planning and list of test requirements for the qualification of the HCLL TBM prior to ITER was defined. A preliminary testing programme for the HCLL TBMs in ITER has been proposed on the basis of the foreseen ITER scenario and of the TBM testing strategy and mock-ups test objectives.

**THE HELIUM COOLED LITHIUM LEAD (HCLL) INTEGRAL TBM (IN-TBM): DESIGN AND ANALYSES**

The In-TBM looks alike a generic HCLL breeder blanket module for DEMO. It features a steel box cooled by horizontal multi-passes rectangular cross section channels and closed by top and bottom cooled covers and, in the rear, by 4 steel plates acting also as distributing/collecting chambers for the He coolant. An exploded view of the TBM is shown in the figure 1.

The box is stiffened by poloidal radial and toroidal radial cooled plates (vertical and horizontal stiffening plates, SPs) in order to withstand the internal pressurization at 8 MPa in case of accident (loss of coolant inside the TBM). The grid also stiffens the box against the torques acting on it during disruptions.

The grid forms radial cells in which circulates the multiplier/breeder Pb-Li, so allowing external tritium extraction. In each cell is inserted a breeder cooling unit (BU), ensuring the heat recovering from the breeding zone. Each BU consists of five radial toroidal plates (Cooling Plates, CPs) cooled by internal double U rectangular channels and welded to the BU back plate. Two BU collectors located behind the BU back plate distribute/collect the He circulating in the CPs.

The manifolding back plate is reinforced by stiffening steel rods for pressure withstanding. In the present reference design the rods has a tubular cross-section with larger overall diameter compared to the equivalent full rods. This new design allows either to use the rods as an access to the module body for the instrumentation connections, or to use some of them as thread for the bolts of the attachment system. This tubular rod design presents also the great advantage that structural function (relying on threads and conical surfaces) and tightening function (relying on welding) are decoupled.

One He circuit is envisaged to cool both the FW and the breeder zone. In the DEMO blanket module the "cold" He ( $T_{in} = 300^\circ$ ) cools in parallel the FW and the SPs, recovering all the power deposited as heat flux (HF) on the FW and a small percentage of the nuclear power deposited in the breeder zone (BZ). Then the He passes in the CPs in which it recovers the largest part of the nuclear power deposited in the BZ and finally it exits at  $500^\circ\text{C}$ .

This cooling scheme was adopted also in the first TBM 0, in which the ratio between the thermal power deposited on the FW and the one deposited on the BZ (0.27/0.78) was of the same order as the DEMO one (0.5/2.2). Recently, because of uncertainties on plasma control, ITER Team has requested TBMs to be designed to withstand a surface heat flux of  $0.5 \text{ MWm}^{-2}$ . The He cooling scheme has then been modified in a way that the FW is cooled at first and then the SPs and the CPs are cooled in parallel. This allows to reduce the He temperature at the FW outlet and then the thermal sink temperature so guaranteeing the recovering of the high heat flux on the FW with moderate total He mass flow (see later § Structural and thermo-mechanical analyses).

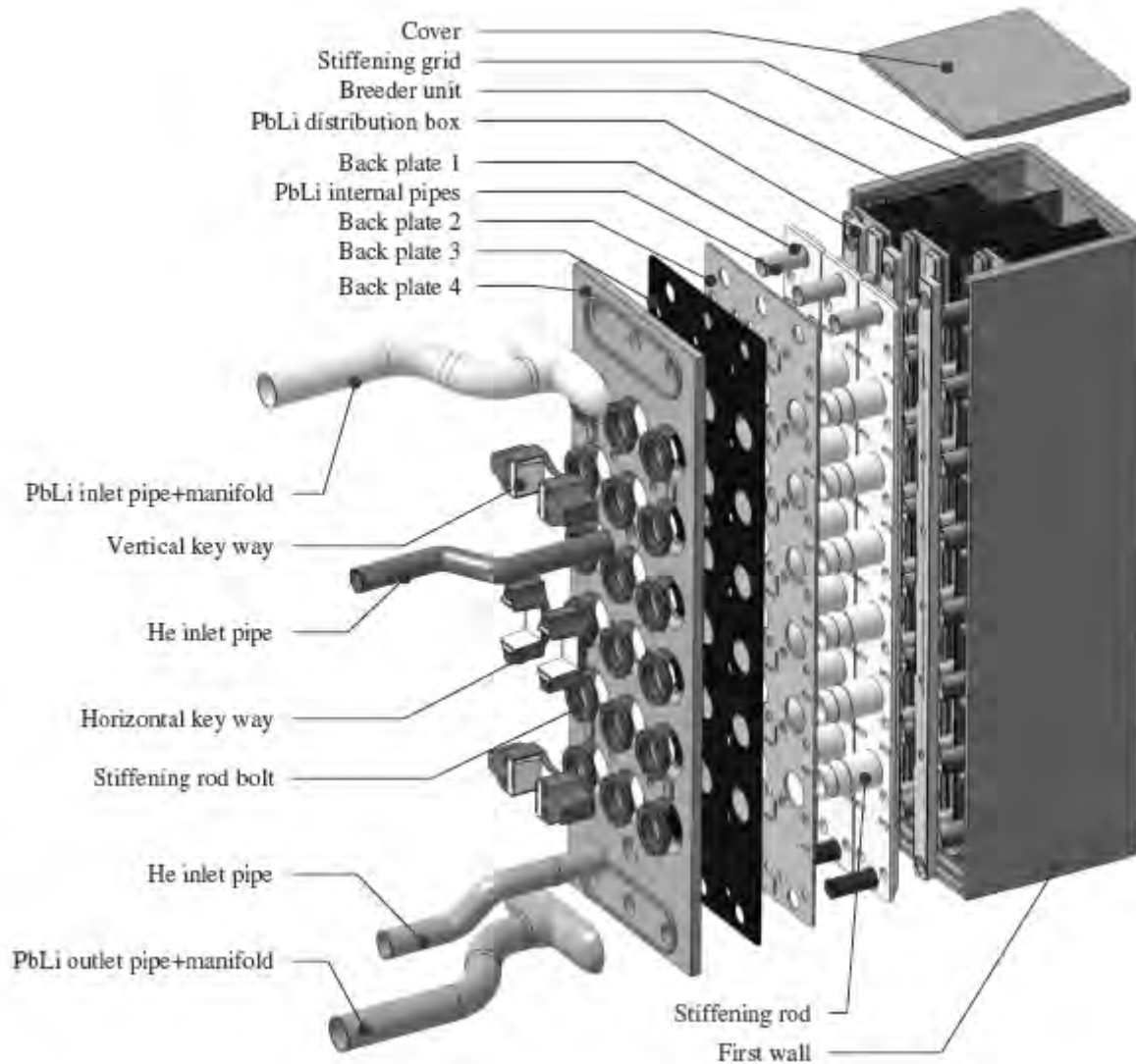


Figure 1 : Exploded view of the HCLL TBM

Recent studies carried out in the frame of the Power Plant Conceptual Study have shown that the configuration previously foreseen for the HCLL DEMO generic blanket module in which the Pb-Li passes in series through all BU of a vertical column meandering between one BU and the one immediately below would lead to too high liquid metal velocities and MHD pressure drops.

As a consequence, an improved liquid metal flow path has been envisaged which allows higher re-circulation rates avoiding excessive LiPb velocities.

The liquid metal enters from the external collector and then it is distributed in some intermediate vertical distributing boxes located behind the BU. It enters in a BU and exits from the one below, feeding in this way the BU in parallel (par couple). The vertical collectors have been integrated in the TBM design as vertical parallelepiped chambers located behind the BU, between the BU He collectors and separated to form the inlet and outlet legs by an oblique internal wall.

The Pb-Li draining is realized from the TBM bottom, to allow the draining by gravity so improving safety.

When draining PbLi from the module, it is necessary to insure that, in case of residual Pb-Li, its solidification does not lead to wall failures. This has led to lower as much as possible the exit pipes used for the draining, and to suppress the lowest cooling plate of the bottom BUs, in order to avoid its potential interaction with residual Pb-Li.

Being the Pb-Li mass flow rate lower than in previous version, the dimensions of Pb-Li external feeding pipes and consequently of the external collectors have been reduced, so increasing the available place for the mechanical attachments on the last back plate.

### Integration into the frame

The number of the TBM pipes leaving the TBM from the rear has been fixed to four, two for the cooling helium (inlet pipe having  $\varnothing_{in} = 60$  mm, outlet pipe having  $\varnothing_{in} = 70$  mm) and two for the liquid metal ( $\varnothing_{in} = 87$  mm). That allows to reduce the time for connection/disconnection and the number of passing through the frame. The pipes are curved in the crossing of the frame in order to limit the neutron streaming.

For the connection of the TBM to the frame, mechanical attachments of the same type as those used for the ITER outboard shielding modules are foreseen, consisting of:

- A flexible fixation (flexible cartridges) on 4 points to recover the radial mechanical loads while authorizing the thermal expansion in the poloidal and toroidal directions.
- A gliding shear keys system along a cross-shaped key way on the external back plate, to lock up the module displacements in poloidal and toroidal directions during the disruption loads, the thermal expansion in these directions being free; it also contributes to bear the weight of the module.

The whole system is positioned on the external plate of the module's back collector. The bolts of the system of flexible cartridges are screwed in four of the stiffening rods of the back collector (the cartridges being screwed in the frame). The key ways are laid out on the back plate according to a cross centred on the module, the shear keys being fixed on the frame.

The attachments have been dimensioned to resist to a maximum torque of 1.5 MNm, value estimated considering a safety factor of three on the resulting forces obtained for the HCPB-TBM. A detail of the TBM in its frame with a cut of the attachment system is shown in figure 2.

**In-TBM Manufacturing sequence**

A preliminary TBM manufacturing sequence has been defined: the main mounting steps for the assembly of the basic components (First Wall, Stiffening Plates, Cooling Plates) have been identified with their specific requirements

(tightness, mechanical resistance, etc.) and illustrated with 3D drawings. This proposal has been submitted to industry expertise intended to evaluate its feasibility and the sequence has then been updated, on the basis of the industry suggestions. A complete set of drawings has been issued showing the manufacturing sequence steps and indicating the operation to be accomplished. The possible main concerns and key points have been also noticed. All welding preparations have been indicated in the drawings, taking into account the chamfrain, where needed, in accord with the envisaged welding technique.

The TBM design has been furthermore modified adopting the following design guidelines:

- Avoid welding triple points.
- Avoid sharp points on some welding trajectories.
- Avoid thickness variations along some welding trajectories.
- Avoid possible interference between welding beams and welded parts.
- Avoid welding of thick to thin components.
- Separate mechanical and tightening function.

**Structural and thermo-mechanical analyses**

The first In-TBM was designed to resist to a surface Heat Flux (HF) = 0.27 MW/m<sup>2</sup> and to a Neutron Wall Loading (NWL) = 0.78 MW/m<sup>2</sup>. Recently, ITER Team has requested TBMs to be designed to withstand a surface heat flux of 0.5 MWm<sup>-2</sup>, even if most of the time the real heat flux will be lower so the previous design has been modified.

Steady state analyses, thermal, thermal-hydraulic and mechanical, have been performed to adapt the outline design to these new "dimensioning loading conditions".

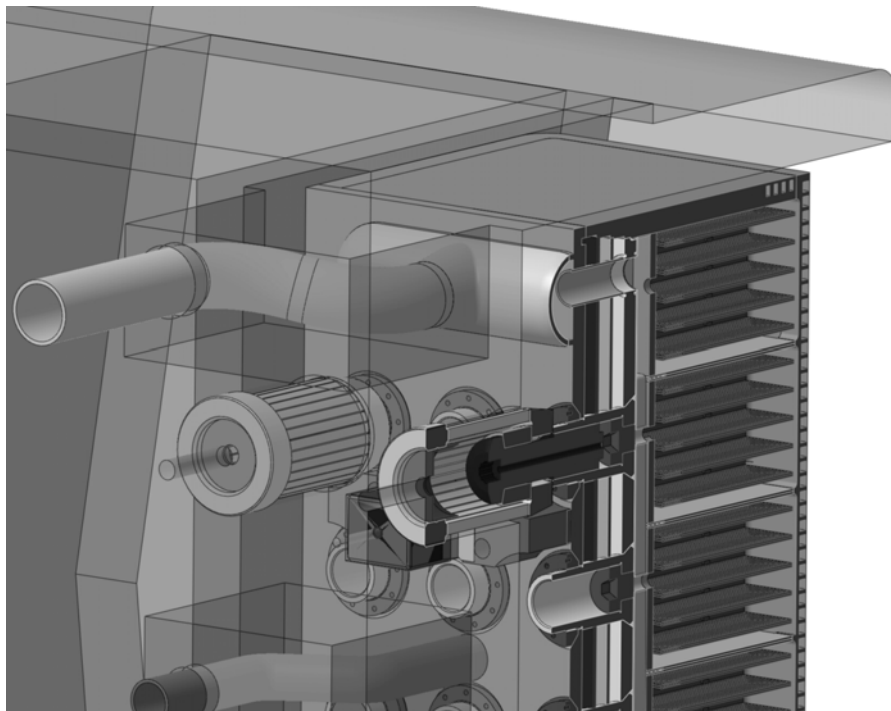


Figure 2 : Detail of the TBM inserted in the ITER frame, with the attachment system

1.2 MW are deposited on the TBM of which about 0.7 MW on the FW and 0.5 MW on the breeder zone (CPs, SPs and liquid metal). Due to higher ratio between the HF and the NWL (0.5/0.78 against 0.5/2.4 in DEMO) neither the cooling schema nor the He parameters adopted in DEMO are fully suitable for the TBM.

In order to recover the 0.5 MW/m<sup>2</sup> impacting on the FW without exceed 550°C in the steel, a He velocity of about 70 m/s is needed with a He maximum temperature of 413°C. Taking into account this requirement, the He flow schema and mass flow and the FW channels cross section have then been modified and optimised with regard to the pumping power in the He circuit.

In the optimised configuration the FW channels have a cross section of 15x10.5 mm<sup>2</sup> (poloidal x radial) and 1.3 kg/s of He circulates in the TBM. The He enters in the FW at 300°C, then passes in the SPs, the covers and the CPs which are cooled in parallel. The percentage of the He circulating in the CPs (37%) is chosen in a way that the He temperature at the exit of the CP channels is 500°C. That will allow to obtain in the CPs steel temperatures of the same order of magnitude as those obtained in DEMO so guarantying a good relevance in terms of T permeation. He exits from the TBMs between 440-460 °C (depending on the derivation scheme).

Pressure drops are evaluated at 0.222 MPa in the FW, 0.0040 MPa in the parallel CPs//SPs//covers (in particular it is in the SPs that take place max pressure drops), and 0.9 MPa in the region between the TBM and the ITER Heat

Recovery System (HRS). 200 m of 100 mm Øin pipes have been assumed between the TBM and the HRS with ten 90° corners. The total pressure drops (including those in the back plate region) amount to 0.38 MPa, leading to a pumping power of about 100 KW.

Mechanical analyses have been furthermore carried out to evaluate the resistance of the module in accidental conditions. It has been assumed that the rupture either of a CP or a SP would imply the pressurization of the entire box to the He pressure (8 MPa).

Analyses showed that (see figure 3), according to the IISDC criteria, the box will be able to withstand this type of load.

Transient analyses have then been carried out considering an ITER pulse with a duty cycle of 400 s/ 1800 s and showed that in terms of thermo-mechanical behaviour, stationary conditions would be reached in the TBM front regions, where maximum temperatures and stresses are located, after some tens of seconds (60 in the FW).

### PLANNING FOR THE TBM DESIGN AND R&D

A planning and list of test requirements for the qualification of the HCLL TBM prior to ITER has been defined.

It is based on a progressive qualification of the TBM, from the qualification of the fabrication techniques and technology of the basic sub-components (FW, CPs, SPs), to the functional qualification of the systems at different scale until a 1:1 scale mock-up.

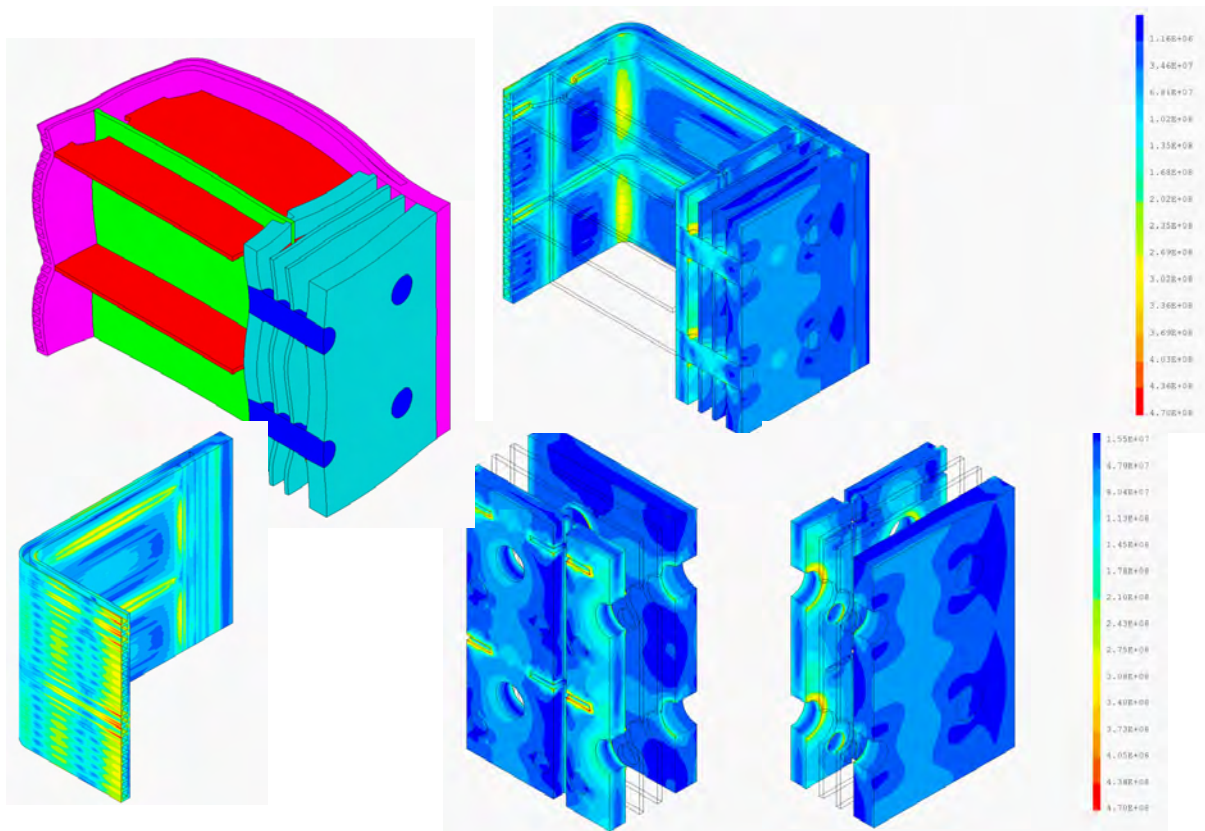


Figure 3 : Von Mises stresses distribution (MPa) in faulted conditions

This planning allows to highlight the need for future He test facilities and will be used within the HCLL/HCPB projects to better define the R&D timeschedule.

On the other hand, some interactions with fabrication R&D have initiated complementary design analyses. The foreseen manufacturing sequence is indeed featured by the assembly of basic components the fabrication of which assumes, thus, a fundamental role in the fabrication feasibility. Various techniques are actually retained for further development for the fabrication of the FW, the CPs and the SPs. The applicability of some of these requires small modifications of the design (i.e. increase of the rib between the CPs channels), the impact of which on the TBM behaviour is under assessment.

Being the Eurofer especially developed for the use in fusion device, the material data base is still under completion. In particular, the data on its weldability with various techniques (EB, laser, TIG), comprising the mechanical behaviour of the welded regions and the post welding treatment needs should be investigated with an appropriate R&D campaign.

### TESTING PROGRAMME IN ITER

A preliminary testing program to test and validate the Helium Cooled Lithium Lead breeder blanket concept in the ITER machine has been defined, taking into account the chosen testing strategy, the TBMs objectives and the ITER operating scenario during the first 10 years of ITER operation.

The proposal envisages four different test mock-ups or modules, adapted for qualifying single or combined effects and whose design makes large use of engineering scaling for compensating the differences between the testing conditions and those expected in DEMO (e.g., neutron wall load, heat flux, pulsed operating conditions):

- EM-TBM: Electromagnetic TBM (plasma H-H).
- NT-TBM: Neutronic TBM (plasma D-D and first period of the D-T low cycle phase).
- TT-TBM: Thermo-mechanic & Tritium Control TBM (last period of the D-T low cycle and first period of the D-T high duty cycle phase).
- IN-TBM: Integral TBM (last period of the high duty cycle D-T phase).

With the first two types of modules, useful information can be obtained about the impact of the TBM on the plasma stability, as well as on the TBM structural integrity and system functionality. The provisional capability of the calculation tools (neutronic, EM, MHD) can be furthermore validated and sources can be calibrated for the following phases.

The two others types of modules will allow to complete the code validation (thermo-mechanic), the tritium control, up to the integral qualification of the HCLL blanket and of PbLi and He coolant circuit components under DEMO relevant conditions.

The He parameters can be varied to achieve the DEMO relevancy under different loading conditions, compatibly with the response time of the system regulators. Therefore, the meaningfulness of most of the tests in the D-T phase, in particular for the TT-TBM and for the In-TBM, will depend on the capability to predict the actual surface heat load with sufficient advance and to keep it constant for a sufficient long time.

The feasibility of the tests foreseen for the various envisaged TBMs will depend from the possibility of measure the meaningful physical properties (temperature in the material structure, in the He and in the liquid metal, He pressure, lithium lead velocity in the various regions of the TBM, deformations in the structure and in the attachments, etc.) with required accuracy, sensibility, response time, etc.

The characteristics of available measurement tools have been explored paying special attention to their adaptability to the ITER working conditions, as well as to their installation in the TBM.

A part from some instruments specifically developed in the frame of this work programme (tritium concentration measure in the LiPb), most of the needed instruments tools are available on shell. Their installation and use in the TBM is not, however, always obvious. The installation of thermocouples or deformation gauges in the FW, p.i. could not be compatible with the TBM manufacturing sequence, in the sense that if the sensor are installed before the welding of the manifolding back plate, they should be undamaged by post thermal treatment. Another issue could be the signal transmission to the treatment system, which could be perturbed by the varying magnetic field.

### REFERENCES

---

- [1] A. Li Puma et al. - HCLL TBM for ITER – Status of the design, analyses and test programme in ITER - CEA report SERMA/RT/04-3350/A, 10/2004.

### REPORTS AND PUBLICATIONS

---

G. Rampal et al. - Helium Cooled Lithium-Lead test blanket module for ITER - reference document for a mounting sequence - CEA Report, SEMT/BCCR/RT/04-016/A, April 2004.

Y. Poitevin et al. - He testing requirement and planning for the development and qualification of HCLL TBM - CEA report SERMA/04-3470/A, 09/2004.

A. Li Puma et al. - Helium Cooled Lithium Lead Test Blanket Module for ITER Engineering design, analyses and test programme & needs - Task EFDA TW2-TTBC001-D01 - Final Report on sub deliverables 1d, 1e, 1g and 1h, CEA report SERMA/RT/05-3568/A, 03/2005.

A. Li Puma, Y. Poitevin, L. Giancarli - The Helium Cooled Lithium Lead blanket test proposal in ITER and requirements on Test Blanket Modules instrumentation - to be published in Fus Eng Des.

G. Rampal, A. Li Puma, Y. Poitevin, E. Rigal, J. Szczepanski, C. Boudot - HCLL TBM for ITER - Design studies", to be published in Fus Eng Des.

Y. Poitevin, L. Boccaccini, A. Cardella et al. - The EU Breeding Blankets development and the test strategy in ITER - to be published in Fus Eng Des.

L.V. Boccaccini, J-F. Salavy, R. Lässer, A. Li Puma, R. Meyder, H. Neuberger, Y. Poitevin, G. Rampal - The european test blanket module systems: design and integration in ITER - Proceeding ISFNT-7 (invited paper) - to be published in Fus Eng Des.

G.Rampal, D. Gatelet, L. Giancarli, G. Laffont, A. Li-Puma, J.F. Salavy, E. Rigal - Design approach for the main ITER Test Blanket Modules for the EU Helium Cooled Lithium-Lead blankets - Proceeding ISFNT-7 - to be published in Fus Eng Des.

## **TASK LEADER**

---

Antonella LI PUMA

DEN/DM2S/SERMA  
CEA-Saclay  
F-91191 Gif-sur-Yvette Cedex

Tél. : 33 1 69 08 79 76  
Fax : 33 1 69 08 99 35

E-mail : [alipuma@cea.fr](mailto:alipuma@cea.fr)

Not available on line

## TW4-TTMS-005-D01

---

### Task Title: **RULES FOR DESIGN, FABRICATION AND INSPECTION** **Update Data Base and Appendix A of DEMO-SDC**

---

#### INTRODUCTION

---

Eurofer is a reduced activation ferritic / martensitic steel that has been selected as the European reference structural material for ITER Test Blanket Modules and DEMO reactor. Several industrial heats of this steel have been produced and tested within the framework of EFDA programme. The ultimate goal of these tasks is to propose materials properties allowables for design and licensing of components fabricated with the Eurofer steel.

TW4-TTMS-005 is one of the EFDA tasks that specifically targets structural materials rules, design and inspection. Its scope is extended since the year 2003 to include metallurgical and mechanical properties characterization actions that were previously carried out.

This report presents a summary of the work done during the year 2004 at CEA for the TW4-TTMS-005-D01. The work done is also part of an international collaboration, coordinated under the fusion materials implementing agreement of the International Energy Agency (IEA).

The main objective of the TW4-TTMS 005-D01 is to collect, validate and harmonize the results of Eurofer steel, in continuation of the earlier work done on the conventional 9Cr-1Mo steel and the RAFM steel grade produced in Japan (F82H), and propose materials properties allowables through an Eurofer steel specific Appendix A.

#### 2004 ACTIVITIES

---

All actions and deliverables foreseen under the terms of TW4-TTMS-005-D01 have been fulfilled in time. In 2004, the database of Eurofer steel was updated, particularly with the RAFM data and analysis resulting from the work done at FZK / Germany.

With the addition of the new Eurofer steel data in 2004, the collection of relational databases for RAFM steels contains:

- Products database: 571 records including 118 on Eurofer.
- Compositions database: 475 records including 26 on Eurofer.
- Tensile database: 1018 records including 258 on Eurofer.

- Impact database: 1520 records including 467 on Eurofer.
- Impact plots: 161 records including 45 on Eurofer.
- Creep database: 205 records including 81 on Eurofer.
- Fatigue database: 181 records including 70 on Eurofer.
- Fracture toughness database: 78 records, including 48 records on Eurofer steel. 8 files are generated for a group of tests and 3 Master curves are plotted.
- Summary database of all above databases that allows sorting of all available test results for a given heat, product or sub-product.

Notice that each record contains many fields.

For instance, a single record of one tension test contains fields with inputs from specimen origin and geometry, its heat treatment and irradiation back ground, testing conditions and all the usual materials properties derived from such tests.

The updated database was then used to revise the Appendix A for Eurofer steel. Some missing design criteria were added. The full package sent to EFDA at the end of 2004 work contained:

- An updated Appendix A of the Eurofer steel referenced CEA-DMN/Dir TN 2004-02.
- A CD-Rom containing the Runtime Solution version 3.0 of the RAFM databases and related documents.
- A Getting Started note explaining how to use the Solution.

#### CONCLUSIONS

---

All deliverables foreseen in this action have been met. The revised Appendix A and its accompanying CD-Rom Runtime solution have been sent to EFDA and are now available to ITER and reactor design teams. In 2005 updating of the databases will continue, particularly with the post-irradiation test results, and data from ODS steels.

## REPORTS AND PUBLICATIONS

---

F. Tavassoli - Fusion Demo Interim Structural Design Criteria (DISDC): Appendix A Material Design Limit Data - A3.S18E Eurofer Steel, EFDA Task TW4-TTMS-005-D01, CEA DMN/Dir TN 2004-02/A, Dec. 2004.

F. Tavassoli - Getting started with the RAFM Database Runtime Solution V. 3.0, EFDA Task TW4-TTMS-005-D01, CEA/Saclay, DMN/Dir, Oct. 14, 2004.

CD-Rom containing the Runtime Solution version 3.0 of the RAFM databases and related documents.

## TASK LEADER

---

Farhad TAVASSOLI

DEN/DMN  
CEA-Saclay  
F-91191 Gif-sur-Yvette Cedex

Tél. : 33 1 69 08 60 21

Fax : 33 1 69 08 80 70

E-mail : [tavassoli@cea.fr](mailto:tavassoli@cea.fr)

## Task Title: **MODELISATION OF IRRADIATION EFFECTS** **Ab-initio defect energy calculations in the Fe-He system**

### INTRODUCTION

Ferritic steels are proposed as structural material in fusion reactors. When subject to 14 MeV neutron irradiation, large amounts of helium and hydrogen are produced from transmutation in addition to self-defects. High He concentrations in metals are known to induce microstructural changes such as bubble formation and void swelling. The objective of this subtask is to contribute to the modeling of such phenomena by providing a database at the *ab initio* level, i.e. in the framework of the Density Functional Theory (DFT), of energies and structures for a set of characteristic atomic configurations involving helium atoms and vacancies in the  $\alpha$ -Fe lattice.

The present calculations are based on a fast DFT-code, namely SIESTA (Spanish Initiative for Electronic Simulations with Thousands of Atoms): <http://www.uam.es/siesta> [1], [2].

This methodology was set up and validated last year by comparison with reference calculations based on plane-wave basis sets [6]. It has been applied here to predict the migration of interstitial and substitutional He atoms in  $\alpha$ -Fe, and their interaction with other He atoms and with vacancies.

### 2004 ACTIVITIES

The results presented below are obtained at constant pressure, on 128 atom supercells, using 3x3x3 k-point grids for the Brillouin zone integration. All calculations are performed in the spin polarized Generalized Gradient Approximation (GGA).

#### HELIUM MIGRATION

##### Migration of interstitial helium

The migration of interstitial He is relevant to the initial stage after He implantation or He production by transmutation, before it is trapped by vacancies or other defects. According to the present calculations, interstitial He prefers to locate at tetrahedral sites rather than octahedral ones, the difference in solution energy being 0.18 eV. In the body-centred cubic structure, a tetrahedral solute may migrate between two equivalent sites without passing through an octahedral one (figure 1). We find for He a very low energy barrier, namely 0.06 eV, similar to the value of 0.08 eV found with an empirical potential [3]. It can therefore be concluded that the migration of interstitial He is extremely fast.

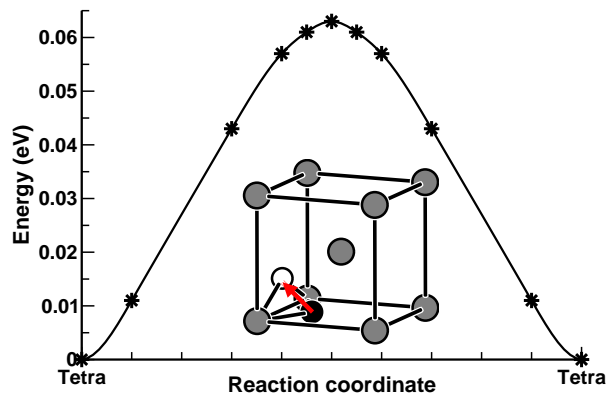


Figure 1 : Migration barrier of interstitial He in iron. The migration jump, between two tetrahedral sites, is schematically represented by the arrow between the initial site (in black) and the final site (in white); the iron atoms are represented in grey

##### Migration of substitutional helium

Two mechanisms are usually considered for the migration of substitutional He, either by vacancy or by dissociation [4]. The first mechanism requires another incoming vacancy. Let's first examine the energetics and local equilibrium geometries of configurations involving a substitutional He and a vacancy, i.e. two vacancies and a He atom. We find that the most stable configuration for the HeV<sub>2</sub> complex is when the two vacancies are first neighbors with a V to HeV binding energy of 0.78 eV, followed by the configuration where they are second neighbors, with a binding energy of 0.37 eV. The interaction between a substitutional He and a vacancy becomes negligible at third neighbor. Concerning the position of the helium atom, it is located midway between the two vacancies in the nearest neighbor case. For the second neighbor case, the helium atom also prefers to be off-site. In this case two degenerate positions exist, located at 0.25 times the lattice parameter from either of the two vacancies; they are separated by a barrier of 0.02 eV.

From the above configurations two competing two-step migration mechanisms can be inferred for the HeV<sub>2</sub> complex (figure 2 (a)-(e)). The first one involves a second neighbor intermediate configuration. First, a nearest neighbor jump of the vacancy transforms the nearest neighbor configuration into a second neighbor one; in the saddle point configuration He occupies a substitutional site (figure 2(d)). Then, by a similar but reverse jump, a nearest neighbor configuration is recovered. The corresponding migration energy is 1.17 eV. The second mechanism involves an intermediate configuration, the third neighbor one - where the He atom sits on one of the two vacancies - this configuration is higher in energy but actually has a slightly lower barrier (1.08 eV).

These barriers for are lower than the lower bound value of the vacancy dissociation energy from HeV<sub>2</sub> (1.45 eV), estimated from the sum of the V to He-V binding energy and the V migration energy (0.67 eV). Therefore the HeV<sub>2</sub> complex is expected to migrate as a unit over appreciable distances.

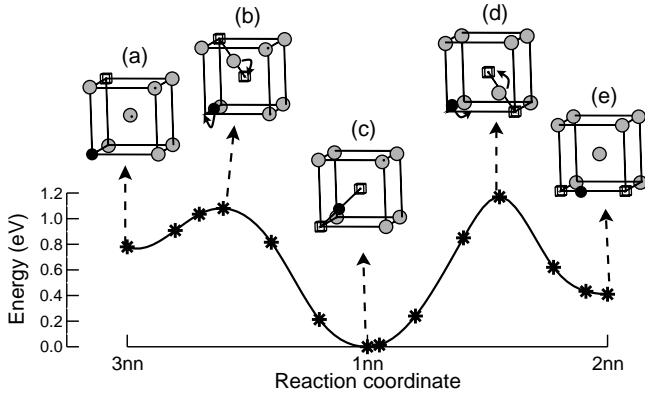


Figure 2 : Schematic representation of the energetic landscape and the most favorable migration mechanisms of the HeV<sub>2</sub> complex:

(c), (e) and (a) represent the most favorable configurations when the He atom is bound to two first, second, and third neighbor vacancies respectively (b) and (d) are the saddle point configurations, the solid arrows indicate atomic jumps yielding configurations (a) and (e) starting from the ground state (c). The atoms (black spheres for He and gray spheres for Fe) are represented at their relaxed positions, vacancies are symbolized by small cubes

The effective migration energies of substitutional He can be discussed for the vacancy mechanisms described above and the dissociation one, i.e. when a substitutional He dissociates from its vacancy to migrate through interstitial sites until trapping at another vacancy. When thermal vacancies dominate, the expressions for these effective migration energies are [5]:

$$E^b(\text{He-V}) + E^m(\text{He}^{\text{int}}) - E^f(\text{V})$$

migration by dissociation

$$E^m(\text{HeV}_2) + E^f(\text{V}) - E^b(\text{He}^{\text{sub}}\text{-V})$$

migration by vacancies

where  $E^b(\text{He-V})$ ,  $E^b(\text{He}^{\text{sub}}\text{-V})$  are the tetrahedral He – vacancy, and substitutional He – vacancy binding energies respectively,  $E^f(\text{V})$  is the vacancy formation energy, and  $E^m(\text{He}^{\text{int}})$ ,  $E^m(\text{HeV}_2)$  are respectively the migration energies of a tetrahedral He and a HeV<sub>2</sub> complex.

The values obtained from the present calculations are 0.24 eV and 2.42 eV respectively.

When thermal vacancies prevail, the dominant diffusion mechanism is expected to be dissociative.

Note that empirical potential studies [3] give higher effective migration energies by dissociation, that is, 2.08 eV instead of 0.24 eV, mainly because of the larger predicted He-V binding energy.

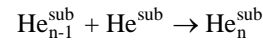
## BINDING OF HELIUM AND VACANCIES TO HELIUM-VACANCY CLUSTERS

### Interaction between interstitial helium atoms

We find that the interaction between interstitial He atoms is attractive. The binding energy is 0.46 eV between the first two He atoms, and it increases with the number of the He atoms. This self-trapping of He atoms together with the fast migration of interstitial He was proposed to be responsible for the formation of He bubbles observed at low temperatures in initially vacancy free lattices.

### Interaction between substitutional helium atoms

We find that two substitutional He atoms prefer to be first nearest neighbors. The binding energy of two substitutional He located at first and second neighboring positions are respectively 1.15 eV and 0.74 eV, this attractive interaction is short ranged, the binding energy becomes negligible beyond second neighbor separation. When more than two substitutional He atoms are present, they tend to form compact clusters. We have investigated the binding energy of small clusters containing n He atoms (n = 2 to 5) according to the reaction:



The resulting values are 1.15 eV, 1.58 eV, 2.25 eV and 2.30 eV respectively, and the most compact clusters are the most favorable energetically

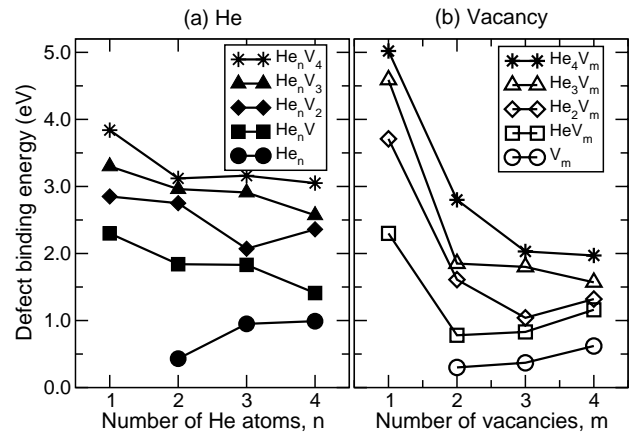


Figure 3 : Binding energies of (a) a He atom and (b) a vacancy to a He<sub>n-1</sub>V<sub>m</sub> and He<sub>n</sub>V<sub>m-1</sub> cluster respectively. Abscises and legends refer to the composition of the resulting helium-vacancy cluster

### Helium-vacancy clusters

More generally the stability of small He<sub>n</sub>V<sub>m</sub> clusters was also investigated for n and m = 0 to 4. The binding energy of a vacancy to the He<sub>n</sub>V<sub>m-1</sub> cluster is defined by:

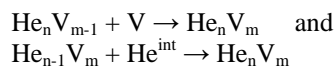
$$E_B(\text{V}) = E([\text{N}-(\text{m}-1)] \text{Fe}, n \text{He}) + E((\text{N}-1) \text{Fe}) - E([\text{N}-\text{m}] \text{Fe}, n \text{He}) - E(\text{N Fe})$$

where E([N-m] Fe, n He) is the energy of the system with (N-m) Fe atoms and a He<sub>n</sub>V<sub>m</sub> cluster.

The binding energy of an interstitial tetrahedral helium atom with a  $\text{He}_{n-1}\text{V}_m$  can be defined in a similar way by:

$$E_B(\text{He}) = E((N-m) \text{Fe}, (n-1) \text{He}) + E(N \text{Fe}, \text{He}) - E((N-m) \text{Fe}, n \text{He})$$

The convention adopted here is a positive sign for an attraction between the vacancy or the helium atom and the initial He-V cluster. They correspond respectively to the reactions:



where  $\text{He}^{\text{int}}$  indicates an interstitial tetrahedral helium atom. The values found are positive for all cases (figure 3). For  $n=1$ , the He binding energy increases as function of the number of vacancies in the cluster,  $m$  (see figure 3); it tends rapidly to the asymptotic value of interstitial He solution energy, i.e. 4.39 eV in the present calculation.

For a given value of  $m$ , the He binding energy decreases as the He content increases, reflecting the increase in cluster pressure caused by the accumulation of He atoms. Empirical potentials show the same trend, and predict a spontaneous emission of He or self-interstitials at larger  $n/m$  ratios [3].

The vacancy to cluster binding energies increase with helium content - again as a consequence of the increase of cluster pressure - and in particular they are always larger with than without helium (figure 3). In other words helium stabilizes vacancy-type clusters by reducing the vacancy emission rates.

This is consistent with the experimental evidence that He atoms enhance the formation of microvoids. For a given number of He atoms,  $n$ , the vacancy binding energy first decreases rapidly when the number of vacancies increases, until  $m-1 \approx n$ , i.e. until the cluster pressure is reduced. Then, it increases slowly (as in the helium-free case), when the cluster surface energy contribution becomes dominant.

## CONCLUSIONS

---

The following conclusions can be drawn from the present *ab initio* calculations on the behaviour of helium in pure  $\alpha$ -Fe, and its interaction with vacancies:

- The migration energy of interstitial He, between two tetrahedral sites, is very low: 0.06 eV.
- The interaction between interstitial He atoms is attractive, with a binding energy of 0.46 eV; this attraction is at the origin of the self-trapping effect proposed for He in metals.
- The interaction between substitutional He atoms is attractive, with a binding energy of 1.15 eV at nearest neighbor and 0.74 eV at second nearest neighbor.

- More generally the binding of He and vacancies to  $\text{He}_n\text{V}_m$  clusters have been determined up to  $n=4$  and  $m=4$ .
- The migration barrier for the  $\text{HeV}_2$  complex has been determined: 1.08 eV. It is involved in the migration mechanism of substitutional He by the vacancy mechanism.

## REFERENCES

---

- [1] J.M. Soler, E. Artacho, J.D. Gale, A. Garcia, J. Junquera, P.Ordejon and D. Sanchez-Portal - J. Phys. Cond. Matter 14, 2745 (2002).
- [2] C.C. Fu, F. Willaime and P. Ordejon - Phy. Rev. Lett. 92, 195503 (2004).
- [3] K. Morishita, R. Sugano, B.D. Wirth and T. Diaz de la Rubia - Nucl. Instr. Meth. B 202, 76 (2003) and references therein.
- [4] L. K. Mansur, E. H. Lee, P. J. Maziasz and A. P. Rowcliffe - J. Nucl. Mater. 141-143, 633 (1986).
- [5] V. Sciani and P. Jung - Rad. Eff. 78, 87 (1988).

## REPORTS AND PUBLICATIONS

---

- [6] F. Willaime and C. C. Fu - Ab initio calculations of helium-vacancy defects in  $\alpha$ -Fe: first results - CEA report DMN/SRMP/2004-002/I.
- [7] C. C. Fu and F. Willaime - Ab initio study of helium in  $\alpha$ -Fe: dissolution, migration and clustering with vacancies - submitted for publication.

## TASK LEADER

---

François WILLAIME

DEN/DMN/SRMP  
CEA-Saclay  
F-91191 Gif-sur-Yvette Cedex

Tél. : 33 1 69 08 43 49  
Fax : 33 1 69 08 68 67

E-mail : fwillaime@cea.fr



**TW3-TTMA-001-D04**  
**TW3-TTMA-002-D04**

## Task Title: SiC/SiC CERAMIC COMPOSITES Divertor and Plasma Facing Materials

### INTRODUCTION

The objective of these tasks is to irradiate in a common rig SiC-SiC ceramic composites and tungsten alloys samples at two temperatures, i.e., 1000°C and a lower temperature approximately of 600-650°C. The dose foreseen is about 5 dpa equivalent Fe. This irradiation experiment will be performed in the OSIRIS reactor at CEA-Saclay.

The first step of this work consists on the design of the corresponding irradiation capsule based on the requirements defined by EFDA for this irradiation experiment, i.e., conditions required, fluence level, temperature distribution, materials, type, number and dimensions of specimens.

As said before, two families of materials are planned to be irradiated in this experiment, that is, several types of SiC<sub>f</sub>/SiC ceramic composites and refractory tungsten-based alloys. All materials will be supplied by EFDA as machined specimens ready for irradiation.

### ACTIVITIES 2004

Activities performed during this period were mainly focused on the definition of the loading plan and the design of the irradiation rig. Also, the design of the gas circuit systems was continued as well as the safety analysis.

This experiment was named "FURIOSO" (FUtion RIg OSiris irradiatiOn).

### LOADING PLAN

After several meeting and discussions, it was agreed the loading plan presented in table 1, which summarises the materials and the characteristics of specimens (type, dimensions and number) that will be irradiated in this experiment. Different nuances of SiC/SiC ceramic composites are considered for irradiation: 2D and 3D-composites supplied by EFDA and manufactured in Europe by MAN; 2D-NITE material from Japan and two types of composites supplied by ORNL (U.S.). These materials are included as specimens for mechanical tests (tensile and bending tests) and as samples for measurements of thermal diffusivity.

Concerning tungsten, two types of alloys will be included in the rig, one containing lanthanum oxide (W-La<sub>2</sub>O<sub>3</sub>) and other with potassium addition (W-K). These materials will

be irradiated as plate tensile specimens and Charpy V subsize (KLST) samples destined to bending tests. The distribution and number of samples as well as the drawings giving the dimensions and the corresponding tolerances for each type of specimens have been communicated to EFDA for approval in october 2004.

### IRRADIATION RIG

The irradiation capsule will be constituted of two sections of the same length, one that will work at 1000°C and the other at 600°C. Figure 1 shows a scheme of one irradiation temperature section of the sample holder. Each section is constituted of six baskets to locate the samples. SiC/SiC composite specimens occupy four baskets and W- samples are distributed in the two others.

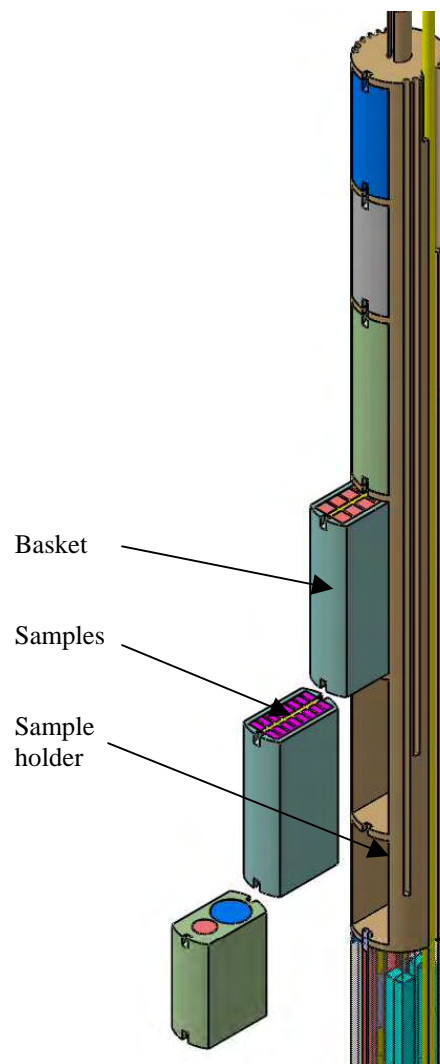


Figure 1 : Scheme of one irradiation temperature section constituted by six baskets for the distribution of different types of specimens

Table 1 : Loading plan : distribution of different materials and specimens in the rig

|                                  |            | Composites SiC / SiC |                |       |        | W- alloys |          |          |          |
|----------------------------------|------------|----------------------|----------------|-------|--------|-----------|----------|----------|----------|
|                                  | Temp. (°C) | Basket #             | EU-3D          | EU-2D | J-NITE | US        | W1       | W2       |          |
| TOP                              | 600°C      | 1                    |                |       |        |           | 5Ch+3T19 |          |          |
|                                  |            | 2                    |                |       |        |           |          | 5Ch+3T19 |          |
|                                  |            | 3                    | 4Bend+<br>5T45 | 5T45  |        |           |          |          |          |
|                                  |            | 4                    | 4Bend          | 6Bend |        |           |          |          |          |
|                                  |            | 5                    |                |       | 8T40   | 8T40      |          |          |          |
|                                  |            | 6                    | 5D10           | 5D10  | 5D6    | 5D6       |          |          |          |
| Isolating region                 |            |                      |                |       |        |           |          |          |          |
| BOTTOM                           | 1000°C     | 7                    | 5D10           | 5D10  | 5D6    | 5D6       |          |          |          |
|                                  |            | 8                    |                |       | 8T40   | 8T40      |          |          |          |
|                                  |            | 9                    | 4Bend          | 6Bend |        |           |          |          |          |
|                                  |            | 10                   | 4Bend+<br>5T45 | 5T45  |        |           |          |          |          |
|                                  |            | 11                   |                |       |        |           |          | 6Ch+3T19 |          |
|                                  |            | 12                   |                |       |        |           |          |          | 6Ch+3T19 |
| Total number of specimens        |            |                      |                |       |        |           |          |          |          |
| T40 : Tensile 4x2x40             |            |                      |                |       | 16     | 16        |          |          |          |
| T45 : Tensile 4x2x45             |            |                      | 10             | 10    |        |           |          |          |          |
| Bend : 4x3.5x45                  |            |                      | 16             | 12    |        |           |          |          |          |
| D6 : Diffusivity 0 6x2.5 thick   |            |                      |                |       | 10     | 10        |          |          |          |
| D10 : Diffusivity 0 10x2.5 thick |            |                      | 10             | 10    |        |           |          |          |          |
| Ch : Charpy KLST                 |            |                      |                |       |        |           | 11       | 11       |          |
| T19 : Tensile 5x1x19             |            |                      |                |       |        |           | 6        | 6        |          |

(dimensions in mm)

The main concern in the design was related to the temperature distribution in the device because the materials behaviour is strongly dependent on the irradiation temperature. This parameter depends on the rig's position in the reactor core (gamma heating) and the geometry of the irradiation capsule.

The calculation and drawing of a powerful furnace were performed to guarantee the regulation and control of specimen's temperature during irradiation. But besides the heating system, the temperature could be also regulated, using a gas flow with an adequate thermal conductivity, inside and outside the sample holder. According to calculations of thermal distribution, a better control and regulation of temperature could be achieved using a flowing mixture of helium-neon for both internal and external gas circuits.

Consequently, inside the capsule, samples will be in contact with a circulating gas mixture of helium and neon. The final configuration of the gas control system is in progress. The monitoring of temperature will be performed with thermocouples located in the sample holder.

## FUTURE WORK

At the present time, the design of the rig is practically finished as regards of the geometry and dimensions of the sample holder. Next time, the manufacturing of the sample holder will be launched. The completion of the design and the installation of the gas system are expected to be carried out in the first half of 2005.

## TASK LEADER

A. ALAMO

DEN/DMN/SRMA  
CEA-Saclay  
F-91191 Gif-sur-Yvette Cedex

Tél. : 33 1 69 08 67 26  
Fax : 33 1 69 08 71 67

E-mail : ana.alamo@cea.fr

**Task Title: MODELLING OF THE MECHANICAL BEHAVIOUR OF  
ADVANCED 3D SiC<sub>f</sub>/SiC COMPOSITE**

**INTRODUCTION**

A previous bibliographic study indicate that modelling of the thermo-mechanical behaviour of SiC<sub>f</sub>/SiC structure with multi-scale methods allows to introduce more physics by describing the phenomena that control its behaviour (damage, creep,...) at the scale at which they takes place [5].

The aim of the work performed in 2004 was to identify and gather the scale change methods, constitutive laws and representative volume elements the most adapted to SiC<sub>f</sub>/SiC woven composites in order to perform their implementation in the finite element code CAST3M. This works results of a collaboration with the ONERA (Office National d'Etudes et de Recherches Aérospatiale) and the LCPC (Laboratoire Central des Ponts et Chaussés).

**2004 ACTIVITIES**

Two sets of constitutive laws (linking the stress to the strains) were chosen in order to allow comparison and mutual enrichment of the models.

Figure 1 shows on the left-hand the detailed structure of SiC<sub>f</sub>/SiC woven composites.

Two successive scale changes at least are necessary. One from the macro (structure) to the meso scale (plies) and one from the meso to the micro scale (fibre, matrix and interface).

The right-hand of figure 1 shows the two sets of chosen representative volume elements at the different scales and indicate the change scale methods we will adopt.

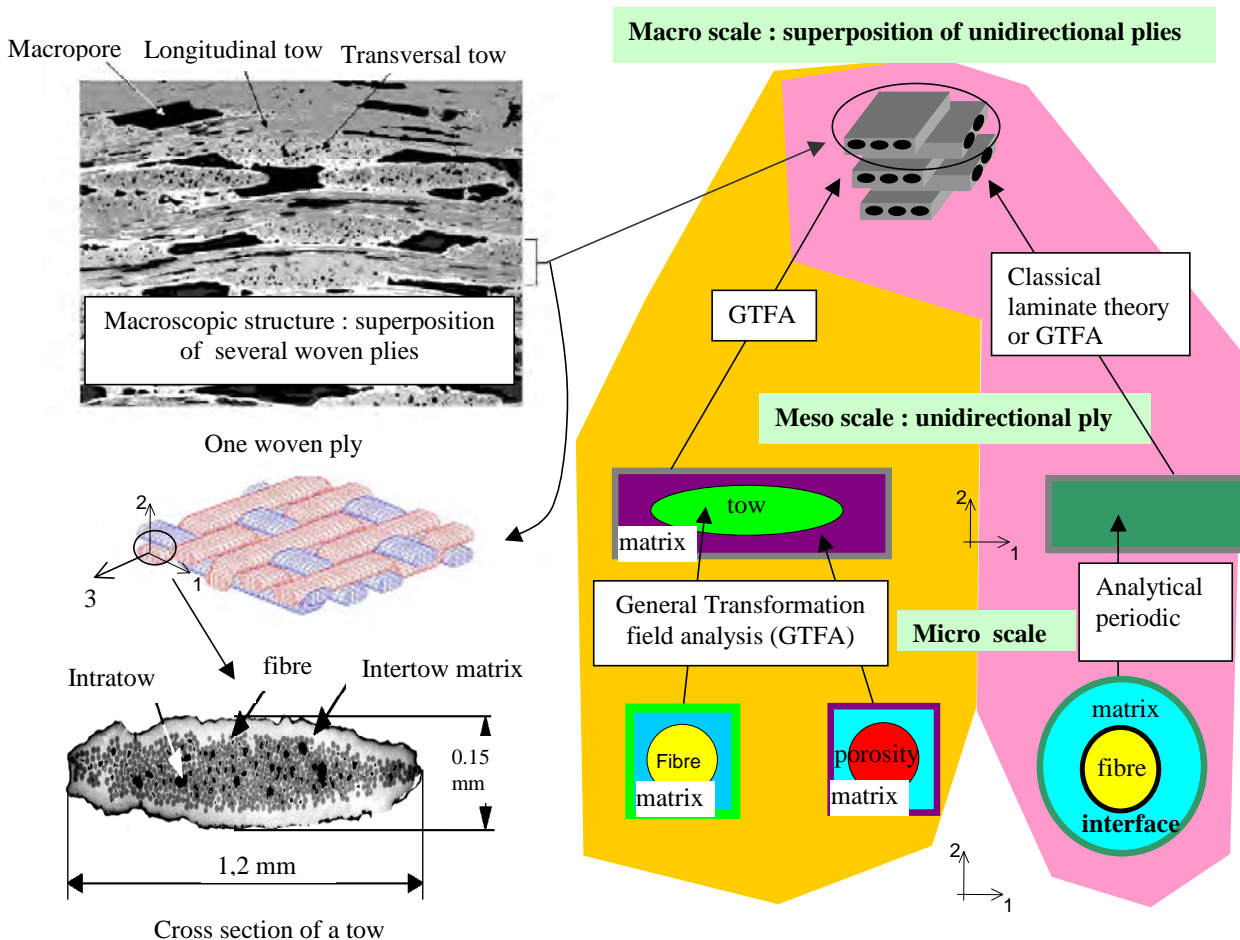


Figure 1 : Left-hand : detailed representation of woven SiC<sub>f</sub>/SiC composite(from [4] [6] and [7])  
Right-hand, representative volume elements and change scale methods chosen for the implementation  
in CAST3M (Yellow: from [6] [7], Pink: from [1] [2])

The first chosen constitutive laws set was reported by C. Rospars et al [1] [2]. These laws take into account the effect of damage at the level of the fibres, interface and matrix.

Their parameters have already been determined by C. Rospars for different SiC<sub>f</sub>/SiC and C/SiC composites. These constitutive laws were moreover successfully applied to modelling of SiC<sub>f</sub>/SiC structures via two scale changes. The other constitutive laws we wish to use were determined by ONERA [6].

They allow to take into account various phenomena observed during ceramic matrix composite testing such as the initial and damage-induced anisotropy (with the eventual lost of orthotropy), damage kinetics for the different cracking modes (different crack families defined by their orientations), damage deactivation, progressive cracks closure and residual strains induced by damage and residual fabrication stresses. These constitutive laws and their parameters are adapted and known for the macroscopic scale.

At lower scale, their parameters could be identified by inverse methods. It can also be envisaged to determine first the thermo-mechanical properties of the tows and the matrix with porosity using a multi-scale approach.

This allows to predict the influence of parameters such as fibres swelling or porosity concentration. Damage is then introduced at the meso-scale corresponding to the ply (sequenced method).

The change scale methods for the localisation step (calculation of the local strains, and corresponding stress, from the global strains) that will be used are the general transformation field analysis (GTFA) [7] and an analytical method for periodic fibre composites from C. Pideri [3] which is adapted to the micro to meso scale change. GTFA allows to perform all the envisaged scale changes. Constitutive laws as well as the change scale methods and the integrations methods are described in [8].

A UMAT procedure (procedure integrating the constitutive law that can be used in CAST3M or ABAQUS finite element code), based on the work of C. Rospars, has already been adapted to CAST3M and allows to calculate a unidirectional plane of SiC<sub>f</sub>/SiC, corresponding to the meso scale.

The work which will be undertaken in the next years consists in the following points:

- Implementation of the GTFA method in CAST3M, including the calculation of the localisation and influence tensors for change scale ( meso ↔ macro) and (micro ↔ meso).
- Implementation of the constitutive laws of ONERA for the scalar and pseudo-tensorial models.
- Tests calculations for the ONERA constitutive laws at the macro-scale.

- Following a sequenced integration method: determination of the thermo-elastic properties of the bundle and the matrix using multi-scale approach, introduction of damage at the meso-scale from the ONERA constitutive laws. Test calculations with scale change from meso to macro-scale
- The GTFA method for the meso to macro scale change (which allow to take into account out-of-plane 3D components) will also be used for test calculation of a realistic woven SiC<sub>f</sub>/SiC composite with the micro to meso scale change and component constitutive laws of C. Rospars.

## REFERENCES

---

- [1] C. Rospars, E. Le Dantec and F. Lecuyer - CMC damage prediction by micro-macro modelling, twelfth international conference on composite materials - Paris, France, 5th-9th (july 1999) - ICCM-12.
- [2] C. Rospars, E. Le Dantec and F. Lecuyer - Composites Science and Technology - 60 (2000) 1095-1102.
- [3] C. Pideri - Matériaux composites élastiques - Thèse de l'université de Pierre et Marie Curie - Paris 6 - soutenue le 10 novembre 1987.
- [4] V. Clard - Approches statistiques-probabilistes du comportement mécanique des composites à matrice céramique - Thesis n° 1948 - University of Bordeaux I - France, (1998).

## REPORTS AND PUBLICATIONS

---

- [5] C. Guerin - Multi-scale modelling for SiC<sub>f</sub>/SiC composites - Preliminary considerations to an implementation in CAST3M - CEA report DRN/DMT SEMT/LM2S/RT/04-001/A - January 2004.
- [6] J. F. Maire and N. Carrere - Modélisation multi-échelles des composites SiC<sub>f</sub>/SiC - Définition des potentiels thermodynamiques et de dissipation pour les différents constituants du composites SiC<sub>f</sub>/SiC (to be published).
- [7] N. Carrere and J. F. Maire - Modélisation multi-échelles des composites SiC<sub>f</sub>/SiC. Fourniture des éléments nécessaires à l'implémentation d'une méthode de changement d'échelle pour les passages micro-méso et méso-macro adaptée au SiC<sub>f</sub>/SiC (to be published).
- [8] C. Guerin - Multi-scale modelling of the thermo-mechanical behaviour of SiC<sub>f</sub>/SiC advanced composite - 2004 Activity report - Definition of the constitutive laws and gathering of the data necessary for the implementation in CAST3M (to be published).

## **TASK LEADER**

---

Caroline GUERIN

DRN/DMT/SEMT/LM2S  
CEA-Saclay  
F-91191 Gif-sur-Yvette Cedex

Tél. : 33 1 69 08 53 52  
Fax : 33 1 69 08 86 84

E-mail : [cguerin@cea.fr](mailto:cguerin@cea.fr)



---

**Task Title: IFMIF ACCELERATOR FACILITIES**  
**Accelerator system design**

---

**INTRODUCTION**

---

The mission of IFMIF is to provide an accelerator-based, D-Li neutron source to produce high energy neutrons at sufficient intensity and irradiation volume to test samples of candidate materials up to about a full lifetime of anticipated use in fusion energy reactors. IFMIF would also provide calibration and validation of data from fission reactor and other accelerator-based irradiation tests. It would generate an engineering base of material-specific activation and radiological properties data, and support the analysis of materials for use in safety, maintenance, recycling, decommissioning, and waste disposal systems.

The basic approach is to provide two linacs modules, each delivering 125 mA at 40 MeV to a common target. This approach presents availability and operational flexibility advantages.

The Transition year(s) were initiated in 2003 with the objective of continuing the “Key Element Technology Phase” (KEP). The activities defined here concentrate on a follow up of the previous work, delivery to the other team of the previous works, transition meetings, reflection on the present design and its possible evolution.

The IFMIF work is carried out at the CEA in the framework of a considerably larger activity presently undergoing in the field of high-intensity linear accelerators [1], [2], [3].

**2004 ACTIVITIES**

---

**THE REFERENCE DESIGN**

The ion source generates a Continuous Wave (CW) 140-mA deuteron beam at 95 keV. A Low Energy Beam Transport (LEBT) guides the deuteron beam from the operating source to a Radio Frequency Quadrupole (RFQ). The RFQ bunches the beam and accelerates 125 mA to 5 MeV. The 5 MeV RFQ beam is injected directly into a Room Temperature (RT), Drift-Tube-Linac (DTL) of the conventional Alvarez type with post couplers, where it is accelerated to 40 MeV.

The rf power system for the IFMIF accelerator is based on a diacode amplifier operated at a power level of 1.0 MW and a frequency of 175 MHz. Operation of both the RFQ and the DTL at the same relatively low frequency is a conservative approach for delivering the high current deuteron beam with low beam loss in the accelerator. The use of only one rf frequency also provides some operational simplification.

Beam loss in the accelerator is to be limited so that maintenance can be “hands-on”, i.e., not requiring remote manipulators. However, the accelerator facility will be designed in such a way that remote maintenance is not precluded. As shown later, the DTL output beam is carried to the target by a High Energy Beam-Transport (HEBT) that also provides the desired target spot distribution tailoring and energy dispersion. This HEBT must perform a variety of functions, complicated by the presence of strong space-charge forces within the beam.

The design improved since the referenced CDA in 1996. Several options were evaluated, and the work led to the selection of a single reference for each subcomponent. There is no showstopper in the present reference design, but it does not mean that this 10 MW accelerator will be easy to build. Each subsystem will have to be carefully built and assembled. The project remains one of the most powerful in the world. The reference design is based on a conservative basis for this reason, most of the subcomponents having been fully tested or used. The design did not significantly change during the year 2004. The most interesting points are a confirmation on some choices.

Even if the reference design exists, the delays observed in the process of decision can be profitably used in exploring new possibilities, which will have to prove their ability to replace the present choices.

**The ECR Source**

The ECR source was selected as a result of the IFMIF KEP development program. This choice has been validated after extensive parallel development in Europe (CEA-Saclay and Frankfurt) and in Japan (JAERI). It has been selected mostly because of its intrinsic availability compared to other source types, and its efficiency. No further development on the D<sup>+</sup> source is required.

We need to use H<sub>2</sub><sup>+</sup> particles instead of D<sup>+</sup> during the commissioning of the accelerator in order to minimize the activation during the tuning. Therefore work was provided on this basis in CEA-Saclay and IAP-Frankfurt. In both places, the results are not in accordance with the objectives. The source is optimized for atomic ions production and extraction; it remains extremely difficult to tune it for molecular ions production. Around 30 mA can be extracted at the cost of a big amount of other species.

Opinion was received that H<sup>+</sup> could be used by running the accelerator at half voltage, thus avoiding the need for H<sub>2</sub><sup>+</sup> injector which requires development. The Accelerator Team does not fully agree with this position as it ignores the most important aspect of reliability. At half-voltage, the accelerator is not at its operating condition.

Extensive experience at LEDA showed that the most difficult conditioning and tuning problems occurred within 10% of the design conditions. The main (only ?) advantages of running  $H^+$  is to check the obvious errors like quadrupoles misplugged or badly misaligned.

The requirement for an  $H_2^+$  injector for commissioning and tuning will remain on the requirements list. This supposes the development of a new source, which has to start very soon in order to meet the requirement on time for the commissioning. As this new source will be used only during commissioning, it has to be easily plugged. Also one has to understand that the beam parameters (like emittance) will be different from the final source. A complete study will have to be made during EVEDA to assess the gain of such source. If no solution could be found, the commissioning will have to be made in pulsed mode to minimize the activation. The acceptable losses vs beam duty factor will have to be calculated by the safety group during EVEDA.

The whole accelerator has to be able to work also in pulsed mode, and this includes the source, the RF system and diagnostics.

### Beam diagnostics

The development of diagnostics continues but is clearly not sufficient. The IFMIF program may profit from other project like SPIRAL2 [3], IPHI [1] or SNS [4], J-Park [5] and GSI [6] in order to develop non interceptive diagnostics. Some techniques are promising like the Doppler shifted line analyses or the backscattered particles detection that will be used during the IPHI tests in Saclay, or the profiler based on residual gas ionization in use in GANIL.

Nevertheless the specificity of the IFMIF accelerators (very high beam power, low energy) makes the development crucial. They are also difficulties in finding good diagnostics for the longitudinal plane (transition RFQ-DTL and DTL tanks). It appears that the beam footprint monitoring instrumentation is not needed any more. This is a good point that needs to be clarified, as it is a crucial point at the intersection of 2 groups : target and accelerator.

Beam diagnostics specific to IFMIF have to be developed during EVEDA.

### RFQ

RFQ are expensive components. They are also crucial to bunch and accelerate the beam. The output beam energy has been part of an optimization of the whole design, and decreased from 8 to 5 MeV in 1999.

There are 2 designs available, with similar performances. They were compared with different codes. It is important to know that only one of the 2 (the Saclay design) was used in the end-to-end error study performed by the Saclay group, including the HEBT. Also the Saclay team has performed SUPERFISH calculations and 2D shape optimizations which provided good RF power consumption.

The tuning knowledge of 4-vanes RFQ was a result of a strong CEA effort. It might be exported.

Two types of cavity were evaluated for the IFMIF accelerator: 4-vanes and 4-rods types. One can quote that:

- Four vanes structures are the less consuming structures.
- Four rods RFQs show a very high peak power loss. The value cannot be easily managed and induces engineering difficulties and possible deformations in CW mode.

The Frankfurt team looked seriously in the 4-rod options and recommends, as us, using 4-vane RFQ.

Taking these results into account, we reinforce our recommendation using the 4-vane RFQ type.

The 2-D transverse section is completely defined. The optimization leads to an RF consumption estimated to  $\approx 1600$  kW, "everything" included. One RF source has been saved.

The work that needs to be done concerns the RF coupling in the cavity (engineering), the optimization of the 3D extremities, detailed design and integration. A high power RFQ cavity load must be build. It will help the design and will be useful as a load for the RF system and coupling loop tests. Tests using beam injection should also be included. Obviously, if the budget profile allows a fully-constructed RFQ, time and money will be saved.

### DTL

A good and conservative design exists. It was included in the multiparticle end-to-end beam simulations performed in 2003. A hot model had good success in proving the feasibility. This hot model was developed at 352 MHz with similar or stricter parameters.

Detailed design and integration have to be performed. Engineering prototypes at the right frequency for manufacture of the DTL is now required. The RF coupling to the cavity has also to be studied.

### The IFMIF High Energy Beam Transport line

The HEBT was studied based on the reference concept (multipole expanders). It reaches performances close to the requirements. Nevertheless the differences need to be validated by the target group.

The detailed design and integration of the line needs to be done. This will include the magnet specifications. The HEBT scrapers must be studied, and may have an impact on the line length (shielding).

We already know that the magnetic elements of the end part of the line will have to be aligned with concepts coming from the 4<sup>th</sup> generation electron light machine. Their placement and displacement will have to be monitored with an active system (2  $\mu$ m).

A cheaper solution may exist with a raster scanner technique. A safe and rigorous system may be built with a good benefit for the project.

**RF system**

We now have at least one manufacturer able to deliver a 1MW CW tube at 175MHz. The tube was tested for more than 1000 hours on a dummy load with success.

The RF system remains the most expensive part of the accelerator. Therefore it is necessary to have a good control of the costing of these elements. We recommend to quickly developed, buy and test a full RF system. An experienced team is already working on this topics, it is a good point to maintain.

The test can be made on the RFQ hot cavity, with beam coming in (test of the RF low level, RF high level, and beam injection capability). This supposes the availability of a test stand, as always stated by the accelerator group.

**Miscellaneous**

- The first point concerns the test stand. As stated by R. Jameson: “Probably the largest “hole” in the EVDA definition is that the costs for the engineering validation tests assume the existence and underwriting of a powerful test facility, capable of installing and operating the D<sup>+</sup> and H<sub>2</sub><sup>+</sup> injectors, RFQ load cavity, complete RF system with one coupler, and beam diagnostics instrumentation (.../...) as a test stand”.
- The safety analysis should start as soon as possible. It has a big impact on the accelerator and building designs. Experience with other projects showed that it may also lead to huge planning delays if not started on time. A call for work package was tendered by EFDA.
- The main beam parameters are defined at low energy. So, if one wants to qualify the accelerator, it is necessary to build and test a source, LEBT, full RFQ and the first tank of the DTL. This will have to be followed by a diagnostic line. Doing so, each sub-component is fully tested (the first DTL tanks is the most difficult one), as well as the transitions which are crucial in a high-intensity/high-power accelerator (space charge regime).

**Other development**

The project is a 2x5 MW beam power project. This is one of the most powerful projects in the world (with ILC-International Linear Collider). Therefore it was always based on conservative specifications.

As the project is delayed, it might be interesting to support new developments like design based on superconducting cavities. This supposes that the new options **MUST** be compared at the same level than the reference design, to be able to prove their advantages.

The technical baseline will be frozen with the construction decision phase.

**Other**

During the year 2004, reviews were made on the present design, next R&D, schedule and costing with the Ad-Hoc committee and some of the accelerator team members.

One of the point explained by the Ad-Hoc Committee in the “technical assessment report” is that “In an aggressive realisation scenario it should be possible to shorten significantly the total time planned for the EVEDA, construction and commissioning phases (currently 15 years to full exploitation), which would be in the best interest of the Project’s mission.”. It is necessary to keep in mind that the EVEDA phase was proposed to allow a spreading of the investment over the years. It was also pointed out at the time of the suggestion that it could lead to a global cost increase.

**CONCLUSIONS**

We have a reference design. This design has to enter in a detailed study phase, with prototypes or final parts. Integration, RF system, engineering models have to be made. This supposes a major investment and a decision on ITER/IFMIF has to be pronounced. Such an “announce effect” might be crucial for the project.

The team needs to be reinforced, once the construction decision is made. The CEA-Saclay team is on a “waiting position”. Even if the CEA-Saclay team is not directly involved in the near future development, they can answer questions that may arise on the linac design. The main contact persons are:

|  |                             |
|--|-----------------------------|
| Pascal DEBU:<br>pdebu@cea.fr                     | Head of the SACM laboratory |
| Pierre-Yves BEAUVAIS:<br>pybeauvais@cea.fr       | IPHI project leader         |
| Pierre-Emmanuel BERNAUDIN:<br>pebernaudin@cea.fr | DTL hot model               |
| Aline CURTONI:<br>acurtoni@cea.fr                | 2D RFQ optimization         |
| Michel DESMONS:<br>mdesmons@cea.fr               | RF                          |
| Romuald DUPERRIER:<br>rduperrier@cea.fr          | Beam dynamics – end-to-end  |
| Robin FERDINAND:<br>robin.ferdinand@cea.fr       | former task leader          |
| Alain FRANCE:<br>afrance@cea.fr                  | RFQ tuning                  |
| Raphael GOBIN:<br>rjgobin@cea.fr                 | ECR source                  |
| Jacques PAYET:<br>jpayet@cea.fr                  | HEBT                        |
| Didier URIOT:<br>duriot@cea.fr                   | Beam dynamics – end-to-end  |

## REFERENCES

---

- [1] P-Y. Beauvais - Status report on the construction of the French high intensity proton injector (IPHI) - proceeding of EPAC 2002, Paris, page 539-541.
- [2] R. Gobin et al. - High intensity ECR ion source (H+, D+, H-) developments at CEA Saclay - ISIS2001 conference, RSI, Vol.73, n°2, February 2002 (922).
- [3] SPIRAL 2 white book - To be published in May.
- [4] SNS Beam commissioning status - S. Henderson et al. - Proc. EPAC 2004, p. 1524.
- [5] Beam Dynamics and Commissioning of the J-PARC Linac - Y. Yamazaki et al. - Proc. EPAC 2004, p. 1351.
- [6] The GSI synchrotron facility proposal for acceleration of high intensity ion and proton beams - P. Spiller et al. Proc. PAC 2003, p. 589.

## TASK LEADER

---

Robin FERDINAND

DSM/DAPNIA/SACM  
CEA-Saclay  
F-91191 Gif-sur-Yvette Cedex

Tél. : 33 1 69 08 96 91  
Fax : 33 1 69 08 14 30

E-mail : robin.ferdinand@cea.fr

---

**Task Title: VALIDATION OF COMPUTER CODES AND MODELS**


---



---

**INTRODUCTION**


---

The Activated Corrosion Products (ACP) in the ITER Primary Heat Transfer Systems (PHTS) or Tokamak Water Cooling Systems (TCWS) can be of major concern as contributor to the source term of potential released activity to the environment in case of accident (LOCA for instance) and to the ORE (Occupational Radiological Exposure) during the normal operation of ITER.

The PACTITER code, an adaptation of the PACTOLE code developed for Pressurized Water Reactor, has been used for predicting the ACP activities in the various PHTS or TCWS since 1995 [1].

On the other hand CORELE experiments have been performed in 2001 to test the capability of PACTITER V2 to reproduce measured release rates [2].

However some experimental artifacts have appeared during this tests campaign and shed a doubt on the relevance of the obtained results.

An important effort has then been produced to qualify the functioning of this loop [3] [4] and the objective of the new 2004 tests campaign was thus to definitely determine release rates in order to validate the PACTITER V2.1 version.

---

**2004 ACTIVITIES**


---

**STAINLESS STEEL RELEASE RATE EVALUATION IN THE CORELE LOOP**
**Experimental**

For TCWS operating conditions wall temperatures range between 100°C and 150°C and the coolant velocity from 0.04 m/s to 11 m/s. From a chemical point of view ITER operates under temperature at a pH equivalent to a neutral pH25°C. The 2004 CORELE test matrix proposed three tests devoted to the study of the influence of both temperature and flow rate in the same operating conditions of the 2001 tests campaign and corresponding to the ITER TCWS specifications (see table1).

The tube sections are made of stainless steel SS316L(N)IG manufactured using industrial processes. They are activated in the OSIRIS reactor and then connected to the main circuit of the CORELE loop. Having circulated in the irradiated tubes, the coolant is purified by passing through mixed beds of ion-exchange resins. As far as no release can exist in the loop (cold part in polypropylene, hot part in zircaloy) except in the test sections the activity trapped in the resins is solely due the released radioactive ions.

Due to the composition of the tested alloy, the main radio nuclides created by neutron irradiation in OSIRIS reactor and detected by gamma spectrometry in the beds of resins are  $^{60}\text{Co}$ ,  $^{58}\text{Co}$ ,  $^{51}\text{Cr}$  and  $^{54}\text{Mn}$ .

Table 1 : 2004 test matrix

|                                      | ITER 2004- 01                          |             | ITER 2004-02                         |             | ITER 2004-03                       |             |
|--------------------------------------|--|-------------|--------------------------------------|-------------|------------------------------------|-------------|
|                                      | SE1                                    | SE2         | SE1                                  | SE2         | SE3                                | SE4         |
|                                      | insert                                 | No insert   | insert                               | No insert   | insert                             | No insert   |
| Operating conditions                 | <b>150°C / 150 bar</b>                 |             | <b>100°C / 150 bar</b>               |             | <b>100°C / 120 bar</b>             |             |
| Velocity V (m/s)                     | <b>4.12</b>                            | <b>1.02</b> | <b>3.96</b>                          | <b>0.95</b> | <b>3.82</b>                        | <b>1.01</b> |
| Duration (hours)                     | <b>353</b>                             |             | <b>332</b>                           |             | <b>335</b>                         |             |
| O <sub>2</sub> concentration (ppb)   | <b>4.15 &lt;O<sub>2</sub>&lt; 22.5</b> |             | <b>9&lt;O<sub>2</sub>&lt;24</b>      |             | <b>3 &lt;O<sub>2</sub>&lt; 4</b>   |             |
| H <sub>2</sub> concentration (cc/kg) | <b>23.7&lt;H<sub>2</sub>&lt;26</b>     |             | <b>23.5&lt;H<sub>2</sub>&lt;25.5</b> |             | <b>23.5&lt;H<sub>2</sub>&lt;25</b> |             |
| Li (ppm)                             | <b>0.21</b>                            |             | <b>0.195</b>                         |             | <b>0.23</b>                        |             |
| pH <sub>25°C</sub> measured          | <b>6.6</b>                             |             | <b>6.85</b>                          |             | <b>6.6</b>                         |             |

**Results**

The two first tests were performed with a same pair of tubes (SE1 and SE2) although the last one was performed with a new freshly irradiated pair of tubes (SE3 and SE4). The following figure 1 gives the release rate of each element detected for ITER 2004-01 test and figure 2 compares the results of the two tests campaign at 100°C ITER 2004-02 and 03. The global release rate is the sum of the different release rates relative to each radionuclide measured in the resins

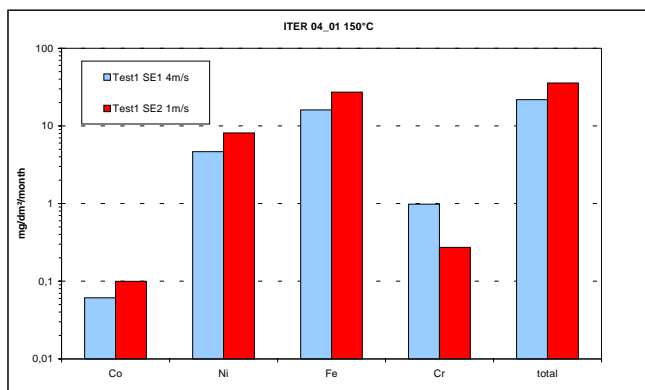


Figure 1 : ITER 04  
Test Results at 150°C operating conditions

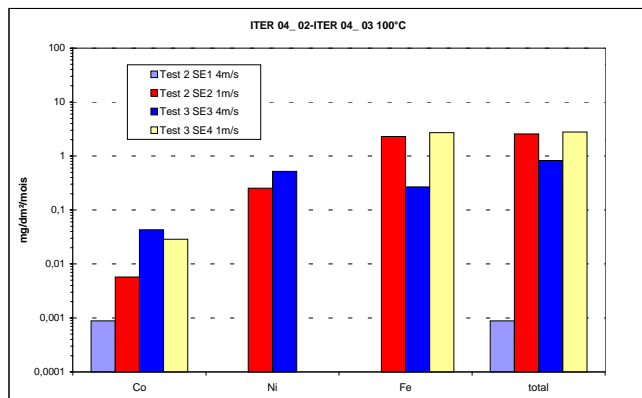


Figure 2 : ITER 04  
Test Results at 100°C operating conditions

**Discussion**

*Release of chromium*

Chromium was detected during test 2004-01 and was only trapped in measurement resin thus indicating the presence of a soluble form of chromium. This detection could thus be linked to the temperature of the test (150°C) and to the slight presence of oxygen which could favor the formation of mixed oxide of the chromite type (MCr<sub>2</sub>O<sub>4</sub>, where M = Fe, Ni).

The existence of such MCr<sub>2</sub>O<sub>4</sub> layer is coherent with experimental results indicating the release of Fe and Ni (upon the assumption that <sup>58</sup>Co is representative of Ni) It is worth noting that when the temperature is lower (100°C) no soluble chromium is detected whatever the O<sub>2</sub> content in the fluid.

*Influence of temperature*

The values of the release rate measured during this 2004 tests campaign are in fair agreement with those obtained during the 2001 campaign. Globally it can be seen that the lower the temperature the lower the release rate. These results could be explained by the existence of a diffusion barrier (possibly a mixed oxide as chromite for instance) at the interface fluid/stainless steel. At low temperature (say less than 100°C) the solid diffusion of atomic oxygen in this layer could be considerably reduced thus limiting the further formation of oxides (corrosion) and then the associated releases. As an example the thickness of this layer is commonly of the order of a nanometer (L=10<sup>-9</sup> m). Considering a solid diffusion coefficient, D, of 10<sup>-21</sup> m<sup>2</sup>/s (common value) leads to a characteristic diffusion time (L<sup>2</sup>/D) of 20 minutes compared to more than 300 hours of duration of the tests. Dividing D by 1000 when T is lowered from 150°C (423 K) to 100°C (373 K) could be possible if E would be higher than 180 kJ/mol.

*Influence of velocity*

From the comparison of the different tests conducted at about 1 m/s and 4 m/s (at the same temperature) one can conclude that the lower the velocity the slightly higher the release rate.

The velocity is a key parameter in the release global process as it is responsible for erosion of the deposits and for mass transfer limitation in the hydraulic diffusion layer. The erosion depends directly on the velocity whatever the temperature and the wall roughness in the ITER 2001 and 2004 tests conditions. No particles having been detected one must conclude that in the 2004 tests conditions erosion is not a relevant mechanism. On another hand the mass transfer coefficient in the diffusion layer is given through the Nusselt number calculated for instance by the Dittus-Boelter correlation. It appears that an increase in coolant velocity due to the reduction in the hydraulic diameter globally lowers the mass transfer - and then the release rate.

Finally two types of mass transfer limitations can be put forward in order to interpret the whole CORELE experiments :

- the thermally activated solid diffusion of oxygen in a surface barrier (possibly a mixed oxide as chromite for instance) which reduces the potential source of release by corrosion,
- the hydraulic diffusion which depends solely on Reynolds number instead of the velocity.

**SIMULATIONS**

**Neutronic and Activation simulations**

Prior to PACTITER calculations it is necessary to know the specific activities of the tubes (total and isotope-related) at the end of irradiation phase and the reaction rates related to the nuclear reactions responsible for the production of relevant radioisotopes.

A neutronic model has been set up to simulate the CORELE test tubes irradiation in OSIRIS reactor and to reproduce, as far as possible, the neutron fluxes in the different zones of the OSIRIS experimental area. From the analysis of table 2 which compares calculated and experimental isotope activities, one can conclude that the ANITA-2000 code is reliable enough for PACTITER calculations and more refined calculations seem not necessary [6].

Table 2 : Comparison of CORELE test tube experimental and calculated isotope activities

| Activity (Bq) for the 127 g tube | Experiment 26-3-2004 | ANITA-2000 calculations |
|----------------------------------|----------------------|-------------------------|
| Co-60                            | 1.13E+07             | 9.95E+06                |
| Co-58                            | 1.20E+07             | 3.30E+06                |
| Mn-54                            | 1.72E+06             | 6.90E+05                |
| Fe-59                            | 1.49E+07             | 1.27E+07                |
| Cr-51                            | 7.00E+08             | 6.00E+08                |

### PACTITER V2.1 simulations

First simulations with PACTITER V2.1 indicate that simultaneous conditions of Li content and pH are not reproducible. As an example the experimental Li contents yield to a calculated pH value ranging from 7.9 to 9.01 instead of the 6.6 measured.

Simulations of the whole CORELE experiments by PACTITER V2.1 also require the knowledge of the porosity of the oxide layer at the surface of the inner tube (POROS).

Unfortunately no measurement of such key parameter is available. Using respectively 40% and 80% when the temperature is respectively 100 and 150°C enables a fair agreement between experimental and calculated release rates (R in mg/dm<sup>2</sup>.month) as depicted in table 3.

Table 3 : Comparison between experimental and calculated release rates R (in mg/dm<sup>2</sup>.month)

| T [°C]                 | 100       |           | 150      |          |
|------------------------|-----------|-----------|----------|----------|
| POROS                  | 0.4       |           | 0.8      |          |
| Coolant velocity (m/s) | 3.82      | 1.01      | 4.12     | 1.02     |
| Re                     | 3,62E+04  | 5,77E+04  | 5,93E+04 | 8,55E+04 |
| R (PACTITER)           | 1,05      | 1,55      | 19,40    | 24,50    |
| R experimental         | 0,8 ± 0,3 | 2,8 ± 1,5 | 22 ± 3   | 36 ± 2   |

The simulation of CORELE 2004 experimental tests provided encouraging results : dependency of SS316L release rate from Re (and not from fluid velocity), important role of the fluid temperature.

Nevertheless it has been shown that the release model in PACTITER V2.1 (or in PACTOLE V2) is questionable (no experimental validation of the POROS parameter for instance) [6]. Therefore a new version of PACTOLE (PACTOLE V3.1) will be released in the next future and will benefit of many improvements (chemistry module, parametric expression of the corrosion and release rates, treatment of oxidizing conditions, numerical method). The reference version of PACTITER will then be version 3.1.

## REFERENCES

- [1] D. Tarabelli - PACTITER (PACTOLE VERSION FOR ITER) - Final Report - CEA Technical Report - DEC/SECA/LTC/98-150, June 1998.
- [2] T. Duverneix, V. Biscay - Report on ITER 01 and ITER 02 tests in the CORELE 2 loop CEA Technical report DEC/S3C/ 01 - 139 Ind. 0 - December 2001.
- [3] D. Tarabelli, S. Anthoni, D. Féron, Ph. Ridoux, L. Guinard, Ch. Brun, A. Long - Status and future plans of the PACTOLE code predicting the activation and transport of corrosion products in PWRs - Proc. of the Japan Atomic Industrial Forum International Conference on Water Chemistry in Nuclear Power Plants - Kashiwasaki, October 13-16, JAIF, Tokyo (1998) 301-305.

## REPORTS AND PUBLICATIONS

- [4] V. Biscay, M. Girard, F. Dacquait - Qualification de la boucle CORELE : Essai sur le système de rétention des ions - CEA Technical report DEC/S3C/02-145 ind. 0.
- [5] F. Dacquait, V. Biscay, M. Girard - Qualification du système de rétentions d'ions de la boucle CORELE - CEA Technical report DEC/S3C/03-162 Ind 0.
- [6] G. Cambi, D.G. Cepraga, M. Frisoni - OSIRIS neutronic and activation simulation with Scalene-ANITA in support of PACTITER/CORELE analyses - Memo 1/2005/ENEA/FIS-MET - February 2005.
- [7] P. Schindler et al. - Stainless steel realize rate evaluation in ITER operating conditions DTN/STRI/LTCD04-020 - December 2004.

## **TASK LEADER**

---

Patricia SCHINDLER

DTN/STRI/LTCD  
CEA-Cadarache  
F-13108 Saint-Paul-Lez-Durance Cedex

Tél. : 33 4 42 25 73 62  
Fax : 33 4 42 25 47 77

E-mail : [patricia.schindler@cea.fr](mailto:patricia.schindler@cea.fr)

---

## **Task Title: WASTE AND DECOMMISSIONING STRATEGY**

---

### **INTRODUCTION**

---

Within the framework of waste management strategy, it has been demonstrated that one way to reduce the high level waste is detritiation. This detritiation could be applied to steel waste. The knowledge of mechanisms involved in tritium trapping and desorption will allow to choose the most appropriate procedure. The working program deals with the management of tritiated steels and the way to reduce tritium transfer. This work is divided into 4 tasks:

- Task 1 : Lowering of desorption kinetics of the residual tritium.
- Task 2 : Lowering of the residual tritium concentration.
- Task 3 : Validation of tritium loading technique in solid phase.
- Task 4 : Role of microstructure on the tritium desorption.

In 2003, only the task 1, 3 and 4 have been undertaken. The tasks 1 and 3 use ingots from CEA Valduc. These ingots are obtained by melting under vacuum of waste composed with tritiated austenitic stainless steels. The results of this studies detailed in [1] have been presented last year.

In 2004 this study has been completed by the achievement of tasks 2 and 4 , so all tasks have been fulfilled.

### **2004 ACTIVITIES**

---

The goal of the first task is to develop thermal treatment in solid phase to:

- Lower the residual tritium concentration (by desorption reheating).
- Reduce the diffusivity of residual tritium (by changing the microstructure).
- Reduce the kinetic of residual tritium desorption (by forming of barrier films).

### **TASK 2**

The objective of task 2 was to characterize the residual tritium content and the desorption flow at ambient temperature in stainless steel samples detritiated using a new process recently implemented by the CEA at Valduc.

As these samples were not available, a study was recently launched – as part of task 2 – using samples that were detritiated by the CEA at Cadarache (DEN/ STPA/ LPC).

The final report [2] provides a review of tasks 2 & 4 results; future prospects vis-à-vis the extension of this study are also discussed

This study aims at testing the validity of a detritiation process that was implemented by the CEA at Cadarache (DEN/ STPA/ LPC). More specifically, the study aims at comparing results previously obtained from task 1 [1]. With new results obtained under the same conditions and using the same materials following detritiation at Cadarache.

CEA Valduc stainless steel (batch A) was used in this study. This steel was characterized prior to testing [1] with its residual tritium content being below 100 kBq/g. Six 11×6×0.6 mm samples were cut using a micro-saw and polished using 1200-grit sandpaper.

Before sending these samples to the CEA for detritiation, the surface activities of all sample surfaces were recorded and desorption measurements at 20°C were taken over a period of 60 minutes to determine the average desorption flow.

Following detritiation by the CEA, the surface activities and residual tritium desorption flows of certain samples were measured again. All measurements were carried out using the same procedures as those previously described [1].

### **RESULTS**

#### **Surface activities and average desorption flows before detritiation**

The results are illustrated in table 1. The surface activity corresponds to the average value of the measurements taken on both sides of each sample.

Except for sample 6, good reproducibility was observed in the sample surface activities and average desorption flows at 20°C for 60 minutes.

Furthermore, these values proved to be very similar to those previously measured on samples taken from the same stainless steel ingot [1].

The profiles representing the accumulated quantity of desorbed tritium at 20°C over 60 minutes are illustrated in figure 1. Except for sample 6, good reproducibility of tritium desorption profiles from one sample to another can also be observed.

Table 1 : Surface activities and average desorption flows before detritiation (Valduc steel, batch A)

| Sample (weight in grams) | Surface activity (Bq/cm <sup>2</sup> ) | Average desorption flow (60 min) (Bq/cm <sup>2</sup> /s) |
|--------------------------|--|--|
| 1 (0.2740)               | 3.3                                    | 1.44 10 <sup>-3</sup>                                    |
| 2 (0.2842)               | 4.6                                    | 1.57 10 <sup>-3</sup>                                    |
| 3 (0.3148)               | 4.5                                    | 1.64 10 <sup>-3</sup>                                    |
| 4 (0.3153)               | 3.4                                    | 1.59 10 <sup>-3</sup>                                    |
| 5 (0.3108)               | 3.6                                    | 1.42 10 <sup>-3</sup>                                    |
| 6 (0.2973)               | 2.5                                    | 0.84 10 <sup>-3</sup>                                    |

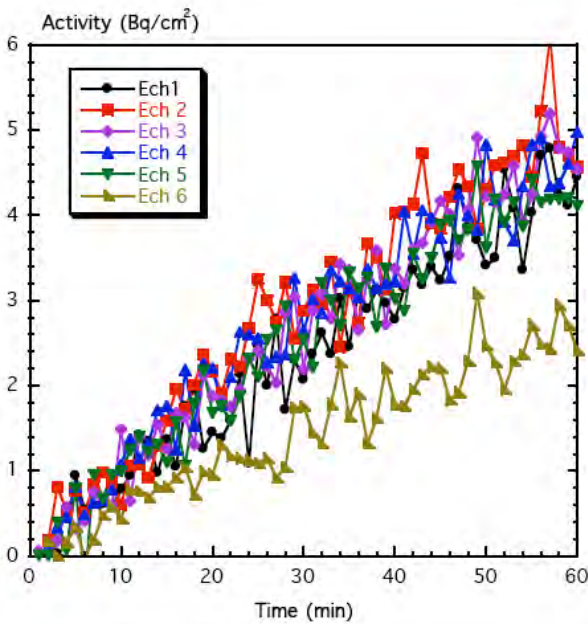


Figure 1 : Tritium desorption profiles of samples before detritiation (Valduc steel, batch A, profiles are corrected based on the value of the surface activity at t = 0)

**Surface activities and average desorption flows after detritiation**

Detritiation conditions were chosen based on previously obtained results [1] (Task 3), which made it possible to illustrate an almost total detritiation of the samples subjected successively to annealing at 600°C for 20 hours in a sealed phial, the oxidized surface being twice polished, and annealing at 600°C for 4 hours two more times – with polishing operation between annealing – in a moist air environment. The two detritiated samples were available at the end of december 2004. The detritiation tests were conducted with Hytec gas in the LPC<sup>1</sup> using two different annealing conditions:

- Sample 1: 600°C, 20 h + 600°C, 4h + 600°C, 4 h with polishing operation between each annealing to eliminate oxide films.
- Sample 2: 600°C, 20h.

Measurements were carried out on each sample 1) before eliminating the oxide film that appears following detritiation annealing and 2) after having eliminated this film by polishing operation with 1200-grit sandpaper.

The results are indicated in table 2. The values measured before eliminating the oxide film are indicated in italics. These results reveal the existence of residual tritium activity on the surface of the detritiated samples coated with an oxide film. In conformity with previous results [1], this activity is much lower in sample 1, which had undergone complete detritiation. These results also reveal – for both detritiation conditions – that surface activities and tritium desorption at ambient temperature are almost non-existent after annealing and polished operation. The desorption profiles (in figure 2) illustrate the absence of tritium desorption at 20°C following annealing (the accumulated tritium quantity does not increase).

Table 2 : Surface activity and average desorption flow after detritiation (Valduc steel, batch A)

| Sample | Detritiation conditions                           | Surface activity (Bq/cm <sup>2</sup> ) | Average desorption flow (60 min) (Bq/cm <sup>2</sup> /s) |
|--------|---|--|--|
| 1      | 600°C, 20 h + pol. + 600°C, 4h + pol. + 600°C, 4h | <i>8.1 10<sup>-2</sup>, &lt; DT</i>    | < DT, < DT   |
| 2      | 600°C, 20 h                                       | 2.6, < DT                              | < DT, < DT   |

DT: detection threshold  
pol.: polishing

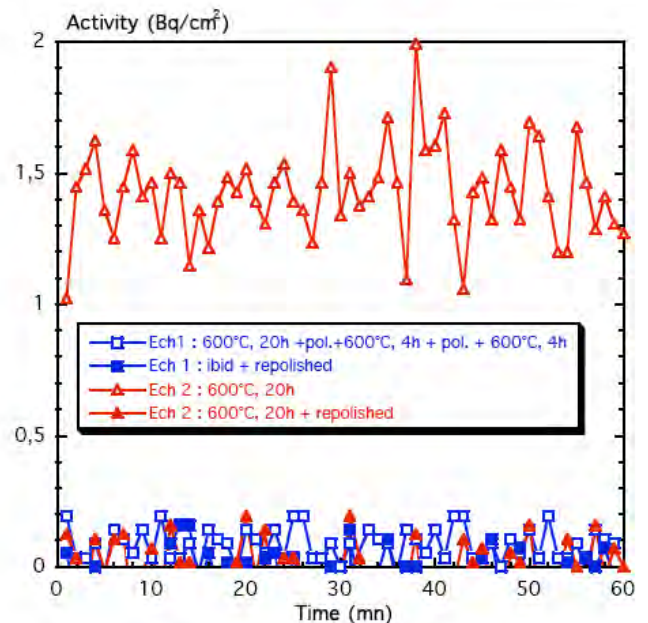


Figure 2 : Tritium desorption profiles of samples 1 & 2 after detritiation annealing (Valduc steel, batch A)

Such results tend to reduce the total tritium degassing from a cask of waste and then final disposal specifications could be easier to reach.

<sup>1</sup> Laboratoire Procédés physico-chimique sur les Caloporteurs ≈ Laboratory studying physico-chemical procedures on coolants

## TASK 4

It is important to remember that this study aims at examining the influence of micro-structural defects in stainless steels upon tritium absorption and tritium desorption at ambient temperature. In the continuity of work carried out in 2003 ([1], tasks 3 & 4), a comparative study was launched, focusing on the influence of different standard microstructures upon:

- The quantity of hydrogen introduced under given cathodic hydrogenation conditions and the residual hydrogen content after desorption annealing.
- Surface activities and tritium desorption kinetics at 20°C respectively after a) having introduced tritium into these different structures by cathodic charging at 150°C under the previously described conditions ([1], Task 3) and b) desorption annealing.

The comparative study focuses on five different microstructures of three different austenitic stainless steel grades. The microstructures can be described as such:

- Recrystallized 316 LN steel (1 h, 1,090°C + water quench).
- Sensitized 316 LN steel (1 h, 1,090°C + water quench + 30 % rolling + 5 h, 700°C).
- Recrystallized 321 steel (1 h, 1,200°C + water quench).
- Recrystallized 321 steel (1 h, 1,200°C + water quench + 5 h, 800°C).
- Valduc steel (batch A, remelt rough-cast microstructure + detritiation 20 h, 600°C + 4 h, 600°C + 4 h, 600°C).

These different microstructures contain precipitate phases of differing chemical compositions, morphologies and volume fractions. To begin with, the influence of each microstructure upon hydrogen absorption and desorption was investigated using a quantitative analysis technique by melting. The effect of microstructures was then studied using liquid scintillation counting (LSC) on the tritiated samples.

### **Influence of microstructures on hydrogen absorption & desorption**

This section of the study aims at revealing any possible effects of the microstructure upon the quantity of absorbed hydrogen or the residual hydrogen content after desorption annealing. In order to do this, a direct quantitative analysis technique was applied by melting the total quantity of the hydrogen introduced into the material by cathodic hydrogenation in molten salts.

In terms of austenitic stainless steels, difficulties lay in the low diffusivity of hydrogen and its isotopes [3]. A plane millimeter-thin plate and a hydrogenation temperature of about 300°C were therefore required to hydrogenate to saturation point in a reasonable time limit.

The choice of the best hydrogenation and desorption conditions is detailed in [2]. Two hydrogenation temperatures have been tested : 150°C and 300°C

The following hypotheses make it possible to explain the absence of any significant effects of the microstructures upon the hydrogen contents measured after hydrogenation at 150°C and 300°C:

- The effects of hydrogen trapping on the micro-structural defects are limited owing to the low H-trapping interaction energy levels. Consequently, the introduced hydrogen concentration at these temperatures is – for given hydrogenation conditions (temperature, equivalent hydrogen pressure) – controlled by the solubility of hydrogen in the material, with this solubility mainly depending on the chemical composition of the material.
- The quantity of hydrogen trapped in the micro-structural defects would therefore be low at such temperatures and variations in hydrogen quantities in relation to the microstructure are masked by the high concentration of lattice hydrogen.

### **Influence of microstructures on tritium absorption & desorption**

For each microstructure, two or four samples of equivalent geometry were tritiated, all surfaces were polished in an identical manner and surface activity measurements were taken. The accumulated quantity of tritium desorbed at 20°C was then recorded during 60 minutes and 900 minutes.

A first series of measurements was carried out less than 48 hours after having introduced the tritium. A second series of measurements was carried out 10 to 20 days after hydrogenation to test the influence of the microstructures on the variations in surface activities and desorption kinetics in relation to the ageing time at -20°C.

The surface activity of each sample surface was first measured before measuring only one surface of the samples successively to quantify the dispersion of the surface activity values. Prior to taking the each measurement, the sample surface was polished using 4000-grit sandpaper for 15 seconds in order to eliminate any possibly absorbed species, without however significantly grinding the surface.

Except the considerably lower values measured in the sensitized 316 LN steel, which remain to be validated, comparable surface activities show that the influence of the microstructure on the surface activity is minor.

Comparison of the desorption profiles (20°C, 900 min) indicated in figure 3 for two samples of each microstructure however point to an influence of the microstructure upon desorption. More specifically, the average desorption flow is clearly higher for the recrystallized 316 LN steel in which the precipitation of carbides or carbonitrides is extremely minimal.

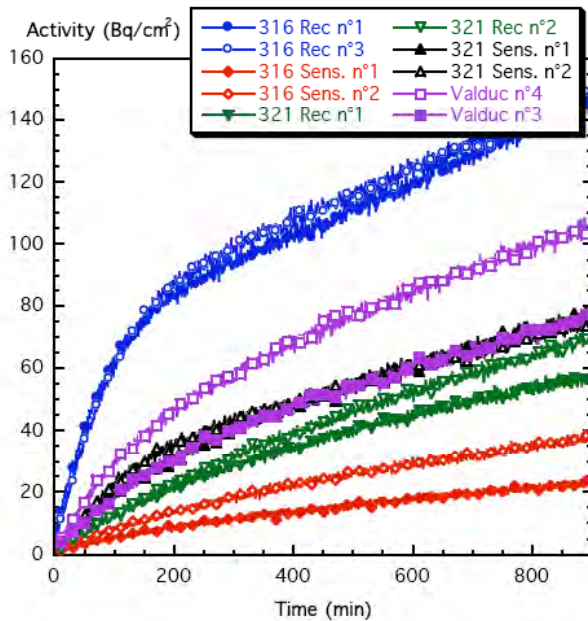


Figure 3 : Tritium desorption profiles (20°C, 900 min) of various 316 LN, 321 and Valduc steel samples with different microstructures

The results of measurements carried out on Valduc steel samples that were detritiated (20 h, 600°C + 4 h, 600°C + 4 h, 600°C) and then recharged in tritium (3 h, 150°C) are illustrated in table 2. These results reveal comparable variations in surface activities and average desorption flows in relation to sample ageing.

Figure 3 illustrates both the reproducibility of the desorption measurements (20°C, 900 min) and the influence of ageing upon the samples. These results show that the surface activities and the average desorption flows remain high after 10 months of ageing at -20°C. Such results validate observations also made concerning 316 LN and 321 steel samples, according to which the decrease in the desorption flow combined with the ageing effect is mainly be observed during the first few days after hydrogenation.

#### Influence of desorption annealing on surface activities and average desorption flows at 20°C

Tritiated samples were annealed under conditions similar to those applied to determine hydrogen concentrations in order to measure – after tritium desorption under the given temperature/ time conditions – the surface activity representative of the residual tritium content and the average desorption flow at 20°C of the residual tritium. The results of the first series of measurements taken after 70 hours of annealing at 150°C are detailed in [2].

In terms of the surface activity, the relatively high values measured on the non-polished surface after annealing indicate enrichment in tritium in the thin oxy-hydroxide film formed during annealing. These observations corroborate previous results (Task 2, and [1], Tasks 1 & 3).

After having eliminated the oxide film, the very low but significant activities were measured in all the microstructures except for the precipitate-free microstructure (recrystallized 316 LN steel). These values indicate that the residual tritium content is low (1% to 10% of the initial value).

After annealing, desorption of the residual tritium can only be observed in the sensitized 321 and Valduc steel samples; in both cases however, this desorption is extremely low. These results comply with the hydrogen concentration results and imply that the Valduc and 321 steels (particularly the sensitized microstructure) are the most suitable steels when it comes to maintaining small quantities of trapped tritium after annealing at 150°C.

## CONCLUSIONS

The first series of measurements carried out during Task 2 confirm the results obtained in [1] revealing high detritiation in the Valduc steel after annealing at 600°C with a detritiation factor with single annealing treatment above 30.

Detritiation seems more effective in tests carried out at in the last tests as only one annealing at 600°C for 20 hours was required to lower the surface activity below the detection threshold. This most probably results from the atmosphere in which the treatment was performed (circulation of a gas). Comparison of these measurements with the residual hydrogen contents measured in samples after chemical dissolution remains to be done.

Work carried out during Task 4 made it possible to test the validity of a cathodic hydrogenation technique in molten salts at 300°C designed to saturate the millimeter-thick austenitic stainless steel samples with hydrogen.

The hydrogen concentrations obtained after hydrogenation at this temperature point to the absence of any marked effect of the microstructure upon the hydrogen content introduced into these steels.

The measurements performed on the hydrogenated samples after degassing at moderate temperature (100°C to 200°C) indicate the absence of any significant hydrogen trapping in the microstructures in question when the degassing temperatures exceeds 150°C.

It is important to remember that the small mass of the samples, combined with the high fabrication-produced hydrogen content present in the standard non-hydrogenated samples, makes it difficult to measure small quantities of trapped hydrogen with this technique.

Measurements nevertheless reveal high residual hydrogen content in the complex Valduc microstructure following degassing at 100°C and 150°C.

In terms of the samples tritiated at 150°C (3h), interpreting the surface activity measurements proves to be difficult owing to a) the heterogeneous tritium concentration in the sample thickness and b) variations in measurements in relation to the ageing time of the samples at storage temperature (-20°C).

The high sensitivity of the  $\beta$  LSC technique makes it possible to show that a low fraction – of about 1% – of hydrogen remains trapped in the steel after degassing at 150°C. In order to more accurately quantify this residual tritium content, it would be necessary to multiply the number of measurements under conditions making it possible to improve their precision while conducting measurements by chemical dissolution in parallel.

The quantities used to characterize tritium desorption at 20°C (quantity of desorbed tritium in a given time, desorption profiles) as well as variations in these quantities in relation to the sample ageing time at -20°C, point to an influence of the microstructure upon desorption. More specifically, the accumulated quantity of desorbed tritium is greater in the microstructure whose precipitate content is low (316 LN in solution for 1 hour at 1,090°C).

Generally speaking, results tend to reveal the existence of a low fraction of hydrogen trapped in the microstructures containing precipitates (sensitized 316, 321, sensitized 321 and Valduc steels). This trapping is apparent by both the low content of residual tritium in the microstructures after degassing at moderate temperature (below 150°C) and the decrease in the average desorption flow of diffusible tritium in the presence of these precipitates. However, the fact that the effect of trapping above 150°C almost completely disappears seems to suggest that the tritium/ precipitate trapping energies are low. More pronounced trapping effects could be observed in the complex Valduc microstructures obtained by twice melting waste.

Quantitative analysis of these trapping phenomena and their influence upon tritium desorption kinetics would imply the systematic study of hydrogen or tritium trapping by thermal-desorption in relation to the nature and density of the micro-structural defects in the steel microstructures.

Last of all, deformation products (dislocations,  $\epsilon$  and  $\alpha'$  martensites, etc.) represent another family of micro-structural defects for which study has not been launched and whose effect upon tritium desorption (trapping and diffusion short-circuits) deserves to be characterized and quantified.

---

## REPORTS AND PUBLICATIONS

---

- [1] J. Chêne, A.M. Brass, A. Lassoued, O. Gastaldi, P. Trabuc - Management of tritiated wastes - Stainless steel detritiation studies - Note technique DTN/STPA/LPC 04/069.
- [2] A-M Brass, J. Chêne, P. Trabuc, O. Gastaldi - Tritiated steel management - Note technique DTN/STPA/LPC - to be published.

---

## REFERENCES

---

- [3] P. Tison - Influence de l'hydrogène sur le comportement des métaux - Rapport CEA R-5240, 1984.

---

## TASK LEADER

---

Olivier GASTALDI

DEN/DTN/STPA/LPC  
CEA-Cadarache  
F-13108 Saint-Paul-Lez-Durance Cedex

Tél. : 33 4 42 25 37 87  
Fax : 33 4 42 25 72 87

E-mail : olivier.gastaldi@cea.fr



**Task Title: ICE FORMATION ON CRYOGENIC SURFACES**

**INTRODUCTION**

The computer codes which are used for the analysis of the accidental sequences in ITER should have good quality assurance level. The EVITA facility (figure 1) has been designed for the simulation of the physical phenomena occurring during a coolant ingress into the cryostat of ITER reactor, which is one of the identified accidental sequence in the ITER safety report. Studied physical phenomena are namely ice formation on a cryogenic structure, heat transfer coefficient between walls and fluid, flashing, two-phase critical flow. The comparison between calculations and experiments allows the ability of the computer codes to treat the relevant physical phenomena to be assessed.

The EVITA programme is supported by EFDA and it is also an item of an implementing agreement under the auspices of the International Energy Agency. The main experimental results are the pressure evolution in the vacuum vessel, the different heat exchanges and the ice formation on the cryogenic surface.

**2004 ACTIVITIES**

**EXPERIMENTS**

The EVITA device has been adapted by the end 2003 in order to carry out cryogenic experiments [1] with the measurement of steam condensation on cryogenic surfaces in the presence of non condensable gas (gaseous nitrogen), and the test matrix (11 tests) was defined. These tests were completed in 2004 [2].

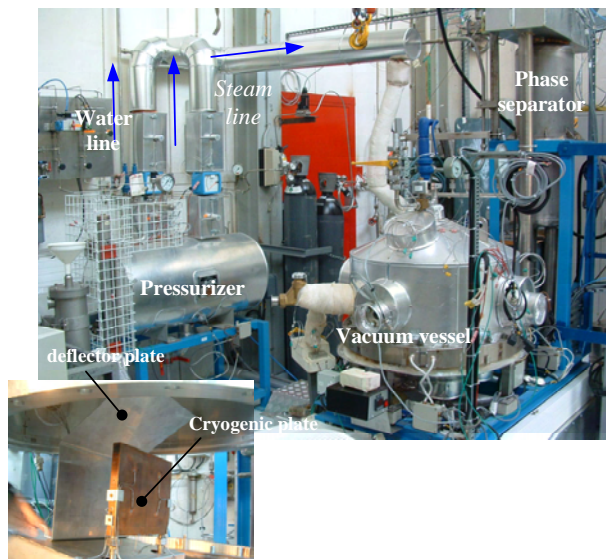


Figure 1 : View of the EVITA facility

**MAIN RESULTS**

These tests highlighted that the presence of non condensable gas with the steam or pressurized water is important for the physical phenomena occurred in the EVITA facility, and so in accidental situation in ITER:

- The kinetic of the ice layer formation : injection of non condensable gas seems to increase the velocity of the ice layer formation. The ice mass formed (figure 2) is the same for a given steam /water flow rate with or without non condensable gas but it takes about two minutes to reach stalized layer of ice comparing to those ten minutes during the tests without non condensable gas.
- The heat transfers to the nitrogen in the cryogenic plate are also modified during the injections with non condensable gas. The heat transfer to the liquid nitrogen is lower during a simultaneous steam/water - non condensable gas injection than in a single steam or water injection.
- The vacuum vessel pressurization is also affected by the presence of the non condensable gas, the final stabilized pressure in the vessel is about half of the previous value measured in the tests without non condensable gas injection (see figures 3 and 4).

Concerning the pressurization of the vacuum vessel, the tests without non condensable gas are conservatives whereas the tests with non condensable gas injection are conservatives from the ice mass formation point of view.

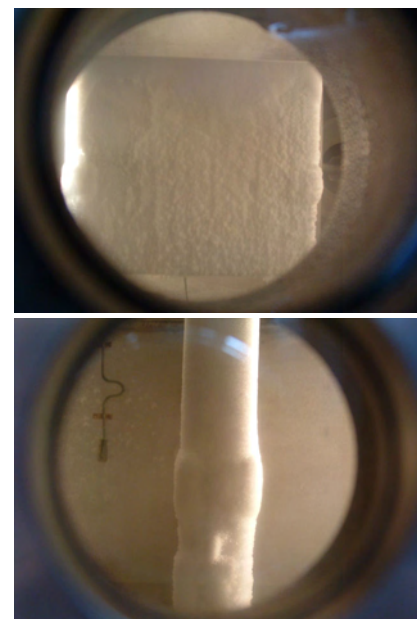


Figure 2 : Views of the cryogenic plate with the ice layer formed on it

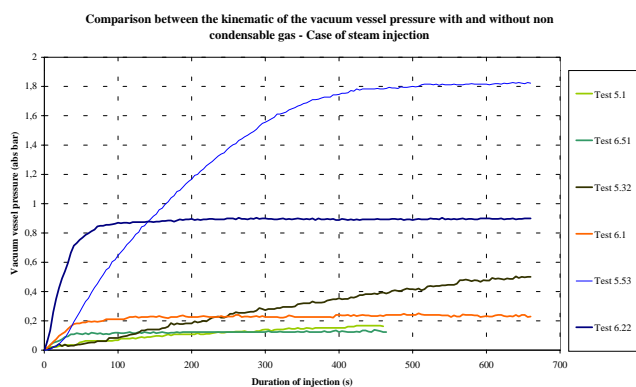


Figure 3 : Comparison of the pressure evolutions in the vacuum vessel in the case of pressurized water injection with and without non condensable gas

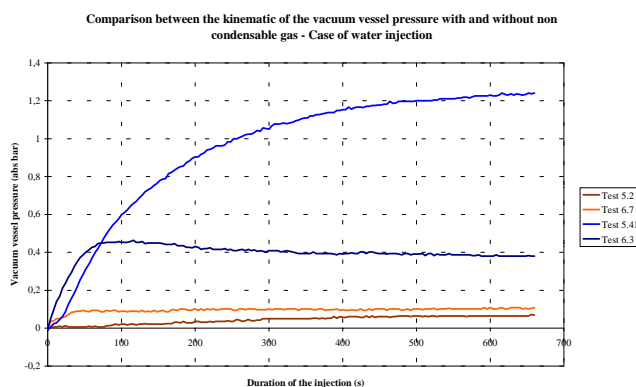


Figure 4 : Comparison of the pressure evolutions in the vacuum vessel in the case of steam injection with and without non condensable gas

## CONCLUSIONS

These tests show that the presence of non condensable gas have an influence of on physical phenomena which occurred in the vacuum vessel (heat exchanges, ice formation and pressure evolution).

A more detailed study of those physical phenomena like the ice formation on the cryogenic surface and condensation on the ice layer, which play an important role in the kinetic of the pressurization of the vessel, should be out of interest in the frame of our experimental program.

Selected tests (with and/or without incondensable gas) should be performed (2005 program) several times with different durations in order to assess ice and condensate masses at different steps of the process for a given set of experimental parameters.

This could be out of interest to characterize their influence on the vacuum vessel pressure evolution (vaporization of the condensate, formation of a water pool at the bottom of the vessel,...).

## REPORTS AND PUBLICATIONS

- [1] L. Ayrault - EVITA, Preparation of the cryogenic tests with steam injection in presence of non condensable gas - Technical note DER/STR/LCET NT 03-035, 20/10/2003, CEA, France.
- [2] L. Ayrault, F. Challet - EVITA : Results of the cryogenic test campaign with injection of non condensable gas - CEA report DTN/STPA/LTCG 04/035.
- [3] P. Sardain, L. Ayrault, G. Laffont, F. Challet, L.B. Marie, B. Merrill, M.T. Porfiri, G. Caruso - The EVITA programme: experimental and numerical simulation of a fluid ingress in the cryostat of a water-cooled fusion reactor - SOFT 2004.

## TASK LEADER

Laurent AYRAULT

DEN/DTN/STPA/LTCG  
CEA-Cadarache  
F-13108 Saint-Paul-Lez-Durance Cedex

Tél. : 33 4 42 25 44 72

Fax : 33 4 42 25 66 38

E-mail : laurent.ayrault@cea

**Task Title: ASSESSMENT OF RADIOACTIVE WASTE IN ITER HOT CELL FACILITY**

**INTRODUCTION**

Within the framework of the ITER project and in order to improve the assessment done on the waste production coming from hot cell and to determine the best way to manage the produced waste, a specific study has been launched on this topic.

The objectives of the study are the quantification and the characterization of operational waste (process and housekeeping) coming from hot cells facility.

The main goal of this task is to perform a detailed assessment of the amount and type of radioactive waste produced during maintenance and refurbishing activities. The task is divided into two parts:

- Investigation and summing up of the refurbishing and maintenance activities in order to quantify the amount and type of radioactive waste including identification of nuclides of special interest (3H, Be, ...).
- Categorisation of the waste according to the specific regulations for radioactive waste disposal at the European candidate site.

The first part is done by CEA and the second one by VR Studsvik.

To treat the first part, based on ITER documentation, a synthesis of operating conditions has been done to determine the main functions each part of the hot cell facility which leads to specify the waste type and to highlight the used tools inducing house keeping waste.

After this qualitative analysis and quantitative one is done. Afterwards, the housekeeping waste production is estimated. To do that, the experimental feedback of different hot cell facilities has been used. The facilities are JET, PHENIX (French fast breeder reactor) and LECA STAR (hot cells facility in CEA Cadarache).

**2004 ACTIVITIES**

The first phase of this task has been the determination of the operating conditions, the maintenance and refurbishment needs and the used tools in the hot cells. The study of the needs of maintenance and refurbishment allows to determine the main components leading to a waste flux in term of amount.

From an analysis of the operations foreseen in ITER hot cells, the main components to handle with are:

- Modules (first wall and blanket).
- Divertor (standard divertor cassette, second divertor cassette, diagnostics divertor cassette).
- Port limiter.
- Test blanket modules.
- Cryopump and cryogenic valves.
- ICH&CD Module.
- ECH&CD module.
- NB injector (ion source, filaments, 12 holders, Caesium oven).
- Diagnostics (Equatorial port, diagnostic plug/ RH port plug).
- Upper port.
- Divertor port.
- VV seal plates.
- IVV/GDC probes.

Some of them are producing a very low amount of them, but for the others, a detailed analysis has been done.

The following table summarises the estimated waste masses from component replacements. The assumptions leading to this table are given in [1].

| <b>Component/material</b>           | <b>Waste mass (t)</b> |
|-------------------------------------|-----------------------|
| <b>Divertor</b>                     |                       |
| Steel                               | 330                   |
| Copper                              | 90                    |
| Tungsten                            | 95                    |
| Carbon (CFC)                        | 8                     |
| Total                               | 523                   |
| <b>Shielding blanket first wall</b> |                       |
| Steel                               | 15                    |
| Copper                              | 7.5                   |
| Beryllium                           | 0.7                   |
| Total                               | 23                    |
| <b>Limiter front parts</b>          |                       |
| Copper                              | 1.4                   |
| Beryllium                           | 0.051                 |
| Total                               | 1.5                   |
| <b>ECH&amp;CD front parts</b>       |                       |
| Expected to be mostly steel         | 4.1                   |
| <b>ICH&amp;CH front parts</b>       |                       |
| Expected to be mostly steel         | 4.8                   |

|                                       |            |
|---------------------------------------|------------|
| <b>NBH&amp;CH front parts</b>         |            |
| Expected to be mostly steel           | 21         |
| <b>Diagnostics front parts</b>        |            |
| Expected to be mostly steel           | 82         |
| <b>Test blanket module first wall</b> |            |
| Expected to be mostly steel           | 40         |
| <b>Fuelling system equipment</b>      |            |
| Possibly mostly steel-like            | 7.0        |
| <b>Tritium plant equipment</b>        |            |
| Possibly mostly steel-like            | 38         |
| <b>Remote handling equipment</b>      |            |
| Possibly mostly steel-like            | 1.0        |
| <b>Hot cell equipment</b>             |            |
| Possibly mostly steel-like            | 1.0        |
| <b>Total</b>                          | <b>750</b> |

To determine the induced housekeeping waste production, analogy with existing facilities is done. But to obtain an efficient comparison, these facilities are chosen if they are using some comparable tools and if the treated components are of the same nature (when it is possible).

The determination of the used tools is done by the analysis of the life cycle of the different parts of the hot cell building, which is described in appendix 1.

The main tools used are:

- Casks for transfer (different type)
- Remote manipulators
- Vacuum brush tool for dust cleaning (with bag filters)
- Cranes
- Lifting tool
- Heavy manipulators
- Testing equipment (leak),
- Welding tools
- Cutting tools
- Monorail hoist, ...

In comparison, some other hot cells facility have been studied to determine the ratio between initial waste flux and induced housekeeping waste flux. The better available experimental feedback is Phenix (French Liquid Metal Fast Breeder Reactor) one.

The Phenix larger hot cell (CEI) volume is about 1000 m<sup>3</sup>. The operations with this cell have started in 1974. So we can benefit of an important experience. More than 1300 assemblies have been dismantled. Many operations can be achieved in the CEI and in the annex cell (specially machining in this cell):

- Non destructive control with different tools:
  - . Neutron radiography.
  - . Eddy currents.
  - . Gamma spectrometry.

- Maintenance, reconditioning and dismantling with different tools:

- . Cleaning pits.
- . Hoisting tools.
- . Machining: sawing, milling, ...
- . Sorting, conditioning and sealing.

So the operations to achieve are quite similar to the one foreseen in ITER hot cells.

### WASTE PRODUCTION

These cells receives different elements coming from the reactor vessel. These elements are leading to waste which can be sorted into two categories:

1. Assemblies structure, lateral neutronic protection; fuel pin, ...which are of French B category waste.
2. Housekeeping waste composed of tools (saws, fuel pin thimbles, rubber, remote handling, ...). This last category can be divided into three sub categories:
  - Organic, plastics and rags.
  - Cables.
  - Metallic housekeeping.

Most of the produced waste are B type. For housekeeping the difficulty is to separate each type. In fact it has been noticed that housekeeping would be A type waste, at least, but in the case of Phénix, sorting is difficult due to the hot cell conception.

In term of waste flux, during the two last years around 20 casks were produced by the treatment of the assemblies (one cask represents about 300 kg waste). Among them two were filled with various housekeeping waste. Then, it is possible to have an approximate ratio of the housekeeping waste flux versus the global waste flux: around 10 %. Earlier experiences were mentioned in the document [2]. From this document, the following data can be extracted: among 768 casks, 68 were classified into the flammable category which represents the major part of housekeeping waste produced. Currently a production of 30 casks per year is foreseen with about 4 casks filled with housekeeping.

This ratio can vary during the life of the facility. For example, remote handling needs more maintenance after many years of use, dismantling operations are also producing more housekeeping waste than normal operations.

### WASTE SPECIFIC ACTIVITY

For each type of component an analysis of main radionuclides has been done based on the activation calculation made in [3]. These calculations are considering on homogeneous material and are using 1 D model.

The detailed values of the activity for each nuclide in a specific component are given in [1].

Taking into account, the French waste classification which is presented in [1], the following table summarizes which component will be in a specified category. This part will be detailed in further studies.

| Components  | Type of waste |
|---|---------------|
| Modules<br>(first wall and blanket)   | B type        |
| Divertor<br>(standard divertor cassette,<br>second divertor cassette,<br>diagnostics divertor cassette) | B type        |
| Port limiter  | A type        |
| Test blanket modules  | B type        |
| Cryopump<br>and cryogenic valves  |               |
| ICH&CD Module   | B type        |
| ECH&CD module   | B type        |
| NB injector<br>(ion source, filaments,<br>12 holders, Caesium oven)                                     | A type        |
| Diagnostics<br>(Equatorial port, diagnostic<br>plug/ RH port plug)                                      | A type        |

## CONCLUSIONS

This work summarises the amount of foreseen waste production which comes from the ITER hot cells. Based on main maintenance analysis and refurbishment frequency, the masses of each components has been determined.

Based on operational experience of mainly Phénix hot cells a ratio between waste production (directly linked to the maintenance frequency) and induced housekeeping waste production has been established. This ratio is between 10 to 15 % in volume.

The following table summarize the amount of waste of each type of components during the maintenance phases.

| Component/System  | Global waste mass [t]                    |
|---|--|
| Divertor cassettes  | 523                                      |
| Blanket module (first wall)   | 23                                       |
| Diagnostics (equatorial port<br>plug and upper port plug)   | 82                                       |
| Heating systems   | 30                                       |
| Port limiters   | 1.5                                      |
| Cryopumps valves  | Included in fuelling<br>system equipment |
| Test blanket modules  | 40                                       |
| Fuelling system equipment   | 7  |
| Tritium plant equipment   | 38                                       |
| Remote handling + hot cell<br>equipment   | 2  |
| Associated housekeeping<br>waste ~10 – 15 % in volume<br>(mass calculated with a<br>packing <sup>2</sup> factor of 1) | ~100                                     |
| Dust  | 0.5                                      |
| <b>Total</b>  | ~850                                     |

## REPORTS AND PUBLICATIONS

- [1] O. Gastaldi, C. Lacrosonniere - Source, quantity and type of radioactive waste coming from ITER hot cells - Technical document DTN/STPA/LPC 2004/070.
- [2] Bilan des poubelles de déchets Phénix envoyées à COGEMA/TCD/TDS/CDS entre 1974 et 1998 (PA 6925 XD 46849 /B).
- [3] G. Cambi, D.G. Cepraga, M. Frisoni, R. Forrest - Work on source term for ITER-FEAT (D451) - Sub-task 1 : activation calculation.

## TASK LEADER

Olivier GASTALDI

DEN/DTN/STPA/LPC  
CEA-Cadarache  
F-13108 Saint-Paul-Lez-Durance Cedex

Tél. : 33 4 42 25 37 87  
Fax : 33 4 42 25 72 87

E-mail : olivier.gastaldi@cea.fr



## TW4-TSS-SEA5.5-D02&D05

# Task Title: VALIDATION OF THE PAXITR AND PACTITER CODE AGAINST FUSION-SPECIFIC EXPERIMENTS

## INTRODUCTION

### OBJECTIVE OF THE FEASIBILITY STUDY

This document is carried out for the task TW4-TSS-SEA 5.5 related to the validation of the PACTITER computer code which could be used for safety assessments of ITER or future fusion power plants. The possibility to improve the validation level of the PACTITER code against CIRENE tests is here studied, knowing that until now, the CIRENE loop is dedicated to the understanding and quantification of corrosion product deposition in Pressurized Water Reactor conditions [1] [2] [3].

A feasibility study has been launched for estimating the interest of the CIRENE facility for the experimental simulation of ITER - like CRUD deposition in the ITER Tokamak Cooling Water Systems (TCWS) operating conditions. Thus, the following items have been studied : thermal-hydraulic data, chemistry of the coolant, volumes and surfaces of the circuit, materials, keeping in mind that the TCWS have water cooled copper and stainless steel components that lead to Activated Corrosion Products (ACP) and corrosion species different from those encountered in PWR circuits.

### CHECKED PARAMETERS FOR ITER

The PACTITER code estimates the masses and activities of the corrosion products deposited on the surfaces of the different components using reactor design and operation data. The validation of the PACTITER code requires experiments carried out under the specific conditions of the ITER TCWS or Primary Heat Transfer System (PHTS) [4] whose main characteristics are :

- In terms of materials : most of the components in contact with the coolant are made in 304, 316 L stainless steels and CuCrZr alloys which may release corrosion products in the coolant. Further neutron activation of these chemical species yields to radioactive oxide deposits which may contribute to the source term of the potential released activity to the environment in case of accident and to the ORE (Occupational Radiological Exposure) during the normal operation of ITER.
- A coolant with a pH equivalent to a neutral pH<sub>25°C</sub>; the Water Chemistry Specifications for ACP Analyses gives a pH<sub>20°C</sub> = 7, with [H<sub>2</sub>] ~ 25 cm<sup>3</sup>/kg and [O<sub>2</sub>] ~ 10 µg/kg, up to 100 µg/kg for the Vacuum Vessel [5].
- From a thermal-hydraulic point of view : the PHTS coolant flow rates in the channels range from 0.04 m/s (Vacuum vessel) to 11 m/s (Limiters/Divertors) and the fluid temperatures between 50°C and 240°C.
- Operational scenarios : the ITER operating scenarios include different operational periods for the three types of PHTS (FW/blanket shield, divertor and vacuum vessel) as for example the following one related to the FW/blanket shield loop (SA1\_acp scenario) [4] :

*Table 1 : ITER SA1 operating scenario (TCWS coolant temperature)*

| Cold standby | Baking   | Hot standby | Plasma burn         | Dwell    |
|--------------|----------|-------------|---------------------|----------|
| 50°C         | 240°C    | 100°C       | ΔT :<br>100 - 150°C | 50°C     |
| 450 days     | 450 days | 305 days    | 155 days            | 360 days |

*Table 2 : Required modifications of CIRENE for ITER tests*

|                     | CIRENE outlines for PWR tests   | CIRENE outlines for DIV/LIM tests   |
|---------------------|---|---|
| Under flux section  | Zy4 claddings area / heating rods<br>Thermal flux section<br>ΔT ~ 30 - 50°C and v ~ 3 - 4 m/s | Stainless steel and CuCrZr alloy area<br>Thermal and neutronic flux section<br><b>design to define for ΔT ~ 50°C and velocity : ~ 1 to 11 m/s</b> |
| Out-of-flux section | Stainless steel pipes   | idem  |
| Heat exchanger      | Ni based alloy, S.G tubes<br>ΔT ~ 30°C  | Stainless steel<br><b>design to define for ΔT up to 50°C velocity : ~ 0.02 to 1 m/s</b>   |
| Circulation pump    | Fixed flow rate   | Variable flow rate  |
| Implemented devices | Ion and radionuclide injections<br>Adapted to PWR corrosion products                          | Idem Fe, Ni, Co and Cu<br>Adapted to TWCS corrosion products  |

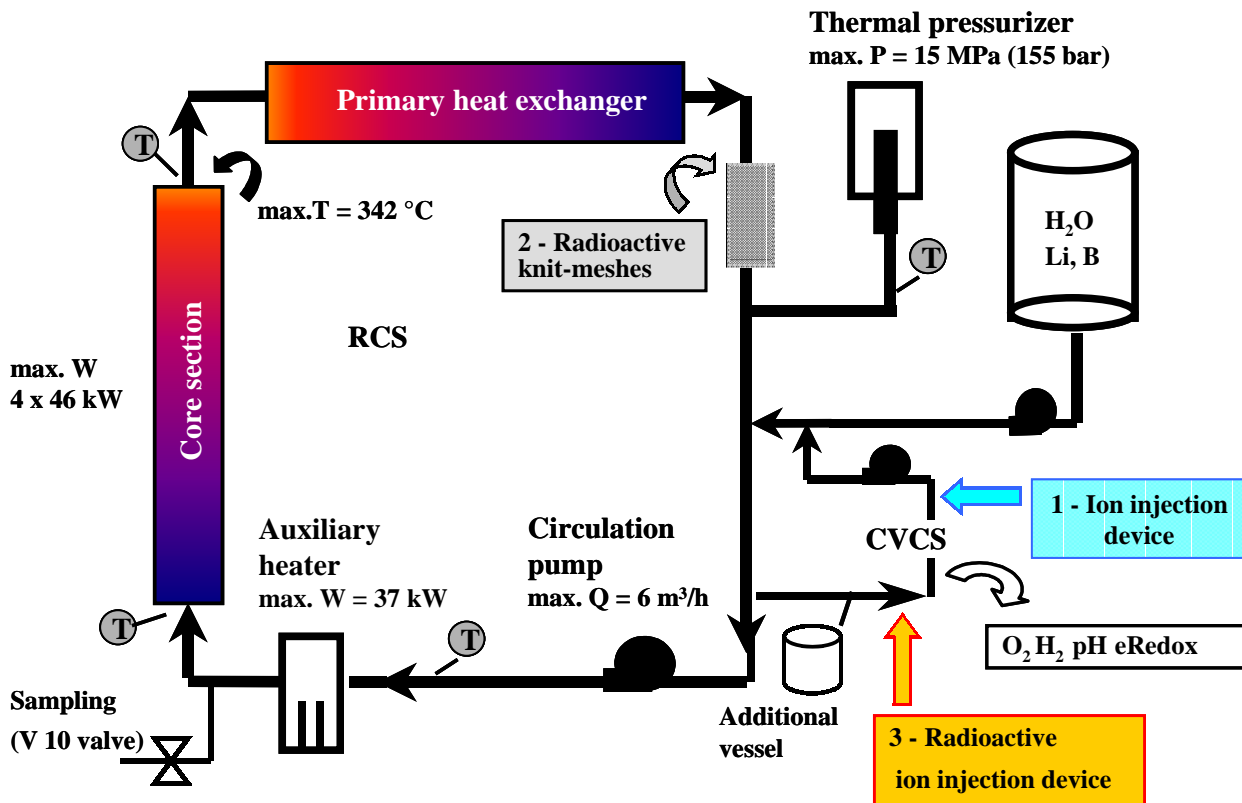


Figure 1 : CIRENE loop outlines

## PROPOSALS FOR MODIFICATIONS OF THE CIRENE LOOP

According to all the elements identified above we suggest in table 2 the following modifications for the CIRENE loop (see figure 1) in order to perform tests under ITER TCWS specifications.

The purpose of the ion injection device is to reproduce the concentration of metallic elements released in the coolant of the TCWS. Thus, we intend to inject under soluble state, Fe, Ni, Co and Cu elements only if the available stainless steel and copper areas are not sufficient. The external injection rate has to be calculated using the required exchange area of the material and the corresponding release rate. This approach is similar to the one used for PWR deposition studies and requires not only the perfect control of the injection rate but also to be as representative as possible of the request released concentrations in the coolant during the time of the experiment. In that sense the "boundary conditions" are well known during the test ensuring the possibility for validating the deposition modelling in the PACTITER code. On the other hand this external injection may be questionable in terms of similarity with actual ITER release rates (especially for Cu). The required properties of the TCWS under flux section can led to the two following designs :

1) a central section made of stainless steel and Cu alloy claddings is inserted in a square stainless steel pipe in which circulates the fluid. When necessary the request heating flux is applied to the rods to reach the thermal gradient between the inlet and the outlet of this section. This design is quite similar to the updated one which maintains the fluid velocity around 3 - 4m/s,

2) in this case, the stainless steel and Cu - alloy section is heating by means of an external device, the inner wall is sized to reach high values of fluid velocity as 12 m/s on Cu areas. This design is more adapted to  $\gamma$  spectrometry analyses, in term of interpretations : deposition occurs on only one area, i.e., on the inner surface of the stainless steel and copper section while for the design 1/, deposition can occur on the stainless steel - Cu alloy claddings and/or on the inner surface of the stainless steel pipe.

## RELEVANT CHARACTERIZATIONS

All the analyses proposed for the ITER tests which would be performed in the CIRENE loop are presented in this chapter.

### Chemical analyses of the coolant in operation

2 liter - samples can be taken with the V10 valve (see figure 1) in order to analyse the composition of the primary coolant :

- metallic element contents : samples are passed through a 0.45  $\mu\text{m}$  Millipore filter and two ion-exchanger filters in order to increase measurement sensitivity and to quantify the soluble and particle proportions in metallic elements, i.e. in Fe, Co, Ni, Cr, Mn and Cu. Filter analyses are performed by X-ray fluorescent spectrometry. It can be noticed that these samplings can be performed at any stage of the test enabling a better monitoring of the evolution of the fluid composition. The detection limits are currently of the ppb order ( $10^{-9}$  kg/kgH<sub>2</sub>O ) and should be adapted to the requested concentrations in the fluid for the main CP elements in study (see the equilibrium solubilities of Cu alloy in [6]) ;

- impurities : impurities analyses involved coupling-plasma emission spectrometry, atomic absorption spectrometry and ion chromatography. This type of analyses is only performed at the beginning and at the end of the test, the relevant impurities being Al, Ca, Cl, F, SO<sub>4</sub>, Na and Mg.

### Nuclear measurements in operation

The possible ITER radionuclides are <sup>58</sup>Co, <sup>59</sup>Fe, <sup>64</sup>Cu, <sup>60</sup>Co and <sup>54</sup>Mn :

- The use of <sup>60</sup>Co and <sup>54</sup>Mn radionuclides which have a long radioactive half-time (respectively 5.3 years and 312 days), will lead to a global contamination of the RCS main pipes, that represents a major inconvenience with regard to the next tests undertaken in the loop.
- The possibly interesting gamma isotopes of Cu (<sup>62</sup>Cu, <sup>64</sup>Cu and <sup>66</sup>Cu) have very short radioactive half-time periods [7] that prevent them to be prepared in advance and injected through the ion injection device. Then further investigations are required to evaluate if in-situ measurements of copper through local neutron bombardment and  $\gamma$  spectrometry analysis [8] could be performed to measure the deposition of this corrosion product. Among the different nuclear reactions, the (n,  $\gamma$ ) reactions on <sup>63</sup>Cu (which gives <sup>64</sup>Cu) or on <sup>65</sup>Cu (which gives <sup>66</sup>Cu) are the lone whose activation cross sections (expressed in barns) may be sufficient. Nevertheless the gamma emission percentages range from very low (0.6% for <sup>64</sup>Cu) to low (7.6% for <sup>66</sup>Cu) that requiring a more complete study for this potentiality. Another way to perform such characterization could be to identify a transfer correlation between a well-known gamma emitter and Cu : for instance theoretical considerations could allow one to identify a co-released or co-deposited element. However experimental validation of such correlation should be required. For that purpose the CORELE loop could be used by inserting an irradiated copper based alloy in its test section and measuring both the released Cu content by chemical means and the released gamma emitter activities. Further study should be undertaken to better estimate that potentiality and particularly the relevance of the correspondence between co-release and co-deposit.

Thus, considering their radioactive half-times and the relevant in-line gamma spectrometry application, three radionuclides - <sup>58</sup>Co, <sup>59</sup>Fe and <sup>51</sup>Cr - can be selected for ACP study with the current measurement methodology of the CIRENE loop : radionuclide injection device, and in-line  $\gamma$  spectrometry measurements [9]. The measured areas could be the under flux section with stainless steel and Cu materials and an out-of-flux section with stainless steel material. The materials and design of these sections must be completely adapted to  $\gamma$  spectrometry investigations.

### Radiochemical measurements after shutdown

Radioactivity of the deposits on the RCS can be measured through gamma-ray spectrometry at the end of the ITER test, at ambient temperature.

The relevant studied areas could be the same that those in operation.

### Scrapings after the shutdown

The relative composition of the remained deposits, i.e. the composition in metallic elements as Fe, Co, Ni, Cr, Mn, Cu and in Ca mineral impurity can be obtained by means of X-ray fluorescent spectrometry analyses of CRUD scrapings. The weighing of the samples can give an indication of the residual CRUD density. Besides, CRUD scrapings could also be subjected to radiochemical measurements. Additional analyses can be proposed if the remained CRUD densities turn out to be sufficient (oxide analysis, crystallography...).

**Remark** : the CRUD scraping areas must be determined on sections which do not need any disassembly.

### CONCLUDING REMARKS

#### Validation of the tcws corrosion product deposition modelling of pactiter

At present time the CORELE loop is devoted to release rate measurements but presents some particular features. The most interesting concerns the fact that all the components of this loop, excepted the test section, are made of inert materials (polypropylene in the cold parts, zircalloy in the hot ones) that ensuring no release of these components in the circuits of the loop. Thus as far as the "radioactive" injection device of the CIRENE loop could be easily adapted to CORELE, the boundary conditions (in terms of concentrations, flow rates, temperature, pressure...) would be perfectly controlled (and known). This could be of great interest for the validation of the deposition modelling of PACTITER. Obviously the possibility of measuring deposition of ACP in CORELE requires some adaptations of the loop which are to be quantified as for instance the bypass of the resin beds or the in-line nuclear measurements mentioned above.

#### Global Validation of the Pactiter code

As previously mentioned, the external injection of ACP can be justified for the validation of the particular deposition modelling of the PACTITER code but is not relevant when dealing with a global validation of the code. Effectively the actual release rates in ITER conditions should vary during operations essentially due to the fact that the corrosion rates vary with time in more or less high proportions. Thus a global validation which aims to be representative of the whole ITER scenarios requires the measurement of all the mechanisms of ACP migration from the formation/release to the deposition. This can exclusively be performed in a dedicated loop in which all these phenomena can be reproduced in closest as possible ITER TCWS conditions. This feasibility study brings some answers regarding the possibility of using the CIRENE loop for that purpose, but the design of a new facility should be considered in order for example to take into account the electromagnetic field which could possibly influence the ACP migration.

## REFERENCES

---

- [1] M. Girard - Report of the 2000/02-03 CIRENE test - Note technique DEC/S3C/01 - 012.
- [2] Th. Duverneix, M. Girard, M. Sabatier - Définition et simulation d'essais de qualification du code PACTOLE dans la boucle CIRENE - Note technique DEC/S3C/02 – 125.
- [3] M. Sabatier, F. Nguyen, H. Marteau - Simulation par le code PACTOLE V3.0 des Essais 2000/03 et 2001/02 de la boucle CIRENE - Note Technique DEC/S3C/03 - 084.
- [4] L. Di Pace - ACP evaluation for the ITER TCWS DIV/LIM loop using PACTITER V2.1 - Final report - FUS-TN-SA-SE-R079 - October 2003.
- [5] H.W. Bartels - Specifications for Activated Corrosion Product Assessment for ITER-FEAT (Version 1.0) - Safety, Environmental and Health Group ITER - Garching JWS, November 24th, 1999.
- [6] L. Di Pace, D. Tarabelli, You D. - Development of the PACTITER code and its application to the assessment of the ITER Divertor cooling loop corrosion products - Fusion Technology Vol.34, No.3 part 2, pp733 - 737, 1998.
- [7] A.I. Aliev, U.I. Drynkin, D.I. Leipunskaya, V.A. Kasatkin - Handbook of nuclear data for neutron activation analysis, 1970.
- [8] M. Girard - Mesure du bore par interrogation neutronique active (INA) - Adaptation d'un montage sur la boucle CIRENE - Dossier de faisabilité - Note Technique DEC/S3C/02 – 055.
- [9] M. Girard, F. Dacquait, R. Chatelet - Injection d'ions actifs dans le circuit primaire de la boucle CIRENE - Dossier de faisabilité - Note Technique DEC/S3C/03-104.

## TASK LEADER

---

Marianne GIRARD

DEN/DTN/STRI

CEA-Cadarache

F-13108 Saint-Paul-Lez-Durance Cedex

Tél. : 33 4 42 25 45 54

Fax : 33 4 42 25 47 77

E-mail : marianne.girard@cea.fr

**Task Title: VALIDATION OF THE PACTITER CODE AGAINST FUSION-SPECIFIC EXPERIMENTS**  
**Development of the PACTITER code**

**INTRODUCTION**

The Activated Corrosion Products (ACP) in the ITER Primary Heat Transfer Systems (PHTS) can be of major concern as contributor to the Occupational Radiological Exposure (ORE) during the normal operation of ITER.

For almost 30 years, the PACTOLE code has been developed to predict the level of ACP in the PWR primary systems [1]. The code has been adapted for the ITER heat transfer systems by taking into account their specific operating conditions, material composition and water chemistry since 1995 [4]. The modified PACTOLE code is called PACTITER.

**2004 ACTIVITIES**

Following a comparison of results between PACTITER V2 and PACTITER V2.1 [2], in-depth investigations [5] have led to conclude that the PACTITER code, version V2 or V2.1, based on PACTOLE V2, gives overestimated results, but should definitively be improved and validated with dedicated experiments.

Indeed, a corrective factor was applied to the corrosion product solubilities at low temperatures ( $T < 200^{\circ}\text{C}$ ) in the PACTOLE V2 and PACTITER V2.1 codes. This solubility correction allows to fit the release rates to the experimental values at low temperatures without modifying the release model. However, it also affects dissolution and precipitation of corrosion products. Although this is not a problem for a PWR simulation (temperatures below  $200^{\circ}\text{C}$  are only encountered in the Chemical and Volume Control System, which has just a purification function for a PACTOLE calculation), it has an impact on contamination of the ITER heat transfer systems since the release value fitting has changed the dissolution and precipitation values.

This release model should be changed for ITER simulations, and that has been done in the PACTITER V3.0 code.

The PACTOLE V2 code has shown some lacks of modelling [3], particularly the release model. Therefore, a new code version released in 2003, namely PACTOLE V3.0, has been designed to account for recent developments relevant to the behaviour of corrosion products in PWR [3]. In 2004, the PACTITER V3.0 code has been developed from PACTOLE V3.0.

The PACTOLE and PACTITER V3.0 codes are still based on a control volume approach, the primary circuit is represented by an arrangement of several volumes in which mass balance equations are solved :

$$\frac{\partial m_i}{\partial t} + (\dot{m}_s - \dot{m}_e) = \sum_{\text{Source}} J_m - \sum_{\text{Sink}} J_m$$

Where  $m_i$  is the mass of the  $i^{\text{th}}$  isotope in a considered medium defined as a form for the corrosion products,  $t$  is the time,  $\dot{m}_s - \dot{m}_e$  is the convective term (balance between input and output) and except for nuclear reactions, which are mass production/loss within the considered medium,  $J_m$  is an exchange mass rate between two different media.

Seven different media are taken into account in a control volume: metal, inner oxide, outer oxide, deposit, fluid (containing ionic species), particle and filter&resin. All the media are represented in figure 1.

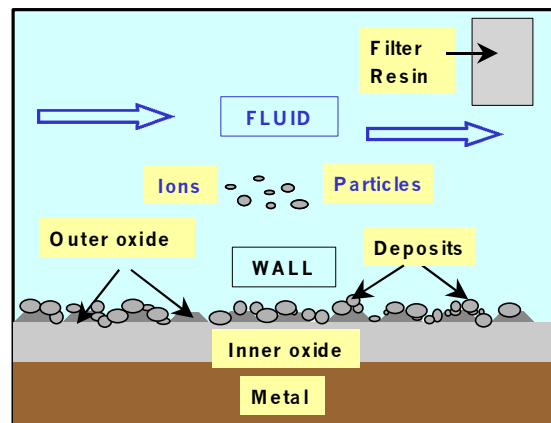


*Figure 1 : Media in a control volume for a PACTOLE representation*

The transfer mechanisms, which are modelled in the mass balance equations, between all the considered media, are summarised in figure 2.

The PACTOLE V3.0 code (and PACTITER V3.0) has been totally rewritten in a fully object oriented programming language (C++). It solves time-dependent mass balance equations in order to be able to simulate transient phenomena. Thanks to its architecture, new models can be easily tested and the class management process allows a non-limited number of isotopes. In this version, the release model has been reviewed, but there are still both existing models to improve and new models to implement. The making of a willful workprogram for improving the physical models and the data is under way.

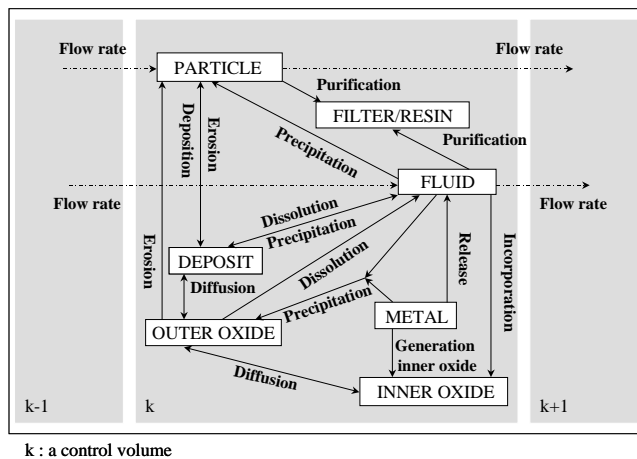


Figure 2 : Transfer processes between media in a control volume

A feasibility study has been launched for estimating the interest of the CIRENE facility for the experimental simulation of ITER - like crud deposition [7]. This type of tests would improve the validation level of the PACTITER code. This study has led to the following conclusions:

- The main components of the current CIRENE loop (core section, heat exchanger and the circulation pump) must be modified in order to be really representative of the ITER conditions. These modifications concern not only the design but also the used materials.
- For the corrosion products potentially released from materials,  $^{58}\text{Co}$ ,  $^{59}\text{Fe}$  and  $^{51}\text{Cr}$  can be used as gamma tracers with the current CIRENE measurement methodology.
- A complementary study should be undertaken to estimate the feasibility of in-line monitoring of Cu by in-situ neutron activation or whether a transfer correlation could exist between Cu and another measured radionuclide ( $^{58}\text{Co}$ ,  $^{59}\text{Fe}$  and  $^{51}\text{Cr}$ ).
- The need for release rates of copper (CuCrZr) and stainless steel in the overall spectrum of the ITER operating conditions (thermal-hydraulic and chemical conditions) has also been identified.
- A complementary study could be undertaken to estimate whether the CORELE loop could be adapted to the validation of the deposition modelling of PACTITER, or even if a new facility should be designed for the global validation of the code in as close as possible ITER conditions.

## CONCLUSIONS

In 2004, the PACTITER V3.0 code was developed from the PACTOLE V3.0 code. The first results are encouraging [6]. Nevertheless, as the PACTOLE V3.1 code will be greatly improved in 2005 (chemistry module, parametric expression of the corrosion and release rates, treatment of oxidizing conditions, numerical method), the reference version of PACTITER will be version 3.1.

## REFERENCES

- [1] P. Beslu, G. Frejaville, and A. Lalet - A computer code PACTOLE to predict activation and transport of corrosion product in PWR - Proceedings of an international conference organized by the British Nuclear Energy Society - Bournemouth, 24-27 October 1977. BNES, London, 1978, pp. 195-201.
- [2] L. Di Pace - Tasks TW1-TSS-SEA5 - Validation of computer codes and models, Presentation of results within delivery 10 - Report on status of 2002 PACTITER validation of task - Review meeting on ITER TA81-01, Dust mobilisation and removal from the vacuum vessel and ITER TA81-04 - Activation corrosion product assessment, Frascati, 30<sup>th</sup> September 2003.
- [3] F. N'Guyen, D. Tarabelli, H. Marteau, F. Dacquait, N. Perot, G. Ranchoux, L. Guinard, A. Long, C. Viala - First numerical simulations of contamination of the PWR primary circuit by activated corrosion products with the PACTOLE V3.0 code. - Proceedings of the International Conference on Water Chemistry of Nuclear Reactors Systems - San Francisco, October 11-14, 2004, p. 562-571.
- [4] J.C. Robin - Adaptation of PACTOLE for fusion application - Note Technique DEC/SECA/LTC/95-255, décembre 1995.

## REPORTS AND PUBLICATIONS

- [5] F. Dacquait, - Status of PACTITER - Note Technique DTN/SMTM/2004-117 - décembre 2004.
- [6] F. Dacquait, B. Larat, F. N'Guyen - Status of the PACTITER development - Meeting on PACTITER, Cadarache, 25-26/01/05.
- [7] M. Girard, V. Blet, F. Dacquait - Final report - Validation of EU Safety Computer codes: validation of PACTITER on the CIRENE experiment - Feasibility study - Note Technique DTN/STRI/LTCD 04-021 - décembre 2004.
- [8] P. Shindler, Y. Philibert, V. Blet - ITER 2004 tests report - Stainless steel Release rate evaluation in ITER operating conditions - Note technique DTN/STRI/LTCD 04-020 - décembre 2004.

## TASK LEADER

Frédéric DACQUAIT

DEN/DTN/SMTM/LMTR  
CEA-Cadarache  
F-13108 Saint-Paul-Lez-Durance Cedex

Tél. : 33 4 42 25 75 74  
Fax : 33 4 42 25 77 67

E-mail : frederic.dacquait@cea.fr

**TW2-TRP-PPCS15-D03****Task Title: WASTE MANAGEMENT STRATEGY ON MODE A AND B****INTRODUCTION**

In order to reduce the quantity of wastes from PPCS (Power Plant Conceptual Study) reactors and optimize the final disposal, the waste management strategy is based on a selective segmenting as well as on the application of specific treatments aimed at reducing the volume and activity (fusion, incineration, detritiation, decontamination...).

The main objective of the CEA contribution to this task is to suggest a waste management strategy for PPCS fusion reactor.

This task is in continuation of the previous work performed in the framework of TW1-TRP-PPCS5-D03.

**2004 ACTIVITIES**

Based on the different classifications obtained in 2002, a strategy of waste management is proposed for each component. The different classifications show that it is interesting to increase the duration of an interim storage of the waste. Then they can the waste category can change, namely because of the tritium decay.

For each components an analysis has been done.

**TF COILS***PPCS A –PPCS B*

This large component is made of steel of superconducting coil type (steel alloy, chromium, nickel). Its mass represents about 70 % of the total reactor mass.

After 50 years, the waste from this component are classified for the outboard part, into Non-Active Waste (NAW) and for the inboard part, into Simple Recycled Material (SRM). After 100 years, the classification of waste from the inboard part is identical to that after 50 years (wastes classified as SRM).

The very low activity of TF coils allows this component to be fully recycled after 50 years. It does not seem necessary to wait for a longer period of time for the inboard part, as there is no possible declassification.

The clearance being lower than 1, the outboard part can thus be cleaned in the public domain. And the inboard part can be recycled using Remote Handling Recycling (RHR). This component is thus easy to manage.

**VACUUM VESSEL***PPCS A –PPCS B*

This large component is made of steel 316 S and boron. Its mass represents about 10% of the total reactor mass.

After 50 years, the waste from this component can be classified for the outboard part into SRM and for the inboard part into Complex Recycled Material (CRM) wastes. They have thus to be dismantled by using remote handling. After 100 years, the component (inboard or outboard parts) is classified SRM and only the outboard part of PPCS A can benefit from simplified dismantling procedures.

The activity of this component is due to nickel 63 (beta emitter), to decay heat, to dose rate and to cobalt 60. The cobalt content in steel 316 S is of 0.09 % (mass) i.e. 900 ppm. Cobalt 60 comes from the activation of cobalt. In order to reduce the dose rate of cobalt 60, the contents of the cobalt element in steel 316 S could be reduced.

VV being only slightly active, it seems preferable to treat this component as soon as possible using RHR.

**SHIELD**

This component is made of eurofer (steel, chromium, manganese). The behaviours of PPCS A and PPCS B are different.

*For PPCS A*

After 50 years, the waste from this component are classified for the outboard part, into SRM wastes and for the inboard part into CRM wastes. After 100 years, the component (both parts) is classified SRM.

The activity, the decay heat and the dose rate of this component are due to cobalt 60. The cobalt present in this Eurofer is in an impure state, its content is of 0.005 % i.e. 50 ppm. It therefore does not seem feasible to reduce this content further.

The waste from the outboard part can be completely recycled, after 50 years using Remote Handling Recycling (RHR). A longer time (100 years) provides for an easier recycling (Hands On Recycling (HOR) type). For the inboard part, the activity being significant, no recycling is considered. A longer time would be necessary (100 years) to be able to recycle them in the same way.

*For PPCS B*, the shield is divided into two parts : the Low Temperature (LT) shield and the High Temperature (HT) shield.

After 50 years, the waste from the LT and HT shields are classified, for the outboard and inboard parts into Permanent Disposal Waste (PDW), non-recyclable. After 100 years, the waste from the LT shield (in and outboard) are classified CRM and the wastes from the HT shield are classified SRM.

The HT shield waste can be recycled after 100 years using heavy means. After 100 years, 90 % of the LT shield could still not be recycled.

A temporary storage of these components thus does not seem to be the best solution since the decrease of the activities is slow, especially for the LT shield. These waste could therefore be directly treated after cutting and be sent to their final destination, namely a geological disposal site.

## MANIFOLD

This is made of eurofer (steel, chromium and manganese). This component is more active for PPCS A than for PPCS B.

### *PPCS A*

After 50 years, the waste from the outboard part are classified into CRM, recyclable by remote handling and from the inboard part, into PDW, in other words, non-recyclable. After 100 years, the entire component is an SRM waste, which can be recycled by remote handling.

There are two dismantling strategies for this component : either clean, after 50 years, the outboard part and wait 100 years for the inboard part, or wait 100 years and clean the entire component.

### *PPCS B*

After 50 years, the whole component is classified SRM. It is thus recycled by remote handling. After 100 years the outboard part can benefit from lighter treatments (HOR).

The manifold only being slightly active, it would seem preferable to treat it as soon as possible by using RHR.

## BREEDER / BLANKET AND FW

### *PPCS A – PPCS B*

These are made of eurofer, LiPb for PPCS A and of eurofer and LiSiO<sub>4</sub> for PPCS B. FW is only composed of eurofer.

The waste from these components are very active and are classified after 50 years into non-recyclable PDW.

After 100 years, for PPCS A, the waste are classified as SRM and for PPCS B, as CRM.

These are metallic wastes, tritiated and activated (cobalt 60) with significant decay heat. A Remote Handling Recycling (RHR) is possible if the entire component is temporarily stored (for 100 years).

The activity is mainly due to tritium, so a detritiation of these components could be possible so as to declassify them more rapidly. The Eurofer cobalt content already being very low, it does not seem feasible to reduce it.

The presence of a toxic element such as beryllium is concept B will require particular attention, but could be associated to specific treatments such as detritiation or decontamination.

## CONCLUSIONS

---

The quantity of wastes to be managed during the dismantling of a nuclear facility depends on many criteria, including the process itself (design, materials used...) and on the operating conditions (maintenance schedule, replacement of components).

This document presents a waste balance for two fusion reactor concepts : PPCS A and PPCS B. PPCS A is a concept using a liquid LiPb blanket cooled by water whereas PPCS B is a concept using a solid LiSiO<sub>4</sub> cover cooled by helium.

The results of this study show that the mass balance of the waste to be treated corresponding to the dismantling of a reactor as well as to the treatment of those components replaced during maintenance operations, namely 5 blankets and 10 divertors, is respectively for PPCS A and PPCS B of  $1,63.10^5$  and  $7,41.10^4$  tons of wastes.

The distribution of wastes is as follows :

### *For PPCS A*

After 50 years :

2,67.10<sup>4</sup> tons are PDW, so 35,10 %  
 3,69.10<sup>4</sup> tons are CRM, so 25,89 %  
 4,22.10<sup>4</sup> tons are SRM, so 22,63 %  
 5,72.10<sup>4</sup> tons are NAW, so 16,38 %

After 100 years :

no PDW  
 1,54.10<sup>4</sup> tons are CRM, so 9,45 %  
 8,78.10<sup>4</sup> tons are SRM, so 53,91 %  
 5,97.10<sup>4</sup> tons are NAW, so 36,64 %

### *For PPCS B*

After 50 years :

1,37.10<sup>4</sup> tons are PDW, so 18,54 %  
 1,13.10<sup>4</sup> tons are CRM, so 15,24 %  
 1,69.10<sup>4</sup> tons are SRM, so 22,89 %  
 3,21.10<sup>4</sup> tons are NAW, so 43,33 %

After 100 years :

no PDW  
 7,74.10<sup>3</sup> tons are CRM, so 10,44 %  
 3,04.10<sup>4</sup> tons are SRM, so 41,01 %  
 3,60.10<sup>4</sup> tons are NAW, so 48,55 %

Based on these results, if the management of PDW has to be eliminated, it will be necessary for some components to wait 100 years.

The low activity of TF coils and of the Vacuum Vessel allows these two components to be recycled after 50 years and in their entirety (inboard and outboard parts). The validation of the clearance index will be required to be able to place in the domain (which domain?) the TF coil component. The wastes coming from the breeder, blanket and first wall are only recyclable after 100 years using Remote Handling. Lastly, the wastes from the outboard part of these shield components can be recycled after 50 years whereas for the inboard part these require waiting for 100 years. Only the LT shield component cannot be recycled even after 100 years.

The main radionuclides involved in the activation of materials (breeder, blanket, first wall plus shield pour PPCS B) and penalizing for dismantling are tritium and cobalt 60.

The use of eurofer, a material with very low cobalt content as a structural material in both concepts does not allow to consider a reduction of cobalt 60 in the wastes. Only a temporary storage and a detritiation process could allow for a faster and easier recycling of these wastes, when tritium is the most penalizing isotope.

## REFERENCES

---

- [1] C. Lacressonniere - Waste management in a future fusion power plant TW1-TRP-PPCS5-D03 - Technical report CEA/DER/STR/LCEP NT 02/050.

## REPORTS AND PUBLICATIONS

---

- [2] C. Lacressonniere - Waste management in fusion power plant PPCS (task TW2-TRP-PPCS15-D3) - Technical report CEA/DTN/STPA/LPC NT 04/065.

## TASK LEADER

---

Christelle LACRESSONNIERE

DEN/DTN/STPA/LPC  
CEA-Cadarache  
F-13108 Saint-Paul-Lez-Durance Cedex

Tél. : 33 4 42 25 35 50  
Fax : 33 4 42 25 72 87

E-mail : christelle.lacressonniere@cea.fr



---

**Task Title: CONCEPTUAL DESIGN OF A HCLL REACTOR  
Tritium control & management analysis, thermo-hydraulic and  
thermo-mechanical analyses**

---

**INTRODUCTION**

Within the framework of the European Power Plant Conceptual Studies (PPCS), one of the reactor models, the model AB, is based on a Helium-Cooled Lithium-Lead (HCLL) blanket [1]. A view of the corresponding blanket module and of the detail of a Breeder Unit (BU) is shown in figure 1.

The integration and the design of the HCLL blanket and associated circuits and components within the model AB reactor plant has been addressed and performed in another parallel subtask [2], [3].

The mechanical, thermo-mechanical and thermo-hydraulic analyses for the HCLL have been based on the similar analyses performed for the HCLL DEMO blanket modules [4] taking into account the larger size of the PPCS reactor.

The objective of this task was to check validity of the analyses performed for DEMO when extrapolated to the PPCS specifications and to assess the T-management and control in the HCLL blanket and associated systems.

The latter has been clearly identified as one of the critical issues for HCLL blankets and, was never addressed in details in past. Most of the subtask activity has therefore been devoted to this item.

**2004 ACTIVITIES**

The performed activities focused on the verification of the thermo-hydraulic and thermo-mechanics data compared to the DEMO HCLL blanket [4] and to the assessment of T-management in the blanket and associated systems.

**THERMO-MECHANICAL AND THERMO-HYDRAULIC EVALUATION**

Based on the PPCS HCLL modules design and specifications [2], [3] and after several iterations, the temperatures distribution, mechanical stresses, flow rates of He-coolant and PbLi breeders, coolant pressure drops have checked and/or estimated. The most significant results are listed in table 1. On the basis of neutronic calculations results, the He mass flow in each blanket module has been estimated and, for each sub-components, first wall (FW), stiffening plates (SPs), and cooling plates (CPs), the He velocities and temperatures have been derived.

Thermo-mechanical resistance of the equatorial blanket module (the most solicited region because of the maximum heat flux on the FW) has thus been verified on the basis of the analyses carried out on the generic DEMO blanket module [4] since He parameters, blanket geometry and loading conditions are quite similar. It has been shown that stresses are everywhere below the maximum limits for the appropriate temperatures.

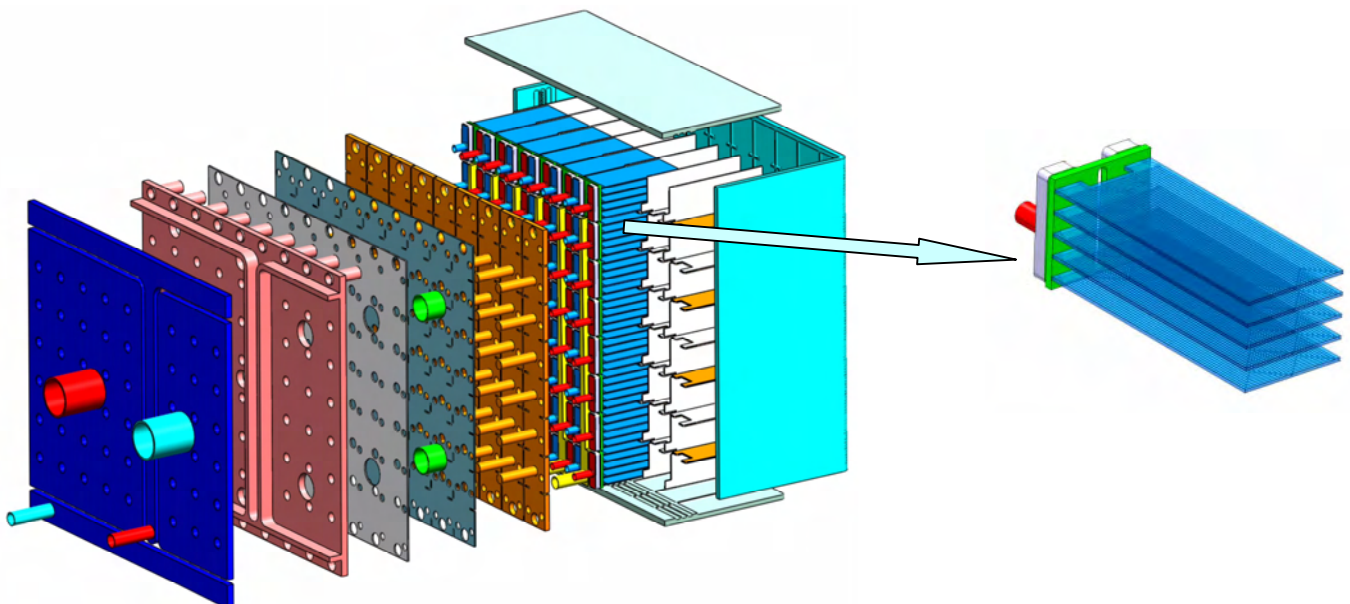


Figure 1 : Detailed views of a HCLL blanket module and of a Breeding Unit

Table 1 : Relevant specifications and main obtained results

|   |          |
|---|----------|
| Number of blanket modules                                   | 180      |
| Max. Neutron Wall Loading on FW (MW/m <sup>2</sup> )        | 2.58     |
| Heat flux on FW (MW/m <sup>2</sup> )                        | 0.5      |
| Helium pressure (MPa)                                       | 8        |
| Blanket He inlet/outlet T (°C)                              | 300/500  |
| Blanket He flow rate (kg/s)                                 | 4070     |
| Pumping Power (MW)  | 400      |
| Min/max EUROFER T (°C)                                      | 330/550  |
| Max EUROFER/PbLi interface T (°C)                           | ~ 510    |
| Average PbLi velocity (mm/s) in breeder units/feeding pipes | 0.18/100 |
| PbLi flowrate (m <sup>3</sup> /s)                           | 0.07     |
| Number of Steam Generators                                  | 9        |

The pressure drops in each blanket module have been estimated evaluating separately the contribution of the various sub-components in the module itself (FW, back plate, CPs) and in the manifolds. A large uncertainty is present in the estimation of the pressure drop in the back plate chambers because of the very complex geometry and the consequent complex He flow path in this region.

The highest pressure drop occurs in the lower inlet blanket module, due to the larger manifold length and is about 0.33 MPa. To take into account the calculation uncertainties, a pressure drop of 0.35 MPa has been assumed for the blanket.

**TRITIUM CONTROL AND MANAGEMENT**

Figure 2 gives a sketch of the main systems of a HCLL blanket for a nuclear fusion power plant. The main T-flows are reported (J1 to J5), where: J1 = production rate, J2 = extraction rate from PbLi, J3 = permeation rate towards He coolant, J4 = extraction rate from the He coolant, J5 = release rate to the environment from the He loop. The maximum authorized T-release to the environment is assumed to be 27 Curies/day, equivalent to 1 g/year. However, this allowance will be for the whole plant, including other sources of tritium like reactor refuelling, divertor pumping etc. Even taking the whole allowance for the breeding blanket system, the tritium isolation ratio J1 / J5 is to be as high as 200 000, with the assumption of a reaction availability of 82 % (300 operating days per year). Therefore, a detailed analysis of all contributions is required in order to identify potential reduction of each of them. The preliminary considerations about the main contributions are given hereafter. In order to evaluate T-permeation in the blanket, the details of the PbLi flow has been evaluated. The PbLi inventory and mass flow in each type of module (assuming 10 renewals per day, which represents the basic assumption for PbLi flow) are summarized in the table 2.

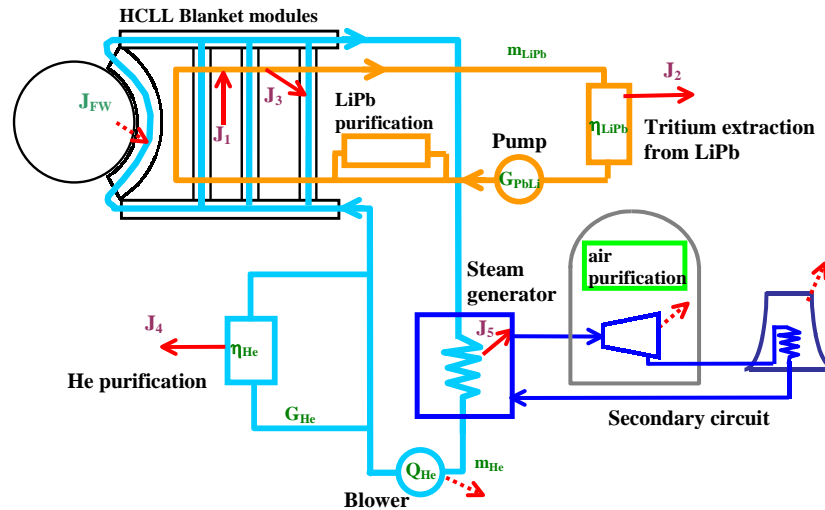


Figure 2 : Scheme of the main tritium-related system and corresponding tritium flow in a HCLL fusion reactor

Table 2 : PbLi inventory and mass flow in the reactor

| Module type | N of modules | N of BU per module | PbLi volume (m <sup>3</sup> ) | PbLi mass flow at T = 450°C, (kg/s), 10 rec/day |
|-------------|--------------|--------------------|-------------------------------|---|
| 1           | 18           | 140                | 38                            | 41  |
| 2           | 18           | 140                | 38                            | 41  |
| 3           | 27           | 72                 | 29                            | 31  |
| 4           | 36           | 168                | 162                           | 173   |
| 5           | 45           | 140                | 169                           | 180   |
| 6           | 36           | 154                | 149                           | 159   |
| total       | 180          | 24876              | 585                           | 625   |

Assuming an internal diameter of 75 mm, the liquid metal velocity in the modules feeding pipes ranges between 5 cm/s (modules 1 and 2) and 12 cm/s (module 4). A suitable electrical insulation should then be foreseen in that region of the PbLi manifold pipes located inside the magnetic field, in order to avoid high MHD pressure drops (assumed equal to zero in the present calculations).

Assuming 360 pipes of 100 m length and 75 mm internal diameter, the PbLi inventory in the pipelines will amount to about 10 m<sup>3</sup>, which is negligible compared to the inventory inside the modules. plates (SPs Stiffening Plates), in order to withstand the He-pressure under accidental conditions and closed in the back by 5 back plates (BPs) ensuring the He collecting/distribution. The SPs form some radial cells in which are inserted the breeder cooling units (BUs). Each BU features 5 radial-toroidal cooling plates (CPs), recovering the thermal power deposited in the breeder zone (BZ). All He and PbLi headers are located in the rear part of the blanket.

The PbLi breeder slowly flows throughout the box for allowing external tritium extraction. It enters at the bottom of the module and it is distributed in parallel to each column. In order to minimize simultaneously PbLi velocity and tritium residence time, in each column the BUs are fed in parallel through a vertical manifold located between the BUs and the 1<sup>st</sup> BP.

The reference PbLi recirculation rate is 10 renewals/day. In the present study, MHD pressure drops have been computed with this value, but it could be interesting, in order to limit T permeation towards He coolant to increase the PbLi velocity. An optimum is to be sought considering PbLi pressure drop and detritiation plant size as well as He purification plant size. With 10 re-circulations per day the PbLi flow to be processed is 0.07 m<sup>3</sup>/s (244 m<sup>3</sup>/h, approx. 625 kg/s, at 450 °C).

The daily tritium production in the PbLi of the HCLL blanket is about 650 g/day. Thanks to the PbLi circulation, the tritium is recovered outside the blanket in a column extractor (for instance, a He bubbles counter-current column [3]). Because of its low solubility in the PbLi, which leads to significant partial pressure, part of the tritium permeates through the steel walls towards the He-coolant. The level of permeation depends on the temperatures, the possible presence of tritium permeation barriers (deposited and/or naturally formed), and on the He-chemistry. The effect of the presence of T-permeation barriers and of the PbLi velocity is shown in figure 3.

The tritium extraction is thus foreseen also from the He, however, only a fraction of the flowing He will be derived to be processed in the Coolant Purification System.

Considering the fugacity of the tritium, particular care should be applied in the PbLi and He cooling circuits design in order to maintain the tritium release to the environment below the allowable value, assumed to be 27 Ci/day for following calculations. The final tritium release rate will depend by the tritium permeation towards

the He coolant in the blanket modules, the PbLi circulation rate, the Tritium Extraction System (TES) efficiency, the tritium permeation in steam generator, the He coolant leak rate, Coolant Purification System (CPS) maximum flow rate and efficiency.

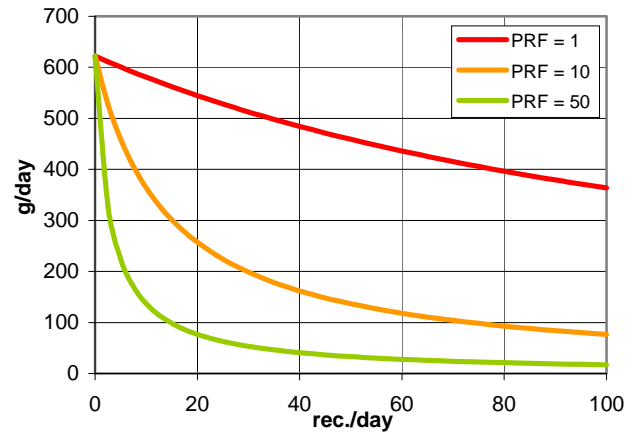


Figure 3 : Tritium permeation rate towards He-coolant in the PPCS HCLL blanket

The He mass flow to be purified in the CPS has been estimated through analytical formulas for several configuration, for several He leakage (10 % and 2 % of the total He inventory) and number of PbLi recirculation/day. The influence of a coating having a Permeation Reduction Factor (PRF) of 10 has also been assessed. In these evaluations a TES efficiency of 80 % and tritium permeation through the steam generator equal to zero have been assumed.

Table 3 : He mass flow to be purified for several leaks, PRF and PbLi renewals/day configurations

| He leak rate % (Nm <sup>3</sup> /h) | PRF | Rec/day (PbLi v) | He to be purified Nm <sup>3</sup> /h |
|-------------------------------------|-----|------------------|--------------------------------------|
| 10 % (2 Nm <sup>3</sup> /h)         | 1   | 10 (0.2 mm/s)    | 5 10 <sup>5</sup>                    |
| 10 % (2 Nm <sup>3</sup> /h)         | 1   | 80 (1.5 mm/s)    | 3 10 <sup>5</sup>                    |
| 10 % (2 Nm <sup>3</sup> /h)         | 10  | 10               | 3 10 <sup>5</sup>                    |
| 10 % (2 Nm <sup>3</sup> /h)         | 10  | 80               | 7 10 <sup>4</sup>                    |
| 2 %                                 | 1   | 10               | 1 10 <sup>5</sup>                    |
| 2 %                                 | 1   | 80               | 8 10 <sup>4</sup>                    |
| 2 %                                 | 10  | 10               | 7 10 <sup>4</sup>                    |
| 2 %                                 | 10  | 80               | 2 10 <sup>4</sup>                    |

## PRELIMINARY CONCLUSIONS ON T-MANAGEMENT AND CONTROL

In conclusion, the capability for the PPCS HCLL blanket system to comply with T-release allowance relies on a combination of the followings items:

- confirmation of a negligible permeation in the steam generator, that can be reached via various measures like:
  - transformation of T<sub>2</sub> in HTO via proper chemistry of the coolant,
  - use of double-walled pipes for the SG [T. Schulenberg, ref. 10 ],

- development of permeation barrier for the SG with a PRF larger than the present considered value of 400, and reliable in time,
2. confirmation of favourable recent measurements for the Tritium Sievert constant,
  3. very efficient blanket permeation reduction factor (PRF at least around 50) to be used in the blanket analytical computation of the permeation (using performing permeation barriers and/or taking into consideration tritium diffusion in the PbLi via finite element modelling),
  4. significant increase of a the PbLi recycling rate (above the present admitted value of 10 recirculations/day)
  5. possibility that the driving factor for permeation in the steam generator becomes a linear function of pressure at low tritium partial pressure (recombination limited permeation) and be no longer proportional to the square root of the partial pressure (diffusion limited permeation). Presently, no data are available about this physical transition threshold, that would tolerate higher tritium partial pressure in He coolant,
  6. possibility to consider a secondary water purification plant and/or have reduced steam leakage in the turbines,
  7. confirmation of the presently assumed low level of T-reach Helium leakages from the circuit components.

A reasonable compromise among the various, often controversial requirements, could be found, if the assumption of successful R&D applied to all the different above items fields will be confirmed. In principle, under PPCS specifications, T-control for HCLL blankets can be managed provided the required improvement can be smoothly distributed over most of the different items listed above, leading in particular to technologically achievable requirements for tritium permeation barriers, tritium extraction systems both from PbLi and He, permeation through the steam generator and leak rates from the He cooling system.

## REFERENCES

---

- [1] A. Li Puma et al. - Breeding Blanket Design and Systems Integration for a Helium-Cooled Lithium-Lead Fusion Power Plant, accepted as oral paper at the ISFNT-7 - to be published in Fus. Eng. & Design.
- [2] Progress Report 2004 for the subtask TW4-TRP-002-D04.
- [3] A. Li Puma, L. Giancarli - Helium-Cooled Lithium-Lead Fusion Power Plant (PPCS model AB) Design and integration of in-vessel components and associated systems Task EFDA TW4-TRP-002-D04 - CEA Report, SERMA/LCA/RT/04-3543/A - February 2005.

- [4] A. Li Puma, Y. Poitevin, L. Giancarli, W. Farabolini, G. Rampal, JF. Salavy, J. Szczepanski, U. Fischer, P. Pereslavitsev - Helium Cooled Lithium Lead blanket module for DEMO: designs and analyses - CEA Report, DM2S/SERMA, September 2003.

## PUBLICATIONS AND REPORTS

---

W. Farabolini et al. - Tritium Control Modeling in a Helium-Cooled Lithium-Lead Blanket for a Fusion Power Reactor, accepted as oral paper at the ISFNT-7 - to be published in Fus. Eng. & Design.

W. Farabolini et al. - Tritium control & management analysis, thermo-hydraulic and thermo-mechanical analyses for the PPCS HCLL Blankets - CEA Report, SERMA/LCA/RT/05-xx - June 2005.

## TASK LEADER

---

Wilfrid FARABOLINI

DEN/DM2S/SERMA  
CEA-Saclay  
F-91191 Gif-sur-Yvette Cedex

Tél. : 33 1 69 08 78 79  
Fax : 33 1 69 08 99 35

E-mail : wfara@soleil.serma.cea.fr

---

## Task Title: CONCEPTUAL DESIGN OF A HCLL REACTOR

### Design Integration

---

#### INTRODUCTION

---

Within the framework of the European Power Plant Conceptual Studies (PPCS), launched in January 2000, four reactor models were developed. Two “near term” models were defined, named A and B, based on limited extrapolations from to-day technology knowledge and plasma physics assumptions and featuring, respectively, a Water-Cooled Lithium-Lead (WCLL) blanket with a water cooled divertor and a Helium-Cooled Ceramic/Be Pebble-Beds (HCPB) blanket with a He cooled divertor. The two other models, consider reactors with higher efficiency, higher availability and, possibly, more aggressive physics. These models, named C and D, feature a Dual Cooled Lithium Lead (DCLL) blanket with a He cooled divertor and on a Self Cooled Lithium Lead blanket with a self cooled lithium lead divertor, respectively [1].

Following a review of its DEMO blanket development programme, Europe decided to consider the Helium-Cooled Lithium-Lead blanket (HCLL) as possible DEMO blanket concept [2]. A view of the corresponding blanket module is shown in figure 1. In this context, a new task has been launched for the definition of a third ‘near term’ fusion power reactor based on the HCLL blanket concept (model AB) featuring a He cooled divertor. In particular, the objective of this deliverable is the design integration of the PPCS model AB reactor.

#### 2004 ACTIVITIES

---

The activities focused on: i) the definition of the blanket segmentation and attachments, ii) the breeding blanket connections and maintenance, iii) the shielding design, available divertor concepts integration, iv) the external circuits and components definition, v) the efficiency evaluation.

The coordination of the whole task results was also included in this deliverable.

The main features of the model AB reactor are in fact the result of successive iterations in parameters definition, neutronic and thermal-hydraulic analyses, as well as of the design integration needs.

#### REACTOR PARAMETERS

The PPCS model AB is based on the same physics assumptions and technologies as the two near-term models, A and B.

The main assumptions are a maximum divertor heat load of 10 MW/m<sup>2</sup> and a First Wall (FW) heat load limit of 0.5 MW/m<sup>2</sup>.

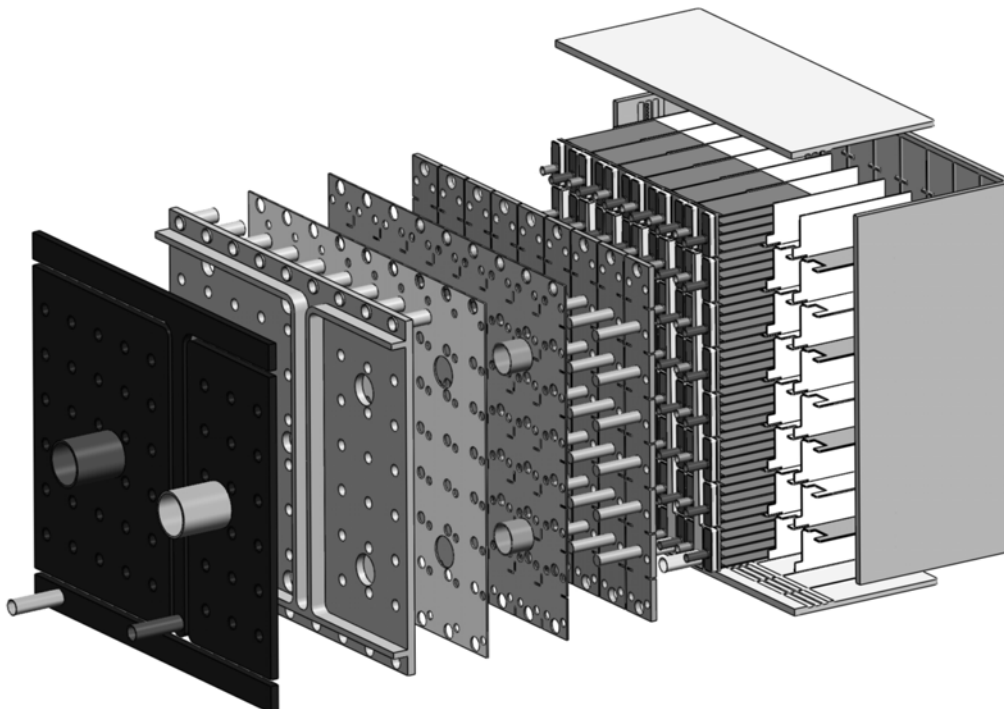


Figure 1 : Exploded view of a generic DEMO HCLL blanket module of 2 m (pol.) × 2 m (tor) × 1 m (rad)

In order to establish the main reactor parameters the other main initial assumptions are: i) an electrical net output of 1500 MW, ii) a blanket energy multiplication factor of 1.18, iii) a conversion efficiency of 43.7 % (not taking into account pumping power), and, iv) a pumping power of 400 MW. These assumptions have been used to define a set of parameters using the PROCESS code [3]. The last iteration results are summarized in table 1.

Table 1 : Parameters of the PPCS AB model reactor

|   |                       |
|---|-----------------------|
| Unit Size (GW <sub>e</sub> )            | 1.5                   |
| Blanket Gain                            | 1.18                  |
| Conversion efficiency                   | 0.437 (gross)         |
| Pumping Power (MW)                      | 400                   |
| Fusion Power (GW)                       | 4.24                  |
| Aspect Ratio                            | 3.0                   |
| Elongation (95% flux)                   | 1.7                   |
| Triangularity (95% flux)                | 0.27                  |
| Major Radius (m)                        | 9.56                  |
| TF on axis (T)                          | 6.7                   |
| TF on the TF coil conductor (T)         | 13.1                  |
| Plasma Current (MA)                     | 30.0                  |
| $\beta_N$ (thermal, total)              | 2.7, 3.5              |
| Average Temperature (keV)               | 21.5                  |
| Temperature peaking factor              | 1.5                   |
| Average Density ( $10^{20}m^{-3}$ )     | 1.05                  |
| Density peaking factor                  | 0.3                   |
| H <sub>H</sub> (IPB98y2)                | 1.2                   |
| Bootstrap Fraction                      | 0.43                  |
| P <sub>add</sub> (MW)                   | 257                   |
| n/n <sub>G</sub>                        | 1.2                   |
| Q                                       | 16.5                  |
| Recirculating power fraction            | 0.38 (pump. included) |
| Average neutron wall load               | 1.84                  |
| Divertor Peak load (MW/m <sup>2</sup> ) | 10                    |
| Z <sub>eff</sub>                        | 2.6                   |

## DESIGN: MAIN RATIONAL AND DESCRIPTION

A poloidal cut of the PPCS AB reactor is shown in figure 2. The following basic guidelines have been considered for the design of this reactor:

- The breeding blanket main parameters and architecture are based on the corresponding DEMO HCLL blanket [2].
- Use of the “large modules maintenance” based on previous EFET evaluation derived from the ITER experience; a possible alternative proposal could be to have small modules 2mx2m installed on a banana-shaped back-plate and vertical maintenance.

- Use of modules vertical orientation (4 m high x 2 m width) in order to keep the same He flow path length in the FW as in DEMO (thermal hydraulics limitations); as a consequence, the modules are assumed to follow the plasma shape in the poloidal direction and to be straight in the toroidal direction.
- Module attachments are located on the side wall (SW), in order to avoid penetrations through FW and breeder zone and to avoid complex design and fabrication of modules internals.
- The shield is divided in two regions: high temperature shield (HTS) called also “manifold zone”, and low temperature shield (LTS). The presence of HTS allows the lateral attachment of the module to be rigid (minimal differential thermal expansion); flexible connections are therefore assumed between HTS and LTS.
- Pb-Li pipes are located at the bottom of the modules to allow the liquid metal draining by gravity to improve safety.
- Connection/disconnection of the He-pipes (two per module, one inlet at 300°C, one outlet at 500°C) is realized with an internal cutting/welding device which is inserted from the collector feeding pipes (in order to locate the connection in a region protected against neutron irradiation by the module itself); a possible alternative proposal would be an access from the front through a hole drilled at the bottom of the rear collector.
- Use of mechanical joints (threaded flange) for the Pb-Li collectors to avoid remote welding of pipes with residual Pb-Li on the surface.
- He and Pb-Li collectors are integrated in the HTS, in order to cool HTS through the He-collector; HTS has therefore to be poloidally continuous; LTS is also poloidally continuous so the attachments between HTS and LTS have an independent location from the module segmentation.

## Blanket design

The HCLL blanket is based on the use of EUROFER as structural material, of Pb-Li (Li at 90% in <sup>6</sup>Li) as breeder, neutron multiplier and tritium carrier, and of He as coolant with inlet/outlet temperature of 300/500°C and 8 MPa pressure.

It consists (see figure 1) of a steel box directly cooled by He flowing in internal channels. The box is reinforced by a stiffening grid of radial-toroidal and radial-poloidal He-cooled plates (SPs Stiffening Plates), in order to withstand the He-pressure under accidental conditions and closed in the back by 5 back plates (BPs) ensuring the He collecting/distribution. The SPs form some radial cells in which are inserted the breeder cooling units (BUs). Each BU features 5 radial-toroidal cooling plates (CPs), recovering the thermal power deposited in the breeder zone (BZ). All He and Pb-Li headers are located in the rear part of the blanket.

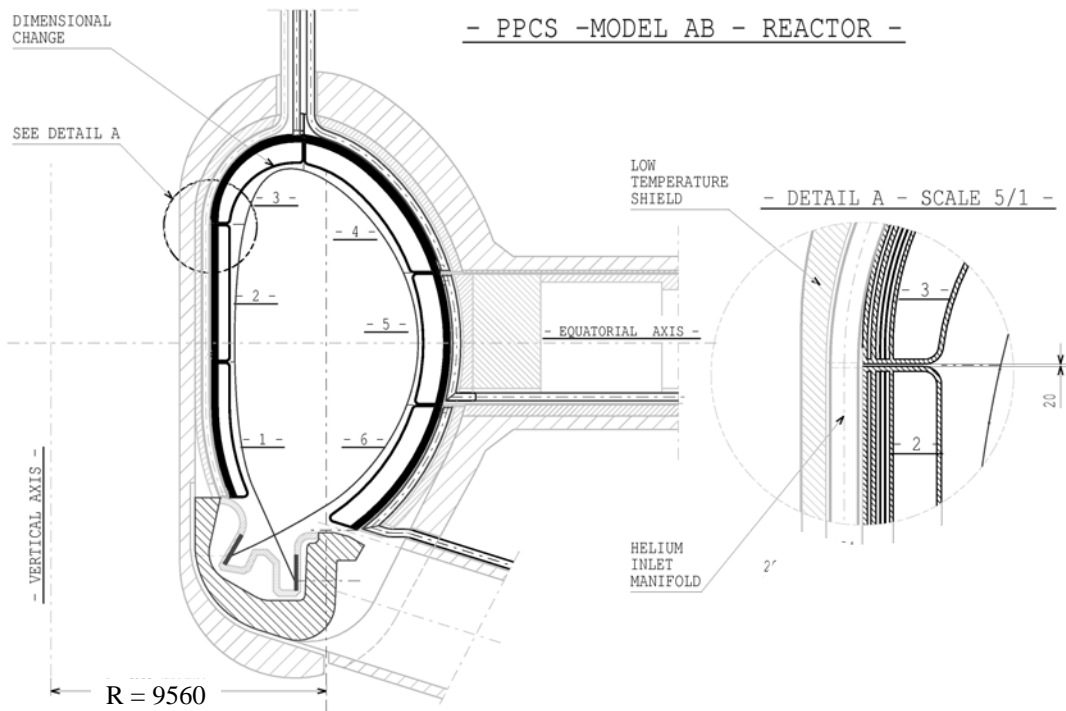


Figure 2 : Vertical section of the PPCS AB reactor

The Pb-Li breeder slowly flows throughout the box for allowing external tritium extraction. It enters at the bottom of the module and it is distributed in parallel to each column. In order to minimize simultaneously Pb-Li velocity and tritium residence time, in each column the BUs are fed in parallel through a vertical manifold located between the BUs and the 1<sup>st</sup> BP. The manifold is vertically divided in an inlet and an outlet chambers by a steel separating wall. The inlet chamber feeds one out of two BUs, then the Pb-Li flows radially towards the FW gradually increasing the tritium concentration, goes to the BU immediately above and then radially flows to the outlet chamber at the back. The liquid metal is then collected in an outlet manifold located in the 5<sup>th</sup> BP from which it leaves the module.

The He cools in parallel the box and the SPs, then passes in the CPs of the BUs.

The BZ thickness has been fixed, on the basis of neutronic analyses (TBR self-sufficiency) and reactor dimensions considerations, at 45 cm for the inboard side and 80 cm for the outboard one.

### Shields and vacuum vessel design

The shield is split in two parts, the HTS and the LTS. The HTS is thick 300 mm in the inboard and 350 in the outboard, the LTS 200 mm in the inboard and 350 mm in the outboard. Both the He and Pb-Li manifolds are integrated in the HTS made of Eurofer. To improve shielding efficiency the LTS is made of Eurofer and Tungsten Carbide (WC) and cooled by water.

To avoid connection holes through the FW and the BZ, the blanket modules are fixed to the HTS by lateral attachments. The HTS has the same average temperature as the blanket modules back plate, which avoids differential thermal expansion and allows the use of rigid attachments. The HTS can be then connected to the LTS by attachments accommodating the different thermal dilatation.

The shield of the module located in the front of the port is specially designed and removed with the module.

The HTS is moreover appropriately shaped behind the top inboard module in order to adapt it to the transition from two equatorial to three top inboard modules (in a 40° sector) and allow the passage of the pipes.

### Piping and connections

Both for He and Pb-Li, the modules are connected in parallel in a way that the mass flow can be regulated separately in each module, in order to compensate the differences in deposited power and in tritium production.

The Pb-Li pipes are connected with a remotely operated connector consisting in a clamp which can be remotely opened and closed by a screw mechanism. The liquid metal connections are located at the bottom of the modules, so that the draining will be performed by gravity. The access for the connection/disconnection tool is realized from the bottom, so the modules of a toroidal ring can be disconnected when those of the ring below have been removed.

The He collectors ensure the heat recovering for the HTS. The He pipes are connected by welding. A laser cutting/welding tool, similar to that developed for ITER shield blanket modules, will make connection/disconnection operations. The laser head will reach the appropriate location sliding inside the large-diameter He pipes (internal diameter > 20 cm).

The welding/cutting region is located in the gap between the modules and the HTS. This region is shielded by the blanket module, however, because of the low blanket shielding efficiency, the local He-production in the steel of this region after 5 years of operation (corresponding to the assumed blanket replacement time) will be about 5 appm.

To reduce this value to the “re-welding” limit of 1 appm, a special local shielding will have to be developed. This issue could also be solved by choosing to replace the HTS with the blanket. Because of the poloidal continuity of the HTS, this choice is possible if vertical maintenance from the top port is adopted.

### Divertor design

A He-cooled, high-temperature, low pressure-drop divertor is envisaged, based on W as armour material and W-alloy as pressure-retaining boundary [4], [5].

The 10 MPa pressure He enters in the divertor cassette at 541 °C, and exits at 717 °C, cooling the cassette at first. In these conditions the W-alloy remains within the acceptable operating temperature window of 600 - 1300 °C. The target is expected to survive to about 10-100 cycles between room and operating temperature.

The use of an improved high temperature water-cooled divertor [6] can be envisaged as back up solution.

This concept uses EUROFER as structural material, water coolant pressure and outlet temperature respectively of 15.5 MPa and 325°C, and W-alloy monoblocks as armour. An advanced interface, formed by a thermal barrier in the pipe front part and a compliance layer between W and steel, both made of Carbon-based materials, allows this concept withstanding up to 15 MW/m<sup>2</sup>.

This divertor concept could allow higher maximum heat flux although it will lead to a slight reduction of the reactor efficiency (~ 1 %). The global impact on the reactor major radius has not yet investigated.

### Maintenance scheme

The divertor cassettes will be extracted from the lower port independently from the presence of the blanket modules.

The blanket modules will be extracted from the equatorial ports (4.8 m x 2.18 m). The module placed in the front of the port will be extracted translating it in the radial direction in its original position. Then, lower modules can be disconnected and removed, so allowing the access to the connections of the equatorial ones, and then of the top ones.

### Reactor design point

The reactor design point has been obtained as the result of successive iterations in parameters definition, neutronic, magneto-hydrodynamic (MHD) and thermal-hydraulic analyses, as well as of the design integration needs and considerations on tritium management and He circuit. The PPCS model AB principal working parameters are summarized in the table 2.

*Table 2 : Reference design point for the PPCS AB model reactor*

|                                       |          |
|---------------------------------------|----------|
| Net electric power (GW <sub>e</sub> ) | 1.5      |
| Net Conversion efficiency             | 0.35     |
| Pumping Power (MW)                    | 400      |
| Tritium Breeding Ratio                | 1.13     |
| Max. NWL on FW (MW/m <sup>2</sup> )   | 2.58     |
| Heat flux on FW (MW/m <sup>2</sup> )  | 0.5      |
| Blanket/divertor lifetime (years)     | 5/2      |
| Helium pressure (MPa)                 | 8        |
| Number of blanket modules             | 180      |
| Number of Steam Generators            | 9        |
| Number of blanket circuits            | 9        |
| Blanket He inlet/outlet T (°C)        | 300/500  |
| Blanket He flow rate (kg/s)           | 4070     |
| Min/max EUROFER T (°C)                | 330/550  |
| Max dpa in EUROFER after 5 years      | ~150     |
| Average Pb-Li velocity (mm/s)         |          |
| in breeder unit                       | 0.18     |
| in feeding pipes                      | 100      |
| PbLi flowrate (m <sup>3</sup> /s)     | 0.07     |
| Number of Divertor cassettes          | 72       |
| Number of divertor circuits           | 9        |
| Divertor He inlet/outlet T (°C)       | 540/717  |
| Min/Max structure W-alloy T (C°)      | 600/1300 |
| Divertor He flow rate (kg/s)          | 926      |

### LiPb CIRCUIT AND TRITIUM MANAGEMENT

The daily tritium production in the Pb-Li of the HCLL blanket is about 620 g/day. Thanks to the Pb-Li circulation (about 0.07 m<sup>3</sup>/s considering 10 recirculation/day), the tritium is recovered outside the blanket in a column extractor (a He bubbles counter-current column is envisaged). Because of its low solubility in the Pb-Li, which leads to significant partial pressure, part of the tritium permeates through the steel walls towards the He-coolant.

The level of permeation depends on the temperatures, the possible presence of tritium permeation barriers (deposited and/or naturally formed), and on the He-chemistry.

Therefore also the He-coolant needs to be detritiated using the same detritiation techniques and components as proposed for Model B reactor [7]; however, only a fraction of the flowing He has to be processed in the purification system.

Considering the fugacity of the tritium, particular care should be applied in the Pb-Li and He cooling circuits design in order to maintain the tritium release to the environment below the allowable value, assumed to be 27Ci/day.

The final tritium release rate will depend by the tritium permeation towards the He coolant in the blanket modules, the Pb-Li circulation rate, the Tritium Extraction Unit (TEU) efficiency, the tritium permeation in steam generator, the He coolant leak rate, Helium Purification Unit (HPU) maximum flow rate and efficiency.

A reasonable compromise among the various, often controversial requirements, could be found, leading to technologically achievable requirements for tritium permeation barriers, tritium extraction systems both from Pb-Li and He, and leak rates from the He cooling system.

A purification system will be furthermore needed in the Pb-Li circuit (a fraction of the Pb-Li will be derived) for extracting radioisotopes characterized by high ingestion and inhalation hazard potential in case of accidental release.

### He CIRCUIT AND EFFICIENCY

The power heat deposited on the blanket and HTS (4219 MWth) and in the divertor (926 MWth) is recovered and useful in terms of the energy conversion system, while the one deposited in the LTS and in the VV is lost.

A thermodynamic Hirn cycle has been adopted in which the high temperature He of the divertor cooling loop is used to superheat the steam generated by the colder He coming from the blanket loop.

The cycle parameters (i.e. the mass flow repartition between the three stages of the turbine, etc.) have been optimised using the CYCLOP code [8] so leading to a gross efficiency (defined as the ratio between the total electric power generated and the total thermal charge of the VV) of about 43,7 %.

Although the high efficiency of the thermodynamic cycle, because of the high needed pumping power, both in the blanket and in the divertor, the net efficiency (ratio between the power to the grid and the fusion power) goes down to 35 %.

Both for the blankets and the divertor 9 primary loops have been assumed.

The outline scheme of a loop with related He mass flows and temperatures, recovered thermal power and needed pumping power is shown in figure 3.

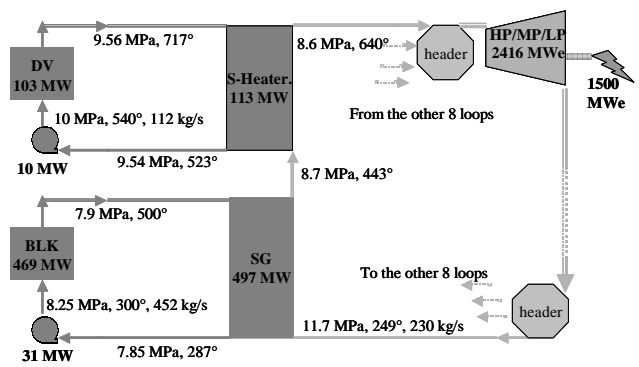


Figure 3 : Scheme of a BLK/DV cooling loop with related parameters

### REFERENCES

- [1] D. Maisonnier et al. - The European Conceptual Power Plant study - proceedings 23rd SOFT, Venice, Italy, September 19-24 2004.
- [2] A. Li Puma, Y. Poitevin, L. Giancarli, W. Farabolini, G. Rampal, J.F. Salavy, J. Szczepanski, U. Fischer, P. Pereslavltssev - Helium Cooled Lithium Lead blanket module for DEMO: designs and analyses - CEA Report, DM2S/SERMA, September 2003.
- [3] T.J. Hender, P.J. Knight, I. Cook - UKAEA FUS 333 (1996).
- [4] A. Pizzuto, P. Karditsas, C. Nardi, S. Papastergiou - HETS performances in Helium cooled power plant divertor - proceedings 23rd SOFT, Venice, Italy, September, 19-24 2004.
- [5] Norajitra et al. - Development of a helium-cooled divertor concept: design-related requirements on materials and fabrication technology - Journal of Nuclear Materials 329-333 (2004) 1594-1598.
- [6] L. Giancarli, A. Li Puma, B. Michel, P. Sardain, J.F. Salavy - Conceptual Design of a High Temperature Water-cooled Divertor for a Fusion Power Reactor - proceedings 23rd SOFT, Venice, Italy, September, 19-24 2004.
- [7] S. Hermsmeyer - Conceptual Design of the Helium Cooled Pebble Bed Blanket Plant Model in the frame of the EU Power Plant Conceptual Study, PPCS/FZK/PPCS2D10, FZK Report, May 2003.
- [8] D. Haubensack, C. Thévenot, P. Dumaz - The COPERNIC/CYCLOP computer tool: pre-conceptual design of generation 4 nuclear systems - HTR 2004, 2<sup>nd</sup> International Topic Conference for the HTGR, Beijing (China), September, 22-24 2004.

## **PUBLICATIONS AND REPORTS**

---

A. Li Puma et al. - Breeding Blanket Design and Systems Integration for a Helium-Cooled Lithium-Lead Fusion Power Plant, accepted as oral paper at the ISFNT-7 - to be published in Fus. Eng. Des.

A. Li Puma, L. Giancarli - Helium-Cooled Lithium-Lead Fusion Power Plant (PPCS model AB) Design and integration of in-vessel components and associated systems Task EFDA TW4-TRP-002-D04 - CEA report, SERMA/LCA/RT/04-3543/A, February 2005.

## **TASK LEADER**

---

Antonella LI PUMA

DEN/DM2S/SERMA  
CEA-Saclay  
F-91191 Gif-sur-Yvette Cedex

Tél. : 33 1 69 08 79 76  
Fax : 33 1 69 08 99 35

E-mail : [alipuma@cea.fr](mailto:alipuma@cea.fr)

**CEFDA03-1069**  
**CEFDA03-1082**  
**CEFDA04-1161**  
**TW4-TES-COLABA**

**Task Title: EUROPEAN ITER SITE STUDIES (EISS)**  
**TW3-TES-EISSg1: EISS 3 generic tasks CEA**  
**TW3-TES-EISS2c: EISS 3 stage 2**  
**TW3-TES-EISS4F: European ITER site study 4 - Cadarache**  
**TW4-TES-COLABA: Cadarache site for ITER -**  
**Collaboration with Local Authorities**

**INTRODUCTION**

EISS activities have their own steering process with regular meetings and exchange of information with EFDA and the Commission. The EISS4 contract covers the period from 1<sup>st</sup> January 2004 to 31<sup>st</sup> March 2005. A main deliverable will be issued end of March 2005 (ref. GA41-DEL-2004-0006). This document will refer to 36 specific deliverables covering all the topics of the EISS4 contract. The reader who would wish extensive information is requested to ask for these documents.

The following pages are given for reminder and are covering only the main aspects of the contracts.

After the choice of Cadarache as the European site for ITER in November 2003, the subsequent choice of the definitive site between Europe and Japan was expected in 2004. The EISS project (and its corresponding tasks) is, as for previous years, structured to progress on all items on the critical path, with an emphasis on the licensing schedule.

**2004 ACTIVITIES**

**SAFETY & LICENSING**

The first version of the main technical document in support of the Safety Authority’s instruction, the “Rapport Préliminaire de Sûreté” is almost completed. Nevertheless, a strong enhancement will be necessary once the generic design will be adapted to the specificities of Cadarache. The writing of this document is supported by many studies, performed at European level in parallel. The R&D needs to complete the writing of the RPrS have been identified. The sketch below (figure 1) illustrates the process that was used all along these safety studies.

The first preliminary studies, based on the whole European know-how, enabled the writing and successful instruction process of “Dossier d’Options de Sûreté” by the Safety Authority. More detailed studies were then performed in order to support the first compulsory document, called “Preliminary Safety Report”, made of two volumes: a description of the installation and then its safety analysis. A synthesis will be made that could be used in support of the public enquiry.

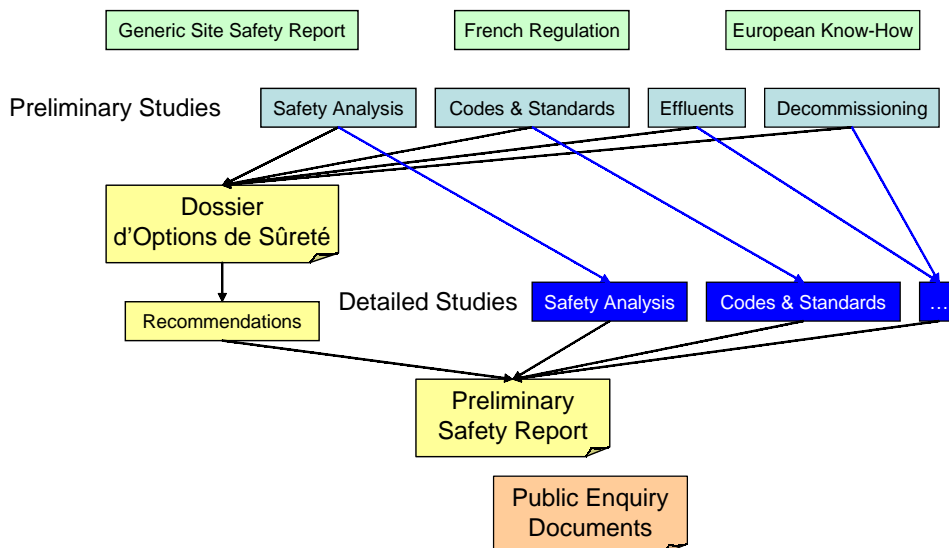


Figure 1 : Process used for safety studies

Here are several examples of studies performed to support this document writing.

The chemical risks including beryllium and chemical zoning aspects have been studied. The fire risk in the nuclear buildings and in particular the tritium building has been evaluated using general descriptions, regulations, fire loads and simulations. Plant states have been defined according to normal operation and incidental and accidental scenarios. Management of waste and casks for mixed waste has been defined. A study to verify the mechanical strength of the ITER tokamak during dismantling has been undertaken. A report on the draft radioprotection zoning was supplied. Work experience in a tritium plant was described.

Management of tritiated waste has been investigated. The activation calculations used by ITER have been evaluated. The handling of mixed waste packages to foreseen depositories has been studied. A specification for the DARPE writing has been provided. And the tritium inventory in the ITER vacuum vessel has been further studied.

## PUBLIC DEBATE

The relevant authorities, the “Commission Particulière du Débat Public” (CPDP) put in place in 2003 to organise the public debate on “ITER en Provence”, has been frozen until a decision on the site choice is taken.

Before this decision, at the request of the president of the CPDP, a contract had been established with the office “IDES consultant” to assure the secretary general of the Public Debate.

An interim issue of the file of the Public Debate has been sent to the Commission Nationale du Débat Public in July 2004. A call for tender has been launched for the realisation of the layout and the printing of 5000 copies of the final file. The first part of this contract has been realized, composed of the graphic chart, the iconography and the layout, as shown hereafter (figure 2).

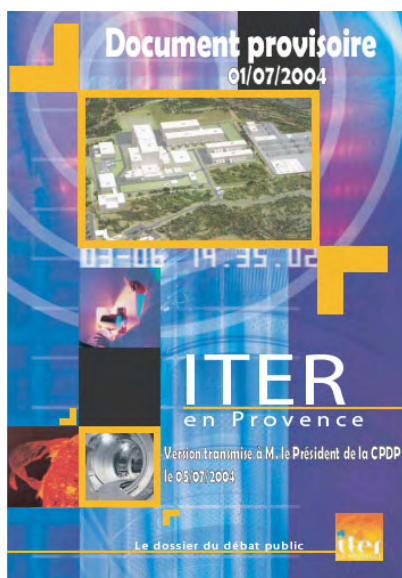


Figure 2 : File of the public debate

Different media have been also prepared for the Public Debate. A multimedia interactive terminal has been purchased to be used on exhibitions and during the Public Debate.

A movie called “ITER, une étoile en Terre de Provence” has been realised, at the intention of the general public (figure 3). A first version of this movie is finished and has been used at several occasions. A few modifications will be asked to the producer. This movie will be showed during the Public Debate and will be distributed on a DVD media.

The movie has been financed by conventions signed with the local authorities and completed by EFDA within the TWA-TES-COLABA task.



Figure 3 : Picture, extracted from the film “ITER, une étoile en Terre de Provence”

## IN-FENCE STUDIES

The technical specification for the “First office building” is ready. The call for tender and the implementation could be launched as soon as the site decision is taken. This building will have around 100 offices, several meeting rooms and will host the ITER team before the construction of the main office buildings and other annex buildings (restaurant, public relation centre, medical building, etc.).

The site drawings have been updated, taking into account the ITER team design evolution. A survey of the hydrogeology is performed, with a synthesis report every year (figure 4). This survey will be used to design the draining system.

A 1/500<sup>th</sup> model of ITER site has been realised for public relation purposes.

## TRANSPORT OF THE HEAVY AND LARGE COMPONENTS

The studies concerning the transport of the ITER components have been continued in the goal to transmit the files to the “Direction Départementale de l’Équipement” (DDE) in charge of the realisation of the work on the roads. These studies have also been financed by the local authorities completed by EFDA within the TWA-TES-COLABA task.

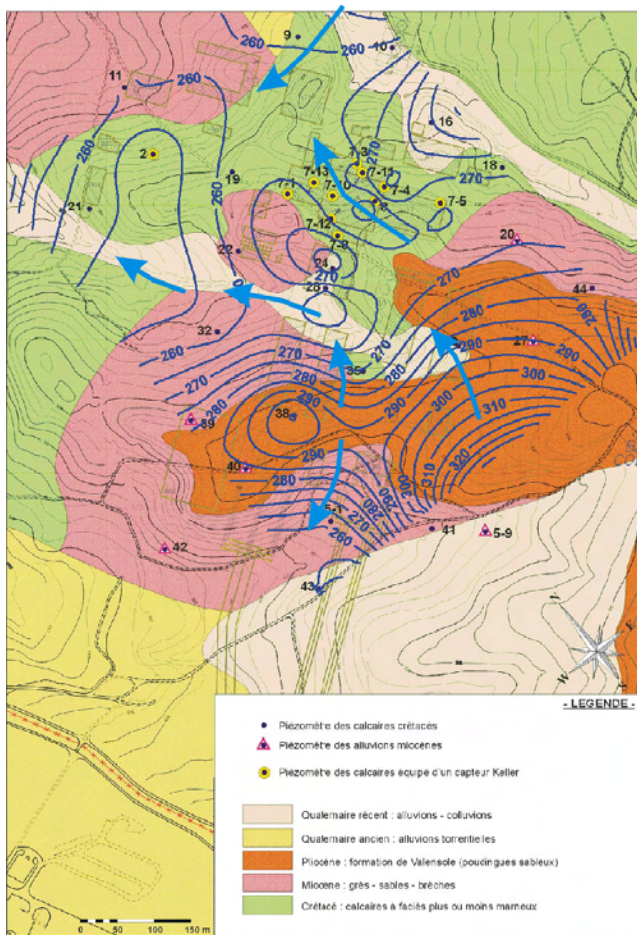


Figure 4 : Hydrologic map recorded in August 2004, by means of the piezometers installed on the site

They concern the ecological survey, characterization of the bridges all along the itinerary, technical studies on unloading quay, feasibility study on a dragging operation, and the detailed profiles of the roads.

Initial state of the environment: following a call for tender with 7 societies, a contract has been established with "Sémaphores" to realise an initial state of the environment on the transport itinerary. The main results of this study take into account the details of the zones requiring some laying-out or creation of trails. An ecological inventory on the natural environment has been made on the four consecutive seasons. This inventory is completed by an inventory on different items like water, housing, patrimony, etc.

Characterization of the bridges: Following a call for tender with 10 companies, a contract with GETEC grouping has been established for this study.

The main items were to analyse the bridges with more of five meters range, to study the effects of the passing by of the ITER loads, and to suggest some solutions for those are not well proportioned.

Technical studies on unloading quay: Five societies have been consulted before to choose INGEROP to realise this study. The main items are to proportion the future quay after geotechnical campaigns, to move 7 pipes of the SHELL facilities, and to lay out the road on the beach.

Feasibility study of a dragging operation: Realised by SAFEGE CETIIS after a call for tender, the objectives of are to list the legal aspects of the operation forecasted, to inventory the initial state, to analyse the sediments to drag and to describe the operation with the destination of the sediments dragged.

Detailed profiles of the roads: The SETEC Company has been chosen after a call for tender to realise this study. The drawing of 77 plans at 1/2000 scale, the study of two examples (a gyratory crossroads and a T crossroads crossing) have been realised with calculation and 3D visualisation of the crossing (figure 5).



Figure 5 : Crane beam transport crossing a roundabout

## REPORTS AND PUBLICATIONS

EISS3 stage 1+2 report delivered in June 2004  
EISS2 final report delivered in March 2004  
EISS4 interim report delivered in January 2005  
EISS4 final report to be delivered in March 2005

## TASKS LEADER

Pascal GARIN

EISS Project Leader  
DSM/DRFC/DIR  
CEA-Cadarache  
F-13108 Saint-Paul-Lez-Durance Cedex

Tél. : 33 4 42 25 45 43

Fax : 33 4 42 25 63 75

E-mail : pascal.garin@cea.fr



---

**Task Title: TW3-TEP-CRYO2:  
DESIGN OF ITER CRYOPLANT/CRYO-DISTRIBUTION  
SYSTEM (AUXILLIARY COLDBOXES, CRYOLINE, ...)**

---

## INTRODUCTION

---

The role of the European Participant working group was to provide technical analysis and design study on the ITER cryogenic system.

Both were based on CEA and CERN available experiences, respectively design and operation of the TORE SUPRA tokamak and large scale cryoplants and cryolines for the LEP and LHC particle accelerators. Each of these installations is supplied by European firms (AIR LIQUIDE or LINDE).

Due to this relevant experience and following previous CEA works for the ITER cryogenic system (see references [1], [2], [3], [4], [5]), ITER International Team (IT) has requested support from European Participants to get technical design for the ITER cryo-distribution and cryoplant system.

The main objective of this task (EFDA 03-1083) is to provide input information for establishing the final dimension details of the main tokamak complex and cryoplant buildings, which are time-critical for ITER construction.

The task was broken down as follows (*see 2004 Activities and Reports*).

- Establishing the overall PFD and then detailed PIDs of the ITER cryo-distribution system
- Development of the conceptual design of a typical Auxiliary Cold Box (ACB) for the ITER magnet system (TF coils).
- Updating the conceptual design of the Torus Cryopump Cold Valve Boxes (CVBs) taking into account the 470 K regeneration requirements.

## 2004 ACTIVITIES

---

This task was the first common ITER cryogenic study of the so called "CEA cryogenic working group for ITER" composed by cryogenic experts from le Service des Basses Températures (SBT) at CEA-Grenoble (France), le Service des Accélérateurs, de Cryogénie et de Magnétisme (SACM), le Service d'Ingénierie des Systèmes (SIS) at CEA-Saclay (France) and le Service Tokamak Exploitation et Pilotage (STEP) at CEA-Cadarache.

The work of this task was performed with an alternation of working periods and progress - review meetings (six at Grenoble and some others at Garching and Karlsruhe) between CEA cryogenic working group and ITER-IT Cryogenic Group, located in Naka (Japan) and followed by the EFDA/CSU responsible officer from Garching (Germany). The main activities performed in 2004 in the framework of the task EFDA 03-1083 are summarized hereafter.

## GENERATION OF PFD/PID FOR ITER CRYO-DISTRIBUTION SYSTEM

The ITER cryogenic distribution is composed of 56 cold boxes (25 under responsibility of cryogenic team / 29 under responsibility of magnet division / 2 under responsibility of 80 K thermal shield team), about 20 cryolines and around 20 warm lines which have to be installed and interconnected at different levels of the tokamak building. To establish PFD/PID, CEA has proposed symbol legend and tag numbering for all components based on ISO standards and its own experiences. The overall PFD and detailed PIDs are now defined (reports [1], [2]) and approved by ITER for all cryo-distribution system with standardization of components (valves, pumps, heaters, ..), instrumentations (temperature, pressure, flow, ...) and functions (helium guard, vacuum group, purge/filling, exchange of circulating pumps, ...). Each diagram is associated with a list of components detailing their position, function and characteristics. The total number of components is 4500 for all cryo-distribution system including 50 % of active components (cryogenic valves, sensors, heaters, pumps,...) and 50 % of passive components (hand valves, pressure relief valves, heat exchangers, ...).

In the present task, CEA has confirmed or introduced the following PID specificities to ensure the highest reliable operation of the ITER cryogenic system:

- The helium guard system for any sub-atmospheric operation for magnets ( $T < 4.3$  K), is a simple system confirmed by tens years of operation at CEA (TORE SUPRA) or at CERN (LHC) and requiring minimum additional costs.
- Each cold box has its own vacuum enclosure separated from cryolines by vacuum barriers. A standalone vacuum group is attached to each cold box of the cryo-distribution system to allow pumping of the vacuum enclosure independently of the ITER Service Vacuum System.

- A purge/filling system is also installed on each cold box for individual conditioning with pure helium before cool-down or after local reparation.
- All cryogenic circuits or vacuum enclosures are protected by pressure safety valves with setting pressure equal to 0.15 MPa for vacuum enclosure and around 2.0 MPa for all cryogenic circuits including the LHe bath. This large value (20 bar) for internal circuits is foreseen to reduce the sizing of the relief valves, to lower the number of relief valve opening and to store the maximum of helium inside the cryogenic circuits. All pressure safety valves for one cold box are collected in a recovery header.

### DESIGN OF TYPICAL AUXILIARY COLD BOX (ACB) FOR TF COILS

Conceptual designs for TF-ACB answer to ITER requirements and are based on classical and proven technology. The ACB report as well as the attached CATIA drawing files (report [3]) summarise the conceptual design and the assembling procedure proposed for TF-ACB as well as industrial validations of the key components.

The key components of this cold box are the large circulating pump for supercritical helium (3 kg/s at 5 K – 5 bar), the immersed heat exchanger between supercritical helium (5 K – 5 bar) and liquid helium (4.2 K – 0.99 bar) to remove heat loads deposited in magnets, the electrical heater to simulate the TF coil heat loads and a set of safety isolation valves to reduce the amount of cold helium release in the tokamak cryostat in case of helium piping leaks.

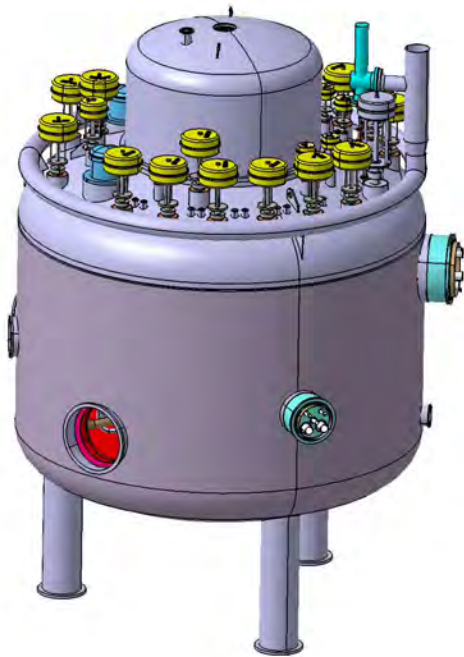


Figure 1 : TF-ACB (4.2 m in diameter)

Specific helium guard system is recommended for all components operating below atmospheric system as detailed in PID study. In addition to these specific components, TF-ACB within a stainless steel vacuum enclosure of about 4.2 m in diameter and 6.5 m in height

for a total weight of 24 tons, contains several internal stainless steel piping with tube bend design (avoiding the use of bellows), one 80 K thermal shield, MLI (multi layer insulation) and a dedicated number of cryogenic valves, pressure safety valves and instrumentation to control the supercritical helium cooling flow for the TF coils.

The thermo-mechanical calculations have given the corresponding heat loads and have validated the mechanical design mainly based on the CODAP French code.

The pressure drop (direct impact on circulating pump power) and heat load calculations have indicated larger values than expected and should be integrated in the future global review of the cryogenic system.

The pressure drops could possibly be reduced through an increase of the piping diameter, however the heat loads (mainly coming from cryogenic valves) will be more difficult to reduce.

### DESIGN OF TYPICAL COLD VALVE BOX (CVB) FOR TORUS CRYOPUMPS

As for TF-ACB studies, conceptual designs for CVBs fulfil present ITER requirements and are based on classical and proven technology. The CVB report as well as the attached CATIA drawing files (report [4]) summarise the conceptual design and the assembling procedure of the Torus Cryopump CVB as well as industrial validations of the key components.

In addition to the constraints associated with the magnetic field and radiation environment existing in the ITER Port Cell where is located the equipment, the CVB has to accept the cyclic regeneration required for the 4.5 K cryopanel at different temperature levels: 100 K, 300 K and seldom at 470 K.

This high temperature imposes the selection of special materials (joints) or components (sensors and insulation) to ensure reliable operation.

Each CVB within a stainless steel vacuum enclosure of about 1.5 m in diameter and 1.8 m in height for a total weight of 3 tons, contains several internal stainless steel piping with tube bend design (avoiding the use of bellows), one 80 K thermal shield, MLI (multi layer insulation) and a dedicated number of valves, pressure safety valves and instrumentation to control the helium cooling flow for the Torus Cryopumps as well as for the Pellet Injection System (PIS).

The thermo-mechanical calculations have given the corresponding heat loads and have validated the mechanical design mainly based on the CODAP French code.

Finally, even if the proposed CVB design fulfils the present requirements, special attention will be required in future for definition and position of standalone vacuum group and recovery header for pressure safety valves, heat flux assessment in cryopumps and PIS interfaces.

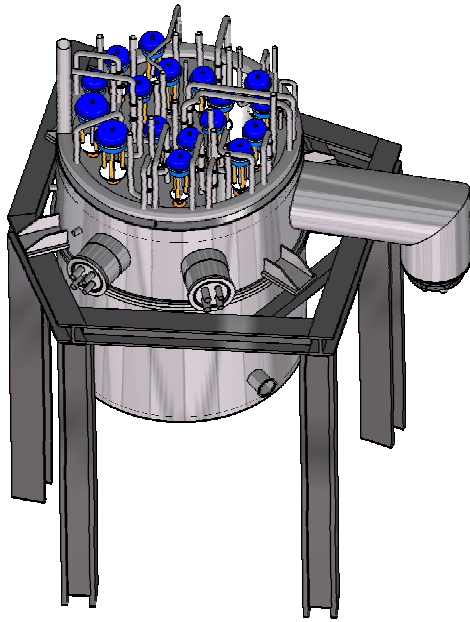


Figure 2 : Torus cryopump CVB (1.5 m in diameter)

## CONCLUSIONS

The proposed overall PFD and detailed PIDs (associated with component lists) for all ITER cryo-distribution system have defined all components and instrumentation required to insure reliable control of the cooling loops for the magnets, cryopumps and 80 K thermal shields. ITER has now adopted a helium guard system to protect all sub-atmospheric circuits based on solutions adopted and validated for years at CEA for TORE SUPRA and at CERN for LHC.

The proposed conceptual design for ACB and CVB is a typical design and dimensions should be adapted to the latest ITER requirements for the 4.5 K SHe cooling loops. For all proposed design of cold boxes, CEA recommends avoiding the use of bellows (risk of leaks) and consequently only U-bend or L-bend shapes are defined for the internal piping.

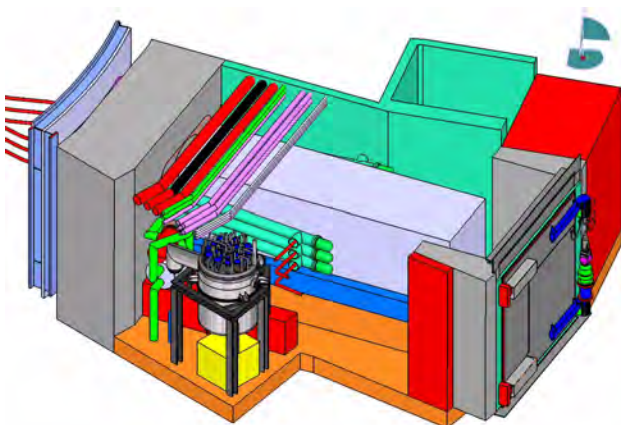


Figure 3 : CVB for Torus Cryopump and PIS installed in one ITER Port Cell

The severe requirements (building constraints / magnetic field / radiation / 470K regeneration for cryopumps) require compact design for ACB and CVB and impose specific selection of components and sensors. One can note that such compact design is risky for any maintenance or reparation during the lifetime of ITER. Furthermore, validations (requiring sometimes specific developments) of cryogenic key components are recommended before the procurement phase to ensure the reliable installation-control-maintenance of the cryogenic system in the tokamak building.

Both ACB and CVB studies were developed with CATIA V5 at CEA and successful exchanges of CATIA files with ITER/Garching were performed in December 2004 opening better integration of CEA works in ITER drawing database and also better understanding of ITER constraints by CEA designers.

Additional works on the ITER cryoplant and cryo-distribution system have to be performed in the coming years to assess the ITER cryogenic system according recent updated requirements such as HTS current leads for magnets and to detail some critical parts of the cryogenic system and associated building layouts. In complement to these design studies, some component and instrumentation qualification campaigns have also to be planned to define potential components and instrumentation for the ITER cryogenic system and also magnet and thermal shield cryogenic loops.

## REFERENCES

- [1] Design Description Document DDD 3.4 : Cryoplant and Cryodistribution System - N 34 DDD 8 R0.2, Vladimir KALININ, 2004.
- [2] Design of ITER-FEAT cryoplant to achieve stable operation over a wide range of experimental parameters and operation scenarios - Proceedings of 21<sup>th</sup> Symposium on Fusion Technology (SOFT-21) - Madrid (Spain), Vladimir KALININ et al, 2000.
- [3] Design and Performance analysis of the ITER cryoplant and cryodistribution - Proceedings of 19<sup>th</sup> International Cryogenic Engineering Conference (ICEC-19) - Grenoble (France), François MILLET et al, 2002.
- [4] Design and operating features of ITER cryoplant, Proceedings of 2003 Cryogenic Engineering Conference (CEC-03) - Anchorage (USA), François MILLET et al, 2003.
- [5] Cryogenic subsystem to provide for nominal operation and fast regeneration of the ITER primary cryo-sorption vacuum pumps - Proceedings of 2003 Cryogenic Engineering Conference (CEC-03), Anchorage (USA), Vladimir KALININ et al., 2003.

## REPORTS AND PUBLICATIONS

---

- [1] CEA Study for Process Flow Diagram (PFD) and Piping Instrumentation Diagram (PID) for the ITER cryo-distribution system (including AUTOCAD drawings and component lists) - Note SBT/04-244/FM, François Millet, November 2004.
- [2] Description of the PFD for the ITER cryo-distribution system - Note SBT/04-58 rev 2/FM, François Millet, November 2004.
- [3] Conceptual Design for Auxiliary Cold Box for Toroidal Magnets (including CATIA drawings) - Technical Report DAPNIA-SACM - Philippe Chesny, March 2005.
- [4] Conceptual Design for Cold Valve Box for Torus Cryopumps and Pellet Injection System (including CATIA drawings) - Note SBT/CT/05-01 - François Millet and Yoann Machizaud - March 2005.

## TASK LEADER

---

François MILLET

DSM/DRFMC/SBT  
CEA-Grenoble  
17, rue des Martyrs  
F-38054 Grenoble Cedex 9

Tél. : 33 4 38 78 36 31  
Fax : 33 4 38 78 51 71

E-mail : fmillet@cea.fr

**Task Title: TW3-TDS-MAGCEA: DETAILED ENGINEERING AND MANUFACTURING STUDIES OF THE ITER MAGNET SYSTEM: POLOIDAL FIELD (PF) COIL WINDINGS AND COLD TEST ASSESSMENT**

**INTRODUCTION**

The purpose of this task, started in 2004, is to review the engineering design of critical areas, assess the manufacturing procedures and techniques, layout of the manufacturing facilities and test options, review the fabrication schedule for the production of the ITER coils and their support structures. In particular, the subject of this study contract refers to:

- 1) Engineering and manufacturing studies of the Poloidal Field (PF) coil winding packs.
- 2) Assessment of the cold test options for the Toroidal Field (TF) coils.

CEA is requested to perform this work with industrial participation to assist EFDA and the ITER International Team in the review of some of the critical features of the design, study the manufacturing procedures and tooling required for winding and impregnation of the PF coils, establish the detailed layout of the manufacturing facilities and schedule, and make an assessment of the need for cold testing of the TF coils.

In order to get industrial support for the engineering and manufacturing studies of the PF coils, CEA has placed a contract with the Alstom company in Belfort (France). The assessment of the cold test options for the TF coils involves participation of the DAPNIA at CEA Saclay and of the DRFMC at CEA Grenoble, and is carried out in close cooperation with FZK at Karlsruhe (Germany).

**2004 ACTIVITIES**

**DETAILED ENGINEERING STUDIES OF PF WINDINGS**

A draft report has been delivered by the Alstom company in December 2004.

**Review of some critical areas**

*He cooling inlets*

Alstom reviewed the ITER design for the helium inlet and found that removal of the cable wrapping would be

difficult, the 0.5 mm radius at the notch end impossible to machine, the machining of a groove on a cambered conductor not easy to perform. Consequently, they proposed several variants, with a preference for that shown in figure 1. Nevertheless, this proposal isn't assessed on any mechanical analysis and therefore needs to be confirmed to check if it is viable.

*Joint area*

A design of the joints between conductors has been developed by Alstom, based on the twin box concept, qualified for NbTi conductors by the manufacture and tests of the PF-FSJS prototype sample, in the framework of Task M50. This design is applicable as well for the connection of the two conductors of the same double pancake module as for the connection of the conductors of adjacent modules (figure 2). The terminal width has been taken at 64 mm, which is similar to that of the PF-FSJS, and it is proposed to take the height at 58.7 mm, which enables to standardize the terminals for all connections but putting a copper shim between the intermodule terminals and no copper shim between the inside-module terminals.

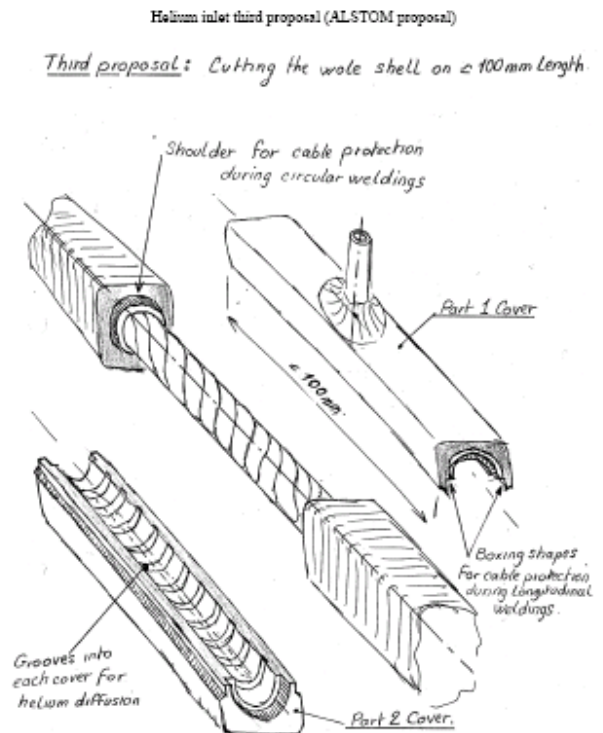


Figure 1 : PF helium cooling inlet (Alstom proposal)

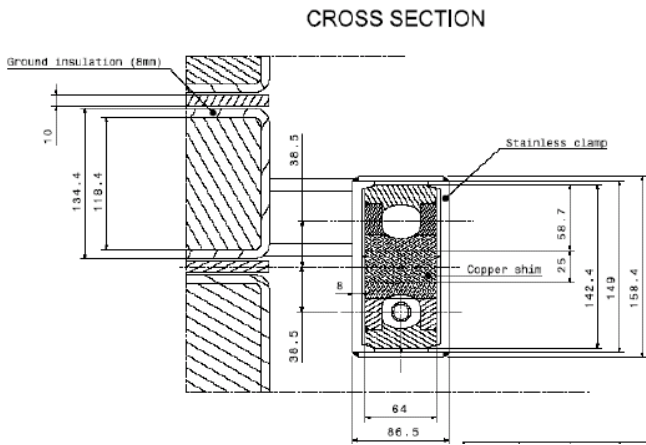


Figure 2 : Transversal cross-section of the PF joint (Alstom proposal)

### Feeders

Derived from their experience in the manufacture and assembly of the ITER TFMC busbars, Alstom proposed to simplify the clamping system of the conductor in the feeder area and to provide a gap between clamp and conductor, which can be filled with insulating material to wedge the conductor for resisting the Laplace force (figure 3).

### Manufacturing procedures

#### Winding technique

The two-in-hand design of the PF coils requires to wind simultaneously two conductors, coming from two spools, located close to the winding table.

The technique recommended by Alstom is to wind the lower pancake from outside to inside and then the upper pancake from inside to outside, avoiding so the need of two reserve spools located on top of the winding table and to wind twice the conductor of the lower pancake.

#### Helium inlet

The Alstom proposal is to perform the machining of the conductor above the winding table after calendaring, by lifting the conductor and protecting the whole area from contamination (figure 4).

#### Separation plates

Instead of manufacturing the separation plates by winding a stainless steel spiral, as designed by the ITER IT, Alstom proposes to use premachined steel sectors, which will allow to have these pieces cut and prepared by a sub-supplier outside the coil manufacturing line and avoid the deformations which could occur with the winding process.

### Manufacturing dimensions and tolerances of PF coils

Alstom analysed the manufacturing dimensions, taking into account their experience of the manufacture of the POLO coil and of the reshaping of the TFMC busbars conductors.

They propose to increase the shim thickness between turns up to 1.4 mm to cope with the tolerances assumed on the conductor and the shim thickness between doubles pancakes in coils PF1, PF2, PF5, PF6 up to 3 mm to cope with unflatness defects on the impregnated modules. For PF3 and PF4 coils, they propose to stack the non impregnated ground insulated DPs and separation plates, which allows to recover the unflatness defects of the DPs without ground insulation.

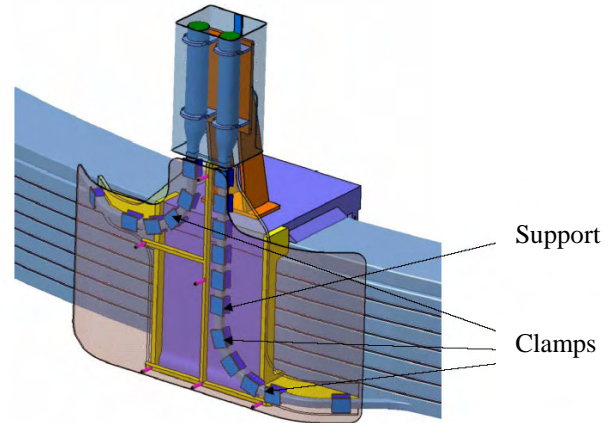


Figure 3 : Conductor clamping in the feeder area (Alstom proposal)

### Manufacturing tooling and equipment

Alstom agrees on the baseline definition of the manufacturing line proposed in a previous study by Ansaldo.

### Review of QA documents and quality control procedures

Alstom delivered comments on the available QA documents.

### ASSESSMENT OF COLD TEST OPTIONS FOR TF COILS

This work has been reported in a poster presentation at the 23<sup>rd</sup> SOFT in Venice [1].

### Assessment of the need for cold test of the TF coils

#### Coil features and properties

The Toroidal Field (TF) magnet will be made of eighteen 350 tons D-shaped coils operating at a temperature of 4.5 K up to a maximum magnetic induction of 11.8 T, using a 68 kA cable-in-conduit Nb<sub>3</sub>Sn conductor inserted in stainless steel radial plates. The manufacturing techniques to be used in the construction of these coils have been qualified by the manufacture and tests of the Toroidal Field Model Coil (TFMC). Nevertheless, this was achieved for a coil of a smaller size (1/3 scale) than the TF coils, which remains up to now the single one of this type ever built. Changing a faulty coil in the torus would cause a major breakdown in the experimental programme and represents a considerable work, which makes compulsory to install only coils the performances of which have been carefully checked.

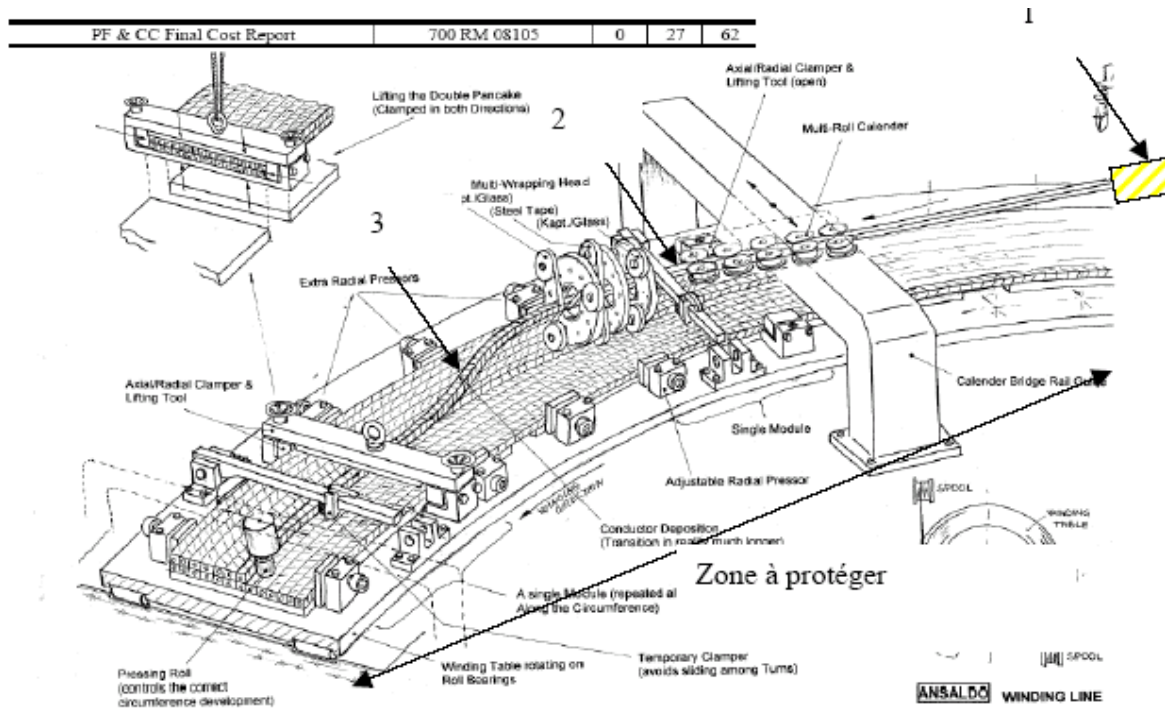


Figure 4 : Manufacture of helium inlet (Alstom proposal)

This means that sufficient knowledge should be acquired on their electromagnetic, thermal, hydraulic, mechanical, insulation properties and operating margins.

*Testing scenarios*

Unfortunately, very limited direct measurements will be available from manufacture due to the limitation of cold testing to LN<sub>2</sub> temperature without current, whereas tests at liquid helium temperature with current would provide much more information. Consequently, the main characteristics can only be derived from the measurements performed on a relevant coil, assuming the reproducibility of the manufacturing process.

This calls clearly for the cryogenic test of a prototype coil, built with the same geometry and materials as the series coils and on the same manufacturing line with the same procedures and toolings. The experience accumulated with the TFMC tests is not totally relevant, since the coil geometry is different, new manufacturing techniques are foreseen, as well as the use of new advanced conductors. Forgetting this step could lead to discover problems at a late stage of manufacture.

Nevertheless, the measurement of the critical electrical properties of the prototype coil cannot be achieved in relevant conditions if this coil is tested alone, since the achievable magnetic field will be much smaller than in the toroidal configuration and could only reach a maximum of 6 T at nominal current.

To reach the critical current needs thus to operate at temperatures above 9 K, assuming a thermal strain of -0.84%, according to the ITER design criteria and neglecting the electromagnetic strain (figure 1).

It is therefore necessary to complete this measurement by the test of a significant length of conductor in relevant magnetic field and temperature, which could be achieved by the test in the Central Solenoid Model Coil (CSMC) test facility of an insert coil using the same type of conductor.

It is recommended to use the strategy usually followed for fusion machines, which is cold testing of all coils, as experienced in the past for Tore Supra or at present for W7-X or EAST, since it provides the most confidence in the coil performances and minimizes the risk of failure. Besides, the same strategy could apply as well to the CS and PF coils.

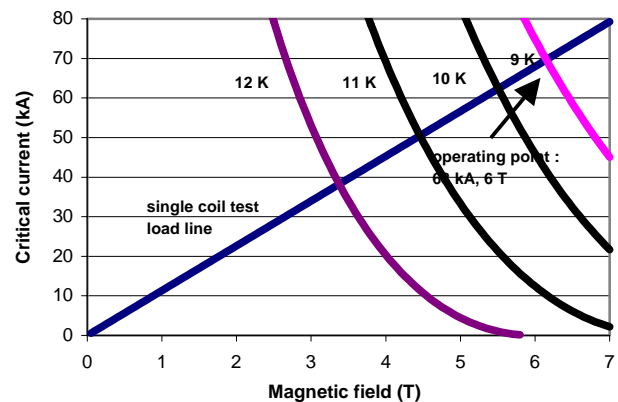


Figure 5 : TF coil critical current versus magnetic induction ( $\epsilon = -0.84\%$ )

**Test configuration**

In a single coil test the coil experiences only in-plane loading whereas in simultaneous operation of two coils, in-plane as out-of-plane loading can arise.

In the two coil configuration, two options may be considered : ramping up the current in both coils simultaneously or successively. In case of simultaneous operation, current limitation or an additional support structure may be required to prevent excessive deformation. On the contrary, if the coils are operated successively, each coil is tested as a single coil with in-plane forces only, but the overall time schedule for the tests can be reduced by saving time for installation, cooldown and warm-up. Figure 6 shows a possible arrangement for the two coil test configuration : the coils are assembled as adjacent coils in the torus allowing the attachment of the coils together, which can provide mechanical support if the current is ramped in both coils simultaneously.

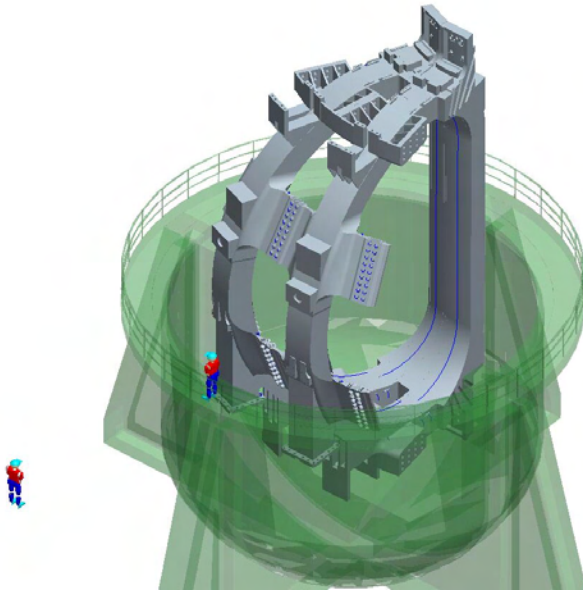


Figure 6 : Two coil test configuration

**Preliminary design of a test facility**

The testing facility will then include a 12.5 m diameter, 20 m high cryostat, a vacuum pumping unit with 15 000 m<sup>3</sup>/h primary and 15 m<sup>3</sup>/s secondary pumping capacity, a 2 kW cryogenic refrigerator [2], a 70 kA power supply with associated switching unit and a 3 mΩ dump resistor unit. The required building will be 50 m long, 20 m wide and 20m high, the lower part of the cryostat being under the ground level and equipped with a 500 t lifting unit (figure 7).

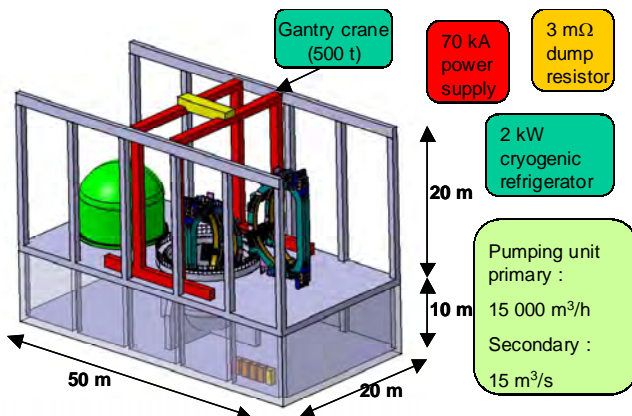


Figure 7 : TF coil cold test facility

**CONCLUSION**

The engineering design of the PF coils has been reviewed in details by Alstom, in the framework of an industrial study contract and a draft report has been delivered by the company. Proposals have been made for the detailed design of critical areas (He inlets, joints, feeders), the tolerances on coil dimensions have been assessed and the manufacturing procedures reviewed.

The need of testing at least a prototype TF coil at low temperature has been argued and the test of all coils at 4 K and nominal current recommended. The preferred testing arrangement is the twin coil test configuration. An overall design of the test facility has been proposed.

Completion of the work is scheduled for April 2005.

**REFERENCES**

- [1] How should we test the ITER TF coils ? - P. Libeyre et al. - 23<sup>rd</sup> SOFT, Venice, 20-24.09.2004.
- [2] G. Zahn et al. - Design of a cooling system for the cold test of the ITER TF coils before installation - Proc. ICEC20, Beijing, 2004, to appear.

**TASK LEADER**

Paul LIBEYRE

DSM/DRFC/STEP  
CEA-Cadarache  
F-13108 Saint-Paul-Lez-Durance Cedex

Tél. : 33 4 42 25 46 03  
Fax : 33 4 42 25 26 61

E-mail : libeyre@cea.fr

**CEDFA03-1031**  
**CEFDA04-1146**

---

**Task Title: JW3-EP-ICRH and JW4-EP-ICRH: CONTRIBUTION TO ICRH COMPONENTS ANTENNA LIMITER**

---

**INTRODUCTION**

---

The scope of the present project is the design and the manufacturing of the ICRH antenna limiter (figure 1) which was to be installed in the JET vessel during the 2004 shutdown.

The contractual activity on the antenna limiters was launched on May 2002 and consisted mainly for the first 1.5 years in designing, engineering, calculations, drawings and procurement specification for the limiter project.

This work is produced in close collaboration with the JET operator and the EFDA CSU JET and has been reported previously.

The task agreement for 2004 was oriented towards the manufacturing activities associated to this project.

**2004 ACTIVITIES**

---

**CFC TILE MACHINING MONITORING**

A contract was awarded by the commission, at the end of 2003, to Carbone Lorraine in Paris for the machining of the antenna limiter tiles (private & poloidal) and for the divertor replacement tiles.

The main activity on this task was the monitoring of this contract following the requirements of the EFDA CSU JET and the UKAEA quality insurance system.

The plasma facing side of every tiles was designed following a 3D contouring allowing for very precise shadowing of all edges in a variety of plasma configuration. Therefore the contour machining was directly processed from the CATIA drawing files. A limited quantity of graphitised Carbone Fiber Composites blocks were available. Consequently the quality plans of all tiles were directed as to allow for control & validation of graphite prototypes before machining the CFC blocks.

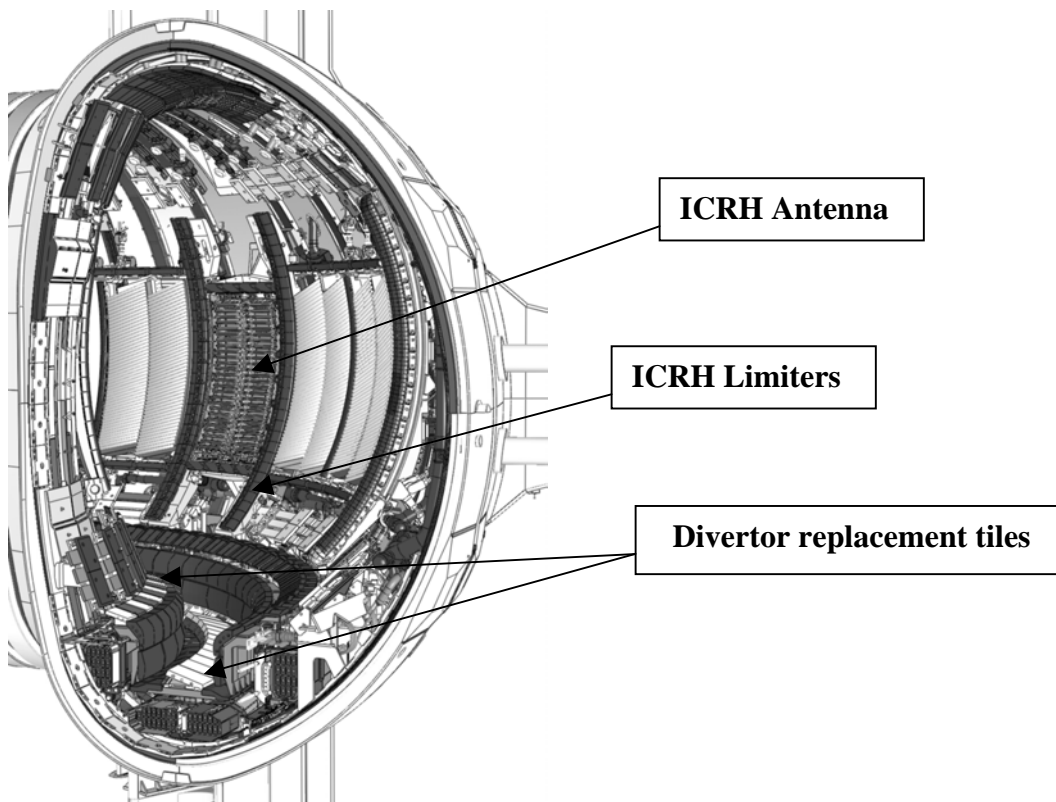


*Figure 1 : Antenna limiter & divertor new configuration*

Progress in manufacturing was followed by a monthly progress report from Carbone Lorraine as well as by Monthly visit, to be added to the hold points decided on the quality plans.

The first divertor tiles were delivered in June 2004, the first poloidal limiter tiles in October 2004 and the last private limiter tiles in December 2004.

## SUPPORT STRUCTURE

The Kick off meeting for the manufacturing contract of the support structuring took place in October 2003. The monitoring of this contract covered also the manufacturing of the metallic supporting structure for the divertor new load bearing septum replacement plate.

The manufacturing contract was allocated to R. Mulheisen Gbmh, a German company based closed to Frankfurt.

The first 4 month of the contract were mainly devoted to the paper work associated to the stringent specification which was written in accordance with the EFDA CSU Jet requirements and following the UKAEA quality Insurance.

After validation of all manufacturing drawing by CEA and approval of the quality plans , the purchase of raw material was allowed.

Close monitoring of the subcontracted company for the welding was done in collaboration with the UKAEA welding engineer allowing for a precise quality plan for all welds, in accordance with the UKAEA QA.

Over 5000 Items were machined for these limiters mainly in Inconel 625.

Other materials such as Alu bronze, Nimonic, Inconel 725 & Nickel 200 were also used.

All elements were fully checked on a 3D measuring device.

The close monitoring of this limiter involved checking all the different subcontractors and validating their quality insurance systems.

All monitoring reports were transmitted to the operator and commented during the numerous projects meetings.

## INSTALLATION

Final delivery of the limiters done on December the 20<sup>th</sup> 2004.

Installation in the machined by the operator was scheduled for the first month of 2005 and started by manual set-up and adjustment of the supporting legs, before separate installation of the beams (poloidal & cross) by remote handling.

All tiles were also to be installed individually by the same means.



*Figure 2 : Final assembly of the supporting structure at the subcontractor*

## CONCLUSIONS

---

All tasks associated with the design and manufacturing of the poloidal ICRH limiters are achieved as well as the monitoring activity for divertor elements. The final paperwork is under process.

The specific design and technical achievements for this project were reported in the Venice 23<sup>rd</sup> SOFT conference.

## REPORTS AND PUBLICATIONS

---

Design of a limiter for the JET EP ICRH Antenna; Ph. Chappuis & Al, 23<sup>rd</sup> SOFT in Venice September 2004.

## TASK LEADER

---

Philippe CHAPPUIS

DSM/DRFC/SIPP  
CEA-Cadarache  
F-13108 Saint-Paul-Lez-Durance Cedex

Tél. : 33 4 42 25 46 62  
Fax : 33 4 42 25 49 90

E-mail : e-mail : philippe.chappuis@cea.fr

---

**Task Title: JW3-EP-IRV: DIAGNOSTICS ENHANCEMENT - WIDE ANGLE IR ENDOSCOPE**

---

**INTRODUCTION**

---

In the framework of the JET-EP project, proposal sent by the Association CEA Cadarache to develop a new diagnostic for thermography analysis was approved by EFDA in 2002. This system will allow to see a large section of the internal components in the vessel such as divertor, main chamber, ICRH antenna etc, aiming at measuring the surface temperature during normal operation and off normal events such as ELMs and disruption. This diagnostic is ITER relevant both for the technology used and for the physic outputs. This system will allow to evaluate the power deposition in the main chamber during transient events and could be used, in the future with implementation of a feed back control, for real time machine protection.

**2004 ACTIVITIES**

---

The scope of the work in 2004 was the following-up of the two Article 7 contracts launched in 2003 for procurement of an infrared camera and an endoscope.

The infrared camera and acquisition system have been manufactured without major problems.

Some technical difficulties occurred on the production of the infrared filters due to the strong optical requirements ; the filters have finally been delivered within the specifications with a few months delay. IR camera has been delivered and tested in CEA Cadarache in November 2004. Software to interface the IR camera and the JET acquisition system is being developed and should be implemented during the first term of 2005.

Prior to the start of the work on the endoscope contract, additional work has been needed to clarify the interface with the JET machine. Then, detailed optical and mechanical designs have been produced by TNO. Further to final approval of the design by the project team, the manufacturing phase could start in November 2004.

Manufacturing phase is now finished for both contracts and the project is now a very likely to be ready in August 2005, as initially expected. Due to delay in the JET Shutdown Plan, the JET EP IRV would be now installed during the Restart and should be operational at the beginning of the C15 Campaign .

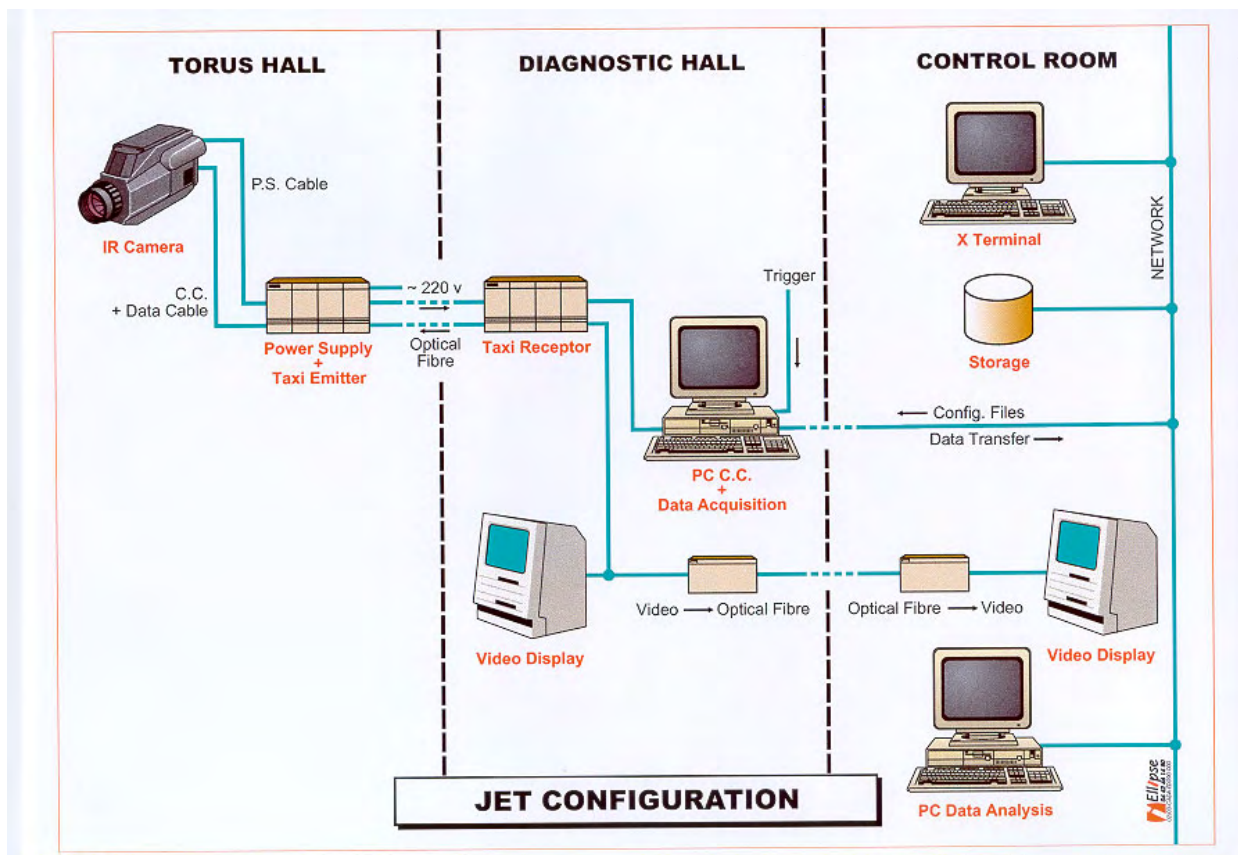


Figure 1 : Schematic layout of the Infrared Camera data acquisition system on JET

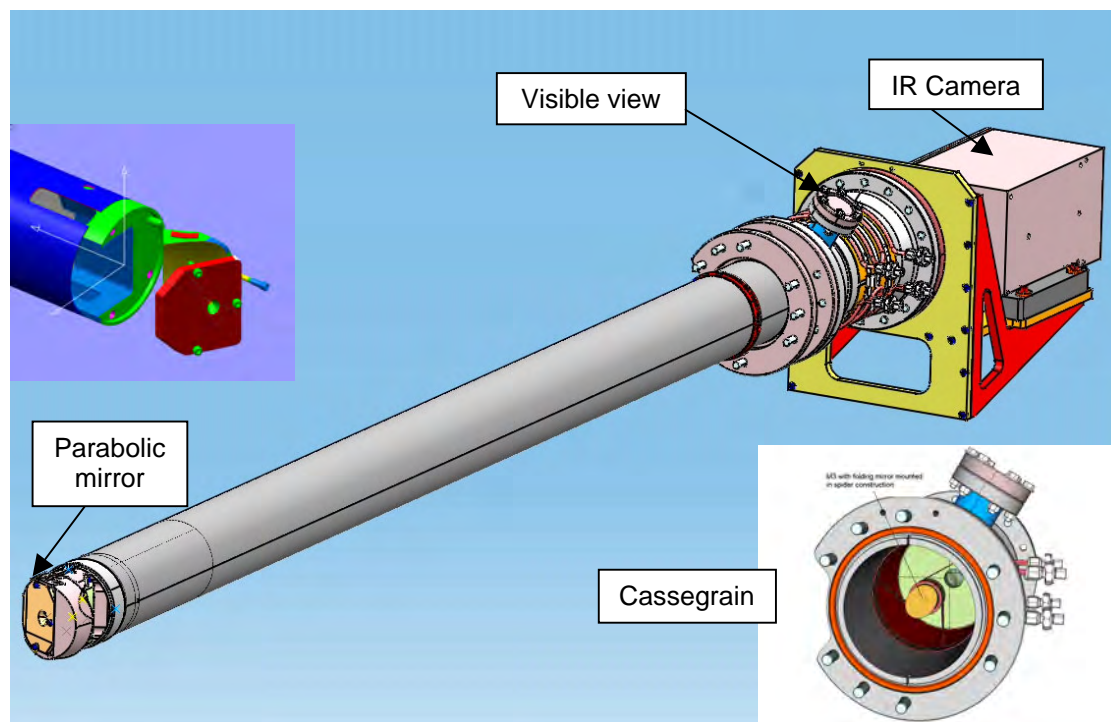


Figure 2 : Schematic layout of the endoscope equipped with the IR camera

## CONCLUSION

---

The manufacturing phase is over and we are now in the assembly and integration phase of the project. The JET EP IRV diagnostic is planned to be commissioned during summer 2005 and should be operational at the start of the C15 Campaign.

## REPORTS AND PUBLICATIONS

---

Technical group evaluation report on analysis of IR endoscope tenders - DIAG/NTT-2004.005 (2004) - E. Gauthier.

Technical specifications of Cudas software for control of the JET-EP IR camera - DIAG/CCH-2004.015 (2004) - E. Gauthier.

Minutes on meeting at CEDIP on 8th April 2004 - DIAG/CRR-2004.016 (2004) - E. Gauthier, H. Roche.

Report on tender evaluation on the IR endoscope Call for Tender - DIAG/NTT-2004.004 (2004) - E. Gauthier.

Minutes of meeting at TNO on 17th march 2004 - DIAG/CRR-2004.009 (2004) - E. Gauthier, J. Migozzi.

Optical design of an infrared endoscope using reflective optics - DIAG/NTT-2004.007 (2004) - E. Gauthier, J. Migozzi.

Minutes of meeting at TNO on 24th march 2004 - DIAG/CRR-2004.010 (2004) - E. Gauthier.

Minutes of meeting hold at JET on 21st October 2004 - DIAG/CRR-2004.043 (2004) - E. Gauthier.

Photometric analysis of the JET-IRV new optical design - DIAG/NTT-2004.011 (2004) - D. Guilhem.

Minutes of kick-off meeting with TNO on infrared endoscope contract FU 06 CT 2004-00023 - EFDA EP IRV 01/09/2004 - E. Gauthier.

Minutes of project Board on 28<sup>th</sup> September 2004 at JET - EFDA EP DIA IRV-R-010 12/10/2004 - J. Gafert.

JET EP INFRARED DIAGNOSTIC PROJECT - Thermomechanical behaviour of Cassegrain telescope system - DIAG/NTT-2004.008 (2004) - M. Missirlian.

## TASK LEADER

---

Eric GAUTHIER

DSM/DRFC/SIPP  
CEA-Cadarache  
F-13108 Saint-Paul-Lez-Durance Cedex

Tél. : 33 4 42 25 42 04  
Fax : 33 4 42 25 49 90

E-mail : gauthier@drfc.cad.cea.fr

**Task Title: INTERNAL PFC COMPONENTS BEHAVIOUR AND MODELLING**

**INTRODUCTION**

Power flux deposition on the divertor during Edge Localised Modes (ELMs) is a crucial issue for the divertor in ITER. Power flux and energy distribution in space and time are key parameters that determine the ablation rate of the material. In present tokamak such as JET, during experimental campaign, the temperature is measured with thermocouples inserted in the tiles and with infrared camera measuring the surface temperature. Then, the power flux is calculated from the surface temperature evolution as function of time.

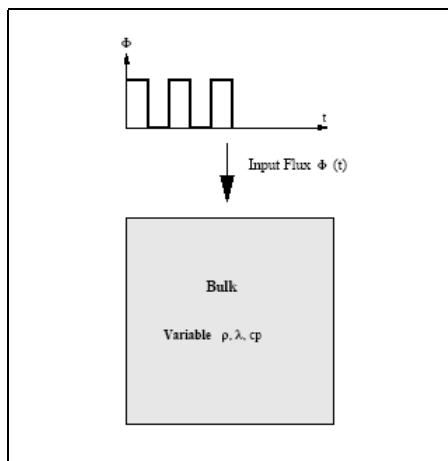
During transient high heat loads the power calculated using standard material properties for PFC is over-estimated [1] due to carbon layer deposition on the tile occurring during plasma operation: surface temperatures are higher than expected on initial PCF material. Moreover, for transient events such as ELMs with a duration in the range of 100-400  $\mu$ s in JET, energy can not be measured from thermocouples due to the long time constant  $\tau = l^2/D$  (where  $l$  is the distance between the thermocouple location and the tile's surface and  $D$  the thermal diffusivity of the material). To compensate this effect, the surface layer has been modelled by introduction of a heat transmission factor [1]. Since the thermo mechanical parameters ( $\rho$ ,  $\lambda$ ,  $C_p$ ) of the surface layer are unknown, the uncertainty on the heat transmission coefficient induces large error bar on the calculated heat load. Moreover, parametric study of the heat transmission coefficient has demonstrated that its value, at a given location of the layer, is not unique but can change with time or temperature during a plasma discharge [2]. In fact, characterization of the redeposited layer cannot be achieved *in situ* in a tokamak since both the power flux and the thermal properties of the layer are unknown.

In order to improve power estimation and provide tools for better power/energy measurements in tokamaks, model validation and experiments on divertor tiles are on going. This work is carried out within the Fusion Technology (FT) Task force (TF) at JET and in the European national laboratories in collaboration with the JET Operator (UKAEA) and is part of the "Internal plasma facing components behaviour and modelling" research topic.

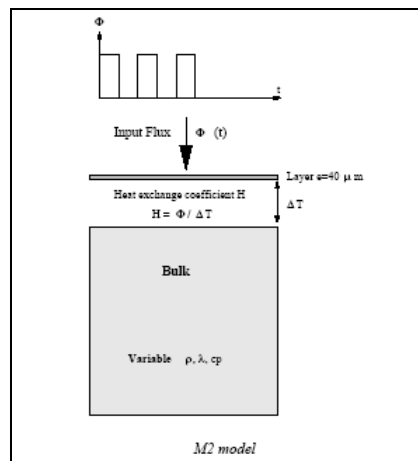
**2004 ACTIVITIES**

Experiments on divertor tiles have been carried out in 2003 within the Fusion Technology (FT) Task force (TF) at JET and in the European national laboratories in collaboration with the JET Operator (UKAEA). Two MkII divertor tiles, installed in JET during the 1995-1996 campaign, one from the inner side showing thick coating layer and one from the outer side showing erosion dominated and thin coating areas, have been selected to be exposed to power flux in the range from 5 to 100MW/m<sup>2</sup>. Both tiles were equipped with 12 thermocouples inserted at different depth from the surface allowing measuring the thermal diffusivity in the bulk and the total energy impinging on the tile. The surface temperature was to be recorded by using a fast infrared camera and a standard IR camera.

In 2004, post-tests thermal calculations of JET divertor tiles have been performed to calculate the surface and in-depth temperature distribution on the actual JET divertor tiles during high frequency energy deposition. These calculations have been reported in [12]. Different tiles configurations have been considered in the numerical simulations taking into account the possible modification of the surface of the tiles (erosion, re-deposition):



M1 model : Fresh tile

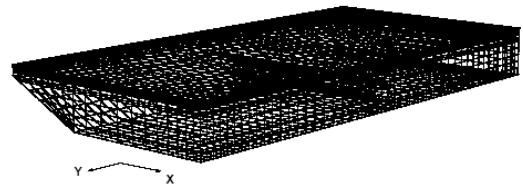


M2 model ; Bulk + deposited layer

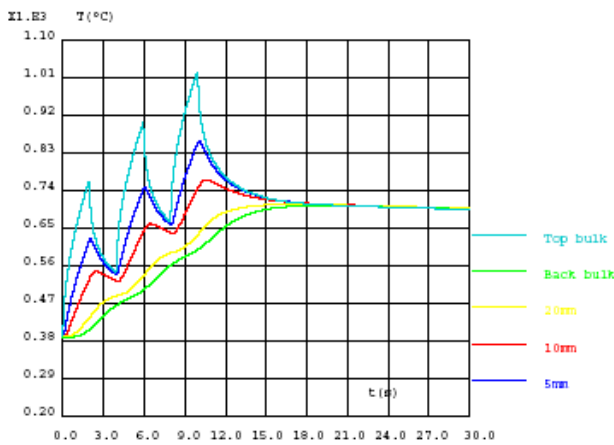
The heat exchange between the layer and the bulk material is an adjustable parameter together with the thermal conductivity of the layer.

In a first step, a simple 1-D model (with CAST3M finite element code developed at CEA, see [6]) was considered to validate the models and to study the influence of the layer and of the heat exchange between the layer and the bulk on bulk surface and in-depth thermocouples temperatures.

Main conclusion about the influence of re-deposited layer on surface temperatures was that it was necessary to consider a model with a heat exchange coefficient between the bulk and the surface layer (M2 model) and the value of heat exchange coefficient is about 50 kW/m<sup>2</sup> with a heat flux of 5 MW/m<sup>2</sup>.

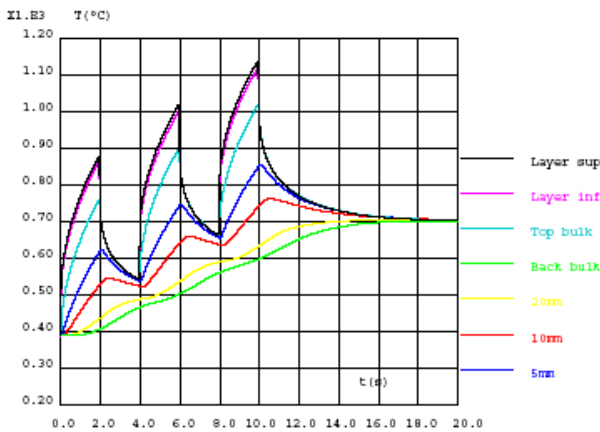


3-D Finite element mesh of the tile type 4 LH with thermocouples positions



Zoom on temperature evolution at different locations

1-D Model M1 : bulk without additional layer

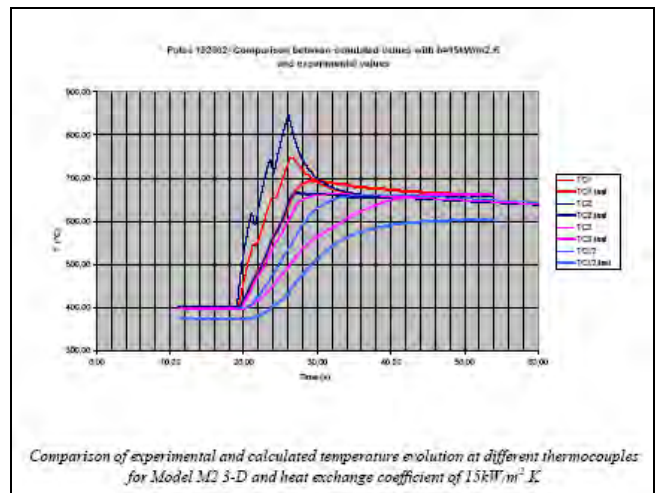


Zoom on temperature evolution at different locations

1-D Model M2 : bulk + additional layer and heat exchange coefficient of 50 kW/m<sup>2</sup>.K

Pulse n°152448 5 MW/m<sup>2</sup> 2s/2s for 3 cycles

In a second step, the real geometry of tiles has been taken into account in a complete 3-D model using the CAST3M code (see also pre tests calculations reported in [10] and [11]) to calculate the surface and in-depth temperature distribution on the actual JET divertor tiles during high frequency energy deposition:



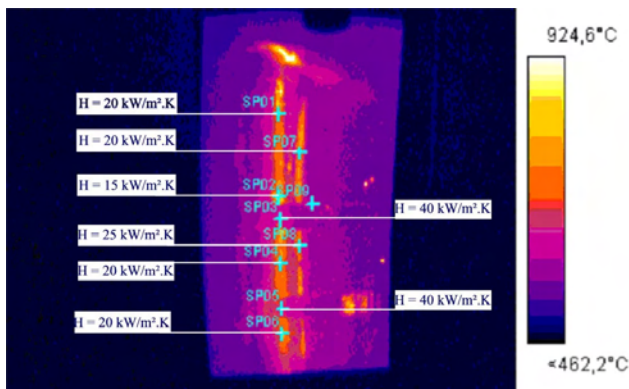
Comparison of experimental and calculated temperature evolution at different thermocouples for Model M2 3-D and heat exchange coefficient of 15kW/m<sup>2</sup>.K

Pulse n°152448 5MW/m<sup>2</sup> 2s/2s for 3 cycles: calculated temperatures for 100 % input flux

All calculations with 90 % of the experimental flux (possible over-estimation of the experimental flux) give a better agreement with equilibrium temperature but there were some discrepancies between experimental and calculated bulk temperatures (possible bad CFC thermal properties).

Modelling of the surface temperature has been successfully achieved using a 2D array variable, the heat exchange coefficient being governed by the co-deposited pattern.

Additionally, it has been shown that the thermal properties of the co-deposited layer changed from shot to shot, due to annealing of the layer inducing structural modification (graphitisation).



*Heat exchange coefficient  $H$  on different location on the tile for pulse 152306 at 5 MW/m<sup>2</sup>*

## CONCLUSIONS

Post-tests 3-D thermal calculations of JET divertor tiles have been performed in 2004. A detailed 3-D model was developed using the CAST3M code to calculate the surface and in-depth temperature distribution on the actual JET divertor tiles during high frequency energy deposition. Different tiles configuration have been envisaged in the numerical simulations taking into account the possible modification of the surface of the tiles (erosion, re-deposition). All calculations with 90% of the experimental flux (possible over-estimation of the experimental flux) give a better agreement with equilibrium temperature but there are still some discrepancies between experimental and calculated bulk temperatures (mainly due to bad thermal contacts between the thermocouples and the tile). Concerning surface temperatures, results obtained with modelling a modification of the surface of the tiles (erosion, re-deposition) with a heat exchange coefficient in the range of 15 to 50 kW/m<sup>2</sup>.K, give good agreement with experimental values.

Results have been presented at the PSI conference in May 2004 and published in Journal of Nuclear Material. Draft report has been sent in June 2004 and after amendments, Final report on FT3.1 task has been accepted in December 2004. The task is now completed.

## REFERENCES

- [1] S. Clement et al - J. Nucl Mat. - 266-269 (1999) 285.
- [2] Y. Corre et al - 30<sup>th</sup> EPS Conference - St Petersburg, 2003.
- [3] P. Andrew et al. - J. Nucl Mat. - 313-316 (2003) 135-139.
- [4] E. Gauthier et al. - Proc. 24th EPS Conf, Berchtesgaden, (1997).
- [5] H.S. Carslaw and J.C. Jaeger - Conduction of heat in solids - second edition Oxford at the Clarendon press.
- [6] CAST3M - see <http://www-cast3m.cea.fr>.
- [7] J.P. Coad et al. - J. Nucl Mat, 313-316, 2003, 419-423.
- [8] E. Gauthier - Thermal behaviour of redeposited layer under high heat flux exposure - J. Nucl. Mat. - 337-339 (2005), 960-964.
- [9] V. Riccardo et al. - PPCF, 2001.
- [10] P. Yala and L. Nicolas - Pre test 3-D thermal calculations of jet divertor tiles - JET Task Fusion Technology JW0-FT-3.1 - CEA report SEMT/LM2S/RT/02.042, November 2002.
- [11] E. Gauthier et al. - Interim report FT3.1 - CEA report CFP/NTT-2003.005, February 2003.
- [12] P. Yala and L. Nicolas - Post test 3-D thermal calculations of jet divertor tiles - JET Task Fusion Technology JW0-FT-3.1 - CEA report SEMT/LM2S/RT/04.027, August 2004.

## REPORTS AND PUBLICATIONS

Compte rendu et analyse préliminaire des expériences de dépôt de puissance sur les tuiles du divertor (Task FT3.1) - DIAG/NTT-2004.028 (2004) - E. Gauthier.

Modélisation des expériences de dépôt de puissance sur des tuiles issues du divertor du JET - CFP/NTT-2004.022 (2004) - S. Dumas, E. Gauthier, M. Missirlian.

P. Yala and L. Nicolas - Post test 3-D thermal calculations of jet divertor tiles - JET Task Fusion Technology JW0-FT-3.1 - CEA report SEMT/LM2S/RT/04.027, August 2004

Final report of JW0-FT-3.1 task - CFP/NTT-2004.031 (2004) - E. Gauthier, S. Dumas, L. Nicolas, P. Yala.

Thermal behaviour of redeposited layer under high heat flux exposure - 16<sup>th</sup> Int. Conf. on Plasma Surface Interaction in Controlled Fusion Devices (2004) - J. Nucl. Mater, 337-339 (2005) 960-964 - E. Gauthier, S. Dumas, J. Matheus, M. Missirlian, Y. Corre, L. Nicolas, P. Yala, J. Coad, P. Andrew, S. Cox, and EfdA-JET team.

## **TASK LEADER**

---

Eric GAUTHIER

DSM/DRFC/SIPP  
CEA-Cadarache  
F-13108 Saint-Paul-Lez-Durance Cedex

Tél. : 33 4 42 25 42 04

Fax : 33 4 42 25 49 90

E-mail : eric.gauthier@cea.fr

In collaboration with :

Laetitia NICOLAS

DEN/DM2S/SEMT  
CEA-Saclay  
F-91191 Gif-sur-Yvette Cedex

Tél. : 33 1 69 08 55 40

Fax : 33 1 69 08 86 84

E-mail : laetitia.nicolas@cea.fr

# JW3-FT-2.15-D01

## Task Title: DETRITIATION OF SOFT HOUSEKEEPING MATERIALS (mainly plastics)

### INTRODUCTION

The aim of this task is to study different ways for chemical detritiation of housekeeping materials (at laboratory scale), the processes that seem to be most efficiency were selected to determine whether further experiments are needed to validate this selection.

These dedicated procedures are proposed for the different type of waste as follow:

- parts of gloves (butyl rubber),
- parts of light coveralls (polyester),
- plastic sheet (PVC or polyurethane),
- parts of seals,
- filaments of paper.

The results of the different detritiations must not create other wastes which are difficult and expensive to treat.

### 2004 ACTIVITIES

A literature review was performed to find different ideas but there is no process actually used. CEA VALDUC, which have the same type of wastes manage them in function of their activities [1].

- introduction in air lock,
- drums emptying,
- counting,
- sorting and control,
- shredding,
- drying (at 90°C, to limit the tritium degas),
- drums filling,
- compacting press,
- closing and control.

Type TFA wastes are evacuated in ANDRA storage.

Type A is stored in hangars.

Type B is stored in ventilated hangars.

Type C with a more important degassing rate is stored in special drums and in more ventilated hangars.

To estimate the degassing rate, all these drums are measured by calorimetry.

Different ways are studied for the housekeeping detritiation without generating other wastes:

- leaching with hot water,
- leaching with acidic solution,
- leaching with basic solution,
- full mineralization in a digester.

With this type of waste, the difficulty of the study is the homogeneity of samples to compare different processes.

An approach with a cryo-grinding treatment with liquid nitrogen shows that it's impossible to transform them as powder. All the samples remain too soft.

So to have comparative decontamination ratio, it is necessary to measure the residual tritium content in the housekeeping material after the detritiation process by full dissolution of samples.

### STUDY OF FULL MINERALIZATION SAMPLE TO MEASURE TRITIUM ACTIVITY

In a reactor connected to different traps for tritium measurement:

- a volume of sulfuric acid during one day at 100°C is used for the dissolution of the housekeeping,
- and another volume of sulfuric acid during 3 days and some drops of hydrogen peroxide.

Acidic and basic solutions are distilled and all the traps solutions are measured with liquid scintillation apparatus. The wiring diagram (figure 1) shows the montage.

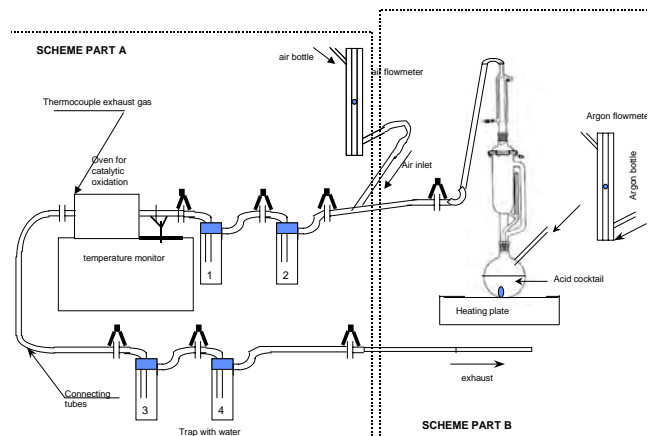


Figure 1 : Wiring diagram

Results : sample 6,4 g of different wastes are treated.

Activity in reactor :  $^3\text{H}$  liq. = 260517 Bq.  
 Activity in different traps :  $^3\text{H}$  gas = 9924 Bq.

Total activity :  $^3\text{H}$  = 42256 Bq/g

The results show that more than 90% of the tritium is not under gas form. The tritium comes from the contamination of the materials after the different experiments. In this case, the tritium contamination can be eliminated with different lixiviation processes.

**DETRITIATION BY LEACHING WITH HOT WATER (100°C)**

Same used montage (figure 1).

After 8 hours : tritium activity = 1289 Bq/g (only in reactor).

After 16 hours : tritium activity still the same as after 8 hours and equal to 1289 Bq/g (only in reactor).

Total activity :  $^3\text{H}$  = 1328 Bq/g (reactor+ traps)

More than 90 % of tritium activity is in the reactor and the rest in traps.

Only 100°C  
 Tritium is not under gas form

Calculation of the decontamination ratio :

Mineralization of the rest of the lixiviated housekeeping

Total tritium activity = 447 Bq/g  
 Decontamination ratio = 75 %

Total tritium activity between first and second experiment is very different. 422256 Bq/g for the first and 1328 Bq/g for the second, which have been done 3 month later. This result shows the heterogeneity of the different wastes and the difficulty of sampling identical samples. The wastes are stored in plastic box, so we have to consider that a lot of tritium is lost by diffusion through the plastic box.

**DETRITIATION BY LEACHING WITH HOT NITRIC ACID (2M)**

After 8 hours : tritium activity = 1202 Bq/g (only in reactor)

After 16 hours : tritium activity still the same as after 8 hours.

Total activity :  $^3\text{H}$  = 1303 Bq/g (reactor+ traps)

More than 90% of tritium activity is in the reactor and the rest in traps

Calculation of the decontamination ratio :

Mineralization of the rest of the lixiviated housekeeping

Total tritium activity = 500 Bq/g  
 Decontamination ratio = 72 %

The decontamination ratio with acid solution is quite the same as water.

**DETRITIATION BY LEACHING WITH HOT SODA (1M)**

After 8 hours : tritium activity = 656 Bq/g (only in reactor)  
 After 16 hours : tritium activity still the same as after 8 hours.

Total activity :  $^3\text{H}$  = 710 Bq/g (reactor+ traps)

More than 90% of tritium activity is in the reactor and the rest in traps

Calculation of the decontamination ratio :

Mineralization of the rest of the leached housekeeping

Total tritium activity = 308 Bq/g  
 Decontamination ratio = 70 %

The decontamination ratio with basic solution is quite the same as water.

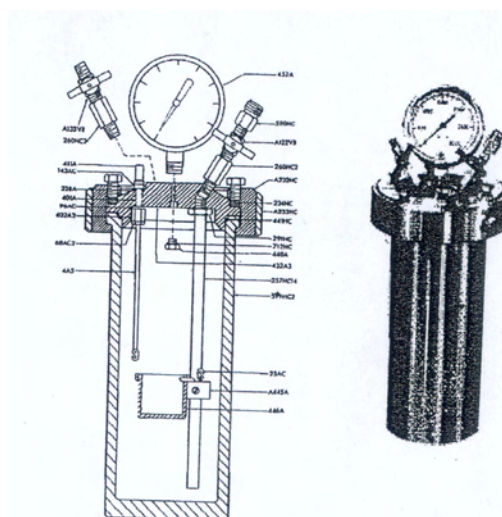
These three leaching types have nearly the same decontamination ratio. They all generate tritiated aqueous solutions. The easiest is the process with water where tritiated water is generated, which have to be stored in polyethylene bottle to avoid corrosion.

For the high activity levels, the water is adsorbed on zeolithe and store in drums.

**FULL MINERALIZATION IN A DIGESTER**

Under oxygen (25 bars), all the organic structure is burned and destroyed. The tritium is recovered under liquid and gas forms.

The next photo shows the mineralization system.



In this case, all the housekeeping materials are burned and 100 % of the tritium is trapped in the bubbles and rinsed water of the mineralization system as tritiated water.

The total tritium activity measured is 1973 Bq/g.  
The decontamination ratio is 100 %.

More than 95 % of the tritium is in the rinsed water phase.  
Only tritiated water is created.

## CONCLUSIONS

---

Even the chemical tests would have been done, the extraction rate is around 70 %.

The easiest is the process with water where tritiated water is generated which have to be stored in polyethylene bottle for having no corrosion.

For the high activity levels, the water is adsorbed on zeolithe and store in drums.

In a digester, 100 % of the tritium is transformed with oxygen as HTO form and trapped in bubbles. Only tritiated water is created.

In both cases tritiated water is easy to manage. It must be stored in polyethylene bottle to avoid corrosion.

For the high activity levels, the water is adsorbed on zeolithes and stored in drums.

CEA VALDUC, which has the same problems doesn't detritiate their housekeeping materials. They manage the storage of the wastes pertaining to their activities. They are stored in different hangars with adapted ventilation levels. The degassing rate is controlled by calorimetry measurement on the drums.

## REFERENCE

---

- [1] Compte rendu de réunion : UKAEA/CEA co-operation on fusion decommissioning - S. Rosanvallon DER/STR/LCEP 2001/309.

## TASK LEADER

---

Pierre TRABUC

DEN/DTN/STPA/LPC  
CEA-Cadarache  
F-13108 Saint-Paul-Lez-Durance Cedex

Tél. : 33 4 42 25 43 05  
Fax : 33 4 42 25 72 87

E-mail : pierre.trabuc@cea.fr



**JW3-FT-2.15-D02****Task Title: DETRITIATION OF VACUUM OIL AND ORGANIC LIQUIDS****INTRODUCTION**

The aim of this task is to study different ways for chemical detritiation of oil and scintillation liquids (at laboratory scale), the processes that seem to be most efficiency were selected to determine whether further experiments are needed to validate this selection.

These dedicated procedures are proposed for the different type of organic liquids:

- Vacuum pump oil : P3 (PFEIFFER VACUUM).
- Scintillation liquid : Optiphase Hisafe @.
- Oxysolve T@.

The results of the different detritiation procedures must not create other wastes that are difficult and expensive to treat.

**2004 ACTIVITIES**

A literature review was performed to find some processes. The only process used is the incineration off-site facility. CEA VALDUC, manage the low activity level oils to an incinerator [1]. The high activity level oils are input in polyethylene drums (to have no corrosion) that are put in stainless steel container which are stored in glove box.

To estimate the degassing rate, all this drums are measured by calorimetry with  $^3\text{He}$  technique (tritium activity in waste drums correlated to the  $^3\text{He}$  escape of the drum).

For the low tritium activity levels of scintillation liquid, CEA Valduc collect and send them to ANDRA, which manages them to an incinerator.

At the beginning a method of full mineralization of oil was studied to measure tritium activity. Then different detritiation ways without generating other wastes are studied:

- Chemical extraction:
  - . hot water,
  - . acidic,
  - . basic,
  - . dehydration.
- Mechanical extraction.

A tritium species was performed to understand the phenomena then a thermal process was studied with a digester.

With the scintillation liquid, the tritium activities are measured ; the different studied processes are:

- chemical extraction:
  - . hot water,
  - . acidic,
  - . basic,
  - . freeze drying.
- thermal procedure:
  - . digester.

**STUDY OF FULL MINERALIZATION OF OIL OR LIQUID SCINTILLATION SAMPLE TO MEASURE TRITIUM ACTIVITY**

In a reactor connected to different traps for tritium measurement:

- a volume of concentrated nitric acid,
- heated under reflux during 6 hours,
- let cool down,
- small quantities of perchloric acid added,
- heat (without reflux) until white smokes and until having clear solution.

Acidic and basic solutions are distilled and all the traps and solutions are measured with liquid scintillation apparatus.

The wiring diagram (figure 1) shows the procedure scheme.

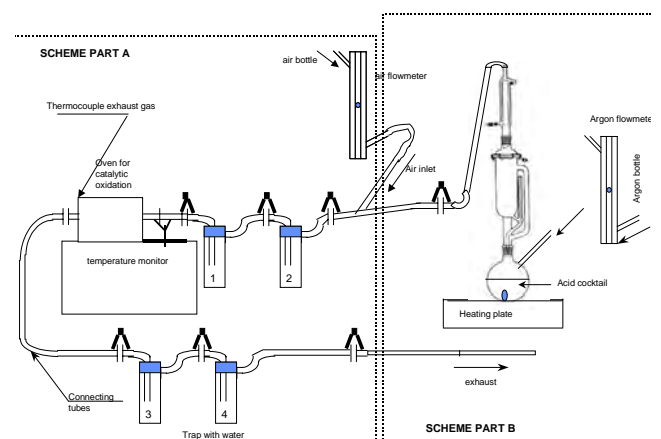


Figure 1 : Wiring diagram

**OIL DETRITIATION****Results of the total tritium activity measurement of P3 oil**

Estimated or measured activity for the sent oil :  
 $^3\text{H}$  activity : 301 kBq/L (unknown date)

Measured activity in our lab :

$^3\text{H}$  activity : 8.8 kBq/L (05/05/04)

New measurement 5 month later :

$^3\text{H}$  activity : 2.2 kBq/L (10/09/04)

New measurement 1 month later :

$^3\text{H}$  activity : 1.8 kBq/L (26/10/04)

The conditioning conditions (plastic bottle) lead to a tritium diffusion through the plastic bottle and a lot of tritium is lost. Oil is self-detririated.

The storage conditions must be the same as it was described for the CEA VALDUC.

### Chemical extractions

Experiment with hot water : 30 mL of oil and 30 mL of water under stirring and heated at 140°C 3 times during 5 hours.

Measurements of tritium activity in the oil before and after the experiment give an extraction rate of about 50 %.

Experiment with water heated under reflux :

Extraction rate : ~ 40 %

Experiment with acidic solution (pH=4)

Extraction rate : ~ 30 %

Different experiments with different volumes with different temperatures, pH (basic to acid) lead to the same extraction rate

Less then 50 % extracted

### Dehydration experiment

Some dehydration tests are done to trap water.

Soda pellets mixed with oil during 18 hours bring no influence.

With  $\text{CaCl}_2$  pellets, there is no influence and  $\text{CaCl}_2$  pellets under ultrasound during 12 hours lead to the same results.

### Mechanical experiment

To confirm that the quantity of water is very low in this oil, some centrifugation experiments are realized.

30 mL of oil are centrifuged at a speed of 3000 rpm during 30 mn. There is no physic modification. Creaming the surface of the oil, the liquid scintillation measurement shows no difference.

30 mL of oil are centrifuged with 30 mL  $\text{H}_2\text{O}$  at a same speed during 6 hours. The liquid scintillation measurement gives a detririation rate of about 33 %.

Industrial process of hot ultra centrifugation exists for used oil of cars that allow recycling 70 % of oil.

This process is used to separate metallic particles. We don't own such an instrument in our lab to test whether it's possible to adapt it to tritium. The expected results seem to be the same as classical centrifugation because there is no water phase to separate as it was observed with the dehydration test.

### Tritium species

Oil is heated in a reactor under argon flow. The outlet of the reactor is connected to air and to the bubbles of MARC 7000 system to trap tritium.

With this type of design, it's possible to define the different species of tritium. In reactor, remains the non volatile tritium (bound tritium), in bubbles 1 and 2 the tritium as HTO and in the bubbles 3 and 4 (after conversion to HTO in the catalytic oven at 450°C), the HT form.

The next photo shows the montage:



Photo 1 : Tritium species montage

The results are after liquid scintillation measurement:

- 25 % of tritium as HTO form,
- 25 % of tritium as HT form,
- 50 % of liquid tritium, which is bound tritium.

### Full mineralization in a digester:

Under oxygen (25 bars), all the oil is destroyed. The tritium is recovered as liquid (a little volume of water is needed in the bottom of the digester) and gas form. The gas is transformed as HTO form with oxygen and thus trapped in bubbles.

The calculated detririation rate is 100 % after the different liquid scintillation measurements.

### Conclusion of the oil detririation:

Even the chemical tests would have been done, the extraction rate is not higher than 50 %. This extracted tritium is labile.

The tritium, which remains in oil, is considered as to be bound tritium.

In a digester, 100 % of the tritium is transformed with oxygen as HTO form and trapped in bubbles. Only tritiated water is created.

CEA VALDUC, which has the same problem, doesn't detritiate oil. They manage the low activity level oils to an incinerator. The high activity level oils are input in polyethylene drums (to have no corrosion) which are put in stainless steel container which are store in glove box.

## SCINTILLATION LIQUID DETRITIATION

### Results of the total tritium activity measurement of HISAFE and OXSOLVE T

Optiphase Hisafe : 4.59 kBq/mL (May 15-2004)

Oxysolve : 2.4 kBq/mL (May 25-2004)

#### Chemical extractions

Experiment with hot water : 20 mL of Hisafe and 30 mL of water under 15 mn stirring then addition of 30mL ultra-pure water for distillation.

Resulting tritium activity of the distillation: 0.05 kBq/mL and a tritium rate of about 1 %.

Same procedure with hot water (close to boiling) leads to an extraction rate of 5 %

Tritium remains in the boiler and a try to continue the distillation is dangerous. A pressure increase has been observed.

Experiment in a vessel with 5 mL of oxysolve plus 5 mL of fresh oxysolve plus 10 mL o water. Heating under air flow with a MARC 7000 downstream. Tritium is mainly recovered as HTO form, but only 30 % of the tritium is extracted.

Experiment with acidic solution or basic solution.

10 mL of Optiphase Hisafe with HCl 6N then a distillation leads to 73 % of tritium extracted. The same operation with soda leads to an extraction rate of 80 %.

Same operation at pH 2 with 10 mL of oxysolve T with 40 mL of acid solution and 48 h of stirring then addition of 100 mL of water and distillation lead to a 96 % rate. However the waste volume increased.

One solution for decreasing the waste volume could be the use of freeze-drying procedure.

#### Mechanical experiment

The same procedure with water, has been done by heating until 80°C under ultrasound stirring and the obtained extraction rate is only 15.8 %.

### Full mineralization in a digester:

Full mineralization in a digester leads to the total destruction of the organic structure and 100 % of the tritium is recovered as HTO form.

In this case, only tritiated water is created.

## CONCLUSIONS

---

### Oil detritiation

Even the chemical tests would have been done, the extraction rate is not higher than 50 %. This extracted tritium is labile.

The tritium, which remains in oil seems to be bound tritium. In a digester, 100 % of the tritium is transformed with oxygen as HTO form and trapped in bubbles.

The advantage is that only tritiated water is created. This waste is clearly identified and easy to store.

CEA VALDUC, which has the same problem, doesn't detritiate oil. They manage the low activity level oils to an incinerator.

The high activity level oils are put in polyethylene drums (to have no corrosion), which are put in stainless steel container, stored in glove box.

### Scintillation liquid

A long time stirring with acid or base addition improves extraction.

Distillation with concentrated scintillation liquid seems explosive.

In a digester, 100 % of the tritium is transformed (with oxygen) as HTO form and trapped in bubbles.

The same advantage as oil is the generation of tritiated water only.

At CEA Valdudc the low level activity samples are collected and sent to ANDRA that manages them to an incinerator.

## REFERENCE

---

- [1] Compte rendu de réunion: UKAEA/CEA co-operation on fusion decommissioning - S. Rosanvallon DER/STR/LCEP 2001/309.

## **TASK LEADER**

---

Pierre TRABUC  
Christian POLETIKO

DEN/DTN/STPA/LPC  
CEA-Cadarache  
F-13108 Saint-Paul-Lez-Durance Cedex

Tél. : 33 4 42 25 43 05  
Tél. : 33 4 42 25 64 93  
Fax : 33 4 42 25 72 87

E-mail : pierre.trabuc@cea.fr  
christian.poletiko@cea.fr

## Task Title: LASER DECONTAMINATION/TRITIUM REMOVAL Studies on Tokamak wall surfaces decontamination by pulsed repetition rate lasers

### INTRODUCTION

The excessive content of tritium in plasma-facing components is seen as a severe problem for the efficient functioning of a fusion reactor [1-3]. Laser decontamination of the plasma facing component surfaces is of a special interest as it can offer a completely optical method of a surface cleaning by its heating or laser ablation. The possibility to transport the laser beam to the cleaning zone by the optical fiber allows both to remove the laser system away from the contaminated zone and to offer detritiation without direct personnel participation. The absence of the direct contact with the contaminated surfaces, the reduced waste volume, and a possible complete automation of the process that can ensure the personnel safety are regarded as the most attractive features of laser decontamination. The developed and commercially available powerful high repetition rate pulsed Nd-YAG lasers where the radiation transport is carried out with the optical fibers are seen as good candidates for decontamination of the vacuum chamber surfaces in Tokamak thermonuclear installations.

In 2002-2003, our laboratory developed the necessary experimental equipment, and the first investigations on the graphite surface de-hydrogenisation with the pulsed repetition rate Nd-YAG laser systems were made [3]. The development of the experimental equipment (vacuum chamber, sealed cells, pyrometer, plasma imaging with the ICCD camera) and methods for co-deposited layer characterization (GD-OES, optical and electron microscopy, ejected gas chromatography and mass spectrometry) was the first step of a 2004-year programme. The next step of our studies was to validate the laser treatment parameters (defined for graphite samples in 2003) and to make ablation tests on decontamination of diagnostics and tools. Ablation thresholds for different metals (diagnostics and tools) and graphite samples were determined experimentally and compared with the theoretical data. The detailed presentation of the developed experimental equipment and the results obtained are presented in our final 2004-year report.

### 2004 ACTIVITIES

The design, development, and tests on the new experimental equipment and tools (vacuum chambers and cells, pyrometer, high repetition rate laser on 1.064  $\mu\text{m}$  with ms pulse duration, high speed plasma imaging) were successfully realized. A small sealed cell was applied to analyse ablated matter (gases, micro particles).

The preliminary temperature measurements of the graphite surface (figure 1) heating by a pulsed repetition rate Nd-YAG laser beam were made with a pyrometer with 15  $\mu\text{s}$  time resolution. It was possible to measure the temperature in 280 – 2300°C range with 0.1°C accuracy.

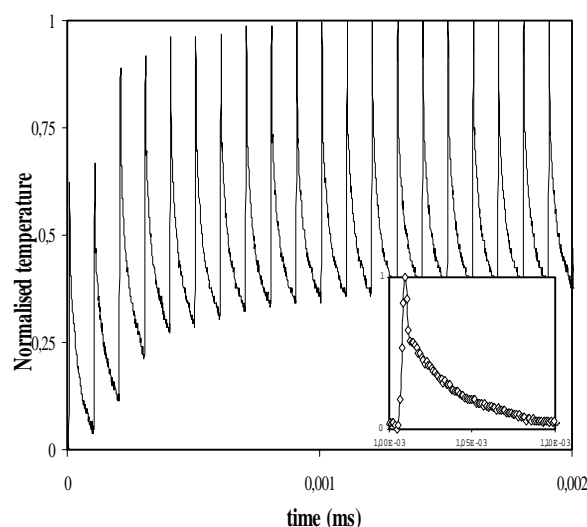


*Figure 1 : Graphite temperature measurement with the pyrometer - Time resolution-15  $\mu\text{s}$ ; space resolution- 0.5 mm - Heating with Nd-YAG laser beam, 10 kHz, 532 nm, 100 ns, 0.6 J/cm<sup>2</sup>, air 1 bar  
Insertion- temperature for one laser pulse heating*

Millisecond pulses on 1064 nm wavelength were obtained after modification of the acoustic-optical switcher regime of Nd-YAG laser. With a longer pulse duration, it was possible to apply the same beam transportation system (optical fiber) even for 200W mean laser power (two-fold increase from 100 W at 532nm to 200W at 1064 nm). For detritiation studies, a simple replacement of some optical elements (mirrors, lenses) was sufficient to provide the operation regime of the high repetition rate laser bench.

With pulsed high repetition rate lasers, the surface shielding by ablated matter was particularly pronounced and, consequently, resulted in decrease of laser ablation efficiency. This was observed in our experiments with 10 KHz repetition rate. To study the ablated matter (gases, micro particles, plasma) properties, the imaging system on the basis of the ICCD gated camera was developed. The system may allow the interaction zone imaging with adjustable time resolution up to several nanoseconds. To synchronise the imaging system to a specified pulse, a special electronic system was developed and applied. It allowed also to synchronise the ICCD camera with any specified laser pulse.

Two methods (heating and laser ablation) were applied to characterize the gases released during de-hydrogenisation of graphite samples with a co-deposited layer. TORE SUPRA co-deposited layer characterization was made by the gas release measurements with a hydrogen analyser RH-404 (LECO Corporation) that is used for measuring hydrogen in inorganic matters. Gas release was obtained with the sample heating in a furnace. A low repetition rate laser bench was used to provide ablation of the TORE-SUPRA graphite samples with a thin co-deposited layer. The samples were put inside a developed sealed stainless cell. With 1 J/cm<sup>2</sup> laser fluence (that corresponds to the ablation threshold of TORE SUPRA graphite with 4 ns pulses), it was possible to obtain only a co-deposited layer ablation.

The cell gas analysis following the co-deposited layer ablation was made with a mass spectrometer. It was possible to make the mass measurements in the range of 1-150 a.u.m. with the ppm accuracy. Approximately the same concentrations of H and D isotopes were obtained. The hydrogen concentration in the ablated layer was comparable with the results obtained with the sample heating in furnace followed by chromatography analysis. The obtained hydrogen contents in TORE SUPRA co-deposited layer is in good agreement with the previous measurements [3] by Glow Discharge–Optical Emission Spectroscopy (GD-OES) method. Thus, the results obtained with three different methods demonstrated a sufficiently good agreement in hydrogen contents in the TORE SUPRA co-deposited layer.

The new results on graphite ablation obtained with a high repetition rate laser bench seem to be very promising. The back side surface of TORE SUPRA graphite samples was ablated with 90 ns pulses of a high repetition rate laser bench. The ablation threshold was determined to be (2.5 ± 0.5) J/cm<sup>2</sup>, that is, 2.5 times higher than the previously determined ablation thresholds of 1 J/cm<sup>2</sup> for 4 ns laser pulses.

This difference in ablation thresholds might be explained by the longer pulse duration of a high repetition rate laser. The graphite surface heating depth can be described as  $L \approx (D \times \tau)^{0.5}$ , where D – thermo diffusivity of graphite,  $\tau$  – laser pulse duration [4-6]. Thus, the longer the laser pulse duration is, the thicker the absorbed energy depth. Our experiments with 4 ns [3] and 90 ns pulse durations confirmed this dependence. For TexTor co-deposited layer, the ablation threshold was determined to be (0.4 ± 0.1) J/cm<sup>2</sup>. In contrast to the backside graphite results, the ablation thresholds for a co-deposited layer were the same for both 5 ns (low repetition rate laser bench) and for 100 ns (high repetition laser rate bench) duration pulses.

Laser ablation thresholds for some metal samples were of particular interest in our studies. Table 1 summarizes the experimental results on the ablation thresholds for different metals (Cu, Al, Fe, Ni, Pb, W) and graphite obtained with 5nsec pulses (532 nm). The ablation thresholds for 100 ns laser pulses were determined by the relation:

$$F_{th}(\tau_1) \approx F_{th}(\tau_2) \times \sqrt{\tau_1 / \tau_2} \quad \text{or} \quad F_{th}(100ns) \cong 4,5 \times F_{th}(5ns)$$

Table 1 : Ablation thresholds for different metal targets with 5 ns and 100 ns laser pulses

| Target | Experimental data for 5 ns (J/cm <sup>2</sup> ) | Estimations for 100 ns (J/cm <sup>2</sup> ) |
|--------|---|---|
| Al     | 1.71  | 7.7   |
| Cu     | 2.09  | 9.1   |
| Fe     | 1.00  | 4.5   |
| Mo     | 2.56  | 11.4  |
| Ni     | 0.941   | 4.2   |
| Zn     | 0.980   | 4.4   |

The ablation thresholds for the metals in our study were in 1-2.5 J/cm<sup>2</sup> range for 5 ns laser pulses. They were determined to be higher than the co-deposited layer ablation threshold of 0.4 J/cm<sup>2</sup>. For 100 ns laser pulses, the ablation thresholds were determined to be five times higher than for 5 ns pulses.

Different ablation thresholds for a substrate and a co-deposited layer could be applied to ensure self-control of laser surface cleaning. This might be obtained if the laser fluence in the interaction zone is chosen to be lower than the ablation threshold of the substrate. Thus, with 100 ns pulses, laser detritiation of diagnostics and tools can be performed with the laser fluence without the substrates damage.

The ablation threshold was not found to depend on the environmental gas contents. Both in air and in the noble gas (argon in our experiments), the ablation thresholds and ablation rates were determined to be of the same value. A slight difference in laser/surface interaction was observed with the laser fluence lower than 0.5 J/cm<sup>2</sup>. No ablation was observed with  $F < 0.5$  J/cm<sup>2</sup> in Ar. In contrast, the co-deposited layer erosion was observed in air.

This erosion might be associated with the surface oxidation with CO<sub>2</sub> gas release. Environmental condition effect manifested itself as a black circular zone around the crater. The circular zone was observed in Ar, but was not detected with ablation in air.

It is considered to be resulting from the graphite powder re-deposition. Ar was considered to keep hydrogen atoms from oxidation. In air, oxygen gave rise to CO<sub>2</sub> formation and, thus, suppressed the graphite powder re-deposition around the crater.

With the developed plasma imaging system, it was possible to observe the important plasma intensity increase in argon figure 2.

This phenomenon is regarded essential for Laser Ablation – Optical Emission Spectroscopy (LA-OES) method for diagnostics and control of co-deposited layer removal and surface characterization.

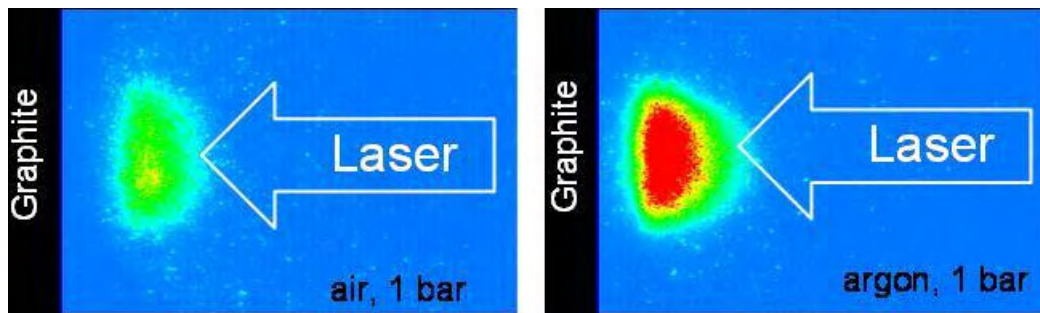


Figure 2 : Plasma images in air and in argon (1 bar at normal temperature). ICCD camera: delay-1 $\mu$ s, gate – 20 $\mu$ s

The obtained optimal conditions for a co-deposited layer ablation (laser fluence of  $F=1-2 \text{ J/cm}^2$ , high repetition rate) were applied for TexTor co-deposited layer cleaning. The  $10 \times 10 \text{ mm}^2$  zones for cleaning were chosen on the TexTor tile surface where the ablation efficiency had already been determined. Ablation was obtained with a high-repetition rate laser with 20W mean power and 20 kHz repetition rate. The laser beam was focused into a spot of 250  $\mu\text{m}$  diameter ( $\text{FWe}^{-2}$ ) with  $2 \text{ J/cm}^2$  maximum fluence and was scanned on the chosen zone of the surface. Figure 3 presents the TexTor tile after laser cleaning. On the right, the decontaminated zone ( $10 \text{ mm} \times 10 \text{ mm}$ ) was obtained by a single scanning over 2 seconds. On the left, the decontaminated zone was obtained with a ten-fold scanning. This zone comprised the surface without a co-deposited layer. It was specially chosen to verify that there was no ablation of graphite surface even with a multiple laser treatment of the surface. The co-deposited layer of 50  $\mu\text{m}$  thickness was almost completely removed with a single scanning of  $10 \times 10 \text{ mm}^2$  surface. The graphite substrate surface was protected and did not suffer any damage (the left cleaned zone on figure 3).

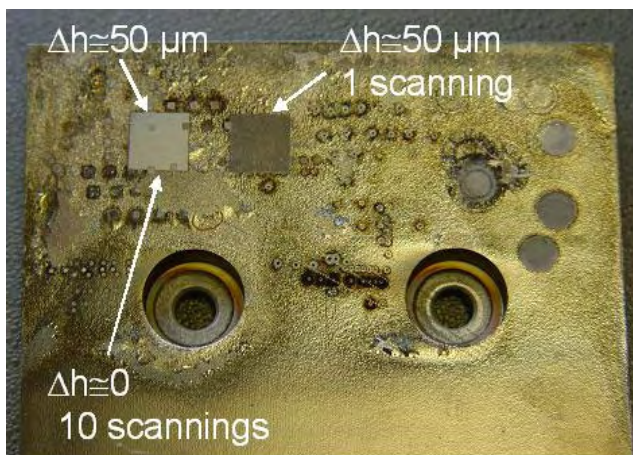


Figure 3 : TexTor tile with co-deposited layer of 50  $\mu\text{m}$  thickness. Interaction parameters: laser fluence  $\sim 2 \text{ J/cm}^2$ , laser mean power - 20 W, high repetition rate – 20 kHz, air 1 bar, scanned zones of  $10 \text{ mm} \times 10 \text{ mm}$  for 2 sec

Even with a ten-fold laser scanning, the graphite substrate surface was not observed to be damaged. The surface of the cleaned zone was found to coincide with the flaked zone. This was confirmed by TexTor tile backside surface cleaning.

A ten-fold scanning of the backside graphite surface (the same conditions as for the left zone of figure 3) was not determined to damage the graphite surface and resulted only in changing the surface color. Thus, the experiments on TexTor co-deposited layer cleaning by laser ablation gave all the reasons to conclude that the laser surface decontamination should be regarded very promising for plasma facing component surfaces detritiation.

## CONCLUSIONS

The design, implementation, and tests of a vacuum chambers and sealed cells were realised. Sealed cells and chambers application allowed to study laser heating and ablation in controlled environmental conditions and also to collect ejected matter and gases for their subsequent analysis. Different analytical methods (ejected gas chromatography and mass spectrometry, GD-OES, optical and electron microscopy) were applied and tested for co-deposited layer and graphite surface characterization.

Validation of the laser treatment parameters (defined in 2003) for graphite samples was performed in the controlled environment (Ar and air). Laser ablation threshold of  $(2.5 \pm 0.5) \text{ J/cm}^2$  for graphite without a co-deposited layer was obtained with 100 ns laser pulses. A specially designed imaging system was applied for laser plasma characterization and for environment effect study. The environmental effect was observed as the important plasma intensity increase in argon. The plasma intensity growth resulted from both the intensity and lifetime increase of the spectral lines. This phenomenon is regarded essential for LA-OES method for diagnostics and control of co-deposited layer removal and for surface characterization. The environmental effect manifested itself as the dark matter re-deposition around the crater in Ar and as the surface erosion with the rate of nm/pulse in air at low laser fluence (low than  $0.5 \text{ J/cm}^2$ ).

A specially developed PYROMETER system was applied for laser heating characterization. A new high repetition rate laser system with 1064 nm wavelength and millisecond pulse duration was developed to study surface heating and ablation. Time resolved temperature measurements with the pyrometer will be possible with the millisecond pulses.

Ablation thresholds for different metals (diagnostics and tools) were determined experimentally for 5 ns pulses.

For the samples under study and applied nanosecond pulses, the ablation thresholds were higher than  $1 \text{ J/cm}^2$ . Theoretical model of high repetition laser heating of a complex surface (graphite or metal with a co-deposited layer) was developed to explain the experimental results and to obtain laser detritiation optimization [6].

The obtained optimal conditions (high pulse repetition regime,  $2 \text{ J/cm}^2$ , ablation rate) were applied for laser cleaning of  $1 \text{ cm}^2$  co-deposited layer on Textor graphite tile without any damage of the graphite substrate. The co-deposited layer of  $50 \text{ }\mu\text{m}$  thickness was almost completely removed with a single scanning of  $10 \times 10 \text{ cm}^2$  surface during two seconds. Thus, with a laser of  $20 \text{ W}$  mean power, it was possible to clean  $0.2 \text{ m}^2$  co-deposited layer of  $50 \text{ }\mu\text{m}$  thickness during one hour. With  $100 \text{ W}$  mean power, it will be possible to clean  $1 \text{ m}^2$  co-deposited layer during the same time (one hour). The comparison of the obtained laser cleaning rate with the data presented in our previous report [3] ( $1 \text{ m}^2$  per hour of  $20 \text{ }\mu\text{m}$  thickness co-deposited layer cleaning with  $250 \text{ W}$  Nd-YAG laser mean power) demonstrates an approximately six-fold increase in the cleaning rate. Further experimental and theoretical studies to explain the cleaning rate increase and to obtain the subsequent optimization of the laser detritiation performances should be made.

## REFERENCES

---

- [1] R. A. Causey - J. Nucl. Mater. - 300 (2002) 91-117.
- [2] M. Friedrich et al. - Nucl. Instr. Meth. in Phys. Res. B, B161 – 163 (2000) 216-220.
- [3] A. Semerok et al, - Studies on graphite surfaces detritiation by pulsed repetition rate nanosecond lasers - CEA report NT DPC/SCP/04-076-A, 2004, pp. 31.
- [4] S. Fomichev and A. Semerok - Etude des Processus Thermiques Survenant Lors de la Microanalyse des Surfaces par la Méthode Raman - Report CEA, DPC/SCPA/NT02-053, 2002, 27 pages.
- [5] A. Semerok and J.-M. Weulersse - Bibliography Study on Theoretical Models of Laser Detritiation Processes - Report CEA, NT DPC/SCP 03-069-A, 2003, 28 pages.
- [6] S. Fomichev, A. Semerok, JM. Weulersse, F. Brygo - Report CEA - NT DPC/SCP 11-069-A, 2004, 77 pages.

## REPORTS AND PUBLICATIONS

---

A. Semerok, JM. Weulersse, F. Brygo, D. Farcage, C. Hubert, C. Lascoutouna, M. Géléoc, P. Wodling, H. Long, F. Champonnois, G. Brunel, G. Vimond, E. Lizon, V. Dauvois, V. Delanne, C. Grisolia, S. Fomichev, M. Hashida - Studies on TOKAMAK wall surfaces decontamination by pulsed repetition rate lasers - CEA report NT DPC/SCP/05-111-A, January 2005, 50 pages.

A. Semerok, F. Le Guern, F. Brygo, C. Grisolia, D. Farcage, C. Hubert, C. Lascoutouna, M. Tabarant, J.M. Weulersse - Studies on graphite surfaces detritiation by pulsed repetition rate nanosecond lasers - presentation on SOFT'2004 conference, 20-24 September 2004, Venice, Italy.

## TASK LEADER

---

Alexandre SEMEROK

DEN/DPC/SCP/LILM  
CEA-Saclay  
F-91191 Gif-sur-Yvette Cedex

Tél. : 33 1 69 08 65 57  
Fax : 33 1 69 08 78 84

E-mail : asemerok@cea.fr

**Task Title: TW3-THHN-IITF1: THE FIRST ITER NB INJECTOR AND THE ITER NB TEST FACILITY: DESIGN**

**INTRODUCTION**

At the time of the last “Technofusion” report the work on the 5 areas of physics design assigned to the DRFC had been completed.

In the period covered by this report the work foreseen under this contract on the infrastructure, including the cryo system and the cooling system, and, the beamline vessel for the Neutral Beam Test Facility (NBTF) has been completed and agreement on the designs reached with EFDA and the other EURATOM Associations involved with this work (ENEA, FZK, IPP and UKAEA).

The main purpose of this task is to make progress with the detailed design of the first ITER Neutral Beam (NB) injector and the conceptual design of the ITER NBTF. The work carried out by the DRFC in 2004 is described briefly below.

**2004 ACTIVITIES**

**SYSTEM DESIGN**

Four design areas of the NBTF have been covered:

**Design of the general infrastructure**

The study of the generic design of the NBTF general infrastructure was launched early 2004. The study of the experimental hall will be completed at the end of 2005. This study includes the test facility itself and the associated auxiliaries such as cooling plant, cryoplant and forepumping system. The NBTF safety requirements (neutron and X-ray production) have to be taken into account. Figure 1 shows the layout of the system.

**Design of the dedicated beam line Vessel (BLV)**

The current design of the dedicated Beam Line Vessel (BLV) allows mixed vertical and horizontal access to the beam line components was proposed and developed by the CEA.

The proposed mixed vertical horizontal option differs mainly from that proposed in 2003 in the cryopump design: This now consists of two (almost) semi-cylindrical cryopumps that are essentially identical to the 2 halves of the ITER NB cryopump. As with the previous BLV option the beamline components may be removed for maintenance either vertically or horizontally.

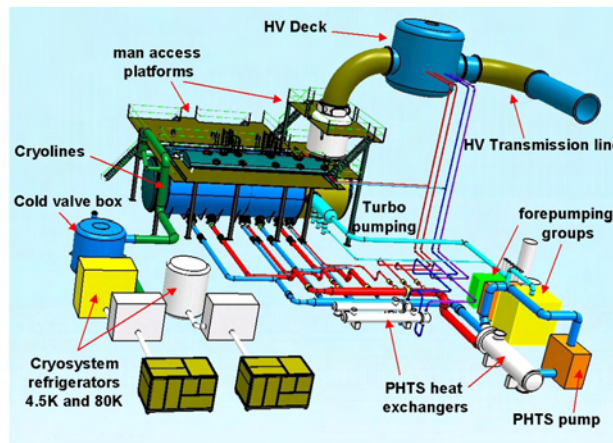


Figure 1 : Neutral beam test facility, general infrastructure (the buildings are hidden)

The upper large opening (9.50 m x 2.55 m) allows vertical maintenance and easy diagnostic and man access (see figure 2 below). The maximum BLV height is limited to 4.4 m for transportability consideration. The elliptic shape is connected to the BSV cylinder through a stiff circular welding. The beam line vessel volume is  $\approx 200 \text{ m}^3$ .

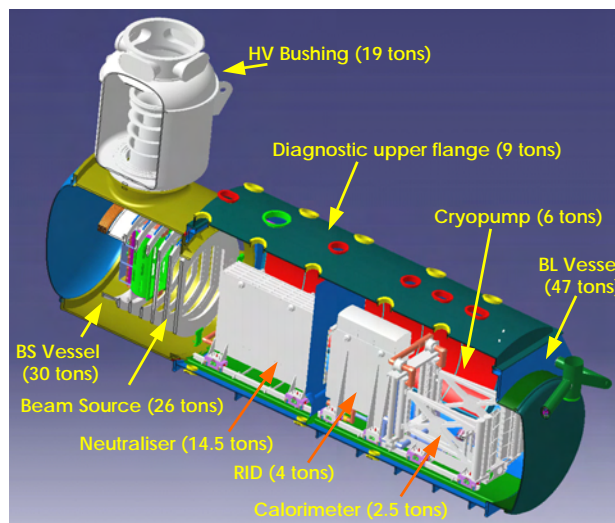


Figure 2 : The NBTF beam line vessel and beam source vessel equipped with the beam line components and semi-cylindrical cryopumps

The proposed “Phase I operation” of the NBTF is dedicated to the qualification of the source and beam line components with short pulse operation ( $\approx 30 \text{ s}$ ). During this phase the flexibility offered by the MVHO (see figure 3.1) is considered a substantial advantage compared to using a system allowing only horizontal maintenance and limited access for diagnostics.

At the end of the Phase I operation, it is foreseen to move to “Phase II”, which will mainly consist of a campaign with long pulses of up to 3600 s, in H<sub>2</sub> and D<sub>2</sub>.

During Phase II the beamline configuration is to be changed (figure 3.2) by linking the two sem-cylindrical cryopumps in order to have the final same configuration as the ITER NB cryopumps. This will require some adaptation of the cryopump support system which is attached to the wall of the BLV.

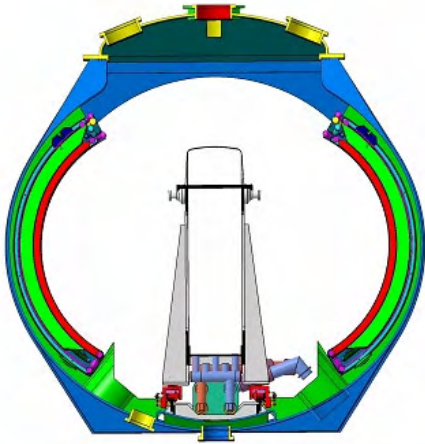


Figure 3.1 : Phase I configuration

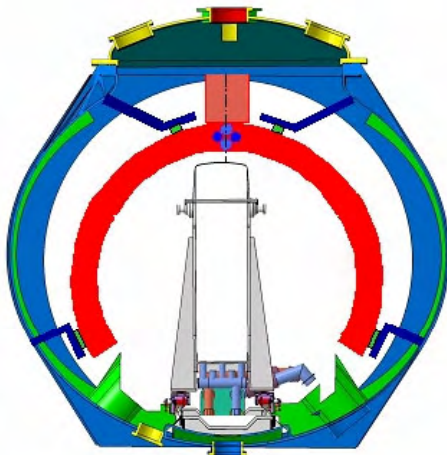


Figure 3.2 : Phase II configuration

**Finalisation of the design of the cryo system**

The ITER NB heating and current drive system is equipped with a cryosorption cryopump (made up of 12 half modules connected in parallel), refrigerated by 4.5 K 0.4 MPa supercritical helium.

The pump is submitted to a non homogeneous flux of H<sub>2</sub> or D<sub>2</sub> molecules, and the absorbed flux varies from 3 Pa.m<sup>3</sup>.s<sup>-1</sup> to 35 Pa.m<sup>3</sup>.s<sup>-1</sup>. A usual and important operation of the cryopumps is the regeneration at 100 K of the cryopanel.

In the framework of the “ITER first injector and test facility”, the successive studies that were performed in 2004 are the following :

- Evaluation of the reference ITER cryogenic system designed to refrigerate the NBI (and torus) cryopumps in ITER operating conditions.
- Definition of a reliable cryogenic system able to refrigerate the NBTF cryopump in “acceptable” and “representative” operating conditions (short 20 s pulses) and long (3600 s pulses), using 4.5 K, 0.4 MPa, super critical helium for the cryopanel, and gaseous helium at 80 K at 1.8 MPa for the thermal shields and baffles.
- Evaluation of the costs and the procurement time of the proposed NBTF cryogenic system.

*The 4.5K refrigerator*

A standard industrial 4.5 K refrigerator, available provides a cold power of 500 W at 4.5 K in pure refrigeration mode and 150 l/h in pure liquefaction mode. The optimization of the thermodynamic process to provide the 160 W required by the cryopump at 4.5 K is to be carried out by the supplier. Such a refrigerator does not supply any cold power at 80 K.

*The 80K refrigerator*

The Brayton cycle used by the proposed refrigerator includes a screw compressor with its oil removal unit, a counter flow exchanger, an expander equipped with an active charcoal filter in order to remove impurities, and a by-pass to adjust the temperature at the inlet of the shields if necessary (see figure 4). However, to minimise the required helium flow rate (0,175 kg/s) and consequently the power supply of the compressor, the Brayton cycle must operate with a large temperature difference (24 K) between the inlet (66 K) and the outlet (90 K) of the shields and the baffles. The Brayton cycle is well adapted to provide a progressive cool down of the shields and the baffles, as the turbo-expander can be by passed. This solution is self contained and of course independent of LN<sub>2</sub> deliveries.

The cryoplant layout is shown schematically in figure 4

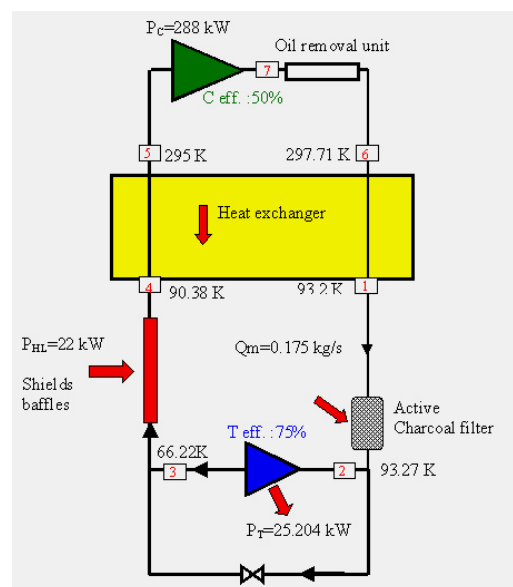


Figure 4 : The 80K Brayton cycle process flow diagram

Table 1 : PHTS characteristics

| Component                                 | Inlet Temperature (°C) | Max Averaged Outlet Temp (°C) | Max outlet Temp (°C) | Saturation Pressure (MPa) | Inlet Pressure (MPa) | In Vessel Pressure drop (MPa) | Outlet Pressure (MPa) |
|---|------------------------|-------------------------------|----------------------|---------------------------|----------------------|-------------------------------|-----------------------|
| Neutraliser leading edge                  | 80                     | 132                           | 175                  | 0.9                       | 2.65                 | 0.06                          | 2.59                  |
| Neutraliser Panels                        | 80                     | 132                           | 140                  | 0.4                       | 2.65                 | 0.25                          | 2.4                   |
| RID                                       | 80                     | 132                           | 205                  | 1.8                       | 2.65                 | 0.07                          | 2.58                  |
| Calorimeter Closed/Open                   | 80                     | 106                           | 128                  | 0.3                       | 2.65                 | 2                             | 0.65                  |
| Ion Source, Filaments and Power Supply    | 20                     | 43.5                          |                      | 0.1                       | 2.65                 | 0.9                           | 1.75                  |
| Acceleration grid, Extractor, Plasma grid | 55                     | 93.3                          |                      | 0.1                       | 2.65                 | 0.9                           | 1.75                  |

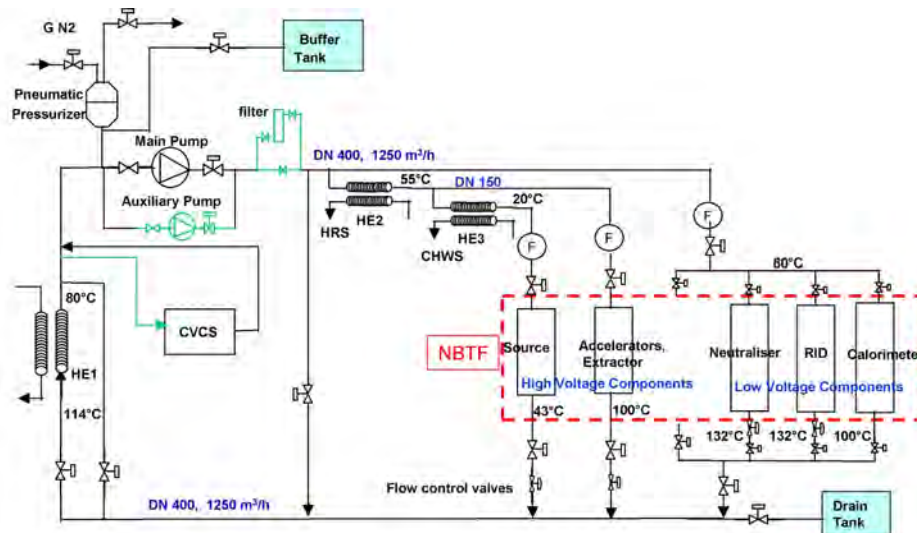


Figure 5 : PHTS process flow diagram

### Final design of the cooling system

The methodology used for the NB injector cooling system starts from the review of the thermo-hydraulic data presented in the various ITER Design Description Documents (the DDD's). Then the operation conditions of the Primary Heat Transfer System (PHTS) were derived, considering that the facility is a dedicated test bed. The study performed in 2004 was divided into 4 successive steps :

- An assessment of the reference cooling plant designed to refrigerate the ITER NB injection system.
- The design of a reliable cooling system, able to refrigerate the NBTF in "acceptable" and "representative" operating conditions for short (20 s) and long (3600 s) pulses. The proposed design covers both the Primary Heat Transfer System (PHTS) and the Heat Rejection System (HRS).
- Design of the layout of the PHTS, the HRS and auxiliary loops dedicated to the NBTF.
- A survey of the potential equipment and an associated cost assessment, including the integration on the site.

The main characteristics of the PHTS are summarised in table 1 and the process flow diagram is shown as figure 5.

### CONCLUSION

This contract was completed and the final reports submitted to EFDA in October 2004. A second contract continuing the design of the NBTF was let by EFDA to the same EURATOM Associations plus the EURATOM Association CIEMAT. The new contract aims at finalising many aspects of the design, such as the BLV, of which the main aspects are described in this report, and to bring to the same level as the reference design (or better) the design of the alternative concepts for the negative ion source and accelerator, both of which are being developed in Europe.

### TASK LEADER

Ronald HEMSWORTH

DSM/DRFC/SCCP/GIDEA  
CEA-Cadarache  
F-13108 Saint-Paul-Lez-Durance Cedex

Tél. : 33 4 42 25 63 45  
Fax : 33 4 42 25 62 33

E-mail : ronald.hemsworth@cea.fr



**Task Title: TW4-THHN-ADSD2: NEUTRAL BEAM DEVELOPMENT FOR EFDA EXTENSION**

**INTRODUCTION**

The KAMABOKO III ion source, is being tested on the MANTIS test stand at the DRFC Cadarache in collaboration with JAERI, Japan, who designed and supplied the ion source. The ion source is attached to a 3 grid 30 keV accelerator (also supplied by JAERI) and the accelerated negative ion current is determined from the energy deposited on a calorimeter located 1.6 m from the source.

**2004 ACTIVITIES**

During 2004 experiments on MANTIS the following adverse effects of long pulse operation were found:

- The negative ion current to the calorimeter is  $\approx 50\%$  of that obtained from short pulse operation.
- The caesium “consumption” is up to 1500 times that expected.

Results presented here indicate that both of these are, at least partially, explained by thermal effects.

**Beam Transmission**

Figure 1 shows the accelerated current and the current to the calorimeter as a function of the arc power. As can be seen from figure 1, only about 50 % of the accelerated current reaches the calorimeter.

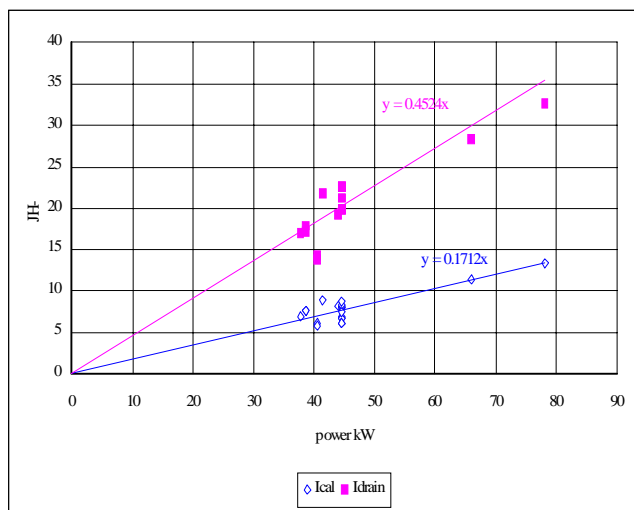


Figure 1

Possible reasons for this poor transmission are:

- a) The “lost” beam is electrons, arising from either accelerated extracted electrons or electrons created by stripping in the accelerator.

*Extracted electrons:* Extracted electrons are deflected onto the surface of the extraction grid by the magnetic field from the filter in the ion source and permanent magnets buried in the extraction grid, but some electrons escape to the extraction region. The fraction of the accelerated electrons has been measured by operating the source in pure argon. In this situation no negative ions are produced in the discharge, but a high electron current (assumed equal to the current to the extraction grid) of 3 A was extracted. No power was recorded on the calorimeter, and the accelerated current, was 30 mA, i.e.  $< 1\%$  of the extracted current. Furthermore the current to the acceleration grid was equal (within the measurement error) to the current drain from the high voltage power supply, which means that most of the accelerated electrons were collected on that grid. As the extracted electron current during H<sub>2</sub> operation is typically  $< 20\%$  of the accelerated current, and approximately equal to the accelerated current in D<sub>2</sub> operation, extracted electrons cannot explain an accelerated electron current that is 50% of the total accelerated current.

*Electrons from stripping:* To a first approximation the fraction of electrons stripped during the passage of the H<sup>-</sup> or D<sup>-</sup> through the accelerator is proportional to the source pressure. Thus if stripping were the cause of the “lost” beam, the transmission should vary strongly with the source filling pressure. Within the experimental errors there is no variation with pressure. (Note that the calculated stripping fraction in the acceleration gap at a source filling pressure of 0.3 Pa is  $\approx 3\%$ ).

- b) The beam optics are extremely bad. Careful simulations of the beam optics have been carried with assumed possible variations and errors in extraction and acceleration gaps, grid misalignment and negative ion current density and magnetic field effects. All the simulations predict beams with adequate optics to achieve transmissions of  $> 90\%$ . However it has recently been realised that the acceleration grid could be bowing under the heat load received from intercepted ions electrons. To test this hypothesis the beam transmission was measured as a function of the pulse length, see figure 2. The measured data give the average transmission for each pulse, and the blue curve on figure 2 is a “by eye” fit to those data figure 2 shows that for very short pulses,  $< 4\text{ s}$  the transmission is  $> 70\%$ .

The transmission degrades to a minimum at about 25 s, and then improves to its long pulse value of  $\approx 55\%$ .

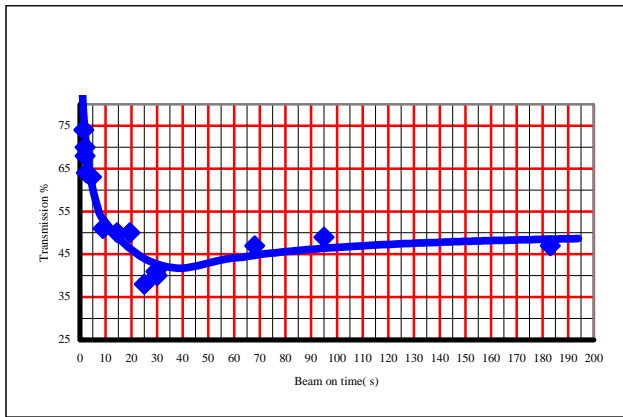


Figure 2

In order to investigate this “lost” power; a new drift duct has been fabricated and installed which is well instrumented to allow the power deposited between the accelerator and the calorimeter, and the spatial distribution of that power, to be determined. This drift duct is made of 6 copper boxes; each box is made up of 4 copper plates. These plates are electrically connected however thermally insulated from each other. Each plate is equipped with 2 thermocouples, which allow a good measurement of the power received on each panel of the duct; giving a good spatial distribution of the “lost” accelerated power. This drift duct can be seen in figure 3.



Figure 3

A new accelerator grid has been designed and the new grids are due to be delivered by the beginning of June. These accelerator grids are designed to allow dilatation under power loading. It is proposed that experimentation with this accelerator be carried out during the summer of 2005.

### Cs Consumption

Very high Cs consumption rates have been found during long pulse operation: the amount of Cs “consumed” per aperture in the PG is up to 1500 times that assumed for the ITER source, which is based on extrapolation from short

pulse operation. A possible, partial, explanation is that during the operation of long pulses ( $>100$  s), the source walls reach thermal equilibrium at a temperature (typically  $75\text{ }^\circ\text{C}$ ) substantially higher than during short pulses ( $\approx 20\text{ }^\circ\text{C}$ ). The increase in the vapour pressure of Cs on the source walls would result in an increase in the Cs flow from the walls into the discharge by up to a factor of 60, see figure 4 [1].

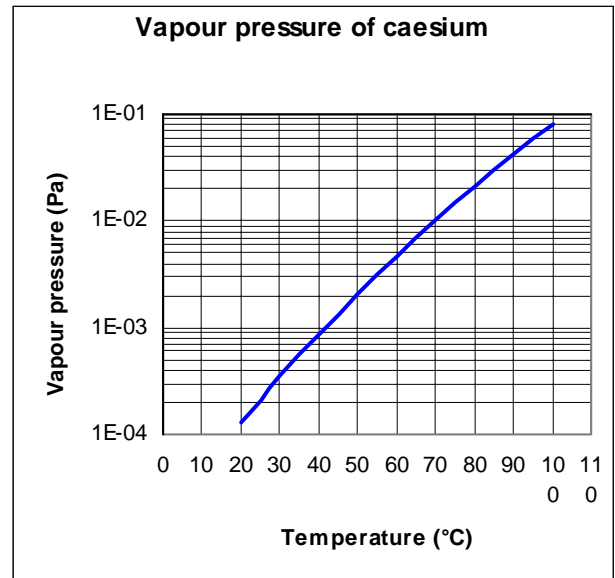


Figure 4

In order to understand better what happens to Cs injected into the ion source, when the ion source was opened after an experimental campaign it was examined carefully. The source itself was covered with what looked like a moist tungsten layer. In order to determine the percentage of Cs left in the source, it was cleaned with water, and the water kept for analysis. Initially the cleaning water was opaque, dark grey, but overnight it became clear with a grey precipitate at the bottom. Chemical analysis of the clear water showed that approx.  $4.5 \pm 0.9$  g of Cs was inside the source when it was cleaned. The grey precipitate is presumed to be tungsten. As  $\approx 5$  g had been injected into the source since it was last cleaned, this shows that essentially all the Cs was still present within the source. This was unexpected as the Cs effect had started to disappear and evaporation and loss through the accelerator apertures alone should have significantly reduced the quantity of Cs in the source. It is speculated that the Cs on the walls of the source was either covered by a layer of evaporated W or trapped in a matrix of W on the wall.

If the Cs is “buried”, or “blocked”, on the wall by W evaporated from the filaments, control of the evaporation of W could prove a key part in the operation of this source for high current density. The W filaments are operated between 2800 and 3000 K in order to obtain the required electron emission current density. At this temperature the evaporation of W from the filaments is significant: It is calculated that the W flux is sufficient to cover all the inner surface of the ion source with a monolayer of W in 125 s of operation.

It is proposed to reduce the operating temperature of the W filaments, reducing the evaporated W into the source. This could be achieved by operating at higher anode-cathode voltages and lower emission current, therefore reducing the filament temperature, or by operating with thoriated tungsten filaments, which would allow for operation at 2100 K with the required electron emission density [2].

## CONCLUSIONS

---

- The KAMABOKO III ion source operates to the ITER specifications during short, 5 s pulses, i.e. the specified current densities of 200 A/m<sup>2</sup> D- and 280 A/m<sup>2</sup> H- have been accelerated and measured on a copper target when the source has been operated at the ITER specifications.
- A low H<sup>-</sup> or D<sup>-</sup> current density measured at the calorimeter on the MANTIS test bed during long pulse operation cannot be explained by lost accelerated electrons arising from either extraction from the ion source or creation by stripping in the accelerator and is attributed to poor transmission due to thermal loading leading to distortion of the acceleration grid. Operation with a new extraction and acceleration grid should alleviate this problem.
- The reduced PG temperature effect measured during long pulse operation could be partly explained by enhanced evaporation of Cs from the source walls at the equilibrium temperature reached during long pulse operation perturbing the dynamic balance between the arrival of Cs from the source walls and the evaporation from the plasma grid.
- The consumption of Cs is many times larger than expected, which may be partly explained by the increased evaporation from the "hot" source walls. However it is found that most of the Cs remains in the source even after it was expected to have been lost from the source. It is speculated that the Cs could be "blocked" on the walls either by burial under layers of tungsten evaporated from the filaments or by being trapped in a loose matrix of tungsten on the source walls.

## REFERENCES

---

- [1] The Evaporation of Atoms, Ions and Electrons from Caesium Films on Tungsten - JB. Taylor and I. Langmuir - Phys. Rev., 44, 6, 1933, pp 423 – 458.
- [2] Thermionic emission investigation of materials for directly heated cathodes of electron tubes - B Gellert and W Rohrbach - XVI International Symposium on Discharges and Electrical Insulation in Vacuum, Moscow to St. Petersburg 1994 pp.501-504.

## REPORTS AND PUBLICATIONS

---

- [1] Development of the Long Pulse Negative Ion Source for ITER - R.S. Hemsworth, D. Boilson, U. Fanz, L. Svensson, H.P.L. de Esch, A. Krylov, P. Massmann, and B. Zaniol - Symposium on the Production and Neutralization of Negative Ions and Beams - Kiev, 13-17 September 2004.
- [2] Negative Ion Yield in Long pulse operation on the KAMABOKO III ion source – D. Boilson, H.P.L. de Esch, R.S. Hemsworth; A. Krylov, P. Massmann and L. Svensson - 23<sup>rd</sup> symposium of fusion technology - 20-24 September 2004.

## TASK LEADER

---

Deirdre BOILSON  
 in collaboration with R.S. HEMSWORTH  
 A. KRYLOV  
 C. GRAND

DSM/DRFC/SCCP/GIDEA  
 CEA-Cadarache  
 F-13108 Saint-Paul-Lez-Durance Cedex

Tél. : 33 4 42 25 62 93  
 Fax : 33 4 42 25 62 33

E-mail : deirdre.boilson@cea.fr



## TW3-THHE-CCGDS1

---

### **Task Title: COAXIAL CAVITY GYROTRON AND TEST FACILITY Design, support to the industrial development and preparation of the technical specifications**

---

#### **INTRODUCTION**

---

In ITER, Electron Cyclotron (EC) heating and current drive is foreseen not only as a principal auxiliary system for plasma heating and as assist for plasma start-up, but is considered essential in meeting the key requirement of neoclassical tearing mode (NTM) stabilisation. The main purpose of the task is to follow the development of this EC power generation system, for which a 2 MW CW coaxial cavity gyrotron at 170 GHz has to be developed, as well as the superconducting magnet, the High Voltage power supplies, the dummy load and the test facility.

#### **2004 ACTIVITIES**

---

The contribution of the Association Euratom-CEA to the Task TW3-THHE-CCGDS1 was in 2003 and 2004 the participation of one professional as an 'expert' to the different design review meetings.

In 2004, there was three meetings: two progress meetings in january in Garching and in june in Karlsruhe, and the final meeting in december in Garching.

Concerning the gyrotron development, the final technical specifications required for the supply contract were prepared and finalized in january. The supply contract between the European Atomic Energy Community and Thales Electron Devices was signed in may, for a total duration of 27 months, with the objective of the delivery of the so-called "coaxial cavity development prototype #1 at 170 GHz, 2 MW, 1 s" in november 2005 at the test bed in CRPP, for a period of nine months in site tests.

The contract negotiations with the selected company (Ansaldo Superconduttori) for the manufacture of the first superconducting magnet, started in march and the final agreement was reached in june. The contract between the European Community and the Supplier was signed in september for a delivery at the test bed in CRPP in november 2005.

The contract for both Main High Voltage Power Supply and Body Power Supply are to be signed by the European Commission at the end of 2004/ beginning of 2005. The planned delivery dates are respectively may 2006 and june 2006, followed for each PS by a delay of one month necessary for the integration at CRPP. For both power supplies, the delivery dates are after the commissioning of the gyrotron.

A temporary MHVPS will then be used for the beginning of the tests, at reduced specifications and without BPS.

The Contract for the High Voltage Solid State Switch was still in the negotiation phase at the end of the year, but this component is needed only for fast on/off modulation, and consequently not required for the first tests.

A spherical water load compatible with the RF power of 2 MW in short pulse duration has been developed by ENEA and should be delivered in time for the gyrotron tests. In parallel, the development of a CW 2 MW load is in progress.

#### **CONCLUSIONS**

---

The contract for the first gyrotron prototype has been signed in may 2004, this first prototype capable of producing an RF power of 2 MW during 1 s, will be delivered at the TEST bed in Lausanne in november 2005, for a test period of 9 months. The Contract for the manufacture of the prototype superconducting magnet was signed in september 2004, and will be delivered at CRPP also in november 2005. Due to the late signature of the contract for the two required High Voltage Power Supplies, they will not be available in time for the beginning of the tests of the gyrotron, an existing power supply in Lausanne will then be used during this phase. A short pulse water load will be available for the tests.

#### **TASK LEADER**

---

Roland MAGNE

DSM/DRFC/SCCP/GCHF  
CEA-Cadarache  
F-13108 Saint-Paul-Lez-Durance Cedex

Tél. : 33 4 42 25 62 81  
Fax : 33 4 42 25 62 33

E-mail : roland.magne@cea.fr



**TW3-THHI-GTFDS1**


---

**Task Title: FUSION DIACRODE, IC RF GENERATOR, IC POWER SUPPLY  
AN IC TEST FACILITY  
Design, support to the industrial development and preparation  
of the technical specifications**

---

**INTRODUCTION**

Ion Cyclotron heating and current drive auxiliary heating method requires a Radio Frequency (RF) power source capable of an efficient continuous operation on a highly variable load, for future experiments in existing European fusion laboratories and for ITER operation.

High Standing Wave Ratio (VSWR) and RF power level are required for auxiliary heating operation in high confinement plasmas such as ITER-relevant high  $\beta$  plasma scenarios.

The RF power source consists of a three stages electronic tubes amplifier driven by a solid-state RF source. Although there is no problem to build low power amplification stages, no existing end stage is yet capable of the required performance. Therefore, the development of a new-generation of RF power sources is needed; it would be both a technical and a financial advantage if one single source could be developed in European Union (EU). Fusion laboratories and ITER could take benefit from it. The aim of this project is the construction by industry of a RF power source capable of the required performance.

In response to a European Fusion Development Agreement (EFDA) call of expression of interest, CEA offers to provide technical assistance to the EFDA development of the RF power source within the more general framework of a coordinated effort among European Associations, with CEA acting as the leading Association. In particular, CEA offers technical assistance as required for the industrial development and testing and full responsibility for construction and operation of a high power steady state test facility at Tore Supra (TS) Cadarache site.

A CCFW subgroup, including all interested Fusion Associations representatives has defined and agreed detailed technical specifications for a high power RF source. Everybody agreed that a technological step is required to meet the specifications of high power RF sources, which will be used on future fusion experiments as ITER, W7X, JET-EP or Tore Supra CIMES project.

The alternative using of a high power diacrode® leads to a simpler generator with less components for which maintenance and reliability appear more attractive. A call for tender has been done and EFDA is now ready to place an order for a prototype of RF high power source. The first step of the task is now completed, however, the task has been suspended as long as ITER negotiations haven't been completed.

**CONCLUSIONS**

Today, many parts of the task are completed. Technical specification have been written, a call for tender have been done and EFDA received an offer from the industry on July 2003.

The Technical Evaluation Group meeting took place on July 2003 and EFDA is now ready to place an order for the IC RF generator.

At the same time the ICRF system is a matter of negotiations for ITER. So EFDA decided on September 2003 to put on standby the ICRF generator R&D, pending the ITER decision, and to extend task TW3-THHI-GTFDS1 of one year till the end of 2005.

**REFERENCES**

- 
- ITER Design - Task EU-D350 (DEC 1999) and associated NET Task.
  - New power gridded tube in fusion applications - Thomson Tubes Electroniques - Second Europhysics Topical Conference on RF Heating and Current Drive of Fusion Devices - Brussels - 20-23 January 1998.
  - A new generation of gridded tubes for cw operation on new fusion magnetic machines applications - Thomson Tubes Electroniques - 1997 Symposium on Fusion Engineering - San Diego, California - October 6-10, 1997.
  - Joint USDOE/General Atomics and Varian Power Grid and X-RAY Tube products Development Project for X2242/X2274 Anode Cooling Upgrade and Improved Grid RF performance - December 1990.
  - EIMAC 4CM2500KG tetrode data sheet.
  - Thales Electron Devices TH525 and TH526 tetrodes data sheets.

## REPORTS AND PUBLICATIONS

---

- Note CH/CCH 2003/015 - Tâche EFDA TW3.THHI. GTFDS1 - Cahier des charges du Fusion Diacrode Assembly - 28 may 2003.
- Note CH/CRM 2003/001 - Tâche EFDA TW3.THHI. GTFDS1 - First intermediate report and review meeting - EFDA GARCHING (Germany) - 31 january 2003.
- Note CH/CRM 2003/003 - Tâche EFDA TW3.THHI. GTFDS1 - Intermediate report and review meeting. Technical Evaluation Group - EFDA GARCHING (Germany) - 24 july 2003.
- Note CH/CCH 2003/016 - Spécifications techniques d'une charge HF 3 MW pour le test d'un prototype de générateur FCI pour ITER. - 16 june 2003.
- Note CH/CRM 2003/002 - Tâche EFDA TW3.THHI. GTFDS1 - Compte rendu de réunion dans les locaux de la société Thales Electron Devices - Thonon les bains - 03 april 2003.

## TASK LEADER

---

Patrick MOLLARD

DSM/DRFC/SCCP

CEA-Cadarache

F-13108 Saint-Paul-Lez-Durance Cedex

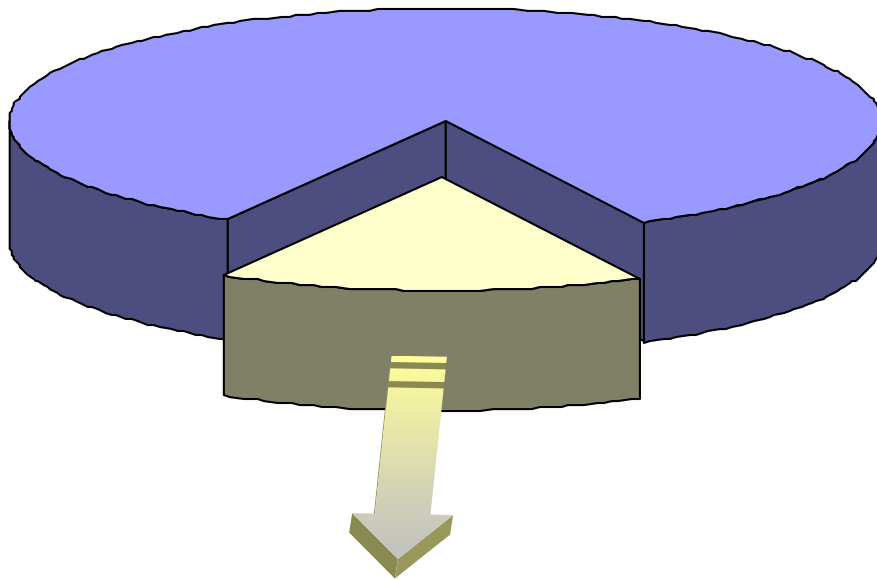
Tél. : 33 4 42 25 32 54

Fax : 33 4 42 25 62 33

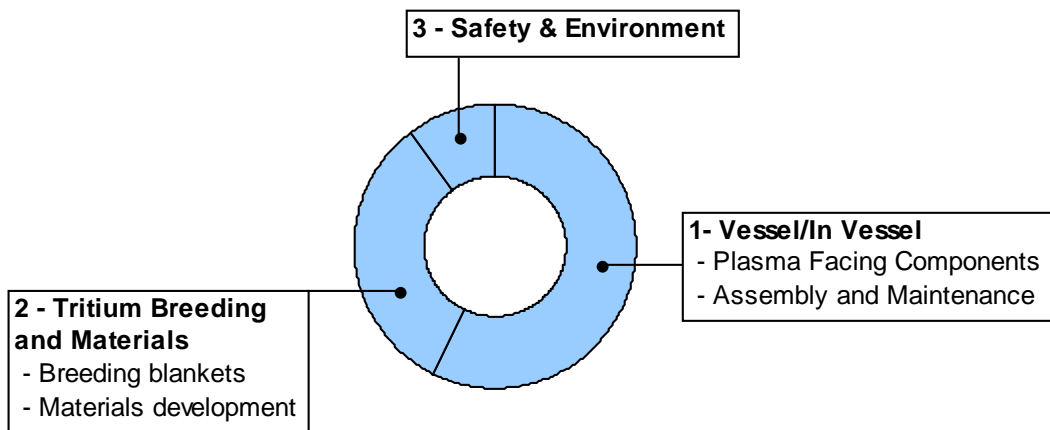
E-mail : [patrick.mollard@cea.fr](mailto:patrick.mollard@cea.fr)

# UNDERLYING TECHNOLOGY PROGRAMME

EFDA  
Technology



Underlying Technology





## UT-VIV/PFC-Damage

### Task Title: STUDY OF DAMAGE MECHANISMS IN PLASMA FACING COMPONENTS

#### INTRODUCTION

Plasma Facing Components (PFC) for future fusion reactors should withstand high heat flux. The component developed for TORE SUPRA included a high thermal conductivity material (a composite made with carbon matrix reinforced by carbon fibres) mechanically bonded to a copper heat sink and able to remove incident stationary heat flux of 10 MW/m<sup>2</sup> [a]. In order to reach a value of 20 MW/m<sup>2</sup> for the divertor component of the ITER machine, the lifetime of this assembly submitted to considerable thermal stress must be increased. Based on the analyses already performed by the TORE SUPRA team and the knowledge of the LCTS laboratory, the objectives of this activity are (i) providing a study of damage mechanisms of the CFC bond, (ii) proposing an optimization of the bond and (iii) possibly giving a tile damage ratio depending on the history of its loading.

#### 2004 ACTIVITIES

During this period the three studies foreseen on the task action sheet were achieved: review of constitutive laws for CFC materials and finite elements simulations at various scales to estimate the stress field in the PFC.

#### EXISTING CONSTITUTIVE LAWS FOR CFC MATERIALS AND POSSIBLE EXTENSION TO N11 AND NB31 [1]

A literature review was performed to analyse the various constitutive laws, which could be used to describe the mechanical behaviour of a carbon/carbon composite. The damage mechanics theory is well suited to reproduce the non-linear behaviour that results from the well distributed micro-cracks which develop in this kind of material subjected to mechanical loads [2]. As it was previously shown that the damage does not modify the initial orthotropy, a scalar damage model can be used and the relevant identification procedure has been defined.

#### ANALYSIS OF LOCAL CRACKING MECHANISMS [2][3]

At the microscopic scale, it is to be pointed out that the bond between the copper and the composite tile is obtained with the help of an original concept: the tile surface is machined with a laser to produce micro-holes (cone shaped: 300 microns diameter and 500 microns deep) before casting the copper. Computations performed at the microscopic scale reveal that the fabrication phase of the PFC induces (i) a stress concentration in the composite tile ahead of a copper spike, (ii) a positive de-bond stress along the

interface between a copper spike and the composite (figure 1). These results correlate well with micrographic observations, which show that damage can initiate within the composite ahead of a copper spike and propagate along the copper/composite interface.

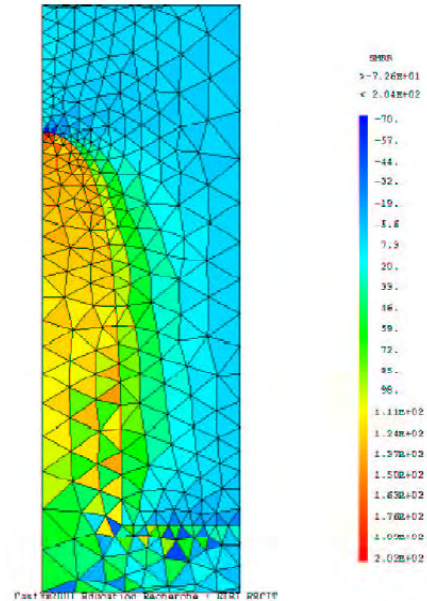


Figure 1 : Radial stress at the microscopic scale during the cooling step from 470°C to 20°C

#### CALCULATIONS OF RESIDUAL AND UNDER-FLUX STRESSES [4]

At the macroscopic scale (figure 2), the composite tile is mainly submitted to compression as a result of the residual stress field that is induced by the fabrication phase (figure 3). However, a very localised traction component is observed near the edge tile (figure 4) and could give rise to damage initiation within the composite.

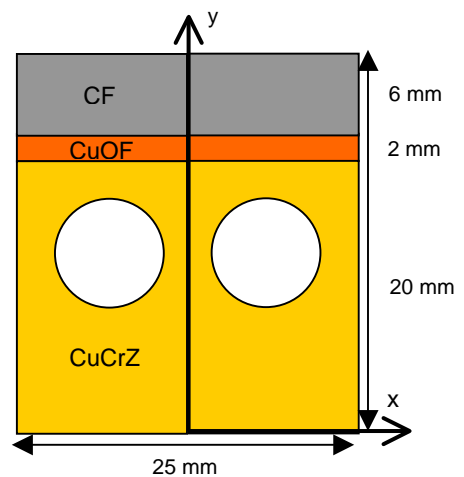


Figure 2 : Geometry of the PFC. The coordinates of the centres of the cooling channels (8 mm diameter) are  $x = \pm 5 \text{ mm}$  and  $y = 13 \text{ mm}$

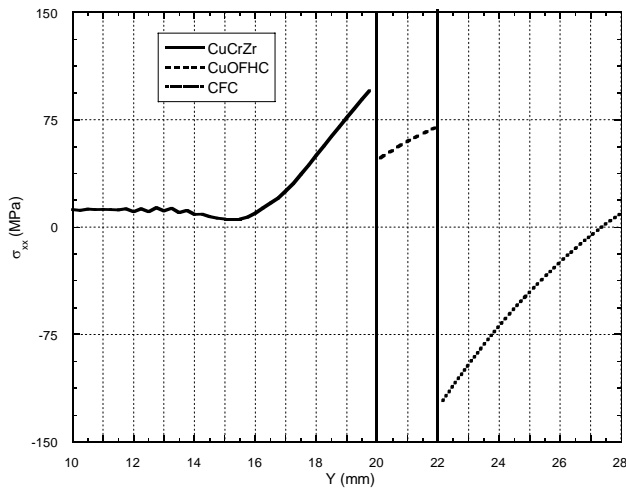


Figure 3 : Longitudinal stress  $\sigma_{xx}$  in the centre of the PFC following a cooling step from 470°C to 20°C

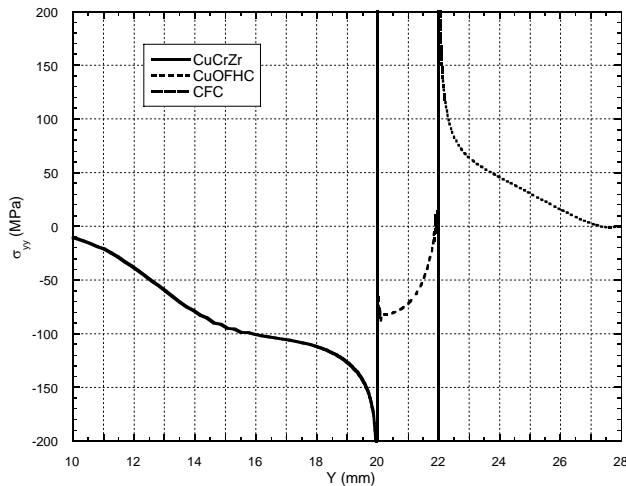


Figure 4 : Longitudinal stress  $\sigma_{yy}$  at the edge of the PFC, following a cooling step from 470°C to 20°C

## CONCLUSIONS

The reports corresponding to these activities have been delivered. The work will continue in 2005 with (i) tests on CFC samples to identify a constitutive law, (ii) observations and analyses of damage mechanisms, (iii) optimization of the edge geometry and (iv) modelling of the crack propagation.

## REFERENCES

- [a] J. Schlosser, P. Chappuis, A. Durocher, L. Moncel, P. Garin - Development of actively cooled components for the Tore Supra toroidal pump limiter - Physica Scripta, TIC 116, 1-4, 2001.

## REPORTS AND PUBLICATIONS

- [1] G. Camus - Endommagement et rupture dans les assemblages des composants face au plasma, Identification d'une loi de comportement thermomécanique pour composites 3D C/C : application aux matériaux N11 et NB31. Lois de comportement disponibles pour les C/C et extension possible aux matériaux N11 et NB31 - Rapport 1a, Projet P6, 01/12/04.
- [2] D. Leguillon, C. Henninger - Endommagement et rupture dans les assemblages des composants face au plasma, Analyse de l'endommagement de la liaison CFC-Cu à l'échelle microscopique : Analyse des mécanismes d'amorçage - Rapport 2a, Projet P6, 20/12/04.
- [3] D. Leguillon, C. Henninger - Endommagement et rupture dans les assemblages des composants face au plasma, Analyse de l'endommagement de la liaison CFC-Cu à l'échelle microscopique : Analyse des mécanismes locaux de fissuration - Rapport 2a-bis, Projet P6, 20/12/04.
- [4] E. Martin - Endommagement et rupture dans les assemblages des composants face au plasma - Analyse des mécanismes d'endommagement de l'assemblage à l'échelle macroscopique : Calcul des contraintes résiduelles et des contraintes sous chargement de flux thermique - Rapport 3a-bis, Projet P6, 1/12/04.

## TASK LEADER

Eric MARTIN

LCTS, UMR 5801 (CNRS-Snecma-CEA – UB1)  
 Domaine Universitaire  
 3 Allée de la Boétie  
 33600 Pessac

Tél. : 33 5 56 84 47 00  
 Fax : 33 5 56 84 12 25

E-mail : martin@lcts-u.bordeaux1.fr

Not available on line

## UT-VIV/PFC-Pyro

### Task Title: APPLICATION OF A TRICOLOUR PYROREFLECTOMETER TO PLASMA FACING COMPONENTS IN-SITU INFRARED MONITORING

#### INTRODUCTION

The plasma-facing components in tokamaks are observed by infrared thermography to provide security against overheating.

The results depend on the emissivity of the surface which is not known a priori and may be a function of temperature, viewing direction, wavelength and physical state of the surface.

The latter changes in the course of the interaction with the plasma. Particularly important is this question for low emissivity metallic surfaces as tungsten and beryllium, which are presently foreseen for ITER alongside with carbon, that causes less problems due to its high emissivity.

The main aim of this collaboration is to develop a tri color pyroreflectometer technique [1] capable of measuring in-situ and in real-time the emissivity of the monitored materials. The main steps are:

- A) For 2004 : use the multi colour pyroreflectometry method on materials samples typical of fusion devices (Carbon Fiber Composite CFC or Tungsten W, new and used) to determine unambiguously their temperature and deduce the emissivity in the near infrared range ( $0.84 - 1.5 \mu\text{m}$ ) and by additional luminance measurements at  $5 \mu\text{m}$  and  $8-12 \mu\text{m}$  to investigate the possibility to measure temperatures lower than  $500^\circ\text{C}$ .
- B) For 2005 : evaluate the possibility to implement the pyroreflectometer in the FE200 high heat flux station of CEA situated in Le Creusot and implement it for a testing campaign.
- C) For 2006 : evaluate the possibility to implement the pyroreflectometer in Tore Supra or another tokamak and eventually commission and implement it; and prepare a study of feasibility for ITER application.

#### 2004 ACTIVITIES

#### EXPERIMENTAL SETUP

The experimental set up used for the first experiments (figure 1) is MEDIASE, one of the solar extreme test facilities of the laboratory [2].

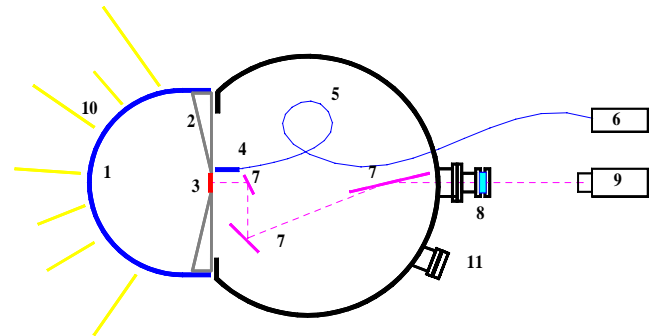


Figure 1 : MEDIASE test facility

The setup comprises:

- 1) hemispherical silica window
- 2) water-cooled front shield
- 3) sample
- 4) moving probe equipped with an hemispherical probe
- 5) optical fibers
- 6) bicolor pyroreflectometer
- 7) 3-mirrors goniometer
- 8) view port
- 9) radiometer equipped with specific filter
- 10) concentrated sun radiation
- 11) connection to vacuum device

The sample (3) is heated by the concentrated solar flux (10) on its front face and instrumented on the rear face. The moving probe (4) can be located on the rear face of the sample or in its side. The probe is a reflecting hemisphere equipped with two optical fibers (5) linked to the bi-color pyroreflectometer (6) for normal normal reflectivity measurements.

Angular resolved reflectivity measurements are not possible with this set-up. The radiometer (9) can be equipped with filter at  $5$  and  $8-12 \mu\text{m}$  to measure the directional radiance temperature  $Tr(\lambda, \theta)$  of the sample through a window (8) and a 3-mirrors internal goniometer (7). During these experiments, MEDIASE was operated under residual pressure of  $10^{-5}$  mbar (see vacuum device (11)).

Four cylindrical samples (diam. 25 mm, thick. 2 mm) were delivered by CEA to CNRS in may 2004 : two samples of pure W from Plansee GmbH. One of the W samples was glass-blasted in Cadarache before sending to CNRS (sample 1), the other one was "clean" (sample 2), two samples of CFC N11 from manufacturing of Tore Supra LPT (samples 3 and 4).

**METHOD**

The bi [3] or tri [1] color pyroreflectometry is a new concept developed at the CNRS Odeillo to determine the true temperature for opaque material. The main principle is to measure simultaneously and for two or three working wavelengths the radiance temperature  $Tr(\lambda)$  and the bi-directional reflectivities on the normal position. The main hypothesis is to consider that the instrumented sample has the same B.R.D.F. (bi-directional reflectivity distribution function) at the working wavelengths. Taking into account these two points the true temperature is obtained solving a system of two or three equations based on a relation:

$$1/T = 1/Tr(\lambda) + \lambda/C_2 \ln(1 - \eta(T)\rho^{0,0}(\lambda, T)) \quad (1)$$

where  $\eta$  is the diffusivity factor which is the ratio of hemispherical reflectivity  $\rho^{0,\wedge}(\lambda, T)$  to normal normal reflectivity:

$$\eta(T) = \rho^{0,\wedge}(\lambda, T) / \rho^{0,0}(\lambda, T) \quad (2)$$

Consequently  $\rho^{0,\wedge}(\lambda, T)$  and  $\varepsilon^0(\lambda, T)$  can also be determined.

The figure 2 presents an example of a graphical determination of solution the true temperature for a W sample heated at the solar furnace.  $Tc_a$ ,  $Trr_a$ ,  $Trb_a$  are the measured apparent (colour and radiance) temperatures and  $\rho_r_a$  and  $\rho_b_a$  the measured apparent normal normal reflectivities (r indicate 1.55 $\mu$ m et b 1.3 $\mu$ m).

The resulting convergence temperature  $T^*$  is assumed to be equal to the true temperature  $T$  at a corresponding apparent value  $\eta^*_a$  and the apparent emissivities  $\varepsilon_r_a$  and  $\varepsilon_b_a$ . This method worked well for the tungsten targets. For the carbon targets the reflectivity was too low. Hence we assumed identical emissivity at the two wavelengths (1.3 and 1.55  $\mu$ m) and determined the ‘true’ temperature via bi color pyrometry. After the true temperature of the samples had been determined further passive measurement were performed to determine the directional emissivity  $\varepsilon(T, \lambda, \theta)$  at 5 and 8-12 $\mu$ m. In this case the method is a direct method:

$$\varepsilon(T, \lambda, \theta) = L^\circ(Tr(\lambda, \theta)) / L^\circ(T, \lambda) \quad (3)$$

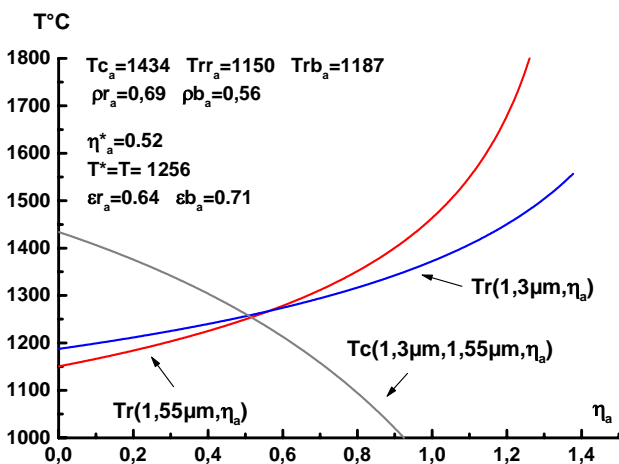


Figure 2 : Example of analysis of bi-color pyro reflectometry measurements

**RESULTS**

Figures 3 and 4 show the results obtained with the pyroreflectometry method on the tungsten samples. In the case of the glass-blasted tungsten (figure 3)  $\varepsilon_r_a$ ,  $\varepsilon_b_a$ ,  $\eta^*_a$  values were different during the first and the following heating cycles. Such differences may be attributed to a modification of the state of the surface (outgassing of impurities, cleaning of surface) during the first temperature rise. The values for clean tungsten did not change from one cycle to another.

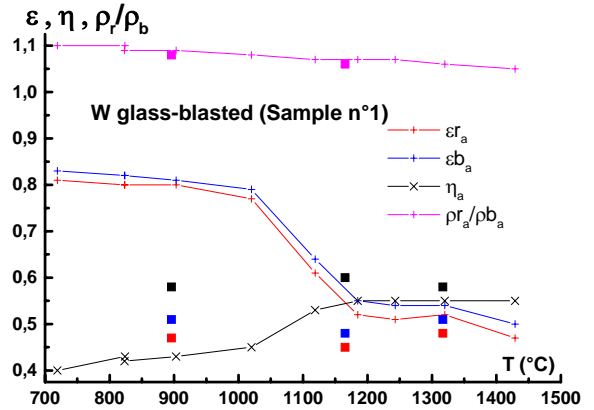


Figure 3 : Glass blasted tungsten: Curves and cross: first increasing cycle – Squares: a further increasing cycle

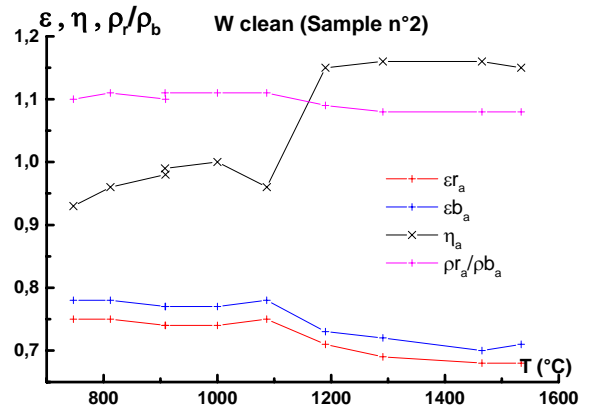


Figure 4 : Clean tungsten during a later increasing cycle

The angular resolved emissivity measurements at 5 and 8-12  $\mu$ m are shown in the figures 5-12.

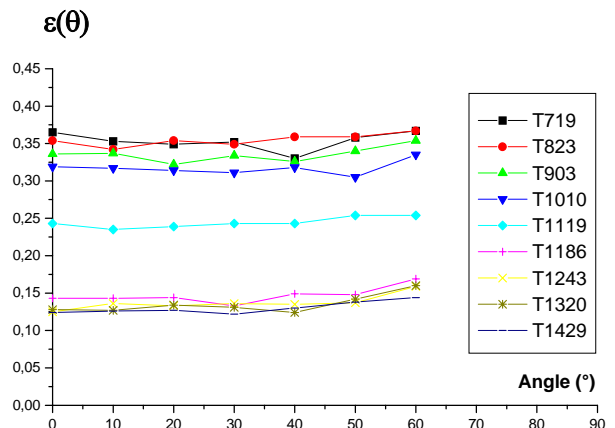


Figure 5 : Glass blasted tungsten at 5 $\mu$ m: first temperature rise

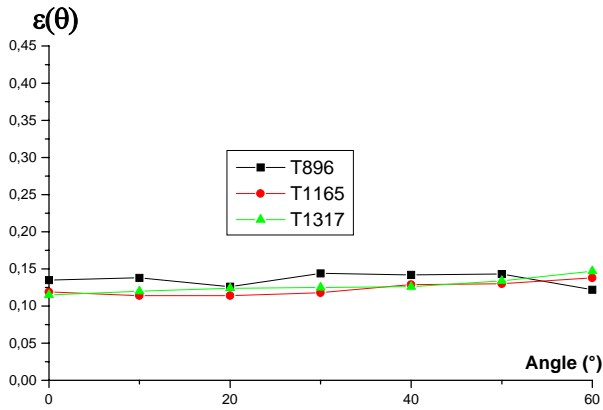


Figure 6 : Glass-blasted tungsten at 5  $\mu\text{m}$  during later cycle

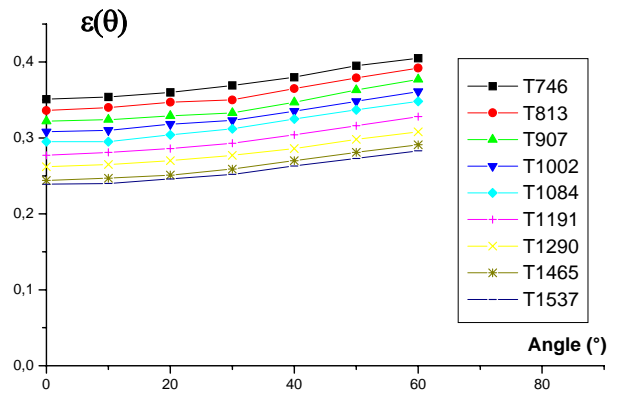


Figure 10 : Clean tungsten at 8-12  $\mu\text{m}$

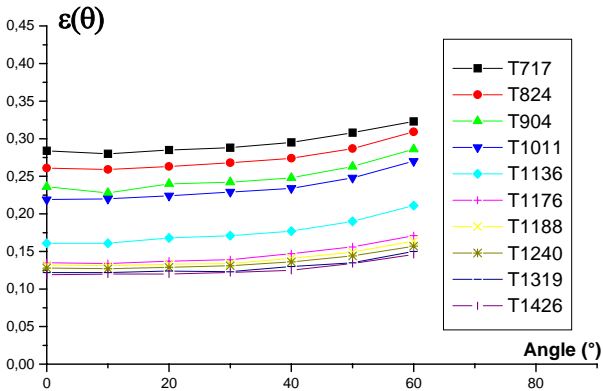


Figure 7 : Glass-blasted tungsten at 8-12  $\mu\text{m}$  during first temperature rise

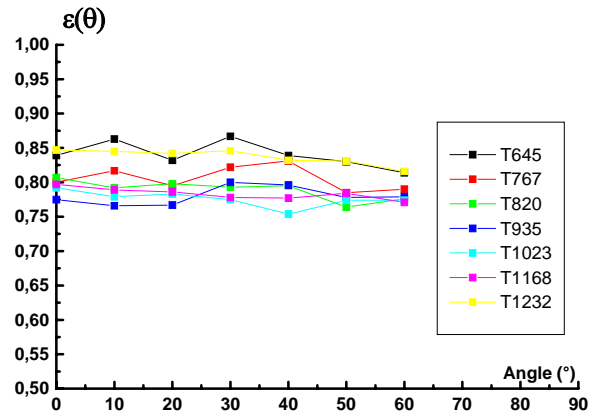


Figure 11 : CFC N11 at 5  $\mu\text{m}$

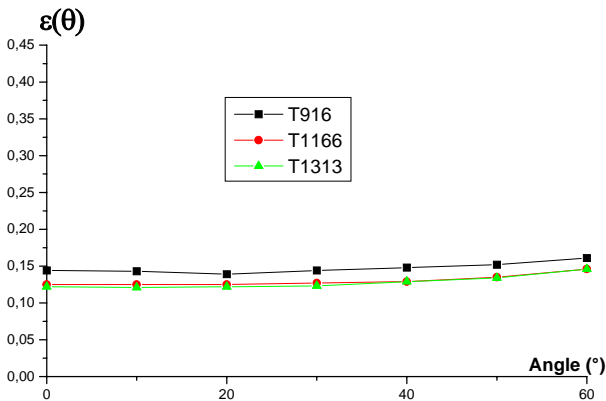


Figure 8 : Glass-blasted tungsten at 8-12  $\mu\text{m}$  during later cycle

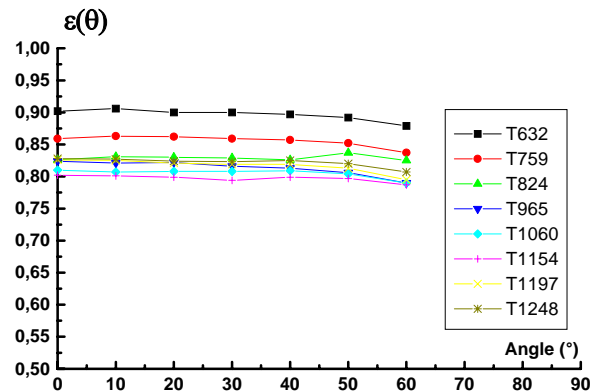


Figure 12 : CFC N11 at 8-12  $\mu\text{m}$

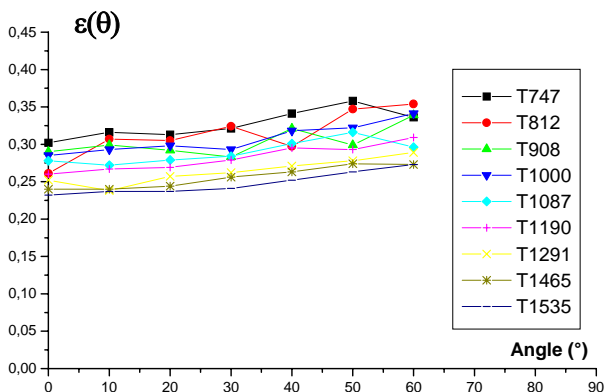


Figure 9 : Clean tungsten at 5  $\mu\text{m}$

## CONCLUSION

Tungsten and Carbon Fiber Composite CFC N11 samples from CEA Cadarache were tested at the MEDIASE facility. Bi-color pyroreflectometry could be used to measure both the true temperature and the emissivity on tungsten but not on CFC N11.

The use of a spherical probe prohibited emissivity measurements at 1.3 and 1.55 microns. These measurements are planned for 2005 using a dedicated experimental set-up called DISCO.

Emissivity of W and CFC N11 were measured at 5 and 8-12 microns. At 5 microns, the results obtained for W (emissivity as low as 0.10-0.40 for  $750 < T(^{\circ}\text{C}) < 1550$ ) are consistent with results obtained at FE200 facility with an infrared device working in the range 3-5 microns.

The results for CFC N11 (emissivity as high as 0.75-0.90 for  $600 < T(^{\circ}\text{C}) < 1250$ ) are consistent with results obtained at FE200 facility with an infrared device working in the range 3-5 microns and at SATIR facility with an infrared device working in the range 8-12 microns. The glass blasted tungsten yielded in the first heating cycle different values than later. The other samples did not show such variations.

## REFERENCES

---

- [1] D. Hernandez - A new concept to determine the true temperature of opaque materials using a tricolor pyroreflectometer - publication accepted in 2004 to be published in 2005 in Review of Scientific Instruments.
- [2] M. Balat-Pichelin, D. Hernandez - Concentrated Solar Energy as a diagnostic tool to study materials under extreme conditions - Journal of Solar Energy Engineering Vol. 124 pp 215-222 august 2002.
- [3] D. Hernandez, et al. - Bicolor pyroreflectometer using an optical fibre probe - Rev. Sci. Instr. 66 (1995), 5548.

## REPORTS AND PUBLICATIONS

---

Application of a tricolour pyroreflectometer to plasma facing components in-situ infrared monitoring, Contract C.E.A. et P.R.O.M.E.S. - C.N.R.S. Ref : V3448.001, Report A2, Experiments at odeillo solar furnace, november 2004, Daniel Hernandez - Jean Louis Sans.

## TASK LEADER

---

Daniel HERNANDEZ

CNRS/IMP

Institut de science et de Génie des Matériaux et Procédés  
Avenue du Professeur Trombe  
Boîte Postale 5  
F-66120 Font-Romeu

Tél. : 33 4 68 30 77 19

Fax : 33 4 68 30 29 40

E-mail : danielh@imp.cnrs.fr

# Task Title: REMOTE HANDLING TECHNIQUES Radiation effects on electronic components

## INTRODUCTION

The well-known method commonly named “carrier current principle”, often implemented on consumer applications (home control instrumentation using electrical nets, data transfer using phone nets) has also proven its capacity for data exchange in severe environments and wires number limitations protocols.

Some experiments of this method were conducted a few years ago to control embedded video camera parameters inside low-dose level cells [1]. A more recent development concerned an absolute position encoder readings involved on hot cells cranes driving [2]. 2004 works focus on the availability to apply these realizations to a more complex situation such as encountered with remote control of maintenance tools of ITER and high level of temperature and radiation. The present document first describes the main points of the previous experiments. Then, the design of a new mock-up is presented as well as laboratory tests and temperature experiments.

## 2004 ACTIVITIES

### BRIEF “STATE OF THE ART” STUDY

To increase the quality of the images of objects situated inside reprocessing cells, acquired by an embedded video camera, some parameters were remotely controlled using supply wires (easier than video cable).

The scheme represented on figure 1 shows a full data link using carrier current transmission between an emitter, which frames digital data and insert them in the supply link, and a receiver which extracts the frame from the global signal received on the supply link, but also reconstitutes supply voltage for its inner electronic modules.

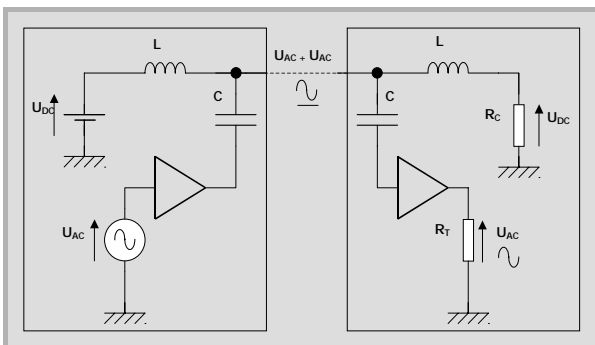


Figure 1 : Basic principles of carrier current transmission

The emitter, in this project a Man-Machine Interface, regularly generates (4 ms) a 16 bits frame based on operator requirements for the embedded parameters.

For those very simple and slow dialogs, the high level duration of a reference digital signal is modulated to assume the coding of “0” and “1” binary digits, which avoids the inclusion of an independent clock signal.

The digital signal is then sent to the FSK system (Frequency Shift Keying) to be converted into an analog signal UAC (one frequency for each of the two digital levels).

This last signal is mixed with the supply signal, UDC, through solenoids and capacitors and sent as UDC+UAC on the bifilar support to the receiver. The receiver, an embedded electronic module of the camera, separates UAC+UDC. UDC is necessary for all supply voltages and data are extracted from UAC to activate the necessary functions.

The expected low dose environment (less than 2 kGy) enabled us to report FSK modulation and demodulation on dedicated integrated components XR-2211 and XR-2206 which delivers a precise continuous phase shifting.

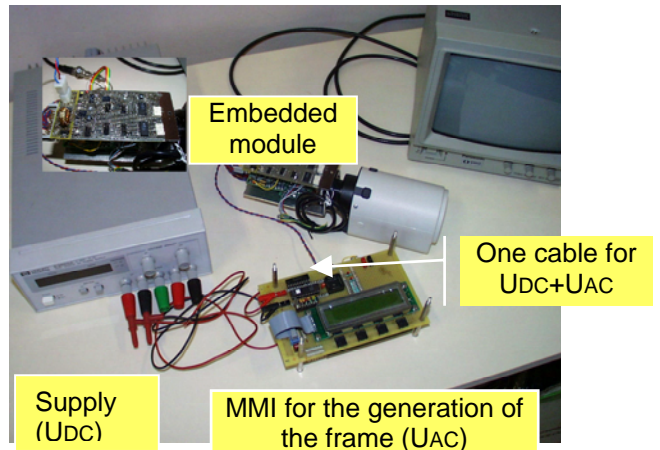


Figure 2 : Full experimental mock-up

The full mock-up test bench, presented on figure 2 was experimented under radiation with on-line measurements up to 2 kGy. No failures were observed during the irradiation period. Some chronograms registered during the experiment. On figure 3, GENE and DEMODU curves show the nominal frame generated by the MMI module and the finale frame issued from the demodulator. CLK curve is generated from the rising fronts of the received signal and reconstituted to deliver a usual clock signal. This signal is then used to transfer the frame to buffers and, later, sensors and actuators of the camera.

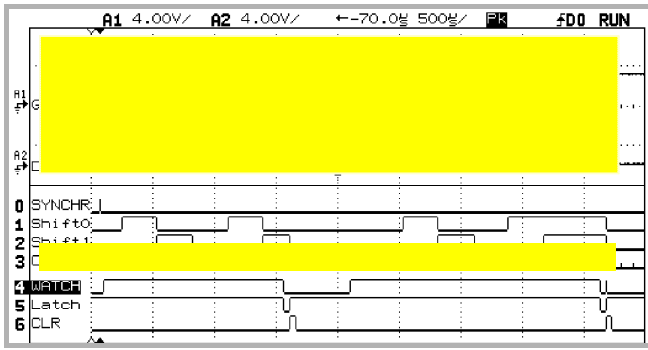


Figure 3 : Chronograms registered during experimental tests

The second development was needed for on-cell encoders readings expected to encounter total dose over 100 kGy which can not be solved by components such as those selected above. The solution was firstly to define and design a “discrete” modulation/demodulation system using proprietary oscillators and switching mechanisms.

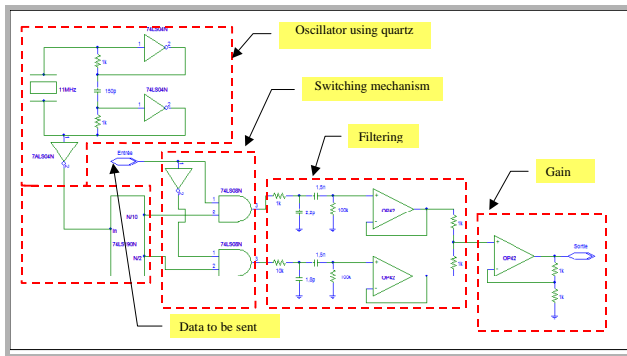


Figure 4 : Modulation module with discrete components

The electronic functions of the modulation modules are represented on figure 4. The two chosen frequencies (F1 5.5 MHz for high level “1” and F2 1.3 MHz for low level “0”) are defined through a common 11 MHz quartz oscillator and some logic components. Then, two filters centred on each frequency convert square logic signals to their analog sinusoidal form while eliminating secondary harmonics. The last gain stage assumes summation of the two sinusoidal signals and delivers the FSK modulated signal. Demodulation must be done with care. To reduce the number of wires, it is not possible to transfer FSK frequencies between modules. These signals must be locally reconstituted or retrieved through FSK signals with adapted filters.

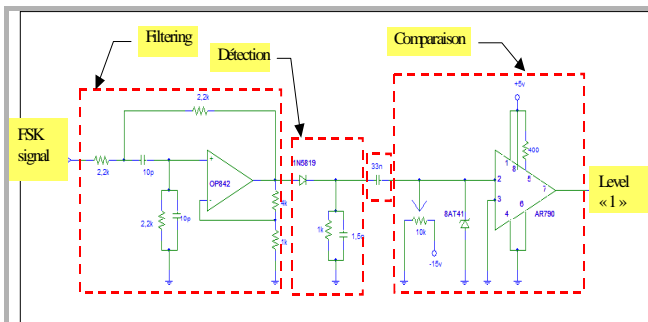


Figure 5 : Demodulation of “1” logic level frequency

Typically, in figure 5, a 2<sup>nd</sup> order Sallen-Key cell band pass filter with 5.5 MHz central frequency provides the FSK modulated “1” signal. The detection cell with a diode and RC components ensures a correct peak detection of the modulation signal F1 without significant unwanted effect during the null signal time.

Based on these operational electronic modules, a full duplex transmission using a single wire was realised with a OOK (On-Off keying) modulation for each way (only one level is translated into sinusoidal signals, the other being set to ground).

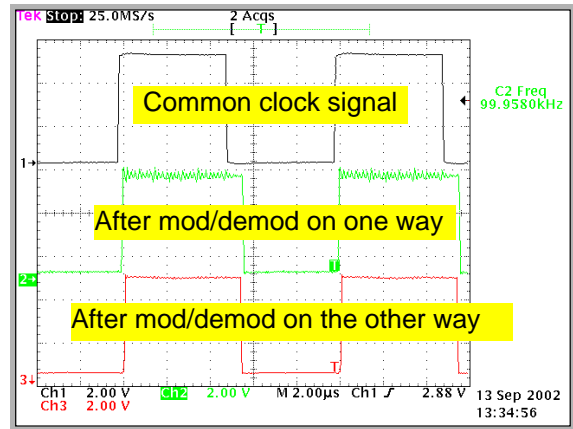


Figure 6 : Mod/demod of a clock signal

Laboratory tests of the line transmission made with a common clock signal sent to each modulator (F1 or F2 FSK frequencies), gives, after demodulation on each side, signals which are similar to the initial ones (see figure 6).

For this experiment, most components were issued from radiation tolerance tests.

**ON-GOING DEVELOPMENTS**

The developments of a full carrier current link with both data and supply, available under high temperature and dose environments, are initiated by the remotely handled camera development with most of the techniques proposed by the second example to mitigate the lack of FSK integrated circuits.

Some of the results coming from fusion tasks [3] [4] were also kept to actualise the design of the mock-up with components robust to high level of radiation and temperature.

Then, the FSK frequencies are limited by the bandwidth of the OPA27/OPA277 needed for these sub-modules. A reasonable agreement could be a high value of about 300 kHz.

Starting with a clock signal issued of a 4MHz quartz, the signal was derived through simple AUC flip-flops up to reach the two FSK frequencies signals of 250 kHz (logic “1” level) and 125 kHz (logic “0” level).

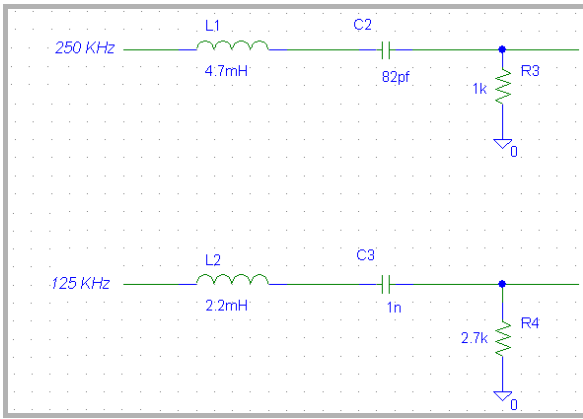


Figure 7 : Pass band 2<sup>nd</sup> order filter

These two signals are sent to a simple AUC logic switching mechanism to be separated and clocked on the data signal input. A simple passive 2<sup>nd</sup> order pass band filter is used (see figure 7) on each branch to generate the corresponding FSK sinusoidal signals. Then these two analog signals are added to deliver the full FSK data signal as represented on figure 8.

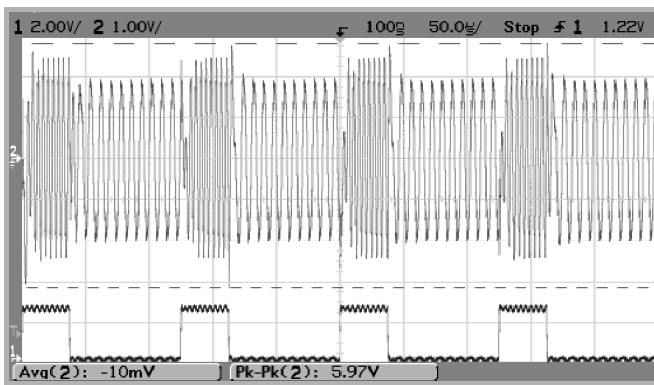


Figure 8 : FSK modulation and data signals

**ADAPTATION TO THE SUPPLY LINE**

A positive +7.5V supply and a negative -7.5V is applied to the mock-up.

By itself, the modulated signal cannot drive the positive supply line for carrier current transmission. A push-pull power amplifier is associated with an OPA mounted to control the switching distortion. It delivers enough current to attack and modulate the supply line voltage.

The adaptation to the line is realised by a simple filter cell inserted at each end of the line (here, a 10 meters twisted pair of wires). The C4 capacitor of figure 9 avoids continuous supply current to enter the FSK modules while the inductance avoids FSK modulation current to perturb the continuous supply.

At the end of the line, the FSK modulated signal is extracted while the supply signal is set free for applications (symbolised by the load point). No further development was made to precisely define the values of the cell.

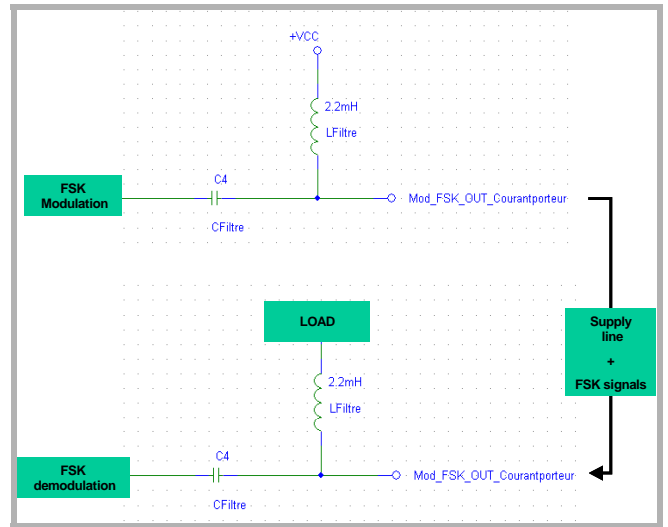


Figure 9 : Modulation and demodulation line adaptation

When no load is connected to the extremity or when the load does not perturb the signals on the line, the forms of these signals are very similar to those of figure 8.

The FSK demodulation is still correctly triggered by the digital data to transfer.

However, more aggressive loads such a PC supply fan let appear some defaults on the demodulated signal.

An induced oscillation on the supply signal was added to the FSK and detected at the demodulation (see figure 10).

The real influence of such degradations must be done with the final use of the FSK carrier current module.

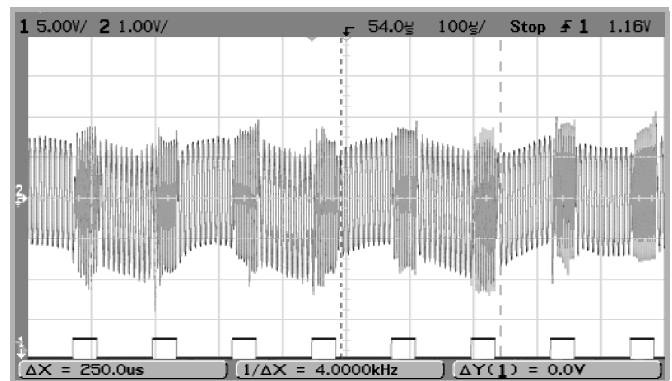


Figure 10 : Load influence on the demodulated FSK signal

The signal carried by the line is presented on figure 11.

The alternative F1 and F2 FSK signals are mixed with the positive +7.5V supply with amplitude modulation near 4V peak to peak.

The limited gain-bandwidth product of these OPAs affects the quality of sinusoidal signals. Nevertheless, this should not create a critical problem for the demodulation because the fundamental frequencies F1 and F2 are preserved.

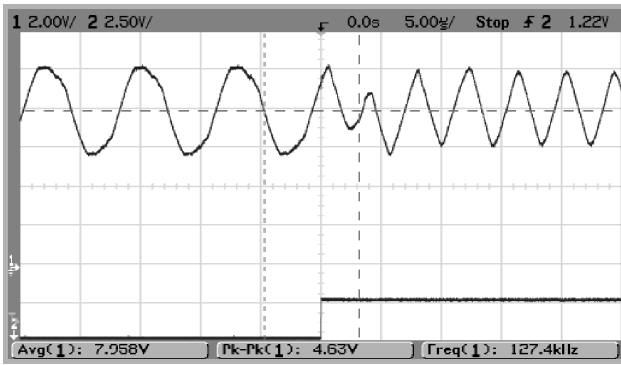


Figure 11 : Evolution of signal on the 10 m line

Care should be made to verify that the additional spectrum created by the AOP limitation does not interfere with others signals on the supply line.

It should also be possible to exchange OPAs with better ones like AD711 with the restriction of a non certified very high total dose tolerance.

The remaining of the work was done, when needed, with these components.

The mock-up developed to validate FSK and carrier current supply principles is presented on figure 12.

The driving of an embedded sensor, like LVDT position encoder, needs some new modules validated on some of ITER functions [5].

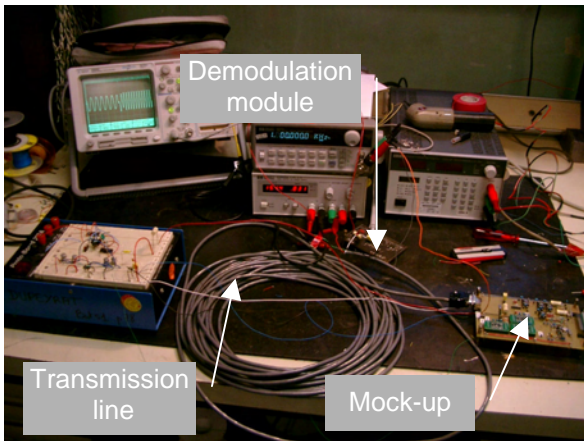


Figure 12 : Test bed to validate FSK and carrier current supply

**ADAPTATION TO THE FLOATING GROUND SUPPLY**

To supply the sensor with a single wire, it is necessary to replace external double supplies by an embedded floating ground supply able to deliver +/-7.5V from external 15V.

The study conducted under RADTOL developments was modified in order to take into account carrier current developments as detailed on figure 13.

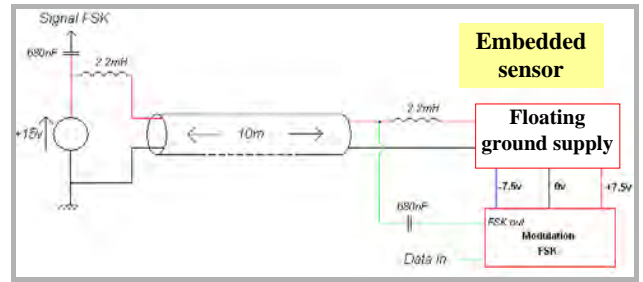


Figure 13 : Floating ground and carrier current association

No significant problems were occurred to realise the adaptation of the two developments. A load current of about 200 mA did not affect the stability of the internal supplies (+/-7.5V) and the FSK signals.

The different registered signals on figure 14 show the correct evolution of the FSK signals from modulation to demodulation via the supply line.

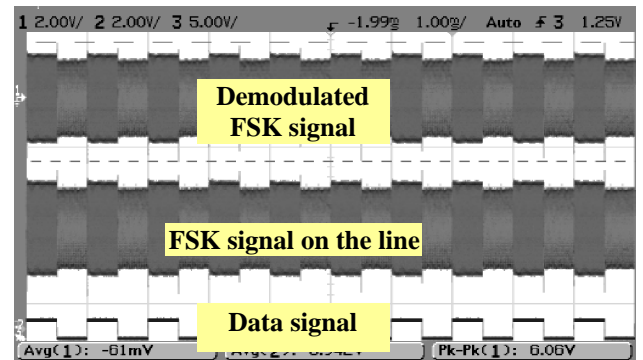


Figure 14 : Chronograms of FSK signals

**PWM CODING**

As for the remote control of the camera, the clock management must be integrated within the transmitted signal in order to limit wires number. Associated with FSK modulation and relatively slow frame communications, the coding of binary digits as duration of a clock base signal to deliver is very simple and useful (see figure 15).

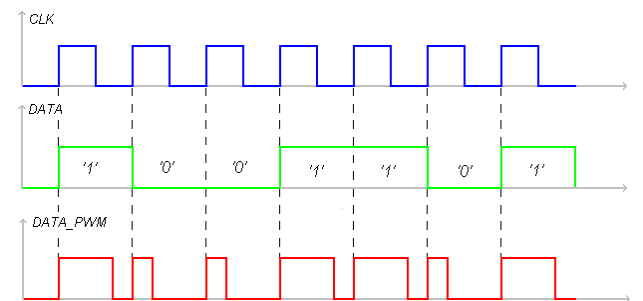


Figure 15 : PWM coding

The robustness to dose effects of most of the necessary components enables to define, starting from FSK timers, an efficient additional logic module able to convert data to

data PWM (see figure 15), that last data becoming the input of FSK modulation. The resulting chronograms are shown on figure 16.

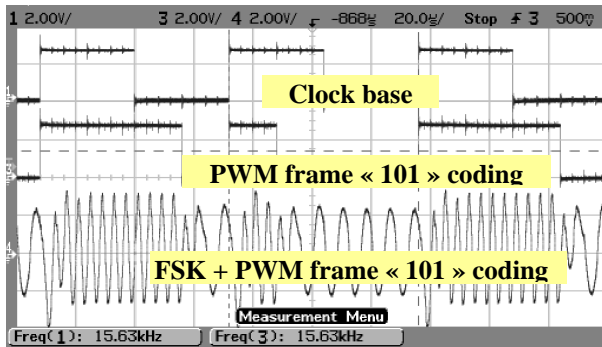


Figure 16 : PWM and FSK modulation

The full demodulation module, also achieved, provides, on figure 17, an operational full data transmission link based on FSK and carrier current principles with a particular PWM coding used to allow clock transfer without any extra wire. The drift observed is mostly inherent to the intermediate stages and can be easily optimised.

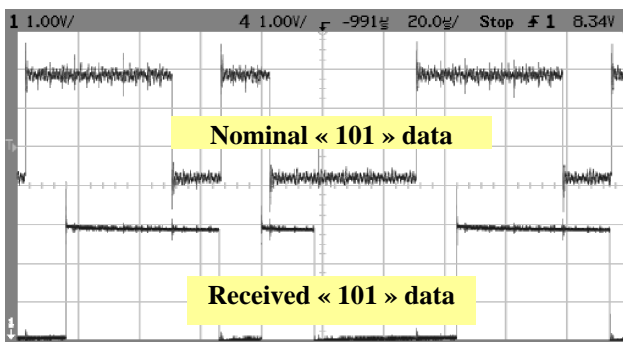


Figure 17 : Full carrier current data link transmission

## TEMPERATURE VALIDATION

The full mock-up was validated up to 150°C with on-line control during long term periods and short stresses without any major incidents or failures. The signals showed a regular stability as can be seen on figure 17.

## CONCLUSION

Works done during this year carried a very simple and robust link to transfer with a medium rate, data from a sensor to a remote control desk. The advanced limitation of wires with embedded supplies and clock masking could offer some answers for data consultings in very severe environments.

The volontaire approach based on previous developments for nuclear activities should be seen also as a logical come back to perform them with emerging technologies and higher performance.



Figure 18 : Full mock-up inside oven

## REPORTS AND PUBLICATIONS

- [1] Michel Robiolle - Télécommande de cameras - Report CEA/DRT/LIST/DTSI/SLA/02-83.
- [2] Julien Coudon - Réalisation d'une transmission de type modulation FSK en environnement durci - internal report.
- [3] Fusion Technology Annual Report 2003 EURATOM CEA pp 113-117.
- [4] Fusion Technology Annual Report 2002.
- [5] Fusion Technology Annual Report 2004.

## TASK LEADER

Alain GIRAUD

DRT/LIST/DTSI/SARC/LCSD  
CEA-Saclay  
F-91191 Gif-sur-Yvette Cedex

Tél. : 33 1 69 08 64 30

Fax : 33 1 69 08 20 82

E-mail : alain.giraud@cea.fr



---

## Task Title: TECHNOLOGIES AND CONTROL FOR REMOTE HANDLING SYSTEMS

---

### INTRODUCTION

---

CEA in collaboration with CYBERNETIX and IFREMER has developed the advanced hydraulic robot MAESTRO. Control laws developed in the TAO 2000 controller made possible the use of the MAESTRO in a force reflective master-slave configuration.

Development around the actuating technology of the MAESTRO's hydraulic arm successfully proved on servo-valves prototypes the interest to use pressure control servo-valve instead of flow control servo-valve. The control is directly made on the pressure, i.e. the force which makes real improvement during force control modes which are extensively used in remote handling techniques.

In-LHC (French servo-valve manufacturer), developed a pressure servo-valve prototype that fits the MAESTRO's space constraints.

Operating in a fusion reactor requires a cleanliness level that oil hydraulic cannot ensure. Pure water hydraulics therefore proposes a good alternative and developments are today focusing in that direction. Although basic hydraulic elements like pumps, valves, filters running with pure water are already available on the market, the number of actuation means like servo-valves is very low. The existing products are big, their design was sometimes quickly adapted to water without real endurance tests and their reliability steel needs to be tested.

Collaboration between CEA and In-LHC was started to evaluate the feasibility to accommodate the existing design of the oil pressure control servo-valve to a prototype running with water.

### 2004 ACTIVITIES

---

#### NEW CONSIDERATIONS DUE TO WATER USE

New interactions between hydraulic components and the fluid are to be considered when an oil-designed component has to be used with water.

The list below gives some of the main identified area of improvement: Corrosion, erosion, cavitation, scale deposit, temperature influence, pH influence, viscosity, bulk modulus, poor lubrication, and long lasting stops of the hydraulic system.

Materials of the servovalve are adapted to reduce the effect of corrosion.

A good balance must be found between materials providing good corrosion resistance but low hardness compared to that required in the main elements of the valve. Coatings are sometimes providing a good answer but surface roughness also play a major role in the development of corrosion. Reduction of the effects of water can be expected with modifications of the design. An improved design can reduce the effect of low viscosity, cavitation and casket corrosion. Modifications will focus on:

- Reduction of clearances.
- Avoid sudden section widening.
- Introduction of a sleeve in the valve body.

#### NUMERICAL MODELS OF THE SERVOVALVE

The Experimental feedback gained on operations with the oil version of the pressure control servo-valve developed for the Maestro manipulator can provide helpful information for the design of the water servo-valve. According to In-LHC's know-how, a 1D model of the oil version of the pressure control servo-valve was built in the AMESIM software. The two stages of the valve are described:

- The pilot stage with the torque motor, and the flapper nozzle assembly.
- The power stage composed of the spool and main body of the valve.

The model takes into account:

- The fluid properties:
  - . density,
  - . viscosity,
  - . bulk modulus
  - . ...
- The geometry of the valve:
  - . ports diameters,
  - . pressure losses,
  - . clearances,
  - . ...

Parameters of the model were fitted according to the experimental results of the oil servo-valve.

Fluid parameters were then modified to evaluate the behaviour of the water version.

Analysis of the 1D model provided information on the:

- Pressure gain
- Internal leaks
- Flow response for a given pressure step
- Dynamic response

After tuning, estimations of the servovalve behaviour is summarized in the figure 1 to figure 3.

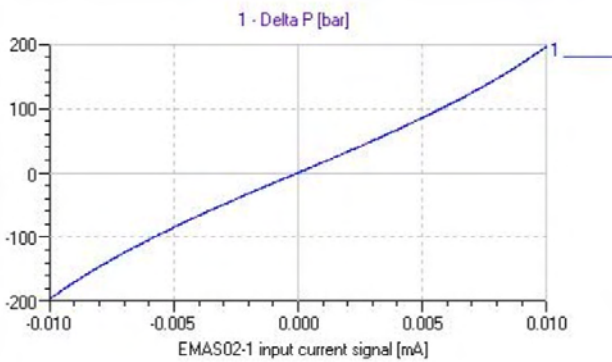


Figure 1 : Computed pressure gain of the water servovalve

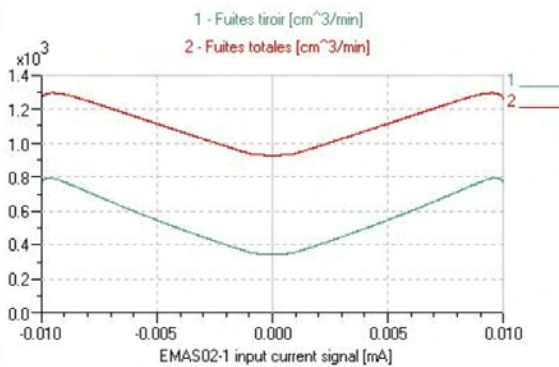


Figure 2 : Computed leaks of the water servovalve

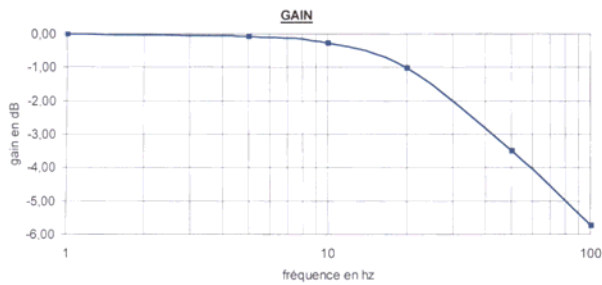


Figure 3 : Computed dynamic response

Compared to oil, the saturation pressure of water is very low and it is necessary to check that cavitation can not occur in local areas with high pressure drops. The ports and nozzle areas are considered to be zones with high cavitation risk. 3D flows can be modeled in the FloWorks software. A local model of the port area was built according to the dimensions and clearances defined with help of the 1D model. Due to symmetries in the system, simplification of the 3D architecture of the port area to a 2D plane model is possible. Representation of the model is detailed on figure 4.

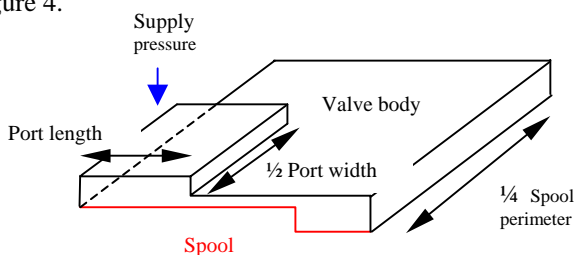


Figure 4 : FloWorks model for cavitation area

## CORROSION TESTS

Corrosion tests were performed on bushings, bodies and spools of servo-valves from the standard series.

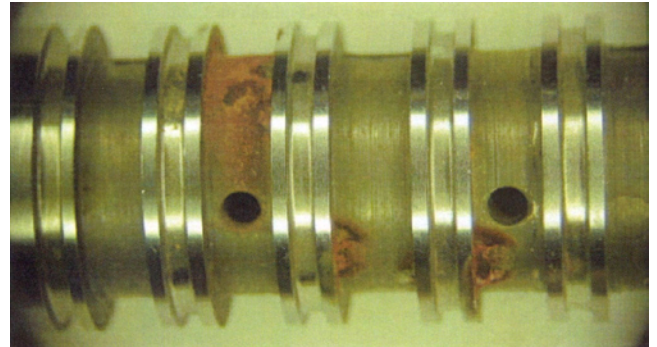


Figure 5 : Corrosion tests on standard servovalve bushing

The same material in different conditions has very distinct behaviours. It seems like for materials with good corrosion resistance, the result becomes more dependent to the properties of water than to the material itself.

## CONCLUSIONS

According to simulation results and corrosion tests, a new prototype of servo-valve was designed by the manufacturer In-LHC. Providing the fact that the conductivity of the water used in the hydraulic systems remains low and that a stabilization of the pH is made, this prototypes should provide performances suitable with robotics application. Manufacture and testing of this new product could be made during year 2005.

## REPORTS AND PUBLICATIONS

DTSI/SCRI/LPR/05RT003 - Preliminary study of a 'pressure control' water hydraulics servovalve.

DTSI/SCRI/LPR/05RT010 - Feasibility assessment of a 'pressure control' water hydraulics servovalve

## TASK LEADER

Jean-Pierre FRICONNEAU

DTSI/SCRI/LPR  
CEA-Fontenay aux Roses  
Boîte Postale 6  
F-92265 Fontenay aux Roses Cedex

Tél. : 33 1 46 54 89 66  
Fax : 33 1 46 54 75 80

E-mail : jean-pierre.friconneau@cea.fr

## UT-VIV/AM-Vacuum

---

# Task Title: TECHNOLOGIES FOR VACUUM AND TEMPERATURE AND MAGNETIC FIELD CONDITIONS FOR REMOTE HANDLING SYSTEMS

---

## INTRODUCTION

---

This project takes place within the framework of the Underlying Technology (UT) programme for Remote Handling (RH).

In-vessel Inspection devices are being studied and developed within the L7 Project to perform inspections inside the ITER vessel. They intend to perform an inspection operation under vacuum and temperature. Due to the requirements to operate the magnet system, inspection under magnetic field is being assessed.

The combination of severe conditions induces high limitations in the technology available. As an inspection device requires use of joints to operate properly in a reactor like ITER, a review of feasibility is required to assess this issue.

The maintenance work of the system involves handling for inspection purpose under the condition just after shutdown of the machine. In-Vessel conditions induce to sustain vacuum, high temperature, dose rate and high-level magnetic field

First phase of the work concerned the analysis of the requirements to perform a realistic operation inside the Vacuum Vessel (VV) conditioning with ultra high vacuum, temperature and magnetic field.

Work then focused on the analysis of the influence of the magnetic field on the components involved in the design of a remote handling system and reviewed the technologies available for these components.

Second phase of the work states for a detailed specification of a remote handling manipulator joint based on reasonably achievable techniques and the conceptual design of this joint.

## 2004 ACTIVITIES

---

### DETAILED SPECIFICATION OF A RH JOINT FOR VACUUM AND TEMPERATURE & MAGNETIC FIELD

The maintenance work of the system involves handling for inspection purpose under the condition just after shutdown of the machine.

In-vessel conditions induce to sustain vacuum, high temperature, dose rate and high-level magnetic field.

The most critical components require sustaining the following conditions:

- vacuum :  $10^{-7}$  Pa with pollution avoidance,
- 120 °C (including 240°C of baking temperature),
- magnetic field from 4 to 8 T.

The RH joint is considered as a base joint of a manipulator arm. It should fit with some performance requirements summarized as follow:

Payload: 20 kg.

Length in the VV: 5 meters.

Kinematics in the VV: 1 to some degrees of freedom.

Accuracy: 0.5 meter absolute accuracy, 0.05 meter repeatability and no vibration.

Speed: 1 meter/minute maximum.

The most constrained parts are those which are present in ITER VV, instead of those which could be located in a control room.

Then, study will be focused on technologies directly involved in the design of the in-vessel part of the robot.

Main required issues will be structure, actuators, position sensors, and data / energy transfer which should be fully compatible with ITER most severe constrains of vacuum, temperature, magnetic field and radiations.

### CONCEPTUAL DESIGN OF A RH JOINT FOR VACUUM AND TEMPERATURE & MAGNETIC FIELD

The selected technology for the actuator is water hydraulics which exists with rotary motors and cylinders.

The best solution is to use a linear actuator and amplify the effort by a lever effect as shown in figure 1.

From the performance requirements, we calculate the requirements of the cylinder. We obtain that the maximal value is about 29000 N for a total stroke of 283 mm. These performances can be obtained with a 63 mm diameter cylinder, the largest size in the standard catalogue.

The state of the art in the use of water hydraulics recommends keeping the pressure inside the circuit under 150 bars. Here, only 93 are required, so, the solution is valuable for standard conditions.

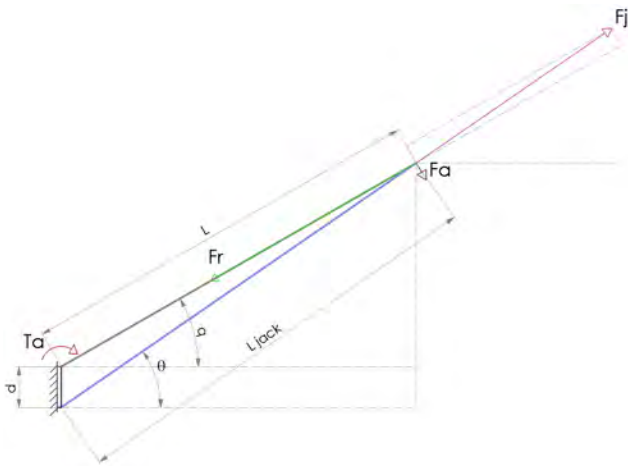


Figure 1 : Design of a RH joint with cylinder

With the precedent work, it has been demonstrated that the magnetic field have a very low incidence on the water hydraulic systems.

However, the existing technology cannot be used directly, it will be necessary to adapt a standard jack to the tokamak conditions. This upgrade mainly concerns material for the seals and the low pressure to avoid steam and cavitation in the circuit. In normal conditions, at 120°C the water is at a vapour state. But it is possible to maintain it liquid if we increase sufficiently the pressure inside the water circuit.

Indeed, it is impossible to control a hydraulic circuit if the fluid is in two phases at the same time and especially if the liquid water turns in steam. We can estimate the minimal pressure with the phase diagram of water.

With a pressure greater than 2 bars for the temperature of 120°C, and 16 bars for 200°C, the storage temperature, water is liquid. Then it is possible to use a water circuit with an offset of pressure in the output circuit.

An other way to avoid the temperature constrain could be to cool the body of the jack in order to keep a reasonable pressure in the hydraulic circuit.

It could be possible with a secondary water hydraulic circuit dedicated to the control of temperature.

The usable materials for the design have been identified in the first phase of the studies with the associated consequences due to the magnetic field.

For the design of the seals, we could also add the PEEK and the Vespel to the list because they have been validated for temperature and vacuum.

So, with quite standards seals, it could be possible to work under the thermal sollicitation.

One other problem is that the stem of the jack must always be lubricated, but it implies that the sealing of the jack's body will not be efficient to answer to the need of low degasification in vacuum atmosphere.

So it will be necessary to close this part inside bellows as shown on figure 2.

This kind of design could be a solution of a water hydraulic cylinder for supporting the constraints of high vacuum, temperature and magnetic field.

At least, there is no standard solution for the need. It will be necessary to joint different elements of the water hydraulic industry and joint them into a suitable proposition.

For now, there is no significant and blocking point in the study, but it will be necessary to test and validate some sub-assemblies to ensure a secure answer.

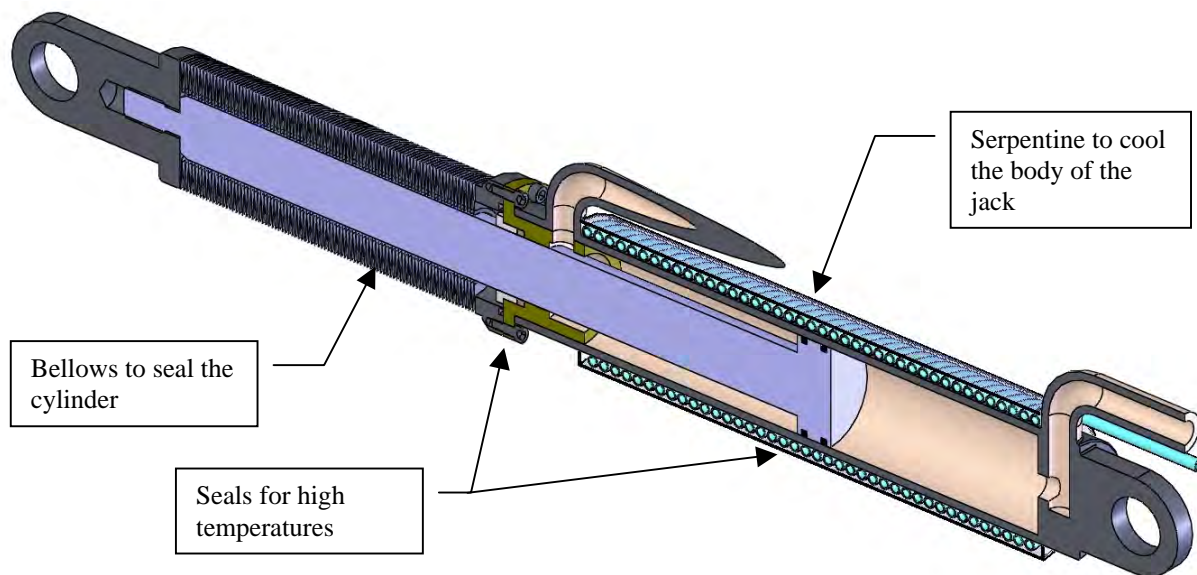


Figure 2 : Design of an adapted water hydraulic cylinder

## CONCLUSIONS

---

The combination of severe conditions induces high limitations in the technology available. The present study proposes a detailed specification of a remote handling manipulator joint based on reasonably achievable techniques and then describes the conceptual design of this joint.

Water hydraulics appears the best candidates to provide high forces and torques under magnetic field conditions.

A lot of points remain to be assessed, specially to address a full robot design with full operating conditions constrains (vacuum, temperature) and to try to estimate the level of performance such a system can reach.

## REFERENCES

---

European Fusion Technology Programme - Task UT-VIV/AM-Vacuum "Technologies for vacuum and temperature and magnetic field conditions for remote handling systems" june 17<sup>th</sup> 2002.

## PUBLICATIONS

---

Report DTSI/SRSI/LPR 04RT 097 UT-VIV/AM-Vacuum, "specification and conceptual design of a manipulator joint for remote handling under vaccum, temperature and magnetic field".

## TASK LEADER

---

Jean-Pierre FRICONNEAU

DRT/LIST/DTSI/SRSI  
CEA-Fontenay aux Roses  
Boîte Postale 6  
F-92265 Fontenay aux Roses Cedex

Tél. : 33 1 46 54 89 66

Fax : 33 1 46 54 75 80

E-mail : jean.pierre.friconneau@cea.fr



**Task Title: HELIUM COMPONENTS TECHNOLOGY PROBLEMS AND OUTLINE OF SOLUTIONS**

**INTRODUCTION**

A review of problems related to helium technology, and a proposal of studies and experiments had been done in the previous year (2003).

Four subjects have been addressed in 2004.

First, the leaks of helium and of tritium have to be evaluated, for a typical design, in order to know which points must be improved, and/or which mitigation systems must be designed, in order to reduce tritium release to admissible values. The task was, in 2004, to evaluate leaks other than by permeation, this aspect being dealt with by CEA/DEN/DM2S, in 2004.

Second, tribological materials must be identified, and tested. In 2004, experiments on several of them have been done.

Third, the leak tightness of commercial or prototype static seals must be tested. A bench called HETIQ (figures 1 and 2) has been built, for this. It has been commissioned in 2004.

Fourth, the pipe containing helium from the divertor will convey a gas at about 740°C, 9.65 MPa.

A technological solution deduced from helium cooled fission reactors might consist in protecting the pressure vessel by an Inner Thermal Barrier (ITB). A mock-up called HETHIMO (figures 3 and 4) has been commissioned in 2004, in order to test several designs of ITBs.

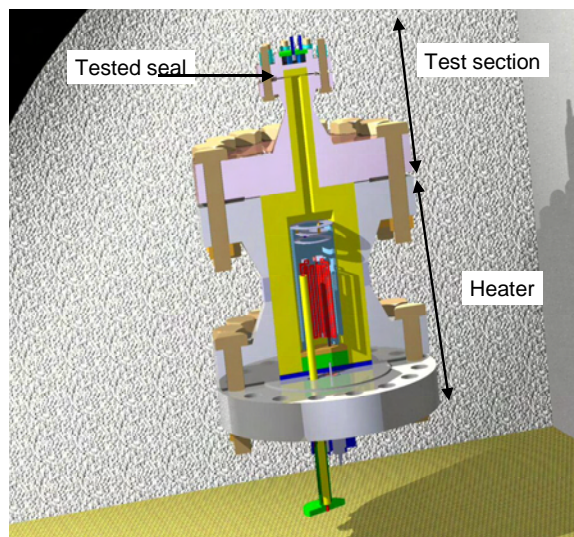


Figure 1 : HETIQ / principle

**2004 ACTIVITIES**

The helium leak flow of blanket cooling circuits of a 1500 MWe PPCS has been evaluated, for all leaks but those by permeation. Since rotating seals lead either to high leak flows, or to complicated circuit designs, it was assumed that these seals will be eliminated by using immersed electric motors. For other elementary leak sources, elementary data from fission reactors were extrapolated. The following table gives the detail of the leak flows. It leads to a global leak of 0.4 Nm<sup>3</sup> per hour, which is equivalent to a loss of 2% of the total inventory per year.

Recapitulation of helium losses of PPCS BKT and DV cooling circuits, other than by permeation

|                                     | Total leaks in m <sup>3</sup> /h at Normal conditions      | Comments  | Possibility of reduction                                    |
|-------------------------------------|--|---|---|
| Static seals                        | 9.72 x 10 <sup>-6</sup>                                    |   | Yes (welding)   |
| Rotating seals                      | 0  | Electric motors immersed in helium                                    |   |
| Steam generator                     | ε  | Depends on the detection capability of measurements in the water side |   |
| Maintenance operations              | 0.24   |   | Yes (lower the pressure to a fraction of p <sub>atm</sub> ) |
| Isolating components                | 0.19   |   |   |
| Purification & inventory management | 0  | Cost of 0 leak to be evaluated  | No : can only increase                                      |
| <b>Total</b>                        | <b>0.4 Nm<sup>3</sup>/h</b><br>2 x 10 <sup>-2</sup> inv./y |   |   |



Figure 2 : HETHIMO / photograph

The experience of past gas cooled fission reactors shows that leak flows have often been severely underestimated at the draft stage (by a factor 5 at DRAGON, and 20 at Fort-St-Vrain), which shows that great care must be taken for all potential leak sources.

The helium TRIBOMETER allows experiments at temperatures up to 1000°C, with controlled impurity content.

The first tests in 2004 have shown that friction materials have difficulties to go beyond 800°C, for instance with zirconia with contact pressures of 2 MPa.

This is disappointing, when compared with the performances seen in the literature, showing tests performed on zirconia at 950°C and 5 MPa of contact pressure without excessive damages. Nevertheless, this leaves some hope even for the higher DV helium temperatures (720°C or 740°C), but with a moderate margin.

The leak tightness bench, called HETIQ (Helium TIGHTness Qualification) and the Inner thermal Barrier Bench, called HETHIMO (Helium THERmal Insulation Qualification) have been commissioned this year.

They were tested at 1000°C, 5 bars and at 20°C, 100 bars, but not at both 1000° and 100 bars. The outer wall of the pressure vessel is at about 100°C, when helium is at 1000°C, 10 bars.

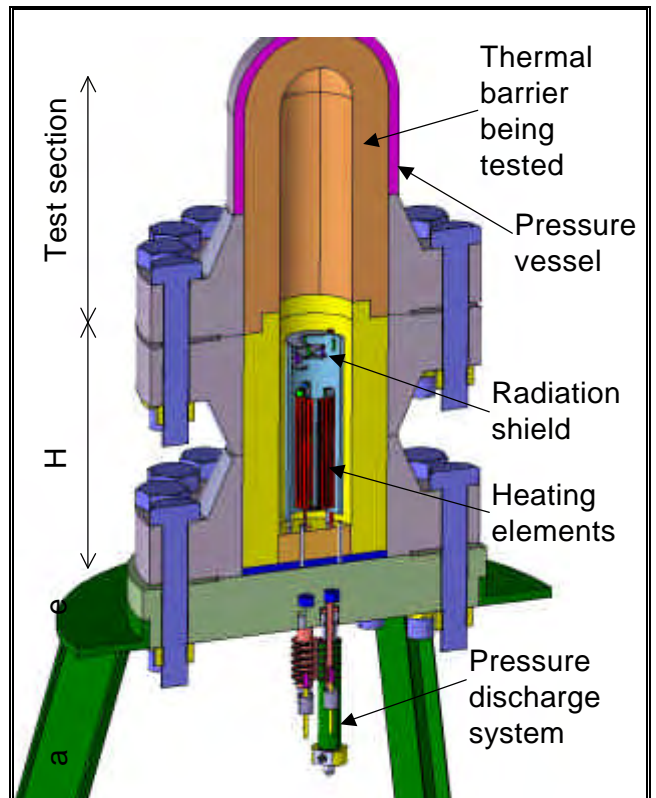


Figure 3 : HETHIMO / principle



Figure 4 : HETHIMO / photograph

After a few temperature cycles, two problems occurred:

- 1) Cracks several centimetres long were found in the thermal barrier of the heating section, which was made of a solid material.
- 2) The composite graphite resistor was oxidised, to a point where it was broken.

Solutions have been found, namely, the thermal barrier is now ceramic felt, maintained by a Ni base alloy liner, and a new start-up procedure is applied, in order to avoid burning the graphite resistor. If necessary, the resistor would be changed for new materials like MoSi<sub>2</sub>, or SiC, for example.

## CONCLUSIONS

---

It seems possible to limit the leaks of the PPCs, other than permeation, to about 0.4 Nm<sup>3</sup>/h, provided that great care be taken for the design and realization of the circuits. This assumes also that immersed rotors be used.

Candidate materials have been found for friction parts in helium. Fortunately, the higher temperatures in the PPCS are lower than 720°C or 740°C, which is lower than the limit of use of friction materials which were tested. This limit seems to be 800°C, according to the provisory results obtained.

The benches for seal tests and for internal thermal barriers tests have been commissioned, and youth problems are hopefully solved. Experiments should give first results during year 2005.

## REPORTS AND PUBLICATIONS

---

- [1] J.L. Berton - Helium and tritium leaks in the PPCs BKT & DV cooling circuits - CEA Report NT DEN/DTN/STPA/LTCG/04/032, august 2004.
- [2] J.L. Berton - Report of experiments on static benches - CEA report NT DEN/DTN/STPA/LTCG/04/069, december 2004.

## TASK LEADER

---

Jean-Luc BERTON

DTN/STPA/LTCG  
CEA-Cadarache  
F-13108 Saint-Paul-Lez-Durance Cedex

Tél. : 33 4 42 25 77 93  
Fax : 33 4 42 25 66 38

E-mail : jean-luc.berton@cea.fr



## Task Title: DEVELOPMENT OF NEW RAFM STEELS WITH REGARD TO CREEP PROPERTIES

### INTRODUCTION

Martensitic 8-12Cr steels, because of their excellent dimensional stability under irradiation, are being developed as candidate materials for structures subjected to a significant neutron flux at high temperature and under stress. Certain of the elements used to confer good high-temperature properties on martensitic steels for conventional power generation, such as Mo, Nb and Co, must be forbidden in nuclear applications because of their high radiological impact or transmutation to undesirable products under irradiation. Existing reduced-activation (RA) steels have only moderate creep resistance at high temperatures, so there is interest in improving this by means of compositional modification.

With this aim, three new compositions were proposed with the aid of thermodynamic and statistical modelling as well as information from the literature. Strengthening is achieved by means of MX carbonitrides such as vanadium nitride (VN) or titanium carbide (TiC) which stabilise the dislocation network, coupled with tungsten to provide solid-solution strengthening [1]. The compositions are detailed in table 1.

Table 1 : Compositions of designed alloys V1, V2 and Ti1, in wt. %

|     | C    | N     | Cr | W   | V    | Ti  |
|-----|------|-------|----|-----|------|-----|
| V1  | 0.1  | 0.085 | 9  | 1.5 | 0.32 |     |
| V2  | 0.1  | 0.07  | 8  | 2.5 | 0.35 |     |
| Ti1 | 0.05 |       | 8  | 1   |      | 0.2 |

Ingots of alloys V1, V2 and Ti1 were fabricated by Aubert et Duval. Ti1 did not present any problems but macroscopic porosity was observed in V1 and V2.

The thermodynamic modelling software Thermo-Calc was used to compare phase stabilities at equilibrium in the V1 and V2 with those in other, successfully fabricated alloys of similar composition (notably a high nitrogen content) [2]. Porosity was found to occur only in alloys which had a temperature range for which high-temperature (delta) ferrite and nitrogen gas were the only stable phases. The existence of such a domain can therefore be taken as an indication that porosity problems may occur. Phase stability calculations showed that the domain was expanded by elements known to be ferrite-stabilisers, and contracted by austenite-stabilisers. This information should facilitate compositional modifications to avoid porosity while maintaining the desired mechanical properties.

### 2004 ACTIVITIES

#### VANADIUM-RICH STEELS: MODIFIED COMPOSITIONS

The thermodynamic analysis indicated that it may be possible to avoid porosity by eliminating the phase domain in which only delta-ferrite and gas are stable. Reduction of the size of this domain can be achieved by decreasing the tungsten content, increasing the carbon content, or adding manganese or nickel. As lowering the amount of tungsten would reduce the solid-solution strengthening effect, and manganese and nickel are believed to reduce the creep strength, these options were rejected. The addition of carbon favours the formation of  $M_{23}C_6$  phase, which is chromium-rich and removes chromium from the matrix. Hence, an increase in the carbon content must be balanced by an increase in chromium to maintain the resistance to oxidation provided by chromium in solid solution.

#### 1. High-nitrogen, high-carbon steel

The first modified composition suggested was chosen on the basis of thermodynamic calculations using Thermo-Calc, aiming firstly to maximise the amount of vanadium nitride precipitated, secondly to ensure that the dissolution temperature of this phase is below that of the onset of formation of the brittle delta-ferrite phase, and thirdly to avoid the region believed to be associated with porosity. After determination of suitable composition ranges, predictions of the creep rupture strength were obtained using the neural network model originally used in [1] and minor adjustments to the composition made based on this.

A casting of this alloy was made without any problems of porosity being noted. However, after forging, cracks were found to be present.

#### 2. Boron-strengthened alloy

One of the promising methods found in recent literature for the improvement of creep properties is the addition of a small amount of boron, which dissolves into  $M_{23}C_6$  and reduces its coarsening rate (e.g. [3]).

Two isotopes of boron, B-10 and B-11, are found in nature, and B-10 predominates. However, under irradiation, this isotope transmutes to helium, so it is unsuitable for use as in steels for nuclear applications. B-11, however, does not behave in this way.

Contact was made with Eagle-Picher, Ltd., a company supplying isotopically separated boron products, and a suitable amount of B-11 was obtained in the form of iron boride to facilitate addition to the melt.

The new boron-strengthened alloy also contains vanadium nitride, but the nitrogen content is set lower than that of the original V1 and V2, because of concerns about the formation of boron nitride and also to avoid any possible porosity evolution.

This alloy has been fabricated successfully. Normalised and normalised-tempered samples have been obtained and can now be characterized metallographically and tested.

**CHARACTERIZATION OF TITANIUM-STRENGTHENED ALLOY**

Characterization of the titanium-containing alloy Ti1 has been started. Metallographic examination showed a typical lath martensite microstructure after normalisation (1200°C, 30 min, oil quench). The austenite grains were rather large and there were some second-phase particles present after quenching. These were determined by EDX to be titanium-rich, so can be considered to be titanium carbonitrides. After tempering (720°C, 10 hours) the hardness compared favourably with that of existing 9Cr-type alloys such as T91.

A study of the phase transformations in this alloy using dilatometry and calorimetry showed that the martensite-start temperature ( $M_s$ ) increased with decreasing cooling rate from the austenitisation temperature. This indicates that the carbon content in solution is reduced in the case of a slower quench; this could be due either to decarburisation or to carbide precipitation.

Decarburisation was indeed observed in certain samples, but even in those where it was not seen, the  $M_s$  temperature depended on the cooling rate. It could therefore be concluded that the kinetics of carbide formation were extremely rapid, and at least part of the precipitation took place during the quench. This is in agreement with the observation that titanium carbide particles were present even in the austenitised and quenched sample of Ti1.

Models of the dependence of  $M_s$  on the alloying element content of the matrix were used to determine whether this effect could indeed be explained by the precipitation of TiC. These were compared with measurements of thermoelectric power, which is sensitive to variations in matrix carbon content [4]. The agreement between model and experiment was not particularly good, possibly because the models do not take account of the effect of titanium on the  $M_s$  temperature.

The critical cooling rate for the avoidance of ferrite formation is relatively high in this alloy, which may restrict its utility for thick-section applications.

In order to optimise the heat treatment to provide a fine, stable and homogeneous distribution of TiC particles, a number of experimental heat treatments have been carried out and the characterization of the particle distribution in these samples is under way. Concurrently, modelling of the precipitation kinetics is being undertaken using a new piece of software available from the University of Graz, Austria.

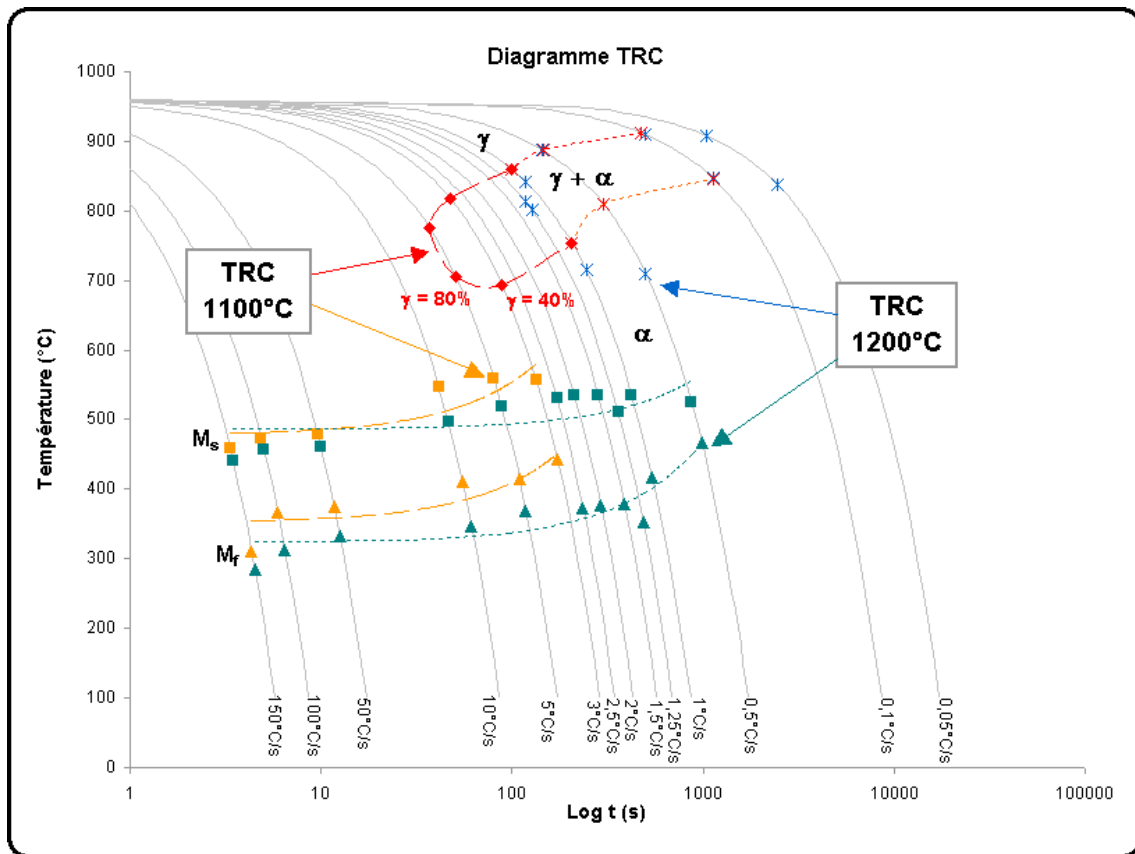


Figure 1 : Continuous Cooling Transformation diagram showing the increase in martensite-start ( $M_s$ ) temperature with decreasing cooling rate and the critical cooling rate to avoid ferrite formation. Points marked as asterisks rather than solid markers indicate samples in which decarburisation was observed

## REFERENCES

---

- [3] F. Abe, T. Horiuchi, M. Taneike, K. Sawada - Improvement of Creep Strength by Boron and Nano-Sized Nitrides for Tempered Martensitic 9Cr-3W-3Co-VNb Steel at 650°C - Parsons 2003 : Engineering Issues in Turbine Machinery, Power Plant and Renewables - Proceedings of the Sixth International Charles Parsons Turbine Conference - 16-18 september 2003, Trinity College Dublin, Ireland, ed. A. Strang et al., p. 379-396.
- [4] J.C. Brachet - Correlation between thermoelectric power (TEP) and martensite start temperature (Ms) measurements of 9Cr-W-V-(Ta) martensitic steels - Journal de Physique IV, supplément au Journal de Physique III, Volume 5 (1995).

## REPORTS AND PUBLICATIONS

---

- [1] Y. de Carlan - Conception de nouveaux alliages ferritiques-martensitiques à activation réduite optimisés pour la résistance au fluage - Final Report UT-TBM/MAT-LAM/DES - CEA report, NT SRMA 03-2526, february 2003.
- [2] V.A. Yardley - Progress in Fabrication of Experimental 9Cr Steel Compositions Optimised for Creep Resistance, Proposed Solutions - CEA report, DMN/SRMA/LA2M/NT/04-2642/A.

V.A. Yardley, Y. de Carlan - Design Criteria for High-Temperature Steels Strengthened with Vanadium Nitride - submitted to special issue 'User Aspects of Phase Diagrams' of Journal of Phase Equilibria and Diffusion.

## TASK LEADER

---

Yann de CARLAN

DEN/DMN/SRMA  
CEA-Saclay  
F-91191 Gif-sur-Yvette Cedex

Tél. : 33 1 69 08 61 75  
Fax : 33 1 69 08 71 30

E-mail: [yann.decarlan@cea.fr](mailto:yann.decarlan@cea.fr)



**Task Title: PULSED IRRADIATION OF THE MARTENSITIC ALLOY EUROFER**  
**Irradiations by krypton ions at 350 and 550°C at high flux during short time**

**INTRODUCTION**

In the framework of the study of irradiation microstructures in ferritic stainless steel, the purpose is to investigate the secondary defects distribution to test the influence of the flux mode. Three modes are experimented at the same damage (3 dpa), two during the same time: cyclic (pulsed), continuous, and the third is a short time. The results in Eurofer are compared to irradiation in a model alloy.

**2004 ACTIVITIES**

**MATERIAL AND IRRADIATION CONDITIONS**

The Eurofer97 (table 1) is delivered by SRMA (A. Alamo), [1].

*Table 1 : Chemical composition of Eurofer97*

| element | weight percent |
|---------|----------------|
| C       | 0.12           |
| Cr      | 8.96           |
| W       | 1.04           |
| Ta      | 0.15           |
| V       | 0.18           |
| Mn      | 0.48           |
| Si      | 0.03           |
| Ni      | 0.06           |
| N       | 0.022          |
| Nb      | <0.002         |

The model ferritic alloy (Fe/9% w. Cr) is elaborated at the SRMP by high frequency heating of high purity Fe (99.999 %) and Cr (99.99 %).

In the Eurofer, the microstructure is very similar from one foil to the other. It consists in laths containing a high density of dislocations. The model alloy is fully ferritic and only scarce dislocation lines are visible at the microscope scale. The Irradiations are performed in the Van de Graaff accelerator of the SRMP (table 2). The sample are irradiated as disks for transmission electron microscope holders (diameter: 3 mm) extracted from the foil by punching. Then, they are thinned in a double jet device (Tenupol 2 from STRUERS).

*Table 2 : Irradiation conditions aimed*

|         |   |
|---------|---|
| ion     | Kr <sup>++</sup>                            |
| Energy  | 700 keV                                     |
| Damage  | 3 dpa                                       |
| Fluence | 9.64.10 <sup>14</sup> ions.cm <sup>-2</sup> |
| Time    | 18 mn                                       |
| dpa/s   | 2.8.10 <sup>-3</sup>                        |

**IRRADIATION MICROSTRUCTURE**

**Irradiation at 350°C**

In Eurofer, the lath microstructure and the dislocation network does not show evolution after the irradiation. Between the lines, despite a fine investigation, no clusters have been detected.

Controversially, the model alloy show a homogeneous distribution of small loops visible as black dots.

Moreover, some dislocation lines show a climb configuration attributed to the absorption of point defects (figure 1).

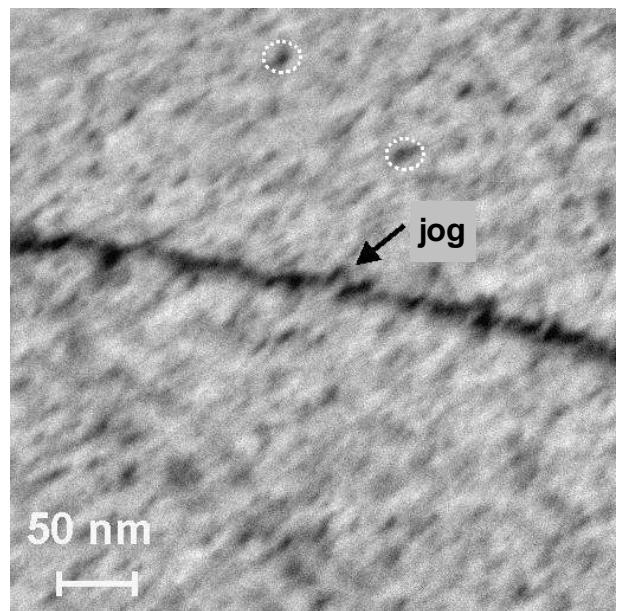


*Figure 1 : Model alloy irradiated at 350°C*

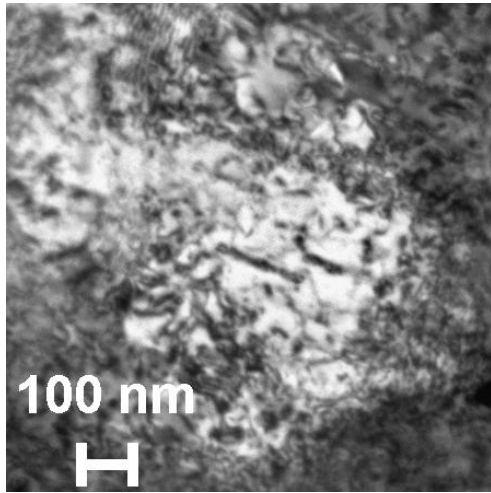


Figure 2 : Eurofer irradiated at 550°C

### Irradiation at 550°C

At this temperature, in the Eurofer, the observation inside laths becomes difficult because the total number of dislocation lines has increased. This comes from two origins. First, it seems that the density of the dislocation network has increased (likely by climb), secondly, large clusters located in {100} plane are present (figure 2) as large dislocation loops (> 80 nm).

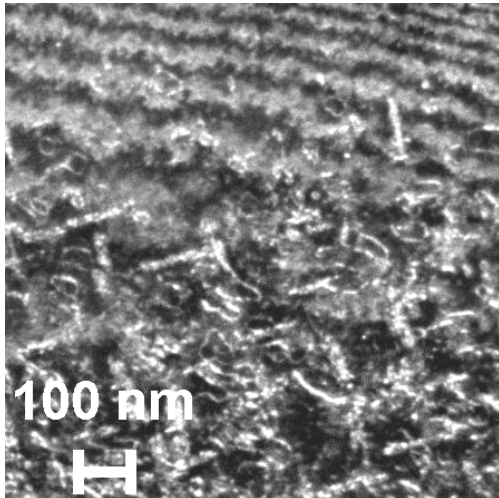


Figure 3 : Model alloy irradiated at 550°C :  
loops edge on

In the model alloy, the initial microstructure makes it easy to detect the loops that are homogeneously distributed. They are similar to the one present in the Eurofer (figure 3).

The shape of loops can be clearly observed and reveals indentation along the line limiting the loop (figure 4). Some smaller loops with straight dislocation lines are visible close the foil edge.

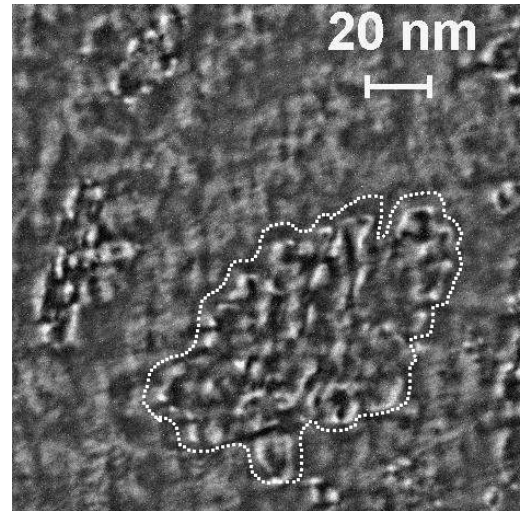


Figure 4 : Model alloy irradiated at 550°C :  
loops tilted showing indentations

### POST IRRADIATION ANNEALING

The annealing has been performed inside the transmission electron microscope by use of a GATAN double tilt holder.

We realized isochronal annealing that consists in heating at various temperatures and then come back to room temperature to make a fine observation of the eventual evolution.

In the Eurofer, the evolution begins at 550°C. At that temperature resolved loops are presents. The same evolution is present in the model alloy but at lower temperature (450°C).

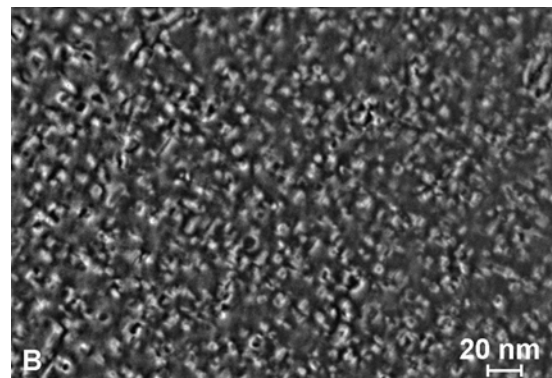
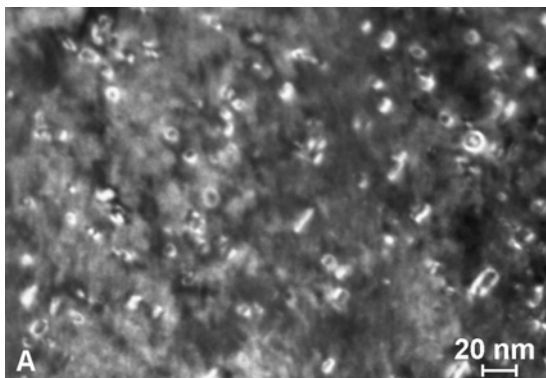


Figure 5 : Dislocation loops in the Eurofer after irradiation and annealing at 550°C, G = 250 k  
A : thin region, B : thick region (3 times thicker)

The figure 5 shows the loops in a thin region and in a close other one, 3 times thicker. The distribution of sizes is equivalent in the two regions; the density is different. This excludes a spurious effect as injection of vacancies from weak oxidation of the surfaces. More precisely, as the surface is similar for the two regions, an injection of defects (vacancies) from the surface would lead to larger clusters in the thin region.

## CONCLUSIONS

---

The irradiations at 350°C and 550°C have been performed at high flux and short time. In the Eurofer, no secondary defects are present at the lowest temperature. At 550°C, large loops in {100} plans are present showing a flower like shape.

A post irradiation annealing at 550°C, induces the condensation into large loops of the defects (individual or as clusters) that have been accumulated during the irradiation.

The model alloy shows roughly the same behaviour. The migration of species is faster because, after irradiation at 350°C, loops are present and their growth occurs at a lower temperature, 450°C instead of 550°C for Eurofer. The lack of defects in Eurofer is in agreement with slower species.

The perspectives are to determine the nature of loops in all cases and the Burgers vectors after annealing.

## REFERENCES

---

- [1] Metallurgical characterization of as-received Eurofer97 products - C. A. Danon, S. Urvoy, A. Alamo - CEA report, NT SRMA 01-2418, March 2001.

## REPORTS AND PUBLICATION

---

Preparation of Eurofer samples for pulsed irradiations - L. Boulanger and Y. Serruys - CEA report, NT DEN/SAC/DMN/SRMP 2004-01.

Monotonous short time irradiation of Eurofer at 350 and 550°C - L. Boulanger and Y. Serruys - CEA report, NT DEN/SAC/DMN/SRMP 2004-012.

Annealing of Eurofer irradiated at 350°C - L. Boulanger and Y. Serruys - CEA report, NT DEN/SAC/DMN/SRMP 2004-to be issued.

## TASK LEADER

---

Loic BOULANGER

DEN/DMN/SRMP  
CEA-Saclay  
F-91191 Gif-sur-Yvette Cedex

Tél. : 33 1 69 08 64 19

Fax : 33 1 69 08 68 67

E-mail : loic.boulanger@cea.fr



**Task Title: LASER DECONTAMINATION/TRITIUM REMOVAL**  
**Modelling of lasers surface heating**

**INTRODUCTION**

Laser surface cleaning and decontamination is seen very promising for nuclear technology and industry. The controllable-in-depth laser heating of thermonuclear reactor surface can remove tritium from the wall with a co-deposited layer without wall surface destruction. Tritium removal may be realized either by laser ablation of a co-deposited layer or by its sufficient heating resulting in tritium release.

The surface temperature depends on laser parameters (power, wavelength, focusing, pulse duration) and on thermo-physical properties (specific heat, thermoconductivity, coefficients of reflection and absorption of laser radiation and so on) of both the co-deposited layer and the substrate. It also depends on the layer/substrate interface properties. Generally, the cleaned surface comprises a micrometric (1 – 1000 μm thickness) layer deposited on a substrate with different thermo-physical and optical properties.

To control laser decontamination, it seems useful to develop a model to evaluate the surface temperature under different conditions. This model development was the aim of our studies. The model can allow to find the optimal conditions of the surface cleaning and to explain some particular properties of the laser heating of the surface with a co-deposited layer.

**2004 ACTIVITIES**

For laser heating, the calculations of the surface temperature are generally associated with solution of a complex nonlinear thermo-physical problem involving the temperature dependence of thermo-physical and optical properties of the surface substances [1-3]. In general, with a moving laser beam, it can be made only by direct space-time (3+1 dimensional) numerical simulations by finite-difference methods. The complete system of the heat equations (in the cylindrical coordinates) to describe the temperature distribution  $T(r, z, t)$  over space and time is the following:

$$c_l(T) \frac{\partial T}{\partial t} = k_l(T) \left( \frac{\partial^2 T}{\partial z^2} + \frac{\partial^2 T}{\partial r^2} + \frac{1}{r} \frac{\partial T}{\partial r} \right) + \frac{dk_l(T)}{dT} \left( \left( \frac{\partial T}{\partial z} \right)^2 + \left( \frac{\partial T}{\partial r} \right)^2 \right) + Q_l(t, r, z) \tag{1a}$$

$$c_s(T) \frac{\partial T}{\partial t} = k_s(T) \left( \frac{\partial^2 T}{\partial z^2} + \frac{\partial^2 T}{\partial r^2} + \frac{1}{r} \frac{\partial T}{\partial r} \right) + \frac{dk_s(T)}{dT} \left( \left( \frac{\partial T}{\partial z} \right)^2 + \left( \frac{\partial T}{\partial r} \right)^2 \right) + Q_s(t, r, z) \tag{1b}$$

Equation (1a) corresponds to the co-deposited layer ( $0 < z < d$ ) with thickness  $d$ . Equation (1b) corresponds to substrate ( $z > d$ ). The laser energy that is released into the layer and the substrate can be presented as follows:

$$Q_l(t, r, z) = A_l \alpha_l I(r, t) \{ \exp(-\alpha_l z) + R_s \exp[\alpha_l(z - 2d)] \}, \tag{2a}$$

$$Q_s(t, r, z) = A_l A_s \alpha_s I(r, t) \exp[-\alpha_s(z - d) - \alpha_l d], \tag{2b}$$

where  $I(r, t)$  is radial ( $r$ ) distribution of time-dependent ( $t$ ) laser intensity at  $z = 0$ ,  $A_l$  is the transmittance of the layer surface at  $z = 0$ ,  $\alpha_l$  is the layer absorption coefficient,  $A_s$  is transmittance on the boundary between the layer and substrate at  $z = d$ ,  $\alpha_s$  is substrate absorption coefficient. The set of equations (1a) and (1b) is solved with the boundary conditions:

$$-k_l(T) \frac{\partial T(t, r, z)}{\partial z} \Big|_{z=d-0} = -k_s(T) \frac{\partial T(t, r, z)}{\partial z} \Big|_{z=d+0}, \tag{3a}$$

$$T(t, r, z = d - 0) = T(t, r, z = d + 0), \tag{3b}$$

$$\frac{\partial T(t, r, z)}{\partial z} \Big|_{z=0} = 0 \tag{3c}$$

The boundary conditions (3a) and (3b) correspond to a perfect thermal contact on the layer/substrate interface. For a poor heat contact, the condition (3a) should be replaced by condition:

$$-k_l(T) \frac{\partial T(t, r, z)}{\partial z} \Big|_{z=d-0} = 0. \tag{3d}$$

Different spatio-temporal regimes of laser radiation are considered in the source terms  $I(r, t)$  (either continuous or pulsed laser radiation). The spatial distribution of the focused laser radiation can be either Gaussian or homogeneous flat-top.

The case of temperature-independent values of the thermo-physical and optical parameters of the layer and the substrate was considered. The «analytical solution» of the linear laser heating was obtained, analyzed, and used for the relatively fast simulations of laser heating on a long space-time scale with the developed MATLAB-code (our annual report).

Some of the theoretical results obtained are presented on figure 1 and figure 2.

Figure 1 presents the results for 100 ns laser pulses (10 kHz repetition rate) and pure graphite heating by homogeneous or Gaussian laser beam of  $2r_0 = 1$  mm diameter.

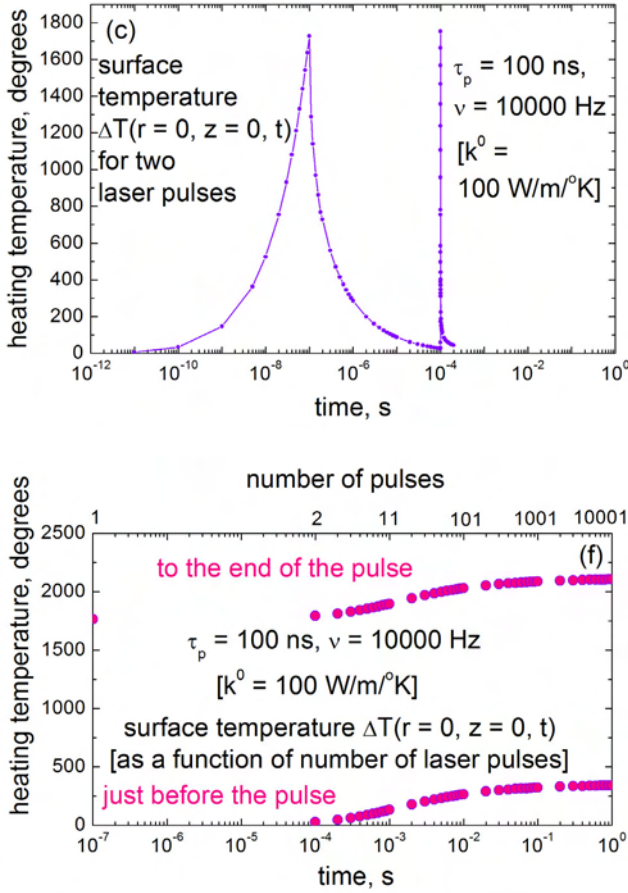


Figure 1 : The temperature of the surface of technical graphite (with  $k^0 = 100 \text{ W/m}^2\text{K}$ ) by laser radiation with repeating pulses ( $F = 1 \text{ J/cm}^2$ ,  $2r_0 = 1$  mm)

Given that the graphite sublimation temperature is  $\approx 3900^\circ\text{C}$  and defining the graphite ablation threshold as the laser fluence that is required to reach the graphite sublimation, the ablation threshold for 100 ns pulses can be estimated as  $F_{\text{thresh}} \approx 2.2 \text{ J/cm}^2$ . The calculated ablation threshold was compared with the experimental one ( $2.5 \text{ J/cm}^2$  for 100 ns laser pulses at 10000 Hz repetition rate [4]) and demonstrated good agreement.

Figure 2 presents the temperature depth dependence for graphite with a co-deposited layer of 100  $\mu\text{m}$  thickness at different moments (just after 1<sup>st</sup>, 101<sup>st</sup>, and 1001<sup>st</sup> pulse).

The results obtained with constant thermo-physical parameters and the simulation results of nonlinear laser heating with temperature-dependent parameters were compared.

The comparison justified the “analytical” model with constant thermo-physical and optical parameters.

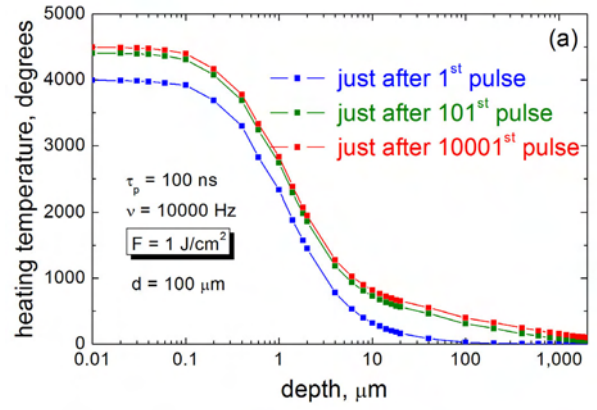


Figure 2 : The temperature depth distributions at different times for graphite with a co-deposited layer of thickness  $d = 100 \mu\text{m}$  ( $\tau_p = 100$  ns,  $F = 1 \text{ J/cm}^2$ ,  $2r_0 = 1$  mm, 10 kHz repetition rate laser)

## CONCLUSIONS

A model for the laser heating of complex surfaces with a layer (1 – 1000  $\mu\text{m}$ ) of different substances on a substrate was developed. Much attention was paid to a three-dimensional “analytical” model with constant optical and thermo-physical parameters to determine the heating temperature on a large space-time scale. On the basis of the developed analytical model, a computing MATLAB code was written to calculate a surface heating temperature under different conditions.

The simulations were made for the laser heating of graphite surfaces without and with a co-deposited layer. Only two adjustable parameters (porosity and thermal conductivity) for normal technical graphite and for the co-deposited layer were used in the calculations.

Different heating regimes with a pulse laser radiation (5 ns – 50 ns pulse duration and 20 – 10000 Hz pulse repetition rate) and a cw laser were considered. For different regimes of laser heating, the ablation thresholds were estimated on the basis of the results obtained. For a normal graphite surface for 5 ns and 100 ns laser pulses, the estimated ablation thresholds were found in agreement with the experimental results.

For the high repetition rate lasers (10000 Hz), the heat energy accumulation from pulse to pulse was investigated. During the heating, the laser beam was either immobile or could move along the surface. The calculations with the moving laser spot on the surface at different velocities of the laser scanning can estimate the effective number of laser shots on a given place of the surface. Different temporal and spatial distributions of laser radiation on the surface were implemented in the code.

For graphite surface with a co-deposited layer, the dependences of the surface heating temperature on the layer thickness were calculated for different regimes of laser heating (for cw laser radiation and for pulsed lasers).

Two limiting cases of the heat contact between the friable co-deposited layer and the graphite substrate were considered. For the perfect heat contact between the layer and the substrate, the ablation threshold for the layer thickness  $> 10 \mu\text{m}$  can be evaluated as two times lower than for the normal technical graphite surface. With the decrease in a layer thickness, the heating temperature decreases and tends to be the same as for the normal graphite surface. For a poor heat contact between the layer and the substrate, the ablation threshold will be very low. In this case, the heating temperature increases considerably with the decrease in a layer thickness.

To validate the calculations based on the mean constant temperature-independent graphite properties, the known temperature dependences of the thermo-physical parameters of graphite are considered in the direct numerical solution of heat equations. The corresponding calculation code was written on Dufort-Frankel algorithm [5]. The test simulations of nonlinear laser heating were compared with the results obtained with constant mean thermo-physical parameters. The results justify the "analytical" model of laser heating with the mean constant thermo-physical and optical parameters. It can be applied for both qualitative and quantitative estimations of the surface temperature during the laser heating of complex surfaces.

Thus, the developed code allows to simulate the laser heating of the graphite surface without and with a co-deposited layer. It may also be applied to study the laser heating of any other surface with different properties. The code can be easily generalized by involving the diffusive scattering of the laser light in turbid media, for example. In this case, it would be required to change just some parameters in the laser heating source terms.

The developed model will be applied to choose the relevant validation experiments. The experiments are planned to be made with the Pyrometer method that is under development in our Laboratory (CEA Saclay, DEN/DPC/SCP/LILM).

## REFERENCES

---

- [1] H. S. Carslaw and J. C. Jaeger - Conduction of Heat in Solids - 2<sup>nd</sup> edition (Oxford, Oxford University Press, 1959).
- [2] S. V. Fomichev and A. Semerok - Etude des Processus Thermiques Survenant Lors de la Microanalyse des Surfaces par la Méthode Raman - Report CEA, DPC/SCPA/NT02-053, 2002, 27 pages.
- [3] A. Semerok and J.-M. Weulersse - Bibliography Study on Theoretical Models of Laser Detritiation Processes - Report CEA, NT DPC/SCP 03-069-A, 2003, 28 pages.

- [4] A. Semerok, J.M. Weulersse, F. Brygo, D. Farcage, C. Hubert, C. Lascoutouna, M. Géléoc, P. Wodling, H. Long, F. Champonnois, G. Brunel, G. Vimond, E. Lizon, V. Dauvois, V. Delanne, C. Grisolia, S. Fomichev, M. Hashida - Studies on TOKAMAK wall surfaces decontamination by pulsed repetition rate lasers - CEA report NT DPC/SCP/05-111-A - january 2005, 50 pages.

- [5] D. Potter - Computational Physics (Wiley, NY, 1973).

## REPORTS AND PUBLICATIONS

---

- S. Fomichev, A. Semerok, J.M. Weulersse, F. Brygo - Report CEA, NT DPC/SCP 11-069-A, 2004, 77 pages.

## TASK LEADER

---

Alexandre SEMEROK

DEN/DPC/SCP/LILM  
CEA-Saclay  
F-91191 Gif-sur-Yvette Cedex

Tél. : 33 1 69 08 65 57  
Fax : 33 1 69 08 78 84

E-mail : asemerok@cea.fr



## Task Title: RECALCULATION OF THE LIFUS EXPERIMENT (INTERACTION BETWEEN LITHIUM-LEAD AND WATER) WITH THE 3D VERSION OF SIMMER

### INTRODUCTION

Lithium lead is a candidate as breeding material in a fusion reactor. Water could be used as coolant of the breeding blanket or at least as coolant for the shielding part. In the case of ITER, the EU Test Module Blanket (TBM) will be He cooled but the use of water as coolant is foreseen for all the in-vessel components.

The contact between water and lithium lead could produce a strong and rapid interaction.

A series of interaction tests between lithium-lead liquid metal and water have therefore been carried out at the ENEA Brasimone Institute (Italia) with the LIFUS facility. The phenomenology of the interaction between lithium-lead and water for various operating conditions (temperature, pressure, duration of the water injection) has been dealt with.

These tests were modeled in 2003 with the two dimensional SIMMER code, a software which was previously used for the analysis of severe accidents in the field of the sodium cooled fast reactors.

The calculation results agreed well with the experimental ones except for the pressure level reached during the interaction, which was underestimated by SIMMER. Nevertheless, it was concluded that the SIMMER code was well suited to describe the phenomenology of the accident. Hypotheses were proposed to explain the discrepancy. The pressure evolution was however not significantly improved.

The 2004 task is aimed at reviewing the effect of a better description of the interaction vessel geometry by a three dimensional approach. This comparison is now made possible with the new 3D version of SIMMER, which allows a refined modeling of the LIFUS facility.

### RECALL OF THE PREVIOUS SIMULATION

#### LIFUS test

The test n°4 of the LIFUS program was modeled using a Cartesian representation, following a previous work carried out at CEA on the BURTY experiment, in order to take into account the non-symmetry of the facility [1]. Using the two dimensional version of SIMMER, the results showed that the Cartesian approach provided a good estimation of the time delay of the expansion vessel pressurization, directly correlated to the amount of injected water.

A modeling limitation was however found in the two dimensional SIMMER code, resulting in a lower pressure level than the pressure reached in the experiment [2].

The main difficulty was to represent the different parts of the experimental facility. The interaction vessel is made of four different compartments separated by walls (figure 1). The fluid can circulate between these compartments through the gaps. The injector and cooling tubes are located in one of these compartments and the injector is not in the central part. Each compartment is also equipped with an expansion pipe, connected to a unique expansion vessel.

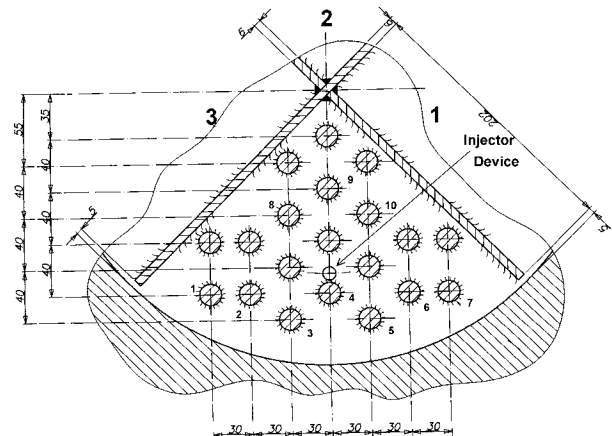


Figure 1 : Location of the tube bundle and the injector in the interaction vessel

### 2D approach

In order to represent this complex geometry, simplifications were necessary in the two dimensional approach. As the pressure level reached during the interaction is directly dependent on the free volume available for the fluid, the results are sensitive to the description of the interaction vessel.

It was pointed out that the modeling must be modified to better take into account the geometry of the LIFUS facility. Particularly, the position of the injector device must be correctly represented since it is not on the same axis as the expansion tube. A finer meshing must also be made in order to simulate the jet flow kinetics without introducing too important numerical diffusion effects. The transfers between structure and fluid must be represented by wall laws is necessary in order to take into account the fluid/structure frictions and interactions.

### 2004 ACTIVITIES

In order to improve the simulation of the interaction, the LIFUS test n°4 is recalculated thanks to the 3D SIMMER code.

### 3D MODELING

The modeling of the interaction vessel in 3D, represented in figure 2, is made in the Cartesian representation [3]. The boundary conditions are imposed at the inlet of the interaction vessel by simulating the injected water, and at the outlet by imposing the pressure of the mixture going to the expansion vessel. The purpose is to show the capability of the SIMMER 3D version to better calculate the behaviour of the mixture in the interaction vessel.

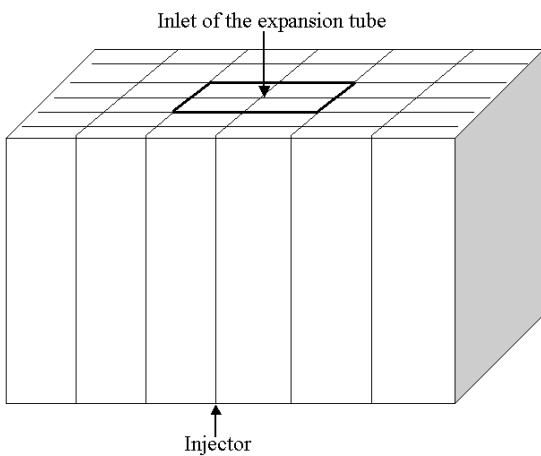


Figure 2 : Interaction vessel

### SIMMER RESULTS

The pressure is evaluated at the top of the interaction vessel below the expansion vessel. As shown in figure 3, the calculated pressure is in agreement with the experimental values reached during the thermal interaction between the lithium-lead alloy and water.

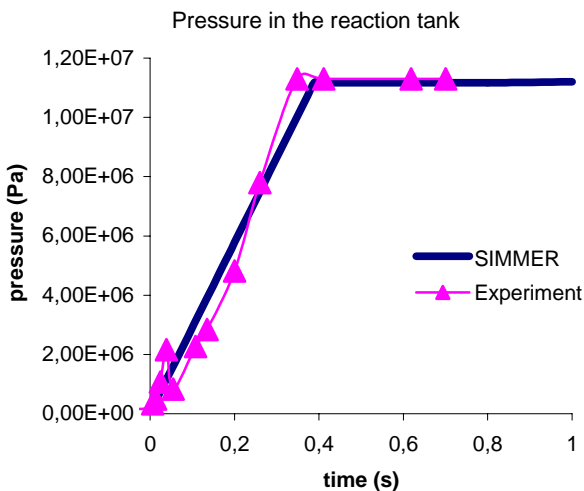


Figure 3 : Pressure evolution in the reactor vessel

The pressure evolution is well reproduced in the interaction vessel in time and magnitude, even though the calculated pressure has a smoother slope than the experimental one. The pressure peak, due to a water hammer effect and a water vaporization, reaches a maximum value of 115 bars after 370 ms.

The second phase is characterized by a pressure stagnation in all sectors of the interaction vessel because of the free flow of gases into the expansion vessel, balanced by an equivalent injection of water from the injection device. This second phase lasts for about 250 ms.

### COMPARISON BETWEEN THE 2D/3D APPROACH

In comparison to the previous approach based on the two dimensional Cartesian calculation, the three dimensional approach takes into account the spatial motion of the lithium-lead and water mixture during the interaction. As the pressure is inversely proportional to the free volume, the correct representation of the geometry is essential to determine the kinetics and the magnitude of the pressure in the vessel. With this approach, the temperature evolution is also correctly obtained.

### CONCLUSION

The experimental campaign on LIFUS facility was aimed at giving a clear understanding of the interaction between lithium-lead alloy and water in the blanket module. The effects of thermal-hydraulics parameters and the geometrical features on the pressure and temperature evolution in the interaction vessel were particularly investigated. A SIMMER modeling of the LIFUS was achieved, based on the experience gained from the previous validation with the two dimensional approach. The injector, the interaction vessel and the connection to the expansion tubes were represented. Even though the phenomenology of the interaction was evidenced in the 2D SIMMER calculation, a discrepancy was observed for the pressure variation.

Taking into account the three dimensional geometry of the sole interaction vessel, the evolution of pressure can be better reproduced by the code by a 3D description of the available volume for the expansion of the lithium-lead and water mixture. The whole kinetics of the interaction phenomenon, temperature and pressure evolutions are in agreement with the experimental results. These results show the potentialities of SIMMER 3D, which could be relevantly used on the whole representation of the facility and not only the reaction vessel, as presented here. This activity could be fruitfully continued in 2005 on the test n°3 of the LIFUS program. This test is characterized by different conditions in terms of pressure and temperature of the injected water. This recalculation could be used as a complement to the validation of the current work. The modeling could also be more complete in order to have a better description of the LIFUS facility, in particular for the expansion vessel.

## REPORTS AND PUBLICATIONS

---

- [1] Phase 2 code assessment of SIMMER-III, a computer program for LMFR core disruptive accident analysis - Japan Nuclear Cycle Development Institute - O-Arai Engineering Center - JNC TN9400 2000-105 september 2000.
  
- [2] Modeling of the interaction between lithium-lead and water using the SIMMER-III code - january 2004 - CEA report by Thierry Cadiou - NT DER/SESI/LCSI 03/403.
  
- [3] Recalculation of the LIFUS experiment (interaction between lithium-lead and water) with the 3D version of SIMMER - february 2005 - CEA report by Thierry CADIOU - CEA/DEN/CAD/DER/SESI/LCSI/NT DO1 14/01/05.

## TASK LEADER

---

Thierry CADIOU

DEN/DER/SESI/LCSI

CEA-Cadarache

F-13108 Saint-Paul-Lez-Durance Cedex

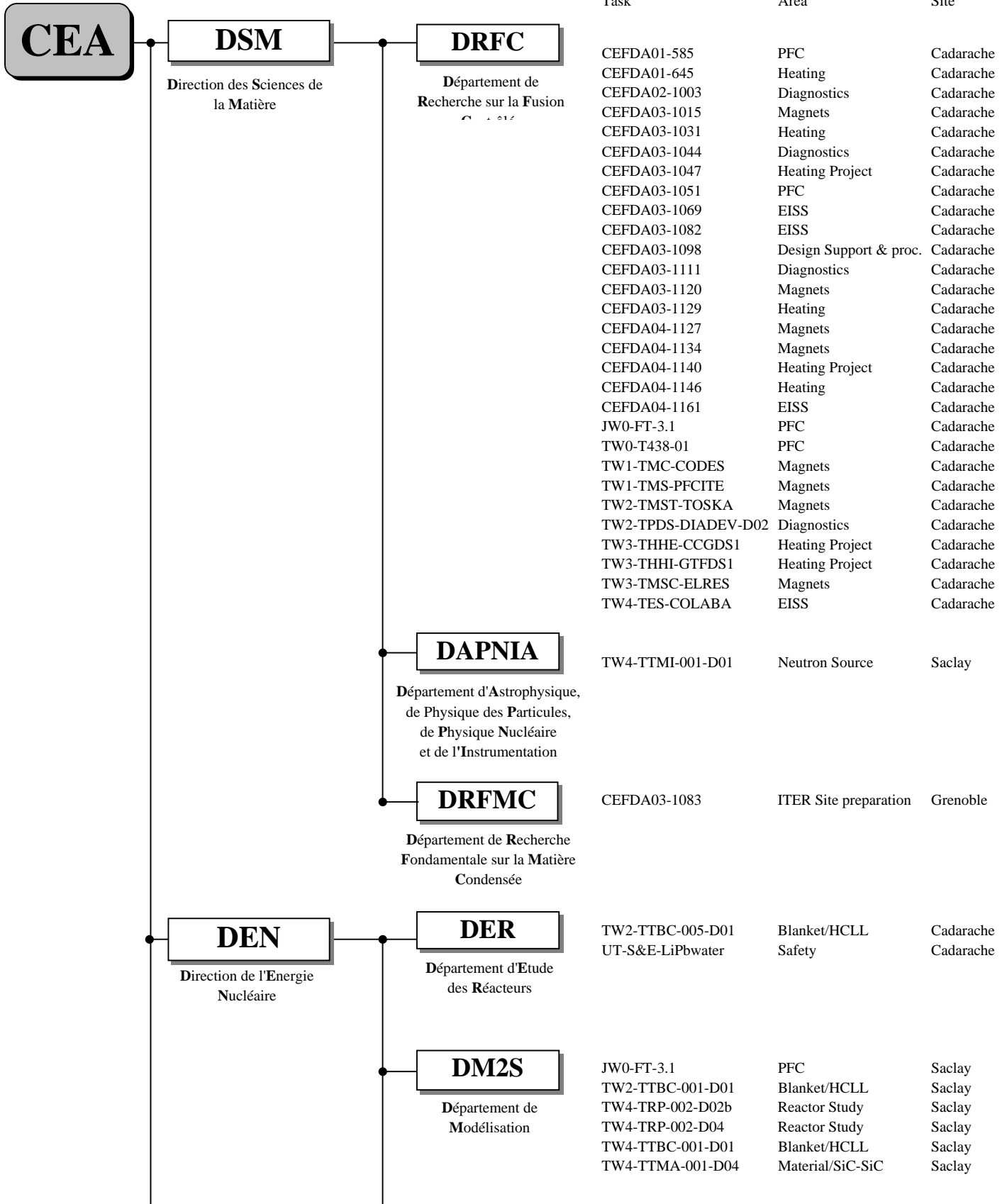
Tél. : 33 1 42 25 66 17

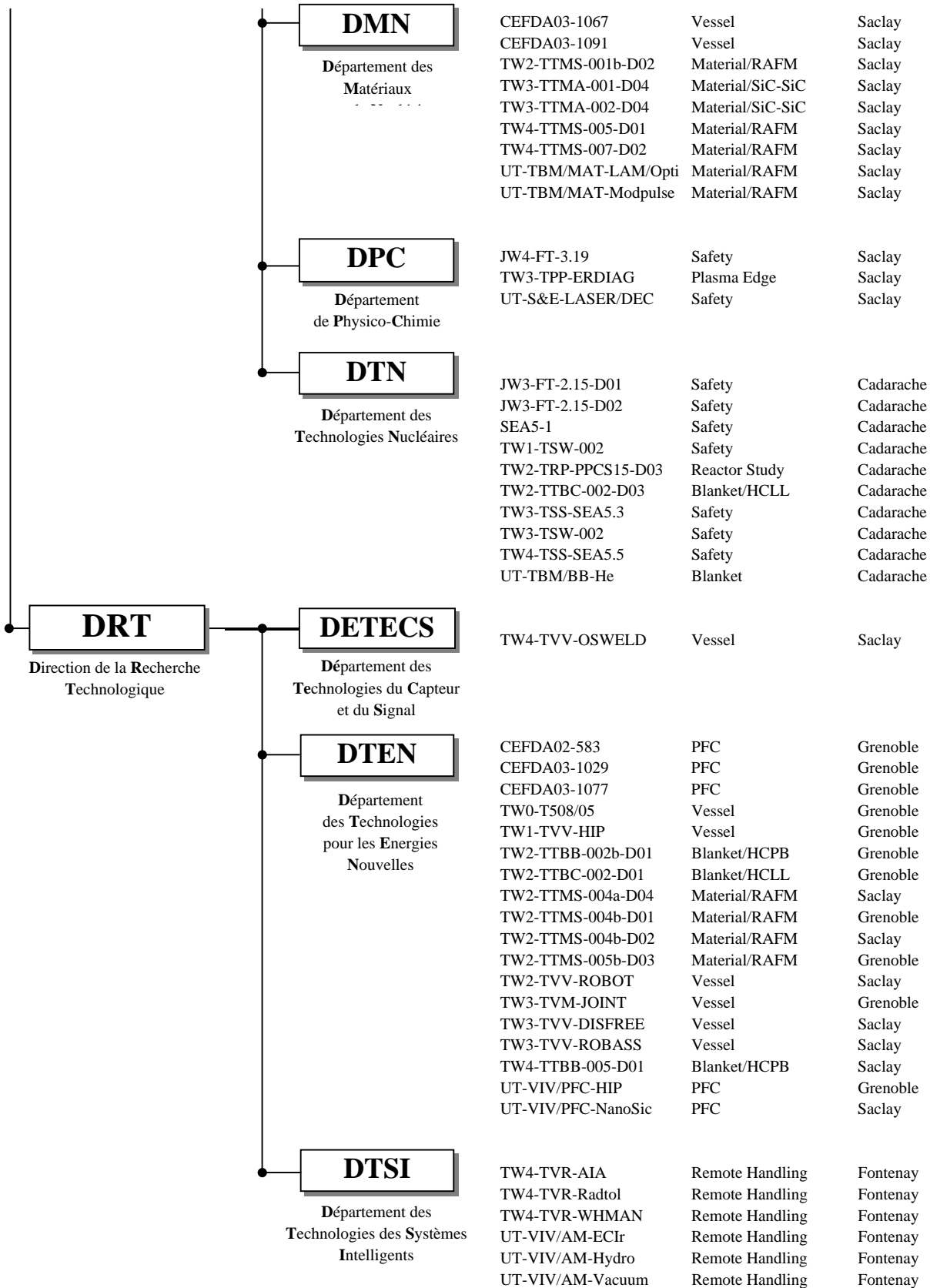
Fax : 33 1 42 25 71 87

E-mail : [cadiou@drncad.cea.fr](mailto:cadiou@drncad.cea.fr)



# APPENDIX 1 : DIRECTIONS CONTRIBUTION TO THE FUSION PROGRAMME





## EXTERNAL COLLABORATIONS

**CNRS (French National Centre  
for Scientific Research)**

UT-VIV/PFC-Damage  
UT-VIV/PFC-Pyro

PFC  
PFC

Pessac  
Font Romeu

**Technicatome**  
(Collaboration with CEA)

TW2-TTBC-005-D01

Blanket/HCLL

Aix en Pce



## APPENDIX 2 : ALLOCATIONS OF TASKS

| EFDA TECHNOLOGY PROGRAMME           |   | Unit   | Site      | Investigator   |
|-------------------------------------|---|--------|-----------|----------------|
| <b>Physics Integration</b>          |   |        |           |                |
| <b>Plasma Edge</b>                  |   |        |           |                |
| TW3-TPP-ERDIAG                      | Evaluation of Laser Ablation Optical Emission Spectroscopy (LA-OES) Method for graphite co-deposited layer characterization                       | DPC    | Saclay    | Semerok A.     |
| <b>Heating and Current Drive</b>    |   |        |           |                |
| CEFDA01-645                         | TW2-TPHN-NBDES1 : Support to neutral beam physics and testing 1   | DRFC   | Cadarache | Svensson L.    |
| CEFDA03-1129                        | TW3-TPHI-ICRDES1 : ITER ICRF Antenna and Matching System  | DRFC   | Cadarache | Bosia G.       |
| <b>Diagnostics</b>                  |   |        |           |                |
| CEFDA02-1003<br>CEFDA03-1111        | TW2-TPDS-DIASUP4 and TW3-TPDS-DIASUP1 : Support to the ITER diagnostic design   | DRFC   | Cadarache | Stott P.       |
| TW2-TPDS-DIADEV-D02                 | Development of diagnostic components : First mirrors study  | DRFC   | Cadarache | Lipa M.        |
| <b>Vessel-In Vessel</b>             |   |        |           |                |
| <b>Vessel-Blanket and Materials</b> |   |        |           |                |
| CEFDA03-1067                        | TW3-TVM-MDB : Rules for design, fabrication and inspection Establishment and maintenance of a material data for licensing TBM's design rules      | DMN    | Saclay    | Tavassoli F.   |
| CEFDA03-1091                        | TW2-TVM-LIP : Rules for design, fabrication and inspection Modification of ITER material documents and assessment of materials data for licensing | DMN    | Saclay    | Tavassoli F.   |
| TW0-T508/05                         | Development of Be/CuCrCz brazing techniques   | DTEN   | Grenoble  | Bucci P.       |
| TW1-TVV-HIP                         | Improvements of HIP Fabrication Techniques  | DTEN   | Grenoble  | Bucci P.       |
| TW2-TVV-ROBOT                       | Dynamic test rig for Intersector Welding Robot (IWR) for VV sector field joining  | DTEN   | Saclay    | Aubert P.      |
| TW3-TVM-JOINT                       | Characterization of the CuCrZr/SS junction strength for different blanket manufacturing conditions  | DTEN   | Grenoble  | Gillia O.      |
| TW3-TVV-DISFREE                     | Further development of the hybrid MIG/Laser welding technique for VV sector field joining   | DTEN   | Saclay    | De Dinechin G. |
| TW3-TVV-ROBASS                      | Long Detection Range Seam Tracker   | DTEN   | Saclay    | Aubert P.      |
| TW4-TVV-OSWELD                      | Qualification of multiple phased array UT for one sided welds during VV manufacture   | DETECS | Saclay    | Bredif Ph.     |
| <b>Plasma Facing Components</b>     |   |        |           |                |
| CEFDA01-585                         | TW1-TVP-TESTAN : Monitoring and analysis of the thermal fatigue testing of divertor prototypes - 200 kW electron beam gun test                    | DRFC   | Cadarache | Escourbiac F.  |
| CEFDA02-583                         | TW1-TVV-DES : Destructive examination of primary first wall panels and mock-ups   | DTEN   | Grenoble  | Bucci P.       |

|                        |  |      |           |                 |
|------------------------|--|------|-----------|-----------------|
| CEFDA03-1029           | TW3-TVB-JOINOP : Optimization of Be/Cu alloy joints for primary first wall panels    | DTEN | Grenoble  | Bucci P.        |
| CEFDA03-1051           | TW4-TVD-ACCEPT : Study on acceptance criteria for the ITER divertor vertical target  | DRFC | Cadarache | Schlosser J.    |
| CEFDA03-1077           | TW3-TVB-INMOCK : fabrication of primary first wall mock-ups for in-pile experiments  | DTEN | Grenoble  | Bucci P.        |
| TW0-T438-01            | Development and testing of time resolved erosion detecting techniques                | DRFC | Cadarache | Gauthier E.     |
| <b>Remote Handling</b> |  |      |           |                 |
| TW4-TVR-AIA            | Articulated inspection arm (AIA)   | DTSI | Fontenay  | Friconneau J.P. |
| TW4-TVR-Radtol         | Radiation tolerance assessment of standard electronic components for Remote Handling | DTSI | Fontenay  | Giraud A.       |
| TW4-TVR-WHMAN          | Development of a water hydraulic manipulator   | DTSI | Fontenay  | Friconneau J.P. |

## Magnet Structure & Integration

### Magnet Structure

|                |  |      |           |                |
|----------------|--|------|-----------|----------------|
| CEFDA03-1015   | TW2-TMSM-COOLIN : Mock-ups for the TF and CS Terminal regions and Cooling Inlets   | DRFC | Cadarache | Decool P.      |
| CEFDA03-1120   | TW3-TMSC-ASTEST : Tests of advanced Nb <sub>3</sub> Sn strands - Extensive characterization of industrial advanced Nb <sub>3</sub> Sn strands developed for ITER TF Coils system   | DRFC | Cadarache | Zani L.        |
| CEFDA04-1127   | TW4-TMSC-SAMAN1 : manufacture of sub-size samples  | DRFC | Cadarache | Duchateau J.L. |
| CEFDA04-1134   | TW4-TMSC-BARBEN : Bending strain effects of single strands - Study of bending strain effect on critical properties of Nb <sub>3</sub> Sn strands jacketed with stainless steel for various bending amplitudes and temperatures | DRFC | Cadarache | Zani L.        |
| TW1-TMC-CODES  | Design and Interpretation Codes  | DRFC | Cadarache | Decool P.      |
| TW1-TMS-PFCITE | Poloidal Field Conductor Insert (PFCI)   | DRFC | Cadarache | Ciazynski D.   |
| TW2-TMST-TOSKA | TFMC testing with the LCT coil   | DRFC | Cadarache | Duchateau J.L. |
| TW3-TMSC-ELRES | Experimental assessment of the effect of electrical resistances on the V-I characteristics of superconductive cables   | DRFC | Cadarache | Ciazynski D.   |

## Tritium Breeding and Materials

### Breeding Blanket

#### Helium Cooled Pebble Bed (HCPB) Blanket

|                   |  |      |          |               |
|-------------------|--|------|----------|---------------|
| TW2-TTBB-002b-D01 | Blanket manufacturing techniques - First wall HIPping with open channels   | DTEN | Grenoble | Rigal E.      |
| TW4-TTBB-005-D01  | HCPB breeder and neutron multiplier materials<br>Procurement and quality control of Li <sub>2</sub> TiO <sub>3</sub> pebbles | DTEN | Saclay   | Lulewicz J.D. |

#### Helium Cooled Lithium Lead (HCLL) Blanket

|                  |  |      |           |            |
|------------------|--|------|-----------|------------|
| TW2-TTBC-001-D01 | Helium Cooled Lithium Lead - TBM design, integration and analysis - Blanket system design and analysis - Integration and testing in ITER | DM2S | Saclay    | Li Puma A. |
| TW2-TTBC-002-D01 | Blanket manufacturing techniques - Fabrication processes for HCLL and HCPB TBMs  | DTEN | Grenoble  | Rigal E.   |
| TW2-TTBC-002-D03 | Testing of small-scale mocks-ups to qualify manufacturing technologies   | DTN  | Cadarache | Cachon L.  |

|                  |  |          |                        |                            |
|------------------|--|----------|------------------------|----------------------------|
| TW2-TTBC-005-D01 | Helium Cooled Lithium Lead - Safety and Licensing - Test Blanket Module (TBM) accidental safety study                    | DER + TA | Cadarache + Aix en Pce | Schmidt N.,<br>La Lumia V. |
| TW4-TTBC-001-D01 | TBM design, integration and analysis - Testing programme and engineering design of the first HCLL TBM for ITER H-H phase | DM2S     | Saclay                 | Farabolini W.              |

### Structural Materials Development

#### Reduced Activation Ferritic Martensitic (RAFM) Steels

|                   |   |      |          |              |
|-------------------|---|------|----------|--------------|
| TW2-TTMS-001b-D02 | Irradiation performance - Neutron irradiation to 70 dpa at 325°C and PIE  | DMN  | Saclay   | Alamo A.     |
| TW2-TTMS-004a-D04 | Eurofer : Fusion welds development - Evaluation of a welding process adapted to the Test Blanket Module's geometry : Assembly of the horizontal cooling plates with the continuous wave YAG laser welding process | DTEN | Saclay   | Forest L.    |
| TW2-TTMS-004b-D01 | Tubing process qualification - Advanced process development and testing for the production of TBM's cooling channels  | DTEN | Grenoble | Rigal E.     |
| TW2-TTMS-004b-D02 | Qualification of fabrication processes - Processing of high quality welds according to TBM design   | DTEN | Saclay   | Asserin O.   |
| TW2-TTMS-005b-D03 | Rules for design, Fabrication, Inspection - Fracture mechanics assessments of TBM's   | DTEN | Grenoble | Couturier R. |
| TW4-TTMS-005-D01  | Rules for design, fabrication and inspection<br>Update Data Base and Appendix A of DEMO-SDC   | DMN  | Saclay   | Tavassoli F. |
| TW4-TTMS-007-D02  | Modelisation of irradiation effect - Ab initio defect energy calculations in the Fe-He system   | DMN  | Saclay   | Willaime F.  |

#### Advanced Materials

|                                      |   |      |        |           |
|--------------------------------------|---|------|--------|-----------|
| TW3-TTMA-001-D04<br>TW3-TTMA-002-D04 | SiC/SiC ceramic composites - Divertor and plasma facing materials       | DMN  | Saclay | Alamo A.  |
| TW4-TTMA-001-D04                     | Modelling of the mechanical behaviour of advanced 3D SiCf/SiC composite | DM2S | Saclay | Guérin C. |

### Neutron Source

|                  |  |        |        |              |
|------------------|--|--------|--------|--------------|
| TW4-TTMI-001-D01 | IFMIF accelerator facilities : accelerator system design | DAPNIA | Saclay | Ferdinand R. |
|------------------|--|--------|--------|--------------|

### Safety and Environment

|                        |   |     |           |              |
|------------------------|---|-----|-----------|--------------|
| SEA5-1                 | Validation of computer codes and models   | DTN | Cadarache | Schindler P. |
| TW1-TSW-002            | Waste and decommissioning strategy  | DTN | Cadarache | Gastaldi O.  |
| TW3-TSS-SEA5.3         | Ice formation on cryogenics surfaces  | DTN | Cadarache | Ayrault L.   |
| TW3-TSW-002            | Assessment of radioactive waste in ITER hot cell facility   | DTN | Cadarache | Gastaldi O.  |
| TW4-TSS-SEA5.5-D02&D05 | Validation of the PAXITR and PACITR code against fusion-specific experiments (ICE, EVITA, CORELE, CIRENE) | DTN | Cadarache | Girard M.    |
| TW4-TSS-SEA5.5-D11     | Validation of the PACTITER code against fusion-specific experiments - Development of the PACTITER code    | DTN | Cadarache | Dacquait F.  |

### System studies

#### Power Plant Conceptual Studies (PPCS)

|                    |  |      |           |                   |
|--------------------|--|------|-----------|-------------------|
| TW2-TRP-PPCS15-D03 | Waste management strategy on model A and B   | DTN  | Cadarache | Lacressonnière C. |
| TW4-TRP-002-D02b   | Conceptual design of a HCLL reactor - Tritium control and management analysis, thermo-hydraulic and thermo-mechanical analyses | DM2S | Saclay    | Farabolini W.     |

|   |  |        |             |                         |
|---|--|--------|-------------|-------------------------|
| TW4-TRP-002-D04                           | Conceptual design of a HCLL reactor - Design integration   | DM2S   | Saclay      | Li Puma A.              |
| <b>ITER Site Preparation</b>              |  |        |             |                         |
| <b>European ITER Site Studies</b>         |  |        |             |                         |
| CEFDA03-1069                              | TW3-TES-EISSg1 : EISS 3 : generic tasks CEA  | DRFC   | Cadarache   | Garin P.                |
| CEFDA03-1082                              | TW3-TES-EISS2c : EISS 3, stage 2   |        |             |                         |
| CEFDA04-1161                              | TW4-TES-EISS4F : European ITER site study 4 - Cadarache  |        |             |                         |
| TW4-TES-COLABA                            | Cadarache site for ITER, collaboration with local authorities  |        |             |                         |
| <b>Site and Plant Layout</b>              |  |        |             |                         |
| CEFDA03-1083                              | TW3-TEP-CRYO2 : Design of ITER cryoplant/cryodistribution system (auxilliary cold boxes, cryoline...)  | DRFMC  | Grenoble    | Millet F.               |
| <b>Design Support and Procurement</b>     |  |        |             |                         |
| CEFDA03-1098                              | TW3-TDS-MAG : Detailed engineering and manufacturing studies of the ITER magnet system : Poloidal Field (PF) coil windings and cold test assessment              | DRFC   | Cadarache   | Libeyre P.              |
| <b>JET</b>                                |  |        |             |                         |
| <b>Physics Integration</b>                |  |        |             |                         |
| <b>Heating Systems</b>                    |  |        |             |                         |
| CEFDA03-1031                              | JW3-EP-ICRH and JW4-EP-ICRH : contribution to ICRH components  | DRFC   | Cadarache   | Chapuis P.              |
| CEFDA04-1146                              | antenna limiter  |        |             |                         |
| <b>Diagnostics</b>                        |  |        |             |                         |
| CEFDA03-1044                              | JW3-EP-IRV : Diagnostics enhancement - Wide angle IR Endoscope   | DRFC   | Cadarache   | Gauthier E.             |
| <b>Vessel/In-Vessel</b>                   |  |        |             |                         |
| <b>Plasma Facing Components</b>           |  |        |             |                         |
| JW0-FT-3.1                                | Internal PFC components behaviour and modeling   | DRFC + | Cadarache + | Gauthier E.,            |
| <b>Safety and Environment</b>             |  |        |             |                         |
| JW3-FT-2.15-D01                           | Detritiation of soft housekeeping materials (mainly plastics)  | DTN    | Cadarache   | Trabuc P.               |
| JW3-FT-2.15-D02                           | Detritiation of vacuum oil and organic liquids   | DTN    | Cadarache   | Trabuc P. & Poletiko C. |
| JW4-FT-3.19                               | Laser decontamination/Tritium removal - Studies on tokamak wall surfaces decontamination by pulsed repetition rate lasers  | DPC    | Saclay      | Semerok A.              |
| <b>Heating Systems Technology Project</b> |  |        |             |                         |
| CEFDA03-1047                              | TW3-THHN-IITF1 : The first ITER NB Injector and the ITER NB Test Facility : design   | DRFC   | Cadarache   | Hemsworth R.            |
| CEFDA04-1140                              | TW4-THHN-ADSD2 : Neutral beam development for EFDA Extension   | DRFC   | Cadarache   | Boilson                 |
| TW3-THHE-CCGDS1                           | Coaxial cavity gyrotron and test facility - Design, support to the industrial development and preparation of the technical specifications                        | DRFC   | Cadarache   | Magne R.                |
| TW3-THHI-GTFDS1                           | Fusion diacode, ICRF generator, IC power supply and IC test facility : design, support to industrial development and preparation of the technical specifications | DRFC   | Cadarache   | Mollard P.              |

## UNDERLYING TECHNOLOGY PROGRAMME

### Vessel/In-Vessel

#### Plasma Facing Components

|                    |  |           |            |              |
|--------------------|--|-----------|------------|--------------|
| UT-VIV/PFC-Damage  | Study of damage mechanisms in Plasma Facing Components   | CNRS-LCTS | Pessac     | Martin E.    |
| UT-VIV/PFC-HIP     | Improvement of the reliability, performance and industrial relevancy of HIP processes for PFC components | DTEN      | Grenoble   | Chabrol C.   |
| UT-VIV/PFC-NanoSiC | Nano crystalline silicon carbide (SiC) - Optimization of the preparation of Nano-SiC                     | DTEN      | Saclay     | Ténégal F.   |
| UT-VIV/PFC-Pyro    | Application of a tricolour pyroreflectometer to plasma facing components in-situ infrared monitoring     | CNRS-IMP  | Font Romeu | Hernandez D. |

#### Remote Handling

|                  |  |      |          |                 |
|------------------|--|------|----------|-----------------|
| UT-VIV/AM-ECIr   | Remote Handling techniques - Radiation effects on electronic components                        | DTSI | Fontenay | Giraud A.       |
| UT-VIV/AM-Hydro  | Technologies and control for remote handling systems   | DTSI | Fontenay | Friconneau J.P. |
| UT-VIV/AM-Vacuum | Technologies for vacuum, temperature and magnetic field conditions for remote handling systems | DTSI | Fontenay | Friconneau J.P. |

### Tritium Breeding and Materials

#### Breeding Blanket

|              |  |     |         |             |
|--------------|--|-----|---------|-------------|
| UT-TBM/BB-He | Helium components technology - problems and outline of solutions | DTN | Cadache | Berton J.L. |
|--------------|--|-----|---------|-------------|

#### Materials Development

##### Structural Materials

|                     |  |     |        |               |
|---------------------|--|-----|--------|---------------|
| UT-TBM/MAT-LAM/Opti | Development of new RAFM steels with regard to creep properties   | DMN | Saclay | De Carlan Y.  |
| UT-TBM/MAT-Modpulse | Pulsed irradiation of the martensitic alloy Eurofer - Irradiations by krypton ions at 350 and 550°C at high flux during short time | DMN | Saclay | Boulangier L. |

### Safety and Environment

|                  |  |     |         |            |
|------------------|--|-----|---------|------------|
| UT-S&E-LASER/DEC | Laser decontamination : Tritium removal  | DPC | Saclay  | Semerok A. |
| UT-S&E-LiPbwater | Recalculation of the LIFUS experiment (interaction between lithium-lead and water) with the 3D version of SIMMER | DER | Cadache | Cadiou T.  |



# APPENDIX 3 : REPORTS AND PUBLICATIONS

## EFDA TECHNOLOGY PROGRAMME

### Physics Integration

#### Heating and Current Drive

|              |  |   |
|--------------|--|---|
| CEFDA01-645  | Experimental results with the new ITER-like 1 MV SINGAP accelerator<br>10th International Symposium on the Production and Neutralization of<br>Negative Ions and Beams, Kiev, 13-17 September 2004 | L. Svensson, D. Boilson,<br>H.P.L. de Esch, R.S. Hemsworth<br>and P. Massmann |
| CEFDA03-1129 | Proposals for upgrades to the ITER Reference design<br>CEA CNN/NTT (2004)  | G. Bosia  |

#### Diagnostics

|                     |  |                                     |
|---------------------|--|-------------------------------------|
| TW2-TPDS-DIADEV-D02 | First mirror study in Tore Supra<br>TW2-TPDS-DIADEV-D02 Final report, January 2005 | M. Lipa, B. Schunke, Ch. Gil et al. |
|---------------------|--|-------------------------------------|

### Vessel/In-Vessel

#### Vessel-Blanket and Materials

|                              |   |  |
|------------------------------|---|--|
| CEFDA03-1067<br>CEFDA03-1091 | EU contributions to the ITER Materials Properties Data Assessment<br>SOFT, Venice, 20-24 September 2004   | A.T. Peacock, V. Barabash,<br>F. Gillemot, P. Karditsas,<br>G. Lloyd, J.W. Rensman,<br>A.A. F. Tavassoli and<br>M. Walters |
| CEFDA03-1067<br>CEFDA03-1091 | EU Materials properties Database / Data analysis meeting<br>EFDA Garching, 24-25 June 2004  |  |
| TW0-T508/05                  | Development of Be/CuCrZr/SS brazing techniques<br>Rapport technique DTEN/DL/2004/089  | Ph. Bucci, J.M. Leibold, F. Vidotto  |
| TW1-TVV-HIP                  | Improvement of HIP Fabrication Technique<br>Rapport technique DTEN/DR/2004/094  | P. Bucci, J.M. Leibold, F. Vidotto   |
| TW3-TVV-DISFREE              | Assessment of the hybrid process to weld the ITER vacuum vessel<br>DTEN/DL/2005/008   | G. de Dinechin, F. Janin,<br>S. Moran  |
| TW3-TVV-ROBASS               | Long range tracking system<br>Technical report CEA/DTEN/DL/2005/005, 20 January 2005  | D. Sabourin  |
| TW4-TVV-OSWELD               | Development of phased array techniques for the inspection<br>of one sided welds in ITER vacuum vessel<br>SYSSC/04-RT0143/Rev. 0, September 2004 |  |

#### Plasma Facing Components

|              |   |  |
|--------------|---|--|
| CEFDA01-585  | A mature industrial solution for ITER divertor plasma facing<br>components: hypervapotron cooling concept adapted to Tore Supra flat<br>tile technology<br>Proc. 23rd SOFT-23, 20-24 Sept., Venice, Italy | F. Escourbiac, I. Bobin-Vastra,<br>V. Kuznetsov, M. Missirlian,<br>B. Schedler, J. Schlosser |
| CEFDA01-585  | Contract EFDA 01/585 - Final report<br>CFP/NTT-2005.008, March 2005   | F. Escourbiac  |
| CEFDA01-585  | Results and analysis of high heat flux tests on a full scale vertical target<br>prototype of ITER divertor<br>Proc. SOFT-23, 20-24 Sept., Venice, Italy   | M. Missirlian, F. Escourbiac,<br>M. Merola, I. Bobin-Vastra,<br>J. Schlosser, A. Durocher    |
| CEFDA03-1051 | Study of acceptance criteria for the ITER divertor: summary report of<br>the progress meeting on the 7th December 2004, Cadarache<br>CFP/CRR-2004.014   | M. Merola, S. Fouquet  |
| CEFDA03-1051 | Study on acceptance criteria for the ITER divertor, Final report<br>CFP/NTT-2004.035  | S. Fouquet, J. Schlosser   |
| CEFDA03-1051 | Study on acceptance criteria for the ITER divertor,<br>Intermediate report 2:experimental database<br>CFP/NTT-2004.014  | S. Fouquet   |

|              |  |                          |
|--------------|--|--------------------------|
| CEFDA03-1051 | Study on acceptance criteria for the ITER divertor, Intermediate report 3: Thermal calculations for CFC and W monoblocks<br>CFP/NTT-2004.030                                 | C. Portafaix, S. Fouquet |
| CEFDA03-1051 | Synthesis of non-destructive testing of the baffles prototypes designed for the ITER divertor (panels B and C)<br>CFP/NTT-2004.015   | S. Fouquet               |
| CEFDA03-1077 | Fabrication of primary first wall mock-ups for in-pile experiments<br>Task TW3-TV-B-INMOCK, Rapport technique DTEN/DL/2005/016, march 2005                                   | Ph. Bucci et al.         |
| TW0-T438-01  | Procédure d'entretien du laser en salle blanche du bâtiment 507<br>DIAG/NTT-2004.015 (2004)  | P. Dore                  |
| TW0-T438-01  | Mesure de Vibration sur le Limiteur Pompé Toroïdal<br>DIAG/NTT-2004.016 (2004)   | P. Dore                  |
| TW0-T438-01  | Mesure de Vibration sur le Limiteur Pompé Toroïdal (en choc et hors choc)<br>DIAG/NTT-2004.031 (2004)  | P. Dore                  |
| TW0-T438-01  | Final report TW0-T438-01<br>CFP/NTT-2004.033 (2004)  | E. Gauthier, P. Dore     |
| TW0-T438-01  | Etude de l'érosion des composants face au plasma par interférométrie de speckle<br>5ème Colloque Int. Francophone : Méthodes et Techniques Optiques pour l'Industrie, (2004) | P. Dore, E. Gauthier     |

## Remote Handling

|                |   |
|----------------|---|
| TW4-TVR-AIA    | Articulated Inspection Arm, AIA prototype module test campaign report<br>CEA/DTSI/SRSI/LPR/04RT.103/ Issue 0                        |
| TW4-TVR-AIA    | Articulated Inspection Arm, Deployer design report<br>CEA/DTSI/SRSI/LPR/04RT.104/ Issue 0   |
| TW4-TVR-AIA    | Articulated Inspection Arm, Manufacture report<br>CEA/DTSI/SRSI/LPR/03RT.104/ Issue 0   |
| TW4-TVR-AIA    | ITER Articulated Inspection Arm (AIA) : Geometric calibration issues of a long-reach flexible robot<br>SOFT 2004 Paper 389          |
| TW4-TVR-AIA    | ITER Articulated Inspection Arm (AIA): R&d progress on Vacuum and Temperature technology for remote handling<br>SOFT 2004 Paper 393 |
| TW4-TVR-RADTOL | December report DRT/LIST/DTSI/SARC/04-042/AG  |
| TW4-TVR-RADTOL | June report DRT/LIST/DTSI/SARC/04-335/AG  |
| TW4-TVR-WHMAN  | Water hydraulic manipulator. Definition of a single axis water hydraulic mock-up<br>DTSI/SCRI/LPR/05RT006                           |

## Magnet Structure

|                |   |   |
|----------------|---|---|
| CEFDA03-1015   | CS cooling inlets comparison between a full and a half mock-up<br>Note AIM/NTT/2004.004   | P. Decool   |
| CEFDA03-1120   | TW3-TMSC-ASTEST Deliverable 1 : Intermediate report on test of advanced Nb <sub>3</sub> Sn strands<br>Note AIM/NTT-2004.014 (2004)  | L. Zani, H. Cloez, C. Meuris,<br>P. Chesny, J.M. Gheller,<br>L. Kulbicki, L. Vieillard                |
| CEFDA04-1134   | Tâche BARBEN : qualification du système de régulation du cryostat à température variable en configuration Nb <sub>3</sub> Sn<br>Note AIM/NTT-2005.003, 2005   | L. Zani, M. Tena, H. Cloez,<br>J.P. Serries, S. Girard  |
| TW1-TMC-CODES  | Experimental investigation to determine the heat transfer coefficient between annular area and the central channel of ITER-FEAT conductors as an input to codes development<br>Task CODES Deliverable 4 : AIM/NTT-2004.017, August 2004 | S. Nicollet, H. Cloez, P. Decool,<br>J.L. Duchateau, A. Martinez,<br>M. Tena, B. Renard, J.P. Serries |
| TW2-TMST-TOSKA | Evaluation of the ITER cable-in-conduit conductor heat transfer presented at 20th Int. Cryo. Eng. Conf. Beijing, 2004   | S. Nicollet et al.  |

|                |   |                        |
|----------------|---|------------------------|
| TW2-TMST-TOSKA | Final report on the testing of a full size joint sample (Deliverable 4)<br>February 2005 Internal CEA Note AIM/NTT- 2005.002                      | J.L. Duchateau et al.  |
| TW3-TMSC-ELRES | TW3-TMSC-ELRES : Milestone #2 Manufacturing of Samples<br>(Cable and Joints)<br>CEA Note DRFC (STEP/GCRY), AIM/NTT-2004.029,<br>December 15, 2004 | P. Decool and H. Cloez |

## Tritium Breeding and Materials

### Breeding Blanket

#### Helium Cooled Pebble Bed (HCPB) Blanket

|                   |   |                              |
|-------------------|---|------------------------------|
| TW4-TTBB-005-D01  | Final report : Procurement and quality control of $\text{Li}_2\text{TiO}_3$ pebbles<br>Internal report CEA/DTEN/DL/2004/027, September 2004 | J.D. Lulewicz                |
| TW2-TTBB-002b-D01 | The manufacturing technologies of the European breeding blankets<br>ICFRM-11, Journal of Nuclear Materials 329–333 (2004) 133–140           | A. Cardella, E. Rigal et al. |

#### Helium Cooled Lithium Lead (HCLL) Blanket

|                  |   |                              |
|------------------|---|------------------------------|
| TW2-TTBC-001-D01 | He testing requirement and planning for the development and<br>qualification of HCLL TBM<br>CEA report SERMA/04-3470/A, 09/2004   | Y. Poitevin et al.           |
| TW2-TTBC-001-D01 | Helium Cooled Lithium Lead Test Blanket Module for ITER Engineering<br>design, analyses and test programme & needs<br>Final Report on sub-deliverables 1d, 1e, 1g and 1h, CEA report<br>SERMA/RT/05-3568/A, 03/2005 | A. Li Puma et al.            |
| TW2-TTBC-001-D01 | Helium Cooled Lithium-Lead test blanket module for ITER - reference<br>document for a mounting sequence<br>CEA Report, SEMT/BCCR/RT/04-016/A, April 2004  | G. Rampal et al.             |
| TW2-TTBC-002-D01 | Fabrication processes for HCLL and HCPB TBMs<br>Second interim report, Rapport technique DTEN/DL/2005/006,<br>28/02/2005  | E. Rigal et al.              |
| TW2-TTBC-002-D01 | The manufacturing technologies of the European breeding blankets<br>ICFRM-11, Journal of Nuclear Materials 329–333 (2004) 133–140   | A. Cardella, E. Rigal et al. |
| TW2-TTBC-002-D03 | APS d'une section d'essais en PbLi pour CP sur DIADEMO HCLL<br>NT DTN/STPA/LTCG 04-028  | F. Delasalle et al.          |
| TW2-TTBC-005-D01 | ITER – Outlines of the TBM for ITER calculations<br>CEA/DEN/CAD/DER/SESI/LESA/NT D0 14  | N. Schmidt                   |

### Structural Materials development

#### Reduced Activation Ferritic Martensitic (RAFM) Steels

|                   |   |   |
|-------------------|---|---|
| TW2-TTMS-001b-D02 | Status of irradiation experiments performed in BOR 60 reactor at<br>325°C. Post-irradiation examinations of materials irradiated up<br>to 42 dpa: 1st part<br>CEA Progress Report DMN/SRMA/N.T. SRMA 2004-2679, Dec. 2004 | A. Alamo, J.L. Bertin   |
| TW2-TTMS-004a-D04 | CEA weldability developments on RAFM steels in the period<br>1994-2003<br>UTIAC/04-RT-16, 24 June 2004  | G. De Dinechin, C. Chagnot,<br>P. Aubert                                    |
| TW2-TTMS-004a-D04 | Fusion welds development test blanket module's welding procedures :<br>assembly of the horizontal cooling plates to the vertical plates with the<br>plasma arc welding process<br>UTA/04-RT-43, 9 January 2004            | L. Forest   |
| TW2-TTMS-005b-D03 | Structural materials : Rules for design, fabrication, inspection. Fracture<br>mechanics assessments of TBM's<br>Final Report, RT DTEN/DL/2004/041, march 2005   | R. Couturier, L. Briottet,<br>S. Di Iorio, H. Giraud,<br>P. Lemoine, I. Chu |

|                  |  |              |
|------------------|--|--------------|
| TW4-TTMS-005-D01 | Fusion Demo Interim Structural Design Criteria (DISDC): Appendix A Material Design Limit Data - A3.S18E Eurofer Steel<br>CEA/DMN/Dir TN 2004-02/A, Dec. 2004 | F. Tavassoli |
| TW4-TTMS-005-D01 | Getting started with the RAFM Database Runtime Solution V. 3.0<br>EFDA Task TW4-TTMS-005-D01, CEA/Saclay, DMN/Dir, Oct. 14, 2004                             | F. Tavassoli |

## Safety and Environment

|                    |  |   |
|--------------------|--|---|
| SEA5-1             | Stainless steel release rate evaluation in ITER operating conditions<br>DTN/STRI/LTCD04-020, December 2004   | P. Schindler et al.   |
| TW1-TSW-002        | Management of tritiated wastes – Stainless steel detritiation studies<br>Note technique DTN/STPA/LPC 04/069  | J. Chêne, A.M. Brass,<br>A. Lassoued, O.Gastaldi,   |
| TW3-TSS-SEA5.3     | EVITA : Results of the cryogenic test campaign with injection of non condensable gas<br>CEA report DTN/STPA/LTCG 04/035  | L. Ayrault, F.Challet   |
| TW3-TSS-SEA5.3     | The EVITA programme: experimental and numerical simulation of a fluid ingress in the cryostat of a water-cooled fusion reactor<br>SOFT 2004                                      | P. Sardain, L. Ayrault, G. Laffont,<br>F. Challet, L.B. Marie, B. Merrill,<br>M.T. Porfiri, G. Caruso |
| TW3-TSW-002        | Bilan des poubelles de déchets Phénix envoyées à<br>COGEMA/TCD/TDS/CDS entre 1974 et 1998 (PA 6925 XD 46849 /B)  |   |
| TW3-TSW-002        | Source, quantity and type of radioactive waste coming from ITER hot cells<br>Technical document DTN/STPA/LPC 2004/070  | O. Gastaldi, C. Lacressonnière  |
| TW4-TSS-SEA5.5-D11 | Status of PACTITER<br>Note Technique DTN/SMTM/2004-117, décembre 2004  | F. Dacquait   |
| TW4-TSS-SEA5.5-D11 | Status of the PACTITER development<br>Meeting on PACTITER, Cadarache, 25-26/01/05.   | F. Dacquait, B. Larat, F. Nguyen  |
| TW4-TSS-SEA5.5-D11 | Final report - Validation of EU Safety Computer codes: validation of PACTITER on the CIRENE experiment - Feasibility study<br>Note Technique DTN/STRI/LTCD 04-021, décembre 2004 | M. Girard, V. Blet, F. Dacquait   |
| TW4-TSS-SEA5.5-D11 | ITER 2004 tests report – Stainless steel Release rate evaluation in ITER operating conditions<br>Note technique DTN/STRI/LTCD 04-020, décembre 2004                              | P. Shindler, Y. Philibert, V. Blet  |

## System Studies

### Power Plant Conceptual Studies (PPCS)

|                    |   |                          |
|--------------------|---|--------------------------|
| TW2-TRP-PPCS15-D03 | Waste management in fusion power plant PPCS<br>Technical report CEA/DTN/STPA/LPC NT 04/065  | C. Lacressonnière        |
| TW4-TRP-002-D04    | Helium-Cooled Lithium-Lead Fusion Power Plant (PPCS model A and B) Design and integration of in-vessel components and associated systems<br>CEA report, SERMA/LCA/RT/04-3543/A, February 2005 | A. Li Puma, L. Giancarli |

## ITER Site Preparation

### European ITER Site Studies

|                 |  |
|-----------------|--|
| CEFDA03-1069    | EISS3 stage 1+2 report delivered in June 2004    |
| CEFDA03-1082    | EISS2 final report delivered in March 2004       |
| CEFDA04-1161    | EISS4 interim report delivered in January 2005   |
| TW4-TESS-COLABA | EISS4 final report to be delivered in March 2005 |

## Site and Plant Layout

|              |   |                            |
|--------------|---|----------------------------|
| CEFDA03-1083 | CEA Study for Process Flow Diagram (PFD) and Piping Instrumentation Diagram (PID) for the ITER cryo-distribution system (including AUTOCAD drawings and component lists)<br>Note SBT/04-244/FM, November 2004 | F. Millet                  |
| CEFDA03-1083 | Conceptual Design for Auxiliary Cold Box for Toroidal Magnets (including CATIA drawings)<br>Technical Report DAPNIA-SACM, March 2005  | P. Chesny                  |
| CEFDA03-1083 | Conceptual design for cold valve box for torus cryopumps and pellet injection system (including CATIA drawings)<br>Note SBT/CT/05-01, March 2005  | F. Millet and Y. Machizaud |
| CEFDA03-1083 | Description of the PFD for the ITER cryo-distribution system<br>Note SBT/04-58 rev 2/FM<br>November 2004  | F. Millet                  |

## JET Technology

### Physics Integration

#### Heating Systems

|              |  |                     |
|--------------|--|---------------------|
| CEFDA03-1031 | Design of a limiter for the JET-EP-ICRH Antenna<br>23rd SOFT in Venice September 2004. | Ph. Chappuis et al. |
|--------------|--|---------------------|

#### Diagnostics

|              |  |                         |
|--------------|--|-------------------------|
| CEFDA03-1044 | Technical group evaluation report on analysis of IR endoscope tenders<br>DIAG/NTT-2004.005 (2004)                            | E. Gauthier             |
| CEFDA03-1044 | Technical specifications of Cudas software for control of the JET-EP IR camera<br>DIAG/CCH-2004.015 (2004)                   | E. Gauthier             |
| CEFDA03-1044 | Minutes on meeting at CEDIP on 8th April 2004<br>DIAG/CRR-2004.016 (2004)  | E. Gauthier, H. Roche   |
| CEFDA03-1044 | Report on tender evaluation on the IR endoscope Call for Tender<br>DIAG/NTT-2004.004 (2004)                                  | E. Gauthier             |
| CEFDA03-1044 | Minutes of meeting at TNO on 17th march 2004<br>DIAG/CRR-2004.009 (2004)   | E. Gauthier, J. Migozzi |
| CEFDA03-1044 | Optical design of an infrared endoscope using reflective optics<br>DIAG/NTT-2004.007 (2004)                                  | E. Gauthier, J. Migozzi |
| CEFDA03-1044 | Minutes of meeting at TNO on 24th march 2004<br>DIAG/CRR-2004.010 (2004)   | E. Gauthier             |
| CEFDA03-1044 | Minutes of meeting hold at JET on 21st October 2004<br>DIAG/CRR-2004.043 (2004)  | E. Gauthier             |
| CEFDA03-1044 | Photometric analysis of the JET-IRV new optical design<br>DIAG/NTT-2004.011 (2004)   | D. Guilhem              |
| CEFDA03-1044 | Minutes of kick-off meeting with TNO on infrared endoscope contract<br>FU 06 CT 2004-00023<br>EFDA EP IRV 01/09/2004         | E. Gauthier             |
| CEFDA03-1044 | Minutes of project Board on 28th September 2004 at JET<br>EFDA EP DIA IRV-R-010 12/10/2004                                   | J. Gafert               |
| CEFDA03-1044 | JET EP INFRARED DIAGNOSTIC PROJECT - Thermomechanical behaviour of Cassegrain telescope system -<br>DIAG/NTT-2004.008 (2004) | M. Missirlian           |

## Vessel/In-Vessel

### Plasma Facing Components

|            |  |  |
|------------|--|--|
| JW0-FT-3.1 | Post test 3-D thermal calculations of jet divertor tiles<br>CEA report SEMT/LM2S/RT/04.027, August 2004  | P. Yala and L. Nicolas   |
| JW0-FT-3.1 | Compte rendu et analyse préliminaire des expériences de dépôt de puissance sur les tuiles du divertor<br>DIAG/NTT-2004.028 (2004)  | E. Gauthier  |
| JW0-FT-3.1 | Modélisation des expériences de dépôt de puissance sur des tuiles issues du divertor du JET<br>CFP/NTT-2004.022 (2004)   | S. Dumas, E. Gauthier, M. Missirlian   |
| JW0-FT-3.1 | Final report of JW0-FT-FT3.1 task<br>CFP/NTT-2004.031 (2004)   | E. Gauthier, S. Dumas, L. Nicolas, P. Yala   |
| JW0-FT-3.1 | Thermal behaviour of redeposited layer under high heat flux exposure<br>16th Int. Conf. on Plasma Surface Interaction in Controlled Fusion Devices (2004), J. Nucl. Mater., 337-339 (2005) 960-964 | E. Gauthier, S. Dumas, J. Matheus, M. Missirlian, Y. Corre, L. Nicolas, P. Yala, J. Coad, P. Andrew, S. Cox, and Efdá-JET team |

### Safety and Environment

|             |  |   |
|-------------|--|---|
| JW4-FT-3.19 | Studies on graphite surfaces detritiation by pulsed repetition rate nanosecond lasers<br>Presentation on SOFT'2004 conference, 20-24 September 2004, Venice, Italy | A. Semerok, F. Le Guern, F. Brygo, C. Grisolia, D. Farcage, C. Hubert, C. Lascoutouna, M. Tabarant, J.M. Weulersse  |
| JW4-FT-3.19 | Studies on tokamak wall surfaces decontamination by pulsed repetition rate lasers<br>CEA report NT DPC/SCP/05-111-A, January 2005, 50 pages                        | A. Semerok, J.M. Weulersse, F. Brygo, D. Farcage, C. Hubert, C. Lascoutouna, M. Géléoc, P. Wodling, H. Long, F. Champonnois, G. Brunel, G. Vimond, E. Lizon, V. Dauvois, V. Delanne, C. Grisolia, S. Fomichev, M. Hashida |

## Heating Systems Technology Project

|              |   |  |
|--------------|---|--|
| CEFDA04-1140 | Design and Fabrication of the "ITER-like" SINGAP D- Acceleration System<br>23rd symposium of fusion technology 20-24 September 2004                                 | P. Massmann, L. Svensson, H.P.L. de Esch and R.S. Hemsworth  |
| CEFDA04-1140 | Development of the Long Pulse Negative Ion Source for ITER<br>Symposium on the Production and Neutralization of Negative Ions and Beams, Kiev, 13-17 September 2004 | R.S. Hemsworth, D. Boilson, U. Fanz, L. Svensson, H.P.L. de Esch, A. Krylov, P. Massmann and B. Zaniol |
| CEFDA04-1140 | Negative Ion Yield in Long pulse operation on the KAMABOKO III ion source<br>23rd symposium of fusion technology 20-24 September 2004                               | D. Boilson, H.P.L. de Esch, R.S. Hemsworth, A. Krylov, P. Massmann and L. Svensson                     |

## UNDERLYING TECHNOLOGY PROGRAMME

### Vessel/In Vessel

#### Plasma Facing Components

|                   |   |                            |
|-------------------|---|----------------------------|
| UT-VIV/PFC-Damage | Endommagement et rupture dans les assemblages des composants face au plasma, Analyse de l'endommagement de la liaison CFC-Cu à l'échelle microscopique : Analyse des mécanismes d'amorçage<br>Rapport 2a, Projet P6, 20/12/04 | D. Leguillon, C. Henninger |
|-------------------|---|----------------------------|

|                    |  |  |
|--------------------|--|--|
| UT-VIV/PFC-Damage  | Endommagement et rupture dans les assemblages des composants face au plasma, Analyse de l'endommagement de la liaison CFC-Cu à l'échelle microscopique : Analyse des mécanismes locaux de fissuration<br>Rapport 2a-bis, Projet P6, 20/12/04   | D. Leguillon, C. Henninger                                       |
| UT-VIV/PFC-Damage  | Endommagement et rupture dans les assemblages des composants face au plasma, Analyse des mécanismes d'endommagement de l'assemblage à l'échelle macroscopique : Calcul des contraintes résiduelles et des contraintes sous chargement de flux thermique<br>Rapport 3a-bis, Projet P6, 1/12/04  | E. Martin  |
| UT-VIV/PFC-Damage  | Endommagement et rupture dans les assemblages des composants face au plasma, Identification d'une loi de comportement thermomécanique pour composites 3D C/C : application aux matériaux N11 et NB31. Lois de comportement disponibles pour les C/C et extension possible aux matériaux N11 et NB31<br>Rapport 1a, Projet P6, 01/12/04 | G. Camus   |
| UT-VIV/PFC-HIP     | Improvement of the reliability, performance and relevancy of HIP processes for PFC components<br>rapport technique DTEN/DL/2005/015, march 2005  | E. Rigal, C. Chabrol,<br>O. Gillia et al.                        |
| UT-VIV/PFC-NanoSic | Densification of SiC nanometric powders: 2004 final report<br>CEA report, DTEN/DL/2004/044 (01/2005)   | F. Ténégal   |
| UT-VIV/PFC-NanoSic | Elaboration of nanocrystalline silicon carbide by hot isostatic pressing (HIP)<br>NANO 2004, Wiesbaden (06/2004)   | F. Ténégal, N. Herlin, D. Gosset,<br>L. Boulanger, S. Poissonnet |
| UT-VIV/PFC-NanoSic | Nanocrystalline silicon carbide (SiC): 2004 interim report<br>CEA report, DTEN/DL/2004/021 (07/2004)   | F. Ténégal   |
| UT-VIV/PFC-Pyro    | Application of a tricolour pyroreflectometer to plasma facing components in-situ infrared monitoring<br>Contract CEA et PROMES-CNRS Ref : V3448.001, REPORT A2, Experiments at Odeillo solar furnace, Nov. 2004  | D. Hernandez, J.L. Sans  |

## Remote Handling

|                  |  |           |
|------------------|--|-----------|
| UT-VIV/AM-ECIr   | Réalisation d'une transmission de type modulation FSK en environnement durci<br>internal report  | J. Coudon |
| UT-VIV/AM-Hydro  | Feasibility assessment of a 'pressure control' water hydraulics servovalve<br>DTSI/SCRI/LPR/05RT010  |           |
| UT-VIV/AM-Hydro  | Preliminary study of a 'pressure control' water hydraulics servovalve<br>DTSI/SCRI/LPR/05RT003   |           |
| UT-VIV/AM-Vacuum | Specification and conceptual design of a manipulator joint for remote handling under vacuum, temperature and magnetic field<br>Report DTSI/SRSI/LPR 04RT 097 |           |

## Tritium Breeding and Materials

### Breeding Blanket

|              |   |             |
|--------------|---|-------------|
| UT-TBM/BB-He | Helium and tritium leaks in the PPCS BKT & DV cooling circuits<br>CEA Report NT DEN/DTN/STPA/LTCG/04/032, August 2004 | J.L. Berton |
| UT-TBM/BB-He | Report of experiments on static benches<br>CEA report NT DEN/DTN/STPA/LTCG/04/069, December 2004                      | J.L. Berton |

### Materials Development

#### Structural Materials

|                     |   |                            |
|---------------------|---|----------------------------|
| UT-TBM/MAT-Modpulse | Monotonous short time irradiation of Eurofer at 350 and 550°C<br>CEA report, NT DEN/SAC/DMN/SRMP 2004-012 | L. Boulanger and Y.Serruys |
|---------------------|---|----------------------------|

## Safety and Environment

UT-S&E-LiPbwater

Recalculation of the LIFUS experiment (interaction between lithium-lead and water) with the 3D version of SIMMER  
February 2005, CEA report CEA/DEN/CAD/DER/SESI/LCSI/NT DO1  
14/01/05

T. Cadiou

## APPENDIX 4 : CEA TASKS IN ALPHABETICAL ORDER

| <i>Task</i>  | <i>Title</i>  | <i>Prog.</i> | <i>Field</i> | <i>Area</i> | <i>Unit</i> | <i>Site</i>        | <i>Task Leader</i>         | <i>Page</i> |
|--|---|--------------|--------------|-------------|-------------|--------------------|----------------------------|-------------|
| CEFDA01-585  | TW1-TVP-TESTAN: Monitoring and analysis of the thermal fatigue testing of divertor prototypes - 200 kW electron beam gun test   | EFDA         | VIV          | PFC         | DRFC        | Cadarache          | Escourbiac F.              | 49          |
| CEFDA01-645  | TW2-TPHN-NBDES1: Support to neutral beam physics and testing 1  | EFDA         | PI           | Hea         | DRFC        | Cadarache          | Svensson L.                | 9           |
| CEFDA02-1003<br>CEFDA03-1111                                   | TW2-TPDS-DIASUP4 and TW3-TPDS-DIASUP1: Support to the ITER diagnostic design  | EFDA         | PI           | Diag        | DRFC        | Cadarache          | Stott P.                   | 17          |
| CEFDA02-583  | TW1-TVV-DES: Destructive examination of primary first wall panels and mock-ups  | EFDA         | VIV          | PFC         | DTEN        | Grenoble           | Bucci P.                   | 55          |
| CEFDA03-1015   | TW2-TMSM-COOLINL: Mock-ups for the TF and CS Terminal regions and Cooling Inlets  | EFDA         | MAG          | MAG         | DRFC        | Cadarache          | Decool P.                  | 87          |
| CEFDA03-1029   | TW3-TVB-JOINOP: Optimization of Be/Cu alloy joints for primary first wall panels  | EFDA         | VIV          | PFC         | DTEN        | Grenoble           | Bucci P.                   | 59          |
| CEFDA03-1031<br>CEFDA04-1146                                   | JW3-EP-ICRH and JW4-EP-ICRH: Contribution to ICRH components antenna limiter  | EFDA         | PI           | Hea         | DRFC        | Cadarache          | Chapuis P.                 | 219         |
| CEFDA03-1044   | JW3-EP-IRV: Diagnostics enhancement - Wide angle IR endoscope   | EFDA         | PI           | Diag        | DRFC        | Cadarache          | Gauthier E.                | 221         |
| CEFDA03-1047   | TW3-THHN-IITF1: The first ITER NB injector and the ITER NB test facility: design  | EFDA         | HSTP         | HSTP        | DRFC        | Cadarache          | Hemsworth R.               | 239         |
| CEFDA03-1051   | TW4-TVD-ACCEPT: Study on acceptance criteria for the ITER divertor vertical target  | EFDA         | VIV          | PFC         | DRFC        | Cadarache          | Schlosser J.               | 63          |
| CEFDA03-1067   | TW3-TVM-MDB: Rules for design, fabrication and inspection Establishment and Operation of a Material Database  | EFDA         | VIV          | V/B         | DMN         | Saclay             | Tavassoli F.               | 23          |
| CEFDA03-1069<br>CEFDA03-1082<br>CEFDA04-1161<br>TW4-TES-COLABA | European ITER Site Studies (EISS)<br>TW3-TES-EISSg1: EISS 3 generic tasks CEA<br>TW3-TES-EISS2c: EISS 3 stage 2<br>TW4-TES-EISS4F: European ITER site study 4 - Cadarache<br>TW4-TES-COLABA: Cadarache site for ITER - Collaboration with Local Authorities | EFDA         | ISP          | EISS        | DRFC        | Cadarache          | Garin P.                   | 207         |
| CEFDA03-1077   | TW3-TVB-INMOCK: Fabrication of primary first wall mock-ups for in-pile experiments  | EFDA         | VIV          | PFC         | DTEN        | Grenoble           | Bucci P.                   | 67          |
| CEFDA03-1083   | TW3-TEP-CRYO2: Design of ITER cryoplant/cryo-distribution system (auxilliary coldboxes, cryoline...)  | EFDA         | ISP          | SPL         | DRFMC       | Grenoble           | Millet F.                  | 211         |
| CEFDA03-1091   | TW4-TVM-LIP: Rules for design, fabrication and inspection Modification of ITER materials documents and assessment of material data for licensing TBM's design rules   | EFDA         | VIV          | V/B         | DMN         | Saclay             | Tavassoli F.               | 25          |
| CEFDA03-1098   | TW3-TDS-MAGCEA: Detailed engineering and manufacturing studies of the ITER magnet system: Poloidal Field (PF) coil windings and cold test assessment  | EFDA         | DSP          | DSP         | DRFC        | Cadarache          | Libeyre P.                 | 215         |
| CEFDA03-1120   | TW3-TMSC-ASTEST: Tests of advanced Nb <sub>3</sub> Sn strands - Extensive characterization of industrial advanced Nb <sub>3</sub> Sn strands developed for ITER TF coils system   | EFDA         | MAG          | MAG         | DRFC        | Cadarache          | Zani L.                    | 91          |
| CEFDA03-1129   | TW3-TPHI-ICRDES1: ITER ICRF Antenna and matching system design  | EFDA         | PI           | Hea         | DRFC        | Cadarache          | Bosia G.                   | 13          |
| CEFDA04-1127   | TW4-TMSC-SAMAN1: Manufacture of sub-size samples  | EFDA         | MAG          | MAG         | DRFC        | Cadarache          | Duchateau JL.              | 93          |
| CEFDA04-1134   | TW4-TMSC-BARBEN: Bending strain effects of single strands - Study of bending strain effect on critical properties of Nb <sub>3</sub> Sn strands jacketed with stainless steel for various bending amplitudes and temperatures                               | EFDA         | MAG          | MAG         | DRFC        | Cadarache          | Zani L.                    | 95          |
| CEFDA04-1140   | TW4-THHN-ADSD2: Neutral beam development for EFDA extension   | EFDA         | HSTP         | HSTP        | DRFC        | Cadarache          | Boilson                    | 243         |
| JW0-FT-3.1   | Internal PFC components behaviour and modelling   | EFDA         | VIV          | PFC         | DRFC + DM2S | Cadarache + Saclay | Gauthier E.,<br>Nicolas L. | 223         |
| JW3-FT-2.15-D01  | Detritiation of soft housekeeping materials (mainly plastics)   | EFDA         | S&E          | Safety      | DTN         | Cadarache          | Trabuc P.                  | 227         |

| <i>Task</i>         | <i>Title</i>  | <i>Prog.</i> | <i>Field</i> | <i>Area</i> | <i>Unit</i> | <i>Site</i>            | <i>Task Leader</i>      | <i>Page</i> |
|---------------------|---|--------------|--------------|-------------|-------------|------------------------|-------------------------|-------------|
| JW3-FT-2.15-D02     | Detritiation of vacuum oil and organic liquids  | EFDA         | S&E          | Safety      | DTN         | Cadarache              | Trabuc P. & Poletiko C. | 231         |
| JW4-FT-3.19         | Laser decontamination/Tritium removal - Studies on Tokamak wall surfaces decontamination by pulsed repetition rate lasers   | EFDA         | S&E          | Safety      | DPC         | Saclay                 | Semerok A.              | 235         |
| SEA5-1              | Validation of computer codes and models   | EFDA         | S&E          | Safety      | DTN         | Cadarache              | Schindler P.            | 171         |
| TW0-T438-01         | Development and testing of time resolved erosion detecting techniques   | EFDA         | VIV          | PFC         | DRFC        | Cadarache              | Gauthier E.             | 71          |
| TW0-T508/05         | Development of Be/CuCrZr brazing techniques   | EFDA         | VIV          | V/B         | DTEN        | Grenoble               | Bucci P.                | 27          |
| TW1-TMC-CODES       | Design and Interpretation Codes - Determination of thermohydraulic properties of cable-in-conduit conductors with a central channel   | EFDA         | MAG          | MAG         | DRFC        | Cadarache              | Decool P.               | 99          |
| TW1-TMS-PFCITE      | Poloidal Field Conductor Insert (PFCI)  | EFDA         | MAG          | MAG         | DRFC        | Cadarache              | Ciazynski D.            | 103         |
| TW1-TSW-002         | Waste and decommissioning strategy  | EFDA         | S&E          | Safety      | DTN         | Cadarache              | Gastaldi O.             | 175         |
| TW1-TVV-HIP         | Improvement of HIP Fabrication techniques   | EFDA         | VIV          | V/B         | DTEN        | Grenoble               | Bucci P.                | 31          |
| TW2-TMST-TOSKA      | TFMC testing with the LCT coil  | EFDA         | MAG          | MAG         | DRFC        | Cadarache              | Duchateau J.L.          | 105         |
| TW2-TPDS-DIADEV-D02 | Development of diagnostic components - First mirror study   | EFDA         | PI           | Diag        | DRFC        | Cadarache              | Lipa M.                 | 19          |
| TW2-TRP-PPCS15-D03  | Waste management strategy on model A and B  | EFDA         | SS           | PPCS        | DTN         | Cadarache              | Lacressonnière C.       | 193         |
| TW2-TTBB-002b-D01   | Blanket manufacturing techniques - First wall HIPping with open channels  | EFDA         | TBM          | HCPB        | DTEN        | Grenoble               | Rigal E.                | 113         |
| TW2-TTBC-001-D01    | Helium Cooled Lithium Lead - TBM design, integration and analysis - Blanket system design and analysis - Integration and testing in ITER  | EFDA         | TBM          | HCLL        | DM2S        | Saclay                 | Li Puma A.              | 117         |
| TW2-TTBC-002-D01    | Blanket manufacturing techniques - Fabrication processes for HCLL and HCPB TBMs   | EFDA         | TBM          | HCLL        | DTEN        | Grenoble               | Rigal E.                | 123         |
| TW2-TTBC-002-D03    | Testing of small-scale mocks-ups to qualify manufacturing technologies  | EFDA         | TBM          | HCLL        | DTN         | Cadarache              | Cachon L.               | 127         |
| TW2-TTBC-005-D01    | Helium Cooled Lithium Lead - Safety and Licensing - Test Blanket Module (TBM) accidental safety study   | EFDA         | TBM          | HCLL        | DER + TA    | Cadarache + Aix en Pce | Schmidt N., La Lumia    | 129         |
| TW2-TTMS-001b-D02   | Irradiation performance - Neutron irradiation to 70 dpa at 325°C and PIE  | EFDA         | TBM          | RAFM        | DMN         | Saclay                 | Alamo A.                | 135         |
| TW2-TTMS-004a-D04   | Eurofer : Fusion welds development - Evaluation of a welding process adapted to the Test Blanket Module's geometry : Assembly of the horizontal cooling plates with the continuous wave YAG laser welding process | EFDA         | TBM          | RAFM        | DTEN        | Saclay                 | Forest L.               | 139         |
| TW2-TTMS-004b-D01   | Tubing process qualification - Advanced process development and testing for the production of TBM's cooling channels  | EFDA         | TBM          | RAFM        | DTEN        | Grenoble               | Rigal E.                | 143         |
| TW2-TTMS-004b-D02   | Qualification of fabrication processes - Processing of high quality welds according to TBM design   | EFDA         | TBM          | RAFM        | DTEN        | Saclay                 | Asserin O.              | 145         |
| TW2-TTMS-005b-D03   | Rules for design, fabrication, inspection Fracture Mechanics Assessments of TBM's   | EFDA         | TBM          | RAFM        | DTEN        | Grenoble               | Couturier R.            | 151         |
| TW2-TVV-ROBOT       | Dynamic test rig for Intersector Welding Robot (IWR) for VV sector field joining  | EFDA         | VIV          | V/B         | DTEN        | Saclay                 | Aubert P.               | 33          |
| TW3-THHE-CCGDS1     | Coaxial cavity gyrotron and test facility - Design, support to the industrial development and preparation of the technical specifications   | EFDA         | HSTP         | HSTP        | DRFC        | Cadarache              | Magne R.                | 247         |
| TW3-THHI-GTFDS1     | Fusion diacode, IC RF generator, IC power supply and IC test facility - Design, support to industrial development and preparation of the technical specifications   | EFDA         | HSTP         | HSTP        | DRFC        | Cadarache              | Mollard P.              | 249         |
| TW3-TMSC-ELRES      | Experimental assessment of the effect of electrical resistances on the V-I characteristics of superconductive cables  | EFDA         | MAG          | MAG         | DRFC        | Cadarache              | Ciazynski D.            | 109         |
| TW3-TPP-ERDIAG      | Evaluation of Laser Ablation Optical Emission Spectroscopy (LA-OES) method for graphite co-deposited layer characterization   | EFDA         | PI           | Edge        | DPC         | Saclay                 | Semerok A.              | 5           |

| <i>Task</i>                          | <i>Title</i>   | <i>Prog.</i> | <i>Field</i> | <i>Area</i> | <i>Unit</i> | <i>Site</i> | <i>Task Leader</i> | <i>Page</i> |
|--------------------------------------|--|--------------|--------------|-------------|-------------|-------------|--------------------|-------------|
| TW3-TSS-SEA5.3                       | Ice formation on cryogenic surfaces  | EFDA         | S&E          | Safety      | DTN         | Cadarache   | Ayrault L.         | 181         |
| TW3-TSW-002                          | Assessment of radioactive waste in ITER hot cell facility  | EFDA         | S&E          | Safety      | DTN         | Cadarache   | Gastaldi O.        | 183         |
| TW3-TTMA-001-D04<br>TW3-TTMA-002-D04 | SiC/SiC ceramic composites - Divertor and Plasma Facing Materials  | EFDA         | TBM          | ADV         | DMN         | Saclay      | Alamo A.           | 161         |
| TW3-TVM-JOINT                        | Characterization of the CuCrZr/SS junction strength for different blanket manufacturing conditions                                 | EFDA         | VIV          | V/B         | DTEN        | Grenoble    | Gillia O.          | 35          |
| TW3-TVV-DISFREE                      | Further development of the hybrid MIG/Laser welding technique for VV sector field joining  | EFDA         | VIV          | V/B         | DTEN        | Saclay      | De Dinechin G.     | 39          |
| TW3-TVV-ROBASS                       | Long detection range seam tracker  | EFDA         | VIV          | V/B         | DTEN        | Saclay      | Aubert P.          | 43          |
| TW4-TRP-002-D02b                     | Conceptual design of a HCLL reactor - Tritium control & management analysis, thermo-hydraulic and thermo-mechanical analyses       | EFDA         | SS           | PPCS        | DM2S        | Saclay      | Farabolini W.      | 197         |
| TW4-TRP-002-D04                      | Conceptual design of a HCLL reactor - Design Integration   | EFDA         | SS           | PPCS        | DM2S        | Saclay      | Li Puma A.         | 201         |
| TW4-TSS-SEA5.5-D02&D05               | Validation of the PAXITR and PACTITER code against fusion-specific experiments   | EFDA         | S&E          | Safety      | DTN         | Cadarache   | Girard M.          | 187         |
| TW4-TSS-SEA5.5-D11                   | Validation of the PACTITER code against fusion-specific experiments - Development of the PACTITER code                             | EFDA         | S&E          | Safety      | DTN         | Cadarache   | Dacquait F.        | 191         |
| TW4-TTBB-005-D01                     | HCPB breeder and neutrons multiplier materials<br>Procurement and quality control of Li <sub>2</sub> TiO <sub>3</sub> pebbles      | EFDA         | TBM          | HCPB        | DTEN        | Saclay      | Lulewicz J.D.      | 115         |
| TW4-TTBC-001-D01                     | TBM design, integration and analysis - Testing programme and engineering design of the first HCLL TBM for ITER H-H phase           | EFDA         | TBM          | HCLL        | DM2S        | Saclay      | Farabolini W.      | 133         |
| TW4-TTMA-001-D04                     | Modelling of the mechanical behaviour of advanced 3D SiC <sub>f</sub> /SiC composite   | EFDA         | TBM          | ADV         | DM2S        | Saclay      | Guérin C.          | 163         |
| TW4-TTMI-001-D01                     | IFMIF accelerator facilities - Accelerator system design   | EFDA         | TBM          | NS          | DAPNIA      | Saclay      | Ferdinand R.       | 167         |
| TW4-TTMS-005-D01                     | Rules for design, fabrication and inspection<br>Update Data Base and Appendix A of DEMO-SDC  | EFDA         | TBM          | RAFM        | DMN         | Saclay      | Tavassoli F.       | 155         |
| TW4-TTMS-007-D02                     | Modelisation of irradiation effect<br>Ab-initio defect energy calculations in the Fe-He system                                     | EFDA         | TBM          | RAFM        | DMN         | Saclay      | Willaime F.        | 157         |
| TW4-TVR-AIA                          | Articulated Inspection Arm (AIA)   | EFDA         | VIV          | RH          | DTSI        | Fontenay    | Friconneau J.P.    | 73          |
| TW4-TVR-Radtol                       | Radiation tolerance assessment of standard electronic components for remote handling   | EFDA         | VIV          | RH          | DTSI        | Fontenay    | Giraud A.          | 77          |
| TW4-TVR-WHMAN                        | Development of a water hydraulic manipulator   | EFDA         | VIV          | RH          | DTSI        | Fontenay    | Friconneau J.P.    | 83          |
| TW4-TVV-OSWELD                       | Qualification of multiple phased array UT for one sided welds during VV manufacture  | EFDA         | VIV          | V/B         | DETECS      | Saclay      | Bredif Ph.         | 45          |
| UT-S&E-LASER/DEC                     | Laser decontamination/Tritium removal - Modelling of lasers surface heating  | UT           | S&E          | Safety      | DPC         | Saclay      | Semerok A.         | 291         |
| UT-S&E-LiPbwater                     | Recalculation of the LIFUS experiment (interaction between lithium-lead and water) with the 3D version of SIMMER                   | UT           | S&E          | Safety      | DER         | Cadarache   | Cadiou T.          | 295         |
| UT-TBM/BB-He                         | Helium components technology - Problems and outline of solutions   | UT           | TBM          | BLK         | DTN         | Cadarache   | Berton J.L.        | 279         |
| UT-TBM/MAT-LAM/Opti                  | Development of new RAFM steels with regard to creep properties   | UT           | TBM          | MAT         | DMN         | Saclay      | De Carlan Y.       | 283         |
| UT-TBM/MAT-Modpulse                  | Pulsed irradiation of the martensitic alloy Eurofer - Irradiations by krypton ions at 350 and 550°C at high flux during short time | UT           | TBM          | MAT         | DMN         | Saclay      | Boulangier L.      | 287         |
| UT-VIV/AM-ECIrr                      | Remote handling techniques - Radiation effects on electronic components  | UT           | VIV          | RH          | DTSI        | Fontenay    | Giraud A.          | 267         |
| UT-VIV/AM-Hydro                      | Technologies and control for remote handling systems   | UT           | VIV          | RH          | DTSI        | Fontenay    | Friconneau J.P.    | 273         |
| UT-VIV/AM-Vacuum                     | Technologies for vacuum and temperature and magnetic field conditions for remote handling systems                                  | UT           | VIV          | RH          | DTSI        | Fontenay    | Friconneau J.P.    | 275         |

| <i>Task</i>        | <i>Title</i>   | <i>Prog.</i> | <i>Field</i> | <i>Area</i> | <i>Unit</i> | <i>Site</i> | <i>Task Leader</i> | <i>Page</i> |
|--------------------|--|--------------|--------------|-------------|-------------|-------------|--------------------|-------------|
| UT-VIV/PFC-Damage  | Study of damage mechanisms in plasma facing components   | UT           | VIV          | PFC         | CNRS-LCTS   | Pessac      | Martin E.          | 253         |
| UT-VIV/PFC-HIP     | Improvement of reliability, performance and industrial relevancy of HIP processes for PFC components | UT           | VIV          | PFC         | DTEN        | Grenoble    | Chabrol C.         | 255         |
| UT-VIV/PFC-NanoSiC | Nanocrystalline silicon carbide (SiC) - Optimization of the preparation of NanoSiC                   | UT           | VIV          | PFC         | DTEN        | Saclay      | Ténégal F.         | 259         |
| UT-VIV/PFC-Pyro    | Application of a tricolour pyroreflectometer to plasma facing components in-situ infrared monitoring | UT           | VIV          | PFC         | CNRS-IMP    | Font Romeu  | Hernandez D.       | 263         |

**Programme**

EFDA = EFDA Technology Programme  
 UT = Underlying Technology Programme

**Field**

PI = Physic Integration  
 VIV = Vessel - In Vessel  
 MAG = Magnets  
 TBM = Tritium Breeding & Materials  
 S&E = Safety & Environment  
 SS = System Studies  
 ISP = ITER Site Preparation  
 DSP = Design Support and Procurement  
 HSTP = Heating Systems Technology Project

**Area**

Edge = Plasma Edge  
 Hea = Heating and Current Drive  
 Diag = Diagnostics  
 V/B = Vessel/Blanket and Materials  
 PFC = Plasma Facing Components  
 RH = Remote Handling  
 MAG = Magnets  
 BLK = Blanket  
 HCPB = Helium Cooled Pebble Bed Blanket  
 HCLL = Helium Cooled Lithium Lead Blanket  
 MAT = Materials  
 RAFM = Reduced Activation Ferritic Martensitic steels  
 ADV = Advanced Materials  
 NS = Neutron Source  
 Safety = Safety and environment  
 PPCS = Power Plant Conceptual Studies  
 EISS = European ITER Site Studies  
 SPL = Site and Plant Layout  
 DSP = Design Support and Procurement  
 HSTP = Heating Systems Technology Project

## APPENDIX 5 : CEA SITES

